

„Synthese und Untersuchung von
peptidischen Substraten der
Histondeacetylasen“

Dissertation

zur Erlangung des
Doktorgrades der Naturwissenschaften (doctor rerum naturalium)

der

Naturwissenschaftlichen Fakultät I
Biowissenschaften
der Martin-Luther-Universität
Halle-Wittenberg

vorgelegt von
Herrn Matthes Zessin

Gutachter:

Prof. Dr. Mike Schutkowski

Prof. Dr. Wolfgang Sippl

Prof. Dr. Manfred Jung

Termin der öffentlichen Verteidigung: 20.02.2024

Inhaltsverzeichnis

Inhaltsverzeichnis	iii
Abkürzungsverzeichnis.....	v
1 Einleitung.....	1
1.1 Epigenetische Regulation	1
1.2 Posttranslationale Modifikationen – Ac(et)ylierung an Histonen.....	1
1.3 Klassifizierung und zelluläre Lokalisation der Histondeacetylasen.....	2
1.4 Substrate und Substratspezifität der HDACs.....	3
1.4.1 Acylspezifität der HDACs	4
1.4.2 Bedeutung der PTMs am Beispiel der Lysinlactoylierung	6
1.4.3 Proteinsubstrate und biologische Bedeutung der HDACs.....	8
1.5 Struktur und Katalysemechanismus der Histondeacetylasen	9
1.5.1 Struktur der Zn ²⁺ -abhängigen Histondeacetylasen	10
1.5.2 Reaktionsmechanismus Zn ²⁺ -abhängiger HDACs.....	11
1.5.3 Struktur der Sirtuine und die Bindung an die Substrate	12
1.5.4 Reaktionsmechanismus der Sirtuine	13
1.6 Messung der enzymatischen Aktivität von HDACs	15
1.6.1 Quantifizierung durch Trennung von Substrat und Produkt.....	16
1.6.2 Enzym-gekoppelte Messsysteme.....	17
1.6.3 Chemisch gekoppelte Messsysteme	20
1.6.4 Intramolekulare Umlagerung.....	23
1.6.5 Direkte und kontinuierliche Messsysteme	24
1.6.6 Fluoreszenzsonden.....	25
2 Zielstellung.....	27
3 Ergebnisse	28
3.1 Continuous Activity Assay for HDAC11 Enabling Reevaluation of HDAC Inhibitors..	28
3.2 One-Atom-Substitution Enables Direct and Continuous Monitoring of Histone Deacetylase Activity	39
3.3 Continuous Sirtuin/HDAC (histone deacetylase) activity assay using thioamides as PET (Photoinduced Electron Transfer)–based fluorescence quencher	53
3.4 Continuous Histone Deacetylase Activity Assays	68
3.5 Continuous Fluorescent Sirtuin Activity Assay Based on Fatty Acylated Lysines	87
3.6 Uncovering robust delactoylase and depyruvylase activities of HDAC isoforms ...	107
4 Diskussion und Zusammenfassung der Ergebnisse.....	120

4.1	Messung der HDAC-Aktivität	120
4.1.1	FRET-basierter HDAC11 Assay	121
4.1.2	Messung der HDAC-Aktivität durch Hydrolyse des Thioacylrests	123
4.1.3	Substrate mit Thioamiden als PET-basierte Fluoreszenzquencher	126
4.1.4	Fluoreszenzbasierter Assays mit Myristoylrest	130
4.1.5	Betrachtung bekannter HDAC-Assays	132
4.2	Lactoyl- und Pyruvoylmodifikationen an Lysinen	134
5	Zusammenfassung und Ausblick	139
6	Literaturverzeichnis	141
	Danksagung	159
	Publikationsliste	160
	Lebenslauf	162
	Selbstständigkeitserklärung	163

Abkürzungsverzeichnis

3-NY	3-Nitrotyrosin
5-CF	5-Carboxyfluorescein
Abz	Aminobenzoessäure
Ac	Acetylrest
ADPr	ADP-Ribose
AGE	<i>advanced glycolated endproduct</i>
AMA	1-Aminoanthracen
AMC	Aminomethylcoumarin
APC	Antigen-präsentierende Zellen
AS	Aminosäuren
bhb	β -Hydroxybutyrylrest
Brdt	Bromodomain testis-specific protein
CoA	Coenzym A
Cy5	Cyanin5
Dansyl	5-(Dimethylamino)-naphtalin-1-sulfonsäure
DLAT	Dihydrolipoyl-Transacetylase
EGFP	<i>enhanced green fluorescent protein</i>
FAHA	2-Furylacryloylhydroxamat
FDA	<i>Food and Drug Administration</i>
FID	<i>fluorescence indicator displacement assay</i>
FITC	Fluoresceinisothiocyanat
FRET	Förster-Resonanzenergietransfers
GDH	Glutamatdehydrogenase
GO	Glyoxal
GSH	Glutathion
H3K9-Ac	Histon 3 mit Acetylierung am Lysin 9
HAT	Histonacetyltransferasen
HCC	Hepatozelluläres Karzinom
HDAC	Histondeacetylase
HDACi	HDAC Inhibitor
HMG	Hydroxymethylglutaryl
HPLC	Hochleistungsflüssigkeitschromatographie
HTS	<i>high throughput screening</i>
KDAC	Lysin-deacetylasen
Lac	Lactoylrest
LGS	Lactoglutathion
Mesna	2-Mercaptoethansulfonat-Natrium
MGO	Methylglyoxal
MS	Massenspektrometrie
Myr	Myristoylrest
NAD ⁺	Nicotinamidadeninukleotid
NAM	Nicotinamid
NBD	Nitrobenzoxadiazole

nc-RNA	nicht-codierende RNA
NCOR	Nuclear receptor co-repressor
NDA	Naphtalen-2,3-dialdehyd
NES	Nukleus-Exportsequenzen
O-AADPr	O-Acetyl-ADPribose
Pal	Palmitoylrest
PET	Photoinduzierter Elektronentransfer
PHD	<i>plant homeodomain</i>
PKM2	Pyruvatkinase M2
PTM	Posttranslationale Modifikation
Pyr	Pyruvylrest
QD	<i>quantum dots</i> (Quantenpunkte)
Q _E	Quenchingeffizienz
rpHPLC	reversed phase HPLC
SAHA	Suberoylanilid-Hydroxamsäure
SILAC	<i>stable isotope labeling by amino acids in cell culture</i>
Sir2	<i>silent information regulator 2</i>
SIRT	Sirtuine (wenn nicht anders beschrieben humane Isoformen)
TFA	Trifluoracetylrest
TNF α	Tumornekrosefaktor- α
TSA	Trichostatin A

1 Einleitung

1.1 Epigenetische Regulation

Echte vielzellige Organismen bestehen aus verschiedenen spezialisierten Gewebetypen, welche eine Vielzahl verschiedener Aufgaben im Organismus erfüllen. All diese Zellen besitzen nahezu die gleiche in der DNA kodierte Information. Um ihre spezifischen Funktionen zu erfüllen, differenzieren sich diese Zellen in verschiedene Zelltypen. Dies geschieht durch Zelltyp-spezifische Genexpression und wird durch epigenetische Modifikationen gesteuert. Dabei erfolgt eine Veränderung der Zelllinienbildung (Differenzierung), die nicht durch Änderung der DNA (Mutagenese) entsteht (1). Es gibt verschiedene Mechanismen, welche die Genaktivität erhöhen oder unterdrücken. Die wichtigsten epigenetischen Mechanismen sind DNA-Methylierung, nicht-codierende RNAs (nc-RNA), die Konformation des Chromatins und die Modifikation von Histonproteinen (2).

Die DNA eukaryotischer Zellen ist in deren Zellkern in Chromatin verpackt. Das Chromatin besteht aus Nukleosomen, welche sich aus 145-147 DNA-Basenpaaren zusammensetzen, die wiederum um ein Heterooktamer gewickelt sind. Dieses Oktamer setzt sich aus je zwei Kopien der globulären Histonproteine H2A, H2B, H3 und H4 zusammen. Dieser hoch konservierte Proteinkomplex tritt ungefähr alle 200 Basenpaare auf (3, 4). Der N-terminale Teil der Histonproteine liegt ungeordnet vor und ragt aus der Nukleosom- bzw. Chromatinstruktur heraus und ist damit für die Interaktion mit anderen Proteinen zugänglich. Diese Interaktionen und die Chromatinstruktur können durch verschiedene Modifikationen des N-terminalen Histonteils gesteuert werden. Diese Modifikationen entstehen nach der Proteinbiosynthese (Translation), weshalb sie posttranslationale Modifikationen (PTMs) genannt werden. Typische PTMs sind Phosphorylierungen, Methylierungen, SUMOylierung, Ubiquitinylierung, ADP-ribosylierung und Ac(et)ylierung (5, 6). Die Gesamtheit der PTMs bildet zusammen den sogenannten Histon-Code. Der Histon-Code wirkt auf verschiedene zelluläre Prozesse, die durch das Chromatin gesteuert werden (4).

1.2 Posttranslationale Modifikationen – Ac(et)ylierung an Histonen

Der ungeordnete N-terminale Teil der Histone ist reich an den basischen Aminosäuren (AS) Arginin und Lysin und somit unter physiologischen Bedingungen positiv geladen. Daher kommt es mit der negativ geladenen DNA zur Ausbildung ionischer Wechselwirkungen, was zu einer festen Chromatinstruktur führt. Die darunterliegenden Gene weisen dann eine geringe Genaktivität auf (7, 8). Werden die positiv geladenen Teile des Histons durch Modifikationen „maskiert“, verringern sich die Wechselwirkungen und die Chromatinstruktur ist gelockert. Dadurch haben z.B. Transkriptionsfaktoren oder die RNA-Polymerase einen besseren Zugang zu den darunter liegenden Genen und die Genaktivität ist erhöht (8). Die PTM, die diese Maskierung steuert, ist die Ac(et)ylierung der ϵ -Aminogruppe von Lysinen im Histon. Die Gesamtheit aller Ac(et)ylierungen am Chromosom wird als Acetylierungsstatus bezeichnet. Dieser ist hochdynamisch und wird vornehmlich durch zwei Enzymklassen reguliert (9).

Zum einen gibt es die als *writer* bezeichneten Histonacetyltransferasen (HAT, EC: 2.3.1.48). HATs katalysieren die Ac(et)ylierung der ϵ -Aminogruppe von Lysinen, indem sie den Ac(et)ylrest von Ac(et)yl-Coenzym A (Ac-CoA) auf den Lysinrest übertragen (10). Durch die lockere

Chromatinstruktur erhöht sich die Genaktivität. Zum anderen gibt es die *eraser*, die sogenannten Histondeacetylasen (HDAC). HDACs katalysieren die Rückreaktion und entfernen den Ac(et)ylrest von der Lysinseitenkette. Die Chromatinstruktur kondensiert und die Genaktivität sinkt wieder (11). Neben dem Einfluss auf die Chromatinstruktur können Lysinac(et)ylierungen auch durch die sogenannten *reader* „erkannt“ werden, indem diese die entsprechende Modifikation binden (10, 12). Die Bromodomänen sind vermutlich am wichtigsten für die Lysinacetylierung und daher auch die am besten untersuchten Vertreter dieser Gruppe. Oft sind sie entweder Bestandteil größerer Proteinkomplexe oder Domänen von Proteinen, wie z.B. Helicasen, HATs, *ATP dependent chromatin remodelling proteins*, Helicasen, Methyltransferasen und Transkriptionskoaktivatoren (8). Weitere *reader* von PTMs sind *plant homeodomain* (PHD)-Domänen und YEATS-Domänen.

1.3 Klassifizierung und zelluläre Lokalisation der Histondeacetylasen

Die Familie der Histondeacetylasen besteht im *Homo sapiens* aus 18 Enzymen, welche sich aufgrund der Phylogenetik in vier Klassen aufteilen lassen (Abbildung 1) (13). Die Mitglieder der Klasse I (HDAC1, HDAC2, HDAC3 und HDAC8), der Klasse IIa (HDAC4, HDAC5, HDAC7 und HDAC9), der Klasse IIb (HDAC6 und HDAC10) und der Klasse IV (HDAC11) sind die elf Zn²⁺-abhängigen HDACs (EC: 3.5.1.98, (13)). Die Klasse III besteht aus den sieben NAD⁺-abhängigen HDACs (EC: 2.3.1.286), den sogenannten Sirtuinen (SIRT). Der Name entstammt dem zuerst in *Saccharomyces cerevisiae* nachgewiesenen *silent information regulator 2* (Sir2) Protein. Sirtuine sind Homologe von Sir2 und unterscheiden sich sowohl strukturell als auch im Reaktionsmechanismus von den Zn²⁺-abhängigen HDACs. Sie nutzen NAD⁺ als Cosubstrat. Die Sirtuine lassen sich aufgrund von phylogenetischen Untersuchungen in vier Unterklassen aufteilen. Die Unterklasse I besteht aus SIRT1, SIRT2 und SIRT3, die Unterklasse II aus SIRT4, die Unterklasse III besteht aus SIRT5. Die Unterklasse IV wird aus SIRT6 und SIRT7 gebildet (14).

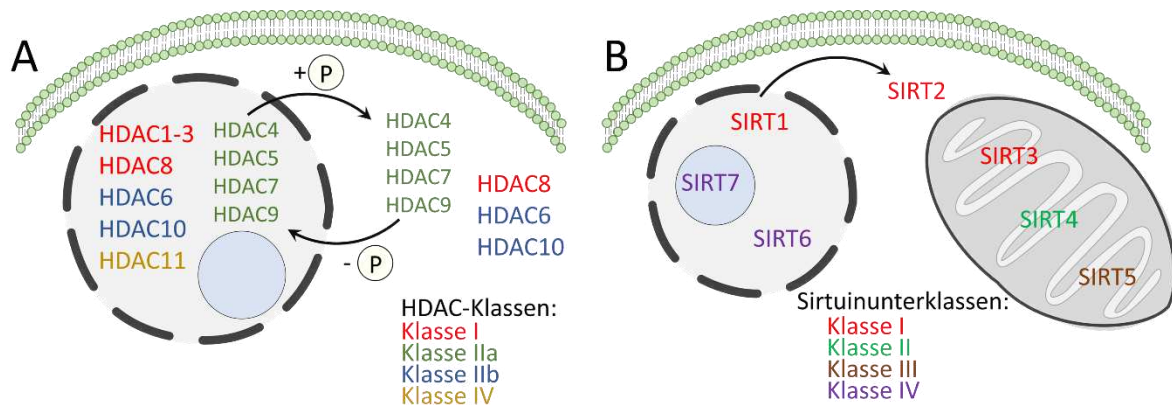


Abbildung 1. A. Subzelluläre Lokalisation und Klassifizierung der Zn²⁺-abhängigen HDACs. Das eingekreiste P zeigt eine Phosphorylierung. B. Subzelluläre Lokalisation und Klassifizierung der Sirtuine (Klasse III der HDACs).

Neben den Histonen gehört eine Vielzahl an verschiedenen Proteinen zu den Substraten der HDACs. Deswegen werden HDACs in der Literatur richtigerweise oftmals auch als Lysindeacetylasen bezeichnet (KDAC). Da HDAC aber der historisch gewachsene und gebräuchlichere Begriff ist, werden sie in dieser Arbeit weiterhin so bezeichnet. Die Substrate der HDACs befinden sich in verschiedenen Kompartimenten der Zelle. Somit lassen sich die HDACs

neben der phylogenetischen Klassifizierung auch nach ihrer zellulären Lokalisation unterscheiden.

Wie in Abbildung 1A dargestellt, sind die HDACs der Klasse I und IV vornehmlich im Nukleus und die HDACs der Klasse IIb im Cytoplasma lokalisiert (15). Die HDACs der Klasse IIa treten sowohl im Nukleus als auch im Cytoplasma auf (16). Die Lokalisation ist dynamisch und wird über Nukleus-Lokalisations- bzw. Nukleus-Exportsequenzen (NES), den Phosphorylierungsstatus und der daraus folgenden Bindung an das 14-3-3 Protein gesteuert (17, 18). Auch für HDAC8 (Klasse I) sind cytosolische Substrate bekannt (19, 20), was den Schluss nahe legt, dass HDAC8 auch im Cytoplasma vorkommt. Ebenso können die HDACs der Klasse IIb neben ihrer cytoplasmatischen Lokalisation auch im Nukleus vorkommen. Zum Beispiel wurde murine HDAC6 nach Unterbrechung der Zellproliferation im Nukleus nachgewiesen (21). Nichtsdestotrotz weist HDAC6 drei NES-Sequenzen auf und ist fast ausschließlich im Cytoplasma zu finden (21).

Die Sirtuine verteilen sich auf verschiedene Kompartimente (Abbildung 1B). SIRT1 und SIRT6 sind im Nukleus lokalisiert, SIRT7 im Nucleolus (22) und SIRT2 im Cytoplasma. Wurde SIRT2 in HeLa-Zellen überexprimiert, konnte es teilweise auch im Nukleus nachgewiesen werden (23). Außerdem scheint SIRT2 während der Mitose am Chromatin assoziiert zu sein (23, 24). Ebenso kann SIRT1 im Cytoplasma lokalisiert sein. Dies ist scheinbar vom Differenzierungsgrad der Zelle abhängig (25). Die letzten drei Sirtuine, SIRT3, SIRT4 und SIRT5, sind im Mitochondrium lokalisiert und weisen jeweils eine Importsequenz für das Mitochondrium auf (26–28). Einzelne HDACs wurden neben den oben genannten Lokalisationen auch in anderen Zellkompartimenten nachgewiesen. Die hier genannten Lokalisationen spiegeln die typische Verteilung der HDACs wider.

1.4 Substrate und Substratspezifität der HDACs

Neben den bis jetzt erwähnten Acetylresten gibt es eine Vielzahl an Acylmodifikationen für Lysinreste, die *in vivo* auftreten (Abbildung 2A). Dazu gehören kleinere Modifikationen wie Formyl- (29), Glyoxalyl- (30), Propionyl- (31), Butyryl- (32), Crotonyl- (33), Lactoyl- (34), Pyruvoyl- (30), Malonyl- (35), Succinyl- (35), Glutaryl- (36), β -Hydroxybutyryl- (bhb) (37), Hydroxyisobutyryl- (38), 3-Hydroxy-3-Methylglutaryl- (HMG) (39), Benzoylreste (40) oder auch längere Fettsäurereste wie Myristoyl- (41) oder Lipoylreste (42). Die Isoformen der HDACs weisen für die entsprechenden Reste verschiedene Spezifitäten auf.

Die Acylreste können als Lysinmodifikationen an den Histonen, aber auch an vielen anderen Proteinen gefunden werden. Diese Proteine können auch an verschiedenen Stellen mit Acylresten modifiziert werden. Weiterhin kann eine Acylierungsstelle auch verschiedene Acylmodifikationen (bzw. auch verschiedene PTMs) tragen.

Beispielsweise scheint die kompetitive Acetylierung und Buturylierung am Lysin5 des Histons 4 (H4K5) und H4K8 in aktiven Promotorregionen eine wichtige regulatorische Rolle während der Spermatogenese einzunehmen (43).

Dadurch ergibt sich eine Vielzahl an Kombinationen für mögliche HDAC-Substrate. Über einige typische Substrate bzw. die Substratspezifität der einzelnen HDACs für die verschiedenen Acylreste wird im nächsten Abschnitt ein Überblick gegeben. Nicht für alle bekannten Spezifitäten für Acylmodifikationen gibt es eine nachgewiesene biologische Relevanz, da diese oft aus *in vitro*-Messungen an Peptidsubstraten stammen. Andersherum gibt es auch *in vivo*-Studien, welche durch *knock-down*-Experimente, Überexpressions- und Inhibitor-Studien Substrate

nachgewiesen haben, ohne dass die Aktivität *in vitro* für die entsprechenden Enzyme beobachtet wurde.

Zusätzlich zur Spezifität für die Acylreste besitzen HDACs eine Spezifität für den Träger der Acylmodifikation, also das Peptid, das Protein oder das Polyamin. Insbesondere hat sich erwiesen, dass in Peptid- und Proteinsubstraten die Peptidsequenz in direkter Nachbarschaft zum modifizierten Lysin für die Substrateigenschaften gegenüber HDACs relevant ist. So wurden für die HDACs der Klasse I Peptidmikroarray-Untersuchungen der Substratsequenz auf der Grundlage von 206 Histonpeptiden durchgeführt. Dabei zeigten HDAC1, HDAC2 und HDAC8 eine hohe Sequenzspezifität. HDAC3 hingegen wies eine geringere Sensitivität für die Peptidsequenz auf (44). Auch HDAC6 weist eine hohe Sequenzspezifität in Peptidmikroarray-Analysen auf (45). Die HDACs der Klasse IIa bevorzugen vor allem aromatische AS in allen untersuchten Positionen (46).

Sirtuine sind eher unspezifisch, was die Peptidsequenz angeht. Die Bindung des Peptids im aktiven Zentrum erfolgt hauptsächlich über Wasserstoffbrückenbindungen zum Peptidrückgrat (47). In einer Untersuchung der Sequenzspezifität mittels Peptidmikroarray wurde gezeigt, dass Sirtuine grundsätzlich Isoform-spezifische Sequenzpräferenzen aufweisen (48). Diese *in vitro* Daten lassen sich nicht immer direkt in den *in vivo*-Kontext übertragen. So befindet sich in einem guten *in vivo* SIRT6 Substrat ein Arginin N-terminal zum modifizierten Lysin (47). Dahingegen erwies sich Arginin an dieser Stelle als nicht bevorzugt in den Mikroarraystudien (48). Bei HDAC1 haben die Interaktionspartner ebenso einen großen Einfluss auf die Sequenzspezifität wie im nächsten Abschnitt beschrieben. Klare Sequenzmotive wie bei manchen Proteasen weisen HDACs nicht auf.

1.4.1 Acylspezifität der HDACs

Die HDACs der Klasse I weisen eine robuste Deacetylaseaktivität auf, wobei HDAC8 für Peptide mit diesem Rest sehr hohe K_M -Werte aufweist (49–51). HDAC1-3 zeigen ebenso auch Deformylaseaktivität, mit deutlich höheren K_M -Werten als für acetylierte Substrate (49). Zusätzlich können sie auch Propionylreste und kürzere Acylreste, die sterisch anspruchsvoller sind, deacylieren, wie z.B. Crotonylreste (52, 53) oder bhb-Reste (54). HDAC3 weist dabei die breiteste Aktivität für diese Acylreste auf (49, 50). HDAC8 ist in der Lage, auch lange Fettsäurereste von Lysinen zu entfernen (51). HDAC1-3 treten *in vivo* vor allem in großen Proteinkomplexen auf, welche ihre Aktivität und ihre Spezifität beeinflussen. Beispielsweise weist die HDAC3 nur Deacetylaseaktivität auf, wenn sie mit dem *Nuclear receptor co-repressor* (NCOR) oder dem SMRT Komplex eingesetzt wird (55). Auch HDAC1 besitzt verschiedene Acylspezifitäten in Abhängigkeit von den entsprechenden Bindungspartnern. Im MiDAC-Komplex ist die HDAC1-Deacetylaseaktivität für das acetylierte H2K11 (H2K11-Ac) im assemblierten Nukleosom über 2 000-fach größer als HDAC1 gebunden im Sin3A-Komplex. Ohne Bindung an einen Proteinkomplex konnte gar keine Deacetylaseaktivität gegenüber H2K11-Ac im Nukleosom gemessen werden (56).

Eine Sonderrolle nehmen die HDACs der Klasse IIa ein. Sie zeigen *in vitro* keine oder nur sehr schwache Deacetylaseaktivität. Das ist darauf zurückzuführen, dass sich im aktiven Zentrum ein Histidin befindet. Im Gegensatz dazu befindet sich im aktiven Zentrum der anderen Zn^{2+} -abhängigen HDACs an dieser Stelle ein konserviertes Tyrosin. (siehe 1.5.2, HDAC-Mechanismus, (57)). Gegenüber trifluoracetylierten (TFA)-Substraten mit deutlich reaktiveren Amidbindungen weisen sie dagegen eine hohe Deacetylaseaktivität auf (57). Über die *in vivo*

Substrate der HDACs der Klasse IIa ist wenig bekannt. Es konnte jedoch für HDAC4 nachgewiesen werden, dass die Deacetylierung eines potentiellen *in vivo* HDAC4-Substrats von der katalytischen Aktivität der HDAC4 abhängt (58). Es könnte sein, dass die HDACs der Klasse IIa vornehmlich nicht als Deacetylasen wirken und stattdessen in der biologischen Funktion als Acetyllysin *reader* auftreten. Wie die HDACs der Klasse I sind sie oft Bestandteil von großen Multiproteinkomplexen (59). Oft kommen in den Komplexen auch HDACs der Klasse I vor, welche dann die Deacetylaseaktivität beisteuern könnten. Erst kürzlich konnte gezeigt werden, dass HDAC7 ein Acetyllysin bindet und dadurch die Dissoziation vom HDAC3/NCOR-Komplex initiiert, was eine Aktivierung von Androgenrezeptor-regulierenden Genen zur Folge hat (60).

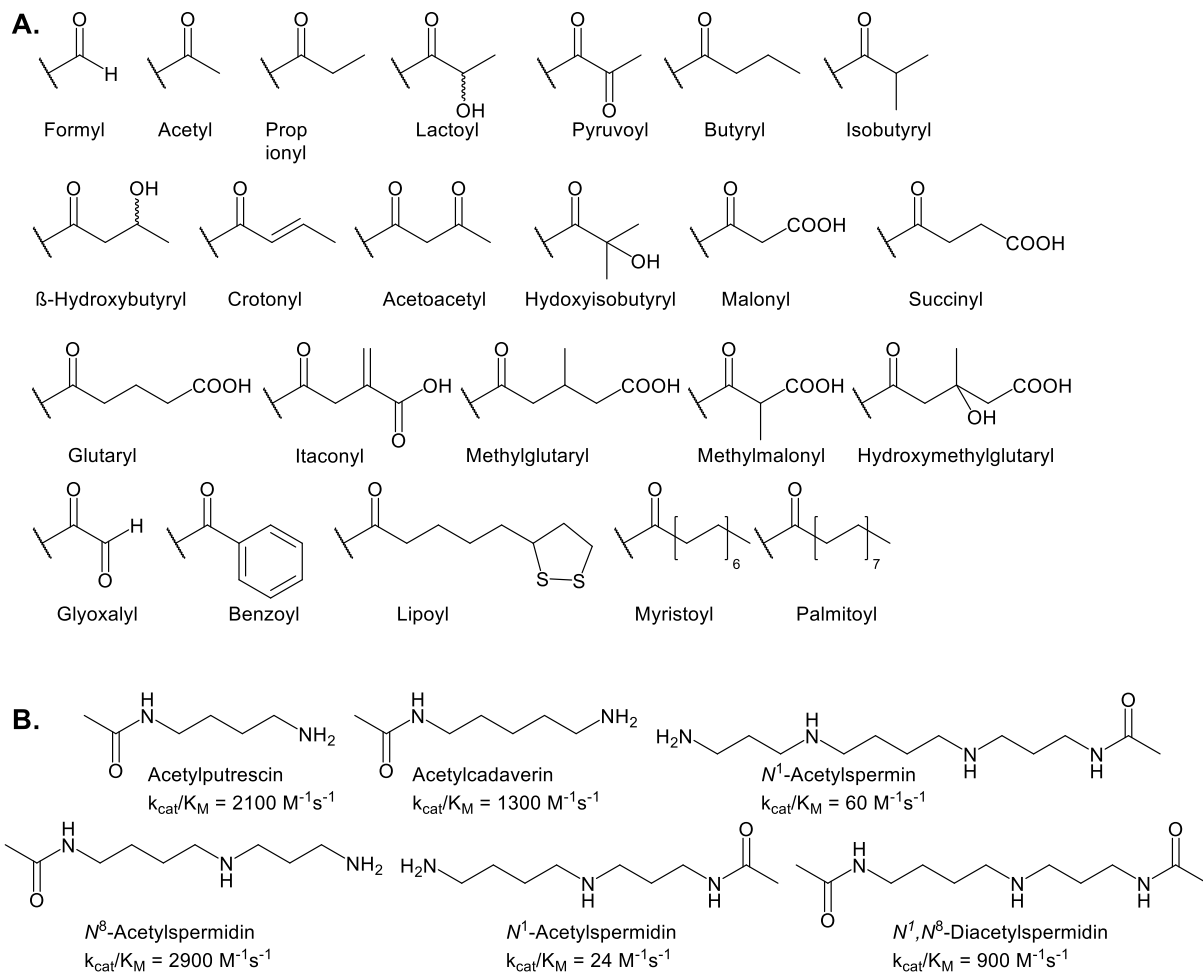


Abbildung 2. A. Struktur der *in vivo* nachgewiesenen N^ϵ -Lysinmodifikationen. **B.** Struktur der acetylierten Polyamine als Substrate für HDAC10.

Die zur Klasse IIb gehörende HDAC6 besteht aus zwei Untereinheiten, CD1 und CD2, welche unterschiedliche Substratspezifitäten aufweisen. HDAC6 ist eine starke Deacetylase mit katalytischer Effizienz bis zu $185\,000 \text{ M}^{-1}\text{s}^{-1}$ und einer guten Deformylaseaktivität mit einem k_{cat}/K_M -Wert von $97\,000 \text{ M}^{-1}\text{s}^{-1}$ mit der gleichen Peptidsequenz. Wird der Rest um eine Methylgruppe länger, also zu einem Propionylrest, verringert sich die Deacylaseaktivität dramatisch auf einen k_{cat}/K_M -Wert $1\,700 \text{ M}^{-1}\text{s}^{-1}$ (45). Längere Reste scheint die HDAC6 nicht zu entfernen (49). Diese Aktivitäten sind auf die CD2 zurückzuführen. CD1 ist sehr spezifisch für

N-terminale Acetyllysine mit Präferenzen für Glycin oder positiv geladenen AS in der -1 Position (45).

HDAC10, die zweite Deacetylase der Klasse IIb, ist dahingehend besonders, dass sie keine Proteine bzw. Peptide, sondern acetylierte Polyamine als Substrate bevorzugt. Damit ist HDAC10 eine Acetyl-Polyamindeacetylase (Abbildung 2B). Die höchste katalytische Effizienz weist HDAC10 für N⁸-Acetyl-Spermidin auf (Abbildung 2B).

HDAC11, die einzige HDAC der Klasse IV, zeigt keine messbare Deacetylaseaktivität. Dafür ist HDAC11 in der Lage, längere Fettsäurereste (ab Hexanoylrest) von Lysinresten zu entfernen. Ihre katalytische Effizienz steigt zunächst, mit zunehmender Länge des Acylrests und erreicht ihr Maximum für Dodecanoyl- bzw. für Myristoylreste. Bei weiterer Zunahme der Kettenlänge zu Palmitoyl- und Stearylresten, sinkt die katalytische Effizienz aufgrund der starken Erhöhung des K_M-Werts wieder deutlich (61–63).

Die Sirtuine der Klasse I (SIRT1, SIRT2 und SIRT3) weisen eine sehr robuste Deacetylase- und eine etwas schwächere Depropionylaseaktivität auf (50, 64). Weiterhin zeigen sie eine relativ breite Deacetylaseaktivität gegen Fettsäurereste wie Myristoylreste (64). SIRT2 akzeptiert dabei ein relativ großes Spektrum an Acylresten als Substrate wie z.B. Lactoyl- (65), Benzoyl- (40) und 4-Oxononanylreste (66).

Für SIRT4 wurde *in vivo* eine Deacetylaseaktivität nachgewiesen. Diese ist *in vitro* mit einer katalytischen Effizienz von 3,7 M⁻¹s⁻¹ allerdings relativ schwach ausgeprägt (67, 68). Dahingegen erkennt SIRT4 Peptide mit HMG-, Methylglutaryl- (39, 68) und Lipoylresten als Substrate mit deutlich besseren kinetischen Konstanten (42). Auch Succinyl- und Glutarylreste werden von SIRT4 als Substrate akzeptiert.

SIRT5 hat eine hohe Substratspezifität für die Dicarbonsäurereste Malonyl-, Succinyl-, Glutarylreste (36, 69, 70). SIRT6 hingegen zeigt *in vitro* eine starke Spezifität für längere Fettsäurereste und weist eine außerordentlich geringe Deacetylaseaktivität auf (41, 71). *In vivo* hingegen konnte für SIRT6 für spezifische Reste (H3K9-Ac und H3K54-Ac) auch eine Deacetylaseaktivität gezeigt werden (72, 73). Wurden vollständige acetylierte Nukleosomen als Substrate genutzt, konnte diese Aktivität auch *in vitro* reproduziert werden. Wurde hingegen nur das acetylierte Histon-Oktamer ohne DNA als Substrat dargeboten, konnte keine Deacetylierung durch SIRT6 beobachtet werden (74). Ähnliche Beobachtungen wurden für SIRT7 gemacht. Zuerst wurden bei SIRT7 nahezu keine Deacetylaseaktivität an Peptidsubstraten *in vitro* gemessen, obwohl einige acetylierte *in vivo*-Substrate, wie z.B. H3K18-Ac (75) und GA *binding protein* β1 (76), nachgewiesen wurden. Es konnte dann aber gezeigt werden, dass die SIRT7-Aktivität für acetylierte, buturylierte und myristoylierte H3K18-Peptide durch DNA bzw. tRNA-Zugabe deutlich gesteigert werden konnte (77, 78). Im Gegensatz dazu konnten andere Arbeiten die Deacetylaseaktivität von SIRT7 nur an vollständigen Nukleosomen nachweisen (79, 80). SIRT7 scheint hierbei sehr ortsspezifisch nur die Reste H3K18-Ac und H3K36-Ac zu deacetylieren (79, 81).

1.4.2 Bedeutung der PTMs am Beispiel der Lysinlactoylierung

Die Lysinlactoylierung ist eine der zuletzt entdeckten PTMs. 2015 wurde die Lysinlactoylierung bei den Untersuchungen der Proteinglykolierung in der Linse des humanen Auges *in vivo* als Proteinmodifikation entdeckt (82). Hierbei wurde vermutet, dass es als *advanced glycolated endproduct* (AGE) aus Methylglyoxal (MGO) entsteht. MGO wiederum ist ein Nebenprodukt der Glykolyse und entsteht aus Glycerinaldehyd-3-phosphat und

Dihydroxyacetonphosphat. Da die Lysinlactoylierung aus der *in vivo* Maillardreaktion stammt, wurde angenommen, dass die Lactoylierung altersbedingt oder krankheitsbedingt (Katarakt) erhöht ist. So konnte eine lineare Korrelation der Gesamtmenge der Lysinlactoylierung mit dem Alter ($r^2 = 0,729$, $n = 25$) nachgewiesen werden (82). In einer ähnlichen Untersuchung konnte zusätzlich demonstriert werden, dass sich die Gesamtmenge der Lysinlactoylierung der löslichen Proteinfraction aus der Leber von drei Monate alten Ratten zu 22 Monate alten Ratten verdoppelte (30).

Zhang *et al.* wiesen 2019 nach, dass die Lysinlactoylierung auch am Histon auftritt. Die Menge der Histonlactoylierung ist dabei vor allem von der Lactatkonzentration in der Zelle abhängig. Die Lysinlactoylierung wird ähnlich wie die Lysinacetylierung an aktiven Genen gefunden. Das deutet auf einen ähnlichen Wirkmechanismus wie bei Lysinacetylierung (Chromatinlockerung und Aktivierung der darunter liegenden Gene) hin. Die Lysinlactoylierungen aktivierten dabei eine Reihe von spezifischen Genen, welche nicht durch die Lysinacetylierungen aktiviert werden (34). Die Verknüpfung der Histonlactoylierung mit der Abundanz freien Lactats in der Zelle ist interessant, weil Krebszellen ihren Stoffwechselweg oft von der oxidativen Phosphorylierung auf Glykolyse als Hauptenergielieferanten umstellen und dadurch große Mengen freies Lactat produzieren. Dieser Vorgang ist als Warburg-Effekt bekannt. Lactat wiederum erzeugt viele Stoffwechselsignale, welche verschiedene Stoffwechselwege aktivieren, die die Tumormetastasierung, die Tumordinvasion und die Immunevasion von Tumorzellen begünstigen (83). Zhang *et al.* haben 28 Lysinlactoylierungen an den Kernhistonen in humanen Zellen und Mauszellen gefunden. Darauf basierend, erstellten sie ein Modell, bei dem sie die M1-Makrophagenpolarisation nach einer Infektion mit gram-negativen Bakterien nachstellten. Proinflammatorische M1-Makrophagen wechseln nach Beginn einer Infektion zur aeroben Glykolyse (siehe Warburg Effekt), was eine Erhöhung der Lactatkonzentration zur Folge hat. Aus diesem Grund konnte eine Erhöhung der Lysinlactoylierung nach 16-24h beobachtet werden. Im Gegensatz dazu sank die Lysinacetylierung. Die Lactoylierung erzeugte eine Genexpression, welche typisch für die M2 Homöostase ist. Diese verzögerte Genexpression durch Lysinlactoylierung bezeichnen die Autoren als Lactat-Timer, der das Expressionsmuster nach dem Bakterienbefall ändert (34).

Außerdem konnte gezeigt werden, dass p300 eine potenzielle HAT für die Lactoylierung ist, wobei Lactoyl-CoA als Substrat genutzt wird. Eine weitere Studie konnte die These für p300 als Histon-Lactoyltransferase bestätigen (84). Weitere Proteine wurden neben den Histonen als Ziele für die Lysinlactoylierung gefunden. Zum Beispiel tritt SNAIL1 bei Hypoxie nach einem Herzinfarkt lactoyliert auf. Auch die Pyruvatkinase M2 (PKM2) wird am Lys62 lactoyliert (84, 85). Diese Lactoylierung am Lys62 wird durch exogene Lactatgabe erhöht und hat einen Einfluss auf die Wundheilung. Da diese Lactoylierung aus dem Metabolismus entstammt, wird angenommen, dass es sich um L-Lactoylierung handelt.

Bei einem alternativen Reaktionsweg ist das Ausgangsprodukt ebenso das reaktive MGO, welches durch die Glyoxalase I auf Glutathion (GSH) übertragen wird. Dadurch entsteht Lactoglutathion (LGSH). Dieses wird durch die Glyoxalase II unter Bildung von D-Lactate und GSH hydrolysiert. LGSH kann auch nicht-enzymatisch den D-Lactoylrest auf Lysinreste übertragen (86). Vor allem Proteine der Glykolyse waren von der D-Lactoylierung betroffen. Da das durch die Glykolyse entstandene MGO nicht mehr durch die Glyoxalasen abgebaut werden kann, lässt sich auf einen möglichen Feedback Mechanismus schließen (86). Versuche an humanen Gehirnzellen deuteten neuronale Erregung und sozialen Stress als weitere Quellen für erhöhte Lysinlactoylierungen an (87).

SIRT2 war das erste Enzym, für welches eine Delactoylaseaktivität *in vitro* und *in vivo* gezeigt werden konnte. Für ein PKM2-basiertes lactoyliertes Peptidsubstrat betrug die katalytische Effizienz $1 \text{ M}^{-1}\text{s}^{-1}$ (65) und für Histon-basierte Peptide (H4K91-Lac) $66 \text{ M}^{-1}\text{s}^{-1}$ (88). In der zweiten Studie zeigten auch SIRT1, SIRT3 und SIRT5 eine schwache Delactoylaseaktivität (88).

Im Gegensatz zu GLO2^{-/-}-Zellen, in denen nur die Glyoxalase II fehlt, zeigten SIRT2^{-/-}/GLO2^{-/-}-Zellen bei *in vivo* SIRT2 *knock-down* Experimenten erhöhte Lysinlactoylierung (65). Des Weiteren konnte nachgewiesen werden, dass der SIRT2 *knock-down* in Neuroblastom (NB)-Zellen signifikant die Histonlactoylierung erhöht, was wiederum die Zellproliferation und Migration ansteigen lässt. Diese Effekte konnten durch SIRT2-Supplementierung aufgehoben werden, was auf eine wichtige Regulation von SIRT2 als Tumorsuppressor über die Histonlactoylierung und die damit verbundene Tumorgenese von NB hindeutet (88). Eine ähnliche Tumorpromotion durch Histonlactoylierung konnte auch für Augenmelanomzellen und im Mausmodell festgestellt werden (89).

In einer weiteren Arbeit wurde gezeigt, dass HDAC1-3 deutlich effizientere Delactoylasen als die Sirtuine sind. Die höchste katalytische Effizienz besitzt dabei HDAC3 mit $2\,600 \text{ M}^{-1}\text{s}^{-1}$ für ein L-lactoyliertes Peptid und $6\,000 \text{ M}^{-1}\text{s}^{-1}$ für ein D-lactoyliertes Peptid. Insgesamt scheinen die HDACs der Klasse I L-Lactoyllysin etwas schlechter zu erkennen als D-Lactoyllysin. Das gleiche Ergebnis wurde für HDAC3 mit D- und L-bhb-Peptiden erzielt. Auch *in vivo knock-down*- und Inhibierungsexperimente zeigten eine *in vivo* Delactoylaseaktivität für HDAC1 und HDAC3, mit starker Präferenz für H4K5-Lac (50).

Seit der Entdeckung der Lysinlactoylierung als PTM wurden durch massenspektrometrische Untersuchungen tausende potenzielle Lactoylierungsstellen in Magenkrebszellen (90) oder auch in *E. coli* gefunden (91). Weitere biologische Bedeutungen dieser PTM sind daher wahrscheinlich.

1.4.3 Proteinsubstrate und biologische Bedeutung der HDACs

Ihre biologische Bedeutung erlangen HDACs als „Gegenspieler“ der HATs und damit zur Aufrechterhaltung des dynamischen Gleichgewichts der Proteinac(et)ylierung. Durch den Einfluss auf Chromatinstruktur und damit auf die Regulierung der Genaktivität sind HDACs in viele (patho)physiologische Prozesse involviert. Typische Beispiele sind die Kontrolle des Zellzyklus, Fettsäureoxidation, Tumorsuppression, Tumorpromotion, Glukosehomöostase, Insulinsekretion, β -Oxidation, Harnstoffzyklus und DNA-Reparatur (16, 92). In den Fokus der Forschung gelangten Sirtuine durch die Steigerung der Lebensspanne von *Saccharomyces cerevisiae* durch Sir2-Überexpression (93, 94). Die Gesamtheit der bereits beschriebenen Substrate der HDACs und deren Regulation zu beschreiben, würde das Ausmaß dieser Einleitung übersteigen.

Vielfältige Beispiele biologischer Substrate für Sirtuine können in dem Review aus dem Jahr 2022 (22) und für Zn²⁺-abhängige HDACs in dem Review aus dem Jahr 2023 (95) gefunden werden. Als Beispiel für ein Enzym, dessen enzymatische *in vitro* Aktivität erst vor sechs Jahren entdeckt wurde, soll die biologischen Funktionen der HDAC11 näher betrachtet werden.

HDAC11 wird im Vergleich zu den anderen HDACs gewebespezifisch im Gehirn, Niere, Skelettmuskel, Herz und Immunzellen, wie Antigen-präsentierenden Zellen (APCs), exprimiert (96). Außerdem ist in verschiedenen Tumorzelllinien und in mit Interleukin-13 behandelten B-Zellen die Expression von HDAC11 erhöht (97–99). HDAC11 beeinflusst auch die Immunantwort, indem es den Promotor von Interleukin-10 bindet und die damit verbundene

Genaktivität inhibiert (100). Außerdem hat HDAC11 einen Einfluss auf die Genomstabilität und den Zellzyklus und auf diverse neuronale und metabolische Funktionen (99, 101).

Für verschiedene Krebsarten wurden unterschiedliche Expressionsmuster für HDAC11 festgestellt. Beispielweise wird HDAC11 im hepatozellulären Karzinom (HCC), Ovarialkarzinom, multiplem Myelom, in akuter lymphatischer Leukämie und bei Lungenkrebs überexprimiert. Dies steht im Zusammenhang mit einer schlechten Patientenprognose. Im Gegensatz dazu führt eine verminderte Expression oder Inhibition von HDAC11 beim Aderhautmelanom, Brustkrebs, *basal-like* Mammakarzinom und Gliomen zur Metastasierung und damit oft ebenso zum kürzeren Überleben (99). Diese Zusammenhänge machen HDAC11 zu einem interessanten Target für die Tumorbehandlung.

Die Fettsäure-Deacylierung der Serinhydroxymethyltransferase 2 (SHMT2) durch HDAC11 ist eines der wenigen Beispiele, bei dem die biologische Bedeutung von HDAC11 als Fettsäuredeacylase nachgewiesen werden konnte. Durch diese Modifikation wird die enzymatische Aktivität von SHMT2 nicht messbar beeinflusst. Dafür scheint die Fettsäuremodifikation die Interaktion des Proteins mit BRISC zu beeinflussen, welcher den Interferonrezeptor-1 deubiquitinyliert. Dadurch kann HDAC11 die Interferon- α Signalkaskade herunterregulieren (63) und könnte so als Target für die Inhibition bei Virusinfektionen dienen, wo eine erhöhte Interferon- α Antwort erwünscht ist.

Des Weiteren wurde HDAC11 im Mausmodell als Repressor des thermogenen Genprogramms im braunen Fettgewebe nachgewiesen. HDAC11-*knock-down*-Mäuse setzen weniger weißes Fettgewebe an, zeigen eine ausgeprägtere kälteinduzierte Thermogenese, weniger Lipidanreicherung und geringere Gewichtszunahme nach fettreicher Fütterung (102). Ebenso konnte der HDAC11 *knock-down* neben der Verringerung der Fettleibigkeit auch deren negativen Folgen, wie Insulinresistenz, erhöhte Glukosetoleranz, Leberschäden und zu hohe Cholesterinwerte, reduzieren (103). Dies zeigt, dass HDAC11 ein interessantes Target für die Behandlung von metabolischen Krankheiten und Übergewicht sein könnte (102). Die enzymatische Aktivität der HDAC11 ist für diese Funktion notwendig und H3K27-Ac wurde als *in vivo* Substrat identifiziert (102). Dabei weist HDAC11 *in vitro* nahezu keine Deacetylaseaktivität auf.

1.5 Struktur und Katalysemechanismus der Histondeacetylasen

Die HDAC-vermittelte Deacylierung funktioniert nach zwei grundsätzlich verschiedenen Mechanismen. Die drei Klassen der Zn^{2+} -abhängigen HDACs (Klasse I, II, IV) sind bei der Deacylierungsreaktion auf ein katalytisches Zn^{2+} -Ion angewiesen. Die Reaktionsprodukte sind ein freier Lysin- und Acylrest (Abbildung 3A, Beispiel für Acetylrest). Die Sirtuine (HDACs der Klasse III) wiederum nutzen NAD^+ als Cosubstrat. Hier entsteht während der Reaktion Nicotinamid (NAM), ein deacylierter Lysinrest und durch die Übertragung des Acylrests auf ADP-Ribose (ADPr) entsteht O-Acyl-ADP-Ribose (O-AADPr, Abbildung 3B) (104, 105). Sirtuine besitzen zusätzlich eine mono-ADP-ribosyltransferase-Aktivität, welche zuerst für Sir2 nachgewiesen werden konnte. Diese alternative enzymatische Aktivität wurde vor allem für SIRT4 und SIRT6 nachgewiesen (106–108, 27). Sie ist für diese Arbeit jedoch unwichtig, weswegen im Folgenden nur die beiden Deacylasereaktionsmechanismen betrachtet werden.

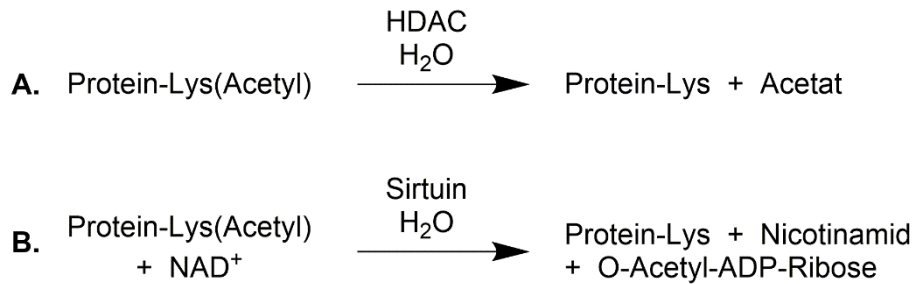


Abbildung 3. Allgemeines Reaktionsschema der Deacetylierung eines acetylierten Lysins für **A.** Zn²⁺-abhängige HDACs und **B.** NAD⁺-abhängige Sirtuine.

1.5.1 Struktur der Zn²⁺-abhängigen Histondeacetylasen

Die humanen Zn²⁺-abhängigen HDACs unterscheiden sich entsprechend ihrer Klassen in der Größe. Die HDACs der Klasse I und IV sind ca. 350 bis 400 AS groß und die HDACs der Klasse II sind ca. 1 000 AS groß. Die humanen Zn²⁺-abhängigen HDACs weisen alle eine gemeinsame Deacetylase-Domäne auf. Diese Domänen sind zwischen 320 AS (Klasse I und IV) und 420 AS (Klasse IIa) groß. Bei den HDACs der Klasse IIa ist die Deacetylase-Domäne C-terminal zu finden und bei den HDACs der Klasse I N-terminal (109). Die beiden HDACs der Klasse IIb weisen zwei Deacetylase-Domänen auf, wobei bei der HDAC10 die zweite Deacetylase-Domäne eine Pseudodeacetylase-Domäne ist, die keine enzymatische Aktivität aufweist (110). HDAC6 besitzt zwei verschiedene katalytische Domänen, CD1 und CD2 (111), mit unterschiedlichen katalytischen Aktivitäten (siehe Abschnitt 1.4.1)

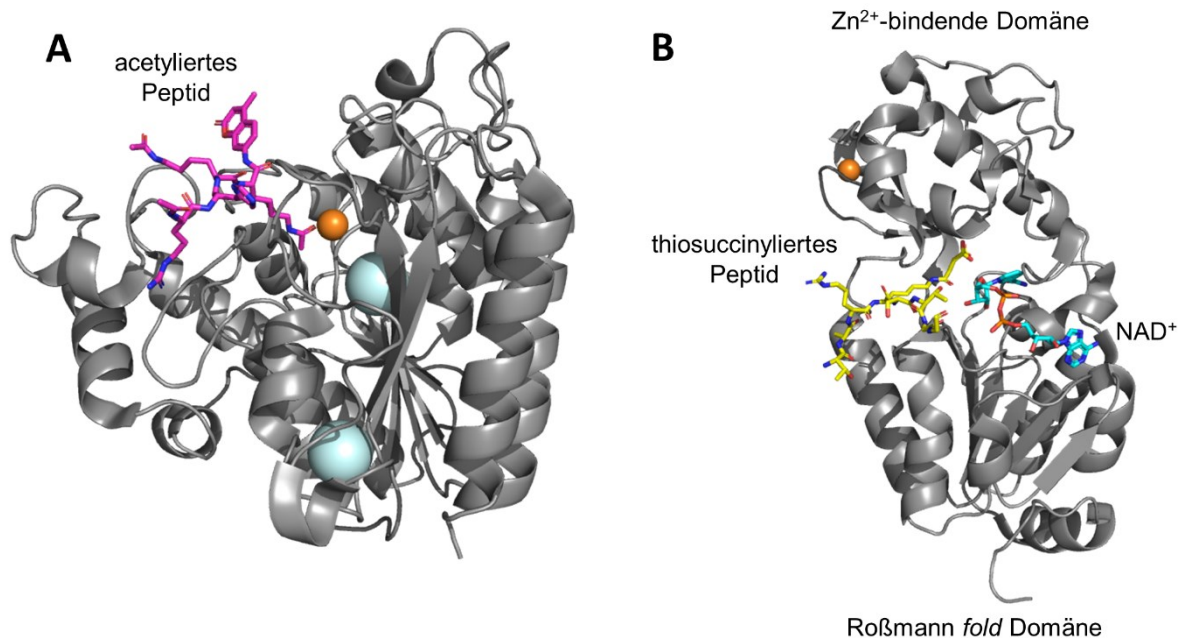


Abbildung 4. Strukturbeispiele der humanen HDAC8 und SIRT5 als Strukturbeispiele. **A.** Cartoon-Darstellung einer inaktiven H143A Variante der humanen HDAC8 (grau, PDB-Code: 3EWF) im Komplex mit einem modifizierten p53-Peptid (violett, Ac-RHK(Ac)K(Ac)-7-Amino-4-methylcumarin (AMC)). Das katalytische Zn²⁺-Ion ist in orange und die beiden K⁺-Ionen in türkise als Sphären dargestellt. **B.** Cartoon-Darstellung von SIRT5 (grau, PDB-Code: 3RIY) im Komplex mit thiosuccinyliertem H3K9-Peptid (gelbe Stickdarstellung, TARK(thiosuccinyl)STGG) und NAD⁺ (türkise Stickdarstellung). Das Zn²⁺-Ion ist als orange Sphäre dargestellt.

Die Deacetylase-Domäne der Zn^{2+} -abhängigen HDACs weist eine α/β -Faltung auf. Diese Faltung konnte zuerst bei der Arginase aus der Leber von Ratten nachgewiesen werden (112–114) und wird daher als Arginase-Deacetylase *fold* bezeichnet (Abbildung 4B). Dieser besteht aus einem zentralen achtsträngigen parallelen β -Faltblatt, das von mehreren α -Helices umgeben ist. Die *loops* L4 und L7 tragen die Reste, die das katalytische Zn^{2+} -Ion koordinieren (115). Die zwei zusätzlichen Bindestellen für monovalente Kationen, werden im Fall von HDAC8 bevorzugt von K^+ -Ionen besetzt (116). Das acetylierte Lysinsubstrat wird in einem hydrophoben Tunnel gebunden, auf dessen Boden das katalytische Zn^{2+} -Ion zu finden ist.

1.5.2 Reaktionsmechanismus Zn^{2+} -abhängiger HDACs

Der Reaktionsmechanismus der Zn^{2+} -abhängigen HDACs ist am Beispiel von HDAC8 in Abbildung 5 dargestellt. Das aktive Zentrum dieser HDACs enthält das katalytische Zn^{2+} -Ion. Dieses ist zwischen einem Histidinrest und zwei Asparaginsäureresten koordiniert. Zusätzlich sind ein (z.B. bei HDAC6 (111)) oder zwei Wassermoleküle am Zn^{2+} -Ion gebunden. Wie in Abbildung 5A zu sehen, sind im Fall von HDAC8 zwei Wassermoleküle am Zn^{2+} -Ion gebunden. Im aktiven Zentrum befinden sich weiterhin zwei His-Asp-Dyaden (hier His142 und His143), welche als generelle Base bzw. Säure während der Katalyse agieren. Des Weiteren ist ein Tyrosinrest im aktiven Zentrum, der das tetrahedrale Intermediat stabilisiert und den Carbonylkohlenstoff aktiviert (Abbildung 5A). Eines der Zn^{2+} -koordinierten Wassermoleküle wird zunächst durch das acetylierte Lysinsubstrat verdrängt (117–120).

Für die Interaktion des Carbonylrests mit dem katalytischen Zn^{2+} -Ion spricht die deutliche Änderung des K_M -Werts bei Änderung des katalytischen Metallions zu Fe^{2+} , Co^{2+} und Ni^{2+} im Fall von HDAC8 (121).

Wie in Abbildung 5B gezeigt, bindet im ersten Schritt der Reaktion das acetylierte Lysinsubstrat an das aktive Zentrum. Der Carbonylsauerstoff koordiniert an das Zn^{2+} -Ion und wird zusätzlich über eine Wasserstoffbrücke mit dem Tyrosinrest stabilisiert (Tyr306). Beide Interaktionen sind essenziell, damit der nukleophile Angriff des Zn^{2+} -gebundenen Wassermoleküls stattfinden kann (122, 123). Einer der Histidinreste agiert als Base um ein Proton des Wassermoleküls zu binden, welches dann den Carbonylkohlenstoff des Acetylrests nukleophil angreift. Es bildet sich das tetrahedrale Intermediat (Abbildung 5C). Dieses wird durch den Tyrosinrest (Tyr306) und das Zn^{2+} -Ion stabilisiert. Im Fall von HDAC8 wirkt His143 nun als katalytische Säure und greift den Carbonylkohlenstoff an. Das tetrahedrale Intermediat kollabiert und es entsteht freies Acetat und der deacetylierte Lysinrest (Abbildung 5D).

Für HDAC8 konnte durch enzymatische und durch QM/MM-Studien gezeigt werden, dass His143 sowohl als Base als auch als Säure wirkt. Der zweite Histidinrest (His142) dient der elektrostatischen Stabilisierung des tetrahedralen Intermediats und der Übergangszustände (124, 125). Diese funktionale Aufteilung der Histidinreste stellt sich bei anderen Isoformen anders da. Bei HDAC6 wirkt His573 als generelle Base und His574 als generelle Säure während der Katalyse (111). Eine ähnliche Aufteilung der Histidinreste des aktiven Zentrums wie bei HDAC6 wurde auch für HDAC10 gefunden (126).

Eine Ausnahme von diesem Mechanismus bilden die HDACs der Klasse IIa. Der konservierte Tyrosinrest im aktiven Zentrum ist hier durch ein Histidin ersetzt. Dieser ist zu kurz, um im aktiven Zentrum mit der Amidbindung zu interagieren und ist nicht in der Lage, den Übergangszustand zu stabilisieren. Dies führt zu einer sehr schwachen bis keiner Deacetylaseaktivität der HDACs der Klasse IIa (57, 127). Dafür können sie effizienter TFA-Reste

entfernen, welche einen reaktiveren Carbonylkohlenstoff aufweisen. Wurden die Histidinreste im aktiven Zentrum von HDAC4 und HDAC7 durch Tyrosin ersetzt, konnte eine robuste Deacetylaseaktivität hergestellt werden (57, 127). Analog dazu kann man für HDACs der anderen Klassen eine Verringerung der Deacetylaseaktivität beobachten, wenn der Tyrosinrest durch einen Phenylalaninrest ersetzt wird (110, 111, 118, 128, 129).

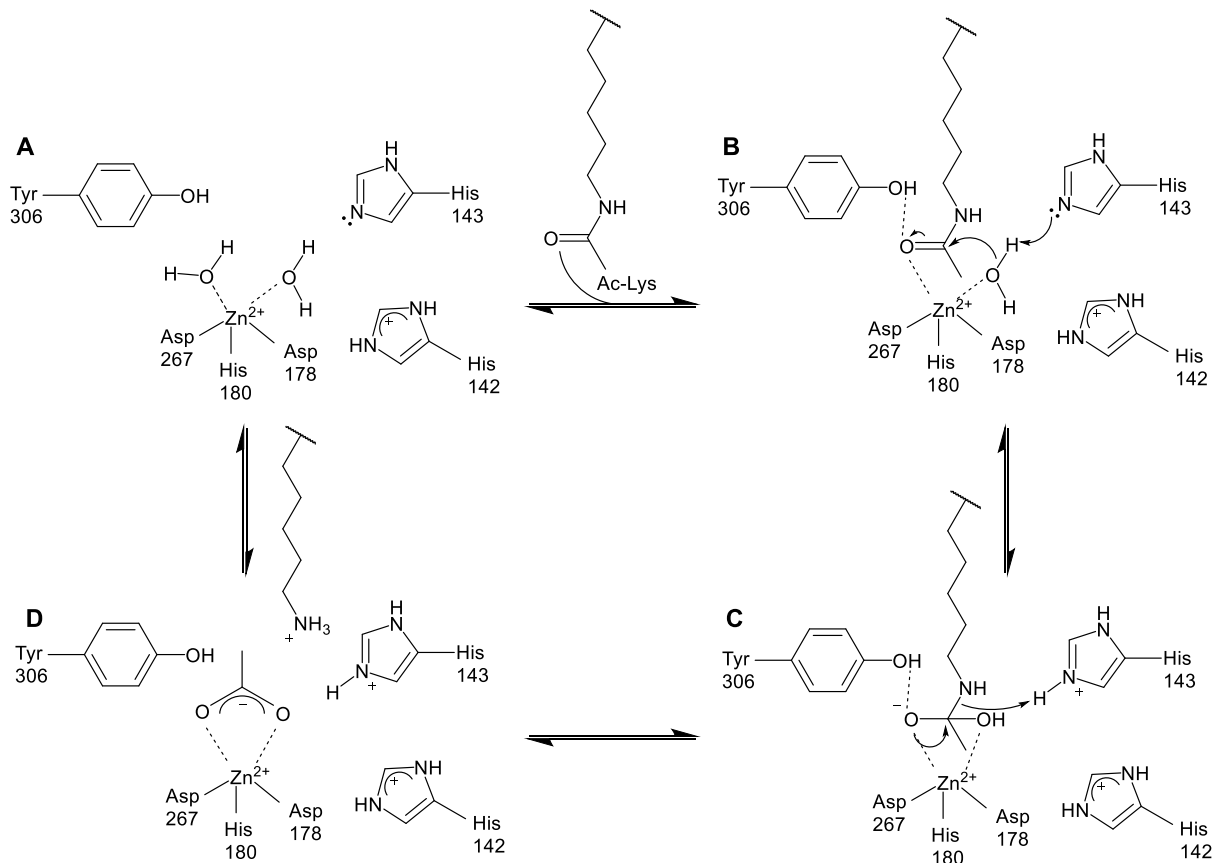


Abbildung 5. Reaktionsmechanismus der HDACs am Beispiel von HDAC8. Die Nummerierung der AS orientiert sich an der Sequenz von HDAC8. Die gezeigten Reste sind für alle humanen Zn^{2+} -abhängigen HDACs konserviert. Die einzige Ausnahme bilden die HDACs der Klasse IIa, welche anstelle des Tyrosinrests einen Histidinrest aufweisen.

1.5.3 Struktur der Sirtuine und die Bindung an die Substrate

Die verschiedenen Vertreter der Sirtuine teilen sich eine konservierte katalytische Kernregion, die aus ca. 250 AS besteht und sich in zwei verschiedene Domänen unterteilen lässt. Die größere der beiden Domänen nimmt eine Rossmann *fold*-artige Faltung ein, welche ein typisches Nukleotid-Bindungsmotiv ist und in vielen NAD^+ / $NADH$ -bindenden Proteinen auftritt (130). Die kleinere der beiden Domänen ist eine Zn^{2+} -bindende Domäne und besitzt vier konservierte Cysteinreste, welche für die Bindung eines Zn^{2+} -Ions verantwortlich sind. Diese Domäne und das Zn^{2+} -Ion besitzen vor allem eine strukturelle Bedeutung (131). Diverse *loops* verbinden die beiden Domänen und bilden so eine ausgedehnte Spalte. Hier befindet sich das aktive Zentrum. Die beiden Substrate, das acetylierte Lysinsubstrat und NAD^+ binden auf den entgegengesetzten Seiten des aktiven Zentrums (131).

Der Reaktionsmechanismus der Sirtuine ist ein sequenzieller Mechanismus (132). Zuerst bindet das acetylierte Lysinsubstrat und anschließend das Cosubstrat NAD⁺ an das Sirtuin (132, 133, 92). Das flankierende Peptidrückgrat (relativ zum modifizierten Lysin) geht β -Faltblatt Interaktionen mit dem FGE *loop* (benannt nach dem konservierten FGExL Motiv) und einem *loop* aus der Roßmann *fold* Domäne ein. Dadurch bildet sich ein dreisträngiges antiparalleles β -Faltblatt aus, der sogenannte *β -stapel* (134, 135). Diese Interaktionen positionieren den acetylierten Lysinrest in einem hydrophoben Tunnel, wo er diverse Van-der-Waals-Kontakte mit hydrophoben Resten eingeht. Interessanterweise scheint sich die Struktur des hydrophoben Tunnels abhängig von der Natur des Acylrests zu ändern (136). Der ϵ -Stickstoff der Lysinseitenkette geht eine Wasserstoffbrücke mit einem konservierten Valin ein. Die Bindung vom acetylierten Lysinsubstrat forciert eine Konformationsänderung, wodurch die Zn²⁺-bindende Domäne räumlich näher an die größere Roßmann *fold* Domäne kommt und somit die korrekte Bindung von NAD⁺ unterstützt (134, 137, 138).

NAD⁺ kann in manchen Fällen auch unabhängig vom acetylierten Lysinsubstrat an das Enzym binden, was aber zu einem nicht produktiven NAD⁺-Enzymkomplex führt (133, 139, 140). Ursache hierfür ist die Bindung von NAD⁺ an das Enzym in einer anderen Konformation, die eine Bindung des acetylierten Lysinsubstrats verhindert (133, 139). SIRT6 bindet NAD⁺ mit vergleichsweise hoher Affinität ($K_D = 27 \mu\text{M}$), ohne vorher das acylierte Substrat gebunden zu haben (141). Im Vergleich dazu zeigt sich bei 10 mM NAD⁺ keine Bindung an SIRT3 bei entsprechenden Kristallstrukturen (138).

Haben beide Substrate in der richtigen Konformation an das Sirtuin gebunden, gibt es eine Konformationsänderung des größten *loops* im aktiven Zentrum, des sogenannte *cofaktor binding loop*, wodurch beide Substrate im aktiven Zentrum orientiert und fixiert werden (133, 138). Teile des *loops* bilden Teile der C-Tasche, wo der NAM-Teil des NAD⁺ bindet.

1.5.4 Reaktionsmechanismus der Sirtuine

Abbildung 6 zeigt den Reaktionsmechanismus der Sirtuine. Im ersten Schritt der Deacetylierungsreaktion greift der Carbonylsauerstoff der Acetylgruppe auf der α -Seite das C1'-Atom des NAD⁺ an. Es wird NAM von der ADP-Ribose abgespalten und es bildet sich das sogenannte 1'-O-Alkylimidat-Intermediat. Wie in Schritt 1 zu sehen (Abbildung 6), ist NAM das erste Reaktionsprodukt, welches dissoziiert (132, 142–144). Für den Mechanismus dieses Schritts werden in der Literatur drei Möglichkeiten diskutiert, um das Imidat auszubilden. Für jede Möglichkeit ergibt sich eine andere Struktur des Übergangszustands (145).

Die erste Möglichkeit ist der Reaktionsverlauf nach einem assoziativen S_N2 Mechanismus, welcher über ein pentakoordiniertes Intermediat im Übergangszustand abläuft. Vor allem kinetische Studien mit Substitutionen am C α -Atom der Acetylgruppe, die die Elektrophilie des Carbonylsauerstoff senken und die Reaktionsgeschwindigkeit deutlich verringern, unterstützen diese Theorie (146).

Die zweite Möglichkeit ist ein dissoziativer S_N1-Mechanismus, wobei vor dem Angriff auf das C1'-Atom das NAM vollständig dissoziiert und ein stabiles Oxocarbeniumion im Übergangszustand entsteht, welches durch das Enzym stabilisiert wird. Anschließend geschieht der Angriff durch den Acetylrest (147).

Die dritte Möglichkeit ist ein gemischter S_N1-S_N2-Mechanismus, wobei im Übergangszustand ebenso ein Oxocarbeniumion entsteht. Es bildet sich kein diskretes Zwischenprodukt im Übergangszustand. Die Bindung zur Abgangsgruppe ist größtenteils gespalten (aber noch

vorhanden) und die Bindungsbildung mit dem Nukleophil hat schon begonnen (148, 149). Wie der tatsächliche Übergangszustand aussieht, ist noch nicht geklärt und muss durch zukünftige Studien gezeigt werden.

Ausgehend von diesem Intermediat gibt es zwei mögliche Reaktionswege. Der Erste ist die offensichtliche Deacetylierungsreaktion, rot dargestellt in Abbildung 6. Die zweite Möglichkeit ist die Rückreaktion durch einen Angriff von NAM auf das Imidat-Intermediat, auch als *base exchange* Reaktion bezeichnet (blau dargestellt in Abbildung 6). Auch diese Rückreaktion benötigt die Anwesenheit des acetylierten Substrats und findet bevorzugt unter hohen NAM Konzentrationen statt (143, 150, 151). Dies wurde durch die Zugabe von ^{14}C -NAM zum Reaktionsansatz gezeigt. Diese radioaktiven ^{14}C -Isotope wurden auf NAD^+ übertragen (143, 152). Ein konservierter Phenylalaninrest schützt das Imidat durch eine Konformationsänderung im Vergleich zum Michaeliskomplex vor dem Angriff von NAM, wie sich bei der Analyse von Kristallstrukturen des Sir2Tm mit gebundenen Thioalkylimidat-Intermediat zeigte. Bei der Verwendung einer katalytisch deutlich gehemmten F33A-Variante des Sir2Tm verbesserte sich der IC_{50} gegenüber NAM im Vergleich zum Wildtyp um das 4 800 fache (153).

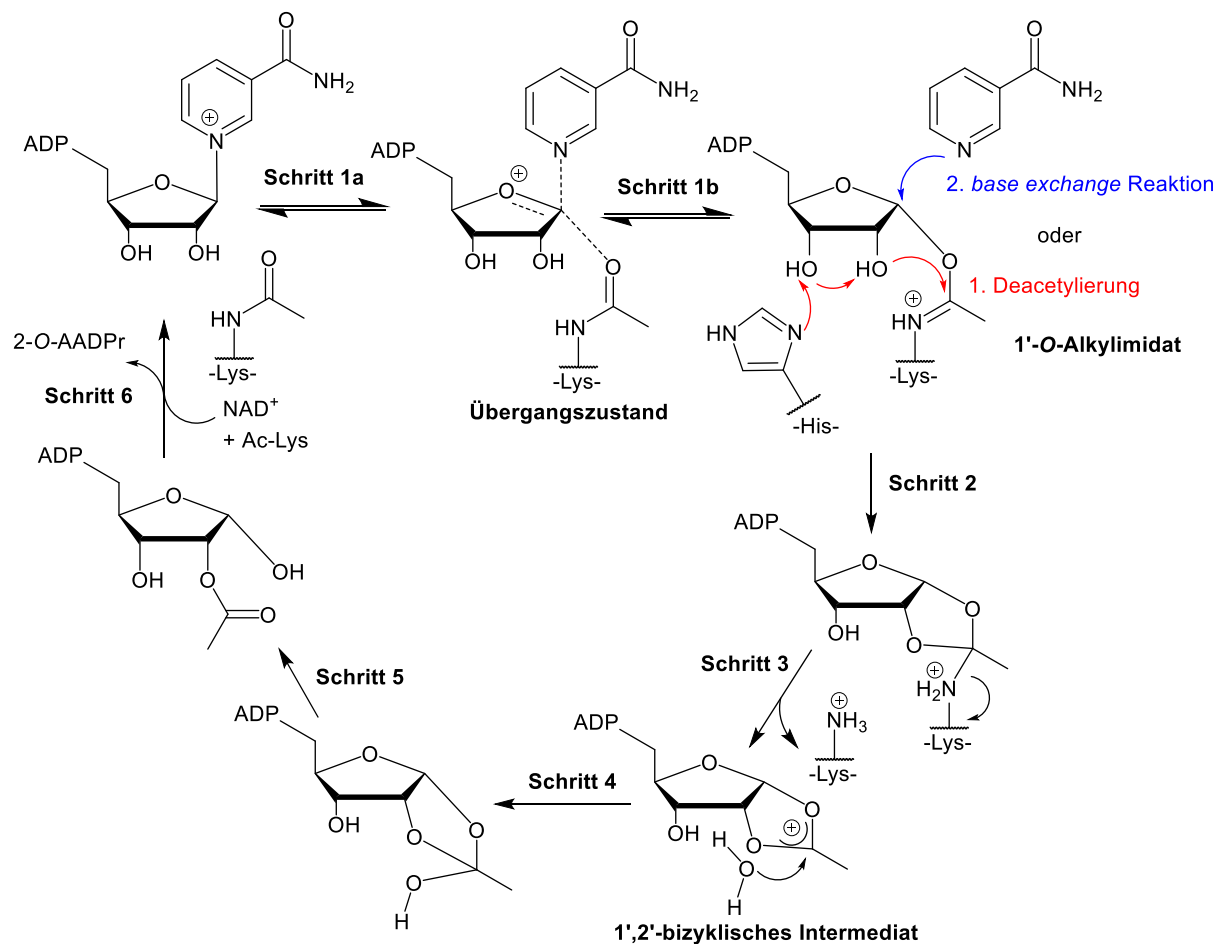


Abbildung 6. Reaktionsmechanismus für Sirtuine. **Schritt 1:** Zeigt die Bildung des 1'-O-Alkylimidat Intermediats und eine mögliche Struktur des Übergangszustands. Von dem 1'-O-Alkylimidat findet die Deacetylierungsreaktion statt (rot) oder es kann die Rückreaktion stattfinden, die sogenannte *base exchange* Reaktion (blau). Es bildet sich in **Schritt 2** und **Schritt 3** das bicyklische Intermediat unter Abspaltung und Freisetzung des deacetylierten Lysinprodukts. Die **Schritte 4-6** zeigen die Hydrolyse zu dem finalen Endprodukt 2-O-Acetyl-ADPRibose.

Im nächsten Schritt der Deacylierungsreaktion aktiviert ein katalytischer Histidinrest die 2'-Hydroxylgruppe der Ribose. Der Histidinrest deprotoniert vermutlich über die 3'-Hydroxylgruppe die 2'-Hydroxylgruppe (Abbildung 6, Schritt 2). Diese greift den Carbonylkohlenstoff des Imidats an, woraufhin sich das tetrahedrale 1',2'-bicyklische Intermediat bildet (154, 155). Anschließend erfolgt die Freisetzung des deacetylierten Lysinproduktes und es bildet sich ein Dioxoniumion (Abbildung 6, Schritt 3). Dieses wird durch Wasser angegriffen und es bildet sich das finale Reaktionsprodukt 2'-O-AADPr (Abbildung 3, Schritt 4-6) (156). Das Wasser greift das Carbonylkohlenstoff des Acetylrests an, was durch Benutzung von $H_2^{18}O$ gezeigt werden konnte (142). Durch Strukturanalysen konnte gezeigt werden, dass 2'-O-AADPr das eigentliche Reaktionsprodukt ist und, dass sich in Lösung ein enzymunabhängiges Gleichgewicht zwischen 2'-O-AADPr-Ribose und 3'-O-AADPr einstellt (157).

1.6 Messung der enzymatischen Aktivität von HDACs

HDACs sind bekannt als epigenetische Regulatoren der Lysinacylierung an Histonen und Nicht-Histon-Proteinen, wo sie an einer Vielzahl physiologischer Prozesse beteiligt sind, wie in Kapitel 1.4.3 bereits beschrieben. Sie sind deshalb ein vielversprechendes Ziel für die Entwicklung von potentiellen Wirkstoffen für verschiedene pathologische Zustände wie Krebs, Herz-Kreislauf-Erkrankungen, neurodegenerative Krankheiten, Immun- oder Metabolismus Störungen und Infektionen durch Parasiten (158). Für die Zn^{2+} -abhängigen HDACs sind zum jetzigen Zeitpunkt vier verschiedene HDAC-Inhibitoren (HDACi) als Medikamente bei der U.S. amerikanischen *Food and Drug Administration* (FDA) zugelassen: Vorinostat (SAHA) und Romidepsin für die Behandlung von kutanen T-Zell-Lymphomen, Belinostat für die Behandlung von peripheren T-Zell-Lymphomen und Panobinostat für die Behandlung des multiplen Myeloms. Zusätzlich wurde von der chinesischen *National Medical Products Administration* Tucidinostat für die Behandlung von peripheren T-Zell-Lymphomen zugelassen (159, 160). Ein Sirtuininhibitor ist nach bisherigem Kenntnisstand noch nicht zugelassen. Für die weitere Entwicklung von Effektoren der HDAC-Aktivität ist es notwendig, stabile und zuverlässige Messverfahren mit hohem Probendurchsatz zu entwickeln.

Grundsätzliches Problem der Zn^{2+} -abhängigen HDAC- und Sirtuinreaktion ist, dass keines der Reaktionsprodukte oder der Substrate spektrophotometrisch direkt messbar ist. Ein messbares Signal wäre für die kontinuierliche Aktivitätsmessung nötig. Daher ist die Reaktion nicht ohne weitere Modifikation kontinuierlich verfolgbar. Es wurden verschiedene Methoden entwickelt, um die HDAC-Reaktion verfolgen zu können. Die Ansätze lassen sich in zwei Kategorien unterteilen. Die erste Kategorie beruht auf der Trennung von Substrat und Produkt. Anschließend werden die getrennten Stoffe quantifiziert. Typische Beispiele sind hier Kapillarelektrophorese, Hochleistungsflüssigkeitschromatographie (HPLC) oder Massenspektrometrie (MS). In der zweiten Kategorie wird die Reaktion so modifiziert, dass ein messbares Signal entsteht. Dafür können entweder chemische oder enzymatische Reaktionen an die eigentliche Reaktion gekoppelt werden oder die Substrate der Reaktion so modifiziert werden, dass ein messbares Signal entsteht. In diesem Kapitel werden verschiedene Ansätze, die für die Messung der HDAC-Aktivität entwickelt wurden, beschrieben.

1.6.1 Quantifizierung durch Trennung von Substrat und Produkt

Für die klassische Aktivitätsmessung der Zn^{2+} -abhängigen HDACs wurden 3H -acetylierte Histone bzw. Histonpeptide verwendet. Nach der HDAC-Reaktion erfolgt die Trennung durch organische Extraktion des Acetats und die Detektion durch Szintillationszählung (161, 162). Für Sirtuine wurde die Methode angepasst. Vor der Extraktion erfolgte die Bindung der Reaktionsprodukte an Aktivkohle mit anschließender Abspaltung des Acetats von O-AADPr unter basischen Bedingungen und Hitze (163). Die Verwendung von ^{32}P -NAD⁺ oder ^{14}C -NAD⁺ in Kombination mit Dünnschicht-Chromatographie nutzte ebenfalls radioisotope Markierungen für die Sirtuinmessungen (132, 164, 165). Andere Optionen sind die Polyacrylamid-Gelelektrophorese mit ^{14}C -markierten Acetylpeptiden (166), die Kapillarelektrophorese (167–169), die Mikrochip-Elektrophorese (170), mikrofluide Mobilitätsassays (171, 172), HPLC (61, 78, 132, 173, 174), und Bindung an Boronsäure-Harz (175). Alternativ bietet MS die Möglichkeit, Peptidsubstrate nach der Trennung in der Gasphase zu quantifizieren (176–178). MALDI-MS-Messungen wurden in Kombination mit auf Glas immobilisierten Peptidderivaten genutzt, um Substratprofile für verschiedene HDACs zu erstellen (179, 180).

All diese Methoden haben gemeinsam, dass die Reaktion nach einer gewissen Zeit abgestoppt und das Reaktionsgemisch zu diesem Zeitpunkt analysiert wird. Der Nachteil ist, dass die Reaktion dabei nur diskontinuierlich verfolgt werden kann. Der Vorteil dieser Messsysteme ist, dass z.B. Peptidsubstrate ohne zusätzliche Markierung (wie z.B. Fluoreszenzfarbstoffe) messbar sind und diese Verfahren zuverlässig sind. Weitere Nachteile ergeben sich aus der oft aufwendigen Probenvorbereitung und dem damit verbundenen großen Zeitaufwand für die Analysen. Um dieses Problem zu umgehen, wurden unter anderem für MS und auch für Kapillarelektrophorese *high throughput screening* (HTS)-Systeme entwickelt (181, 182). Aber auch hier ergeben sich Nachteile, die vor allem durch komplexe und kostenintensive analytische Messsysteme bedingt sind. In den nächsten Abschnitten werden alternative Messsysteme vorgestellt, die entwickelt wurden, um diese Limitierungen zu umgehen.

1.6.2 Enzym-gekoppelte Messsysteme

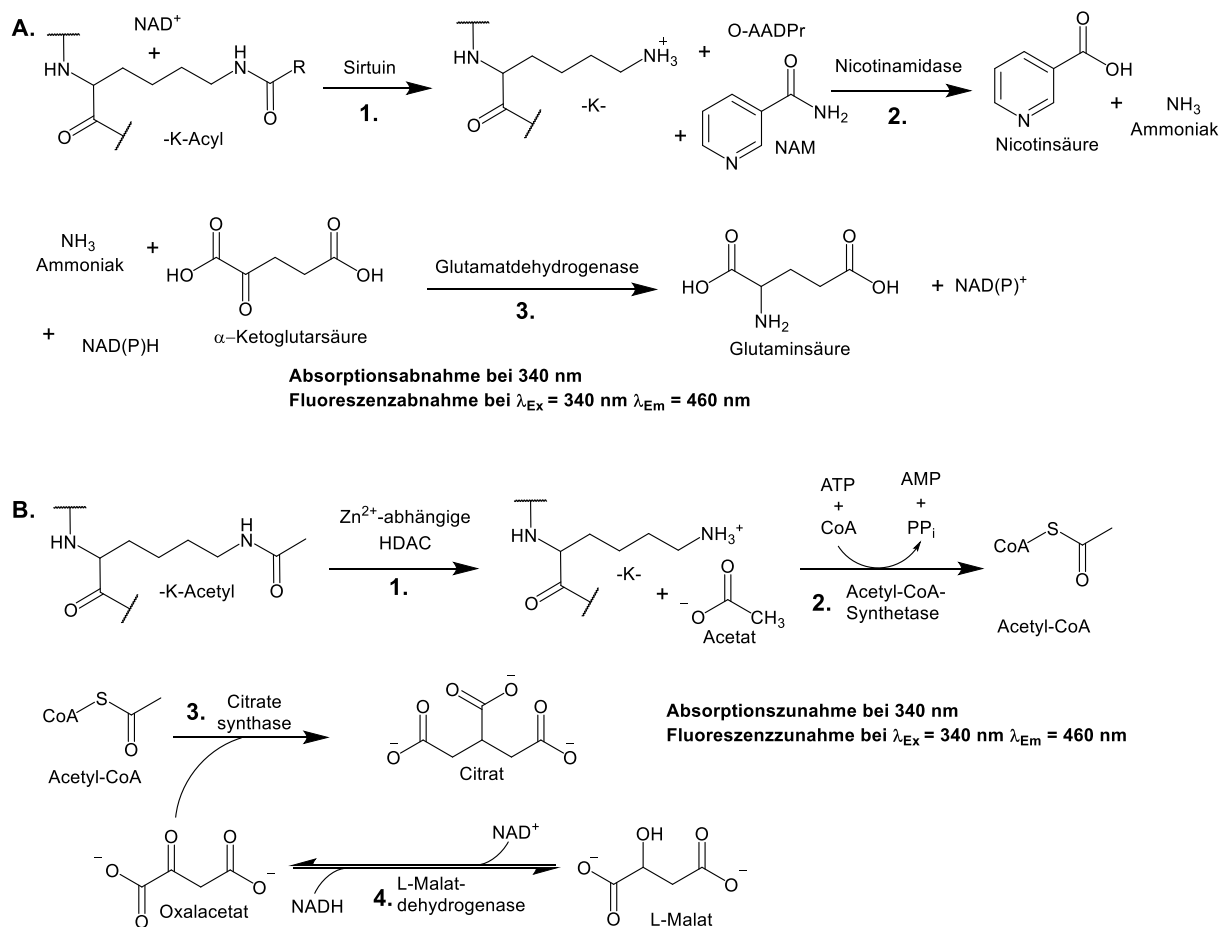


Abbildung 7. Zwei Beispiele für Enzym-gekoppelte HDAC-Assays. **A.** Ein Sirtuin-Aktivitätsassay, der das Produkt NAM nutzt, um über die Reaktion mit der Nicotinamidase (2) und der Glutamatdehydrogenase (3) den NAD(P)H-Verbrauch zu verfolgen. **B.** Acetat-Assay für Zn^{2+} -abhängige Enzyme. Das Acetat wird mittels Acetyl-CoA-Synthetase (2) und Citratsynthase (3) zu Citrat umgesetzt. Das dafür benötigte Oxalacetat wird aus L-Malat durch die L-Malatdehydrogenase (4) synthetisiert und es entsteht NADH.

Durch Enzym-gekoppelte Assays kann die HDAC-Aktivität gemessen werden, indem an deren Reaktion eine oder mehrere Enzymreaktionen gekoppelt werden, die wiederum ein messbares Signal erzeugen. Die Reaktion kann in Abhängigkeit der gekoppelten Reaktion kontinuierlich oder diskontinuierlich verfolgt werden. Bei dieser Art der Assays unterscheiden sich Sirtuine und Zn^{2+} -abhängige HDACs teilweise aufgrund der Reaktionsprodukte. Theoretisch kann jedes Substrat (nur diskontinuierlich) und jedes Reaktionsprodukt enzymatisch so modifiziert werden, dass es ein Messsignal erzeugt.

In Abbildung 7 sind beispielhaft zwei Assays dargestellt. Bei dem Sirtuin-spezifischen Assay werden zwei Enzymreaktionen an die Sirtuinreaktion gekoppelt (Abbildung 7A). Dabei wird das Reaktionsprodukt NAM genutzt. Nach der Sirtuinreaktion wird NAM durch die Nicotinamidase in Nicotinsäure und Ammoniak gespalten. Anschließend wird dieser Ammoniak durch die Glutamatdehydrogenase (GDH) auf α -Ketoglutarat übertragen und es entsteht Glutaminsäure. NAD(P)H wird dabei zu NAD(P)⁺ umgesetzt. Die Detektion erfolgt entweder über die Abnahme der NAD(P)H-Absorption bei 340 nm oder über die Abnahme der NAD(P)H-Fluoreszenz bei 460 nm (183). In einer Abwandlung dieses Assays ist die Nicotinamidase-Reaktion chemisch

gekoppelt an die Reaktion mit Orthophthalaldehyd, Dithiothreitol und Ammoniak. Hier entsteht ein fluoreszierendes 1-Akylthio-Isoindol (184, 185).

In Abbildung 7B ist der Acetat-Assay dargestellt. Dieser Assay ist spezifisch für die Detektion der Aktivität der Zn²⁺-abhängigen HDACs. Hier erfolgt nach der HDAC-Reaktion die Umwandlung des freigesetzten Acetats zu Acetyl-CoA durch die Acetyl-CoA-Synthase. Anschließend überträgt die Citratsynthase den Acetylrest auf Oxalacetat und es entsteht Citrat. Vermittelt durch die L-Malatdehydrogenase steht das Oxalacetat im Gleichgewicht mit L-Malat. Wird dem Gleichgewicht Oxalacetat entzogen, stellt sich dieses wieder unter NADH-Bildung ein. Damit lässt sich diese Reaktion durch die Zunahme der NADH-Konzentration verfolgen (186). Dieser Assay ist durch die Messung des freigesetzten Acetats für alle Acetat-produzierenden Enzyme anwendbar, z.B. auch für die Acetylpolyamin-Amidohydrolyase aus *Pseudomonas aeruginosa* (187). Es existieren weitere Enzym-gekoppelte Assays, welche über die Reaktion mit der Lactatdehydrogenase, der NAD(P)H/FMN-Oxidoreduktase und anschließender Luciferasereaktion ein messbares Lumineszenz-Signal erzeugen, um das nicht reagierende NAD⁺ zu quantifizieren (172).

Ein vor kurzem publizierter Assay nutzt den Effekt, dass die Endonuklease Cas12a durch eine Acetylierung an Lys595 inaktiviert wird. SIRT1 ist in der Lage, diesen Acetylrest zu entfernen und Cas12a zu reaktivieren. Cas12a ist nun in der Lage, zugesetzte Reporter DNA umzusetzen und so ein starkes Fluoreszenzsignal zu erzeugen (188). Ein ähnlicher Ansatz wurde für die Firefly Luciferase verwendet, bei der die Acetylierung von Lys529 die Aktivität der Luciferase inaktiviert. Die Deacetylierung dieses Rests durch verschiedene Sirtuine oder HDAC8 stellt die Aktivität wieder her (189, 190).

In Abbildung 8 ist ein weiterer großer Bereich der Enzym-gekoppelten Assays dargestellt: die Trypsin-gekoppelten Assays. Trypsin ist eine Protease und spaltet Peptidbindungen nach AS mit positiv geladenen Resten, also vor allem Lysin und Arginin. Ist der Lysinrest mit einer Acylgruppe modifiziert, spaltet Trypsin das Peptid an dieser Stelle nicht und es entsteht kein messbares Signal. Nach der Reaktion mit einer HDAC ist der Acylrest entfernt und durch die Spaltung hinter dem Lysin wird ein messbares Signal erzeugt. Diese Assays können in zwei Unterbereiche geteilt werden. Die erste Variante umfasst jegliche Abwandlungen des kommerziell erhältlichen Fluoride-Lys-Assays, wie in Abbildung 8A zu sehen. C-terminal zum modifizierten Lysin ist ein 7-Amino-4-methylcoumarin (AMC)-Rest über eine Amidbindung angebracht. Nach der HDAC-Reaktion wird das AMC vom C-Terminus durch Trypsin gespalten. Die Freisetzung des AMC resultiert in einer Rotverschiebung der Fluoreszenz mit einem Emissionsmaximum von 390 nm zu 440 nm. Entsprechend kann die Zunahme der Fluoreszenzintensität in diesem Wellenlängenbereich gemessen werden. Dieses Assaydesign ist aufgrund der hohen Fluoreszenzänderung durch die Spaltung durch Trypsin die gebräuchlichste Messmethode für die HDAC-Aktivität. Normalerweise wird der Assay diskontinuierlich genutzt (191), kann aber mit optimierter Trypsinkonzentration auch kontinuierlich eingesetzt werden (192). Für SIRT5 konnte dieser Assayansatz auch genutzt werden, um die Enzymaktivität in Zelllysat zu messen (193). Dieser Ansatz wurde in vielen Variationen mit einer großen Anzahl von Peptidsequenzen und verschiedenen Acylmodifikationen zum Inhibitorscreening oder zur Substratanalyse eingesetzt (191–199). Alternativ zum Fluoreszenzassay wurde ein kolometrischer Assay entwickelt, bei welchem 5-Amino-2-Nitrobenzoesäure in das Peptidrückgrat eingebaut wurde. Durch die Spaltung des deacetylierten Peptids durch Trypsin gibt es eine deutliche Farbentwicklung, die bei 405 nm verfolgt werden kann (200).

Wie in Abbildung 8B zu sehen, ist bei der zweiten Variante des Trypsin-gekoppelten Assays jeweils C-terminal und N-terminal vom modifizierten Lysin ein Fluorophor bzw. Quencher angebracht. Es findet im intakten Peptid eine Energieübertragung vom Fluorophor zum Quencher statt, wodurch dessen Fluoreszenzintensität gelöscht wird. Dieser Energietransfer folgt zumeist dem Mechanismus des Förster-Resonanzenergietransfers (FRET). Nach der HDAC-Reaktion und der Trypsinreaktion werden Quencher und Fluorophor räumlich getrennt. Das hat zur Folge, dass die Fluoreszenzintensität steigt. Für die HDAC-Reaktionen genutzte Fluorophor/Quencherpaare sind Aminobenzoessäure (Abz)/3-Nitrotyrosin (3-NY) (201), EDANS/DABCYL und weitere (201–205).

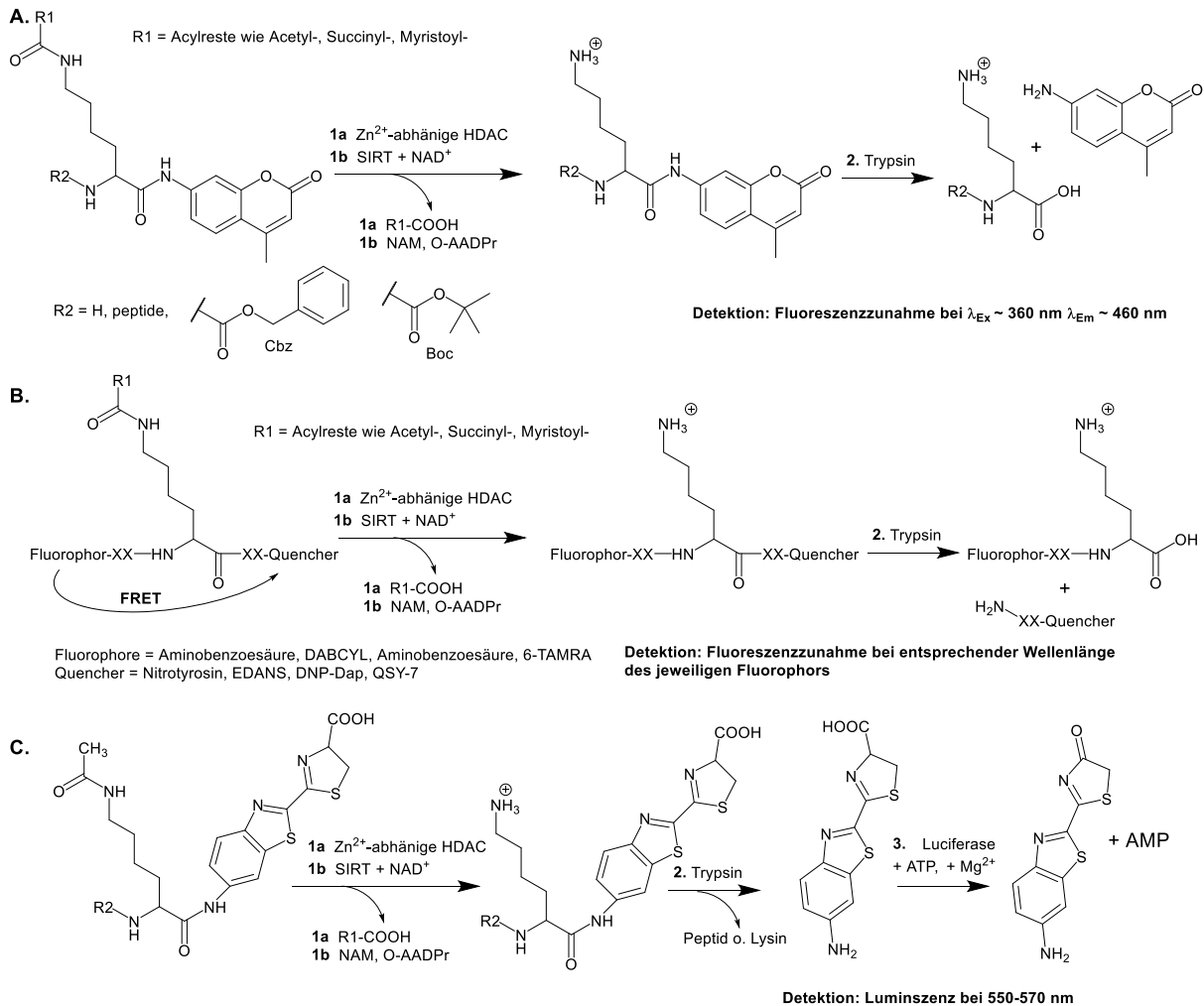


Abbildung 8. Trypsin-gekoppelte Assays zur Messung der HDAC-Aktivität. **A.** Kommerziell erhältliches Fluor-de-Lys-Assay. C-terminal zum modifizierten Lysin befindet sich der 7-Amino-4-methylcoumarinoyl-Rest (AMC), durch Trypsinspaltung wird der Fluorophor freigesetzt und die Fluoreszenzintensität nimmt zu. **B.** Fluorophor und Quencher sind im Peptidrückgrat lokalisiert und über FRET wird die Fluoreszenz gequencht. Durch die Trypsin-vermittelte Spaltung werden Fluorophor und Quencher räumlich getrennt und die Fluoreszenzintensität steigt. DNP-Dap bedeutet 3-(2,4-dinitrophenyl)-l-2,3-diaminopropionsäure. X steht für eine beliebige AS. **C.** Trypsin spaltet ein Luciferasesubstrat vom Peptid ab. Luciferase setzt das Luciferinderivat unter ATP-Verbrauch um und die Intensität der Lumineszenz nimmt zu.

Es existieren noch weitere HDAC-Assays, bei denen die Kopplung von Enzymen genutzt wird. So kann durch die Trypsinreaktion statt des AMC's ein Luciferinderivat freigesetzt werden. Wie in Abbildung 8C dargestellt, wird dieses in einem weiteren enzymatischen Schritt durch die Luciferase umgesetzt, so dass ein messbares Signal entsteht (206, 207). Auch dieser Assay ist kommerziell erhältlich und wird von Promega unter dem Namen HDAC-Glo- bzw. SIRT-Glo-Assay vertrieben. Eine weitere Variation des Trypsin-gekoppelten Assays wurde unter Verwendung eines zweidimensionalen Nanomaterials und einer alternativen Protease entwickelt. Dabei wird ein acetyliertes Peptid, das mit Fluoresceinisothiocyanat (FITC) markiert ist, auf einer Titaniumcarbid (Ti_3C_2)-Schicht immobilisiert. Die Ti_3C_2 -Schicht ist der Quencher für FITC. Wird der Acetylrest durch die HDAC hydrolysiert, kann die zugegebene Carboxypeptidase Y das Peptid abbauen und FITC wird freigesetzt. Es folgt eine räumliche Trennung von der Ti_3C_2 -Schicht und FITC, wodurch die Fluoreszenzintensität steigt (208).

1.6.3 Chemisch gekoppelte Messsysteme

Die chemische Modifikation von Substraten oder Reaktionsprodukten nach der HDAC-Reaktion ist ein weiterer Ansatz, um den Reaktionsfortschritt zu messen. Die Reaktion wird nach einer gewissen Zeit gestoppt und dem Ansatz werden die entsprechenden Chemikalien zugegeben. Aufgrund dessen sind diese Assayansätze normalerweise diskontinuierlich. Eine Übersicht solcher Assays ist in Abbildung 9 dargestellt. Fatkins *et al.* nutzten zum Beispiel aus, dass HDAC8 neben Acetylresten auch artifizielle Thioamidreste hydrolysieren kann (209). Nach der HDAC-Reaktion wird Ellman's Reagenz (DTNB) zugesetzt. Durch die Reaktion mit dem entstandenen Thioacetat bildet sich das Chromophor 2-Nitro-5-thiobenzoat (TNB), was bei einer Wellenlänge von 488 nm verfolgt werden kann (Abbildung 9A).

Eine weitere Möglichkeit ist die Modifikation der entstehenden Aminogruppe. Wichtig ist dabei, dass keine anderen Amine in der Peptidsequenz des Substrates auftreten bzw. mit in die Betrachtung für die Auswertung einbezogen werden. Eine geeignete Substanz ist Fluorescamin. Es reagiert spezifisch mit primären Aminen, d.h. nur mit dem Reaktionsprodukt und nicht mit dem Substrat (Abbildung 9B). Nur das Reaktionsprodukt zeigt hier eine starke Fluoreszenz bei 485 nm (210, 211). Ein weiterer Stoff der zur Modifikation der freigewordenen primären Amine genutzt wurde, ist Dansyl-Chlorid (110).

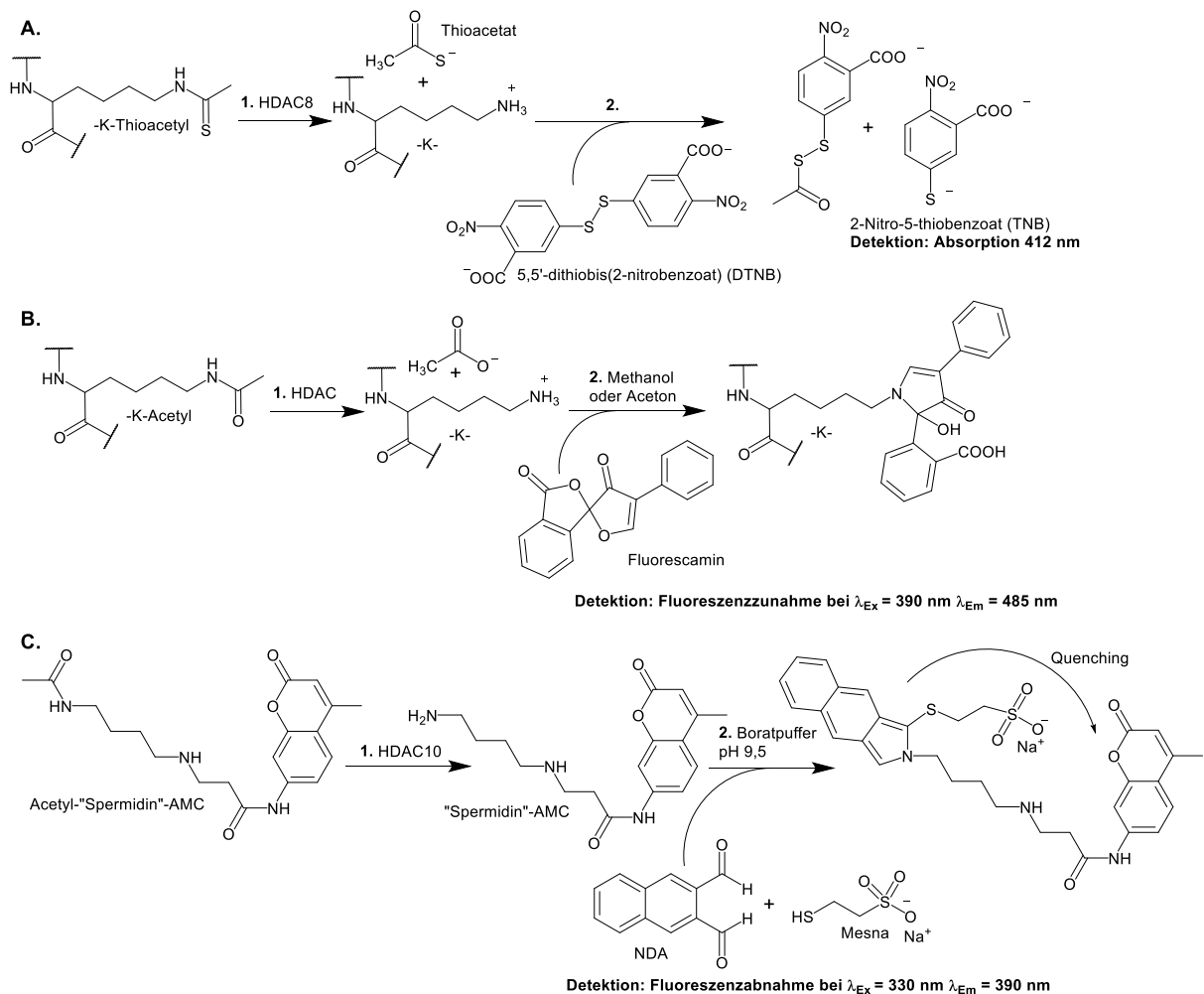


Abbildung 9. Aktivitätsassays, bei denen an die HDAC-Reaktion eine chemische Reaktion gekoppelt ist. **A.** HDAC8-Assay bei dem der Thioacetylrest hydrolysiert wird und das Thioacetat anschließend zugegebenes DTNB spaltet. **B.** Chemische Modifikation der deacetylierten ϵ -Aminogruppe des Lysins durch Fluorescamin. **C.** HDAC10-Assay, um Acetylpolyamindeacetylase-Aktivität zu messen. NDA steht für Naphtalen-2,3-dialdehyd und Mesna für 2-Mercaptoethansulfonat-Natrium.

Ein weiterer chemisch gekoppelter Assay dient der Detektion der HDAC10-Enzymaktivität. Diese Reaktion ist besonders interessant, da HDAC10 vor allem gegen N^8 -Acetylspermidin hohe Deacetylaseaktivität aufweist (110). N^8 -Acetylspermidin und das Produkt Spermidin zeigen bei gängigen Wellenlängen für die HPLC-Detektion (200-220 nm) keine Absorption. Es handelt sich zusätzlich um sehr hydrophile Verbindungen, die bei normaler *reversed phase*- (rp) HPLC im Injektionspeak eluiert werden. Substrat und Produkt können also nicht getrennt werden, weswegen klassische Messsysteme, wie in Abschnitt 1.6.1 beschrieben, schlecht bzw. nicht funktionieren. Ein alternativer Assay ist in Abbildung 9C gezeigt. Das Substrat ist ein AMC-modifiziertes N^8 -Acetylspermidinderivat, welches durch die Anregung bei 330 nm bei 390 nm fluoresziert. Nach der Deacetylierung durch HDAC10 reagiert das primäre Amin mit 2-Mercaptoethansulfonat-Natrium (Mesna) und Naphtalen-2,3-dialdehyd (NDA) und bildet einen Quencher für AMC. Die Fluoreszenzintensität sinkt mit entsprechendem Reaktionsfortschritt. Auch dieser Assay wird diskontinuierlich angewendet (212) und wurde in ähnlicher Form bereits für Peptide verwendet (213).

Bei einem anderen chemisch gekoppelten Assay zur Messung der SIRT1-Aktivität wurde das nicht reagierte NAD^+ chemisch so modifiziert, dass ein starker Fluorophor entstand (214). Für

eine andere Methode wurden Quantenpunkte (*quantum dots*, QD) mit Streptavidin beschichtet. Das acetylierte Peptid wurde mit Cy5 markiert. Nach der SIRT1 Reaktion werden die deacetylierten Lysinreste biotinyliert und können an den mit Streptavidin beschichteten QDs binden. Die nicht deacetylierten Peptide binden entsprechend nicht an die QDs. Werden die QDs zur Fluoreszenz angeregt, findet via FRET eine Energieübertragung der QDs auf Cy5 statt. Der Anstieg der Cy5-Fluoreszenz kann dann gemessen werden (215). Streptavidin beschichtete QDs wurden auch schon deutlich eher als Fluoreszenz-tag genutzt, um SIRT1 Substratspezifität gegen eine Peptidbibliothek zu untersuchen (216).

Im Weiteren werden Assays aufgeführt, bei denen ebenfalls die Fähigkeit von Substraten zur Assoziation mit anderen Biomolekülen in Abhängigkeit von ihrem Acylierungsstatus genutzt wurde. Es handelt sich jedoch nicht um klassische chemische Modifikationen nach der Enzymreaktion. Zum einen sind das die Assays, welche sich die ändernde Affinität zwischen Peptid und DNA abhängig vom Acetylierungsstatus des Peptids zu nutzen machen. Entweder steigt die Fluoreszenz bei DNA-Bindung des deacetylierten Peptids (217) oder sie sinkt bei DNA-Bindung des deacetylierten Peptids, da in die DNA interkaliertes Tb^{3+} durch das Peptid verdrängt wird (218). Zum anderen gibt es Assays, bei denen durch die Deacetylierungsreaktion eine Aggregation der Lysinderivate oder Peptide ausgelöst wird. Die Fluoreszenz steigt durch Aggregations-induzierte Emission. Die Aggregation der Peptide wird durch die Wechselwirkung von einem Sulfonsäure-tag und der positiven Ladung der Aminogruppe des Lysins induziert. Die Fluoreszenzemission wird durch einen Tetraphenylethylen-tag erzeugt (219, 220).

Abschließend wird in diesem Abschnitt ein Assay vorgestellt, der ebenfalls nicht direkt als chemisch gekoppelter Assay gelten kann. Das Besondere ist, dass es sich um eine elektrochemische Detektion handelt, d.h. gemessen wird die Stromstärke. Hierbei wird eine Indiumzinnoxid-Elektrode dreilagig mit Zinn(IV)sulfid, dann mit mit Gold-Nanopartikeln behandeltem Bismutvanadiumoxid und anschließend mit acetyliertem Peptid beschichtet. Nach der SIRT1-Reaktion wird Ascorbinsäure als Elektronendonator und Polyasparaginsäure zugegeben. Polyasparaginsäure geht nur mit dem deacetylierten Peptid ionische Wechselwirkungen ein. Dadurch entsteht eine geordnete Elektrodenoberfläche, welche beim acetylierten Peptid nicht entsteht. An die geordnete Elektrodenoberfläche kann Ascorbinsäure Elektronen abgeben und Strom ist messbar, welcher durch die speziellen Materialeigenschaften und deren Kombination verstärkt wird (221).

1.6.4 Intramolekulare Umlagerung

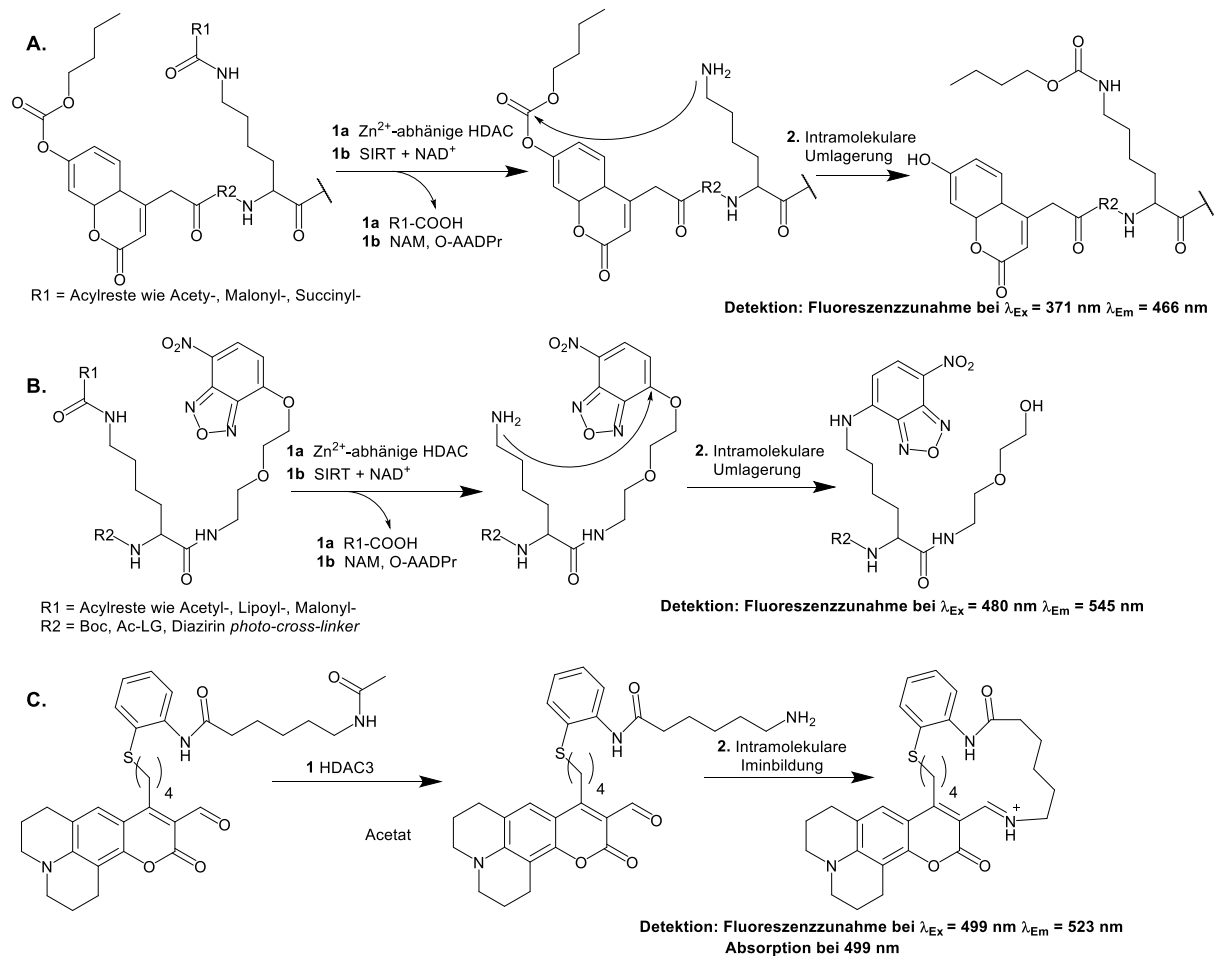


Abbildung 10. Messmethoden, die eine intramolekulare Umlagerung anschließend an die eigentlich Enzymreaktion nutzen.

Eine vielversprechende Methode für die Aktivitätsmessung ist die Kopplung einer intramolekularen Umlagerung an die HDAC-Reaktion, um ein Signal zu erzeugen. Drei Methoden wurden in mehreren Ausführungen publiziert und sind in Abbildung 10 dargestellt. Im ersten Fall wird ein acetyliertes Peptid N-terminal mit einem Cumarinderivat markiert. Dieses Derivat ist zunächst mit einem Kohlensäureester modifiziert und somit nicht zur Fluoreszenzemission fähig. Nach der HDAC-Reaktion findet eine Aminolyse des Esters durch die freie ϵ -Aminogruppe des Lysins statt. Der Kohlensäurerest wird auf die ϵ -Aminogruppe des Lysins übertragen und es entsteht ein Carbamat (Abbildung 10A). Dadurch wird das Cumarinderivat demaskiert und ein starker Fluoreszenzanstieg ist messbar (222). In weiteren Arbeiten wurde der Abstand zwischen Fluorophor und dem acylierten Lysin untersucht. Diese intramolekulare Reaktion funktionierte auch mit größeren Abständen zwischen Fluorophor und modifiziertem Lysin. Ebenso wurden verschiedene Acylreste mit dieser Methode untersucht (223–225).

Bei der zweiten Methode wird das acetylierte Peptid mit O-Nitrobenzoxadiazole (NBD) fluoreszenzmarkiert (Abbildung 10B). O-NBD (NBD als Ether gebunden) kann durch eine Aminogruppe angegriffen werden und es entsteht N-NBD (NBD als Amin gebunden) mit anderen Fluoreszenzeigenschaften. Diese Reaktion findet im Anschluss an die HDAC-Reaktion statt. Der Fluorophor wird auf das deacetylierte Lysin übertragen (226). Auch in diesem Fall wurden verschiedene Acylreste in weiteren Arbeiten getestet. Ebenso konnte der Abstand für die

intramolekulare Reaktion mittels der Peptidlänge variiert werden (227, 228). Außerdem konnte gezeigt werden, das N-NBD auch als FRET-Donor nutzbar ist und damit das N-terminale Cy5 zur Fluoreszenzemission bringen kann (229).

Bei der dritten Variante handelt es sich um eine niedermolekulare Substanz (*small molecule*), welche einen acetylierten Lysinrest imitiert (Abbildung 10C). Nach der HDAC-Reaktion bildet sich ein Imin mit der ϵ -Aminogruppe des Lysins durch intramolekulare Cyclisierungsreaktion. Dies erzeugt einen Fluorophor und die steigende Fluoreszenzintensität ist messbar (230). Dieses Assayprinzip konnte erfolgreich auf ein Peptid übertragen werden (231). Eine ähnliche Cyclisierungsreaktion wurde in einem weiteren Assay genutzt. Auch hier wird ein Fluorophor mit einem Acetyllysin-Imitat konjugiert. Nach der HDAC6-Reaktion spaltet sich durch einen nukleophilen Angriff der deacetylierten Aminogruppe in einer intramolekularen Cyclisierungsreaktion ein Caprolactam ab und es entsteht ein Cyanhydrin-Intermediat, welches spontan zum Fluorophor zerfällt (232). Das gleiche Assayprinzip konnte auf einen Nah-Infrarot-Farbstoff übertragen werden (233, 234) und als Prodrugsystem angewendet werden (234).

Xuan *et al.* verfolgen einen anderen Ansatz für die Messung der HDAC-Aktivität. Statt eines Lysinrests im *enhanced green fluorescent protein* (EGFP) wurde ein acetylierter Lysinrest eingebaut. Der Lysinrest ist essenziell für die Ausbildung des Fluorophors. Ist dieser Lysinrest acetyliert, kann sich der Fluorophor nicht ausbilden. Erst durch die HDAC-vermittelte Deacetylierung kann sich der Fluorophor ausbilden und die Zunahme der Fluoreszenz ist messbar (235). Durch das Expressieren des acetylierten EGFPs in *E. coli*, konnte Aktivität von überexprimierten CobB, SIRT1-3 und SIRT5 gemessen werden. Ebenso konnte die Sirtuin Aktivität unter Nutzung des acetylierten EGFPs in HEK293T-Zellen gemessen werden (235).

1.6.5 Direkte und kontinuierliche Messsysteme

Zur Entwicklung von direkten und kontinuierlichen Messsystemen der enzymatischen Aktivität von HDACs bietet sich die Nutzung der Fluoreszenzlöschung von Fluorophoren durch Quencher an. Infolge der Deacylierungsreaktion werden Fluorophor und Quencher räumlich getrennt und es ergibt sich eine Fluoreszenzänderung. Der Quencher kann im Acylrest integriert werden und der Fluorophor im Peptidrückgrat (Abbildung 11A). Alternativ wird der Fluorophor im Acylrest integriert und der Quencher im Peptidrückgrat (Abbildung 11B). Allerdings bietet der Acylrest wenig Platz und nur geringe Möglichkeiten zur chemischen Modifikation. Zusätzlich werden die Substrateigenschaften des Peptids durch eine solche Modifikation sowohl sterisch als auch chemisch stark verändert.

Eine Möglichkeit ergibt sich daraus, dass Sirtuine (41, 64) und HDAC11 (61–63) auch längere Fettsäurereste hydrolysieren können. In diesen längeren Fettsäureketten ist es möglich, einen Quencher oder einen Fluorophor einzubringen. Der erste direkte und kontinuierliche Assay wurde von Schuster *et al.* für Sirtuine vorgestellt (236). Dabei wurde als Fettsäureimitat Abz als Fluorophor an 11-Aminoundecansäure gekoppelt. Damit ist der Fluorophor weit von der zu spaltenden Amidbindung entfernt und sollte einen geringen Einfluss auf die Sirtuinreaktion haben (Abbildung 11C, R1). In das Peptidrückgrat wurde 3-NY als Quencher eingebaut. Durch die Sirtuinreaktion steigt die Fluoreszenzintensität von Abz an. Das auf die oben beschriebene Weise modifizierte Peptid ist ein sehr gutes SIRT2-Substrat mit einer katalytischen Effizienz von $176\,000\text{ M}^{-1}\text{s}^{-1}$. Für dieses Assay wurde ein Peptid genutzt, das vom Tumornekrosefaktor- α (TNF- α) abstammt, welcher ein natürliches SIRT6 Substrat ist (41). Darauf aufbauend nutzte eine andere Arbeitsgruppe den gleichen Acylrest mit dem gleichen Quencher. Durch die Optimierung

der Peptidsequenz für den Assay konnte ein leicht verbessertes SIRT2-Substrat erhalten werden (237).

Der zweite direkte und kontinuierliche Assay wurde von Kawaguchi *et al.* entwickelt. Dabei ist der gesamte an das Lysin eines H3K9-Nonapeptids gebundene Acylrest ein DABCYL-Derivat (Abbildung 11C, R3) und wirkt als Quencher für ein C-terminal gekoppeltes FITC. Dieses Peptid ist mit einer katalytischen Effizienz von $230\,000\text{ M}^{-1}\text{s}^{-1}$ vor allem für SIRT1 als Substrat geeignet. Durch eine Verkürzung der Peptidkette auf drei AS konnte mit diesem Peptid die Sirtuinaktivität in Zellen gemessen werden (238). In dieser Arbeitsgruppe wurden, ausgehend von diesem Substrat, Substrate für andere Sirtuinisofomne entwickelt. Dazu wurde ein Disperse Red-Derivat als Quencher verwendet (Abbildung 11C, R2). Außerdem wurden alternative Peptidsequenzen genutzt und die FITC-Markierung wurde auf den N-Terminus verschoben. Damit konnte die katalytische Effizienz für SIRT2 um das 24-fache und für SIRT3 um das 154-fache gesteigert werden (239). Für die Zn^{2+} -abhängigen HDACs gab es bis zum Anfertigen dieser Arbeit keine bekannten direkten und kontinuierlichen Aktivitätsassays.

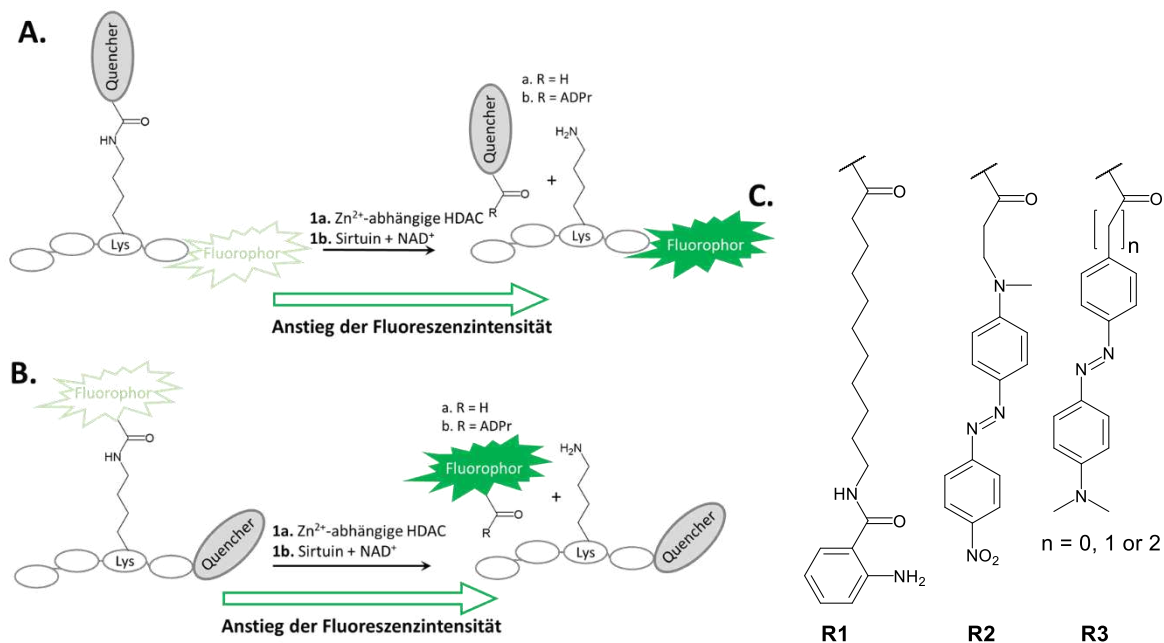


Abbildung 11. Schematische Darstellung für das Prinzip eines kontinuierlichen und direkten Assays für Histondeacetylasen. A. Im Lysinacylrest eingebauter Quencher und am Peptidrückgrat gekoppelter Fluorophor. **B.** Im Lysinacylrest eingebauter Fluorophor und im Peptidrückgrat integrierter Quencher. Bei **A** und **B** wird durch die HDAC vermittelte Deacylierung der Fluorophor vom Quencher getrennt und die Fluoreszenz steigt. **C.** Beispiele für Acylmodifikationen für direkte Messmethoden der HDAC-Aktivität.

1.6.6 Fluoreszenzsonden

Neben den genannten Aktivitätsmessungen existiert die Möglichkeit, Moleküle anhand ihrer Bindungsaffinität an das entsprechende Zielmolekül zu selektieren. Die enzymatische Aktivität spielt hierbei keine Rolle. Diese Messmethoden beruhen darauf, dass sich bei der Bindung einer Sonde an das Zielprotein die Eigenschaften der Sonde messbar ändern. Ein typisches Beispiel dafür sind sogenannte *fluorescence indicator displacement assays* (FID). Die Funktionsweise ist links in Abbildung 12 skizziert. Sie beruht darauf, dass sich die Fluoreszenzintensität oder die Fluoreszenzpolarisation der Sonde im ungebundenen und gebundenen Zustand unterscheidet. Im Ausgangszustand bindet der Fluoreszenzindikator an das Zielmolekül. Nach Zugabe der

Testverbindung konkurriert diese mit der Sonde um die Bindungsstelle am Zielprotein. Die entsprechenden Fluoreszenzeigenschaften ändern sich und erzeugen so ein geändertes Signal. Fluoreszenzsonden sind oft Derivate von bekannten HDACi, wie das SAHA-Derivat, welches an Fluorescein gekoppelt und für die Zn^{2+} -abhängigen HDACs genutzt wurde oder das SirReal2-Derivat, welches an TMARA gekoppelt und für SIRT2 genutzt wurde (211, 240–242). Weitere solcher Sonden wurden in Kombination mit verschiedenen Farbstoffen und Panobinostat (243), Scriptaid (244), SAHA (245) und einem neu entwickelten cyclischen Depsipeptidinhibitor entwickelt (246). Bei solchen Fluoreszenzsonden wird normalerweise die Fluoreszenzpolarisation gemessen. Es besteht auch die Möglichkeit die Eigenschaften von 2-Furylacryloylhydroxamat (FAHA) zu nutzen. FAHA bindet im aktiven Zentrum der Zn^{2+} -abhängigen HDACs und löscht die intrinsische Proteinfluoreszenz aus. Wird FAHA verdrängt, kann die Zunahme der intrinsischen Proteinfluoreszenz gemessen werden (247). 1-Aminoanthracen (AMA) wurde als Sonde mit mäßiger Affinität für SIRT2 ($K_D = 37 \mu M$) vorgestellt, zeigt jedoch bei Bindung an das aktive Zentrum von SIRT2 einen enormen Anstieg der Fluoreszenzintensität. Durch die Co-Bindung eines decanoylierten Peptids konnte die Bindung verbessert werden (248, 249). Eine komplexere Variante dieses Assayprinzips, der unter anderem für SIRT2 und HDAC10 angewendet wurde, ist der Nano-BRET Assay. Hierbei wird an die HDAC ein Luciferase-tag fusioniert. Ist die Fluoreszenzsonde gebunden, wird die durch die Luciferasereaktion erzeugte Energie nicht als Licht emittiert, sondern strahlungslos auf die Fluoreszenzsonde übertragen, die dann Photonen emittiert. Wird die Fluoreszenzsonde verdrängt, kann keine Energieübertragung stattfinden. Der Vorteil dieser Methode ist, dass keine externe Lichtquelle für *in vivo* Messungen benötigt wird (212, 250).

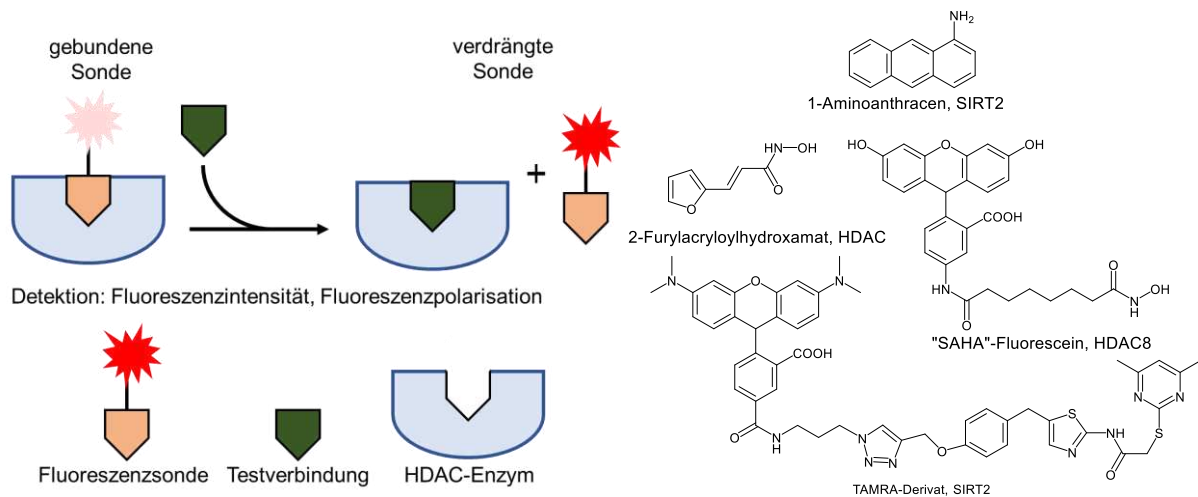


Abbildung 12. Prinzip eines FID-Assays und einige Beispiele für verwendete Sonden für HDAC-Assays.

2 Zielstellung

Das erste Ziel dieser Arbeit ist die Entwicklung neuer Messmethoden für die *in vitro* Aktivität verschiedener Histondeacetylasen. Dafür werden verschiedene Strategien genutzt. Da bekannt ist, dass neben den Sirtuinen auch HDAC11 eine sehr effiziente Deacylase für längere Fettsäurereste wie Myristoyl- und Palmitoylreste ist (61, 62), soll basierend auf einem Sirtuinassay ein direkter und kontinuierlicher Assay entwickelt werden (236).

Weiterhin sollen die speziellen optischen Eigenschaften von Thioamiden genutzt, um die HDAC-Aktivität direkt und kontinuierlich zu messen. Dabei soll die Möglichkeit genutzt werden, dass HDAC8 in der Lage ist, Thioacetylreste mit ähnlicher Effizienz wie Acetylreste zu entfernen (209). In einem für HDAC8 entwickelten Assay wurde eine chemisch gekoppelte Reaktion genutzt (209). Thioamide zeichnen sich dadurch aus, dass sie eine starke Absorption bei 260 nm aufweisen (251). Diese Eigenschaft soll beim zweiten Ziel dieser Arbeit genutzt werden, der Entwicklung eines HDAC-Aktivitätsassays zur direkten und kontinuierlichen Messung. Dafür werden verschiedene Peptide mit der gleichen Aminosäuresequenz synthetisiert. Die Peptide unterscheiden sich jedoch anhand unterschiedlicher Acylreste und der entsprechenden Thioacylreste. Über den Mechanismus des Photoinduzierten Elektronentransfers (PET) können Thioamide als Quencher für Fluorophore wirken (252, 253). Deswegen soll untersucht werden, ob die Thioamidbindung auch als Quencher für Fluorophore dienen kann, um einen fluoreszenzbasierten Assay zu entwickeln.

Das dritte Ziel dieser Arbeit ist die Entwicklung eines Aktivitätsassay für HDACs, die Fettsäurereste hydrolysieren. Dafür werden Thioamide als Quencher für verschiedene Fluorophore eingesetzt. Thioamidbindungen als zu hydrolysierende Bindung lassen sich für die Aktivitätsmessung der Sirtuine nicht verwenden, da sie als Inhibitoren für Sirtuine wirken (254). Um trotzdem das PET-Quenching für einen fluoreszenzbasierten Assay nutzen zu können, soll die Thioamidbindung in einem Myristoylrest „maskiert“ werden. Es soll dafür eine Reihe verschiedener Peptide, die den Thioamidacylrest tragen, synthetisiert werden. Zuerst sollte die Position des Fluorophors im Peptidrückgrat untersucht werden. Anschließend sollten verschiedene Fluorophore an der optimalen Position getestet werden.

Das vierte Ziel dieser Arbeit ist die Untersuchung, ob die Fluoreszenzintensität von umgebungssensitiven Fluorophoren in Peptiden direkt durch Fettsäurereste moduliert werden kann. Alle Peptide sollen auf ihre Substrateigenschaften für die verschiedenen HDACs untersucht werden und spektroskopisch charakterisiert werden. Anschließend sollten sie kinetisch charakterisiert werden. Für die verschiedenen Ansätze sollen Assays für die Messung der Aktivität entwickelt und durch Messungen mit verschiedenen bekannten Inhibitoren validiert werden.

Das fünfte Ziel dieser Arbeit ist, verschiedene kurze Acylreste, welche *in vivo* nachgewiesen wurden, als Substrate für die verschiedenen HDACs zu untersuchen. Dafür sollen Modellpeptide, die diese Acylreste tragen, kinetisch für die verschiedenen HDAC Isoformen charakterisiert und mit dem entsprechenden acetylierten Peptid verglichen werden.

3 Ergebnisse

3.1 Continuous Activity Assay for HDAC11 Enabling Reevaluation of HDAC Inhibitors

Zsófia Kutil, Jana Mikešova, **Matthes Zessin**, Marat Meleshin, Zora Nováková, Glenda Alquicer, Alan Kozikowski, Wolfgang Sippl, Cyril Bařinka und Mike Schutkowski

ACS OMEGA, 2019, 4, 19895-19904
DOI: <https://doi.org/10.1021/acsomega.9b02808>

Abstract:

Histone deacetylase 11 (HDAC11) preferentially removes fatty acid residues from lysine side chains in a peptide or protein environment. Here, we report the development and validation of a continuous fluorescence-based activity assay using an internally quenched TNF α -derived peptide derivative as a substrate. The threonine residue in the +1 position was replaced by the quencher amino acid 3'-nitro-l-tyrosine and the fatty acyl moiety substituted by 2-aminobenzoylated 11-aminoundecanoic acid. The resulting peptide substrate enables fluorescence-based direct and continuous readout of HDAC11-mediated amide bond cleavage fully compatible with high-throughput screening formats. The Z' -factor is higher than 0.85 for the 15 μ M substrate concentration, and the signal-to-noise ratio exceeds 150 for 384-well plates. In the absence of NAD $^+$, this substrate is specific for HDAC11. Reevaluation of inhibitory data using our novel assay revealed limited potency and selectivity of known HDAC inhibitors, including Elevenostat, a putative HDAC11-specific inhibitor.

Continuous Activity Assay for HDAC11 Enabling Reevaluation of HDAC Inhibitors

Zsófia Kutil,[†] Jana Mikešová,[†] Matthes Zessin,[‡] Marat Meleshin,[§] Zora Nováková,[†] Glenda Alquicer,^{†,⊥} Alan Kozikowski,^{||} Wolfgang Sippl,[‡] Cyril Barinka,^{*,†} and Mike Schutkowski^{*,§}

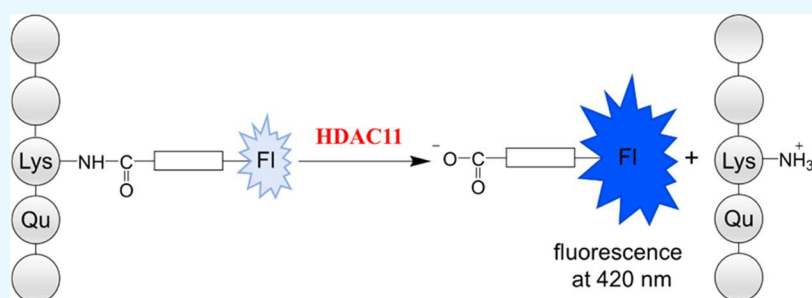
[†]Institute of Biotechnology of the Czech Academy of Sciences, BIOCEV, Prumyslova 595, 252 50 Vestec, Czech Republic

[‡]Department of Medicinal Chemistry, Institute of Pharmacy, Martin-Luther-University Halle-Wittenberg, 06120 Halle (Saale), Germany

[§]Department of Enzymology, Institute of Biochemistry and Biotechnology, Charles Tanford Protein Centre, Martin Luther University Halle-Wittenberg, Kurt-Mothes-Straße 3a, 06120 Halle (Saale), Germany

^{||}StarWise Therapeutics LLC, 505 S Rosa Road, Suite 27, Madison, Wisconsin 53719-1235, United States

Supporting Information



ABSTRACT: Histone deacetylase 11 (HDAC11) preferentially removes fatty acid residues from lysine side chains in a peptide or protein environment. Here, we report the development and validation of a continuous fluorescence-based activity assay using an internally quenched TNF α -derived peptide derivative as a substrate. The threonine residue in the +1 position was replaced by the quencher amino acid 3'-nitro-L-tyrosine and the fatty acyl moiety substituted by 2-aminobenzoylated 11-aminoundecanoic acid. The resulting peptide substrate enables fluorescence-based direct and continuous readout of HDAC11-mediated amide bond cleavage fully compatible with high-throughput screening formats. The Z' -factor is higher than 0.85 for the 15 μ M substrate concentration, and the signal-to-noise ratio exceeds 150 for 384-well plates. In the absence of NAD⁺, this substrate is specific for HDAC11. Reevaluation of inhibitory data using our novel assay revealed limited potency and selectivity of known HDAC inhibitors, including Elevenostat, a putative HDAC11-specific inhibitor.

INTRODUCTION

Reversible ac(et)ylation of lysine side chains has emerged as one of the major regulatory mechanisms in living organisms. It is involved in the modulation of protein–protein interactions, protein localization and degradation, and moreover in chromatin assembly, DNA repair, and metabolic stress response. Acyl residues are introduced either by the action of acetyltransferases using acyl-CoAs as cosubstrates or by spontaneous reactions of acyl-CoA thioesters with the lysine side chains. In the past 10 years, other types of acyl modifications, propionylation,¹ butyrylation,^{2,3} malonylation,⁴ succinylation,⁵ glutarylation,⁶ crotonylation,⁷ 3-hydroxybutyrylation,^{8,9} 4-oxo-nonaoylation,¹⁰ hydroxyisobutyrylation,^{11,12} 3-hydroxy-3-methyl-glutarylation,^{11,12} 3-methyl-glutarylation,^{11,12} 3-methyl-glutaconylation,^{11,12} 3-phosphoglyceroylation,¹³ benzoylation,¹⁴ myristoylation,¹⁵ and stearoylation¹⁶ have been identified, thereby dramatically expanding the portfolio of post-translation modifications controlling a number of cellular processes.^{17,18}

Removal of acyl residues from lysines is catalyzed by histone deacetylases (HDACs). This reaction is more tightly regulated by the substrate and acyl specificities of individual HDACs and their spatiotemporal distribution within the cell. HDACs are evolutionarily conserved among organisms. Based on sequence homology and enzymatic mechanism, HDACs can be divided into 4 classes. Members of classes I (HDAC 1, 2, 3, and 8), II (HDAC4–7, 9 and 10), and IV (HDAC11) are Zn²⁺-dependent hydrolases, while class III proteins (called sirtuins; SIRT 1–7) use NAD⁺ as the cosubstrate for the transfer of the acyl moiety from the lysine side chain to the ADP-ribose fragment of NAD⁺ generating nicotinamide as the third product of the reaction.¹⁹ Recently, our group and others identified a robust defatty acylase activity for HDAC11,^{20–22} which may represent the major enzymatic activity of HDAC11

Received: August 30, 2019

Accepted: October 18, 2019

Published: November 15, 2019

in vivo. HDAC11 is involved in the regulation of the immune system and the modulation of cancer growth,^{19,23} and very recently, it has been demonstrated that HDAC11 knock-out protects mice from high-fat diet-induced obesity and metabolic syndrome,²⁴ making HDAC11 an interesting target for the treatment of cancer and obesity-related diseases.

There is only limited information on the development and use of HDAC11-specific inhibitors. In 2017, Huang et al. reported Elevenostat (compound JB3-22), the putative HDAC11-specific inhibitor, to be effective in pharmacologic modulation of functions of T-regulatory cells.²⁵ Very recently, the development of FT895, a hydroxamate-based small-molecule compound, has been described by Martin et al.,²⁶ and 2-carboxamidothiophene-based zinc ion chelating carbonylhydrazides were shown to be selective HDAC11 inhibitors active in vivo.²⁷ Additionally, several pan-HDAC inhibitors used in clinical trials, including romidepsin and trichostatin A (TSA), are reported to have nanomolar potency for HDAC11. At the same time, however, inhibitory constants of these and other small molecules toward HDAC11 listed in the ChemBL database are somewhat inconsistent, and these inconsistencies may stem from different assay conditions (pH values, the presence of additives like bovine serum albumin (BSA) or detergents, and substrate concentrations) as well as the use of suboptimal substrates like acetylated peptides, which are very poorly accepted by HDAC11. Consequently, we believe that reevaluation of some of these findings would be valuable for the scientific community focused on biological experiments in the future.

The detection of HDAC activity is often coupled to a separation of a substrate and its reaction product. Different methods are used for such separation steps, including capillary electrophoresis,²⁸ microchip electrophoresis,²⁹ microfluidic mobility assay,^{30,31} polyacrylamide gel electrophoresis,³² high-performance liquid chromatography (HPLC),^{33–36} thin-layer chromatography,³⁷ charcoal-binding,³⁸ binding to boronic acid resins,³⁹ and extraction with organic solvents.⁴⁰ Owing to this additional separation step, the resulting assay format is discontinuous and not suited for high-throughput applications. Alternatively, mass spectrometry could be used for the separation of the substrate and the reaction product.^{41,42} Matrix assisted laser desorption ionization-time of flight mass spectrometry readout, in combination with peptide derivatives immobilized on glass surfaces, was used for the systematic profiling of substrate specificity of HDAC2, HDAC3, and HDAC8.^{43,44} Additionally, HDAC activity patterns could be determined in cell lysates using this technique.⁴⁵ Moreover, the same technology uncovered the dependence of the HDAC8 substrate specificity on the nature of the metal ion within the active site.⁴⁶ Alternative approaches make use of reagents sensing either the acetylated substrates, like acetyllysine recognizing antibodies,^{47–52} or the reaction products. The release of radioisotopically labeled acetate was used to analyze HDAC activity.^{53–56} More recently, acetate could be captured by coupling to an enzymatic reaction,⁵⁷ and a chemical reaction was used to trap the HDAC8-mediated release of thioacetate yielding a chromophore.⁵⁸ Reagents for the detection of the generated primary amine in the peptide product could either be chemicals, like biotin-containing active esters or activated fluorescent dyes, reacting with the lysine side chain^{59,60} or intramolecular reactions, like transesterification with a coumarin dye,⁶¹ which is only possible if the lysine side chain is released by HDAC activity.^{62–65} Additionally,

aggregation-induced emission^{66,67} and modulation of binding to DNA^{68,69} were used to probe HDAC activity.

An interesting alternative is the coupling of the HDAC-mediated reaction to a proteolytic reaction using proteases, specific for the free lysine side chain in the reaction product.^{34,56,70,71} The fluorescence-based readout for the proteolytic reaction is common to increase the sensitivity of the assay. Commercially available HDAC substrates are fused to 7-amino-4-methylcoumarin, resulting in bright fluorescence subsequent to cleavage of the lysinyl-coumaryl amide bond.^{72–78} However, as the proteolytic stability of different HDACs against the developer proteases is limited, most protease-coupled HDAC assays have to be performed in a discontinuous manner. The additional disadvantage stems from the fact that the substituted coumaryl moiety represents an artificial residue within the HDAC substrate preventing the investigation of substrate specificities in +1, +2, etc. positions. Moreover, it was demonstrated that profiling of HDAC activity with substrates containing coumaryl fluorophores yielded results different from screening results with more natural substrates, including artificially enhanced affinity to the active site (HDAC6) or loss of sequence specificity (HDAC4).⁷⁹ Additionally, substrates of this type are characterized by suboptimal K_M -values in the high micromolar range.

Continuous assays without coupling to enzymatic or chemical reactions are described for sirtuins.^{80,81} In these cases, a fluorophore or a quencher is an integral part of the acyl moiety linked to the lysine side chain. Such an approach is not feasible for HDACs of classes I and II because their narrow acyl binding pockets cannot accommodate acyl groups decorated with bulky fluorophore moieties. In contrast, HDAC11 is able to remove hydrophobic, long-chain acyl residues from lysine side chains,^{20–22} and therefore, we wondered if continuous substrates described for sirtuins are suitable for the determination of HDAC11 activity. Here, we report the development of a continuous and direct activity assay for HDAC11 based on internal fluorescence quenching. Using this novel HDAC11 activity assay in comparison to the data generated using a commercially available trifluoroacetylated lysine derivative, we were able to reevaluate the potency of known HDAC inhibitors including Elevenostat, Pracinostat, Quisinostat, Dacinostat, Trapoxin A, and Romidepsin. Additionally, we were able to demonstrate that this HDAC11 activity assay is fully compatible with high-throughput screening formats.

RESULTS

Continuous and Direct Activity Assay for HDAC11. HDAC11 is able to remove decanoyl, dodecanoyl, and myristoyl residues from lysine side chains in the sequence context of a substrate sequence derived from peptide microarray experiments.²² We wondered if the active site of HDAC11 could adopt an aminoundecanoic acid residue, which is acylated by anthranilic acid. In the past, we were able to demonstrate that such modification of the acyl moiety is well tolerated by most of the class III HDACs (sirtuins).⁸¹ Fluorescence of the anthraniloylamide is efficiently quenched by a 3-nitrotyrosine residue in the +1 position of a TNF α -derived peptide substrate 1, resulting in an increase of fluorescence subsequent to HDAC11 treatment (Figure S2). We used substrate 1 (see Figure 1) because it is derived from a known in vivo myristoylation site.⁸² First, we analyzed the substrate properties using human HDAC11 in combination

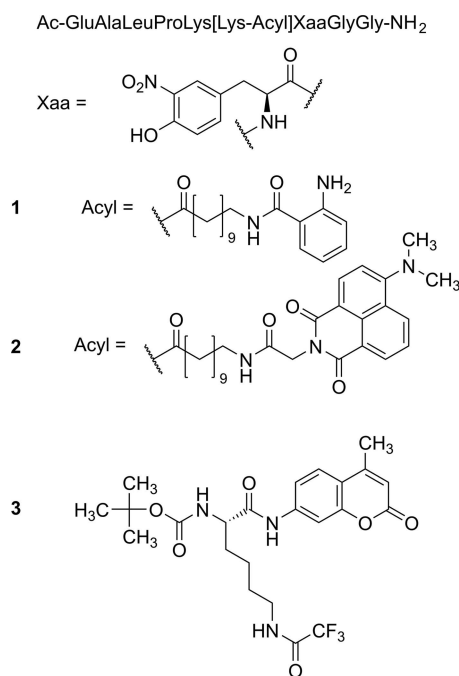


Figure 1. General structure of the substrates. Peptide substrates 1 and 2 were derived from the known myristoylation site TNF α -Lys20.¹⁵ The naturally occurring threonine residue in +1 position is replaced by the quencher L-3-nitrotyrosine. The lysine side chain corresponding to Lys20 of TNF α is acylated with fluorescent N-anthraniloylated (peptide 1) or N-(4,N,N-dimethylamino-1,8-naphthalimido)acetyl (peptide 2) 11-aminoundecanoic acid. Lysine derivative 3 represents the commercially available trifluoroacetylated HDAC substrate.

with an HPLC-based assay as described.²⁰ Substrate 1 is well accepted by HDAC11 with a specificity constant very similar to the values for trifluoroacetylated substrates used in protease-coupled assay formats. To increase the wavelength used for the excitation of fluorescence, we generated peptidic substrate 2 (Figure 1) equipped with a sterically more demanding fluorophore. Using an HPLC-based activity assay, we were able to demonstrate the cleavage of the amide bond at the side chain of the lysine residue but with very poor kinetics (Figure S3). After treatment with 500 nM HDAC11 for 1 h, around 6% substrate conversion could be detected. Obviously, the hydrophobic pocket of HDAC11 accepting the acyl lysine is sensitive to sterically more demanding moieties, at least at the distal positions.

When fluorescence change was monitored over time, the resulting progress curves at different concentrations of HDAC11 were linear up to 25% conversion of the substrate. In the absence of HDAC11, a slight fluorescence decrease of 7% of the total fluorescence intensity is detectable after 30 min (Figure 1a). The slope of the fluorescence increases of reaction solutions containing 1 and HDAC11 is dependent on the enzyme concentration, resulting in a linear correlation between the HDAC11 amount and the reaction rate (Figure 1b). This dependence on enzyme concentration demonstrates that the measured signal increase is caused by the enzyme-mediated cleavage of the amide bond and not by fluorescence artifacts. Therefore, peptide derivative 1 could be used for the recording of HDAC11 activity in a continuous format. For the generation of appropriate calibration curves, N-(2-aminobenzoyl)-11-aminoundecanoic acid, the reaction product, was used. We found a pronounced dependence of HDAC11 activity on the

concentration of bovine serum albumin (BSA) in the assay buffer (Figure 2c). Therefore, all measurements were performed in the presence of 2 mg/mL of BSA. To ensure that this concentration of BSA does not affect the inhibitor's potency, we have tested the quisinostat as a representative of moderately active inhibitors in different concentrations of BSA in the buffer. No decisive effect of BSA on the activity of the inhibitor was observed at concentrations tested (Supporting Information Figure S5). To demonstrate that the activity assay is useful for high-throughput screenings, we performed measurements in 96-, 384-, and 1536-well microtiter plates (Figure 2d) yielding excellent Z'-factors of 0.85 for 1 at 15 μ M concentration. The K_M values determined using the different microtiter plate formats are very similar, and the resulting specificity constants are in the range of 11 000 to 13 000 M⁻¹ s⁻¹ (Figure 2).

Because HDAC8 is the only other Zn²⁺-dependent HDAC, which is able to accept longer acyl moieties, we tested peptides 1 and 2 as HDAC8 substrates using an HPLC-based activity assay. We found less than 1% cleavage using 500 nM HDAC8 for 4 h, with a 20 μ M peptide substrate. Thus, in the absence of NAD⁺, which prevents any action of sirtuins against 1, peptidic substrate 1 could be considered as an HDAC11-specific substrate.

Reevaluation of known HDAC Inhibitors Using Peptidic Substrate 1 and Trifluoroacetyllysine Derivative 3.

Most of the typical HDAC inhibitors are not active against HDAC11. Nevertheless, several inhibitors were described for HDAC11 with IC₅₀ values in the low nanomolar range. Trapoxin A is an inhibitor of HDAC11 activity with an IC₅₀ value of 170 nM and a K_i value of 24 nM if a myristoylated peptidic substrate was used for activity measurements. We determined the IC₅₀-value for Trapoxin A-mediated HDAC11 inhibition using 1 to validate the continuous and fluorescence-based activity assay. We found an IC₅₀ value of 10 nM (Table 1), which is in good agreement with the data from the literature. TSA is an inhibitor for HDAC11 with described affinities between 14 nM⁸³ and 32 μ M.²¹ If measured with an acetylated fluorogenic pentapeptide derived from p53, an IC₅₀ value of 17 nM was reported.⁸⁴ In contrast, no efficient inhibition by TSA could be detected using a myristoylated peptidic derivative with an estimated IC₅₀ value of 32 μ M.²¹ We used 1 to reanalyze the effect of TSA on HDAC11 activity and obtained less than 50% inhibition at 20 μ M inhibitor resulting in an IC₅₀ of 22 μ M (Table 1). This demonstrates that substrate 1 yielded results closer to results found using myristoylated substrates. For comparison, we profiled TSA-mediated inhibition of HDAC11 with the trifluoroacetylated lysine derivative 3 and again found no effective inhibition (an IC₅₀ value of 10 μ M). Similarly, we analyzed romidepsin, a cyclic peptidic inhibitor used in the clinic. An IC₅₀ value of 0.3 nM⁸⁵ could not be confirmed using either substrate 1 or 3 (Table 1). In our hands, romidepsin is active against HDAC11 with the IC₅₀ value in the low μ M range. This finding is supported by the reported IC₅₀ value of higher than 10 μ M if a trifluoroacetylated substrate peptide was used.⁸⁶ To our surprise, several inhibitors that are described to be highly efficient against HDAC11, like Dacinostat, Elevenostat, Pracinostat, Mocetinostat, and Quisinostat, are not so effective if analyzed using substrates 1 and 3 (Table 1). In all cases, the reported values were generated using acetylated substrates. On the other hand, we were able to confirm the efficient inhibition of HDAC11 by fimepinostat using substrate 1, demonstrating

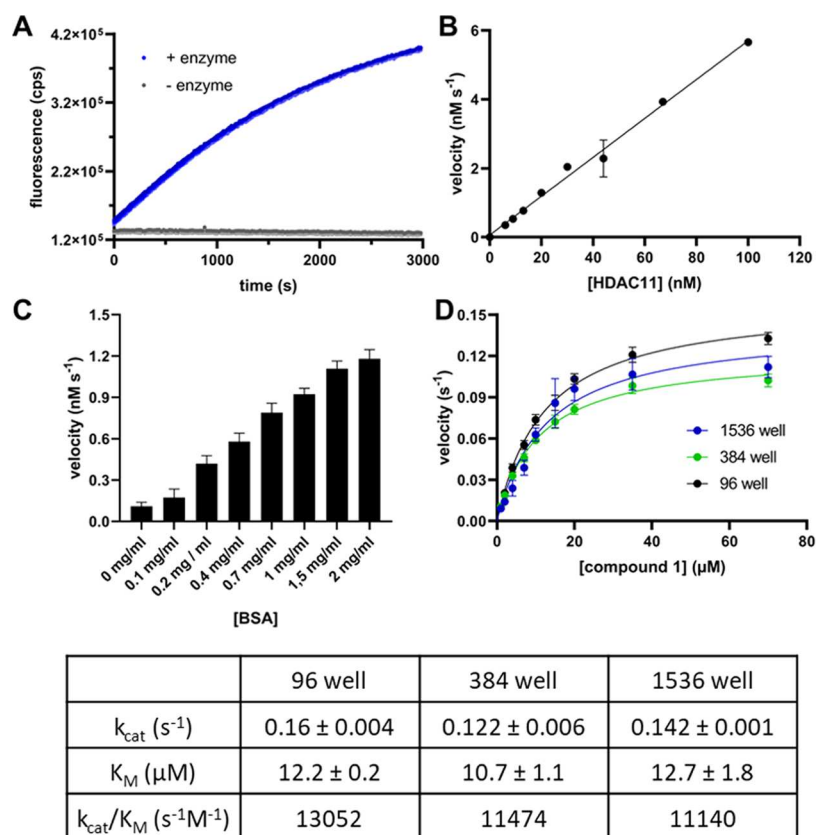


Figure 2. Fluorescence measurements using substrate 1. (A) Fluorescence change as a function of time. The excitation/emission wavelengths were set at $330 \pm 75/430 \pm 8$ nm, respectively. The reaction was performed with the $15 \mu\text{M}$ substrate and 30 nM HDAC11 (blue dots) as well without enzyme (gray dots). (B) Fluorescence change as a function of the HDAC11 concentration. The reactions were performed with 100, 67, 44, 30, 20, 13, 9, and 6 nM HDAC11 and $50 \mu\text{M}$ substrate. (C) Velocity of the product formation as a function of BSA concentration in the buffer. The substrate concentration (peptide 1) was $20 \mu\text{M}$ and HDAC11 concentration was 30 nM . The experiment was performed once with $n = 6$, and the error bars show the standard deviation (SD). (D) Steady-state kinetics of HDAC11 with compound 1. Reactions were performed using 30 nM HDAC11 and varying concentrations of 1 ($0.1\text{--}70 \mu\text{M}$). The results are from two independent experiments, and each experiment was done with $n = 3$ (96 well), $n = 4$ (384 well), and $n = 6$ (1536 well) replicates, and the error bars show the standard deviation. The velocity v means product formation per time unit and per active site. The resulting kinetic constants of the fit are summarized in the table below.

that 1 is suitable for inhibitor screenings resulting in less false positives compared to screenings with acetylated substrates.

DISCUSSION

HDAC11 is one of the least studied HDAC isoforms. To evaluate its biological function, highly efficient tools are needed, like compound selectively inhibiting HDAC11 with high affinity. Screening of large compound libraries is limited by the complex assays known for HDAC activity measurements. Most of the fluorogenic assays are discontinuous because of the limited stability of the HDACs against the developer protease used. Alternative assays, like HPLC-based or MS-based formats, are very time consuming, and therefore not suited for HTS applications. Moreover, HDAC11 is unique in the sense of substrate specificity. It has very poor activity against acetylated substrates but robust activity on trifluoroacetylated substrates and substrates with decanoylated or myristoylated lysine side chains. Based on this knowledge, we developed peptidic substrate 1, which is from the structural point of view closer to the myristoylated *in vivo* substrates. We then used this substrate to reevaluate some of the HDAC inhibitors, especially compounds described to be efficient against HDAC11 (Table 1, Figure 3). There are two major findings. First, effective inhibitors identified using either

trifluoroacetylated substrates (Fimepinostat⁸⁷ or myristoylated substrates (Trapoxin A²¹) could be confirmed using substrate 1. Second, effective compounds identified using acetylated substrates are not so effective if analyzed using either 1 or 3 (Table 1). The very poor activity of HDAC11 against acetylated substrates generates a problem if the enzyme preparation is contaminated with traces of HDACs that are highly active against acetylated substrates. Such contaminations are probably because most of the commercially available HDAC11 preparations have suboptimal purity. Depending on the respective kinetic constants, contaminating HDAC amounts less than 0.1 percent (which is hardly visible in PAGE gels) could generate a robust signal leading to false-positive screening hits. This situation is better if trifluoroacetylated substrates are used because HDAC11 is more active in such cases. Nevertheless, other HDACs like HDAC4, 5, 7, 8, and 9 are known to recognize trifluoroacetyllysine substrates with substantially higher efficacy. Substrate 1 is optimal for HDAC11 measurements because this is the only isoform that is able to handle this acyl moiety. In principle, sirtuins 1–6 can deacetylate substrate 1, but for that reaction, the presence of the NAD^+ cosubstrate is necessary.⁸¹

Careful inspection of the presented IC_{50} values in Table 1 uncovers higher IC_{50} values for measurements performed with substrate 1 compared to lysine derivative 3 resulting in up to 5-

Table 1. IC₅₀ Values for Listed Inhibitors were Determined Using the Peptidic Substrate 1 (15 μM of 1 and 20 nM HDAC11) and Lysine Derivative 3 (10 μM 3 and 60 nM HDAC11) and Compared to IC₅₀ Values found in the Literature

compound	compound class	IC ₅₀ (nM) peptide derivative 1	IC ₅₀ (nM) lysine derivative 3	IC ₅₀ (nM) reported
dacinostat (NVP-LAQ824)	hydroxamic acids	9400 ± 1200	3930 ± 80	5.6 ⁹³
elevenostat (JB3-22)	hydroxamic acids	17 700 ± 2700	5810 ± 470	235 ²⁵
fimepinostat (CUDC-907)	hydroxamic acids	23 ± 3	16 ± 7	5.4 ⁸⁷
mocetinostat (MGCD0103)	benzamidines	>40 000	>40 000	590, ⁹⁴ 195 ⁹⁵
nexturastat A	hydroxamic acids	>40 000	8330 ± 1780	
pracinostat (SB939)	hydroxamic acids	34 800 ± 10 800	28 000 ± 360	93 ⁹⁶
quisinostat (JNJ-26481585)	hydroxamic acids	3270 ± 280	1770 ± 270	0.37 ⁹⁵
ricolinostat (ACY1215)	hydroxamic acids	12 300 ± 1700	5380 ± 360	>10 000 ^{97,98}
romidepsin (FK228)	cyclic peptides	2700 ± 60	4810 ± 40	0.3; ⁸⁵ >10 000 ⁸⁶
trapoxin A	cyclic peptides	10 ± 1.4	78 ± 2	170 ²¹
trichostatin	hydroxamic acids	22 000 ± 6800	10 300 ± 1900	14, ⁸³ 17, ⁸⁴ 25; ⁹⁹ 31; ¹⁰⁰ 15; ¹⁰¹ 32 000 ²¹
valproate	aliphatic acids	>40 000	>40 000	

fold differences. These differences are smaller if the respective K_i -values are calculated because of the much better K_M value of substrate 1 (Figure 4, Table S3). Additionally, differences in inhibition constants depending on the chemical nature of the used substrate are known in the field of sirtuin research⁸⁸ and for HDAC8. Sippl et al. were able to demonstrate that IC₅₀ values can differ up to 10-fold, depending on the used substrate.⁸⁹

In summary, we developed an efficient and HDAC11-selective substrate enabling high-throughput screening of inhibitor libraries yielding reduced false-positive hits.

MATERIALS AND METHODS

Chemicals. All chemicals were purchased from Sigma (Saint Louis) if not denoted otherwise. Trifluoroacetic acid (TFA) was obtained from Roth (Karlsruhe, Germany). Peptidic substrate 1 is commercially available from JPT Peptide Technologies (Berlin, Germany) and lysine derivative 3 was purchased from Bachem (Bubendorf, Switzerland; #4060676).

The synthesis of all peptidic substrates is described.^{20,81} HDAC inhibitors were purchased from Selleckchem and Cayman Chemical.

HDAC11 Expression and Purification. Full-length human HDAC11 was expressed and purified as described previously.²⁰ Briefly, HDAC11 was expressed using HEK-293/T17 cells following transient transfection mediated by linear polyethylene imine (PEI; Polysciences Inc., Warrington, PA). Three days after transfection, cells were harvested by centrifugation at 500g for 10 min and suspended in a lysis buffer (50 mM Tris, 150 mM NaCl, 10 mM KCl, 2 mM MgCl₂, 10% glycerol, pH 8) supplemented with benzonase (2

U/mL; Merck, Darmstadt, Germany) and a cocktail of protease inhibitors (Roche, Basel, Switzerland). Cell lysis was enhanced by the addition of Igepal-630 (final concentration 0.2%), followed by incubation for 30 min at 4 °C. The cell lysate was cleared by centrifugation at 40 000g for 30 min at 4 °C, and the supernatant was loaded on a Strep-Tactin column (IBA, Gottingen, Germany) previously equilibrated in the lysis buffer. The column was first washed with the lysis buffer supplemented with 2 mM ATP and 10 mM MgSO₄, followed by the second wash with the elution buffer (50 mM 4-(2-hydroxyethyl)-1-piperazineethanesulfonic acid (HEPES), 100 mM NaCl, 50 mM KCl, 10% glycerol, pH 7.5). Fusion proteins were eluted with the elution buffer supplemented with 3 mM desthiobiotin. Eluted proteins were concentrated to 2 mg/mL and flash-frozen in liquid nitrogen.

Continuous Fluorescence Assay. The assay was carried out as described previously with a slight modification.⁸¹ The fluorescence measurements were performed using a fluorescence spectrophotometer CLARIOstar (BMG Labtech GmbH, Ortenberg, Germany) at $\lambda_{ex} = 310$ nm and $\lambda_{em} = 405$ nm. The reaction mixture consisted of HDAC11, and the substrate in a reaction buffer comprising 50 mM HEPES, 140 mM NaCl, 10 mM KCl, 2 mg/mL BSA, and 1 mM TCEP, at pH 7.4 was adjusted with NaOH (total volume 50 μL). The reactions were incubated in black 384-well plates for 60 min at 37 °C, and the increase of relative fluorescence reflecting the product formation was monitored. This signal was converted into product concentration via calibration curves of free *N*-(2-aminobenzoyl)-11-aminoundecanoic acid, the product of the reaction. For the determination of kinetic constants, 20 nM HDAC11 and the substrate in the concentration range of 0.04–200 μM were used. The slope of the linear regression of product formation against time yielded the reaction velocity rates in μM/s. Kinetic constants (K_M and k_{cat}) were obtained by nonlinear regression analysis according to Michaelis–Menten.

HPLC-Based Assay. The determination of kinetic constants and IC₅₀ values of inhibitors was carried out in parallel to the continuous fluorescence assay by discontinuous assays analyzed by means of reversed-phase high-performance liquid chromatography (RP-HPLC). The reaction buffer, concentration of enzyme, substrates, and inhibitors were carried out as described above. The reaction was quenched by the addition of 0.5% acetic acid after 30 min of incubation and centrifuged at 2000g at 37 °C for 15 min to remove precipitated BSA and HDAC11. The reactions were analyzed by RP-HPLC (Shimadzu, HPLC Prominence system) with a Kinetex 2.6 μm XB-C18 100 Å column (100 × 3 mm; Phenomenex, Torrance, CA). The mobile phase A was 5% acetonitrile with 0.1% (v/v) TFA and the mobile phase B was 95% acetonitrile with 0.1% (v/v) TFA. The separation of the reaction product from the acylated substrate was performed in a 12-min linear gradient from 10 to 60% of eluent B at a flow rate of 0.6 mL/min. The product and substrate peaks were quantified using the absorbance at 365 nm (absorption of the 3-nitrotyrosyl moiety) to verify the results of the fluorescence assay.

Discontinuous Fluorescence-Based Assay using Boc-Lys(TFA)-7-amino-methylcoumarylamide Derivative. The assay was carried out using the commercially available substrate 3 as described previously with a slight modification.⁹⁰ Briefly, 60 nM HDAC11 was incubated with an inhibitor in the concentration range of 0.006–100 000 nM. The reaction was started with the 10 μM substrate and quenched after 30 min at

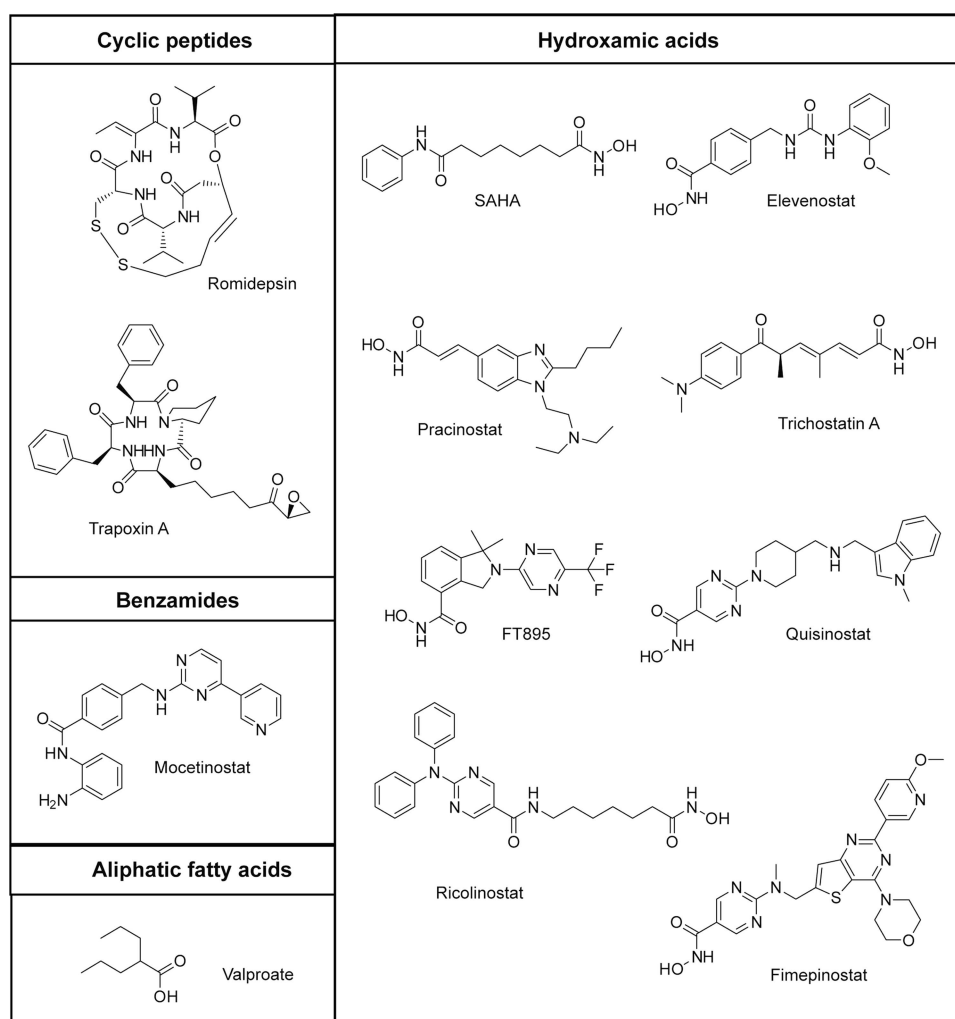


Figure 3. Structures of inhibitors used in this study.

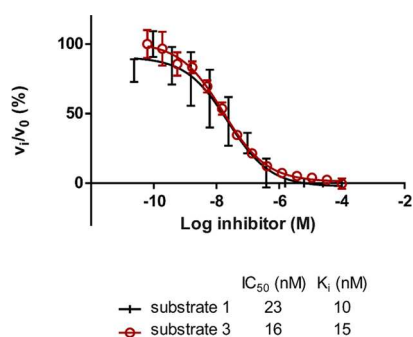


Figure 4. Determination of IC₅₀ values for CUDC-907 using substrates 1 and 3. K_i-values were calculated with the Cheng–Prusoff relationship.¹⁰² The K_M-value used for the calculation for compound 1 was 12 μM and for compound 3 200 μM.

37 °C by the addition of 20 μL of trypsin solution (2 mg/mL trypsin, 20 mM Tris–HCl, 150 mM NaCl, 1 mM EDTA; pH 7.4). Following the 60 min incubation at 37 °C, a fluorescence signal of released aminomethylcoumarin was quantified using a CLARIOstar fluorimeter (BMG Labtech GmbH, Ortenberg, Germany) with excitation/emission wavelengths set at 365/440 nm, respectively.

Determination of Inhibition Constants. For the determination of IC₅₀ values, 20 nM HDAC11 was

preincubated 10 min with an inhibitor in the concentration range of 0.006–100 000 nM, and the reaction was started by the addition of 15 μM of substrate 1. The data were fitted using GraphPad Prism software, and IC₅₀ values were calculated by nonlinear regression analysis. The inhibitor-free and enzyme-free controls were defined as 100 and 0% HDAC11 activity, respectively. All measurements were performed in duplicates.

Determination of Kinetic Constants. The assay was carried out as described previously with a slight modification.⁹¹ The fluorescence measurements were performed with an EnVision 2104 Multilabel reader (Perkin Elmer, Waltham). An excitation filter with λ = 330 ± 75 nm and an emission filter with λ = 430 ± 8 nm (percent of excitation light = 2%, detector gain = 50, flashes per A/D conversion = 1, and number of flashes = 30). The reaction mixture containing peptide 1 in various concentrations and assay buffer (20 mM phosphoric acid pH 7.4 adjusted with NaOH and 2 mg/mL BSA) was incubated at 25 °C in a 96-well plate for at least 5 min. The reaction was started with the addition of HDAC11 to a final concentration of 30 nM and a total volume of 100 μL per well. For the measurements in the 384-well plate and the 1536-well plate, the reaction mixture (composition like above) was incubated for at least 5 min in a clear 96-well plate. The reaction was started with the addition of HDAC11, and the reaction mixture with the enzyme was transferred to the

-appropriate well plate (384-well plate with 20 μL per well and 1536-well plate with 9 μL per well). The increase of relative fluorescence intensity reflecting product formation was monitored and the signal was converted via calibration lines of free *N*-(2-aminobenzoyl)-11-aminoundecanoic acid, the fluorescent product of the reaction. For the determination of kinetic constants, 30 nM HDAC11 and the substrate in the concentration range of 0.04–70 μM were used. The initial slope of the linear regression of product formation against time yielded the reaction velocity rates in $\mu\text{M}/\text{s}$. Kinetic constants (K_{M} and k_{cat}) were obtained by nonlinear regression according to Michaelis–Menten.

Z' Factor Determination. The Z'-factor is a dimensionless statistical parameter for high-throughput screening assays.⁹² The Z'-factor was calculated from the mean of the initial slope from the change of the fluorescence intensity over time with 15 μM peptide 1 and 30 nM HDAC11 (mean (100%)). The negative control was determined in the same way without enzyme (mean (0%)). The standard deviation (SD) was calculated from 3 technical replicates (96-well plate), 6 technical replicates (384-well plate), and 8 replicates (1536-well plate). The fluorescence intensity was measured with an EnVision Multilabel reader as described above. The Z'-factor was determined with the following equation.

$$Z' = 1 - \frac{3\text{SD}(100\%) + 3\text{SD}(0\%)}{|\text{mean}(100\%) - \text{mean}(0\%)|}$$

■ ASSOCIATED CONTENT

● Supporting Information

The Supporting Information is available free of charge on the ACS Publications website at DOI: 10.1021/acsomega.9b02808.

Activity of selected inhibitors against HDAC6; calculated Z' factors and the signal-to-noise ratio of HDAC11 and compound 1; K_{i} values for listed inhibitors; the influence of BSA concentration in the assay buffer on inhibitor potency; comparison of product formation of compound 1 between the multilabel plate reader and HPLC; dose–response curves for inhibitor measurements (PDF)

■ AUTHOR INFORMATION

Corresponding Authors

*E-mail: cyril.barinka@ibt.cas.cz. Tel.: +420-325-873-777 (C.B.).

*E-mail: mike.schutkowski@biochemtech.uni-halle.de. Tel.: +49-345-5524-828 (M.S.).

ORCID

Zora Nováková: 0000-0001-9804-6346

Wolfgang Sippl: 0000-0002-5985-9261

Cyril Barinka: 0000-0003-2751-3060

Mike Schutkowski: 0000-0003-0919-7076

Present Address

[†]Laboratory of Cell Motility, Institute of Molecular Genetics of the ASCR, v. v. i., Vídeňská 1083, Prague (G.A.).

Funding

This work was supported by grants from Deutsche Forschungsgemeinschaft (INST 271/336-1 FUGG) to M.S.Z, the Czech Science Foundation (15-19640S), the CAS (RVO: 86652036), and the project “BIOCEV” (CZ.1.05/

1.1.00/02.0109) from the ERDF. We acknowledge the financial support within the funding program Open Access Publishing by the German Research Foundation (DFG).

Notes

The authors declare no competing financial interest.

■ ACKNOWLEDGMENTS

We are grateful to Ilona Kunze for technical support. We thank Prof. Dr Thomas Kieffhaber at the Martin-Luther University Halle-Wittenberg for giving us access to the single quadrupole LC–MS analyses and the MS-service facility of the Martin-Luther University Halle-Wittenberg for technical assistance during the triple-quadrupole LC–MS experiments.

■ ABBREVIATIONS

RP-HPLC, reverse-phase high-performance liquid chromatography; Abz, 2-aminobenzoyl; TSA, Trichostatin A

■ REFERENCES

- (1) Chen, Y.; Sprung, R.; Tang, Y.; Ball, H.; Sangras, B.; Kim, S. C.; Falck, J. R.; Peng, J.; Gu, W.; Zhao, Y. Lysine propionylation and butyrylation are novel post-translational modifications in histones. *Mol. Cell. Proteomics* **2007**, *6*, 812–819.
- (2) Nishida, Y.; Rardin, M. J.; Carrico, C.; He, W.; Sahu, A. K.; Gut, P.; Najjar, R.; Fitch, M.; Hellerstein, M.; Gibson, B. W.; Verdin, E. SIRT5 Regulates both Cytosolic and Mitochondrial Protein Malonylation with Glycolysis as a Major Target. *Mol. Cell* **2015**, *59*, 321–332.
- (3) Peng, C.; Lu, Z.; Xie, Z.; Cheng, Z.; Chen, Y.; Tan, M.; Luo, H.; Zhang, Y.; He, W.; Yang, K.; Zwaans, B. M. M.; Tishkoff, D.; Ho, L.; Lombard, D.; He, T.-C.; Dai, J.; Verdin, E.; Ye, Y.; Zhao, Y. The first identification of lysine malonylation substrates and its regulatory enzyme. *Mol. Cell. Proteomics* **2011**, *10*, No. M111.012658.
- (4) Zhang, Z.; Tan, M.; Xie, Z.; Dai, L.; Chen, Y.; Zhao, Y. Identification of lysine succinylation as a new post-translational modification. *Nat. Chem. Biol.* **2011**, *7*, 58–63.
- (5) Tan, M.; Peng, C.; Anderson, K. A.; Chhoy, P.; Xie, Z.; Dai, L.; Park, J.; Chen, Y.; Huang, H.; Zhang, Y.; Ro, J.; Wagner, G. R.; Green, M. F.; Madsen, A. S.; Schmiesing, J.; Peterson, B. S.; Xu, G.; Ilkayeva, O. R.; Muehlbauer, M. J.; Brault, T.; Mühlhausen, C.; Backos, D. S.; Olsen, C. A.; McGuire, P. J.; Pletcher, S. D.; Lombard, D. B.; Hirsche, M. D.; Zhao, Y. Lysine glutarylation is a protein posttranslational modification regulated by SIRT5. *Cell Metabol.* **2014**, *19*, 605–617.
- (6) Tan, M.; Luo, H.; Lee, S.; Jin, F.; Yang, J. S.; Montellier, E.; Buchou, T.; Cheng, Z.; Rousseaux, S.; Rajagopal, N.; Lu, Z.; Ye, Z.; Zhu, Q.; Wysocka, J.; Ye, Y.; Khochbin, S.; Ren, B.; Zhao, Y. Identification of 67 histone marks and histone lysine crotonylation as a new type of histone modification. *Cell* **2011**, *146*, 1016–1028.
- (7) Xie, Z.; Zhang, D.; Chung, D.; Tang, Z.; Huang, H.; Dai, L.; Qi, S.; Li, J.; Colak, G.; Chen, Y.; Xia, C.; Peng, C.; Ruan, H.; Kirkey, M.; Wang, D.; Jensen, L. M.; Kwon, O. K.; Lee, S.; Pletcher, S. D.; Tan, M.; Lombard, D. B.; White, K. P.; Zhao, H.; Li, J.; Roeder, R. G.; Yang, X.; Zhao, Y. Metabolic Regulation of Gene Expression by Histone Lysine β -Hydroxybutyrylation. *Mol. Cell* **2016**, *62*, 194–206.
- (8) Cui, Y.; Li, X.; Lin, J.; Hao, Q.; Li, X. D. Histone Ketoamide Adduction by 4-Oxo-2-nonenal Is a Reversible Posttranslational Modification Regulated by Sirt2. *ACS Chem. Biol.* **2017**, *12*, 47–51.
- (9) Galligan, J. J.; Rose, K. L.; Beavers, W. N.; Hill, S.; Tallman, K. A.; Tansey, W. P.; Marnett, L. J. Stable Histone Adduction by 4-Oxo-2-nonenal: A Potential Link between Oxidative Stress and Epigenetics. *J. Am. Chem. Soc.* **2014**, *136*, 11864–11866.
- (10) Dai, L.; Peng, C.; Montellier, E.; Lu, Z.; Chen, Y.; Ishii, H.; Debernardi, A.; Buchou, T.; Rousseaux, S.; Jin, F.; Sabari, B. R.; Deng, Z.; Allis, C. D.; Ren, B.; Khochbin, S.; Zhao, Y. Lysine 2-hydroxyisobutyrylation is a widely distributed active histone mark. *Nat. Chem. Biol.* **2014**, *10*, 365–370.

- (11) Anderson, K. A.; Huynh, F. K.; Fisher-Wellman, K.; Stuart, J. D.; Peterson, B. S.; Douros, J. D.; Wagner, G. R.; Thompson, J. W.; Madsen, A. S.; Green, M. F.; Sivley, R. M.; Ilkayeva, O. R.; Stevens, R. D.; Backos, D. S.; Capra, J. A.; Olsen, C. A.; Campbell, J. E.; Muoio, D. M.; Grimsrud, P. A.; Hirschey, M. D. SIRT4 Is a Lysine Deacetylase that Controls Leucine Metabolism and Insulin Secretion. *Cell Metabol.* **2017**, *25*, 838–855.
- (12) Wagner, G. R.; Bhatt, D. P.; O'Connell, T. M.; Thompson, J. W.; Dubois, L. G.; Backos, D. S.; Yang, H.; Mitchell, G. A.; Ilkayeva, O. R.; Stevens, R. D.; Grimsrud, P. A.; Hirschey, M. D. A Class of Reactive Acyl-CoA Species Reveals the Non-enzymatic Origins of Protein Acylation. *Cell Metabol.* **2017**, *25*, 823–837.
- (13) Moellering, R. E.; Cravatt, B. F. Functional lysine modification by an intrinsically reactive primary glycolytic metabolite. *Science* **2013**, *341*, 549–553.
- (14) Huang, H.; Zhang, Di.; Wang, Y.; Perez-Neut, M.; Han, Z.; Zheng, Y. G.; Hao, Q.; Zhao, Y. Lysine benzylation is a histone mark regulated by SIRT2. *Nat. Commun.* **2018**, *9*, No. 3374.
- (15) Stevenson, F. T.; Bursten, S. L.; Locksley, R. M.; Lovett, D. H. Myristyl acylation of the tumor necrosis factor alpha precursor on specific lysine residues. *J. Exp. Med.* **1992**, *176*, 1053–1062.
- (16) Liu, W.; Zhou, Y.; Peng, T.; Zhou, P.; Ding, X.; Li, Z.; Zhong, H.; Xu, Y.; Chen, S.; Hang, H. C.; Shao, F. Ne-fatty acylation of multiple membrane-associated proteins by Shigella IcsB effector to modulate host function. *Nat. Microbiol.* **2018**, *3*, 996–1009.
- (17) Choudhary, C.; Weinert, B. T.; Nishida, Y.; Verdin, E.; Mann, M. The growing landscape of lysine acetylation links metabolism and cell signalling. *Nat. Rev. Mol. Cell Biol.* **2014**, *15*, 536–550.
- (18) Sabari, B. R.; Zhang, Di.; Allis, C. D.; Zhao, Y. Metabolic regulation of gene expression through histone acylations. *Nat. Rev. Mol. Cell Biol.* **2017**, *18*, 90–101.
- (19) Seto, E.; Yoshida, M. Erasers of histone acetylation: the histone deacetylase enzymes. *Cold Spring Harbor Perspect. Biol.* **2014**, *6*, No. a018713.
- (20) Kutil, Z.; Novakova, Z.; Meleshin, M.; Mikesova, J.; Schutkowski, M.; Barinka, C. Histone Deacetylase 11 Is a Fatty-Acid Deacylase. *ACS Chem. Biol.* **2018**, *13*, 685–693.
- (21) Moreno-Yruela, C.; Galleano, I.; Madsen, A. S.; Olsen, C. A. Histone Deacetylase 11 Is an ϵ -N-Myristoyllysine Hydrolase. *Cell Chem. Biol.* **2018**, *25*, 849–856.
- (22) Cao, J.; Sun, L.; Aramsangtienchai, P.; Spiegelman, N. A.; Zhang, X.; Huang, W.; Seto, E.; Lin, H. HDAC11 regulates type I interferon signaling through defatty-acylation of SHMT2. *Proc. Natl. Acad. Sci. U.S.A.* **2019**, *116*, 5487–5492.
- (23) McCullough, C. E.; Marmorstein, R. Molecular Basis for Histone Acetyltransferase Regulation by Binding Partners, Associated Domains, and Autoacetylation. *ACS Chem. Biol.* **2016**, *11*, 632–642.
- (24) Sun, L.; Marin de Evsikova, C.; Bian, K.; Achille, A.; Telles, E.; Pei, H.; Seto, E. Programming and Regulation of Metabolic Homeostasis by HDAC11. *EBioMedicine* **2018**, *33*, 157–168.
- (25) Huang, J.; Wang, L.; Dahiya, S.; Beier, U. H.; Han, R.; Samanta, A.; Bergman, J.; Sotomayor, E. M.; Seto, E.; Kozikowski, A. P.; Hancock, W. W. Histone/protein deacetylase 11 targeting promotes Foxp3+ Treg function. *Sci. Rep.* **2017**, *7*, No. 8626.
- (26) Martin, M. W.; Lee, J. Y.; Lancia, D. R.; Ng, P. Y.; Han, B.; Thomason, J. R.; Lynes, M. S.; Marshall, C. G.; Conti, C.; Collis, A.; Morales, M. A.; Doshi, K.; Rudnitskaya, A.; Yao, L.; Zheng, X. Discovery of novel N-hydroxy-2-arylisoindoline-4-carboxamides as potent and selective inhibitors of HDAC11. *Bioorg. Med. Chem. Lett.* **2018**, *28*, 2143–2147.
- (27) in Son, S.; Cao, J.; Zhu, C.-L.; Miller, S. P.; Lin, H. Activity-Guided Design of HDAC11-Specific Inhibitors. *ACS Chem. Biol.* **2019**, No. 292.
- (28) Fan, Y.; Scriba, G. K. E. Electrophoretically mediated microanalysis assay for sirtuin enzymes. *Electrophoresis* **2010**, *31*, 3874–3880.
- (29) Ohla, S.; Beyreiss, R.; Scriba, G. K. E.; Fan, Y.; Belder, D. An integrated on-chip sirtuin assay. *Electrophoresis* **2010**, *31*, 3263–3267.
- (30) Blackwell, L.; Norris, J.; Suto, C. M.; Janzen, W. P. The use of diversity profiling to characterize chemical modulators of the histone deacetylases. *Life Sci.* **2008**, *82*, 1050–1058.
- (31) Liu, Y.; Gerber, R.; Wu, J.; Tsuruda, T.; McCarter, J. D. High-throughput assays for sirtuin enzymes: a microfluidic mobility shift assay and a bioluminescence assay. *Anal. Biochem.* **2008**, *378*, 53–59.
- (32) Khan, A. N.; Lewis, P. N. Unstructured conformations are a substrate requirement for the Sir2 family of NAD-dependent protein deacetylases. *J. Biol. Chem.* **2005**, *280*, 36073–36078.
- (33) Du, J.; Zhou, Y.; Su, X.; Yu, J. J.; Khan, S.; Jiang, H.; Kim, J.; Woo, J.; Kim, J. H.; Choi, B. H.; He, B.; Chen, W.; Zhang, S.; Cerione, R. A.; Auwerx, J.; Hao, Q.; Lin, H. Sirt5 is a NAD-dependent protein lysine demalonylase and desuccinylase. *Science* **2011**, *334*, 806–809.
- (34) Marcotte, P. A.; Richardson, P. L.; Richardson, P. R.; Guo, J.; Barrett, L. W.; Xu, N.; Gunasekera, A.; Glaser, K. B. Fluorescence assay of SIRT protein deacetylases using an acetylated peptide substrate and a secondary trypsin reaction. *Anal. Biochem.* **2004**, *332*, 90–99.
- (35) Tanner, K. G.; Landry, J.; Sternglanz, R.; Denu, J. M. Silent information regulator 2 family of NAD-dependent histone/protein deacetylases generates a unique product, 1-O-acetyl-ADP-ribose. *Proc. Natl. Acad. Sci. U.S.A.* **2000**, *97*, 14178–14182.
- (36) Jackson, M. D.; Denu, J. M. Structural identification of 2'- and 3'-O-acetyl-ADP-ribose as novel metabolites derived from the Sir2 family of beta-NAD+-dependent histone/protein deacetylases. *J. Biol. Chem.* **2002**, *277*, 18535–18544.
- (37) Khan, A. N.; Lewis, P. N. Use of substrate analogs and mutagenesis to study substrate binding and catalysis in the Sir2 family of NAD-dependent protein deacetylases. *J. Biol. Chem.* **2006**, *281*, 11702–11711.
- (38) Borra, M. T.; Denu, J. M. Quantitative Assays for Characterization of the Sir2 Family of NAD+-Dependent Deacetylases. In *Chromatin and Chromatin Remodeling Enzymes*; Allis, C. D., Ed.; Elsevier: Amsterdam, 2004; pp 171–187.
- (39) McDonagh, T.; Hixon, J.; DiStefano, P. S.; Curtis, R.; Napper, A. D. Microplate filtration assay for nicotinamide release from NAD using a boronic acid resin. *Methods* **2005**, *36*, 346–350.
- (40) Hoffmann, K.; Heltweg, B.; Jung, M. Improvement and validation of the fluorescence-based histone deacetylase assay using an internal standard. *Arch. Pharm.* **2001**, *334*, 248–252.
- (41) Rye, P. T.; Frick, L. E.; Ozbal, C. C.; Lamarr, W. A. Advances in label-free screening approaches for studying sirtuin-mediated deacetylation. *J. Biomol. Screening* **2011**, *16*, 1217–1226.
- (42) Fischer, F.; Gertz, M.; Suenkel, B.; Lakshminarasimhan, M.; Schutkowski, M.; Steegborn, C. Sirt5 deacylation activities show differential sensitivities to nicotinamide inhibition. *PLoS One* **2012**, *7*, No. e45098.
- (43) Gurard-Levin, Z. A.; Kilian, K. A.; Kim, J.; Bähr, K.; Mrksich, M. Peptide arrays identify isoform-selective substrates for profiling endogenous lysine deacetylase activity. *ACS Chem. Biol.* **2010**, *5*, 863–873.
- (44) Gurard-Levin, Z. A.; Kim, J.; Mrksich, M. Combining mass spectrometry and peptide arrays to profile the specificities of histone deacetylases. *ChemBioChem* **2009**, *10*, 2159–2161.
- (45) Kuo, H.-Y.; DeLuca, T. A.; Miller, W. M.; Mrksich, M. Profiling deacetylase activities in cell lysates with peptide arrays and SAMDI mass spectrometry. *Anal. Chem.* **2013**, *85*, 10635–10642.
- (46) Castaneda, C. A.; Lopez, J. E.; Joseph, C. G.; Scholle, M. D.; Mrksich, M.; Fierke, C. A. Active Site Metal Identity Alters Histone Deacetylase 8 Substrate Selectivity: A Potential Novel Regulatory Mechanism. *Biochemistry* **2017**, *56*, 5663–5670.
- (47) Kutil, Z.; Skultetyova, L.; Rauh, D.; Meleshin, M.; Snajdr, I.; Novakova, Z.; Mikesova, J.; Pavlicek, J.; Hadzima, M.; Baranova, P.; Havlinova, B.; Majer, P.; Schutkowski, M.; Barinka, C. The unraveling of substrate specificity of histone deacetylase 6 domains using acetylome peptide microarrays and peptide libraries. *FASEB J.* **2019**, *33*, 4035–4045.

- (48) Rauh, D.; Fischer, F.; Gertz, M.; Lakshminarasimhan, M.; Bergbrede, T.; Aladini, F.; Kambach, C.; Becker, C. F. W.; Zerweck, J.; Schutkowski, M.; Steegborn, C. An acetylated peptide microarray reveals specificities and deacetylation substrates for all human sirtuin isoforms. *Nat. Commun.* **2013**, *4*, No. 2327.
- (49) Robers, M. B.; Loh, C.; Carlson, C. B.; Yang, H.; Frey, E. A.; Hermanson, S. B.; Bi, K. Measurement of the cellular deacetylase activity of SIRT1 on p53 via LanthaScreen technology. *Mol. Biosyst.* **2011**, *7*, 59–66.
- (50) Dudek, J. M.; Horton, R. A. TR-FRET biochemical assays for detecting posttranslational modifications of p53. *J. Biomol. Screening* **2010**, *15*, 569–575.
- (51) Machleidt, T.; Robers, M. B.; Hermanson, S. B.; Dudek, J. M.; Bi, K. TR-FRET cellular assays for interrogating posttranslational modifications of histone H3. *J. Biomol. Screening* **2011**, *16*, 1236–1246.
- (52) Degorce, F.; Card, A.; Soh, S.; Trinquet, E.; Knapik, G. P.; Xie, B. HTRF: A technology tailored for drug discovery - a review of theoretical aspects and recent applications. *Curr. Chem. Genomics* **2009**, *3*, 22–32.
- (53) Inoue, A.; Fujimoto, D. Enzymatic deacetylation of histone. *Biochem. Biophys. Res. Commun.* **1969**, *36*, 146–150.
- (54) Kölle, D.; Brosch, G.; Lechner, T.; Lusser, A.; Loidl, P. Biochemical methods for analysis of histone deacetylases. *Methods* **1998**, *15*, 323–331.
- (55) Taunton, J.; Hassig, C. A.; Schreiber, S. L. A mammalian histone deacetylase related to the yeast transcriptional regulator Rpd3p. *Science* **1996**, *272*, 408–411.
- (56) Milne, J. C.; Lambert, P. D.; Schenk, S.; Carney, D. P.; Smith, J. J.; Gagne, D. J.; Jin, L.; Boss, O.; Perni, R. B.; Vu, C. B.; Bemis, J. E.; Xie, R.; Disch, J. S.; Ng, P. Y.; Nunes, J. J.; Lynch, A. V.; Yang, H.; Galonek, H.; Israelian, K.; Choy, W.; Iffland, A.; Lavu, S.; Medvedik, O.; Sinclair, D. A.; Olefsky, J. M.; Jirousek, M. R.; Elliott, P. J.; Westphal, C. H. Small molecule activators of SIRT1 as therapeutics for the treatment of type 2 diabetes. *Nature* **2007**, *450*, 712–716.
- (57) Wolfson, N. A.; Pitcairn, C. A.; Sullivan, E. D.; Joseph, C. G.; Fierke, C. A. An enzyme-coupled assay measuring acetate production for profiling histone deacetylase specificity. *Anal. Biochem.* **2014**, *456*, 61–69.
- (58) Fatkins, D. G.; Monnot, A. D.; Zheng, W. Nepsilon-thioacetyllysine: a multi-facet functional probe for enzymatic protein lysine Nepsilon-deacetylation. *Bioorg. Med. Chem. Lett.* **2006**, *16*, 3651–3656.
- (59) Heltweg, B.; Dequiedt, F.; Verdin, E.; Jung, M. Nonisotopic substrate for assaying both human zinc and NAD⁺-dependent histone deacetylases. *Anal. Biochem.* **2003**, *319*, 42–48.
- (60) Toro, T. B.; Watt, T. J. KDAC8 substrate specificity quantified by a biologically relevant, label-free deacetylation assay. Protein science: a publication of the Protein. *Society* **2015**, *24*, 2020–2032.
- (61) Baba, R.; Hori, Y.; Mizukami, S.; Kikuchi, K. Development of a fluorogenic probe with a transesterification switch for detection of histone deacetylase activity. *J. Am. Chem. Soc.* **2012**, *134*, 14310–14313.
- (62) Baba, R.; Hori, Y.; Kikuchi, K. Intramolecular long-distance nucleophilic reactions as a rapid fluorogenic switch applicable to the detection of enzymatic activity. *Chem. - Eur. J.* **2015**, *21*, 4695–4702.
- (63) Rooker, D. R.; Klyubka, Y.; Gautam, R.; Tomat, E.; Buccella, D. Peptide-Based Fluorescent Probes for Deacetylase and Decrotonylase Activity: Toward a General Platform for Real-Time Detection of Lysine Deacetylation. *ChemBioChem* **2018**, *19*, 496–504.
- (64) Liu, X.; Xiang, M.; Tong, Z.; Luo, F.; Chen, W.; Liu, F.; Wang, F.; Yu, R.-Q.; Jiang, J.-H. Activatable Fluorescence Probe via Self-Immolative Intramolecular Cyclization for Histone Deacetylase Imaging in Live Cells and Tissues. *Anal. Chem.* **2018**, *90*, 5534–5539.
- (65) Xie, Y.; Ge, J.; Lei, H.; Peng, B.; Zhang, H.; Wang, D.; Pan, S.; Chen, G.; Chen, L.; Wang, Y.; Hao, Q.; Yao, S. Q.; Sun, H. Fluorescent Probes for Single-Step Detection and Proteomic Profiling of Histone Deacetylases. *J. Am. Chem. Soc.* **2016**, *138*, 15596–15604.
- (66) Yu, C.; Wu, Y.; Zeng, F.; Li, X.; Shi, J.; Wu, S. Hyperbranched polyester-based fluorescent probe for histone deacetylase via aggregation-induced emission. *Biomacromolecules* **2013**, *14*, 4507–4514.
- (67) Dhara, K.; Hori, Y.; Baba, R.; Kikuchi, K. A fluorescent probe for detection of histone deacetylase activity based on aggregation-induced emission. *Chem. Commun.* **2012**, *48*, 11534–11536.
- (68) Minoshima, M.; Matsumoto, T.; Kikuchi, K. Development of a fluorogenic probe based on a DNA staining dye for continuous monitoring of the histone deacetylase reaction. *Anal. Chem.* **2014**, *86*, 7925–7930.
- (69) Han, Y.; Li, H.; Hu, Y.; Li, P.; Wang, H.; Nie, Z.; Yao, S. Time-resolved luminescence biosensor for continuous activity detection of protein acetylation-related enzymes based on DNA-sensitized terbium(III) probes. *Anal. Chem.* **2015**, *87*, 9179–9185.
- (70) Halley, F.; Reinshagen, J.; Ellinger, B.; Wolf, M.; Niles, A. L.; Evans, N. J.; Kirkland, T. A.; Wagner, J. M.; Jung, M.; Gribbon, P.; Gul, S. A bioluminogenic HDAC activity assay: validation and screening. *J. Biomol. Screening* **2011**, *16*, 1227–1235.
- (71) Dose, A.; Jost, J. O.; Spieß, A. C.; Henklein, P.; Beyermann, M.; Schwarzer, D. Facile synthesis of colorimetric histone deacetylase substrates. *Chem. Commun.* **2012**, *48*, 9525–9527.
- (72) Riester, D.; Hildmann, C.; Grünewald, S.; Beckers, T.; Schwienhorst, A. Factors affecting the substrate specificity of histone deacetylases. *Biochem. Biophys. Res. Commun.* **2007**, *357*, 439–445.
- (73) Wegener, D.; Hildmann, C.; Riester, D.; Schober, A.; Meyer-Almes, F.-J.; Deubzer, H. E.; Oehme, I.; Witt, O.; Lang, S.; Jaensch, M.; Makarov, V.; Lange, C.; Busse, B.; Schwienhorst, A. Identification of novel small-molecule histone deacetylase inhibitors by medium-throughput screening using a fluorogenic assay. *Biochem. J.* **2008**, *413*, 143–150.
- (74) Ciossek, T.; Julius, H.; Wieland, H.; Maier, T.; Beckers, T. A homogeneous cellular histone deacetylase assay suitable for compound profiling and robotic screening. *Anal. Biochem.* **2008**, *372*, 72–81.
- (75) Wegener, D.; Hildmann, C.; Riester, D.; Schwienhorst, A. Improved fluorogenic histone deacetylase assay for high-throughput-screening applications. *Anal. Biochem.* **2003**, *321*, 202–208.
- (76) Wegener, D.; Wirsching, F.; Riester, D.; Schwienhorst, A. A fluorogenic histone deacetylase assay well suited for high-throughput activity screening. *Chem. Biol.* **2003**, *10*, 61–68.
- (77) Bradner, J. E.; West, N.; Grachan, M. L.; Greenberg, E. F.; Haggarty, S. J.; Warnow, T.; Mazitschek, R. Chemical phylogenetics of histone deacetylases. *Nat. Chem. Biol.* **2010**, *6*, 238–243.
- (78) Lahm, A.; Paolini, C.; Pallaoro, M.; Nardi, M. C.; Jones, P.; Neddermann, P.; Sambucini, S.; Bottomley, M. J.; Lo Surdo, P.; Carfi, A.; Koch, U.; Francesco, R.; de; Steinkühler, C.; Gallinari, P. Unraveling the hidden catalytic activity of vertebrate class IIa histone deacetylases. *Proc. Natl. Acad. Sci. U.S.A.* **2007**, *104*, 17335–17340.
- (79) Toro, T. B.; Bryant, J. R.; Watt, T. J. Lysine Deacetylases Exhibit Distinct Changes in Activity Profiles Due to Fluorophore Conjugation of Substrates. *Biochemistry* **2017**, *56*, 4549–4558.
- (80) Kawaguchi, M.; Ikegawa, S.; Ieda, N.; Nakagawa, H. A Fluorescent Probe for Imaging Sirtuin Activity in Living Cells, Based on One-Step Cleavage of the Dabcyl Quencher. *ChemBioChem* **2016**, *17*, 1961–1967.
- (81) Schuster, S.; Roessler, C.; Meleshin, M.; Zimmermann, P.; Simic, Z.; Kambach, C.; Schiene-Fischer, C.; Steegborn, C.; Hottiger, M. O.; Schutkowski, M. A continuous sirtuin activity assay without any coupling to enzymatic or chemical reactions. *Sci. Rep.* **2016**, *6*, No. 22643.
- (82) Jiang, H.; Khan, S.; Wang, Y.; Charron, G.; He, B.; Sebastian, C.; Du, J.; Kim, R.; Ge, E.; Mostoslavsky, R.; Hang, H. C.; Hao, Q.; Lin, H. SIRT6 regulates TNF- α secretion through hydrolysis of long-chain fatty acyl lysine. *Nature* **2013**, *496*, 110–113.
- (83) Neelapuru, R.; Holzle, D. L.; Velaparthi, S.; Bai, H.; Brunsteiner, M.; Blond, S. Y.; Petukhov, P. A. Design, synthesis, docking, and biological evaluation of novel diazide-containing

isoxazole- and pyrazole-based histone deacetylase probes. *J. Med. Chem.* **2011**, *54*, 4350–4364.

(84) Yu, C.-W.; Chang, P.-T.; Hsin, L.-W.; Chern, J.-W. Quinazolin-4-one derivatives as selective histone deacetylase-6 inhibitors for the treatment of Alzheimer's disease. *J. Med. Chem.* **2013**, *56*, 6775–6791.

(85) Salvador, L. A.; Park, H.; Al-Awadhi, F. H.; Liu, Y.; Kim, B.; Zeller, S. L.; Chen, Q.-Y.; Hong, J.; Luesch, H. Modulation of Activity Profiles for Largazole-Based HDAC Inhibitors through Alteration of Prodrug Properties. *ACS Med. Chem. Lett.* **2014**, *5*, 905–910.

(86) Yao, Y.; Tu, Z.; Liao, C.; Wang, Z.; Li, S.; Yao, H.; Li, Z.; Jiang, S. Discovery of Novel Class I Histone Deacetylase Inhibitors with Promising in Vitro and in Vivo Antitumor Activities. *J. Med. Chem.* **2015**, *58*, 7672–7680.

(87) Chen, Y.; Wang, X.; Xiang, W.; He, L.; Tang, M.; Wang, F.; Wang, T.; Yang, Z.; Yi, Y.; Wang, H.; Niu, T.; Zheng, L.; Lei, L.; Li, X.; Song, H.; Chen, L. Development of Purine-Based Hydroxamic Acid Derivatives: Potent Histone Deacetylase Inhibitors with Marked in Vitro and in Vivo Antitumor Activities. *J. Med. Chem.* **2016**, *59*, 5488–5504.

(88) Spiegelman, N. A.; Price, I. R.; Jing, H.; Wang, M.; Yang, M.; Cao, J.; Hong, J. Y.; Zhang, X.; Aramsangtienchai, P.; Sathukhan, S.; Lin, H. Direct Comparison of SIRT2 Inhibitors: Potency, Specificity, Activity-Dependent Inhibition, and On-Target Anticancer Activities. *ChemMedChem* **2018**, *13*, 1890–1894.

(89) Kannan, S.; Melesina, J.; Hauser, A.-T.; Chakrabarti, A.; Heimburg, T.; Schmidtkunz, K.; Walter, A.; Marek, M.; Pierce, R. J.; Romier, C.; Jung, M.; Sippl, W. Discovery of inhibitors of *Schistosoma mansoni* HDAC8 by combining homology modeling, virtual screening, and in vitro validation. *J. Chem. Inf. Model.* **2014**, *54*, 3005–3019.

(90) Riester, D.; Wegener, D.; Hildmann, C.; Schwienhorst, A. Members of the histone deacetylase superfamily differ in substrate specificity towards small synthetic substrates. *Biochem. Biophys. Res. Commun.* **2004**, *324*, 1116–1123.

(91) Roessler, C.; Nowak, T.; Pannek, M.; Gertz, M.; Nguyen, G. T. T.; Scharfe, M.; Born, I.; Sippl, W.; Steegborn, C.; Schutkowski, M. Chemical probing of the human sirtuin 5 active site reveals its substrate acyl specificity and peptide-based inhibitors. *Angew. Chem., Int. Ed.* **2014**, *53*, 10728–10732.

(92) Zhang, J. H. A Simple Statistical Parameter for Use in Evaluation and Validation of High Throughput Screening Assays. *J. Biomol. Screening* **1999**, *4*, 67–73.

(93) Auzzas, L.; Larsson, A.; Matera, R.; Baraldi, A.; Deschênes-Simard, B.; Giannini, G.; Cabri, W.; Battistuzzi, G.; Gallo, G.; Ciacci, A.; Vesci, L.; Pisano, C.; Hanessian, S. Non-natural macrocyclic inhibitors of histone deacetylases: design, synthesis, and activity. *J. Med. Chem.* **2010**, *53*, 8387–8399.

(94) Zhou, N.; Moradei, O.; Raeppl, S.; Leit, S.; Frechette, S.; Gaudette, F.; Paquin, I.; Bernstein, N.; Bouchain, G.; Vaisburg, A.; Jin, Z.; Gillespie, J.; Wang, J.; Fournel, M.; Yan, P. T.; Trachy-Bourget, M.-C.; Kalita, A.; Lu, A.; Rahil, J.; MacLeod, A. R.; Li, Z.; Besterman, J. M.; Delorme, D. Discovery of N-(2-aminophenyl)-4-(4-pyridin-3-ylpyrimidin-2-ylamino)methylbenzamide (MGCD0103), an orally active histone deacetylase inhibitor. *J. Med. Chem.* **2008**, *51*, 4072–4075.

(95) Arts, J.; King, P.; Mariën, A.; Floren, W.; Beliën, A.; Janssen, L.; Pilatte, I.; Roux, B.; Decrane, L.; Gilissen, R.; Hickson, I.; Vreys, V.; Cox, E.; Bol, K.; Talloen, W.; Goris, I.; Andries, L.; Du Jardin, M.; Janicot, M.; Page, M.; van Emelen, K.; Angibaud, P. JNJ-26481585, a novel “second-generation” oral histone deacetylase inhibitor, shows broad-spectrum preclinical antitumoral activity. *Clin. Cancer Res.* **2009**, *15*, 6841–6851.

(96) Novotny-Diermayr, V.; Sangthongpitag, K.; Hu, C. Y.; Wu, X.; Sausgruber, N.; Yeo, P.; Greicius, G.; Pettersson, S.; Liang, A. L.; Loh, Y. K.; Bonday, Z.; Goh, K. C.; Hentze, H.; Hart, S.; Wang, H.; Ethirajulu, K.; Wood, J. M. SB939, a novel potent and orally active histone deacetylase inhibitor with high tumor exposure and efficacy in mouse models of colorectal cancer. *Mol. Cancer Ther.* **2010**, *9*, 642–652.

(97) Yang, Z.; Wang, T.; Wang, F.; Niu, T.; Liu, Z.; Chen, X.; Long, C.; Tang, M.; Cao, D.; Wang, X.; Xiang, W.; Yi, Y.; Ma, L.; You, J.; Chen, L. Discovery of Selective Histone Deacetylase 6 Inhibitors Using the Quinazoline as the Cap for the Treatment of Cancer. *J. Med. Chem.* **2016**, *59*, 1455–1470.

(98) Santo, L.; Hideshima, T.; Kung, A. L.; Tseng, J.-C.; Tamang, D.; Yang, M.; Jarpe, M.; van Duzer, J. H.; Mazitschek, R.; Ogier, W. C.; Cirstea, D.; Rodig, S.; Eda, H.; Scullen, T.; Canavese, M.; Bradner, J.; Anderson, K. C.; Jones, S. S.; Raje, N. Preclinical activity, pharmacodynamic, and pharmacokinetic properties of a selective HDAC6 inhibitor, ACY-1215, in combination with bortezomib in multiple myeloma. *Blood* **2012**, *119*, 2579–2589.

(99) Muthyala, R.; Shin, W. S.; Xie, J.; Sham, Y. Y. Discovery of 1-hydroxypyridine-2-thiones as selective histone deacetylase inhibitors and their potential application for treating leukemia. *Bioorg. Med. Chem. Lett.* **2015**, *25*, 4320–4324.

(100) Marek, L.; Hamacher, A.; Hansen, F. K.; Kuna, K.; Gohlke, H.; Kassack, M. U.; Kurz, T. Histone deacetylase (HDAC) inhibitors with a novel connecting unit linker region reveal a selectivity profile for HDAC4 and HDAC5 with improved activity against chemo-resistant cancer cells. *J. Med. Chem.* **2013**, *56*, 427–436.

(101) Cincinelli, R.; Musso, L.; Giannini, G.; Zuco, V.; Cesare, M.; de; Zunino, F.; Dallavalle, S. Influence of the adamantyl moiety on the activity of biphenylacrylohydroxamic acid-based HDAC inhibitors. *Eur. J. Med. Chem.* **2014**, *79*, 251–259.

(102) Yung-Chi, C.; Prusoff, W. H. Relationship between the inhibition constant (KI) and the concentration of inhibitor which causes 50 per cent inhibition (I50) of an enzymatic reaction. *Biochem. Pharm.* **1973**, *22*, 3099–3108.

3.2 One-Atom-Substitution Enables Direct and Continuous Monitoring of Histone Deacetylase Activity

Matthes Zessin, Zsófia Kutil, Marat Meleshin, Zora Nováková, Ehab Ghazy, Diana Kalbas, Martin Marek, Christophe Romier, Wolfgang Sippl, Cyril Bařinka und Mike Schutkowski

Biochemistry, 2019, 58, 4777-4789,
DOI: <https://doi.org/10.1021/acs.biochem.9b00786>

Abstract:

We developed a one-step direct assay for the determination of histone deacetylase (HDAC) activity by substituting the carbonyl oxygen of the acyl moiety with sulfur, resulting in thioacylated lysine side chains. This modification is recognized by class I HDACs with different efficiencies ranging from not accepted for HDAC1 to kinetic constants similar to that of the parent oxo substrate for HDAC8. Class II HDACs can hydrolyze thioacylated substrates with approximately 5–10-fold reduced k_{cat} values, which resembles the effect of thioamide substitution in metallo-protease substrates. Class IV HDAC11 accepts thiomristoyl modification less efficiently with an ~ 5 -fold reduced specificity constant. On the basis of the unique spectroscopic properties of thioamide bonds (strong absorption in spectral range of 260–280 nm and efficient fluorescence quenching), HDAC-mediated cleavage of thioamides could be followed by ultraviolet–visible and fluorescence spectroscopy in a continuous manner. The HDAC activity assay is compatible with microtiter plate-based screening formats up to 1536-well plates with Z' factors of >0.75 and signal-to-noise ratios of >50 . Using thioacylated lysine residues in p53-derived peptides, we optimized substrates for HDAC8 with a catalytic efficiency of $>250000 \text{ M}^{-1} \text{ s}^{-1}$, which are more than 100-fold more effective than most of the known substrates. We determined inhibition constants of several inhibitors for human HDACs using thioacylated peptidic substrates and found good correlation with the values from the literature. On the other hand, we could introduce N-methylated, N-acylated lysine residues as inhibitors for HDACs with an IC_{50} value of $1 \mu\text{M}$ for an N-methylated, N-myristoylated peptide derivative and human HDAC11.

Reprinted (adapted) with permission from One-Atom Substitution Enables Direct and Continuous Monitoring of Histone Deacetylase Activity, Matthes Zessin, Zsófia Kutil, Marat Meleshin, Zora Nováková, Ehab Ghazy, Diana Kalbas, Martin Marek, Christophe Romier, Wolfgang Sippl, Cyril Bařinka, and Mike Schutkowski, *Biochemistry* 2019, 58 (48), 4777-4789, DOI: 10.1021/acs.biochem.9b00786 . Copyright 2019 American Chemical Society.

One-Atom Substitution Enables Direct and Continuous Monitoring of Histone Deacetylase Activity

Matthes Zessin,[†] Zsófia Kutil,[§] Marat Meleshin,[‡] Zora Nováková,[§] Ehab Ghazy,[†] Diana Kalbas,[‡] Martin Marek,^{||} Christophe Romier,^{||} Wolfgang Sippl,^{||} Cyril Bařinka,[§] and Mike Schutkowski^{*,‡,§}

[†]Department of Medicinal Chemistry, Institute of Pharmacy, Martin-Luther-University Halle-Wittenberg, 06120 Halle/Saale, Germany

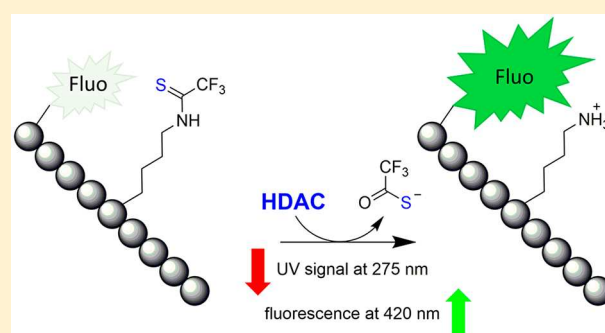
[‡]Department of Enzymology, Institute of Biochemistry and Biotechnology, Charles-Tanford-Protein Center, Martin-Luther-University Halle-Wittenberg, 06120 Halle/Saale, Germany

[§]Institute of Biotechnology of the Czech Academy of Sciences, BIOCEV, Prumyslova 595, 252 50 Vestec, Czech Republic

^{||}Departement de Biologie Structurale Integrative, Institut de Genetique et Biologie Moleculaire et Cellulaire (IGBMC), Universite de Strasbourg (UDS), CNRS, INSERM, 1 rue Laurent Fries, B.P. 10142, 67404 Illkirch Cedex IGBMC, France

Supporting Information

ABSTRACT: We developed a one-step direct assay for the determination of histone deacetylase (HDAC) activity by substituting the carbonyl oxygen of the acyl moiety with sulfur, resulting in thioacylated lysine side chains. This modification is recognized by class I HDACs with different efficiencies ranging from not accepted for HDAC1 to kinetic constants similar to that of the parent oxo substrate for HDAC8. Class II HDACs can hydrolyze thioacylated substrates with approximately 5–10-fold reduced k_{cat} values, which resembles the effect of thioamide substitution in metallo-protease substrates. Class IV HDAC11 accepts thiomristoyl modification less efficiently with an ~ 5 -fold reduced specificity constant. On the basis of the unique spectroscopic properties of thioamide bonds (strong absorption in spectral range of 260–280 nm and efficient fluorescence quenching), HDAC-mediated cleavage of thioamides could be followed by ultraviolet–visible and fluorescence spectroscopy in a continuous manner. The HDAC activity assay is compatible with microtiter plate-based screening formats up to 1536-well plates with Z' factors of >0.75 and signal-to-noise ratios of >50 . Using thioacylated lysine residues in p53-derived peptides, we optimized substrates for HDAC8 with a catalytic efficiency of $>250000 \text{ M}^{-1} \text{ s}^{-1}$, which are more than 100-fold more effective than most of the known substrates. We determined inhibition constants of several inhibitors for human HDACs using thioacylated peptidic substrates and found good correlation with the values from the literature. On the other hand, we could introduce N-methylated, N-acylated lysine residues as inhibitors for HDACs with an IC_{50} value of $1 \mu\text{M}$ for an N-methylated, N-myristoylated peptide derivative and human HDAC11.



Reversible ac(et)ylation of lysine side chains has emerged as a ubiquitous posttranslational modification regulating cellular metabolism as well as many other cellular processes such as protein localization and degradation, chromatin assembly, DNA repair, and metabolic stress response. Either enzymes named acetyltransferases or spontaneous reactions of acyl-CoA derivatives decorate lysine side chains with acyl moieties.^{1,2} Caused by improvements in mass spectrometry, a number of new lysine acylations have been identified *in vivo*, including lysine formylation,^{3,4} propionylation,⁵ butyrylation,⁵ malonylation,^{6,7} succinylation,⁸ glutarylation,⁹ crotonylation,¹⁰ 3-hydroxybutyrylation,¹¹ 4-oxo-nonaoylation,^{12,13} hydroxyisobutyrylation,¹⁴ 3-hydroxy-3-methyl-glutarylation,^{15,16} 3-methyl-glutarylation,^{15,16} 3-methyl-glutaconylation,^{15,16} 3-phosphoglyceroylation,¹⁷ benzoylation,¹⁸ myristoylation,¹⁹ and steary-

lation.²⁰ Several of these modifications could be removed by evolutionarily conserved enzymes introduced as histone deacetylases (HDACs).

On the basis of sequence homology, HDACs can be divided into four classes. Members of class I (HDAC1–3 and -8), class IIa (HDAC4, -5, -7, and -9), class IIb (HDAC6 and -10), and class IV (HDAC11) are Zn^{2+} -dependent hydrolases, while class III proteins (called sirtuins; SIRT 1–7) use NAD^+ as a cosubstrate for the transfer of the acyl moiety from the lysine side chain to the ADP-ribose fragment of the cosubstrate, thereby generating nicotinamide as the third reaction

Received: September 10, 2019

Revised: November 4, 2019

Published: November 4, 2019

product.²¹ HDAC1–3, –6, and –8 show robust deacetylase activity. Class IIa HDACs are nearly inactive on acetylated substrates, but they are highly effective in hydrolyzing trifluoroacetylated peptide derivatives.²² Recently, it was demonstrated that HDAC11 is specific for fatty acyl residues, including octanoyl, decanoyl, dodecanoyl, and myristoyl residues.^{23–25} Demyristoylase activity was demonstrated for HDAC8, too,²⁶ while deformylase activity was detected for HDAC6^{27,28} and HDAC3.²⁸ Additionally, HDAC3 exhibits decrotonylase activity.²⁹ HDAC10 can remove acetyl groups from model peptides, but it has been shown that HDAC10 is much more active if acetylated polyamines like N8-acetyl-spermidin are used as substrates.³⁰

Enzymatic activity of HDACs is involved in a number of processes like cancer progression, regulation of obesity, and immune function. Therefore, several HDAC inhibitors (HDACi) have been approved by the Food and Drug Administration for the treatment of cancer (vorinostat, romidepsin, belinostat, and panobinostat), and a number of clinical trials with HDACi (either natural products or synthetic small molecules) have been started to evaluate their efficacy.^{31,32} Robust and continuous HDAC activity assays compatible with high-throughput screening (HTS) are required for further drug development.

Several assays have been developed and/or optimized for the monitoring of HDAC activity as reviewed in refs 33 and 34. Most of these activity assays are discontinuous [high-performance liquid chromatography (HPLC)-based or mass spectrometry-based assays] or suffering from complex reaction mixtures caused by the coupled enzyme(s) or coupled chemical reaction(s) requiring additional control measurements. Determination of IC_{50} values or K_i values for potential HDACi is therefore time-consuming and cumbersome. In theory, monitoring of the amide bond cleavage followed by ultraviolet (UV) spectroscopy (190–200 nm) can be used for direct measurement of HDAC activity.³⁵ However, in practice, the presence of UV-absorbing buffer ions and proteins makes this setup unfeasible.

To design spectroscopic probes for direct and continuous HDAC assays that can be used for the high-throughput screening platforms in real life, we replaced the oxygen of the amide bond with sulfur. The resulting thioamide bond shows a characteristic red-shifted absorption band at 260 nm for the $\pi-\pi^*$ transition with minimal structural perturbations to a substrate.³⁶ Such thioamide bonds could not be efficiently cleaved by sirtuins due to the formation of a so-called stalled intermediate.^{37,38} Nevertheless, using a discontinuous assay format based on quantification of the released thioacetate by a coupled chemical reaction, Fatkins et al. showed that HDAC8 but not other class I HDACs can hydrolyze thioamide bonds.³⁹

Here, we report that the cleavage of thioacyl groups from lysine side chains by HDACs in model substrates could be followed directly by ultraviolet–visible (UV–vis) spectroscopy. More importantly, modifications of such substrates can yield fluorescence substrates with greatly enhanced sensitivity that can be used in direct and continuous activity assays in the HTS format. Finally, we showed that besides HDAC8, other members of classes IIa, IIb, and IV can hydrolyze thioamide bonds, expanding thus the utility of our findings to the whole family of zinc-dependent HDACs.

■ EXPERIMENTAL PROCEDURES

Chemicals and General Methods. All chemicals were purchased from Sigma (St. Louis, MO) if not denoted otherwise. *N,N*-Dimethylformamide (DMF), piperidine, ethyl (hydroxyimino)cianoacetate (OxymaPure), pentafluorophenol, and Rink amide MBHA resin were obtained from Iris Biotech (Marktredwitz, Germany). 9-Fluorenylmethoxy-carbonyl (Fmoc)-protected amino acid derivatives and *O*-(benzotriazol-1-yl)-*N,N,N',N'*-tetramethyluronium hexafluorophosphate (HBTU) were purchased from Merck (Darmstadt, Germany). Trifluoroacetic acid (TFA) was obtained from Roth (Karlsruhe, Germany). Fmoc-protected β -(7-methoxycoumarin-4-yl)-alanine (Mcm) was purchased from Bachem (Bubendorf, Switzerland). Fmoc-Lys(Ns)-OH was prepared as described elsewhere.⁴⁰ Vorinostat, Trichostatin A, TMP195, TMP269, and KDS170 were purchased from Biomol (Hamburg, Germany).

For HPLC separations, solvents consisting of water (solvent A) and ACN (solvent B), both containing 0.1% trifluoroacetic acid (TFA), were used. Analytical runs were performed on an Agilent 1100 HPLC instrument (Boeblingen, Germany) with a quaternary pump, a well-plate autosampler, and a variable-wavelength detector. Separations were performed on a 3.0 mm \times 50 mm reversed phase column (Phenomenex Kinetex XB C-18, 2.6 μ m) with a flow rate of 0.6 mL/min. **2–5** and **11–13** were separated using a linear gradient from 10% to 60% solvent B within 6 min. **6**, **9**, and **10** were separated using a linear gradient from 5% to 95% solvent B within 6 min. The absorbance of 2-aminobenzoyl residue was used to quantify product and substrate peak areas.

UPLC-MS analysis was performed using either a Waters Acquity UPLC-MS system or a Waters XEVOTQD UPLC-MS system (Milford, MA) with a Waters Acquity-UPLC-MS-BEH C18, 1.7 μ m (2.1 mm \times 50 mm, 30 Å) column. As a mobile phase, 0.1% formic acid in H₂O (solvent A) and 0.1% formic acid in acetonitrile (ACN) (solvent B) solutions were used. A typical gradient from 95:5 to 5:95 (v/v) H₂O:ACN in 6 min was used for the most of the runs. Data analysis was performed using Waters MassLynx software.

Peptides were purified on a Shimadzu LC System with a Phenomenex Kinetex 5 μ m XB-C18 (250 mm \times 21.1 mm, 100 Å) column using different gradients of 0.1% TFA in H₂O (solvent A) and 0.1% TFA in ACN (solvent B) solutions.

Expression Plasmids. Genes encoding individual human HDACs used in this study were obtained from several sources (Table S1). HDAC coding sequences were amplified via polymerase chain reaction using a set of primers listed in Table S1. A Gateway cloning system (Invitrogen, Carlsbad, CA) was used to construct individual HDAC expression plasmids as described previously.⁴¹ Briefly, coding sequences were inserted into the pDONR221 donor plasmid by BP recombination. Expression plasmids were then prepared by LR recombination between the donor plasmid and the destination plasmid bearing the N-terminal TwinStrep-Flag-HALO purification tag (Figure S2).

Expression and Purification of Recombinant HDAC Variants. Large scale expression of human HDACs was carried out essentially as described previously.^{41,23} Briefly, HEK-293/T17 cells were transiently transfected by a given HDAC expression plasmid using linear polyethylene imine (PEI, Polysciences Inc., Warrington, PA). Cells were harvested 3 days post-transfection by centrifugation, and the cell pellet

was resuspended in a lysis buffer [50 mM Tris, 150 mM NaCl, 10 mM KCl, 2 mM MgCl₂, 10% glycerol, and 0.2% Igepal-630 (pH 8)] supplemented with benzonase (2 units/mL; Merck, Darmstadt, Germany) and a cocktail of protease inhibitors (Roche, Basel, Switzerland). The cell suspension was sonicated (30 W, 3 × 20 s) on ice and then incubated on ice for an additional 30 min. The cell lysate was cleared by centrifugation at 40000g for 30 min at 4 °C, and the supernatant was loaded on a Strep-Tactin column (IBA, Gottingen, Germany) previously equilibrated in the lysis buffer. Following the washing step (10 column volumes; the lysis buffer supplemented with 2 mM ATP and 10 mM MgSO₄), fusion proteins were eluted with the elution buffer [50 mM HEPES, 100 mM NaCl, 50 mM KCl, 10% glycerol, and 3 mM desthiobiotin (pH 7.5)]. Eluted proteins were either further purified using the Superdex 16/600 HR200 size exclusion chromatography column (GE Healthcare Bio-Sciences, Little Chalfont, U.K.) with 30 mM HEPES, 140 mM NaCl, 10 mM KCl, 3% glycerol, and 0.25 mM TCEP as the mobile phase or used directly following affinity purification (HDAC1 and -11). The purity of the final HDAC preparations was evaluated by sodium dodecyl sulfate–polyacrylamide gel electrophoresis and is shown in Figure S1. Purified proteins were concentrated to the desired concentration, aliquoted, flash-frozen in liquid nitrogen, and stored at –80 °C until further use.

smHDAC8 was expressed and purified as described previously.⁴²

Solid Phase Peptide Synthesis. The peptides were synthesized using Fmoc-based solid phase peptide synthesis (SPPS) with automated microwave peptide synthesizer Liberty Blue (CEM Corp., Matthews, NC). The coupling of amino acids was performed with DIC/OxymaPure at 90 °C for 2 min. All coupling steps were performed twice. Fmoc deprotection was accomplished with a 20% piperidine solution in DMF at 90 °C for 1 min.

N-Terminal modification was performed with 2-amino-benzoic acid (Abz-OH) (4 equiv), HBTU (4 equiv), and DIPEA (8 equiv) at room temperature in DMF for 1 h. Alternatively, acetylation was performed using an acetic anhydride/DIPEA/DMF [1:2:7 (v/v)] mixture.

Modification of the ε-Amino Group of Lysine. Lysine side chain acylations were performed on the resin after removal of the nosyl protecting group; 100 mg portions of the resin-bound peptide were used for each preparation.

The nosyl group was cleaved using a 1,8-diazabicyclo[5.4.0]-undec-7-ene/thiophenol/DMF solution [1.5:1:7.5 (v/v)] (2 × 90 min). After washing with DMF, the free lysine side chain was modified as described below. (1) The resin was treated with an ethyl dithioacetate (4 equiv) and DIPEA (8 equiv) solution in DMF for 1 h (peptides 2 and 11). (2) The resin was reacted with a solution of trifluorothioacetamide (5 equiv) in DCM overnight (peptides 4, 12, and 13). (3) The resin was treated with a solution of 1-thiododecanoyl-6-nitrobenzotriazole⁴³ in DCM for 1 h (peptide 6). (4) The resin was allowed to react with a solution of myristic acid (4 equiv), HBTU (4 equiv), and DIPEA (8 equiv) in a DMF/DCM [1:1 (v/v)] mixture (peptide 10). (5) The resin was incubated with a solution of carboxymethyl dithiomyristate⁴⁴ (3 equiv) and DIPEA (6 equiv) in DMF for 2 h (peptide 9).

Global Deprotection. Once the reaction proceeded, the resin was washed several times with DCM, MeOH, and DCM before TFA treatment. The resin was further incubated with a TFA/H₂O [90:10 (v/v)] solution for 3–4 h and filtered, and

the volatiles were removed *in vacuo*. The residue was dissolved in an ACN/H₂O solution and purified via HPLC. Fractions containing the pure peptide (as judged by UPLC-MS) were frozen and lyophilized affording pure material.

HPLC-Based Deacylation Assay. Reactions were performed in a total volume of 100 μL in assay buffer, containing 50 mM HEPES, 140 mM NaCl, 10 mM KCl, and 1 mM TCEP (pH 7.4, adjusted with NaOH). To avoid unspecific binding to the reaction vessels, 0.2 mg/mL bovine serum albumin (BSA) was added to the buffer. The peptide (100 μM) was incubated for 7 min at 25 °C. The reaction was started by the addition of 0.1 or 0.01 μM enzyme. After different incubation times (1 and 3 h), the sample was quenched by adding TFA (0.5% final concentration). The cleavage rate was determined by using analytical RP-HPLC. The reaction solution in a volume of ≤100 μL was injected into the HPLC system, and compounds were separated using linear gradients as described above. The absorbance of the 2-aminobenzoyl residue at 320 nm was used to quantify the substrate and the product peak area of 1 to 7, 11, and 12. The consumption of 8 to give 10 and 13 was detected at a wavelength of 220 nm. Product formation was calculated from the product peak area divided by the total peak area (sum of product and substrate peak areas).

UV–vis Spectroscopy. All UV–vis spectra were recorded at 25 °C in assay buffer (composition as described above). Samples were measured in a 150 μL UV cuvette with an optical path length of 1 cm using a model Specord M500 spectrophotometer (Carl Zeiss, Jena, Germany). The peptide concentration was 50 μM. The background of the buffer or the buffer with the corresponding enzyme was subtracted from all spectra. All spectra were measured with a resolution of one data point per nanometer.

Determination of the Molar Extinction Coefficient. The Lambert–Beer law was used to calculate the molar extinction coefficient of the difference spectra for the thioacetyl amide residue (Figure S3) and the thiotrifluoroacetyl amide residue (Figure 2A). A spectrum of free thioacetic acid as the reaction product (corrected against buffer background) and of compound 2 as the substrate (corrected against the absorbance of compound 1, which represents the peptide without lysine modification) was recorded. The absorbance of free thioacetic acid was subtracted from the absorbance of compound 2, resulting in the difference spectra (Figure S3). The difference spectra of free thiotrifluoroacetate (STFAc) and compound 4 were calculated equally. This results in a molar extinction coefficient ϵ_{262} of 6008 L mol⁻¹ cm⁻¹ for thioacetyl amide and an ϵ_{275} of 5556 L mol⁻¹ cm⁻¹ for thiotrifluoroacetyl amide. STFAc was produced by an enzymatic reaction of 4 with 100 nM HDAC7. The full cleavage of peptide 4 was proven by RP-HPLC analysis.

Fluorescence Spectroscopy. All fluorescence spectra were recorded using a compound concentration of 5 μM at 25 °C in a 500 μL cuvette in assay buffer (composition described above). The measurements were performed with a Fluoromax 4 instrument (Horiba, Kyoto, Japan).

Steady-State Measurements. UV Measurements. The kinetic measurements for HDAC4–9 were carried out at 25 °C in assay buffer (composition described above) with varying peptide concentrations (10–1000 μM). The kinetic measurements for HDAC11 were performed at 37 °C in sodium phosphate buffer [20 mM phosphoric acid (pH 7.4, adjusted with NaOH) and 0.2 mg/mL BSA]. Peptide substrates, dissolved in the corresponding buffer, were incubated at

25 °C (or 37 °C for HDAC11) for at least 5 min, and the reaction was started by addition of the enzyme (10–200 nM). The UV measurements were performed in a 150 μ L UV cuvette with an optical path length of 1 cm and in a 150 μ L cuvette with an optical path length of 0.1 cm at the spectrophotometer (Specord M500). For peptides **2** and **9**, the measurement wavelength was 262 nm, and for peptides **4**, **12**, and **13**, the measurement wavelength was 275 nm. The change in absorbance was measured continuously for at least 3 min with one data point per second. At least all measurements were taken in duplicate. The absorbance was plotted against the time, and the initial slope of these curves represents the reaction rate. The Lambert–Beer law and the calculated molar extinction coefficient (see above) were used to calculate the reaction rate in micromolar per second. This reaction rate was plotted as a function of substrate concentration. A nonlinear regression according to the Michaelis–Menten equation was applied for calculation of K_M and k_{cat} values using GraphPad Prism (GraphPad Software, San Diego, CA).

RP-HPLC. The buffer usage and composition for different HDAC isoforms are like those described above. All reactions take place in a 1.5 mL reaction vessel made of polypropylene. The compound was incubated with the appropriate buffer for 7 min. The reaction was started with the addition of an enzyme (1–20 nM). At different time points (1.5–60 min), the reaction was quenched by adding trifluoroacetic acid (0.5% final concentration). The cleavage rate was determined by using analytical RP-HPLC. The reaction solution with a volume of ≤ 100 μ L was injected into the HPLC system. The separation, detection, and quantification of the product were performed as described above. Product formation was plotted as a function of time. The initial slope of this plot represents the reaction rate in micromolar per second. Further analysis ($v/[S]$ plot) was performed as described above.

Fluorescence Measurements. The fluorescence measurements take place in a black 96-microtiter well plate (100 μ L) with a flat bottom from GreinerBioOne (Frickenhausen, Germany, catalog no. 655076). The measurements were performed on an EnVision 2104 Multilabel reader (PerkinElmer, Waltham, MA) with a 330 \pm 75 nm excitation filter and a 430 \pm 8 nm emission filter (1% percent of emission light, 15 flashes, three flashes per AD conversion, and detector gain of 10). The fluorescence signal was converted to a product concentration using calibration curves. The calibration curves were measured using chemically synthesized deacetylated product (10–100 μ M) with the same setting as described above.

Determination of Inhibition Constants. The IC_{50} values are determined in a black 96-microtiter well plate (100 μ L) with a flat bottom from GreinerBioOne (catalog no. 655076). The measurements were performed on an EnVision 2104 Multilabel reader (PerkinElmer) with a 330 \pm 75 nm excitation filter and a 430 \pm 8 nm emission filter (1% percent of emission light, 15 flashes, three flashes per AD conversion, and detector gain of 10). Peptide **4** was incubated with varying inhibitor concentrations (0–2 mM) and 3% DMSO for 7 min, and the deacetylation reaction was started by adding enzyme (10–40 nM). The measurements were taken in triplicate. The fluorescence intensity was plotted as a function of time. The initial slope of these plots was set as activity. The activity in the non-inhibited reaction was assigned to 100%, and the activity in a reaction without enzyme was defined as 0%. The normalized activity was plotted as a function of the logarithm

inhibitor concentration, and the IC_{50} values were calculated using nonlinear regression for normalized dose–response curves with GraphPad Prism and the following equation.

$$Y = \frac{100}{1 + 10^{X - \log IC_{50}}}$$

The measurements for the 384-well plate (GreinerBioOne, catalog no. 784900) run with $n = 4$ and the 1536-well plate (ThermoFisher Scientific, catalog no. 264711) with $n = 8$.

The dose–response curves of HDAC6 were determined with **1**. Product formation was monitored via analytical HPLC as described above. The activity was the initial slope of product formation. All measurements were taken in triplicate.

Z' Factor and Signal/Noise Ratio Analysis. The Z' factor is a dimensionless statistical parameter for HTS assays.⁴⁵ For the analysis, a concentration of 200 μ M peptide **4** as a negative control (mean_{0%}) and a concentration of 200 μ M deacetylated peptide **4** as a positive control (mean_{100%}) were chosen. The fluorescence was detected with the EnVision Multilabel reader as described above. The mean and the standard deviation (SD) were calculated from 40 data points per replicate with three replicates running in 96-well plate, six replicates running in a 384-well plate, and eight replicates running in a 1536-well plate. The Z' factor was determined with the following equation:

$$Z' = 1 - \frac{3SD_{100\%} + 3SD_{0\%}}{|mean_{100\%} - mean_{0\%}|}$$

The signal/noise ratio (S/N) was also calculated with the values described above and with the following equation:⁴⁵

$$S/N \text{ ratio} = \frac{mean_{100\%} - mean_{0\%}}{SD_{0\%}}$$

RESULTS

Thioamide Bond Cleavage Can Be Continuously Monitored by UV Absorption. Recently, we identified an efficient substrate sequence for HDAC6 using a peptide microarray-based approach (**1**).²⁷ We synthesized derivatives of this sequence carrying different acyl groups, including thioacetyl (**2**) and thiotrifluoroacetyl (**4**), together with their respective oxo counterparts **3** and **5** (Figure 1). All compounds are >95% pure as determined by HPLC at 220 nm and showed the expected molecular mass (Figures S24–S32).

Thioamide and thiotrifluoroamide bonds exhibit an intense π – π^* transition at 260 and 275 nm, respectively. Extinction coefficients are 10000 and 9000 $M^{-1} \text{ cm}^{-1}$ for thioacetylated and thiotrifluoroacetylated lysine side chains, respectively,

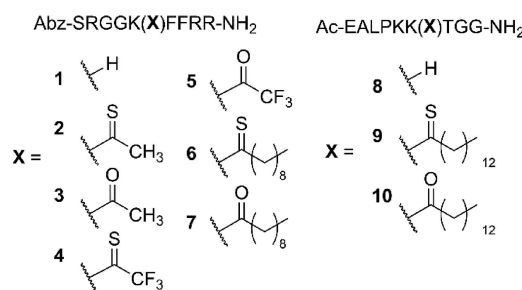


Figure 1. General structure of peptide derivatives used in this study (Abz = 2-aminobenzoyl; Ac = acetyl).

while the thioacetate and thiotrifluoroacetate reaction products show strong absorption in the range of 240–250 nm (Figure 2A and Figure S3). Large absorbance differences at 250 and

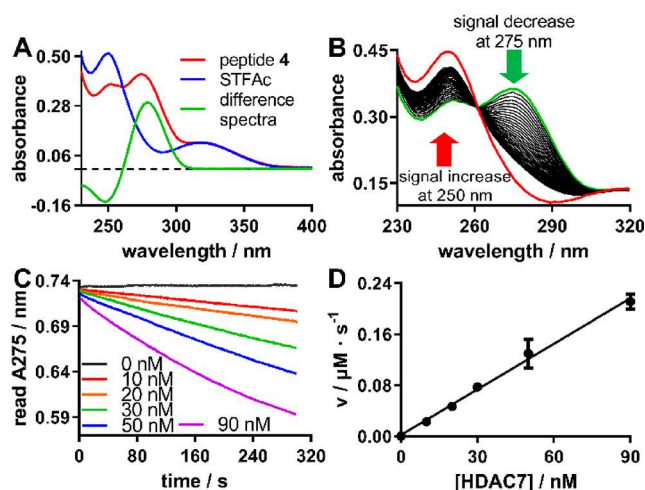


Figure 2. (A) UV–vis spectra of **4** and trifluorothioacetate (STFAC) at a concentration of $50 \mu\text{M}$ and the calculated difference spectrum. (B) UV–vis spectra of **4** treated with 50 nM HDAC7 at 25°C . The green line shows the spectrum immediately after the addition of HDAC7 ($t = 0$). Black lines show the first 30 cycles. UV–vis spectra were recorded every 40 s. The red line shows the UV–vis spectrum of the reaction solution after 66 min (full conversion of **4** verified via HPLC). (C) Progress curves of the conversion of $50 \mu\text{M}$ **4** by HDAC7. The enzyme concentration varies between 10 and 90 nM, and substrate conversion was monitored at 275 nm and 25°C . (D) Rate of reaction of the conversion of **4** by HDAC7 that is linearly dependent on the enzyme concentration at a substrate concentration of $50 \mu\text{M}$. Measurements were taken in duplicate, and error bars show the standard deviation.

275 nm thus allowed us to monitor the HDAC-mediated cleavage of the thiotrifluoroacetylated lysine either by measuring the increase in the intensity of the signal at 250 nm or the decrease in the intensity of the signal at 275 nm. Figure 2B shows recorded UV–vis spectra of a reaction solution containing **4** together with HDAC7. It is obvious that **4** represents a substrate for HDAC7 and that the differences in the UV spectra enable monitoring of the enzymatic reaction as demonstrated in Figure 2C for various concentrations of HDAC7. The slope of the decrease in the intensity of the

signal at 275 nm is dependent on the enzyme concentration, resulting in a linear correlation between the amount of HDAC7 and the reaction rate (Figure 2D). This dependence on enzyme concentration demonstrates that the measured decrease in the intensity of the signal is caused by direct cleavage of the thioamide bond and not cleavage of the normal amide bond subsequent to spontaneous non-enzymatic dethiolation.

Trifluorothioamides Are Superior to Thioamides as HDAC Substrates. Using the set of substrates **2–5**, we evaluated the kinetic parameters of the deacetylase activity of other members of the HDAC family (Table 1 and Table S2) except for HDAC10, as this isoform specifically recognizes acetylated polyamines rather than peptides.³⁰ In agreement with known substrate preferences of HDACs, acetylated peptide **3** was efficiently hydrolyzed only by class I enzymes (HDAC1 and -8) and HDAC6 (Figure S9). Its thioamide analogue, **2**, was efficiently processed by only HDAC8 and HDAC6 (Table S2). HDAC1 was not able to hydrolyze **2**.

On the other hand, trifluoroacetylated peptide **5** and more importantly its trifluorothio analogue, **4**, were more widely accepted making thus trifluorinated (thio)acetyl peptides superior and more versatile substrates for HDAC isoforms. While class IIa HDACs were virtually inactive against thioacetylated derivative **2**, they efficiently removed the trifluorothioacetyl moiety from **4** with high catalytic efficacies ranging from $21000 \text{ M}^{-1} \text{ s}^{-1}$ from HDAC9 to HDAC7, respectively. The K_M values for **4** and **5** are virtually identical for all class IIa isoforms, suggesting that both trifluoroacetyl and trifluorothioacetyl moieties can be well accommodated in the active site. Contrary to the nearly equal K_M values, the catalytic constants are ≤ 10 -fold lower for trifluorothio analogues.

HDAC8 removes the trifluorothioacetyl moiety efficiently, while HDAC1 is inactive against **4** (Table 1). Obviously, the active site of HDAC1 cannot accommodate thioacetyl and thiotrifluoroacetyl residues in a productive conformation. Surprisingly, K_M values for both trifluorothioacetyl and thioacetyl peptides are lower than those of oxo analogues for HDAC8.

HDAC6 accepted the trifluorothioacetyl moiety but with reduced kinetic constants. This effect on HDAC6 is more pronounced for the thioacetyl/acetyl pair of substrates **3** and **2**, where the specificity constant for the thioacetyl substrate is approximately 40-fold lower than that of the oxo analogue **2**,

Table 1. Kinetic Parameters of Trifluoroamide (**5**) and Trifluorothioamide (**4**) Hydrolysis by Different HDAC Isoforms^a

HDAC	peptide 5			peptide 4		
	K_M (μM)	k_{cat} (s^{-1})	k_{cat}/K_M ($\text{M}^{-1} \text{ s}^{-1}$)	K_M (μM)	k_{cat} (s^{-1})	k_{cat}/K_M ($\text{M}^{-1} \text{ s}^{-1}$)
1		no deacetylation ^b			no deacetylation ^b	
4	>400	>40	not determined	290 ± 40	8.3 ± 0.4	29000
5	230 ± 40	80 ± 8	350000	240 ± 70	10 ± 1	31000
6	>400	>1.5	not determined	170 ± 40	0.8 ± 0.3	4800
7	220 ± 40	97 ± 8	450000	240 ± 20	20 ± 5	81000
8	1400 ± 200	440 ± 40	320000	550 ± 50	260 ± 20	470000
9	190 ± 50	11 ± 1	58000	90 ± 30	1.9 ± 0.4	21000
HDAC	peptide 10			peptide 9		
	K_M (μM)	k_{cat} (s^{-1})	k_{cat}/K_M ($\text{M}^{-1} \text{ s}^{-1}$)	K_M (μM)	k_{cat} (s^{-1})	k_{cat}/K_M ($\text{M}^{-1} \text{ s}^{-1}$)
11	7.5 ± 0.2	0.45 ± 0.01	36000	44 ± 13	0.30 ± 0.01	5800

^aData are presented as means \pm standard deviation with $n = 3$. ^bNo deacetylation means <0.5% product formation after 3 h with $0.1 \mu\text{M}$ HDAC and $100 \mu\text{M}$ compound.

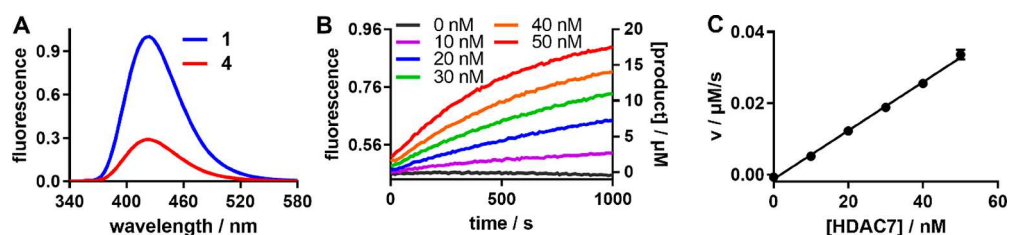


Figure 3. (A) Fluorescence spectra of peptide 4 (red) and 1 (blue). The excitation wavelength was 320 nm, and the compound concentration 5 μM . (B) Progress curves of HDAC7-mediated deacetylation of 4 at different enzyme concentrations at 25 °C. The fluorescence intensity was monitored at 430 ± 8 nm with an excitation wavelength of 330 ± 75 nm. The peptide concentration was 20 μM . (C) Reaction rate of the consumption of 4 as a function of HDAC7 concentration. The peptide concentration was 20 μM , and the error bars show the standard deviation with $n = 3$.

mainly caused by a decrease in catalytic constant k_{cat} . Findings that HDAC6 can accept thioamides, yet prefers their oxo counterparts, were further corroborated by comparing its deformylase and depropionylase activities.²⁷ Here, thioformylated or thiopropionylated substrates were processed with a 30- or 10-fold lower catalytic efficacy, respectively, compared to the formylated or propionylated peptide (Figure S12).

HDAC11 can hydrolyze amide bonds formed by decanoylation or myristoylation of lysine side chains.²³ Therefore, we tested thiodecanoylated peptide 6 and the respective thiomristoylated derivative as substrates for HDAC11. We detected cleavage of the thioacylated amide bonds but were unable to determine catalytic constants K_M and k_{cat} because of solubility problems and/or micelle formation (data not shown). Nevertheless, we were able to show that HDAC11 generates thiomristic acid, yielding a chromophore subsequent to reaction with Ellman's reagent (Figure S8). This result points to direct cleavage of the thiomristoylamide bond mediated by HDAC11. To circumvent the solubility issues and to be closer to myristoylated sites found *in vivo*, we tested peptides derived from naturally occurring TNF α in myristoylated (10) and thiomristoylated (9) forms. We were able to detect efficient cleavage of 10 and ~ 10 -fold less efficient cleavage of the thioamide bond in 9. Surprisingly, in the case of HDAC11, less efficient cleavage of the thioamide bond results from less efficient binding to the active site as mirrored in the K_M values (Table 1).

Fluorescence Quenching by Thioamides Enables the Development of Continuous and Fluorescence-Based HDAC Activity Assays That Are Suitable for High-Throughput Applications. Thioamides represent efficient quenchers for fluorophores excited in the range of 260–330 nm via a FRET-based mechanism.^{46–48} We therefore wondered whether the N-terminal 2-aminobenzoyl fluorophore of 2 and 4 enables the continuous fluorescence-based readout of HDAC-mediated cleavage of thioamide and trifluorothioamide bonds.

Figure 3A shows the fluorescence spectra of 4 and 1 upon excitation of the Abz fluorophore at 320 nm, and the detected large difference in fluorescence intensity verifies an efficient FRET-based quenching of Abz by the trifluorothioamide moiety. Determination of the initial slopes of progress curves (Figure 3B) yielded a linear relationship between the HDAC concentration and the reaction rate as exemplified for HDAC7 in Figure 3C, confirming the utility of this approach for the development of a continuous and fluorescence-based activity assay. On the other hand, 2 shows a much smaller difference in the fluorescence intensity compared to 1, indicating that

thioamides cannot quench the fluorescence of Abz efficiently in this case (Figure S4).

To demonstrate the applicability of our newly developed assays to evaluate inhibitor efficacy in high-throughput screening campaigns, we tested inhibition of HDAC8 by β -Thujaplicin in 96-, 384-, and 1536-well formats (Figure 4A).

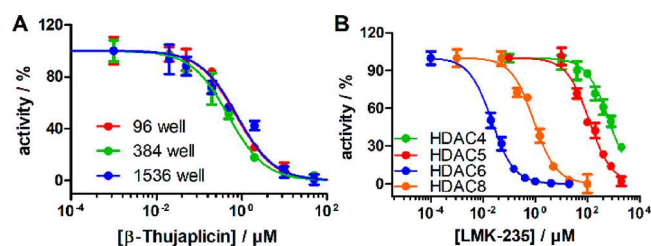


Figure 4. (A) Dose–response curves of HDAC8 with β -Thujaplicin as an inhibitor and 4 as a substrate. The measurements were carried out in 96-well ($\text{IC}_{50} = 0.74 \pm 0.06$ μM , $n = 3$, $Z' = 0.94$, $S/N = 113$), 384-well ($\text{IC}_{50} = 0.49 \pm 0.03$ μM , $n = 4$, $Z' = 0.94$, $S/N = 116$), and 1536-well ($\text{IC}_{50} = 0.78 \pm 0.08$ μM , $n = 8$, $Z' = 0.87$, $S/N = 50$) plates. (B) Dose–response curves of HDAC inhibitor LMK-235 with different HDAC isoforms determined with 4. The error bars show the standard deviation with $n = 3$.

Dose–response curves using the different assay formats provided nearly identical IC_{50} values of 0.74, 0.49, and 0.78 μM for 96-, 384-, and 1536-well plates, respectively, which are in good agreement with the published value of 0.36 μM (calculated from K_i ⁴⁹). Furthermore, the excellent statistical parameters of the assays (Z' score between 0.94 and 0.87 and S/N ratio between 50 and 113) confirmed the scalability and the high-throughput potential of the HDAC activity assay.

Next, we profiled the inhibitory potencies of several known HDACi, including standard HDAC8 inhibitor PCI-34051 and Trichostatin A (TSA), suberoylanilide hydroxamic acid (SAHA), TH42, TH153, KDS170, TMP195, TMP269, and LMK-235, and compared resulting inhibition constants with values reported in the literature (Table 2 and Figure 4B). Overall, there is a very good correlation between the reported inhibition constants and inhibition constants determined in our assay, with the sole exception of LMK235. Here, our IC_{50} values are 5700- and 2800-fold higher for HDAC4 and HDAC5, respectively, as compared to the low nanomolar inhibition constants reported originally.⁵⁰ At the same time, however, a recent report by Choi et al.⁵¹ yielded inhibition constants of LMK-235 against HDAC4 and -5 with high micromolar values that are more consistent with our findings.

The HDAC8 Trifluorothioacetyl “Supersubstrate” Can Be Developed on the Basis of the Modified p53

Table 2. Inhibition Results [IC₅₀ values ± standard deviation (SD) with *n* = 3] for Several HDACi Using Peptide 4 Together with the Respective IC₅₀ Values from the Literature

inhibitor	IC ₅₀ ± SD (nM) of different HDAC isoforms						ref
	HDAC4		HDAC5		HDAC8		
	published	measured	published	measured	published	measured	
SAHA	48300	140000 ± 20000	20000	37000 ± 4000	960	420 ± 80	50
TSA	6590	11000 ± 2000	2170	3900 ± 700	180	120 ± 10	53
β-Thujaplicin	– ^c	– ^c	– ^c	– ^c	356 ^a	740 ± 110	49
TH42	– ^c	– ^c	– ^c	– ^c	69.2	60 ± 10	54
TH153	– ^c	– ^c	– ^c	– ^c	72	86 ± 11	55
KD5170	26	– ^c	950	1000 ± 100	2500	1000 ± 100	56
PCI-34051	– ^c	– ^c	– ^c	– ^c	10	17 ± 4	57
TMP195	111	460 ± 60	106	350 ± 60	– ^c	– ^c	53
TMP269	126	640 ± 150	80	570 ± 100	– ^c	– ^c	53
		282		101			58
LMK-235 ^b	11.9	680000 ± 80000	4.22	120000 ± 20000	1278	880 ± 150	50
	>20000		>20000		1119		51

^aCalculated from the *K_i* value; SD means standard deviation with *n* = 3. ^bIC₅₀ values for HDAC6 are 55.7 nM⁵⁰ and 21 ± 2 nM (determined in this report). ^cNot measured.

Sequence. The catalytic efficacy (*k_{cat}*/*K_M*) of 470000 M^{−1} s^{−1} for HDAC8 and the substrate **4** represents to the best of our knowledge the highest values described so far. To transfer this “supersubstrate” properties into a more native peptide sequence, we introduced thioacetyl (**11**) and trifluorothioacetyl (**12** and **13**) moieties in peptides derived from p53, one of the known *in vivo* HDAC8 substrates (Figure 5). Introduction

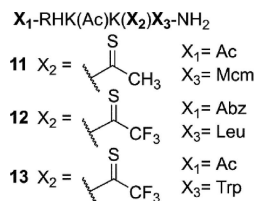


Figure 5. Structure of the p53-derived fluorescent HDAC8 substrates equipped with thioacetyl residues at the lysine side chain. Abbreviations: Mcm, 7-methoxy-coumaryl-L-alanine; Abz, 2-aminobenzoyl; Ac, acetyl.

of the fluorescent amino acid derivative 7-methoxy-coumaryl-L-alanine (Mcm) in the +1 position (**11**), in place of a hydrophobic leucine residue in the wild type sequence, abolished HDAC8-mediated cleavage of the thioamide bond, revealing that this substitution is not tolerated at the +1 position. We thus adjusted our strategy by attaching a fluorophore (Abz) at the N-terminus of the p53-derived sequence in combination with the better accepted trifluorothioacetylated lysine residue leading to **12**. This substrate was hydrolyzed by HDAC8, although with suboptimal kinetic parameters manifested by an ~2-fold increase in the *K_M* value and a 5-fold decreased *k_{cat}* value (Figure 6) maybe caused by the artificial Abz residue at the −4 position. Realizing the preference of HDAC8 for bulky residues at the +1 position,⁵² we next substituted the +1 leucine in **12** with tryptophan and generated substrate **13** with a *k_{cat}*/*K_M* value of >250000 M^{−1} s^{−1} that is more than 100-fold more effective than most of the known substrates reported to date (Figure 6).

It is also interesting to note that, although derivatives **12** and **13** contain a normal acetylated lysine residue at the −1 position close to the trifluorothioacetylated lysine, there is

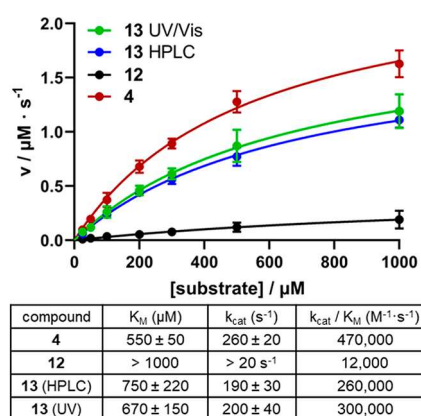


Figure 6. Michaelis–Menten plots of dethioacylation of **4** and of p53-derived substrates **12** and **13** by HDAC8. The error bars show the standard deviation with *n* = 3. The enzyme concentration was 10 nM. Substrate **12** showed suboptimal kinetic constants. Substrate **13** represents one of the best substrates for HDAC8 with *k_{cat}*/*K_M* values of 260000 and 300000 M^{−1} s^{−1} as determined with HPLC-based and UV-based readouts, respectively.

nearly no cleavage of this “normal” acetylated lysine detectable using HPLC-MS even after prolonged reaction times. These findings confirm the critical importance of the +1 position for substrate recognition by HDAC8 (Figure S22).

Monomethylation of the Scissile Amide Bond Converts HDAC Substrates to Inhibitors. The spectral overlap between the thioacetyl amide quencher and the Abz or Mcm fluorophore is not optimal. Therefore, we attempted to improve the spectral overlap by changing the secondary thioamide bond to a tertiary amide bond via introduction of an additional methyl group at the lysine side chain nitrogen of **2**, resulting in a thioacetylated *N*-monomethyl-lysine residue. It is known that the π–π* transition of tertiary thioamides is ~10 nm red-shifted as compared to the respective secondary amides.^{36,59} To our surprise, this peptide derivative was not accepted as a substrate by HDAC8, which was most effective for **2**. Similarly, a peptide containing an *N*-methylated acetyllysine residue was not hydrolyzed by HDAC8 and all four class IIa HDACs. HPLC analysis of peptides containing

acetylated N-monomethyl-lysines revealed that these peptides inhibit enzymatic activity of HDACs with affinities in the range of the K_M values of the respective acetylated substrates (Figure S18). Docking studies with HDAC6 indicated a disturbed binding mode caused by the additional methyl group at the lysine nitrogen (Figure 7). Interestingly, HDAC11 is efficiently inhibited by an N-methylated derivative of a myristoylated substrate with an IC_{50} value of $1.2 \pm 0.24 \mu M$ (Figure S19).

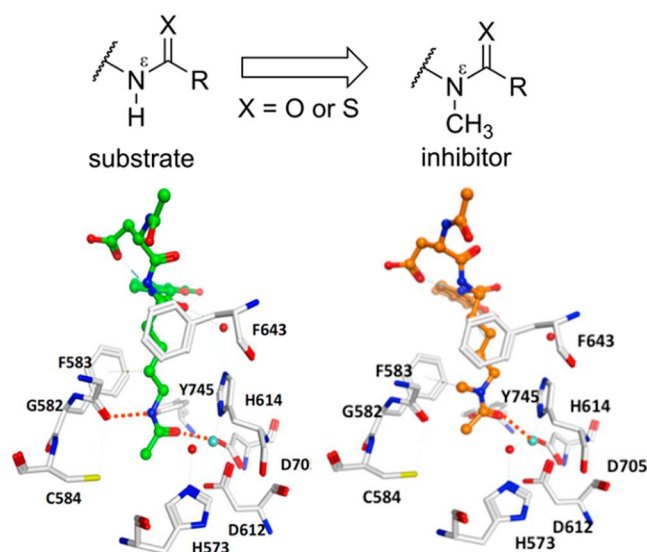


Figure 7. Crystal structure of HDAC6 (*Danio rerio*, Protein Data Bank entry 6EFK) with an acetylated substrate (left, peptide colored green) and the HDAC6 docking pose of a peptide containing an N-methylated, N-acetylated lysine residue (right, peptide colored orange). Cocrystallized water molecules are shown as red spheres, and hydrogen bonds and Zn^{2+} coordinations are shown as red dashed lines.

DISCUSSION

Detection of HDAC activity is often coupled to a separation of a substrate and its reaction product. Different methods are used for such separation steps, including capillary electrophoresis,⁶⁰ microchip electrophoresis,⁶¹ a microfluidic mobility assay,^{62,63} polyacrylamide gel electrophoresis,⁶⁴ high-performance liquid chromatography (HPLC),^{65–68} thin layer chromatography,⁶⁹ charcoal binding,⁷⁰ binding to boronic acid resins,⁷¹ and extraction with organic solvents.⁷² As a result of this additional separation step, the resulting assay format is discontinuous and not suited for high-throughput applications. Alternatively, mass spectrometry could be used for the separation of the substrate and the reaction product.^{73,74} MALDI-MS readout in combination with peptide derivatives immobilized on glass surfaces was used for the systematic profiling of the substrate specificity of HDAC2, HDAC3, and HDAC8.^{52,75} Additionally, HDAC activity patterns could be determined in cell lysates using that technique.⁷⁶ Moreover, the same technology uncovered the dependency of HDAC8 substrate specificity on the nature of the metal ion within the active site.⁷⁷ Alternative approaches make use of reagents sensing either the acetylated substrates, like acetyllysine-recognizing antibodies,^{27,78–82} or the reaction products. The release of radioisotopically labeled acetate was used to analyze enzymatic reactions.^{83–86} More recently, acetate could be captured by coupling to an enzymatic reaction⁸⁷ and a

chemical reaction was used to trap the HDAC8-mediated release of thioacetate yielding a chromophore.³⁸ Reagents for the detection of the generated primary amine in the peptide product could either be added chemicals, like biotin-containing compounds or fluorescent dyes, reacting with the lysine side chain^{88,89} or intramolecular reactions, like transesterification with a coumarine dye,⁹⁰ which is possible only if the lysine side chain is released by HDAC activity.^{91–94} Additionally, aggregation-induced emission^{95,96} and modulation of binding to DNA^{97,98} were used to probe HDAC activity.

An interesting alternative is the coupling of the HDAC reaction to a proteolytic reaction using proteases, specific for the free lysine side chain in the reaction product.^{66,86,99,100} Fluorescence-based readout for the proteolytic reaction is common for increasing the sensitivity of the assay. Commercially available HDAC substrates are fused to 7-amino-4-methylcoumarin, resulting in bright fluorescence subsequent to cleavage of the lysinyl-coumaryl amide bond.^{22,101–106} It was demonstrated that for some sirtuins this assay could be performed in a continuous format^{107,108} but the proteolytic stability of different HDACs against the used proteases is limited. Therefore, most protease-coupled HDAC assays have to be performed in a discontinuous manner. Nevertheless, this assay format has some disadvantages. The substituted coumaryl moiety represents an artificial residue within the HDAC substrate preventing the investigation of substrate specificities in positions +1, +2, etc. Moreover, it was demonstrated that profiling of HDAC activity with substrates containing coumaryl fluorophores yielded results different from screening results with more natural substrates, including an artificially enhanced affinity for the active site (HDAC6) or a loss of sequence specificity (HDAC4).¹⁰⁹

Continuous activity assays are known for sirtuins.^{40,110} A fluorophore (or quencher) is fused to the acyl moiety linked to the lysine side chain. Because of the narrow binding pockets for the acylated lysine side chain of class I and II HDACs, such derivatized acyl residues cannot be accommodated. Nevertheless, thioamides represent a very small quencher enabling either FRET (if the fluorophore absorbs in the range of the thioamide $\pi-\pi^*$ transition at 260 nm)^{47,48,111–115} or PET (if the thioamide bond can make a van der Waals contact with the fluorophore).^{46,116} Therefore, thioacylated substrates in combination with fluorophores like anthranilic amides or tryptophan should yield substrates accepted well by HDACs. Surprisingly, there are differences between the HDAC isoforms ranging from not being accepted as a substrate (HDAC1) to removing thioacyl residues with kinetic constants like the respective acyl residue (class I HDAC8 and class IIa HDAC9).

It is known that metalloproteases and HDACs could be inhibited by thiols caused by coordination to the active site zinc ion. Therefore, we analyzed the effects of sodium thioacetate on the catalysis of different HDACs (Figure S18). We found very minor inhibitory effects (<10% inhibition) on HDAC4 and HDAC7 at 200 μM and between 10% and 20% inhibition of HDAC4 and HDAC7 activity at 2 mM. HDAC8 was inhibited ~20% at 20 μM sodium thioacetate and >80% at 2 mM sodium thioacetate. Nevertheless, in our enzymatic assays, the released thioacetate will not influence the HDAC8 activity because of the short measurements preventing release of more than 20 μM thioacetate.

Analysis of the available crystal structures revealed that the carbonyl oxygen of the acetyl residue is hydrogen bonded to a

conserved tyrosine residue (Tyr306 in HDAC8) and coordinates with the metal ion in the active site. Sulfur is a much weaker hydrogen bond acceptor, and this reduced hydrogen bonding capability could in principle be used to explain the less efficient hydrolysis of thioamide bonds by HDAC1–3, -6, and -11. Class IIa isoforms do not have this tyrosine residue in their active sites and accept thio-trifluoroacetyl residues with similar kinetic constants as compared to trifluoroacetyl residues. Nevertheless, HDAC8 cleaves thioamide bonds very efficiently despite the fact that such hydrogen bonding is important for the reaction mechanism. Tyr306F variants of HDAC8 are “trapping mutants” that bind the acetyllysine-containing peptides but cannot perform the hydrolysis step efficiently.¹¹⁷ There have to be alternatives to explain the reactivity differences against thioamide bonds between the HDAC isoforms.

In general, the ability of some HDAC isoforms to accept thioamides as substrates is interesting because it is known from studies with other enzymes acting on amide bonds that most of these enzymes could not handle thioamides at the scissile bond. Peptides with thioxylylated prolyl bonds represent competitive inhibitors for peptidyl-prolyl *cis/trans* isomerases like cyclophilin¹¹⁸ or Pin1.¹¹⁹ Additionally, sirtuins are potentially inhibited by thioacylated lysine residues^{38,37,120,121} because of the formation of an intermediate that is extremely slowly decomposed to the reaction products.¹²²

Metalloprotease carboxypeptidase A can hydrolyze thioxylylated peptide bonds in dipeptide derivatives with slightly reduced k_{cat} values.^{123–126} Interestingly, activity against thioamide-containing substrates increased remarkably if the active site metal ion was substituted with more thiophilic cadmium or cobalt ions.^{123,125} In contrast, aminopeptidase P can hydrolyze thioxylylated peptide bonds with >1000-fold reduced k_{cat} values.¹²⁷ Additionally, leucine aminopeptidase cannot hydrolyze thioxylylated amide bonds, but such peptide derivatives represent good competitive inhibitors,¹²⁸ showing that these compounds bind in a similar manner to the active site like the respective substrates. Aminopeptidase from *Aeromonas proteolytica* with zinc ions in the active site accepts thioamides with similar kinetics like the (oxo)amides. The respective enzyme equipped with a cadmium ion cleaves the thioamide at the scissile bond exclusively.¹²⁹ Maybe the nature of the metal ion in the active site of HDAC8 is the key for the high efficiency of thioamide bond cleavage. There are discussions that HDAC8 *in vivo* is loaded with divalent metal ions different from Zn²⁺ like Fe²⁺ or Co²⁺.^{77,130,131} Additionally, crystal structures of metallo-substituted HDAC8 complexed to Co²⁺, Mn²⁺, or Fe²⁺ were reported.¹³² If HDAC8 preparations are loaded with a more thiophilic ion, the extraordinary cleavage rates of thioamides by HDAC8 could be explained.

In general, substrates reported so far for HDAC8 are relatively poor with respect to $k_{\text{cat}}/K_{\text{M}}$ values ranging from 10 to 200 M⁻¹ s⁻¹ for acetyllysine-containing N- α -acetylated pentapeptide amides.⁸⁹ Schultz et al. reported for HDAC8 $k_{\text{cat}}/K_{\text{M}}$ values of 60 and 50 M⁻¹ s⁻¹ for Ac-Gly-Ala-Lys(Ac)-fluorophore and Abz-Gly-Ala-Lys(Ac)-Ala-Ala-Dpr(Dnp)-amide, respectively.¹³³ Trifluoroacetylated substrates derived from the histone H4 Lys12 acetylation site [Ac-Leu-Gly-Lys(Tfa)-fluorophore] were published with specificity constants for HDAC8 of 3800 M⁻¹ s⁻¹. For short peptides derived from the acetylated (or doubly acetylated) p53 sequence, including the respective Fluor de Lys substrate, the specificity

constants published are in a similar range^{75,109} or slightly higher.^{29,130} Fatkins et al. determined for an 18meric, thioacetylated p53-derived peptidic substrate a $k_{\text{cat}}/K_{\text{M}}$ value of 7715 M⁻¹ s⁻¹.³⁹ Interestingly, $k_{\text{cat}}/K_{\text{M}}$ values for our trifluoroacetylated substrates **4** are in the range of 450000 M⁻¹ s⁻¹, and these “supersubstrate” properties could be transferred to p53-derived peptide substrate **13**. Substrates **4** and **13** are to the best of our knowledge the most efficient HDAC8 substrates described so far enabling highly effective microtiter plate-based inhibitor screening projects because of the direct and continuous nature of the assay format.

■ ASSOCIATED CONTENT

📄 Supporting Information

The Supporting Information is available free of charge on the ACS Publications website at DOI: 10.1021/acs.biochem.9b00786.

Analytical data, HPLC/MS runs, and additional enzymological data (PDF)

Accession Codes

hHDAC1, Q13547; hHDAC4, P56524; hHDAC5, Q9UQL6 (675–1095); hHDAC6, Q9UBN7; hHDAC7, NM_016596; hHDAC8, Q9BY41; hHDAC9, NM_178425.3; hHDAC11, Q96DB2; smHDAC8, ASH660.

■ AUTHOR INFORMATION

Corresponding Author

*E-mail: mike.schutkowski@biochemtech.uni-halle.de.

ORCID

Zora Nováková: 0000-0001-9804-6346

Martin Marek: 0000-0001-7220-5644

Christophe Romier: 0000-0002-3680-935X

Wolfgang Sippl: 0000-0002-5985-9261

Cyril Bařinka: 0000-0003-2751-3060

Mike Schutkowski: 0000-0003-0919-7076

Present Address

[†]M.M.: Loschmidt Laboratories, Department of Experimental Biology & RECETOX, Faculty of Science, Masaryk University, Kamenice 5/A13, 625 00 Brno, Czech Republic.

Funding

This work was supported by grants from Deutsche Forschungsgemeinschaft (INST 271/336-1 FUGG) to M.S., the Czech Science Foundation (15-19640S), the CAS (RVO: 86652036), and the project “BIOCEV” (CZ.1.05/1.1.00/02.0109) from the ERDF.

Notes

The authors declare no competing financial interest.

■ ACKNOWLEDGMENTS

The authors thank Dr. David Rauh, Sebastian Seiferheld, and Martin Himmelreich for initial experiments and helpful discussions. Moreover, the authors are grateful to Ilona Kunze for technical support. The authors thank Prof. Dr. Thomas Kieflhaber at the Martin-Luther University Halle-Wittenberg for giving us access to the single-quadrupole LC-MS analyses and the MS service facility of the Martin-Luther University Halle-Wittenberg for technical assistance during the triple-quadrupole LC-MS experiments.

■ ABBREVIATIONS

TFA, trifluoroacetic acid; Mcm, 7-methoxy-coumaryl-L-alanine; Abz, 2-aminobenzoyl; Ac, acetyl; HTS, high-throughput screening.

■ REFERENCES

(1) Simic, Z., Weiwad, M., Schierhorn, A., Steegborn, C., and Schutkowski, M. (2015) The ϵ -Amino Group of Protein Lysine Residues Is Highly Susceptible to Nonenzymatic Acylation by Several Physiological Acyl-CoA Thioesters. *ChemBioChem* 16, 2337–2347.

(2) Wagner, G. R., and Payne, R. M. (2013) Widespread and enzyme-independent N ϵ -acetylation and N ϵ -succinylation of proteins in the chemical conditions of the mitochondrial matrix. *J. Biol. Chem.* 288, 29036–29045.

(3) Jiang, T., Zhou, X., Taghizadeh, K., Dong, M., and Dedon, P. C. (2007) N-formylation of lysine in histone proteins as a secondary modification arising from oxidative DNA damage. *Proc. Natl. Acad. Sci. U. S. A.* 104, 60–65.

(4) Wisniewski, J. R., Zougman, A., and Mann, M. (2008) Nepsilon-formylation of lysine is a widespread post-translational modification of nuclear proteins occurring at residues involved in regulation of chromatin function. *Nucleic Acids Res.* 36, 570–577.

(5) Chen, Y., Sprung, R., Tang, Y., Ball, H., Sangras, B., Kim, S. C., Falck, J. R., Peng, J., Gu, W., and Zhao, Y. (2007) Lysine propionylation and butyrylation are novel post-translational modifications in histones. *Mol. Cell. Proteomics* 6, 812–819.

(6) Nishida, Y., Rardin, M. J., Carrico, C., He, W., Sahu, A. K., Gut, P., Najjar, R., Fitch, M., Hellerstein, M., Gibson, B. W., and Verdin, E. (2015) SIRT5 Regulates both Cytosolic and Mitochondrial Protein Malonylation with Glycolysis as a Major Target. *Mol. Cell* 59, 321–332.

(7) Peng, C., Lu, Z., Xie, Z., Cheng, Z., Chen, Y., Tan, M., Luo, H., Zhang, Y., He, W., Yang, K., Zwaans, B. M. M., Tishkoff, D., Ho, L., Lombard, D., He, T.-C., Dai, J., Verdin, E., Ye, Y., and Zhao, Y. (2011) The first identification of lysine malonylation substrates and its regulatory enzyme. *Mol. Cell. Proteomics* 10, M111.012658.

(8) Zhang, Z., Tan, M., Xie, Z., Dai, L., Chen, Y., and Zhao, Y. (2011) Identification of lysine succinylation as a new post-translational modification. *Nat. Chem. Biol.* 7, 58–63.

(9) Tan, M., Peng, C., Anderson, K. A., Chhoy, P., Xie, Z., Dai, L., Park, J., Chen, Y., Huang, H., Zhang, Y., Ro, J., Wagner, G. R., Green, M. F., Madsen, A. S., Schmiesing, J., Peterson, B. S., Xu, G., Ilkayeva, O. R., Muehlbauer, M. J., Braulke, T., Mühlhausen, C., Backos, D. S., Olsen, C. A., McGuire, P. J., Pletcher, S. D., Lombard, D. B., Hirschey, M. D., and Zhao, Y. (2014) Lysine glutarylation is a protein posttranslational modification regulated by SIRT5. *Cell Metab.* 19, 605–617.

(10) Tan, M., Luo, H., Lee, S., Jin, F., Yang, J. S., Montellier, E., Buchou, T., Cheng, Z., Rousseaux, S., Rajagopal, N., Lu, Z., Ye, Z., Zhu, Q., Wysocka, J., Ye, Y., Khochbin, S., Ren, B., and Zhao, Y. (2011) Identification of 67 histone marks and histone lysine crotonylation as a new type of histone modification. *Cell* 146, 1016–1028.

(11) Xie, Z., Zhang, D., Chung, D., Tang, Z., Huang, H., Dai, L., Qi, S., Li, J., Colak, G., Chen, Y., Xia, C., Peng, C., Ruan, H., Kirkey, M., Wang, D., Jensen, L. M., Kwon, O. K., Lee, S., Pletcher, S. D., Tan, M., Lombard, D. B., White, K. P., Zhao, H., Li, J., Roeder, R. G., Yang, X., and Zhao, Y. (2016) Metabolic Regulation of Gene Expression by Histone Lysine β -Hydroxybutyrylation. *Mol. Cell* 62, 194–206.

(12) Cui, Y., Li, X., Lin, J., Hao, Q., and Li, X. D. (2017) Histone Ketoamide Adduction by 4-Oxo-2-nonenal Is a Reversible Post-translational Modification Regulated by Sirt2. *ACS Chem. Biol.* 12, 47–51.

(13) Galligan, J. J., Rose, K. L., Beavers, W. N., Hill, S., Tallman, K. A., Tansey, W. P., and Marnett, L. J. (2014) Stable histone adduction by 4-oxo-2-nonenal: a potential link between oxidative stress and epigenetics. *J. Am. Chem. Soc.* 136, 11864–11866.

(14) Dai, L., Peng, C., Montellier, E., Lu, Z., Chen, Y., Ishii, H., Debernardi, A., Buchou, T., Rousseaux, S., Jin, F., Sabari, B. R., Deng, Z., Allis, C. D., Ren, B., Khochbin, S., and Zhao, Y. (2014) Lysine 2-hydroxyisobutyrylation is a widely distributed active histone mark. *Nat. Chem. Biol.* 10, 365–370.

(15) Anderson, K. A., Huynh, F. K., Fisher-Wellman, K., Stuart, J. D., Peterson, B. S., Douros, J. D., Wagner, G. R., Thompson, J. W., Madsen, A. S., Green, M. F., Sivley, R. M., Ilkayeva, O. R., Stevens, R. D., Backos, D. S., Capra, J. A., Olsen, C. A., Campbell, J. E., Muoio, D. M., Grimsrud, P. A., and Hirschey, M. D. (2017) SIRT4 Is a Lysine Deacetylase that Controls Leucine Metabolism and Insulin Secretion. *Cell Metab.* 25, 838–855.

(16) Wagner, G. R., Bhatt, D. P., O'Connell, T. M., Thompson, J. W., Dubois, L. G., Backos, D. S., Yang, H., Mitchell, G. A., Ilkayeva, O. R., Stevens, R. D., Grimsrud, P. A., and Hirschey, M. D. (2017) A Class of Reactive Acyl-CoA Species Reveals the Non-enzymatic Origins of Protein Acylation. *Cell Metab.* 25, 823–837.

(17) Moellering, R. E., and Cravatt, B. F. (2013) Functional lysine modification by an intrinsically reactive primary glycolytic metabolite. *Science (Washington, DC, U. S.)* 341, 549–553.

(18) Huang, H., Zhang, D., Wang, Y., Perez-Neut, M., Han, Z., Zheng, Y. G., Hao, Q., and Zhao, Y. (2018) Lysine benzoylation is a histone mark regulated by SIRT2. *Nat. Commun.* 9, 3374.

(19) Stevenson, F. T., Bursten, S. L., Locksley, R. M., and Lovett, D. H. (1992) Myristyl acylation of the tumor necrosis factor alpha precursor on specific lysine residues. *J. Exp. Med.* 176, 1053–1062.

(20) Liu, W., Zhou, Y., Peng, T., Zhou, P., Ding, X., Li, Z., Zhong, H., Xu, Y., Chen, S., Hang, H. C., and Shao, F. (2018) N ϵ -fatty acylation of multiple membrane-associated proteins by *Shigella* IcsB effector to modulate host function. *Nature microbiology* 3, 996–1009.

(21) Seto, E., and Yoshida, M. (2014) Erasers of histone acetylation: the histone deacetylase enzymes. *Cold Spring Harbor Perspect. Biol.* 6, No. a018713.

(22) Bradner, J. E., West, N., Grachan, M. L., Greenberg, E. F., Haggarty, S. J., Warnow, T., and Mazitschek, R. (2010) Chemical phylogenetics of histone deacetylases. *Nat. Chem. Biol.* 6, 238–243.

(23) Kutil, Z., Novakova, Z., Meleshin, M., Mikesova, J., Schutkowski, M., and Barinka, C. (2018) Histone Deacetylase 11 Is a Fatty-Acid Deacetylase. *ACS Chem. Biol.* 13, 685–693.

(24) Moreno-Yruela, C., Galleano, I., Madsen, A. S., and Olsen, C. A. (2018) Histone Deacetylase 11 Is an ϵ -N-Myristoyllysine Hydrolase. *Cell chemical biology* 25, 849–856.

(25) Cao, J., Sun, L., Aramsangtienchai, P., Spiegelman, N. A., Zhang, X., Huang, W., Seto, E., and Lin, H. (2019) HDAC11 regulates type I interferon signaling through defatty-acylation of SHMT2. *Proc. Natl. Acad. Sci. U. S. A.* 116, 5487.

(26) Aramsangtienchai, P., Spiegelman, N. A., He, B., Miller, S. P., Dai, L., Zhao, Y., and Lin, H. (2016) HDAC8 Catalyzes the Hydrolysis of Long Chain Fatty Acyl Lysine. *ACS Chem. Biol.* 11, 2685–2692.

(27) Kutil, Z., Skultetyova, L., Rauh, D., Meleshin, M., Snajdr, I., Novakova, Z., Mikesova, J., Pavlicek, J., Hadzima, M., Baranova, P., Havlinova, B., Majer, P., Schutkowski, M., and Barinka, C. (2019) The unraveling of substrate specificity of histone deacetylase 6 domains using acetylome peptide microarrays and peptide libraries. *FASEB J.* 33, 4035–4045.

(28) McClure, J. J., Inks, E. S., Zhang, C., Peterson, Y. K., Li, J., Chundru, K., Lee, B., Buchanan, A., Miao, S., and Chou, C. J. (2017) Comparison of the Deacetylase and Deacetylase Activity of Zinc-Dependent HDACs. *ACS Chem. Biol.* 12, 1644–1655.

(29) Madsen, A. S., and Olsen, C. A. (2012) Profiling of substrates for zinc-dependent lysine deacetylase enzymes: HDAC3 exhibits decrotonylase activity in vitro. *Angew. Chem., Int. Ed.* 51, 9083–9087.

(30) Hai, Y., Shinsky, S. A., Porter, N. J., and Christianson, D. W. (2017) Histone deacetylase 10 structure and molecular function as a polyamine deacetylase. *Nat. Commun.* 8, 15368.

(31) Adhikari, N., Amin, S. A., and Jha, T. (2018) Selective and nonselective HDAC8 inhibitors: a therapeutic patent review. *Pharm. Pat. Anal.* 7, 259–276.

- (32) Li, Y., Wang, F., Chen, X., Wang, J., Zhao, Y., Li, Y., and He, B. (2019) Zinc-dependent deacetylase (HDAC) inhibitors with different ZBG groups. *Curr. Top. Med. Chem.* 19, 223–241.
- (33) Schutkowski, M., Fischer, F., Roessler, C., and Steegborn, C. (2014) New assays and approaches for discovery and design of Sirtuin modulators. *Expert Opin. Drug Discovery* 9, 183–199.
- (34) Suresh, P. S., Devaraj, V. C., Srinivas, N. R., and Mullangi, R. (2017) Review of bioanalytical assays for the quantitation of various HDAC inhibitors such as vorinostat, belinostat, panobinostat, romidepsin and chidamine. *Biomed. Chromatogr.* 31, e3807.
- (35) Lin, L. N., and Brandts, J. F. (1979) Evidence suggesting that some proteolytic enzymes may cleave only the trans form of the peptide bond. *Biochemistry* 18, 43–47.
- (36) Frank, R., Jakob, M., Thuncke, F., Fischer, G., and Schutkowski, M. (2000) Thioxylation as One-Atom-Substitution Generates a Photoswitchable Element within the Peptide Backbone. *Angew. Chem., Int. Ed.* 39, 1120–1122.
- (37) Fatkins, D. G., and Zheng, W. (2008) Substituting N-thioacetyl-lysine for N ϵ -acetyl-lysine in Peptide Substrates as a General Approach to Inhibiting Human NAD $^{+}$ -dependent Protein Deacetylases. *Int. J. Mol. Sci.* 9, 1–11.
- (38) Fatkins, D. G., Monnot, A. D., and Zheng, W. (2006) Nepsilon-thioacetyl-lysine: a multi-facet functional probe for enzymatic protein lysine Nepsilon-deacetylation. *Bioorg. Med. Chem. Lett.* 16, 3651–3656.
- (39) Fatkins, D. G., and Zheng, W. (2008) A spectrophotometric assay for histone deacetylase 8. *Anal. Biochem.* 372, 82–88.
- (40) Schuster, S., Roessler, C., Meleshin, M., Zimmermann, P., Simic, Z., Kambach, C., Schiene-Fischer, C., Steegborn, C., Hottiger, M. O., and Schutkowski, M. (2016) A continuous sirtuin activity assay without any coupling to enzymatic or chemical reactions. *Sci. Rep.* 6, 22643.
- (41) Skultetyova, L., Ustinova, K., Kutil, Z., Novakova, Z., Pavlicek, J., Mikesova, J., Trapl, D., Baranova, P., Havlinova, B., Hubalek, M., Lansky, Z., and Barinka, C. (2017) Human histone deacetylase 6 shows strong preference for tubulin dimers over assembled microtubules. *Sci. Rep.* 7, 11547.
- (42) Marek, M., Kannan, S., Hauser, A.-T., Moraes Mourão, M., Cabby, S., Cura, V., Stolfa, D. A., Schmidtkunz, K., Lancelot, J., Andrade, L., Renaud, J.-P., Oliveira, G., Sippl, W., Jung, M., Cavarelli, J., Pierce, R. J., and Romier, C. (2013) Structural basis for the inhibition of histone deacetylase 8 (HDAC8), a key epigenetic player in the blood fluke *Schistosoma mansoni*. *PLoS Pathog.* 9, No. e1003645.
- (43) Shalaby, M. A., and Rapoport, H. (1999) A General and Efficient Route to Thionoesters via Thionoacyl Nitrobenzotriazoles. *J. Org. Chem.* 64, 1065–1070.
- (44) Leon, N. H. (1976) New compounds: synthesis of carboxymethyl carbodithioates. *J. Pharm. Sci.* 65, 146–148.
- (45) Zhang, Chung, and Oldenburg (1999) A Simple Statistical Parameter for Use in Evaluation and Validation of High Throughput Screening Assays. *J. Biomol. Screening* 4, 67–73.
- (46) Petersson, E. J., Goldberg, J. M., and Wissner, R. F. (2014) On the use of thioamides as fluorescence quenching probes for tracking protein folding and stability. *Phys. Chem. Chem. Phys.* 16, 6827–6837.
- (47) Goldberg, J. M., Batjargal, S., and Petersson, E. J. (2010) Thioamides as fluorescence quenching probes: minimalist chromophores to monitor protein dynamics. *J. Am. Chem. Soc.* 132, 14718–14720.
- (48) Wissner, R. F., Batjargal, S., Fadzen, C. M., and Petersson, E. J. (2013) Labeling proteins with fluorophore/thioamide Förster resonant energy transfer pairs by combining unnatural amino acid mutagenesis and native chemical ligation. *J. Am. Chem. Soc.* 135, 6529–6540.
- (49) Ononye, S. N., VanHeyst, M. D., Oblak, E. Z., Zhou, W., Ammar, M., Anderson, A. C., and Wright, D. L. (2013) Tropolones as lead-like natural products: the development of potent and selective histone deacetylase inhibitors. *ACS Med. Chem. Lett.* 4, 757–761.
- (50) Marek, L., Hamacher, A., Hansen, F. K., Kuna, K., Gohlke, H., Kassack, M. U., and Kurz, T. (2013) Histone deacetylase (HDAC) inhibitors with a novel connecting unit linker region reveal a selectivity profile for HDAC4 and HDAC5 with improved activity against chemoresistant cancer cells. *J. Med. Chem.* 56, 427–436.
- (51) Choi, S. Y., Kee, H. J., Sun, S., Seok, Y. M., Ryu, Y., Kim, G. R., Kee, S.-J., Pflieger, M., Kurz, T., Kassack, M. U., and Jeong, M. H. (2019) Histone deacetylase inhibitor LMK235 attenuates vascular constriction and aortic remodelling in hypertension. *J. Cell. Mol. Med.* 23, 2801–2812.
- (52) Gurard-Levin, Z. A., Kilian, K. A., Kim, J., Bähr, K., and Mrksich, M. (2010) Peptide arrays identify isoform-selective substrates for profiling endogenous lysine deacetylase activity. *ACS Chem. Biol.* 5, 863–873.
- (53) Lobera, M., Madauss, K. P., Pohlhaus, D. T., Wright, Q. G., Trocha, M., Schmidt, D. R., Baloglu, E., Trump, R. P., Head, M. S., Hofmann, G. A., Murray-Thompson, M., Schwartz, B., Chakravorty, S., Wu, Z., Mander, P. K., Kruidenier, L., Reid, R. A., Burkhart, W., Turunen, B. J., Rong, J. X., Wagner, C., Moyer, M. B., Wells, C., Hong, X., Moore, J. T., Williams, J. D., Soler, D., Ghosh, S., and Nolan, M. A. (2013) Selective class IIa histone deacetylase inhibition via a nonchelating zinc-binding group. *Nat. Chem. Biol.* 9, 319–325.
- (54) Heimburg, T., Kolbinger, F. R., Zeyen, P., Ghazy, E., Herp, D., Schmidtkunz, K., Melesina, J., Shaik, T. B., Erdmann, F., Schmidt, M., Romier, C., Robaa, D., Witt, O., Oehme, I., Jung, M., and Sippl, W. (2017) Structure-Based Design and Biological Characterization of Selective Histone Deacetylase 8 (HDAC8) Inhibitors with Anti-Neuroblastoma Activity. *J. Med. Chem.* 60, 10188–10204.
- (55) Heimburg, T., Chakrabarti, A., Lancelot, J., Marek, M., Melesina, J., Hauser, A.-T., Shaik, T. B., Duclaud, S., Robaa, D., Erdmann, F., Schmidt, M., Romier, C., Pierce, R. J., Jung, M., and Sippl, W. (2016) Structure-Based Design and Synthesis of Novel Inhibitors Targeting HDAC8 from *Schistosoma mansoni* for the Treatment of Schistosomiasis. *J. Med. Chem.* 59, 2423–2435.
- (56) Hassig, C. A., Symons, K. T., Guo, X., Nguyen, P.-M., Annable, T., Wash, P. L., Payne, J. E., Jenkins, D. A., Bonnefous, C., Trotter, C., Wang, Y., Anzola, J. V., Milkova, E. L., Hoffman, T. Z., Dozier, S. J., Wiley, B. M., Saven, A., Malecha, J. W., Davis, R. L., Muhammad, J., Shiau, A. K., Noble, S. A., Rao, T. S., Smith, N. D., and Hager, J. H. (2008) KDS170, a novel mercaptoketone-based histone deacetylase inhibitor that exhibits broad spectrum antitumor activity in vitro and in vivo. *Mol. Cancer Ther.* 7, 1054–1065.
- (57) Balasubramanian, S., Ramos, J., Luo, W., Sirisawad, M., Verner, E., and Buggy, J. J. (2008) A novel histone deacetylase 8 (HDAC8)-specific inhibitor PCI-34051 induces apoptosis in T-cell lymphomas. *Leukemia* 22, 1026–1034.
- (58) Kaletsch, A., Pinkerneil, M., Hoffmann, M. J., Jaguva Vasudevan, A. A., Wang, C., Hansen, F. K., Wiek, C., Hanenberg, H., Gertzen, C., Gohlke, H., Kassack, M. U., Kurz, T., Schulz, W. A., and Niegisch, G. (2018) Effects of novel HDAC inhibitors on urothelial carcinoma cells. *Clin. Epigenet.* 10, 100.
- (59) Schutkowski, M., Jakob, M., Landgraf, G., Born, I., Neubert, K., and Fischer, G. (1997) Probing substrate backbone function in prolyl oligopeptidase catalysis—large positional effects of peptide bond monothioxylation. *Eur. J. Biochem.* 245, 381–385.
- (60) Fan, Y., and Scriba, G. K. E. (2010) Electrophoretically mediated microanalysis assay for sirtuin enzymes. *Electrophoresis* 31, 3874–3880.
- (61) Ohla, S., Beyreiss, R., Scriba, G. K. E., Fan, Y., and Belder, D. (2010) An integrated on-chip sirtuin assay. *Electrophoresis* 31, 3263–3267.
- (62) Blackwell, L., Norris, J., Suto, C. M., and Janzen, W. P. (2008) The use of diversity profiling to characterize chemical modulators of the histone deacetylases. *Life Sci.* 82, 1050–1058.
- (63) Liu, Y., Gerber, R., Wu, J., Tsuruda, T., and McCarter, J. D. (2008) High-throughput assays for sirtuin enzymes: a microfluidic mobility shift assay and a bioluminescence assay. *Anal. Biochem.* 378, 53–59.

- (64) Khan, A. N., and Lewis, P. N. (2005) Unstructured conformations are a substrate requirement for the Sir2 family of NAD-dependent protein deacetylases. *J. Biol. Chem.* 280, 36073–36078.
- (65) Du, J., Zhou, Y., Su, X., Yu, J. J., Khan, S., Jiang, H., Kim, J., Woo, J., Kim, J. H., Choi, B. H., He, B., Chen, W., Zhang, S., Cerione, R. A., Auwerx, J., Hao, Q., and Lin, H. (2011) Sirt5 is a NAD-dependent protein lysine demalonylase and desuccinylase. *Science (Washington, DC, U. S.)* 334, 806–809.
- (66) Marcotte, P. A., Richardson, P. R., Guo, J., Barrett, L. W., Xu, N., Gunasekera, A., and Glaser, K. B. (2004) Fluorescence assay of SIRT protein deacetylases using an acetylated peptide substrate and a secondary trypsin reaction. *Anal. Biochem.* 332, 90–99.
- (67) Tanner, K. G., Landry, J., Sternglanz, R., and Denu, J. M. (2000) Silent information regulator 2 family of NAD-dependent histone/protein deacetylases generates a unique product, 1-O-acetyl-ADP-ribose. *Proc. Natl. Acad. Sci. U. S. A.* 97, 14178–14182.
- (68) Jackson, M. D., and Denu, J. M. (2002) Structural identification of 2'- and 3'-O-acetyl-ADP-ribose as novel metabolites derived from the Sir2 family of beta-NAD+-dependent histone/protein deacetylases. *J. Biol. Chem.* 277, 18535–18544.
- (69) Khan, A. N., and Lewis, P. N. (2006) Use of substrate analogs and mutagenesis to study substrate binding and catalysis in the Sir2 family of NAD-dependent protein deacetylases. *J. Biol. Chem.* 281, 11702–11711.
- (70) Borra, M. T., and Denu, J. M. (2004) Quantitative Assays for Characterization of the Sir2 Family of NAD+-Dependent Deacetylases. In *Chromatin and chromatin remodeling enzymes* (Allis, C. D., Ed.) pp 171–187, Elsevier, Amsterdam.
- (71) McDonagh, T., Hixon, J., DiStefano, P. S., Curtis, R., and Napper, A. D. (2005) Microplate filtration assay for nicotinamide release from NAD using a boronic acid resin. *Methods (Amsterdam, Neth.)* 36, 346–350.
- (72) Hoffmann, K., Heltweg, B., and Jung, M. (2001) Improvement and validation of the fluorescence-based histone deacetylase assay using an internal standard. *Arch. Pharm.* 334, 248–252.
- (73) Rye, P. T., Frick, L. E., Ozbal, C. C., and Lamarr, W. A. (2011) Advances in label-free screening approaches for studying siruin-mediated deacetylation. *J. Biomol. Screening* 16, 1217–1226.
- (74) Fischer, F., Gertz, M., Suenkel, B., Lakshminarasimhan, M., Schutkowski, M., and Steegborn, C. (2012) Sirt5 deacetylation activities show differential sensitivities to nicotinamide inhibition. *PLoS One* 7, No. e45098.
- (75) Gurard-Levin, Z. A., Kim, J., and Mrksich, M. (2009) Combining mass spectrometry and peptide arrays to profile the specificities of histone deacetylases. *ChemBioChem* 10, 2159–2161.
- (76) Kuo, H.-Y., DeLuca, T. A., Miller, W. M., and Mrksich, M. (2013) Profiling deacetylase activities in cell lysates with peptide arrays and SAMDI mass spectrometry. *Anal. Chem.* 85, 10635–10642.
- (77) Castaneda, C. A., Lopez, J. E., Joseph, C. G., Scholle, M. D., Mrksich, M., and Fierke, C. A. (2017) Active Site Metal Identity Alters Histone Deacetylase 8 Substrate Selectivity: A Potential Novel Regulatory Mechanism. *Biochemistry* 56, 5663–5670.
- (78) Rauh, D., Fischer, F., Gertz, M., Lakshminarasimhan, M., Bergbrede, T., Aladini, F., Kambach, C., Becker, C. F. W., Zerweck, J., Schutkowski, M., and Steegborn, C. (2013) An acetylome peptide microarray reveals specificities and deacetylation substrates for all human siruin isoforms. *Nat. Commun.* 4, 2327.
- (79) Robers, M. B., Loh, C., Carlson, C. B., Yang, H., Frey, E. A., Hermanson, S. B., and Bi, K. (2011) Measurement of the cellular deacetylase activity of SIRT1 on p53 via Lantha Screen® technology. *Mol. BioSyst.* 7, 59–66.
- (80) Dudek, J. M., and Horton, R. A. (2010) TR-FRET biochemical assays for detecting posttranslational modifications of p53. *J. Biomol. Screening* 15, 569–575.
- (81) Machleidt, T., Robers, M. B., Hermanson, S. B., Dudek, J. M., and Bi, K. (2011) TR-FRET cellular assays for interrogating posttranslational modifications of histone H3. *J. Biomol. Screening* 16, 1236–1246.
- (82) Degorce, F., Card, A., Soh, S., Trinquet, E., Knapik, G. P., and Xie, B. (2009) HTRF: A technology tailored for drug discovery - a review of theoretical aspects and recent applications. *Curr. Chem. Genomics* 3, 22–32.
- (83) Inoue, A., and Fujimoto, D. (1969) Enzymatic deacetylation of histone. *Biochem. Biophys. Res. Commun.* 36, 146–150.
- (84) Kölle, D., Brosch, G., Lechner, T., Lusser, A., and Loidl, P. (1998) Biochemical methods for analysis of histone deacetylases. *Methods (Amsterdam, Neth.)* 15, 323–331.
- (85) Taunton, J., Hassig, C. A., and Schreiber, S. L. (1996) A mammalian histone deacetylase related to the yeast transcriptional regulator Rpd3p. *Science (Washington, DC, U. S.)* 272, 408–411.
- (86) Milne, J. C., Lambert, P. D., Schenk, S., Carney, D. P., Smith, J. J., Gagne, D. J., Jin, L., Boss, O., Perni, R. B., Vu, C. B., Bemis, J. E., Xie, R., Disch, J. S., Ng, P. Y., Nunes, J. J., Lynch, A. V., Yang, H., Galonek, H., Israelian, K., Choy, W., Iffland, A., Lavu, S., Medvedik, O., Sinclair, D. A., Olefsky, J. M., Jirousek, M. R., Elliott, P. J., and Westphal, C. H. (2007) Small molecule activators of SIRT1 as therapeutics for the treatment of type 2 diabetes. *Nature* 450, 712–716.
- (87) Wolfson, N. A., Pitcairn, C. A., Sullivan, E. D., Joseph, C. G., and Fierke, C. A. (2014) An enzyme-coupled assay measuring acetate production for profiling histone deacetylase specificity. *Anal. Biochem.* 456, 61–69.
- (88) Heltweg, B., Dequiedt, F., Verdin, E., and Jung, M. (2003) Nonisotopic substrate for assaying both human zinc and NAD+-dependent histone deacetylases. *Anal. Biochem.* 319, 42–48.
- (89) Toro, T. B., and Watt, T. J. (2015) KDAC8 substrate specificity quantified by a biologically relevant, label-free deacetylation assay. *Protein science: a publication of the Protein Society* 24, 2020–2032.
- (90) Baba, R., Hori, Y., Mizukami, S., and Kikuchi, K. (2012) Development of a fluorogenic probe with a transesterification switch for detection of histone deacetylase activity. *J. Am. Chem. Soc.* 134, 14310–14313.
- (91) Baba, R., Hori, Y., and Kikuchi, K. (2015) Intramolecular long-distance nucleophilic reactions as a rapid fluorogenic switch applicable to the detection of enzymatic activity. *Chem. - Eur. J.* 21, 4695–4702.
- (92) Rooker, D. R., Klyubka, Y., Gautam, R., Tomat, E., and Buccella, D. (2018) Peptide-Based Fluorescent Probes for Deacetylase and Decrotonylase Activity: Toward a General Platform for Real-Time Detection of Lysine Deacetylation. *ChemBioChem* 19, 496–504.
- (93) Liu, X., Xiang, M., Tong, Z., Luo, F., Chen, W., Liu, F., Wang, F., Yu, R.-Q., and Jiang, J.-H. (2018) Activatable Fluorescence Probe via Self-Immolation Intramolecular Cyclization for Histone Deacetylase Imaging in Live Cells and Tissues. *Anal. Chem.* 90, 5534–5539.
- (94) Xie, Y., Ge, J., Lei, H., Peng, B., Zhang, H., Wang, D., Pan, S., Chen, G., Chen, L., Wang, Y., Hao, Q., Yao, S. Q., and Sun, H. (2016) Fluorescent Probes for Single-Step Detection and Proteomic Profiling of Histone Deacetylases. *J. Am. Chem. Soc.* 138, 15596–15604.
- (95) Yu, C., Wu, Y., Zeng, F., Li, X., Shi, J., and Wu, S. (2013) Hyperbranched polyester-based fluorescent probe for histone deacetylase via aggregation-induced emission. *Biomacromolecules* 14, 4507–4514.
- (96) Dhara, K., Hori, Y., Baba, R., and Kikuchi, K. (2012) A fluorescent probe for detection of histone deacetylase activity based on aggregation-induced emission. *Chem. Commun. (Cambridge, U. K.)* 48, 11534–11536.
- (97) Minoshima, M., Matsumoto, T., and Kikuchi, K. (2014) Development of a fluorogenic probe based on a DNA staining dye for continuous monitoring of the histone deacetylase reaction. *Anal. Chem.* 86, 7925–7930.
- (98) Han, Y., Li, H., Hu, Y., Li, P., Wang, H., Nie, Z., and Yao, S. (2015) Time-resolved luminescence biosensor for continuous activity detection of protein acetylation-related enzymes based on DNA-sensitized terbium(III) probes. *Anal. Chem.* 87, 9179–9185.
- (99) Halley, F., Reinshagen, J., Ellinger, B., Wolf, M., Niles, A. L., Evans, N. J., Kirkland, T. A., Wagner, J. M., Jung, M., Gribbon, P., and Gul, S. (2011) A bioluminescent HDAC activity assay: validation and screening. *J. Biomol. Screening* 16, 1227–1235.

- (100) Dose, A., Jost, J. O., Spieß, A. C., Henklein, P., Beyermann, M., and Schwarzer, D. (2012) Facile synthesis of colorimetric histone deacetylase substrates. *Chem. Commun. (Cambridge, U. K.)* 48, 9525–9527.
- (101) Wegener, D., Hildmann, C., Riester, D., and Schwienhorst, A. (2003) Improved fluorogenic histone deacetylase assay for high-throughput-screening applications. *Anal. Biochem.* 321, 202–208.
- (102) Wegener, D., Hildmann, C., Riester, D., Schober, A., Meyer-Almes, F.-J., Deubzer, H. E., Oehme, I., Witt, O., Lang, S., Jaensch, M., Makarov, V., Lange, C., Busse, B., and Schwienhorst, A. (2008) Identification of novel small-molecule histone deacetylase inhibitors by medium-throughput screening using a fluorogenic assay. *Biochem. J.* 413, 143–150.
- (103) Ciossek, T., Julius, H., Wieland, H., Maier, T., and Beckers, T. (2008) A homogeneous cellular histone deacetylase assay suitable for compound profiling and robotic screening. *Anal. Biochem.* 372, 72–81.
- (104) Riester, D., Hildmann, C., Grünwald, S., Beckers, T., and Schwienhorst, A. (2007) Factors affecting the substrate specificity of histone deacetylases. *Biochem. Biophys. Res. Commun.* 357, 439–445.
- (105) Wegener, D., Wirsching, F., Riester, D., and Schwienhorst, A. (2003) A fluorogenic histone deacetylase assay well suited for high-throughput activity screening. *Chem. Biol.* 10, 61–68.
- (106) Lahm, A., Paolini, C., Pallaoro, M., Nardi, M. C., Jones, P., Neddermann, P., Sambucini, S., Bottomley, M. J., Lo Surdo, P., Carfi, A., Koch, U., De Francesco, R., Steinkuhler, C., and Gallinari, P. (2007) Unraveling the hidden catalytic activity of vertebrate class IIa histone deacetylases. *Proc. Natl. Acad. Sci. U. S. A.* 104, 17335–17340.
- (107) Galleano, I., Schiedel, M., Jung, M., Madsen, A. S., and Olsen, C. A. (2016) A Continuous, Fluorogenic Sirtuin 2 Deacetylase Assay: Substrate Screening and Inhibitor Evaluation. *J. Med. Chem.* 59, 1021–1031.
- (108) Roessler, C., Tüting, C., Meleshin, M., Steegborn, C., and Schutkowski, M. (2015) A Novel Continuous Assay for the Deacetylase Sirtuin 5 and Other Deacetylases. *J. Med. Chem.* 58, 7217–7223.
- (109) Toro, T. B., Bryant, J. R., and Watt, T. J. (2017) Lysine Deacetylases Exhibit Distinct Changes in Activity Profiles Due to Fluorophore Conjugation of Substrates. *Biochemistry* 56, 4549–4558.
- (110) Kawaguchi, M., Ikegawa, S., Ieda, N., and Nakagawa, H. (2016) A Fluorescent Probe for Imaging Sirtuin Activity in Living Cells, Based on One-Step Cleavage of the Dabcyl Quencher. *ChemBioChem* 17, 1961–1967.
- (111) Goldberg, J. M., Speight, L. C., Fegley, M. W., and Petersson, E. J. (2012) Minimalist probes for studying protein dynamics: thioamide quenching of selectively excitable fluorescent amino acids. *J. Am. Chem. Soc.* 134, 6088–6091.
- (112) Huang, Y., Ferrie, J. J., Chen, X., Zhang, Y., Szantai-Kis, D. M., Chenoweth, D. M., and Petersson, E. J. (2016) Electronic interactions of $i, i + 1$ dithioamides: increased fluorescence quenching and evidence for n -to- π^* interactions. *Chem. Commun. (Cambridge, U. K.)* 52, 7798–7801.
- (113) Goldberg, J. M., Wissner, R. F., Klein, A. M., and Petersson, E. J. (2012) Thioamide quenching of intrinsic protein fluorescence. *Chem. Commun. (Cambridge, U. K.)* 48, 1550–1552.
- (114) Wissner, R. F., Wagner, A. M., Warner, J. B., and Petersson, E. J. (2013) Efficient, Traceless Semi-Synthesis of α -Synuclein Labeled with a Fluorophore/Thioamide FRET Pair. *Synlett* 24, 2454–2458.
- (115) Goldberg, J. M., Chen, X., Meinhardt, N., Greenbaum, D. C., and Petersson, E. J. (2014) Thioamide-based fluorescent protease sensors. *J. Am. Chem. Soc.* 136, 2086–2093.
- (116) Goldberg, J. M., Batjargal, S., Chen, B. S., and Petersson, E. J. (2013) Thioamide quenching of fluorescent probes through photo-induced electron transfer: mechanistic studies and applications. *J. Am. Chem. Soc.* 135, 18651–18658.
- (117) Vannini, A., Volpari, C., Gallinari, P., Jones, P., Mattu, M., Carfi, A., De Francesco, R., Steinkuhler, C., and Di Marco, S. (2007) Substrate binding to histone deacetylases as shown by the crystal structure of the HDAC8-substrate complex. *EMBO Rep.* 8, 879–884.
- (118) Schutkowski, M., Wöllner, S., and Fischer, G. (1995) Inhibition of peptidyl-prolyl cis/trans isomerase activity by substrate analog structures: thioxo tetrapeptide-4-nitroanilides. *Biochemistry* 34, 13016–13026.
- (119) Zhang, Y., Füssel, S., Reimer, U., Schutkowski, M., and Fischer, G. (2002) Substrate-based design of reversible Pin1 inhibitors. *Biochemistry* 41, 11868–11877.
- (120) He, B., Du, J., and Lin, H. (2012) Thiosuccinyl peptides as Sirt5-specific inhibitors. *J. Am. Chem. Soc.* 134, 1922–1925.
- (121) He, B., Hu, J., Zhang, X., and Lin, H. (2014) Thiomyristoyl peptides as cell-permeable Sirt6 inhibitors. *Org. Biomol. Chem.* 12, 7498–7502.
- (122) Smith, B. C., and Denu, J. M. (2007) Mechanism-based inhibition of Sir2 deacetylases by thioacetyl-lysine peptide. *Biochemistry* 46, 14478–14486.
- (123) Mock, W. L., Chen, J. T., and Tsang, J. W. (1981) Hydrolysis of a thiopeptide by cadmium carboxypeptidase A. *Biochem. Biophys. Res. Commun.* 102, 389–396.
- (124) Bartlett, P. A., Spear, K. L., and Jacobsen, N. E. (1982) A thioamide substrate of carboxypeptidase A. *Biochemistry* 21, 1608–1611.
- (125) Bond, M. D., Holmquist, B., and Vallee, B. L. (1986) Thioamide substrate probes of metal-substrate interactions in carboxypeptidase A catalysis. *J. Inorg. Biochem.* 28, 97–105.
- (126) Campbell, P., and Nashed, N. T. (1982) Carboxypeptidase A catalyzed hydrolysis of thiopeptide and thioester analogs of specific substrates. An effect on k_{cat} for peptide, but not ester, substrates. *J. Am. Chem. Soc.* 104, 5221–5226.
- (127) Schutkowski, M., Neubert, K., and Fischer, G. (1994) Influence on proline-specific enzymes of a substrate containing the thioxoaminoacyl-prolyl peptide bond. *Eur. J. Biochem.* 221, 455–461.
- (128) Beattie, R. E., Elmore, D. T., Williams, C. H., and Guthrie, D. J. (1987) The behaviour of leucine aminopeptidase towards thiono-peptides. *Biochem. J.* 245, 285–288.
- (129) Bienvenue, D. L., Gilner, D., and Holz, R. C. (2002) Hydrolysis of thiono-peptides by the aminopeptidase from *Aeromonas proteolytica*: insight into substrate binding. *Biochemistry* 41, 3712–3719.
- (130) Gantt, S. L., Gattis, S. G., and Fierke, C. A. (2006) Catalytic activity and inhibition of human histone deacetylase 8 is dependent on the identity of the active site metal ion. *Biochemistry* 45, 6170–6178.
- (131) Kim, B., Pithadia, A. S., and Fierke, C. A. (2015) Kinetics and thermodynamics of metal-binding to histone deacetylase 8. *Protein science: a publication of the Protein Society* 24, 354–365.
- (132) Dowling, D. P., Gattis, S. G., Fierke, C. A., and Christianson, D. W. (2010) Structures of metal-substituted human histone deacetylase 8 provide mechanistic inferences on biological function. *Biochemistry* 49, 5048–5056.
- (133) Schultz, B. E., Misialek, S., Wu, J., Tang, J., Conn, M. T., Tahilramani, R., and Wong, L. (2004) Kinetics and comparative reactivity of human class I and class IIb histone deacetylases. *Biochemistry* 43, 11083–11091.

3.3 Continuous Sirtuin/HDAC (histone deacetylase) activity assay using thioamides as PET (Photoinduced Electron Transfer)-based fluorescence quencher

Matthes Zessin, Marat Meleshin, Zeljko Simic, Diana Kalbas, Miriam Arbach, Philip Gebhardt, Jelena Melesina, Sandra Liebscher, Frank Bordusa, Wolfgang Sippl, Cyril Bařinka und Mike Schutkowski

Bioorganic Chemistry, 2021, 117, 105425
DOI: <https://doi.org/10.1016/j.bioorg.2021.105425>

Abstract:

Histone deacylase 11 and human sirtuins are able to remove fatty acid-derived acyl moieties from the ϵ -amino group of lysine residues. Specific substrates are needed for investigating the biological functions of these enzymes. Additionally, appropriate screening systems are required for identification of modulators of enzymatic activities of HDAC11 and sirtuins. We designed and synthesized a set of activity probes by incorporation of a thioamide quencher unit into the fatty acid-derived acyl chain and a fluorophore in the peptide sequence. Systematic variation of both fluorophore and quencher position resulted “super-substrates” with catalytic constants of up to $15,000,000 \text{ M}^{-1}\text{s}^{-1}$ for human sirtuin 2 (Sirt2) enabling measurements using enzyme concentrations down to 100 pM in microtiter plate-based screening formats. It could be demonstrated that the stalled intermediate formed by the reaction of Sirt2-bound thiomristoylated peptide and NAD^+ has IC_{50} values below 200 pM.



Continuous Sirtuin/HDAC (histone deacetylase) activity assay using thioamides as PET (Photoinduced Electron Transfer)–based fluorescence quencher

Matthes Zessin^a, Marat Meleshin^b, Zeljko Simic^b, Diana Kalbas^b, Miriam Arbach^b, Philip Gebhardt^b, Jelena Melesina^a, Sandra Liebscher^c, Frank Bordusa^c, Wolfgang Sippl^a, Cyril Barinka^d, Mike Schutkowski^{b,*}

^a Department of Medicinal Chemistry, Institute of Pharmacy, Martin Luther University Halle-Wittenberg, Halle/Saale, Germany

^b Department of Enzymology, Charles Tanford Protein Center, Institute of Biochemistry and Biotechnology, Martin Luther University Halle-Wittenberg, Halle/Saale, Germany

^c Department of Natural Product Biochemistry, Charles Tanford Protein Center, Institute of Biochemistry and Biotechnology, Martin Luther University Halle-Wittenberg, Halle/Saale, Germany

^d Institute of Biotechnology of the Czech Academy of Sciences, BIOCEV, Prumyslova 595, 252 50 Vestec, Czech Republic

ARTICLE INFO

Keywords:

Sirtuin assay
HDAC11 assay
Thioamide
Photoinduced electron transfer quenching
Microtiter plate-based screening
Histone deacetylase (HDAC) inhibitor

ABSTRACT

Histone deacetylase 11 and human sirtuins are able to remove fatty acid-derived acyl moieties from the ε-amino group of lysine residues. Specific substrates are needed for investigating the biological functions of these enzymes. Additionally, appropriate screening systems are required for identification of modulators of enzymatic activities of HDAC11 and sirtuins. We designed and synthesized a set of activity probes by incorporation of a thioamide quencher unit into the fatty acid-derived acyl chain and a fluorophore in the peptide sequence. Systematic variation of both fluorophore and quencher position resulted “super-substrates” with catalytic constants of up to 15,000,000 M⁻¹s⁻¹ for human sirtuin 2 (Sirt2) enabling measurements using enzyme concentrations down to 100 pM in microtiter plate-based screening formats. It could be demonstrated that the stalled intermediate formed by the reaction of Sirt2-bound thiomirystoylated peptide and NAD⁺ has IC₅₀ values below 200 pM.

1. Introduction

Acylation of lysine side chains in proteins is a widespread post-translational modification regulated by the action of acyltransferases or by the existing metabolic situation. Reversal of such lysine acylations is mediated by evolutionary conserved enzymes known as histone deacetylases (HDACs). Based on sequence homology, HDACs can be divided into 4 classes. Members of class I (HDAC 1, 2, 3, and 8), class IIa (HDAC4, 5, 7 and 9), class IIb (HDAC6 and 10), and class IV (HDAC11) are Zn²⁺ dependent hydrolases, while class III proteins (called sirtuins; Sirt1 – 7) use NAD⁺ as a co-substrate. They transfer the acyl moiety to the ADP-ribosyl fragment of the co-substrate thereby generating 2-O-acetyl-ADP-ribose and nicotinamide as the third reaction product [1].

Enzymatic activity of HDACs is involved in various (patho)physiological processes including cancer progression, regulation of obesity and immune function. Therefore, several HDAC inhibitors have been approved by the Food and Drug Administration for the treatment of cancer (vorinostat, romidepsin, belinostat, and panobinostat) and a number of clinical trials with sirtuin inhibitors (either natural products or synthetic small molecules) have been started to evaluate their efficacy. Robust and continuous sirtuin/HDAC activity assays compatible with high-throughput screening (HTS) are still required for further drug development.

Several assays have been developed for the monitoring of sirtuin and HDAC activity as reviewed in references [2–3]. Most of these activity assays are discontinuous (HPLC-based or mass spectrometry-based

Abbreviations: TFA, trifluoroacetic acid; Mcm, 7-methoxy-coumaryl-L-alanine; Abz, 2-aminobenzoyl; Ac, acetyl; HTS, high-throughput screening. HDAC, histone deacetylase; Sirt, sirtuin; PET, photoinduced electron transfer.

* Corresponding author.

E-mail address: mike.schutkowski@biochemtech.uni-halle.de (M. Schutkowski).

<https://doi.org/10.1016/j.bioorg.2021.105425>

Received 20 July 2021; Received in revised form 7 October 2021; Accepted 9 October 2021

Available online 12 October 2021

0045-2068/© 2021 The Authors. Published by Elsevier Inc. This is an open access article under the CC BY license (<http://creativecommons.org/licenses/by/4.0/>).

assays) or suffering from complex reaction mixtures caused by coupled enzymatic or chemical reactions requiring additional control measurements. Determination of IC_{50} or K_i -values for inhibitors is therefore time-consuming and cumbersome. Nearly all sirtuins have demyristoylation activity [4] and recently it was shown that HDAC11 is a robust demyristoylase as well [5–7]. We were able to demonstrate that the replacement of a myristoylated lysine residue (Fig. 1B) in TNF α -derived substrate peptides by an N-(2-aminobenzoyl)-11-aminoundecanoylated lysine residue (Fig. 1C) generates a quasi-universal sirtuin substrate enabling continuous activity measurements by fluorescence [8]. Recently, we demonstrated that the same peptide derivative is suitable for recording of enzymatic activity of HDAC11, enabling re-evaluation of HDAC11 inhibitors [9]. Nevertheless, attempts to increase the size of the fluorophore in the acyl moiety of the acylated lysine residue of such substrates, in order to allow fluorescence measurements at longer wavelengths, lead to dramatically decreased catalytic efficiency for sirtuins [8] and HDAC11 [9]. Additionally, Kawaguchi *et al.* were able to show that Sirt1-3 and Sirt6 are able to recognize a DABCYL moiety in the acyl chain (Fig. 1D) enabling monitoring of sirtuin activity in living cells [10]. Recently, the DABCYL quencher was replaced by Disperse Red derivative (Fig. 1E) yielding fluorescence probes with improved substrate properties for sirtuin activity measurements [11]. In our search for small quenchers of fluorescence we found thioamides to be ideal candidates. Caused by the soft sulfur atom in the thioamide moiety fluorescence quenching is possible via a mechanism called photoinduced electron transfer (PET) [12]. The Petersson group used this quenching principle for monitoring of protein folding [12–15], recording of proteolytic activities [15–17], investigation of binding events [18] and recently for the analysis of mobility of polyproline ruler peptides [19]. Additionally, we demonstrated that replacement of the scissile bond in fluorescently labeled HDAC substrates by a thioamide bond enabled continuous activity determination of HDAC8 and HDAC11 (Fig. 1F) via

PET fluorescence quenching [3]. Unfortunately, amide to thioamide replacement to the scissile bond leads to very poor substrates for sirtuins because of the generation of a so-called stalled intermediate, slowing down the reaction rate dramatically [20], and thiomylristoyl residue (Fig. 1F) represents a key structural element of efficient inhibitors for Sirt1-3 and Sirt6 [21–23]. To circumvent this problem, we introduced a thioamide bond into the myristoylated lysine residue (Fig. 2, R4) and were able to show that such substrates are well recognized by sirtuins and HDAC11 following the assay principle shown in Fig. 1A. Moreover, incorporation of different fluorophores (Fig. 2) into the peptide chain in combination with thioacetylated 11-aminoundecanoyl lysine residues (Fig. 2, R4) yielded sirtuin and HDAC11 substrates with superior catalytic constants in a continuous and direct activity assay. Such "super-substrates" with catalytic constants of up to $15,000,000 \text{ M}^{-1}\text{s}^{-1}$ for Sirt2 are useful for microtiter plate-based screening in 1,536-well format with Z' -factors higher than 0.88.

2. Results

All the compounds were synthesized based on a short TNF α -derived peptides because this sequence was used as a model substrate [21,24–25] for different sirtuin isoforms (Fig. 2, 1a). Fmoc-based solid phase peptide chemistry was used in combination with the nosyl-protecting group enabling selective on-resin modification of the respective lysine side chain. All compounds have purity greater than 95% as determined by HPLC at 220 nm and showed the expected molecular mass (Figures S1-S26 and Table S1). Peptide 1a (Fig. 2) was reported to be a substrate for Sirt2 and Sirt3 with specificity constants of $53,000 \text{ M}^{-1}\text{s}^{-1}$ and $29,500 \text{ M}^{-1}\text{s}^{-1}$ [8], respectively, and represents the best Sirt6 substrate described so far [24]. The peptide derivatives were synthesized with selectively modified myristoyl residues. In a systematic work, we replaced two adjacent methylene groups by a thioamide group ranging from methylenes 3/4 to 13/14 (a thioamide scan) resulting in 11 peptides with the thioamide moiety in different positions (Table S2). Analyzing substrate properties of these derivatives with Sirt2, Sirt3, Sirt5 and Sirt6 we found that thioamide substitutions in the distal end of the acyl chain are well tolerated (Fig. S27) with an optimum spanning methylenes 11/12, 12/13 and 13/14. Because it was known that acylated 11-aminoundecanoylated lysine residues are well accepted by sirtuins [8] we focused on thioacetylated 11-aminoundecanoyl moieties in this work (R4, Fig. 2). To assess whether a bulky fluorescein residue attached to a cysteine side chain is accepted by sirtuins we generated a control peptide 4b (Fig. 2, R2). To our surprise the modified cysteine at the –2 position was well tolerated by both sirtuins and HDAC11 (Table 2). Additionally, we generated a control peptide 1b with a non-modified amino acid sequence but replacement of the myristoyl residue by the thioacetylated 11-aminoundecanoyl moiety (R4, Fig. 2) to analyze the effect of substitution of two adjacent methylene moieties by a thioamide group on HDAC activity. Again, we found no negative effect on substrate properties for sirtuins and HDAC11 (Table 2). Next, we systematically analyzed efficacy of fluorescein quenching by the thioamide moiety (Table 1) by moving the fluorescein-modified cysteine residue from –5 to +2 position (relative to the acylated lysine) of the substrate resulting in peptide derivatives 1–7 (Fig. 2). The quenching efficacy of these derivatives ranged from 35% for 2 to 48% for 6 (Table 1). As a control, we replaced the thioamide in the peptide 4 by an amide bond yielding 4c, thus abolishing fluorescence quenching as expected (Table 1). Moreover, we also investigated the quenching efficacy for different fluorophores in the +2 position because a bulky residue like fluorescein was well accepted. Therefore, we synthesized derivatives 8–11 and determined the differences in fluorescence as compared to the fully converted assay solution. We found weak quenching for the 7-nitrobenzoxadiazole fluorophore (11) and for the BODIPY 507/545 dye (8). Surprisingly, fluorescence of structurally related BODIPY FL dye in 9 was quenched by more than 50% by the thioamide moiety.

To improve the quenching, we simultaneously substituted two

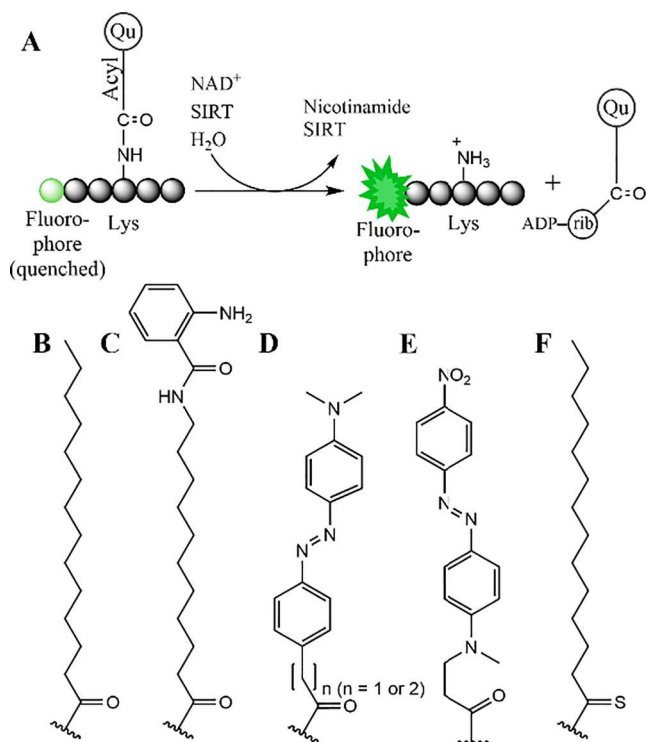


Fig. 1. Scheme of the sirtuin-mediated deacylation reaction. A shows a quencher (Qu)-containing acyl residue being transferred from the lysine side chain to ADP-ribose (ADP-rib) resulting in an increasing fluorescence intensity of the fluorophore incorporated in the peptide backbone. B. shows the naturally occurring myristoyl residue. C-G shows different acyl residues derived of the myristoyl residue used for HDAC/sirtuin activity assays.

"Fluorescein scan"

- 1 Ac-C(FI)ALPKK(R4)TGG-NH₂
- 2 Ac-E C(FI)LPKK(R4)TGG-NH₂
- 3 Ac-EAC(FI)PKK(R4)TGG-NH₂
- 4 Ac-EALC(FI)KK(R4)TGG-NH₂
- 5 Ac-EALPC(FI)K(R4)TGG-NH₂
- 6 Ac-EALPKK(R4)C(FI)GG-NH₂
- 7 Ac-EALPKK(R4)TC(FI)G-NH₂

Control peptides

- 1a Ac-EALPKK(R2)TGG-NH₂
- 1b Ac-EALPKK(R4)TGG-NH₂
- 4a Ac-EALC(FI)KK(R1)TGG-NH₂
- 4b Ac-EALC(FI)KK(R2)TGG-NH₂
- 4c Ac-EALC(FI)KK(R3)TGG-NH₂
- 4d Ac-EALC(FI)KK(R8)TGG-NH₂
- 7a Ac-EALPKK(R1)TC(FI)G-NH₂

Altering acyl residue

- 13 Ac-EALMcmKK(R5)TGG-NH₂
- 14 Ac-EALMcmKK(R6)TGG-NH₂
- 15 Ac-EALMcmKK(R7)TGG-NH₂
- 16 Ac-EALMcmKK(R8)TGG-NH₂
- 17 Ac-EALMcmKK(R9)TGG-NH₂

Altering fluorophore

- 8 Ac-EALPKK(R4)TC(Bp)G-NH₂
- 9 Ac-EALPKK(R4)TC(Bf)G-NH₂
- 10 Ac-EALPKK(R4)TC(Og)G-NH₂
- 11 Ac-EALPKK(R4)TC(Nbd)G-NH₂
- 12 Ac-EALMcmKK(R4)TGG-NH₂

Inhibitor

- 21 Ac-EALPKK(R11)TGG-NH₂

"Sirtuin 5 residue"

- 18 Ac-EALC(FI)KK(R10)TGG-NH₂
- 19 Ac-EALPKK(R10)TC(FI)G-NH₂
- 20 Ac-EALMcmKK(R10)TGG-NH₂

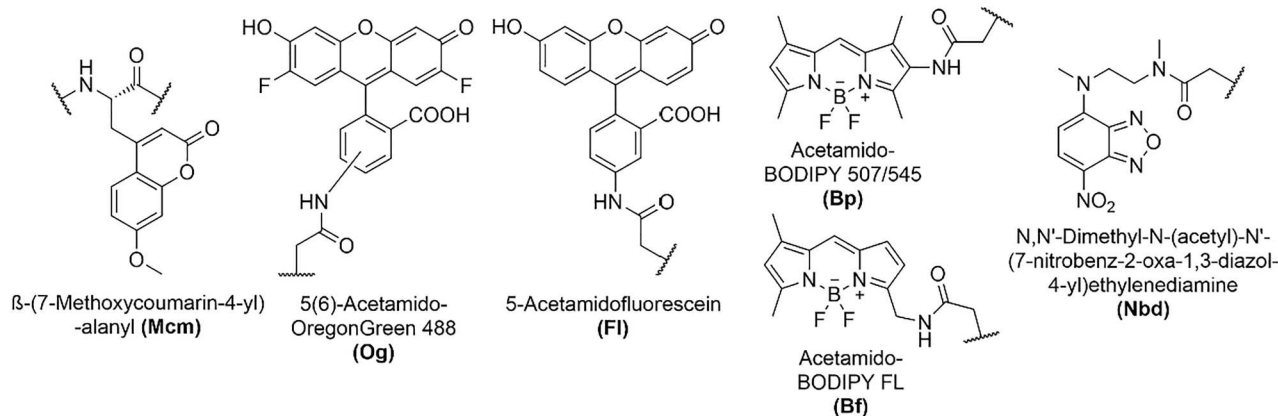
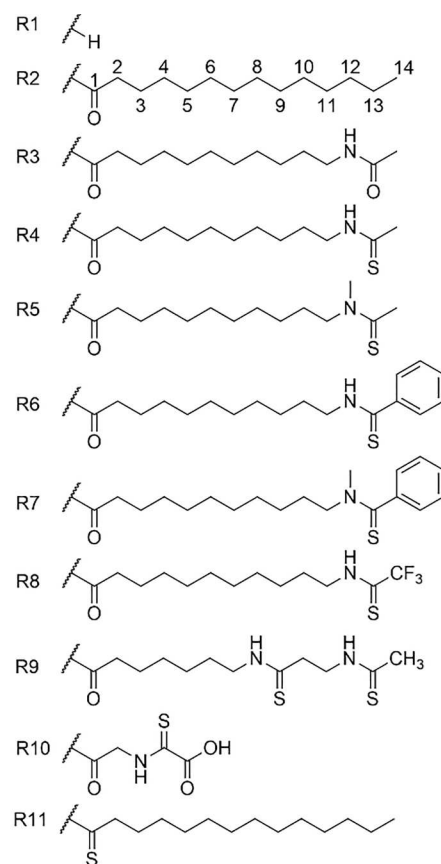


Fig. 2. Overview of the peptide derivatives used in this work. The peptide sequence is derived from TNF α (amino acids 15–22). The fluorophore was incorporated into the peptide backbone either via the cysteine side chain or as amino acid derivative Mcm. The acyl modification of the N^ε-amino group of the lysine residue is marked as R (right).

methylene units (7/8 and 12/13) by thioamide moieties in one acyl chain (Fig. 2, peptide 17). We selected the 7/8 position for the second thioamide in order to create a selective substrate because we had evidence that only Sirt2, but no other sirtuins can accommodate this modification (Fig. S27). As shown in Table 1 the additional second thioamide PET quencher increases the quenching efficacy to 71%.

Efficiency of fluorescence quenching by a PET mechanism, is dependent on the redox potential of both fluorophore and quencher. Additionally, fluorophore and quencher have to be in van der Waals contact to allow dynamic quenching by molecular collisions. In the case of thioamides as PET quencher the fluorophore will be reduced and the thioamide oxidized [26]. Quenching takes place if the free energy of electron transfer is negative [26]. Small structural changes can influence the reduction potential of the fluorophore or the oxidation potential of the thioamide quencher. In a systematic investigation Bordwell *et al.*

could show that the oxidation potential of thioamides could be fine-tuned by modification of both the residues at the thiocarbonyl and the residues at the thiocarbonyl carbon [27]. Substitution at the nitrogen and replacement of a methyl residue by a phenyl residue at the thiocarbonyl carbon increased the oxidation potential [27]. Inspired by this work we analyzed similar substitutions at the PET quencher thioamide moiety in peptide 12 (Fig. 2) which has a quenching efficiency of 55%. Incorporation of a tertiary thioamide bond by methylation of the thioamide nitrogen (Fig. 2 peptide 13) and replacement of the methyl residue at the thiocarbonyl carbon by a trifluoromethyl moiety (Fig. 2, peptide 16) did not improve the quenching efficiency significantly. In contrast, quenching efficiency is much better (Table 1) if a thiobenzoyl residue is attached to the 11-aminoundecanoyl residue (Fig. 2 peptide 14) or N-methylated 11-aminoundecanoyl residue at the lysine side chain (Fig. 2 peptide 15).

Table 1

Quenching efficiency. Q_E is represented as mean of Q_E at 0.5 μM , 1 μM , 1.5 μM , 2.5 μM using a microtiter plate reader to have assay conditions.

compound	Fluorophore	Q_E (%)
1	Fl	46.9
2	Fl	35.7
3	Fl	47.6
4	Fl	43.5
4c	Fl	-2.2
4d	Fl	50.3
5	Fl	46.8
6	Fl	48.3
7	Fl	48.1
8	Bp	6.7 ^a
9	Bf	24.1; 52.5 ^a
10	Og	45.0
11	Nbd	12.2 ^a
12	Mcm	55.1
13	Mcm	58.2
14	Mcm	75.6
15	Mcm	77.2
16	Mcm	57
17	Mcm	71 ^a
18	Fl	7.1 ^a
19	Fl	10.3 ^a
20	Mcm	60.7 ^a

^a Q_E was determined as difference of fluorescence intensity of the peptide with and without lysine modification at emission maximum of the peptide without lysine modification.

Sirt5 is known to specifically hydrolyze malonylated, succinylated and glutarilated lysine residues [28–29]. Therefore, we incorporated a thioamide bond into the glutaryl residue resulting in peptides acylated with thiooxalylglycine (Fig. 2, peptides 18–20). This modification is accepted by human Sirt5 resulting in substrates with k_{cat}/K_M -values in the range of $1000 \text{ M}^{-1}\text{s}^{-1}$ (data not shown). Unfortunately, the quenching efficacy of fluorescein fluorescence in either -2 (18) or +2 position (19) is suboptimal, which is presumably caused by the relatively rigid structure of the thioamide-containing acyl moiety preventing efficient van der Waals contact with the fluorophore. Switching to the coumarin fluorophore in the -2 position (20), we observed 60% quenching of the fluorescence.

Table 2 summarizes the results of our substrates 1–17 treated with HDAC11 or sirtuins 2,3,5, and 6. HDAC11 accepted all substrates with similar turnover (60–90% within one hour). Sirt6 also recognizes all compounds as substrates regardless of the fluorophore position but with significantly lower turnover compared to Sirt2 and Sirt3. No compound was found to be cleaved more effectively through Sirt6 than the fluorescently labeled peptide with natural occurring myristoyl residue (4b). The highest conversion of the other compounds was seen of 4d and 11. Unfortunately, 11 is unusable for a fluorescence approach due to low quenching efficiency. Sirt2 and Sirt3 accept more or less all substrates with some preference for the fluorophore in the +2 position (7) and the -5 position (1), respectively. Also, the changes in the acyl residue (12–16) did not have a clear effect on the substrate preferences. Only compound 17 with two thioamide bonds in the acyl residue seems to be poorly recognized by Sirt3 and still accepted well by Sirt2. In contrast Sirt2 cleaves compound 7 very efficiently with full substrate conversion after 1 h. To our surprise, Sirt5 was able to accept thioamide containing derivatives 1–7 with clear preferences for fluorescein in +2 positions (7). Changing the fluorophore at this position (8–11) has nearly no influence on the cleavage rate of Sirt5. Changing the fluorophore at another position (12) and the acyl residue (13–17) the substrate conversion remains low.

To analyze the substrate properties in more details, we determined the kinetic constants for HDAC11 and Sirt2, 3 and 5 using a microtiter plate fluorescence reader (Table 3). HDAC11 accepts the substrates of the “fluorescein scan” (1–7) with k_{cat}/K_M -values between $13,400 \text{ M}^{-1}\text{s}^{-1}$ and $51,000 \text{ M}^{-1}\text{s}^{-1}$. The specificity constants for 4 is about 4–5-

Table 2

Substrate properties of peptide derivatives 1–20 for HDAC11 and different sirtuin isoforms. Data are represented in % of product formation ($n = 3$) subsequent to treatment with 50 nM HDAC11, 0.1 μM Sirt2, 0.1 μM Sirt3, 0.5 μM Sirt5, and 0.5 μM Sirt6, for 1 h at 37 °C. 0 means product formation < 0.2%. Graphical representation and additional 3 h timepoint are available in supporting information (Fig. S29-S30, Table S3).

compound	HDAC11	Sirt2	Sirt3	Sirt5	Sirt6
1	86 ± 4	60 ± 10	42 ± 4	1.7 ± 0.4	15 ± 1
1b	78 ± 4	16 ± 1	39 ± 1	29 ± 2	10 ± 1
2	84 ± 8	46 ± 3	28 ± 4	1.4 ± 0.5	17 ± 1
3	86 ± 3	43 ± 1	14 ± 1	1 ± 0.1	7.9 ± 0.4
4	89 ± 1	51 ± 7	10 ± 2	3.4 ± 0.6	9.3 ± 0.6
4b	67 ± 6	47 ± 5	46 ± 10	18 ± 3	31 ± 2
4c	69 ± 3	92 ± 5	6 ± 1	1.5 ± 0.1	9.8 ± 1.0
4d	80 ± 5	69 ± 1	29 ± 6	7.4 ± 1.3	22 ± 3
5	64 ± 5	53 ± 4	13 ± 2	1.1 ± 0.2	4.0 ± 0.1
6	81 ± 4	43 ± 6	12 ± 2	3.7 ± 0.6	11 ± 1
7	81 ± 11	100 ± 1	35 ± 5	26 ± 2	11 ± 2
8	83 ± 6	16 ± 1	41 ± 3	27 ± 2	11 ± 2
9	76 ± 7	29 ± 2	21 ± 2	24 ± 2	8.6 ± 2.0
10	84 ± 3	61 ± 4	36 ± 4	19 ± 2	7.7 ± 0.9
11	55 ± 2	16 ± 1	32 ± 1	40 ± 3	25 ± 2
12	89 ± 3	55 ± 5	17 ± 3	3 ± 1	7.6 ± 0.8
13	92 ± 1	69 ± 10	17 ± 2	1.2 ± 0.1	9.4 ± 0.9
14	79 ± 19	60 ± 7	14 ± 3	2.3 ± 0.5	6.7 ± 2.4
15	84 ± 1	50 ± 4	16 ± 3	1.7 ± 0.1	8.8 ± 0.5
16	56 ± 3	52 ± 3	19 ± 3	4.7 ± 0.1	12.6 ± 1.3
17	–	68 ± 5	4 ± 0.4	0.4 ± 0.03	2.4 ± 0.2
18	–	0	0	6.9 ± 0.1	0
19	–	10 ± 1	9.1 ± 0.2	7.3 ± 0.5	0
20	–	1.1 ± 0.2	0.20 ± 0.02	4 ± 0.2	0

fold higher compared to the continuous activity assay based on the same peptide sequence with the 2-aminobenzoylated 11-aminoundecanoyl residue (Fig. 1C) [9] and more than 8-fold higher as compared to a continuous substrate with the thiomristoyl residue (Fig. 1F) [3]. Changing the fluorophore in +2 from fluorescein to BODIPY FL (9) further improves the specificity constant, yielding the most efficient substrate for continuous HDAC11 activity measurements to date. Additionally, this specificity constant is 2.3-fold higher as compared to the myristoylated TNF α -substrate without any fluorophore [3]. As expected from the turnover measurements (Table 2), Sirt3 showed high specificity constants for substrates 1 and 7 with k_{cat}/K_M -values of $79,000 \text{ M}^{-1}\text{s}^{-1}$ and $36,000 \text{ M}^{-1}\text{s}^{-1}$, respectively. The value for 1 is about 28-fold higher as compared to the continuous activity assay based on a very similar peptide sequence with the 2-aminobenzoylated 11-aminoundecanoyl residue (Fig. 1C) [8]. The substrate properties of 7 and 9 for Sirt5 are remarkable. Fluorophores in the +2 position are accepted, resulting in specificity constants between $280 \text{ M}^{-1}\text{s}^{-1}$ and $420 \text{ M}^{-1}\text{s}^{-1}$, respectively. These values are much higher than values reported for non-negatively charged, acetylated substrates like acetylated CPS-1 derived substrate with k_{cat}/K_M -value $16 \text{ M}^{-1}\text{s}^{-1}$ [30].

Inspection of the data presented in Table 3 revealed that thioacylated 11-aminoundecanoyl residues in combination with fluorophores in the peptide sequence yielded “super-substrates” for Sirt2 mainly based on extremely low K_M -values. To our knowledge, resulting specificity constants between $6,800,000 \text{ M}^{-1}\text{s}^{-1}$ for 7 and $15,000,000 \text{ M}^{-1}\text{s}^{-1}$ for 14 represent values never reported so far for any sirtuin. Inspection of kinetic constants for 12 and 13 shows that *N*-methylation of the thioamide moiety has nearly no influence on recognition by HDAC11 or Sirt2. Additionally, substitution of the thioacetyl moiety in 12 and 13 by the more bulky and more hydrophobic thiobenzoyl residues (14 and 15, respectively) results in nearly five-fold better substrates for Sirt2 but not for HDAC11 (Table 3) pointing to differences in the recognition of the hydrophobic acyl chain by the enzymes. This can be explained by the high complementarity of obtained substrates with the Sirt2 substrate binding pocket. Molecular modeling showed that the amino acid residues of the substrates are making multiple hydrogen bonds at the

Table 3

Kinetic parameters for HDAC11 and different sirtuin isoforms measured with Platereader with fluorescence readout, HPLC or fluorescence spectrometer. Concentrations of enzyme used in the assay are shown in parentheses below the enzyme name. Data are represented as mean of 3 independent replicates \pm standard deviation. $v/[S]$ plots could be observed in the supporting information (Fig. S31 – Fig. S37).

Enzyme	Cmpd	K_M (μ M)	k_{cat} (s^{-1})	k_{cat}/K_M ($s^{-1}M^{-1}$)	
HDAC11 (10–20 nM)	1	8.2 \pm 0.5	0.22 \pm 0.01	2.7 $\times 10^4$	
	1*	9.2 \pm 2.6	0.34 \pm 0.01	3.6 $\times 10^4$	
	2	13 \pm 2	0.25 \pm 0.03	1.9 $\times 10^4$	
	3	24 \pm 3	0.59 \pm 0.04	2.5 $\times 10^4$	
	4	5.7 \pm 1.5	0.29 \pm 0.02	5.1 $\times 10^4$	
	4*	5.8 \pm 2.6	0.37 \pm 0.01	6.7 $\times 10^4$	
	5	16 \pm 2	0.22 \pm 0.02	1.3 $\times 10^4$	
	5*	13 \pm 1	0.15 \pm 0.01	1.1 $\times 10^4$	
	6	22 \pm 2	0.4 \pm 0.05	1.8 $\times 10^4$	
	7	14 \pm 3	0.25 \pm 0.04	2.7 $\times 10^4$	
	9	5.8 \pm 0.1	0.47 \pm 0.03	8.1 $\times 10^4$	
	10	13 \pm 2	0.23 \pm 0.03	1.8 $\times 10^4$	
	12	9.5 \pm 0.8	0.26 \pm 0.04	2.7 $\times 10^4$	
	13	3.4 \pm 0.2	0.089 \pm 0.017	2.6 $\times 10^4$	
	14	3.9 \pm 0.9	0.10 \pm 0.02	2.6 $\times 10^4$	
15	2.6 \pm 0.3	0.049 \pm 0.003	1.9 $\times 10^4$		
Sirt2 (0.5–2 nM)	1	0.010 \pm 0.001	0.011 \pm 0.002	1.1 $\times 10^6$	
	2	0.014 \pm 0.001	0.0099 \pm 0.0004	7.1 $\times 10^5$	
	3	0.010 \pm 0.002	0.013 \pm 0.001	1.3 $\times 10^6$	
	4	0.015 \pm 0.002	0.014 \pm 0.003	9.4 $\times 10^5$	
	4d	0.0058 \pm 0.0003	0.0063 \pm 0.001	1.1 $\times 10^6$	
	5	0.054 \pm 0.006	0.013 \pm 0.002	2.4 $\times 10^5$	
	6	0.035 \pm 0.004	0.011 \pm 0.001	2.9 $\times 10^5$	
	7	0.0053 \pm 0.001	0.036 \pm 0.007	6.8 $\times 10^6$	
	10	0.010 \pm 0.001	0.016 \pm 0.003	1.6 $\times 10^6$	
	12 ^a	0.0061 \pm 0.0003	0.019 \pm 0.001	3.0 $\times 10^6$	
	13 ^a	0.0044 \pm 0.0004	0.012 \pm 0.002	2.7 $\times 10^6$	
	14 ^a	0.0011 \pm 0.0001	0.017 \pm 0.002	15 $\times 10^6$	
	15 ^a	0.0012 \pm 0.0002	0.016 \pm 0.003	13 $\times 10^6$	
	16 ^a	0.0015 \pm 0.0003	0.010 \pm 0.001	6.4 $\times 10^6$	
	Sirt3 (10–20 nM)	1	0.28 \pm 0.01	0.022 \pm 0.003	7.9 $\times 10^4$
		7	0.56 \pm 0.01	0.020 \pm 0.003	3.6 $\times 10^4$
10		1.4 \pm 0.3	0.027 \pm 0.001	2.0 $\times 10^4$	
Sirt5 (0.5 μ M)	7	2 \pm 0.2	7.1 $\times 10^{-4} \pm 0.6 \times 10^{-4}$	3.5 $\times 10^2$	
	9	19 \pm 3	7.9 $\times 10^{-3} \pm 1.4 \times 10^{-3}$	4.2 $\times 10^2$	
	10	12 \pm 1	3.3 $\times 10^{-3} \pm 0.2 \times 10^{-3}$	2.8 $\times 10^2$	

* were measured using HPLC;

^a measured using fluorescence spectrometer.

entrance to the substrate binding pocket similar to the co-crystallized peptide. Meanwhile, the long thioacylated 11-aminoundecanoyl lysine residue is placed comfortably in the hydrophobic Sirt2 substrate binding pocket (Fig. 3A). Its scissile amide bond interacts with valine 233 and in the absence of the co-substrate is stabilized by a water molecule. The benzoyl substituent of **14** is embedded into the aromatic cage at the end of the pocket formed by amino acid residues Y139, F143 and F190. Interestingly, this aromatic cage is not observed in the substrate-bound conformation of Sirt3 (Fig. 3B) despite presence of the aromatic amino acid residues at the corresponding positions of the amino acid sequence (Y200, Y204 and F251). The hydrophobic acyl-lysine residues of the substrates point to the allosteric pocket and the benzoyl group of **14** is located near the solvent exposed exit of the tunnel surrounded by non-aromatic residues T150, P155 and D156.

As expected from the results of the “thioamide scan” **17** represents a

Table 4

IC₅₀ values. IC₅₀ values determined with 10 nM **7** and 500 pM Sirt2, 0.27 μ M **1** and 10 nM Sirt3, 2 μ M **7** and 0.5 μ M Sirt5 and 2 μ M **4** and 5 nM HDAC11. Data are represented as mean of 3 independent replicated \pm standard deviation. Dose response curves of IC₅₀ determination could be observed in the supporting information (Fig. S54 – Fig. S57).

Enzyme	Compound	IC ₅₀ (μ M) \pm SD (n = 3)	IC ₅₀ (μ M) reported
Sirt2	S2i5L	0.048 \pm 0.007	0.013 [32], 1.2 ^a [8]
	SirReal2	1.3 \pm 0.1	0.4 [31]
	SirReal2 (K _i)	0.68	0.22 [31]
Sirt3	NAM	198 \pm 31	377 [33], 186 ^a [8]
	3-Typ	168 \pm 4	38 [33]
Sirt5	DK5.1	3.5 \pm 0.8	1.6 [34]
	NAM	210 \pm 30	700 [35]
HDAC11	Trichostatin A (TSA)	2.6 \pm 0.3	0.014 [36], 0.017 [37], 0.025 [38], 0.031 [39], 0.015 [40], 32 [6], 10 [9], 22 [9]
	Panobinostat (LBH-589)	0.37 \pm 0.03	4.4 [27186676]
	Quisinosat (JNJ-26481585)	0.53 \pm 0.23	0.37 [41], 3.3 [9], 1.8 [9]
	CUDC-907	0.040 \pm 0.014	0.023 [9], 0.016 [9], 0.0054 [42]
	(Fimepinostat)		

^a calculated from K_i value.

good substrate for Sirt2 but is not accepted by Sirt3, Sirt5 and Sirt6 (Fig. S27).

We recorded the absorbance spectra for **4a**, **4**, and **4d** and found remarkable differences in the range of 490–502 nm (Fig. S38). In principle these differences are sufficient to monitor sirtuin and HDAC11 activity following absorption at 490 nm (Fig. S38–S41). Fig. 4A shows the fluorescence spectra of **4**, **4a** and **4c**. Fluorescence intensity is much lower for **4** as compared to **4a** and the quenching is dependent on the presence of the thioamide moiety. If the thioamide is replaced by an amide bond (**4c**) resulting fluorescence is similar to **4a**. The observed difference in fluorescence for the substrate and the peptidic cleavage product of the sirtuin reaction enabled recording of progress curves as demonstrated in Fig. 4B for substrate **7** in the presence of different concentrations of Sirt2. In control experiments no significant change in the fluorescence signal over time could be observed either without NAD⁺ in the presence of sirtuin or without sirtuin in the presence of NAD⁺ (Fig. S42). This indicated that the observed fluorescence change results directly from sirtuin-mediated deacylation and not from unspecific interactions between NAD⁺ and/or Sirt2 and **7**. The slope of the fluorescence increase at 535 nm is dependent on the enzyme concentration resulting in a linear correlation between Sirt2 amount and the reaction rate (Fig. 4C). We used a completely converted assay solution (controlled by LC-MS) for the generation of appropriate calibration curves (Fig. S43–S47). Based on the superior properties of substrate **7** we were able to monitor Sirt2 activity down to 0.1 nM concentration (Fig. 4C). Nevertheless, at such low concentrations of enzyme we had to include blocking reagents like bovine serum albumin (BSA) to the reaction solution in order to avoid unspecific binding and inactivation of enzyme and the peptides to the surface of the microtiter plate wells. Fig. 4D summarizes deacylation of substrate **7** by SIRT2 in buffers with increasing BSA concentrations. There, we found no sirtuin activity in the absence of BSA for Sirt2 (Fig. 4D) or Sirt3 (Fig. S48). Overall enzymatic activity is increased stepwise until BSA concentration of 1.3 mg/ml and reached a plateau at 2–3 mg/ml. Similar effects were observed for HDAC11 in previous work, where HDAC11 showed little or no enzyme activity without BSA in the buffer [9].

We measured Sirt2 activity at different concentrations of **7** in 96-, 384-, and 1536-well formats (Fig. 5A) in order to demonstrate the applicability of our newly developed assay to evaluate inhibitor efficacy in high-throughput screening campaigns. The resulting kinetic constants

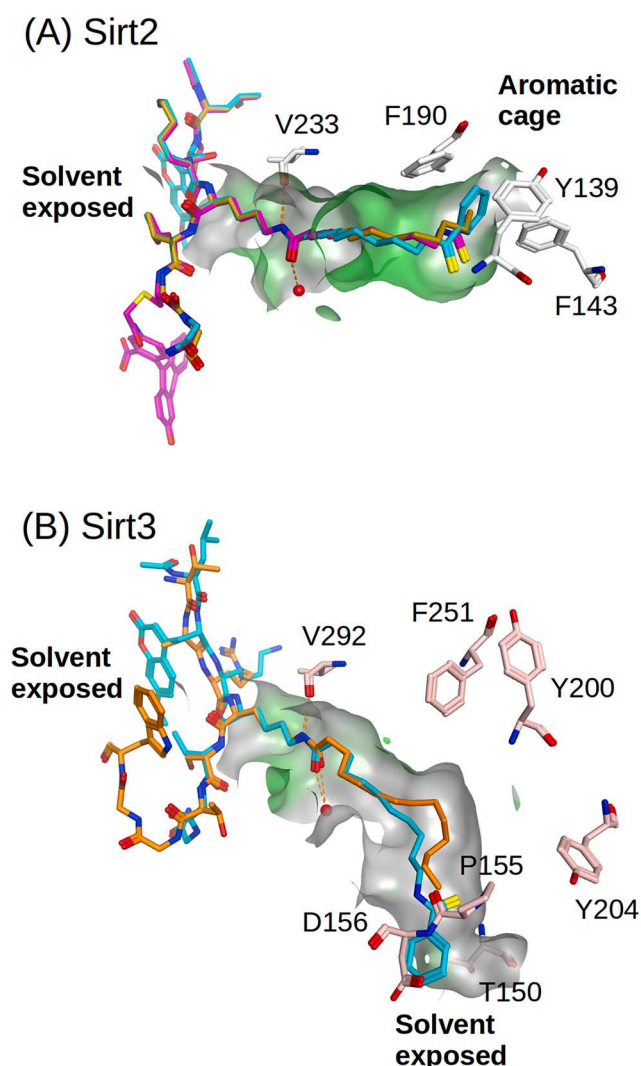


Fig. 3. Binding modes of peptide substrates **7** and **14** in Sirt2 PDB ID 4Y6O (A) and Sirt3 PDB ID 5BWN (B) derived from the docking study. The surface of the substrate binding pocket is colored green for hydrophobic areas and gray for neutral and hydrophilic zones. Relevant amino acid residues of the proteins are shown in stick representation and colored white for Sirt2 and pale pink for Sirt3. Peptide substrates are shown in stick representation with carbon atoms colored as followed: **7** – magenta, **14** – cyan, substrate co-crystallized with Sirt2 – mustard, peptide substrate co-crystallized with Sirt3 – orange. Heteroatoms are colored in a standard way: oxygen – red, nitrogen – blue, sulfur – yellow. Water molecule interacting with the scissile amide bond of the substrate is shown as a red ball. (For interpretation of the references to color in this figure legend, the reader is referred to the web version of this article.)

are comparable and the excellent statistical parameters of the assay Z' factor between 0.90 and 0.88 (and S/N ratio between 75 and 177) confirmed the high-throughput potential of the HDAC11/Sirt2 activity measurements (Fig. 5, Fig. S49–52, Table S4). Next, we profiled the inhibitory potencies of several known Sirt2 inhibitors, including SirReal2 [31] and the cyclic peptide derivative S2i5L [32], using **7** as the substrate. SirReal2 is competitive against the peptide substrate (Fig. 5B) with a K_i -value of 0.68 μM (Fig. 5C) which is in good agreement with the reported value of 0.22 μM [31]. Moreover, we examined inhibitory activity of compounds Trichostatin A (TSA), CUDC-907, Quisinostat, and Panobinostat against HDAC11 using substrate **4** in a 96-well format (Fig. 5D). Again, the determined IC_{50} values correlate well with values determined using a different fluorescence-based and continuous HDAC11 activity assay [9].

Thiomristoylated peptide derivatives represent effective Sirt2

inhibitors caused by the formation of a stalled intermediate reminiscent of a bisubstrate-analog inhibitor. The K_i value of thiomristoylated TNF α derived peptide **21** (Fig. 2) is 80 nM if the enzymatic reaction is started with Sirt2 [8]. Using the substrate **7** we obtained biphasic progress curves resembling slow-binding inhibition yielding IC_{50} values of 4.3 ± 0.6 and 0.9 ± 0.1 nM using either the first phase or the slower phase for calculation, respectively (Fig. S53). In order to determine the IC_{50} value starting off the preformed stalled intermediate we pre-incubated 250 pM Sirt2 with **21** and NAD^+ for 15 min. Starting the enzymatic reaction by adding **7** yielded linear progress curves and enabled us to determine an IC_{50} value of 180 ± 20 pM for the stalled intermediate (Fig. S53B). This value is very close to half-concentration of Sirt2 allowing the speculation, that the assay conditions are still limiting and that the “real” IC_{50} value for the stalled intermediate formed by **21** and ADP-ribose is lower than 180 pM.

If the quenching of the fluorescence is caused by a PET mechanism, the substrates have to be conformationally flexible to allow for the necessary van der Waals contact between the thioamide moiety and the excited fluorophore. On the other hand, quenching via PET should not be possible if the substrate is bound to the active site of Sirt2 due to the spatial separation of the thioamide group and the fluorophore (Fig. 3A). Therefore, we monitored fluorescence intensity of 10 nM **7** in the presence of increasing amounts of Sirt2 (up to 2 μM resulting in 200-fold excess of the enzyme over the substrate). Fig. 6A shows a clear increase in fluorescence depending on the enzyme concentration resembling a titration curve with an inflection point at about 12 nM which is very close to the K_M value of **7**. This observation encouraged us to develop a fluorescent indicator displacement assay for Sirt2. Using a preformed complex of 250 nM Sirt2 and 10 nM of **7** (25-fold excess of Sirt2) we were able to determine a competitive displacement value of 6.8 μM for SirReal2 (Fig. 6B). Using an alternative readout, we were able to show that the change in fluorescence polarization could be used too for determination of binding of **7** to Sirt2 (Fig. 6C) resulting in a similar inflection point like in the fluorescence intensity readout.

3. Discussion

Detection of sirtuin and HDAC activity is often coupled to a separation step enabling independent quantification of a peptidic substrate and a product. Separation methods are different, including capillary electrophoresis [43], microchip electrophoresis [44], microfluidic mobility [45–46], polyacrylamide gel electrophoresis [47], high-performance liquid chromatography [28,48–50], thin layer chromatography [51], charcoal binding [52], binding to boronic acid resins [53] and extraction with organic solvents [54]. Nevertheless, the resulting assay format is discontinuous and therefore not suited for high-throughput applications. Alternatively, mass spectrometry allows quantification of peptidic substrates and products subsequent to separation in the gas phase [35,55–57]. MALDI-MS readout in combination with peptide derivatives immobilized on glass surfaces was used for the systematic profiling of the substrate specificity of Sirt1, Sirt3, HDAC2, HDAC3, and HDAC8 [58–59]. Additionally, sirtuin/HDAC activity patterns could be determined in cell lysates using that technique [60]. Alternative approaches make use of reagents and chemical reactions for sensing either the acetylated substrates, like acetyllysine-recognizing antibodies, [61–66] or the reaction products, like chemical reactions modifying the released primary amino function of the lysine side chain. Such reactions could be acylations with biotin-containing compounds or fluorescent dyes [67], alkylations with fluorescamine [68] or intramolecular reactions, like transesterification with a coumarin dye [69–71], or release of bioluminescent luciferin subsequent to an intramolecular cleavage of an ester bond [72] or intramolecular aldimine formation [73–74]. Additionally, spontaneous chromophore maturation after deacetylation of lysine 85 in enhanced green fluorescent protein enables monitoring of sirtuin activities in living cells via increase in fluorescence [75]. Using a similar approach, active site lysine 529 was

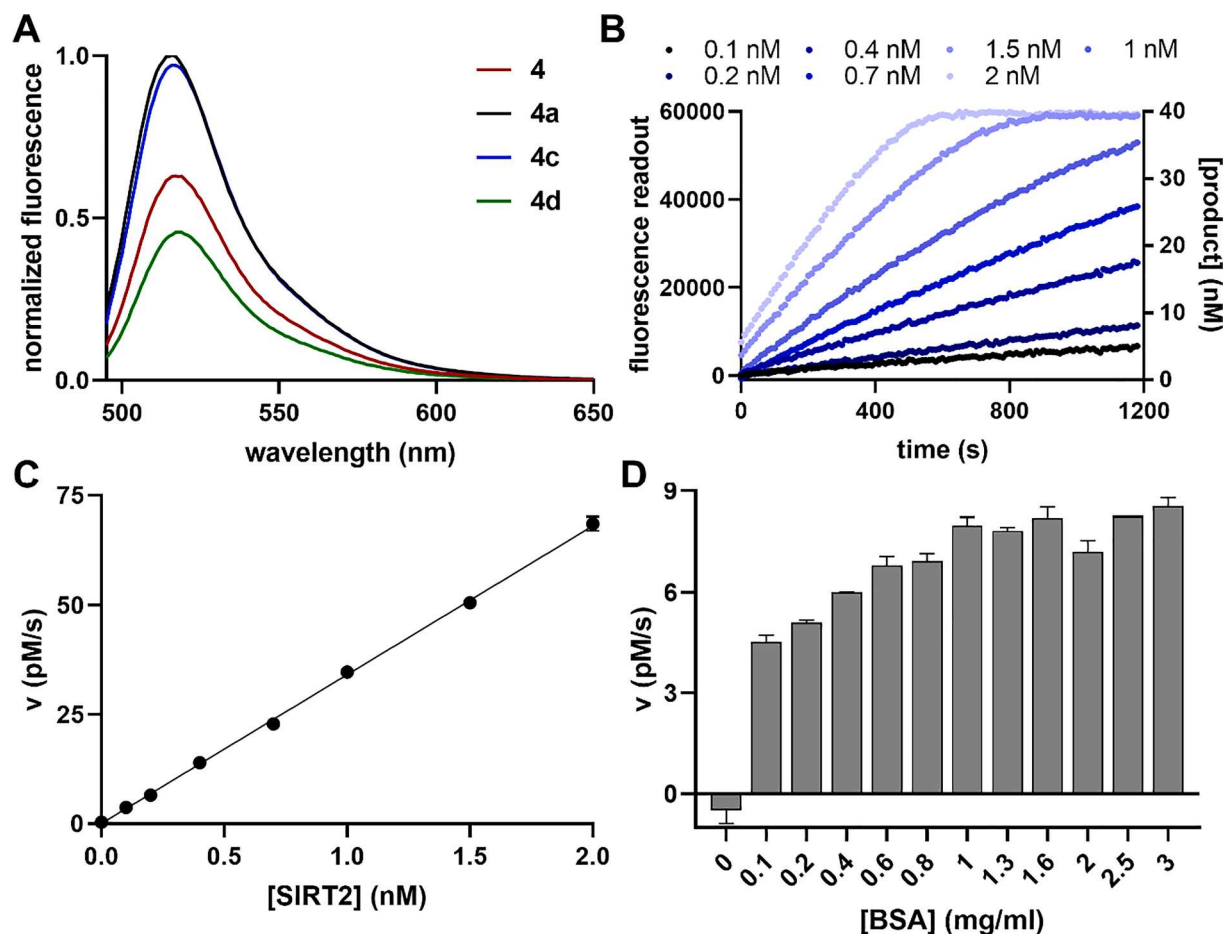


Fig. 4. A. Fluorescence spectra of 4a, 4, 4c, 4d at concentration of 1 μM . Excitation and emission wavelengths were set to 493 nm and 518 nm, respectively. B. Progress curves of Sirt2 mediated cleavage of 7 at 25 $^{\circ}\text{C}$ with 40 nM peptide, 500 μM NAD^+ , and different SIRT2 concentrations ranging from 0.1 to 2 nM. Fluorescence readout was corrected by a negative control without enzyme. Product concentration was calculated using a calibration line (Fig S44). The excitation wavelength was set to 485 ± 14 nm and the emission wavelength to 35 ± 25 nm. C. Reaction rate of 7 from panel B is linearly dependent on the Sirt2-concentration at 40 nM substrate concentration. Error bars show the standard deviation from triplicates of one experiment. D. Reaction rate of Sirt2 mediated cleavage of 7 as a function of BSA-concentration in the reaction mixture at 10 nM of 7 and a Sirt2 concentration of 250 pM.

replaced by acetylated lysine in firefly luciferase yielding an enzymatically inactive enzyme variant. Subsequent to treatment with different sirtuins deacetylation could be monitored in a continuous assay format by restored luciferase activity [76].

Alternatively, physical interactions of positively charged primary amino functions of lysine side chains with negatively charged molecules like DNA were used for monitoring of sirtuin/HDAC activity by aggregation-induced emission [77–78] and modulation of fluorescence properties [79–80].

It was demonstrated that substrates and products of sirtuin/HDAC reaction could be sensed by the coupling to enzymatic reactions either by using proteases, specific for the free lysine side chain of the peptidic product [48,81–83], by using combination of nicotinamidase/glutamate dehydrogenase for indirect spectrophotometric measurements of released nicotinamide [76] and by a cascade of enzymatic reactions to quantify the NAD^+ cosubstrate [46]. One advantage of monitoring the general product nicotinamide or the general cosubstrate NAD^+ is that it allows activity measurements independent of the nature of the peptide substrate. On the other hand, coupling the deacylase reaction to several enzymes makes the assay setup more complex, limits the linear range of the assay and makes the results more prone to artifacts caused by additional interaction of potential sirtuin/HDAC modulators with the coupling enzymes as demonstrated for the Sirt5 inhibitor GW5074 which affects enzymatic activity of the glutamate dehydrogenase [84].

Substrates used for protease coupled sirtuin/HDAC assays are often

fused to substituted coumarins, generating bright fluorescence subsequent to cleavage of the lysyl-coumaryl amide bond [85–90]. Suboptimal proteolytic stability of different HDACs against the used proteases prohibited a continuous assay format, but there are reports for some sirtuins that this assay could be performed in a continuous manner [91–92].

Most of the published sirtuin assays have the limitation, that the substrate properties for the different sirtuin isoforms are suboptimal with regard to both, K_M and k_{cat} values, resulting in k_{cat}/K_M values in the range of $10\text{--}10,000 \text{ M}^{-1}\text{s}^{-1}$. This demands relatively high substrate concentrations and the low k_{cat} values lead to assay protocols with sirtuin concentrations in the range of 500 nM (Sirt2) up to 2 μM for Sirt6 measurements. Such settings limit the validity of the Michaelis-Menten equation and exacerbate correct determination of IC_{50} values for inhibitors binding with high affinity.

In contrast to most HDACs, sirtuins are able to accept longer acyl chains at the lysine side chain [4]. Based on this observation, three fluorescence based and continuous activity assays without any coupling to enzymatic or chemical reaction have been developed for sirtuins [8,10–11]. Subsequently, a similar assay was adapted to monitor HDAC11 activity [9]. In all cases, a fluorophore (or a quencher) is fused to the acyl moiety linked to the lysine side chain. Resulting substrates have good properties for Sirt2 and HDAC11 with k_{cat}/K_M values up to $175,000 \text{ M}^{-1}\text{s}^{-1}$ and $11,000 \text{ M}^{-1}\text{s}^{-1}$, respectively [8]. Recently, we were able to show that replacing the scissile bond by a thioamide bond is

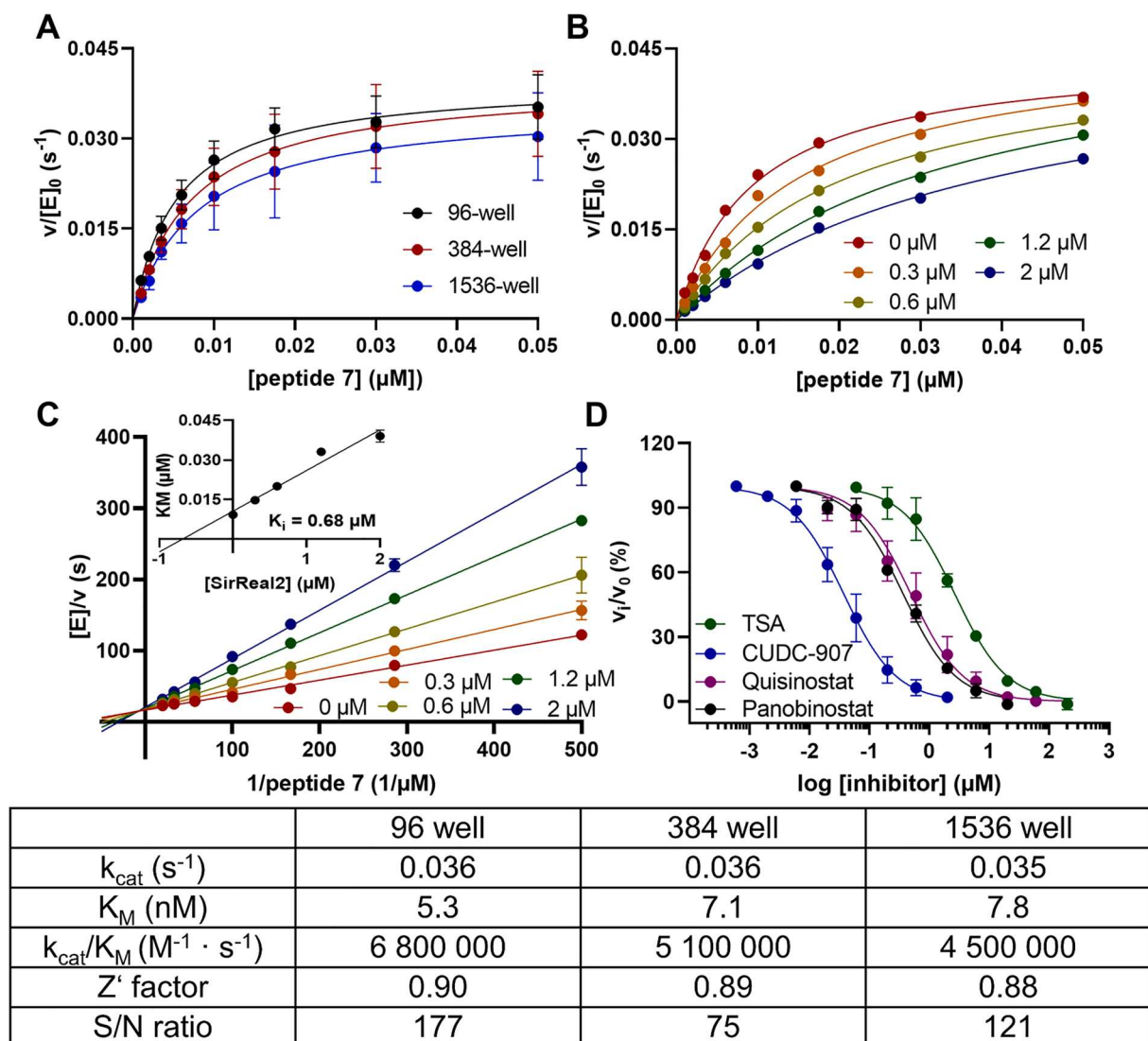


Fig. 5. A. $v/[S]$ plots of 500 pM Sirt2 with different concentrations of 7 and 500 μM NAD^+ in three different well plate types. The resulting kinetic constants, the Z'-factor and the S/N ratio are summarized in the table under the figure. B. $v/[S]$ plots of Sirt2 and 7 with different concentrations of the Sirt2 inhibitor SirReal2 with 500 pM Sirt2, 500 μM NAD^+ and altering concentrations of 7. C. Lineweaver-Burk plot of the steady-state kinetics of B, showing a competitive binding mode of the inhibitor SirReal2, resulting in a K_i value of 0.68 μM . Hanes-Woolf plot and Dixon plot of the inhibitor measurement are shown in the supporting information (Fig. S52). D. Dose-response curves of four known HDAC11 inhibitors using 5 nM HDAC11 and 2 μM of 4. The IC_{50} values are summarized in Table 4.

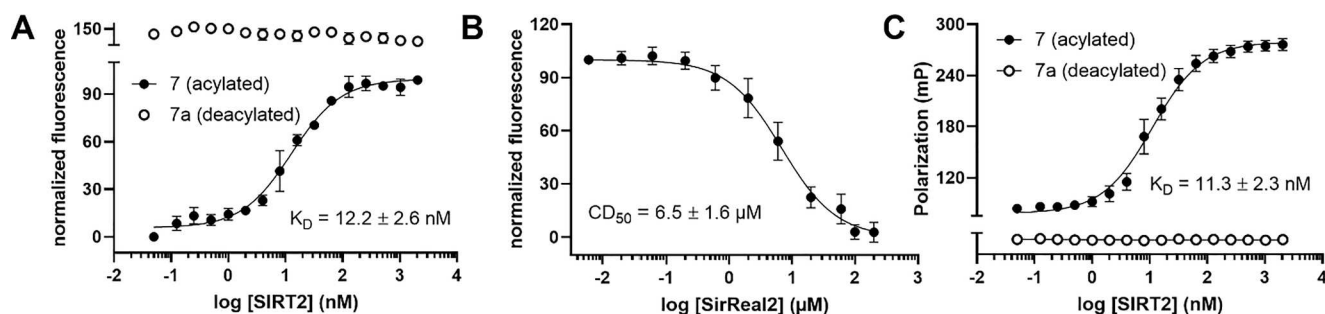


Fig. 6. A. Fluorescence change of 10 nM 7 or 7a subsequent to treatment with increasing amount of Sirt2 (0.05 nM to 2048 nM) but without NAD^+ . B. Binding curve of SirReal2 to Sirt2 generated by displacing 7 from Sirt2 which results in PET-based quenching of fluorescence intensity. The concentration of 7 was 10 nM and Sirt2 excess 25-fold (250 nM). C. Fluorescence polarization change of 10 nM 7 or 7a subsequent to treatment with increasing amount of Sirt2 (0.05 nM to 2048 nM) but without NAD^+ .

accepted by some HDAC isoforms yielding internally fluorescence-quenched HDAC8 super-substrates with $k_{\text{cat}}/K_{\text{M}}$ values up to $450,000 \text{ M}^{-1}\text{s}^{-1}$. A similar replacement in sirtuin substrates is not productive because of the dramatically reduced substrate properties [20]. Therefore, we wondered if we could artificially introduce a thioamide bond into the fatty acid chain of myristoylated peptides (Fig. 2).

In combination with a respective fluorophore in the peptide chain the thioacylated 11-aminoundecanoylated lysine derivatives SIRT2 shows extremely low K_{M} values down to 5.3 nM for **7** and with further minor modifications at the acyl residue down to 1.1 nM (**14**). Known K_{M} values for continuous assay substrates for SIRT2 are 120 nM [8], 520 nM [10] and 41 nM recently shown by Nakajima et al. [11]. Compared with those substrates the K_{M} values for SIRT2 for substrates published in this study are more than 8 to 40 times lower. In contrast, the k_{cat} value with 0.36 s^{-1} (for SIRT2 and **7**) do not decrease significantly despite the low K_{M} values and is comparable to the published k_{cat} value (0.24 s^{-1}) for the aminobenzoylated 11-aminoundecanoyl substrate [8] yielded in a 85 fold increased $k_{\text{cat}}/K_{\text{M}}$ value compared to this substrate.

Additionally, Sirt3, Sirt5 and Sirt6 are also able to recognize substrate **7**. Based on the low K_{M} value the "super-substrate" **7** allows measurements of the Sirt2 activity in a microtiter plate format with enzyme concentrations as low as 100 pM and substrate concentration of 10 nM. To the best of our knowledge this represents the most specific Sirt2 substrates described so far enabling highly effective microtiter plate-based inhibitor screening projects because of the reagent-saving and continuous nature of the assay format. Additionally, this substrate **7** represents a potential candidate for monitoring sirtuin 2 and HDAC11 activity in more complex biological fluids like cell lysates or within cells. Therefore, metabolic stability have to be increased because cleavages of peptide bonds between the fluorophore and the modified lysine residue by proteases will yield a fluorescence signal, too. One possibility is the replacement of single amino acid residues by either D-amino acids or N-methyl amino acids which are known to prevent proteolytic action. In a systematic study we were able to show that sirtuins can tolerate such modifications very well with the exception of the +1 position (data not shown). For cell-based experiments the metabolically stabilized substrate could be fused to oligo-arginines for better cell-penetration. We know that sirtuins recognize peptide substrate fused via the N-terminus to oligo(deca)-D-arginine (data not shown) opening the way of such substrates to be applied in living cells.

We could demonstrate that the underlying mechanism for substrate **7** is quenching by PET. Titrating **7** with Sirt2 in order to force **7** in an enzyme bound state increases the fluorescence up to a value of 70% fluorescence intensity of the corresponding peptide without PET Quencher (**7a**) or peptides derivatives having no PET quencher in their structure (**4c**). If the substrate **7** is bound to Sirt2 van der Waals contact between the thioamide bond and the fluorescein is not possible (Fig. 3A) preventing fluorescence quenching. Interestingly, this fluorescent substrate/enzyme complex could be used in a fluorescent indicator displacement assay format for fluorescence-based screening of inhibitors as demonstrated for the selective Sirt2 inhibitor SirReal2 (Fig. 6B).

In summary, we were able to demonstrate that fluorescence quenching by thioamides via a PET mechanism could be used for the development of highly efficient sirtuin and HDAC11 substrates which can be used for highly effective activity measurements using microtiter plate-based equipment. Moreover, PET mechanism allowed the development of an inhibitor screening based on either fluorescence polarization or fluorescent indicator displacement. Moreover, the developed substrates represent a starting point for the generation of probes enabling monitoring of sirtuin or HDAC11 activity in vivo.

4. Experimental section

4.1. Chemicals and general methods

All chemicals were purchased from Sigma-Aldrich (St. Louis, MO,

USA) if not described otherwise. *N,N*-dimethylformamide (DMF), piperidine, ethyl(hydroxyamino)cyanooacetate (OxymaPure), pentafluorophenol, and Rink amide MBHA were purchased from Iris Biotech (Marktredwitz, Germany). 9-fluorenylmethoxy-carbonyl- (Fmoc) protected amino acid derivatives and *O*-(Benzotriazol-1-yl)-*N,N,N',N'*-tetramethyluronium hexafluorophosphate (HBTU) were purchased from Merck (Darmstadt, Germany). Trifluoroacetic acid (TFA) was obtained from Roth (Karlsruhe, Germany). Fmoc-protected β -(7-methoxycoumarin-4-yl)-alanine (Mcm) was purchased from Bachem (Bubendorf, Switzerland). Fmoc-Lys(Ns)-OH, S2iL5 and DK5.1 were prepared as described before [8,34]. CUDC-907, JNJ-26481585 (Quisnostat), Panobinostat, 3-Typ, Trichostatin A and SirReal2 were purchased from Biomol (Hamburg, Germany). Fluorophores IANBD, 5-Iodoacetamido-fluorescein, BODIPY 507/545-iodoacetamide, BODIPY-FL iodoacetamide, OregonGreen488 iodoacetamide (mixed isomers) were obtained from Thermo Fisher Scientific (Waltham, Massachusetts, USA).

For all HPLC analysis and purifications a system of water supplemented with 0.1% TFA (solvent A) and acetonitrile (ACN) supplemented with 0.1% TFA (solvent B) was used. Analytical runs were performed on an Agilent 1100 system (Boeblingen, Germany) with a quaternary pump, a well-plate autosampler and a diode array detector. Separation was done with a linear gradient from 5% to 95% solvent B within 6 min and a flowrate of 0.6 ml/min on a $3.0 \times 50 \text{ mm}$ reversed phase column (Phenomenex Kinetex XB C-18, 2.6 μm). Purification of peptides was done on Shimadzu LC System with a Phenomenex Kinetex™ 5 μm XB-C18 ($250 \times 21.1 \text{ mm}$, 100 \AA) column using gradients ranging from 10% to 50% solvent B within 45 min to 25–80% solvent B.

UPLC-MS analysis was performed using either Waters Acquity UPLC-MS system or Waters XEVO TQD UPLC-MS system (Milford, USA) with a Waters Acquity-UPLC-MS-BEH C18; 1.7 μm ($2.1 \times 50 \text{ mm}$; 30 \AA) column. As a mobile phase 0.1% formic acid in H_2O (solvent A) and 0.1% formic acid in ACN (solvent B) solutions were used. Typical gradient from 95:5 (v/v) of H_2O :ACN to 5:95 (v/v) of H_2O :ACN in 6 min was used for the most of the runs. Data analysis was performed using Waters MassLynx software.

4.2. Peptide synthesis

All Peptides were synthesized using an automated microwave peptide synthesizer Liberty Blue™ (CEM Corporation, Matthews, NC, USA) and Fmoc-based solid phase peptide synthesis (SPPS). The amino acid coupling was performed twice and with DIC/OxymaPure for 2 min at 90 °C. Fmoc deprotection was done with 20% piperidine solution in DMF for 1 min at 90 °C. N-terminal acetylation was performed with an acetic anhydride/DIPEA/DMF (1:2:7) mixture for 1 h at room temperature.

4.2.1. Modification of ϵ -amino group of lysine

Myristoyl modification was introduced via SPPS as Fmoc-Lys(Myristoyl)-OH building block. Other modification of the ϵ -amino group of lysine were done on the resin after removal of 2-nitrobenzenesulfonyl (nosyl) group. Nosyl protecting group cleavage was done with a mixture of 1,8-diazabicyclo[5.4.0]undec-7-en (DBU)/thiophenol/DMF (1,5:1:7,5 v/v) ($2 \times 90 \text{ min}$). After washing with DMF, free lysine side chain was modified as described below. **1–12**: Resin was treated with Fmoc-11-aminoundecanoic acid (Fmoc-Aun-OH, 3 eq), HBTU (3 eq) and DIPEA (6 eq) in DMF for 1 h. After Fmoc deprotection (20% piperidine in DMF for $2 \times 10 \text{ min}$) and washing ($5 \times 5 \text{ min}$ with DMF), peptides were incubated with 4 eq of ethyl dithioacetate and 4 eq DIPEA in DMF for 1 h. **4a** and **7a**: nosyl protecting group was cleaved like described above. **4c**: After coupling of Fmoc-11-aminoundecanoic acid and Fmoc cleavage, peptide was incubated with an acetic anhydride/DIPEA/DMF (1:2:7) mixture for 1 h at room temperature. **4d** and **16**: After coupling of Fmoc-Aun-OH and Fmoc cleavage, resin was incubated with trifluorothioacetamide (5 eq) in DCM overnight. Then resin was incubated with a saturated solution of H_2S in tetrahydrofuran (THF) for 1 h. These

two steps were repeated once. **13**: After coupling of Fmoc-Aun-OH and Fmoc cleavage resin was incubated with 5 eq 2-nitrobenzenesulfonyl chloride and 10 eq 2,4,6-trimethylpyridine dissolved in *N*-methyl-2-pyrrolidone (NMP) for 15 min. After that, the resulted 2-nitrobenzenesulfonamide of Aun was methylated with triphenylphosphine (5 eq), methanol (MeOH, 10 eq) and diisopropyl azodicarboxylate (DIAD, 5 eq) in DMF for 2 × 30 min. The resin was incubated with 2-mercaptoethanol (10 eq) and DBU (5 eq) in DMF for 2 × 5 min. After washing with DMF resin was allowed to react with a solution of ethyl-dithioacetate (4 eq) and DIPEA (4 eq) overnight. **14**: After Fmoc-Aun-OH coupling and Fmoc-cleavage resin was incubated with *S*-(thiobenzoyl)thioglycolic acid (5 eq) and DIPEA (10 eq) overnight. **15**: After Fmoc-Aun-OH coupling and Fmoc-cleavage resin was incubated with 5 eq 2-nitrobenzenesulfonyl chloride and 10 eq 2,4,6-trimethylpyridine in NMP for 15 min. After that, the resulted nosylamide was methylated with triphenylphosphine (5 eq), MeOH (10 eq) and DIAD (5 eq) in DMF for 2 × 30 min. The resin was incubated with 2-mercaptoethanol (10 eq) and DBU (5 eq) in DMF for 2 × 5 min. After washing with DMF resin was incubated with *S*-(thiobenzoyl)thioglycolic acid (5 eq) and DIPEA (10 eq) overnight. **17**: After nosyl-group cleavage resin was treated with a solution of Fmoc-7-aminoheptanoic acid (4 eq), HBTU (4 eq) and DIPEA (8 eq) in DMF for 1 h, followed by Fmoc deprotection (20% piperidine in DMF, 2 × 10 min incubation) and washing 5 × 5 min with DCM. Then the resin was incubated with Fmoc-thio-β-alanyl-nitrobenzotriazole (3 eq) and DIPEA (1 eq) in DCM for 1 h at room temperature followed by an Fmoc cleavage (20% piperidine in DMF, 2 × 10 min incubation) and washing 5 × 5 min with DCM. Afterwards the resin was incubated with 4 eq ethyl dithioacetate and 4 eq DIPEA for 1 h. **18–20**: After nosyl-group cleavage resin was incubated with Fmoc-glycine (4 eq), HBTU (4 eq) and DIPEA (8 eq) in DMF for 1 h followed by Fmoc cleavage (20% piperidine in DMF, 2 × 10 min incubation) and washing (5 × 5 min) with DCM. Then the resin was treated with *O*-tert-butyl-*S*-methyl-1,1-dithiooxalate (2 eq) dissolved in DCM for 1 h.

4.2.2. Global deprotection

After finishing synthesis on the resin, the resin was washed several times with DCM, then several times with MeOH and again with DCM. The resin was further incubated 2 times for 90 min in a H₂O/TFA/triisopropylsilane (TIPS) [95:2.5:2.5 (v/v/v)] and the volatiles were removed *in vacuo*. The residue was dissolved in a solution of ACN/H₂O [50:50 (v/v)], filtrated and purified with HPLC. Fractions containing the pure peptide (analyzed by UPLC-MS) were united, frozen, and lyophilized. The purity of the lyophilized material was determined with UPLC-MS.

4.2.3. Fluorophore coupling

12–17, **20**: The Fmoc-β-(7-Methoxy-coumarin-4-yl)-Ala-OH was introduced in the peptide backbone while standard SPPS and were ready for further usage after the first purification with HPLC. **1–11**, **18**, **19**: The lyophilized peptide was dissolved DMF and incubated with a solution of the appropriate fluorophore (0.67 eq) and DIPEA (6 eq) for 1 h at room temperature. After complete reaction (verified via UPLC-MS) solution was directly injected in the HPLC system and fraction with pure peptide were combined (judged by UPLC-MS), frozen and, lyophilized. Purity and identity was determined with UPLC-MS.

4.3. Cloning, expression and purification of recombinant enzymes

HDAC11 was cloned, expressed and purified as described [9]. All sirtuin genes were synthesized by Biocat GmbH. Human Sirt5 (34–302) was cloned with protease-cleavable *N*-terminal StrepII-tag [93] into pET-21a(+) vector. Sirt2 (43–356), Sirt3 (114–380) and Sirt6 (1–355 homolog 1) were cloned with protease-cleavable *N*-terminal StrepII-tag into pET-28a(+)-vector. All sirtuins were expressed in *E. coli* BL21 (DE3) in LB media supplemented with ampicillin or kanamycin, respectively. Overexpression was induced by the addition of IPTG in a final

concentration of 0.5 mM at an OD600 of 0.6. Cells were harvested by centrifugation, resuspended in lysis buffer (100 mM Tris-HCl, 250 mM NaCl, 10 mM DTT, 1 mM EDTA, pH 8.0), and lysed by sonification. Cell debris was pelleted by ultracentrifugation and resulting supernatant was loaded onto a StrepTrap column (GE Healthcare, Uppsala, Sweden). The loaded column was intensively washed before elution with 5 mM des-thiobiotin in 100 mM Tris, 250 mM NaCl, pH 8.0. Sirtuin-containing fractions were concentrated and finally separated using a Superdex 75 5/150 gel filtration column (GE Healthcare) equilibrated with 100 mM HEPES, 150 mM NaCl, 10 mM CaCl₂, 1 mM TCEP pH 7.8. All buffers for chromatographic steps were filtrated (0.22 μM) and degassed. Identity and homogeneity were finally confirmed via SDS-Page and LC-MS analysis as depicted in supplementary figures S58 and S59.

4.4. Fluorescence and UV-measurements

The UV measurements were done in a cuvette with an optical path length of 10 mm and a compound concentration 10 μM for peptides **1** to **11**, **18**, **19** and 30 μM for **12** to **17** and **20** at 25 °C in a M500 spectrophotometer (Carl Zeiss, Jena, Germany). The background absorbance of the appropriate buffer was subtracted from all spectra measured. The fluorescence spectra were recorded at a Fluoromax4 (Horiba, Kyoto, Japan) with a compound concentration of 1 μM at 25 °C. The excitation wavelength, excitation slits and emission slits are summarized in Table 5.

4.5. Determination of quenching efficiency

For determination of the quenching efficiency (Q_E) the peptides and the corresponding products were used. The product peptides were produced enzymatically with 50 μM peptide, 500 μM NAD⁺ and 0.5 μM Sirt2 at 37 °C for 5 h. Full cleavage of peptides was confirmed with HPLC. The acylated peptides were treated in the same way but without enzyme. Q_E was determined in a black 96 well plate at 25 °C in a total volume of 100 μl at 0.5 μM, 1 μM, 1.5 μM and 2.5 μM final peptide concentration. Q_E was calculated with the following equation:

$$Q_E(\%) = 100 \frac{\text{product fluorescence} - \text{substrate fluorescence}}{\text{product fluorescence} - \text{background fluorescence}}$$

Background fluorescence is solution of Sirt2 and NAD⁺ in buffer without peptide. The Q_E presented in Table 1 is the mean of Q_E at these 4 concentrations. Q_E for peptide **8**, **9**, **11**, **17**, **18**, **19**, **20** was determined using the fluorescence spectra (Fig. S60-S65) where the product fluorescence is the fluorescence intensity at λ_{max} of the peptide without acyl residue and the substrate fluorescence represents the fluorescence intensity of the peptide (with acyl residue) at the same wavelength.

4.6. HPLC-based deacylation assay

Reactions were performed in a total volume of 70 μl in Sirt-assay buffer containing 20 mM Tris-HCl (pH 7.8), 140 mM NaCl, 10 mM KCl and 2 mg/ml BSA for Sirt2, Sirt3, Sirt5 and Sirt6 or in HDAC11-assay buffer containing 20 mM of phosphoric acid (pH 7.4, adjusted with NaOH) and 2 mg/ml BSA for HDAC11. The peptides with a final concentration of 50 μM and 500 μM NAD⁺ (only for sirtuins) were incubated for 5 min at 37 °C and the reaction was started with the addition of

Table 5
Settings for fluorescence measurements with Fluoromax 4.

Compound	λ _{Ex} (nm)	Exc slit (nm)	Em slit (nm)
1–7 , 10 , 18 , 19	492	0.5	2.5
12–17 , 20	334	1	5
8	507	0.5	5
9	502	0.5	3.5
11	502	1	10

enzyme ([HDAC11] = 50 nM, [Sirt2] = 100 nM, [Sirt3] = 100 nM, [Sirt5] = 500 nM and [Sirt6] = 500 nM final concentrations). After 1 h and after 3 h the reaction was quenched by addition of 1% TFA solution (final concentration at least 0.2%). Analysis of product formation was done with analytical HPLC. The quenched reaction solution was injected in the HPLC system (injection volume 40 μ l) and compounds were separated with a linear gradient 5–95% solvent B in 6 min. Analysis of product peak area and substrate peak area were done with Agilent software Chemstation at 220 nm for **1b**, at 320 nm for **12–17** and **20**, at 450 nm for **1–7**, **9**, **10**, **18** and **19** and at 505 nm for **8** and **11**. Product formation was calculated as the ratio of product peak area to total peak area.

4.7. Steady state measurements

4.7.1. Plate reader

The kinetic measurements were carried out in black 96-well plate with flat bottom. The reaction take place in a total volume of 100 μ l at 25 °C in HDAC11 assay buffer for HDAC11 and in Sirt-assay buffer for sirtuins (buffer composition as described above). For 384-well plate measurements a total volume of 20 μ l and for 1536-well plates a total volume of 10 μ l was used. Peptide substrates were dissolved in DMSO and the DMSO concentration was constant at 2% during the measurements. The peptide was incubated with 500 μ M NAD⁺ (only for sirtuins) in assay buffer for 5 min at 25 °C. The reaction was started with addition of enzyme. HDAC11 concentration was 10 nM for compounds **1** to **10** and 20 nM for **12–16** and peptide concentration varies between 0.25 μ M and 20 μ M. Sirt3 concentration was 20 nM and the peptide concentration varies between 0.05 and 3 μ M. The Sirt5 concentration was 0.5 μ M and the peptide concentration varies between 0.4 and 20 μ M. The Sirt2 concentration was set to 0.25–2 nM depending on the peptide substrate and the peptide concentrations varies between 0.5 nM and 400 nM. The product formation was monitored via the fluorescence intensity, recorded by an Envision 2104 Multilabel Plate Reader (PerkinElmer, Waltham, MA). The filter settings for **1** to **10** was $\lambda_{Ex} = 485 \pm 14$ nm and $\lambda_{Em} = 535 \pm 25$ nm and for **12** to **16** $\lambda_{Ex} = 330 \pm 75$ nm and $\lambda_{Em} = 405 \pm 8$ nm. The fluorescence intensity was plotted vs. the time and the initial slope of these curves represents the reaction rate. The fluorescence intensity was transformed to product concentration using calibration lines as difference between substrate and product fluorescence (Fig. S43–S47). The reaction rate was plotted against the substrate concentration and a nonlinear regression according to the Michaelis-Menten equation was used to determine K_M and k_{cat} values using GraphPad Prism 8 software (San Diego, CA). For determination of kinetic constants K_M and k_{cat} of the HDAC11 reaction with **1–8** and **10** Hanes-Woolf plot was used.

4.7.2. HPLC

The peptide (and 500 μ M NAD⁺ for Sirt2) was preincubated in the appropriate assay buffer (see above) at different concentrations (0.5–40 μ M HDAC11 and 0.25–4 μ M Sirt2) for 5 min at 25 °C in 1.5 ml reaction vessel. The reaction was started with the addition of enzyme (3 nM final concentration). After different time points (5–40 min) the reactions were quenched with 1% TFA (final concentration at least 0.2%). The HPLC-method (injection, separation gradient, detection, and quantification) was like described above. Product concentration was plotted as a function of time and the initial slope of these curves represent the reaction rate. Determination of K_M and k_{cat} values was done like described above with the nonlinear regression according to the Michaelis-Menten equation.

4.7.3. Fluorescence spectrometer

The sensitivity of the Envision Multilabel Plate Reader in this setting was not high enough to determine the K_M and k_{cat} for Sirt2 and **12–16**. The fluorescence spectrometer was the alternative. All measurements were done in a fluorescence cuvette with 10 mm \times 10 mm side length, at 25 °C in modified Sirt-assay buffer (20 mM Tris-HCl (pH 7.8), 140 mM

NaCl, 10 mM KCl and 0.2 mg/ml BSA) at the Fluoromax4 (Horiba, Kyōto, Japan). The reaction solution with peptide (0.25–40 nM) and 500 μ M NAD⁺ was incubated at 25 °C in the cuvette for 5 min. The reaction started with the addition of Sirt2 (2 nM for **12**, **13**, **16** and 1 nM for **14** and **15** final concentration). The product formation was monitored with increase of fluorescence intensity at $\lambda_{Ex} = 334$ nm and $\lambda_{Em} = 397$ nm with an excitation/emission slit at 2/10 nm for **12**, **13** and **16** and with an excitation/emission slit at 2.5/20 nm for **14** and **15**. The fluorescence intensity was plotted against the time and the further determination of K_M and k_{cat} values were done as described in the “Plate Reader” section.

4.8. Determination of inhibition constants (IC_{50} values)

The IC_{50} values were determined in a black 96-well plate (Grainer Bio-One) in a total assay volume of 100 μ l. For sirtuins the substrate was preincubated with altering concentrations of inhibitor and 0.5 mM NAD⁺ in Sirt-assay buffer (as described above) at 25 °C for 5 min. The reaction was started with the addition of enzyme (10% of the total volume). Sirt2 was used with 10 nM of **7** and 500 pM of Sirt2 for Sir-Real2 and S2iL5 and 250 pM for compound **21**. Sirt3 was used with 0.27 μ M **1** and 10 nM of Sirt3. Sirt5 was used with 0.5 μ M Sirt5 and 2 μ M of **7**. For HDAC11 the enzyme (5 nM final concentration) was incubated with different concentrations of inhibitor in HDAC11-assay buffer (as described above) and the reaction was started with the addition of compound **4** as substrate (final concentration 2 μ M). The product formation was monitored with the increase of the fluorescence intensity at $\lambda_{Ex} = 485 \pm 14$ nm and $\lambda_{Em} = 535 \pm 25$ nm in a Perkin Elmer Envision plate reader. The initial rates of product formation were obtained from a linear regression of the plot fluorescence intensity as a function of time. The initial rates were normalized with the uninhibited reaction as 100% and the reaction without enzyme as 0%. The IC_{50} values were calculated with the following nonlinear equation for normalized reaction rates of a dose response curve in GraphPad Prism 8 software from a plot normalized activity as a function of logarithm of inhibitor concentration.

$$Y = \frac{100}{1 + 10^{X - \log IC_{50}}}$$

4.9. Determination of Z' factor and S/N ratio

The Z' factor is a dimensionless statistical parameter to describe the quality of an HTS assay [94]. The Z' factor was calculated using the reaction rates of the Sirt2 deacylation reaction of **7** in different well plate types. The peptide concentration was chosen to be 10 nM like in the IC_{50} determination and 0.5 nM was the Sirt2 concentration. The fluorescence readout was done like described above (steady state measurements). The Z' factor was calculated with the following equation.

$$Z' = 1 - \frac{3SD_{100\%} + 3SD_{0\%}}{|mean_{100\%} - mean_{0\%}|}$$

Mean_{100%} was set as linear slope (reaction rate) of the reaction with 500 pM Sirt2, 500 μ M NAD⁺ and 10 nM **7** from a fluorescence intensity vs. time plot. Mean_{0%} is the negative control of this reaction without enzyme (SD100%) and for the negative control (SD0%) was calculated with n = 3 (samples in one plate) for 96-well plate and with n = 4 (samples in one plate) for 384- and 1536-well plate. The Z' factor presented in this work is the mean of 3 independent assay repeats (Fig. S63).

The signal/noise ratio (S/N) was calculated with the values described above and the following equation [94]:

$$S/N = \frac{mean_{100\%} - mean_{0\%}}{SD_{0\%}}$$

4.10. Binding studies, fluorescence polarization and fluorescence indicator displacement assay

A serial dilution of Sirt2 in Sirt-assay buffer was done with final concentrations from 0.25 nM to 2000 nM Sirt2. **7** was added with a final concentration of 10 nM and then transferred to a black 384-well plate (small volume) with a total volume of 20 μ l. The mixture was incubated for 10 min at 25 °C. The fluorescence readout was done with Envision 2104 Multilabel plate reader (PerkinElmer) with $\lambda_{Ex} = 485 \pm 14$ nm and $\lambda_{Em} = 535 \pm 25$ nm. The fluorescence intensity was normalized with **7** without Sirt2 as 0% and 2 μ M Sirt2 with **7** was set to 100%. The fluorescence polarization readout was done with $\lambda_{Ex} = 485 \pm 14$ nm, $\lambda_{Em} = 535 \pm 40$ nm (S-pol) and $\lambda_{Em} = 535 \pm 40$ nm (P-pol) with the PerkinElmer 2104 Envision Multilabel plate reader and calculation for polarization was done with the device software WallacEnvision Manager. Fluorescence indicator displacement assay was started with a serial dilution of the Sirt2 inhibitor SirReal2 in 5% DMSO in Sirt-assay-buffer from 200 μ M to 6 nM (final concentration). A mixture of 10 nM **7** and 250 nM Sirt2 (final concentration) was added to the inhibitor solution and transferred in a black 384-well plate and incubated for 10 min at 25 °C. Fluorescence readout was done like described above. The fluorescence was normalized with **7** without enzyme as 0% and **7** with Sirt2 but without inhibitor as 100%. Relative fluorescence was plotted as function of lg [inhibitor] and the CD_{50} was determined with the following nonlinear equation.

$$Y = \frac{Bottom + Top - Bottom}{1 + 10^{X - \log CD_{50}}}$$

4.11. Computational studies

Sirt2 (PDB ID 4Y6O, [95]) and Sirt3 (PDB ID 5BWN, [96]) protein structures in complex with myristoylated peptides were downloaded from the Protein Data Bank rcsb.org [97]. The protein structures were prepared by using the Structure Preparation module in MOE2012.01 [98]. Hydrogen atoms were added, for titratable amino acids the protonation state was calculated using the Protonate 3D module in MOE. Protein structures were energy minimized using the AMBER99 force field [99] using a tethering force constant of (3/2) kT / 2 ($\sigma = 0.5$ Å) for all atoms during the minimization. AM1-BCC charges were used for the studied ligands. All molecules except the zinc ion were removed from the structures. Protein-ligand docking was performed using program GOLD5.8.1 [100]. His187 (Sirt2) and His248 (Sirt3) were used to define the size of the grid box (20 Å radius). 100 docking poses were calculated for the docked peptide substrates. To reduce the conformational sampling for the flexible peptide's hydrogen bonds observed between the co-crystallized peptides and Sirt2/3 in the X-ray structures were considered as protein H-bond constraints in GOLD. All other options were left at their default values. One conserved water molecule interacting with the scissile amide bond was considered as part of the protein for the docking. This protocol was correctly reproducing the binding mode of the reference peptides (taken from the Sirt2-peptide complex PDB ID 4Y6O and Sirt3-peptide complex PDB ID 5BWN) with heavy atom RMSD values below 2.5 Å.

Funding

This work was supported by grants from Deutsche Forschungsgemeinschaft (INST 271/336-1 FUGG) to M.S., the Czech Science Foundation (21-31806S to C.B.), the CAS (RVO: 86652036 to C.B.).

Declaration of Competing Interest

The authors declare that they have no known competing financial interests or personal relationships that could have appeared to influence the work reported in this paper.

Acknowledgments

The authors thank Ilona Kunze for excellent technical support. Moreover, the authors are grateful to Petra Baranova and Zsofia Kutil for HDAC11 production. The authors thank Prof. Dr. Thomas Kieffhaber at the Martin Luther University Halle-Wittenberg for giving access to the single-quadrupole LC-MS analyses and the core facility proteomic mass spectrometry of the Martin-Luther University Halle-Wittenberg for technical assistance during the triple-quadrupole LC-MS experiments.

Appendix A. Supplementary material

Supplementary data to this article can be found online at <https://doi.org/10.1016/j.bioorg.2021.105425>.

References

- [1] B.C. Smith, W.C. Hallows, J.M. Denu, Mechanisms and molecular probes of sirtuins, *Chem. Biol.* 15 (10) (2008) 1002–1013, <https://doi.org/10.1016/j.chembiol.2008.09.009>.
- [2] M. Schutkowski, F. Fischer, C. Roessler, C. Steegborn, New assays and approaches for discovery and design of Sirtuin modulators, *Expert Opin. Drug Discov.* 9 (2) (2014) 183–199, <https://doi.org/10.1517/17460441.2014.875526>.
- [3] M. Zessin, Z. Kutil, M. Meleshin, Z. Nováková, E. Ghazy, D. Kalbas, M. Marek, C. Romier, W. Sippl, C. Barinka, M. Schutkowski, One-atom substitution enables direct and continuous monitoring of histone deacetylase activity, *Biochemistry* 58 (48) (2019) 4777–4789, <https://doi.org/10.1021/acs.biochem.9b00786>.
- [4] J.L. Feldman, J. Baeza, J.M. Denu, Activation of the protein deacetylase SIRT6 by long-chain fatty acids and widespread deacetylation by mammalian sirtuins, *J. Biol. Chem.* 288 (43) (2013) 31350–31356, <https://doi.org/10.1074/jbc.C113.511261>.
- [5] Z. Kutil, Z. Novakova, M. Meleshin, J. Mikesova, M. Schutkowski, C. Barinka, Histone deacetylase 11 is a fatty-acid deacetylase, *ACS Chem. Biol.* 13 (3) (2018) 685–693, <https://doi.org/10.1021/acschembio.7b00942>.
- [6] C. Moreno-Yruela, I. Galleano, A.S. Madsen, C.A. Olsen, Histone deacetylase 11 is an ϵ -N-myristoyllysine hydrolase, *Cell. Chem. Biol.* 25 (7) (2018) 849–856.e8, <https://doi.org/10.1016/j.chembiol.2018.04.007>.
- [7] J.i. Cao, L. Sun, P. Aramsangtienchai, N.A. Spiegelman, X. Zhang, W. Huang, E. Seto, H. Lin, HDAC11 regulates type I interferon signaling through defattyacylation of SHMT2, *Proc. Natl. Acad. Sci. U. S. A.* 116 (12) (2019) 5487–5492, <https://doi.org/10.1073/pnas.1815365116>.
- [8] S. Schuster, C. Roessler, M. Meleshin, P. Zimmermann, Z. Simic, C. Kambach, C. Schiene-Fischer, C. Steegborn, M.O. Hottiger, M. Schutkowski, A continuous sirtuin activity assay without any coupling to enzymatic or chemical reactions, *Sci. Rep.* 6 (2016) 22643, <https://doi.org/10.1038/srep22643>.
- [9] Z. Kutil, J. Mikešová, M. Zessin, M. Meleshin, Z. Nováková, G. Alquicer, A. Kozikowski, W. Sippl, C. Barinka, M. Schutkowski, Continuous activity assay for HDAC11 enabling reevaluation of HDAC inhibitors, *ACS Omega* 4 (22) (2019) 19895–19904, <https://doi.org/10.1021/acsomega.9b02808>.
- [10] M. Kawaguchi, S. Ikegawa, N. Ieda, H. Nakagawa, A fluorescent probe for imaging sirtuin activity in living cells, based on one-step cleavage of the dabcylic quencher, *Chembiochem* 17 (20) (2016) 1961–1967, <https://doi.org/10.1002/cbic.v17.2010.1002/cbic.201600374>.
- [11] Y. Nakajima, M. Kawaguchi, N. Ieda, H. Nakagawa, A set of highly sensitive sirtuin fluorescence probes for screening small-molecular sirtuin defattyacylation inhibitors, *ACS Med. Chem. Lett.* 12 (4) (2021) 617–624, <https://doi.org/10.1021/acsmchemlett.1c00010>.
- [12] E.J. Petersson, J.M. Goldberg, R.F. Wissner, On the use of thioamides as fluorescence quenching probes for tracking protein folding and stability, *Phys. Chem. Chem. Phys.* 16 (15) (2014) 6827–6837, <https://doi.org/10.1039/C3CP55525A>.
- [13] J.M. Goldberg, S. Batjargal, E.J. Petersson, Thioamides as fluorescence quenching probes: minimalist chromophores to monitor protein dynamics, *J. Am. Chem. Soc.* 132 (42) (2010) 14718–14720, <https://doi.org/10.1021/ja1044924>.
- [14] J.M. Goldberg, L.C. Speight, M.W. Fegley, E.J. Petersson, Minimalist probes for studying protein dynamics: thioamide quenching of selectively excitable fluorescent amino acids, *J. Am. Chem. Soc.* 134 (14) (2012) 6088–6091, <https://doi.org/10.1021/ja3005094>.
- [15] J.M. Goldberg, S. Batjargal, B.S. Chen, E.J. Petersson, Thioamide quenching of fluorescent probes through photoinduced electron transfer: mechanistic studies and applications, *J. Am. Chem. Soc.* 135 (49) (2013) 18651–18658, <https://doi.org/10.1021/ja409709x>.
- [16] J.M. Goldberg, X. Chen, N. Meinhardt, D.C. Greenbaum, E.J. Petersson, Thioamide-based fluorescent protease sensors, *J. Am. Chem. Soc.* 136 (5) (2014) 2086–2093, <https://doi.org/10.1021/ja412297x>.
- [17] C. Liu, T.M. Barrett, X. Chen, J.J. Ferrie, E.J. Petersson, Fluorescent probes for studying thioamide positional effects on proteolysis reveal insight into resistance

- to cysteine proteases, *ChemBioChem* 20 (16) (2019) 2059–2062, <https://doi.org/10.1002/cbic.v20.1610.1002/cbic.201900115>.
- [18] J.M. Goldberg, R.F. Wissner, A.M. Klein, E.J. Petersson, Thioamide quenching of intrinsic protein fluorescence, *Chem. Commun.* 48 (10) (2012) 1550–1552, <https://doi.org/10.1039/C1CC14708K>.
- [19] D.M. Robkis, E.M. Hoang, P. Po, C.J. Deutsch, E.J. Petersson, Side-chain thioamides as fluorescence quenching probes, *Biopolymers* 112 (1) (2021), <https://doi.org/10.1002/bip.v112.110.1002/bip.23384>.
- [20] B.C. Smith, J.M. Denu, Mechanism-based inhibition of Sir2 deacetylases by thioacetyl-lysine peptide, *Biochemistry* 46 (50) (2007) 14478–14486, <https://doi.org/10.1021/bi7013294>.
- [21] B. He, J. Hu, X. Zhang, H. Lin, Thiomyristoyl peptides as cell-permeable Sirt6 inhibitors, *Org. Biomol. Chem.* 12 (38) (2014) 7498–7502, <https://doi.org/10.1039/C4OB00860J>.
- [22] H. Jing, J. Hu, B. He, Y.L. Negrón Abril, J. Stupinski, K. Weiser, M. Carbonaro, Y.-L. Chiang, T. Southard, P. Giannakakou, R.S. Weiss, H. Lin, A SIRT2-selective inhibitor promotes c-myc oncoprotein degradation and exhibits broad anticancer activity, *Cancer Cell* 29 (3) (2016) 297–310, <https://doi.org/10.1016/j.ccell.2016.02.007>.
- [23] N.A. Spiegelman, J.Y. Hong, J. Hu, H. Jing, M. Wang, I.R. Price, J.i. Cao, M. Yang, X. Zhang, H. Lin, A small-molecule SIRT2 inhibitor that promotes K-Ras4a lysine fatty-acylation, *ChemMedChem* 14 (7) (2019) 744–748, <https://doi.org/10.1002/cmdc.v14.710.1002/cmdc.201800715>.
- [24] H. Jiang, S. Khan, Y.i. Wang, G. Charron, B. He, C. Sebastian, J. Du, R. Kim, E. Ge, R. Mostoslavsky, H.C. Hang, Q. Hao, H. Lin, SIRT6 regulates TNF- α secretion through hydrolysis of long-chain fatty acyl lysine, *Nature* 496 (7443) (2013) 110–113, <https://doi.org/10.1038/nature12038>.
- [25] Y.-B. Teng, H. Jing, P. Aramsangtienchai, B. He, S. Khan, J. Hu, H. Lin, Q. Hao, Efficient demyristoylase activity of SIRT2 revealed by kinetic and structural studies, *Sci. Rep.* 5 (2015) 8529, <https://doi.org/10.1038/srep08529>.
- [26] J.V. Jun, D.M. Chenoweth, E.J. Petersson, Rational design of small molecule fluorescent probes for biological applications, *Org. Biomol. Chem.* 18 (30) (2020) 5747–5763, <https://doi.org/10.1039/D0OB01131B>.
- [27] F.G. Bordwell, D.J. Algrim, J.A. Harrelson, The relative ease of removing a proton, a hydrogen atom, or an electron from carboxamides versus thiocarboxamides, *J. Am. Chem. Soc.* 110 (17) (1988) 5903–5904.
- [28] J. Du, Y. Zhou, X. Su, J.J. Yu, S. Khan, H. Jiang, J. Kim, J. Woo, J.H. Kim, B. H. Choi, B. He, W. Chen, S. Zhang, R.A. Cerione, J. Auwerx, Q. Hao, H. Lin, Sirt5 is a NAD-dependent protein lysine demalonylase and desuccinylase, *Science* 334 (6057) (2011) 806–809, <https://doi.org/10.1126/science.1207861>.
- [29] M. Tan, C. Peng, K. Anderson, P. Chhoy, Z. Xie, L. Dai, J. Park, Y. Chen, H. e. Huang, Y.i. Zhang, J. Ro, G. Wagner, M. Green, A. Madsen, J. Schmiesing, B. Peterson, G. Xu, O. Ilkayeva, M. Muehlbauer, T. Braulke, C. Mühlhausen, D. Backos, C. Olsen, P. McGuire, S. Pletcher, D. Lombard, M. Hirschey, Y. Zhao, Lysine glutarylation is a protein posttranslational modification regulated by SIRT5, *Cell Metab.* 19 (4) (2014) 605–617, <https://doi.org/10.1016/j.cmet.2014.03.014>.
- [30] C. Roessler, T. Nowak, M. Pannek, M. Gertz, G.T.T. Nguyen, M. Scharfe, I. Born, W. Sippl, C. Steegborn, M. Schutkowski, Chemical probing of the human sirtuin 5 active site reveals its substrate acyl specificity and peptide-based inhibitors, *Angew. Chem. Int. Ed Engl.* 53 (40) (2014) 10728–10732, <https://doi.org/10.1002/anie.201402679>.
- [31] T. Rumpf, M. Schiedel, B. Karaman, C. Roessler, B.J. North, A. Lehotzky, J. Oláh, K.I. Ladwein, K. Schmidkunz, M. Gajer, M. Pannek, C. Steegborn, D.A. Sinclair, S. Gerhardt, J. Ovádi, M. Schutkowski, W. Sippl, O. Einsle, M. Jung, Selective Sirt2 inhibition by ligand-induced rearrangement of the active site, *Nat. Commun.* 6 (2015) 6263, <https://doi.org/10.1038/ncomms7263>.
- [32] K. Yamagata, Y. Goto, H. Nishimasu, J. Morimoto, R. Ishitani, N. Dohmae, N. Takeda, R. Nagai, I. Komuro, H. Suga, O. Nureki, Structural basis for potent inhibition of SIRT2 deacetylase by a macrocyclic peptide inducing dynamic structural change, *Structure* 22 (2) (2014) 345–352, <https://doi.org/10.1016/j.str.2013.12.001>.
- [33] U. Galli, O. Mesenzani, C. Coppo, G. Sorba, P.L. Canonico, G.C. Tron, A. Genazzani, Identification of a sirtuin 3 inhibitor that displays selectivity over sirtuin 1 and 2, *Eur. J. Med. Chem.* 55 (2012) 58–66, <https://doi.org/10.1016/j.ejmech.2012.07.001>.
- [34] D. Kalbas, S. Liebscher, T. Nowak, M. Meleshin, M. Pannek, C. Popp, Z. Alhalabi, F. Bordusa, W. Sippl, C. Steegborn, M. Schutkowski, Potent and selective inhibitors of human sirtuin 5, *J. Med. Chem.* 61 (6) (2018) 2460–2471, <https://doi.org/10.1021/acs.jmedchem.7b01648>, <https://doi.org/10.1021/acs.jmedchem.7b01648.s002>.
- [35] F. Fischer, M. Gertz, B. Suenkel, M. Lakshminarasimhan, M. Schutkowski, C. Steegborn, P. Csermely, Sirt5 deacetylation activities show differential sensitivities to nicotinamide inhibition, *PLoS One* 7 (9) (2012) e45098, <https://doi.org/10.1371/journal.pone.0045098>, <https://doi.org/10.1371/journal.pone.0045098.s002>, <https://doi.org/10.1371/journal.pone.0045098.s003>, <https://doi.org/10.1371/journal.pone.0045098.s004>, <https://doi.org/10.1371/journal.pone.0045098.s005>.
- [36] R. Neelarapu, D.L. Holzle, S. Velaparthy, H.e. Bai, M. Brunsteiner, S.Y. Blond, P. A. Petukhov, Design, synthesis, docking, and biological evaluation of novel diazide-containing isoxazole- and pyrazole-based histone deacetylase probes, *J. Med. Chem.* 54 (13) (2011) 4350–4364, <https://doi.org/10.1021/jm2001025>.
- [37] C.-W. Yu, P.-T. Chang, L.-W. Hsin, J.-W. Chern, Quinazolin-4-one derivatives as selective histone deacetylase-6 inhibitors for the treatment of Alzheimer's disease, *J. Med. Chem.* 56 (17) (2013) 6775–6791, <https://doi.org/10.1021/jm400564j>.
- [38] R. Muthyala, W.S. Shin, J. Xie, Y.Y. Sham, Discovery of 1-hydroxypyridine-2-thiones as selective histone deacetylase inhibitors and their potential application for treating leukemia, *Bioorg. Med. Chem. Lett.* 25 (19) (2015) 4320–4324, <https://doi.org/10.1016/j.bmcl.2015.07.065>.
- [39] L. Marek, A. Hamacher, F.K. Hansen, K. Kuna, H. Gohlke, M.U. Kassack, T. Kurz, Histone deacetylase (HDAC) inhibitors with a novel connecting unit linker region reveal a selectivity profile for HDAC4 and HDAC5 with improved activity against chemoresistant cancer cells, *J. Med. Chem.* 56 (2) (2013) 427–436, <https://doi.org/10.1021/jm301254q>.
- [40] R. Cincinelli, L. Musso, G. Giannini, V. Zucco, M. de Cesare, F. Zunino, S. Dallavalle, Influence of the adamantyl moiety on the activity of biphenylacrylohydroxamic acid-based HDAC inhibitors, *Eur. J. Med. Chem.* 79 (2014) 251–259, <https://doi.org/10.1016/j.ejmech.2014.04.021>.
- [41] J. Arts, P. King, A. Mariën, W. Floren, A. Belien, L. Janssen, I. Piltate, B. Roux, L. Decrane, R. Gilissen, I. Hickson, V. Vreys, E. Cox, K. Bol, W. Talloen, I. Goris, L. Andries, M. Du Jardin, M. Janicot, M. Page, K. van Emelen, P. Angibaud, JNJ-26481585, a novel “second-generation” oral histone deacetylase inhibitor, shows broad-spectrum preclinical antitumoral activity, *Clin. Cancer Res.* 15 (22) (2009) 6841–6851, <https://doi.org/10.1158/1078-0432.CCR-09-0547>.
- [42] Y. Chen, X. Wang, W. Xiang, L. He, M. Tang, F. Wang, T. Wang, Z. Yang, Y. Yi, H. Wang, T. Niu, L.i. Zheng, L. Lei, X. Li, H. Song, L. Chen, Development of purine-based hydroxamic acid derivatives: potent histone deacetylase inhibitors with marked in vitro and in vivo antitumor activities, *J. Med. Chem.* 59 (11) (2016) 5488–5504, <https://doi.org/10.1021/acs.jmedchem.6b00579>, <https://doi.org/10.1021/acs.jmedchem.6b00579.s001>.
- [43] Y.i. Fan, G.K.E. Scriba, Electrophoretically mediated microanalysis assay for sirtuin enzymes, *Electrophoresis* 31 (23–24) (2010) 3874–3880, <https://doi.org/10.1002/elps.201000336>.
- [44] S. Ohla, R. Beyreiss, G.K.E. Scriba, Y. Fan, D. Belder, An integrated on-chip sirtuin assay, *Electrophoresis* 31 (2010) 3263–3267, <https://doi.org/10.1002/elps.201000220>.
- [45] L. Blackwell, J. Norris, C.M. Suto, W.P. Janzen, The use of diversity profiling to characterize chemical modulators of the histone deacetylases, *Life Sci.* 82 (21–22) (2008) 1050–1058, <https://doi.org/10.1016/j.lfs.2008.03.004>.
- [46] Y. Liu, R. Gerber, J. Wu, T. Tsuruda, J.D. McCarter, High-throughput assays for sirtuin enzymes: a microfluidic mobility shift assay and a bioluminescence assay, *Anal. Biochem.* 378 (1) (2008) 53–59, <https://doi.org/10.1016/j.ab.2008.02.018>.
- [47] A.N. Khan, P.N. Lewis, Unstructured conformations are a substrate requirement for the Sir2 family of NAD-dependent protein deacetylases, *J. Biol. Chem.* 280 (43) (2005) 36073–36078, <https://doi.org/10.1074/jbc.M508247200>.
- [48] P.A. Marcotte, P.L. Richardson, P.R. Richardson, J. Guo, L.W. Barrett, N. Xu, A. Gunasekera, K.B. Glaser, Fluorescence assay of SIRT protein deacetylases using an acetylated peptide substrate and a secondary trypsin reaction, *Anal. Biochem.* 332 (2004) 90–99, <https://doi.org/10.1016/j.ab.2004.05.039>.
- [49] K.G. Tanner, J. Landry, R. Sternglanz, J.M. Denu, Silent information regulator 2 family of NAD-dependent histone/protein deacetylases generates a unique product, 1-O-acetyl-ADP-ribose, *Proc. Natl. Acad. Sci. U. S. A.* 97 (26) (2000) 14178–14182, <https://doi.org/10.1073/pnas.250422697>.
- [50] M.D. Jackson, J.M. Denu, Structural identification of 2'- and 3'-O-acetyl-ADP-ribose as novel metabolites derived from the Sir2 family of beta-NAD+-dependent histone/protein deacetylases, *J. Biol. Chem.* 277 (2002) 18535–18544, <https://doi.org/10.1074/jbc.M200671200>.
- [51] A.N. Khan, P.N. Lewis, Use of substrate analogs and mutagenesis to study substrate binding and catalysis in the Sir2 family of NAD-dependent protein deacetylases, *J. Biol. Chem.* 281 (17) (2006) 11702–11711, <https://doi.org/10.1074/jbc.M511482200>.
- [52] M.T. Borra, J.M. Denu, Quantitative assays for characterization of the sir2 family of NAD+-dependent deacetylases, in: C.D. Allis, C. Wu (Eds.), *Chromatin and chromatin remodeling enzymes: Part B*, Elsevier Academic Press, Amsterdam, Boston, 2004, pp. 171–187.
- [53] T. McDonagh, J. Hixon, P.S. DiStefano, R. Curtis, A.D. Napper, Microplate filtration assay for nicotinamide release from NAD using a boronic acid resin, *Methods* 36 (4) (2005) 346–350, <https://doi.org/10.1016/j.ymeth.2005.03.005>.
- [54] K. Hoffmann, B. Heltweg, M. Jung, Improvement and validation of the fluorescence-based histone deacetylase assay using an internal standard, *Arch. Pharm. Pharm. Med. Chem.* 334 (2001) 248–252, [https://doi.org/10.1002/1521-4184\(200107\)334:7<248:aid-ardp248>3.0.co;2-k](https://doi.org/10.1002/1521-4184(200107)334:7<248:aid-ardp248>3.0.co;2-k).
- [55] P.T. Rye, L.E. Frick, C.C. Ozbal, W.A. Lamarr, Advances in label-free screening approaches for studying sirtuin-mediated deacetylation, *J. Biomol. Screen.* 16 (10) (2011) 1217–1226, <https://doi.org/10.1177/1087057111420291>.
- [56] S. Holzhauser, A. Freiwald, C. Weise, G. Multhaup, C.-T. Han, S. Sauer, Discovery and characterization of protein-modifying natural products by MALDI mass spectrometry reveal potent SIRT1 and p300 inhibitors, *Angew. Chem. Int. Ed Engl.* 52 (19) (2013) 5171–5174, <https://doi.org/10.1002/anie.v52.1910.1002/anie.201207325>.
- [57] D.i. Shao, C. Yao, M.H. Kim, J. Fry, R.A. Cohen, C.E. Costello, R. Matsui, F. Seta, M.E. McComb, M.M. Bachschmid, Bachschmid, Improved mass spectrometry-based activity assay reveals oxidative and metabolic stress as sirtuin-1 regulators, *Redox Biol.* 22 (2019) 101150, <https://doi.org/10.1016/j.redox.2019.101150>.
- [58] Z.A. Gurard-Levin, K.A. Kilian, J. Kim, K. Bähr, M. Mrksich, Peptide arrays identify isoform-selective substrates for profiling endogenous lysine deacetylase activity, *ACS Chem. Biol.* 5 (9) (2010) 863–873, <https://doi.org/10.1021/cb100088g>.
- [59] Z.A. Gurard-Levin, J. Kim, M. Mrksich, Combining mass spectrometry and peptide arrays to profile the specificities of histone deacetylases, *Chembiochem* 10 (13)

- (2009) 2159–2161, <https://doi.org/10.1002/cbic.v10.1310.1002/cbic.200900417>.
- [60] H.-Y. Kuo, T.A. DeLuca, W.M. Miller, M. Mrksich, Profiling deacetylase activities in cell lysates with peptide arrays and SAMDI mass spectrometry, *Anal. Chem.* 85 (22) (2013) 10635–10642, <https://doi.org/10.1021/ac402614x>.
- [61] Z. Kutil, L. Skultetyova, D. Rauh, M. Meleshin, I. Snajdr, Z. Novakova, J. Mikesova, J. Pavlicek, M. Hadzima, P. Baranova, B. Havlinova, P. Majer, M. Schutkowski, C. Barinka, The unraveling of substrate specificity of histone deacetylase 6 domains using acetylome peptide microarrays and peptide libraries, *FASEB J.* 33 (3) (2019) 4035–4045, <https://doi.org/10.1096/psb2.v33.310.1096/fj.201801680R>.
- [62] D. Rauh, F. Fischer, M. Gertz, M. Lakshminarasimhan, T. Bergbrede, F. Aladini, C. Kambach, C.F.W. Becker, J. Zerweck, M. Schutkowski, C. Steegborn, An acetylome peptide microarray reveals specificities and deacetylation substrates for all human sirtuin isoforms, *Nat. Commun.* 4 (2013) 2327, <https://doi.org/10.1038/ncomms3327>.
- [63] M.B. Robers, C. Loh, C.B. Carlson, H. Yang, E.A. Frey, S.B. Hermanson, K. Bi, Measurement of the cellular deacetylase activity of SIRT1 on p53 via LanthaScreen® technology, *Molecular bioSystems* 7 (1) (2011) 59–66, <https://doi.org/10.1039/C0MB00026D>.
- [64] J.M. Dudek, R.A. Horton, TR-FRET biochemical assays for detecting posttranslational modifications of p53, *J. Biomol. Screen.* 15 (5) (2010) 569–575, <https://doi.org/10.1177/1087057110365898>.
- [65] T. Machleidt, M.B. Robers, S.B. Hermanson, J.M. Dudek, K. Bi, TR-FRET cellular assays for interrogating posttranslational modifications of histone H3, *J. Biomol. Screen.* 16 (10) (2011) 1236–1246, <https://doi.org/10.1177/1087057111422943>.
- [66] F. Degorce, A. Card, S. Soh, E. Trinquet, G.P. Knapik, B. Xie, HTRF: a technology tailored for drug discovery – a review of theoretical aspects and recent applications, *Curr. Chem. Genomics* 3 (2009) 22–32, <https://doi.org/10.2174/1875397300903010022>.
- [67] B. Heltweg, F. Dequiedt, E. Verdin, M. Jung, Nonisotopic substrate for assaying both human zinc and NAD⁺-dependent histone deacetylases, *Anal. Biochem.* 319 (1) (2003) 42–48, [https://doi.org/10.1016/S0003-2697\(03\)00276-8](https://doi.org/10.1016/S0003-2697(03)00276-8).
- [68] T.B. Toro, T.J. Watt, KDAC8 substrate specificity quantified by a biologically relevant, label-free deacetylation assay, *Protein Sci.* 24 (12) (2015) 2020–2032, <https://doi.org/10.1002/pro.2813>.
- [69] R. Baba, Y. Hori, S. Mizukami, K. Kikuchi, Development of a fluorogenic probe with a transesterification switch for detection of histone deacetylase activity, *J. Am. Chem. Soc.* 134 (35) (2012) 14310–14313, <https://doi.org/10.1021/ja306045j>.
- [70] R. Baba, Y. Hori, K. Kikuchi, Intramolecular long-distance nucleophilic reactions as a rapid fluorogenic switch applicable to the detection of enzymatic activity, *Chemistry* 21 (12) (2015) 4695–4702, <https://doi.org/10.1002/chem.201406093>.
- [71] Y. Xie, J. Ge, H. Lei, B.o. Peng, H. Zhang, D. Wang, S. Pan, G. Chen, L. Chen, Y. i. Wang, Q. Hao, S.Q. Yao, H. Sun, Fluorescent probes for single-step detection and proteomic profiling of histone deacetylases, *J. Am. Chem. Soc.* 138 (48) (2016) 15596–15604, <https://doi.org/10.1021/jacs.6b07334>.
- [72] C. Wang, W. Du, T. Zhang, G. Liang, A bioluminescent probe for simultaneously imaging esterase and histone deacetylase activity in a tumor, *Anal. Chem.* 92 (23) (2020) 15275–15279, <https://doi.org/10.1021/acs.analchem.0c04227>.
- [73] D.R. Rooker, D. Buccella, Real-time detection of histone deacetylase activity with a small molecule fluorescent and spectrophotometric probe, *Chem. Sci.* 6 (11) (2015) 6456–6461, <https://doi.org/10.1039/C5SC02704G>.
- [74] D.R. Rooker, Y. Klyubka, R. Gautam, E. Tomat, D. Buccella, Peptide-based fluorescent probes for deacetylase and decrotonylase activity: toward a general platform for real-time detection of lysine deacetylation, *Chembiochem* 19 (5) (2018) 496–504, <https://doi.org/10.1002/cbic.v19.510.1002/cbic.201700582>.
- [75] W. Xuan, A. Yao, P.G. Schultz, Genetically encoded fluorescent probe for detecting sirtuins in living cells, *J. Am. Chem. Soc.* 139 (36) (2017) 12350–12353, <https://doi.org/10.1021/jacs.7b05725>.
- [76] B.C. Smith, W.C. Hallows, J.M. Denu, A continuous microplate assay for sirtuins and nicotinamide-producing enzymes, *Anal. Biochem.* 394 (1) (2009) 101–109, <https://doi.org/10.1016/j.ab.2009.07.019>.
- [77] C. Yu, Y. Wu, F. Zeng, X. Li, J. Shi, S. Wu, Hyperbranched polyester-based fluorescent probe for histone deacetylase via aggregation-induced emission, *Biomacromolecules* 14 (12) (2013) 4507–4514, <https://doi.org/10.1021/bm401548u>.
- [78] K. Dhara, Y. Hori, R. Baba, K. Kikuchi, A fluorescent probe for detection of histone deacetylase activity based on aggregation-induced emission, *Chem. Commun. (Camb)* 48 (2012) 11534–11536, <https://doi.org/10.1039/c2cc36591j>.
- [79] M. Minoshima, T. Matsumoto, K. Kikuchi, Development of a fluorogenic probe based on a DNA staining dye for continuous monitoring of the histone deacetylase reaction, *Anal. Chem.* 86 (15) (2014) 7925–7930, <https://doi.org/10.1021/ac501881s>.
- [80] Y. Han, H. Li, Y. Hu, P. Li, H. Wang, Z. Nie, S. Yao, Time-resolved luminescence biosensor for continuous activity detection of protein acetylation-related enzymes based on DNA-sensitized terbium(III) probes, *Anal. Chem.* 87 (18) (2015) 9179–9185, <https://doi.org/10.1021/acs.analchem.5b01338>.
- [81] J.C. Milne, P.D. Lambert, S. Schenk, D.P. Carney, J.J. Smith, D.J. Gagne, L. Jin, O. Boss, R.B. Perni, C.B. Vu, J.E. Bemis, R. Xie, J.S. Disch, P.Y. Ng, J.J. Nunes, A. V. Lynch, H. Yang, H. Galonek, K. Israellian, W. Choy, A. Iffland, S. Lavu, O. Medvedik, D.A. Sinclair, J.M. Olefsky, M.R. Jirousek, P.J. Elliott, C. H. Westphal, Small molecule activators of SIRT1 as therapeutics for the treatment of type 2 diabetes, *Nature* 450 (7170) (2007) 712–716, <https://doi.org/10.1038/nature06261>.
- [82] F. Halley, J. Reinshagen, B. Ellinger, M. Wolf, A.L. Niles, N.J. Evans, T. A. Kirkland, J.M. Wagner, M. Jung, P. Gribbon, S. Gul, A bioluminogenic HDAC activity assay: validation and screening, *J. Biomol. Screen.* 16 (10) (2011) 1227–1235, <https://doi.org/10.1177/1087057111416004>.
- [83] A. Dose, J.O. Jost, A.C. Spieß, P. Henklein, M. Beyeremann, D. Schwarzer, Facile synthesis of colorimetric histone deacetylase substrates, *Chem. Commun. (Camb)* 48 (2012) 9525–9527, <https://doi.org/10.1039/c2cc34422j>.
- [84] B. Suenkel, F. Fischer, C. Steegborn, Inhibition of the human deacetylase Sirtuin 5 by the indole GW5074, *Bioorg. Med. Chem. Lett.* 23 (1) (2013) 143–146, <https://doi.org/10.1016/j.bmcl.2012.10.136>.
- [85] J.E. Bradner, N. West, M.L. Grachan, E.F. Greenberg, S.J. Haggarty, T. Warnow, R. Mazitschek, Chemical phylogenetics of histone deacetylases, *Nat. Chem. Biol.* 6 (3) (2010) 238–243, <https://doi.org/10.1038/nchembio.313>.
- [86] T. Ciossek, H. Julius, H. Wieland, T. Maier, T. Beckers, A homogeneous cellular histone deacetylase assay suitable for compound profiling and robotic screening, *Anal. Biochem.* 372 (1) (2008) 72–81, <https://doi.org/10.1016/j.ab.2007.07.024>.
- [87] A. Lahm, C. Paolini, M. Pallaoro, M.C. Nardi, P. Jones, P. Neddermann, S. Sambucini, M.J. Bottomley, P. Lo Surdo, A. Carfi, U. Koch, R. De Francesco, C. Steinkühler, P. Gallinari, Unraveling the hidden catalytic activity of vertebrate class IIa histone deacetylases, *Proc. Natl. Acad. Sci. U. S. A.* 104 (2007) 17335–17340.
- [88] D. Wegener, F. Wirsching, D. Riester, A. Schwienhorst, A fluorogenic histone deacetylase assay well suited for high-throughput activity screening, *Chem. Biol.* 10 (1) (2003) 61–68.
- [89] D. Wegener, C. Hildmann, D. Riester, A. Schwienhorst, Improved fluorogenic histone deacetylase assay for high-throughput-screening applications, *Anal. Biochem.* 321 (2003) 202–208.
- [90] D. Wegener, C. Hildmann, D. Riester, A. Schober, F.-J. Meyer-Almes, H. E. Deubzer, I. Oehme, O. Witt, S. Lang, M. Jaensch, V. Makarov, C. Lange, B. Busse, A. Schwienhorst, Identification of novel small-molecule histone deacetylase inhibitors by medium-throughput screening using a fluorogenic assay, *Biochem. J.* 413 (2008) 143–150, <https://doi.org/10.1042/BJ20080536>.
- [91] I. Galleano, M. Schiedel, M. Jung, A.S. Madsen, C.A. Olsen, A. Continuous, Fluorogenic sirtuin 2 deacetylase assay: substrate screening and inhibitor evaluation, *J. Med. Chem.* 59 (2016) 1021–1031, <https://doi.org/10.1021/acs.jmedchem.5b01532>.
- [92] C. Roessler, C. Tüting, M. Meleshin, C. Steegborn, M. Schutkowski, A novel continuous assay for the deacetylase sirtuin 5 and other deacetylases, *J. Med. Chem.* 58 (18) (2015) 7217–7223, <https://doi.org/10.1021/acs.jmedchem.5b00293>.
- [93] T.G.M. Schmidt, A. Skerra, The Strep-tag system for one-step purification and high-affinity detection or capturing of proteins, *Nat. Protoc.* 2 (6) (2007) 1528–1535, <https://doi.org/10.1038/nprot.2007.209>.
- [94] J.-H. Zhang, T.D.Y. Chung, K.R. Oldenburg, A simple statistical parameter for use in evaluation and validation of high throughput screening assays, *J. Biomol. Screen.* 4 (2) (1999) 67–73, <https://doi.org/10.1177/108705719900400206>.
- [95] J.L. Feldman, K.E. Dittenhafer-Reed, N. Kudo, J.N. Thelen, A. Ito, M. Yoshida, J. M. Denu, Kinetic and structural basis for acyl-group selectivity and NAD⁺ dependence in sirtuin-catalyzed deacetylation, *Biochemistry* 54 (19) (2015) 3037–3050, <https://doi.org/10.1021/acs.biochem.5b00150>.
- [96] W. Gai, H.e. Li, H. Jiang, Y. Long, D. Liu, Crystal structures of SIRT3 reveal that the α 2- α 3 loop and α 3-helix affect the interaction with long-chain acyl lysine, *FEBS Lett.* 590 (17) (2016) 3019–3028, <https://doi.org/10.1002/1873-3468.12345>.
- [97] H.M. Berman, J. Westbrook, Z. Feng, G. Gilliland, T.N. Bhat, H. Weissig, I. N. Shindyalov, P.E. Bourne, The protein data bank, *Nucleic Acids Res.* 28 (2000) 235–242, <https://doi.org/10.1093/nar/28.1.235>.
- [98] Molecular Operating Environment (MOE), 2019.01; Chemical Computing Group ULC, 1010 Sherbooke St. West, Suite #910, Montreal, QC, Canada, H3A 2R7, 2021.
- [99] J. Wang, R.M. Wolf, J.W. Caldwell, P.A. Kollman, D.A. Case, Development and testing of a general amber force field, *J. Comput. Chem.* 25 (9) (2004) 1157–1174, [https://doi.org/10.1002/\(ISSN\)1096-987X10.1002/jcc.v25:910.1002/jcc.20035](https://doi.org/10.1002/(ISSN)1096-987X10.1002/jcc.v25:910.1002/jcc.20035).
- [100] G. Jones, P. Willett, R.C. Glen, A.R. Leach, R. Taylor, Development and validation of a genetic algorithm for flexible docking, *J. Mol. Biol.* 267 (1997) 727–748, <https://doi.org/10.1006/jmbi.1996.0897>.

3.4 Continuous Histone Deacetylase Activity Assays

Matthes Zessin, Marat Meleshin, Wolfgang Sippl und Mike Schutkowski

Methods in Molecular Biology, 2023, 2589, 411-428
DOI: https://doi.org/10.1007/978-1-0716-2788-4_27

Abstract:

Protein lysine acylation represents one of the most common post-translational modifications. Obviously, highly reactive metabolic intermediates, like thioesters and mixed anhydrides between phosphoric acid and organic acids, modify lysine residues spontaneously. Additionally, enzymes using acyl-CoAs as co-substrates transfer the acyl residue specifically to defined sequences within proteins. The counteracting enzymes are called histone deacetylases (HDACs), releasing the free lysine side chain. Such enzymatic activities are involved in different cellular processes like tumor progression, immune response, regulation of metabolism, and aging. Modulators of such enzymatic activities represent valuable tools in drug discovery. Therefore, direct and continuous assays to monitor enzymatic activity of HDACs are needed. Here we describe different assay formats allowing both monitoring of Zn²⁺-dependent HDACs via UV-Vis-spectroscopy and NAD⁺-dependent HDACs (sirtuins) by fluorescence-based assay formats. Additionally, we describe methods enabling efficient screening of HDAC-inhibitors via fluorescence displacement assays.

This article is Reproduced with permission of Springer Nature.



Continuous Histone Deacetylase Activity Assays

Matthes Zessin, Marat Meleshin, Wolfgang Sippl ,
and Mike Schutkowski 

Abstract

Protein lysine acylation represents one of the most common post-translational modifications. Obviously, highly reactive metabolic intermediates, like thioesters and mixed anhydrides between phosphoric acid and organic acids, modify lysine residues spontaneously. Additionally, enzymes using acyl-CoAs as co-substrates transfer the acyl residue specifically to defined sequences within proteins. The counteracting enzymes are called histone deacetylases (HDACs), releasing the free lysine side chain. Such enzymatic activities are involved in different cellular processes like tumor progression, immune response, regulation of metabolism, and aging. Modulators of such enzymatic activities represent valuable tools in drug discovery. Therefore, direct and continuous assays to monitor enzymatic activity of HDACs are needed. Here we describe different assay formats allowing both monitoring of Zn^{2+} -dependent HDACs via UV-Vis-spectroscopy and NAD^+ -dependent HDACs (sirtuins) by fluorescence-based assay formats. Additionally, we describe methods enabling efficient screening of HDAC-inhibitors via fluorescence displacement assays.

Key words Histone deacetylase, Sirtuin, Activity assay, Inhibitor measurement

1 Introduction

Acylation of lysine side chains in proteins represents one of the most abundant post-translational modifications in all kingdoms of life. Acyl residues can be introduced either enzymatically by the action of acyltransferases or by the spontaneous reaction with acyl-CoA thioesters [1] or acylphosphates. Acylations of lysine residues can be reversed by the action of two different, evolutionary conserved enzymes both named histone deacetylases or more precisely protein lysine deacylases. On the one hand, there are the Zn^{2+} -dependent histone deacetylases (HDACs) (11 isoforms in the human proteome) and on the other hand the sirtuins (SIRTs) (7 isoforms in the human proteome). Sirtuins are dependent on NAD^+ availability because they act as acyltransferases moving the acyl residue from the lysine side chain to the ADP-ribose part of NAD^+ [2]. Robust deacetylase activity is reported for SIRTs 1–3 and for HDACs 1–3,

6, and 8. Additionally, nearly all SIRT6s are able to remove fatty acid residues [3], and recently it was shown that HDAC11 is a defatty acylase as well [4–6].

Several methods to monitor sirtuin and HDAC11 activity in a continuous and direct format based on Förster resonance fluorescence transfer (FRET) were reported [7–10] and reviewed recently [11]. Nevertheless, relatively large and artificial residues must be incorporated into the long-chain acyl residue for the generation of effective FRET. We wondered if we could use much smaller deviation from the naturally occurring acyl residues by replacing the amide bond by a thioamide bond. Thioamides have unique UV-Vis [12] and CD-spectral properties [13], could be used to switch conformations by UV-light [8, 13], and represent efficient quenchers for different fluorophores mediated by a mechanism called photoinduced electron transfer (PET) [14–18]. Additionally, Fatkins et al. reported efficient cleavage of thioamide bonds by HDAC8 in thioacetylated p53-derived substrate peptides [19], which can be monitored by formation of a colored reaction product formed by the released thioacetic acid and Ellmans reagent [20]. Recently, we demonstrated that replacement of the scissile bond in HDAC substrates (Fig. 2, R1) by a thioacetyl amide bond (Fig. 1, R2) enabled continuous activity determination of HDAC8 and HDAC6 via UV-Vis spectroscopy (Fig. 2a) [15]. In a similar manner, activity of class IIa HDACs 4, 5, 7, and 9 or HDAC11 could be monitored continuously using thiotrifluoroacetylated (Fig. 1, R3) or thiomyrystoylated (Fig. 1, R4) substrates, respectively [15]. Moreover, we were able to extend this assay principle to

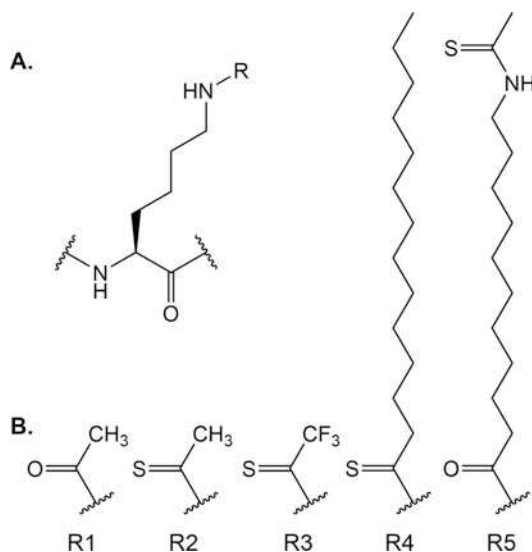


Fig. 1 Different acyl residues that can be used to measure HDAC and sirtuin activity

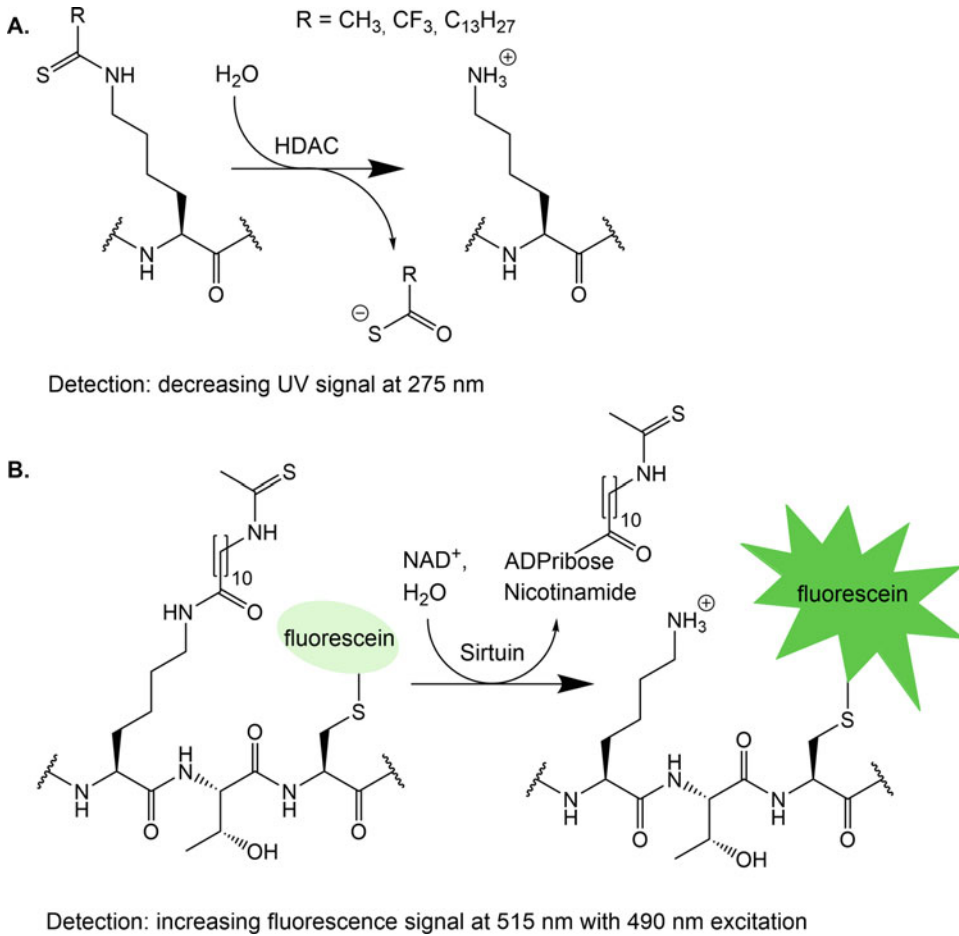


Fig. 2 Assay principle for the UV assay (a) and the fluorescence assay (b). (a) The HDAC enzyme cleaves the thioamide bond, and the product formation is detectable via the decreasing UV-signal at 280 nm. (b) Sirtuin (or HDAC11) cleaves the quencher containing acyl residue of the lysine side chain and the fluorescence intensity of fluorescein (in the peptide) increase

the measurement of HDAC8 activity via a PET-based fluorescence-quenching mechanism yielding some of the most efficient HDAC8 substrates with respect to $k_{\text{cat}}/K_{\text{M}}$ values [15]. Unfortunately, thioamide bonds represent very poor substrates for sirtuins because of the generation of a so-called stalled intermediate slowing down the reaction rate dramatically [21], and thiomristoyl residues (Fig. 1, R4) represent components of efficient inhibitors for SIRT1–3 and SIRT6 [22–24]. To circumvent this problem, we artificially introduced a thioamide bond into the myristoylated lysine residue at different positions and identified (subsequent to a systematical optimization) thioacetylated 11-amino-undecanoyl residues (Fig. 1, R5) as well-recognized substrates by SIRTs and HDAC11 (Fig. 2b) [11].

Here, we describe two different continuous HDAC/SIRT activity assay formats. First, use of thioamide bonds (Fig. 1, R2–R4) as scissile bonds is presented as a unique and continuous assay for monitoring of HDAC activity via UV-Vis spectroscopy. Second, we introduce thioacetylated 11-amino-undecanoylated lysine residues (Fig. 1, R5) in peptide substrates as efficient probes to monitor both sirtuin and HDAC11 enzymatic activity.

2 Materials

2.1 Enzymes

1. Recombinant HDACs (HDAC4, 5, 7, 8, 9, and 11) and sirtuins are commercially available. It might be an alternative to express and purify the recombinant enzymes yourself (protocols could be found for sirtuins in [11], HDAC4, HDAC5, HDAC7, HDAC8, HDAC9 [15], and HDAC11 [4]), (*see Note 1*).

2.2 Peptide Substrates

1. Peptides can be synthesized via solid-phase peptide synthesis in-house or could be purchased commercially from a supplier. A detailed synthesis description could be found in reference [15] for peptides A–C and in reference [11] for peptides D–E. Based on the substrate properties, different peptides should be used for different HDAC isoforms. Peptide A could be used for HDAC8. For HDACs 4, 5, 7, 8, and 9, peptide B should be used. For HDAC11 peptide C (UV assay) or peptide D (fluorescence assay) should be used. Peptide E is recommended to use for SIRT2, SIRT3, and SIRT5. The peptide structure is shown in Table 1. The sequence of substrate peptides A to C is variable. The signal for product formation is generated from the acylated lysine residue.

Table 1
Peptides recommended to be used as substrates for the described activity assays (*see Note 3*)

Peptide	Sequence	Acyl group R (Fig. 1)	Enzyme	K_M (μM)	[enzyme] (nM)
A	(Xaa) _n -K(R)-(Xaa) _m	2	HDAC8	–	20
B	(Xaa) _n -K(R)-(Xaa) _m	3	HDAC IIa HDAC8	–	50 10
C	(Xaa) _n -K(R)-(Xaa) _m	4	HDAC11	–	100
D	Ac-EALC(Fl)KK(R)TGG-NH ₂	5	HDAC11	5.7	5
E	Ac-EALPKK(R)TC(Fl)G-NH ₂	5	SIRT2 SIRT3 SIRT5	0.0053 0.56 2.0	0.5 10 500

C(Fl) means cysteine alkylated with 5-iodoacetamidofluorescein, Xaa means any amino acid

2. Dissolve the peptides in dimethyl sulfoxide (DMSO) with a concentration of 10 mM (or 50 mM for HDAC activity measurements if necessary) (*see Note 2*).

2.3 Compounds Modulating the Deacylase Activities

1. Such compounds could be small molecules, natural products, or peptide derivatives either commercially available or synthesized in-house. Control inhibitors which are commercially available are as follows: for HDACs class IIa, TMP-195; for HDAC8 PCI-34051; for HDAC11 SIS17; and as a pan-HDAC inhibitor, Panobinostat. For sirtuins nicotinamide (NAM) could be used and SirReal2 as SIRT2-specific inhibitor.
2. Prepare a 10-mM stock solution of the compounds in DMSO.

2.4 Buffers and Solutions

1. HDAC assay buffer for HDAC4, 5, 7, 8, and 9: 50 mM of 2-[4-(2-hydroxyethyl)piperazin-1-yl]ethane-1-sulfonic acid (HEPES), 140 mM of NaCl, and 10 mM of KCl, pH 7.4 adjusted with NaOH, supplemented with 1 mM of Tris(2-carboxyethyl)phosphine (TCEP) and 0.2 mg/mL of bovine serum albumin (BSA). It is recommended to add TCEP and BSA fresh from a frozen stock to the buffer for each day.
2. HDAC11-assay buffer: 20 mM of HEPES, pH 7.4 adjusted with NaOH, supplemented with 70 μ M of TCEP and 2 mg/mL of BSA. It is recommended to add TCEP and BSA fresh from a frozen stock to the buffer for each day (*see Note 4*).
3. SIRT assay buffer: 150 mM NaCl, 5 mM $MgCl_2$, and 20 mM Tris base adjusted with HCl to pH 7.8, supplemented with 2 mg/mL of BSA. It is recommended to add BSA fresh from a frozen stock to the buffer for each day.
4. Only for sirtuin measurements: 20 mM of NAD^+ dissolved in SIRT assay buffer aliquoted and store at $-20\text{ }^\circ\text{C}$ for further use.

2.5 Other Equipment

1. Vortex mixer.
2. $37\text{ }^\circ\text{C}$ incubator.
3. Orbital-well plate shaker (maybe combined with the plate reader).
4. Black 96-well fluorescence plate with flat bottom (384-well plate).
5. 384-well plate, black fluorescence plate with flat bottom (with reduced volume).
6. 96-well plate, transparent with V-bottom.
7. Multichannel pipette with 8 or 12 channels.
8. Plate reader with monochromator or filter settings for 480-nm excitation and 520-nm emission.

9. UV-photo spectrometer or a plate reader with the possibility to measure absorbance in the range of 280 nm.
10. UV cuvette with 1-mm or 10-mm pathway (100- μ L volume).
11. Analysis software like GraphPad Prism 8.

3 Methods

Here we describe a method to measure HDAC activity, determining a $v/[S]$ plot and creating a calibration line to calculate product concentration using HDAC4 as an example. The same activity assay could be done with HDACs 5, 7, 8, 9, and 11 using the appropriate substrates (Table 1). The enzyme concentration given in Table 1 are suggestions to start with the measurements. Depending on enzyme concentration and specific activity of the preparation, it is likely that it have to be adjusted. Furthermore, an inhibition measurement with a fluorescence assay (Subheading 3.2) is described for HDAC11. The same assay can be used for sirtuins. The UV-Vis spectroscopic assay could be used for inhibitor measurements, too.

3.1 Assaying HDAC Activity

3.1.1 HDAC Activity Measurement for HDAC4 and Peptide B as Substrate

1. The activity measurement should be done in a 100- μ L cuvette with a pathlength of 1 cm (*see* Notes 4 and 5) at room temperature.
2. Label 1.5-mL tubes according to the number of activity measurements you plan to do. Measurements should be done at least in duplicates. Additionally, make one negative control without enzyme to be sure that the slope of the reaction mixture without enzyme is near to zero or to correct the activity with the slope of the negative control. There are three samples per peptide to be tested. Repeat the complete experiment at least once to get two independent experiments.
3. The reaction volume is 120 μ L, and the reaction mixture consists of the appropriate peptide (50 μ M) and HDAC4 (50nM) in HDAC assay buffer. The reaction started with the addition of enzyme.
4. Add 0.6 μ L of appropriate peptide (peptide B) to 113.4 μ L of HDAC assay buffer, and incubate this mixture for 5 min at room temperature (25°C).
5. Prepare 1 μ M of HDAC4 dissolved in HDAC-assay buffer (20 \times HDAC4). The total volume depends on the number of samples to be measured. Store the enzyme solution always on ice (*see* Note 6).
6. Start the enzymatic reaction by adding 6 μ L of 20 \times HDAC4 to the peptide B, mix it by pipetting up and down, and transfer the mixture to the cuvette.

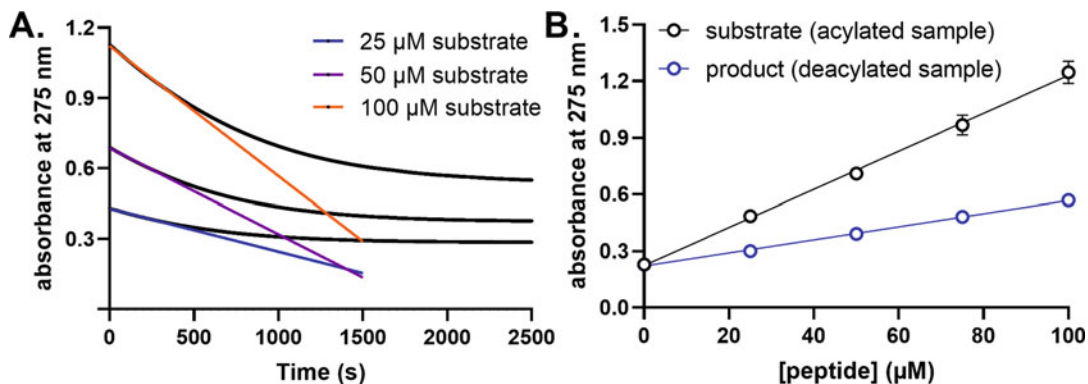


Fig. 3 (a) Example of progression curves of HDAC4-mediated deacylation reaction of peptide B at three different concentrations recorded at an absorbance of 275 nm in UV cuvette with 10-mm pathway at 25 °C. (b) Example for a calibration line of peptide B (the peptide sequence was Abz-SRGGK(R3)FFRR-NH₂) subsequent to treatment with (blue) and without (black) HDAC4

7. Perform the absorbance readout at 280 nm for 3 min. In this time, you can prepare the next substrate solutions. You will measure a decreasing UV signal. Plot the absorbance against the time, and create a linear fit for the linear part of the plot. The absolute value of the slope is proportional to the activity of the enzyme. An example of a progression curve with a linear fit could be found in Fig. 3.
8. Repeat the measurement with the second replicate.
9. The third measurement is the negative control. Add 6 μL of buffer to the mixture, mix it, and transfer it to the cuvette. Measure the absorbance at the same wavelength and for the same time as your measurement with enzyme. Plot the absorbance against the time, and create a linear fit in the same range as done with the enzyme-containing sample. If the slope is not zero, subtract the slope of the negative control from the slope of your sample.

3.1.2 Determining a $v/[S]$ -Plot for HDAC4 and Peptide B as Substrate

To determine a $v/[S]$ -plot of HDAC4 and a peptide substrate, the activity (velocity) of the reaction must be determined at different substrate concentrations. The K_M value of class IIa HDACs to thio trifluoroacetylated peptides is in the higher micromolar range [15]. To stay in a measurable absorbance range (absorbance <2), the $v/[S]$ -plot determination should be done in cuvette with a pathlength of 1 mm. To save time, the whole experiment could be performed in a well plate with UV-transparent bottom.

1. Prepare a substrate dilution series of $1.053 \times$ peptide B in HDAC assay buffer for six to eight different concentrations in triplicates in a volume of 114 μL. Substrate concentration could be ranged between 25 μM and 1000 μM. Be sure that the DMSO concentration is constant in all samples and is not

higher than 5%. Mix the samples and incubate them at room temperature (25 °C).

2. Prepare 1 μM of HDAC4 in HDAC assay buffer (20 \times , *see Note 7*).
3. Add 6 μL of 20 \times HDAC4 to the first substrate concentration, and mix it by pipetting up and down. Transfer the reaction mixture to the cuvette, and start the continuous UV readout at 275 nm for 3 min (*see Note 8*). An example progression curve is given in Fig. 3a.
4. Repeat **step 3** for all substrate concentrations in duplicates.
5. The third sample is for measuring the negative control. Add 6 μL of HDAC assay buffer to the substrate mixture, mix it, and start the UV measurement as in **step 3**. Do this for all substrate concentrations.
6. Plot the absorbance against the time and perform a linear fit. Subtract the slope of the negative control from the slope of the reaction. The corrected slope is your velocity in delta absorbance unit per time unit. To calculate the velocity in $\mu\text{M}/\text{s}$, see Subheading 3.1.3.
7. Plot the velocity against the substrate concentration and perform a nonlinear fit according to the Michaelis-Menten equation.

3.1.3 Peptide Calibration Line (Example: HDAC4 and Peptide B)

1. Thaw the substrate solution (peptide B) at room temperature (*see Note 9*).
2. In order to convert the absorbance signal to the product concentration two calibration lines are necessary, one calibration line for the substrate (acylated peptide) and one calibration line for the product (deacylated peptide + thio trifluoro acetic acid). Both will be prepared out of the same master mix, and one sample is treated with enzyme (deacylated sample) and one without enzyme (acylated sample).
3. Prepare 495 μL of a master mix with 444.4 μM (1.11 \times) peptide B in HDAC assay buffer.
4. Split your master mix into two new tubes by adding 225 μL in every tube. Mark one with acetylated sample and one with deacetylated sample.
5. Prepare 30 μL of 2 μM of HDAC4 in HDAC assay buffer.
6. Add 25 μL of the 2 μM of HDAC4 to the deacetylated sample. The final HDAC4 concentration should be 0.2 μM . Add 25 μL of HDAC assay buffer to the acylated peptide sample. Final concentration of peptide should be 400 μM in both samples.
7. Incubate these samples (acylated and deacylated peptide sample) for at least 3 h at 37 °C with gentle shaking (600 rpm) to reach complete product formation. Full substrate conversion

should be confirmed by HPLC (*see Note 10*). If there is no thermostat shaker available, incubation at room temperature overnight could be an alternative. Vortex the solution for several seconds.

8. Prepare several dilutions of your acylated peptide sample and your deacylated peptide sample in 1.5-mL tubes that covers the absorbance range up to 1 in a total volume of 120 μL in duplicates. Possible peptide concentrations for the serial dilution are 0 μM , 25 μM , 50 μM , 75 μM , and 100 μM in a cuvette with a pathlength of 1 cm.
9. Transfer the mixtures to the cuvette, and measure the absorbance at 275 nm (*see Note 11*) for all concentrations.
10. A standard curve could be created by plotting the absorbance readout of both acylated sample and deacylated sample, against the peptide concentration. Perform a linear fit, and subtract the slope of the acylated sample from the slope of the deacylated sample. This is your factor to calculate the product concentration from the measured absorbance values. An example calibration curve is given in Fig. 3b. The linear calibration line can be also used for measurements in a cuvette with a different pathlength if the factor of the pathlength is considered.

3.2 Determining IC_{50} Value (Example: HDAC11)

IC_{50} value is determined for two compounds against HDAC11. The samples should be assayed in triplicate on the plate. In total you need half of the wells of a 96-well plate. Reaction mixture of each well consists of 20 μL of inhibitor solution (with 5% DMSO final concentration), 70 μL of enzyme solution (5 nM of final concentration), and 10 μL of substrate solution (final concentration 2 μM). A control inhibitor for HDAC11 could be SIS17 or HDAC pan inhibitor Panobinostat.

1. Thaw the appropriate peptide substrate solution (peptide D) and the two compounds of interest at room temperature, and store the HDAC11 enzyme on ice.
2. Prepare 200 μL of a 25% DMSO solution in HDAC11 assay buffer by adding 40 μL of DMSO to 160 μL of HDAC11 assay buffer.
3. Perform a serial dilution of two compounds of interest in 0.5- or 1.5-mL tubes to obtain $5\times$ compound of interest solution for seven different concentrations in a HDAC11 assay buffer/DMSO solution. For example, the final concentrations of your compound are 0.02, 0.06, . . . , and 20 μM the concentration of your compound should be now 0.1, 0.3, . . . , and 100 μM . Make sure that your DMSO concentration in this dilution series is constant for every concentration. For example, if the final DMSO concentration of the assay assigned to be 5%, the DMSO concentration in the $5\times$ compound of interest dilution should be 25%.

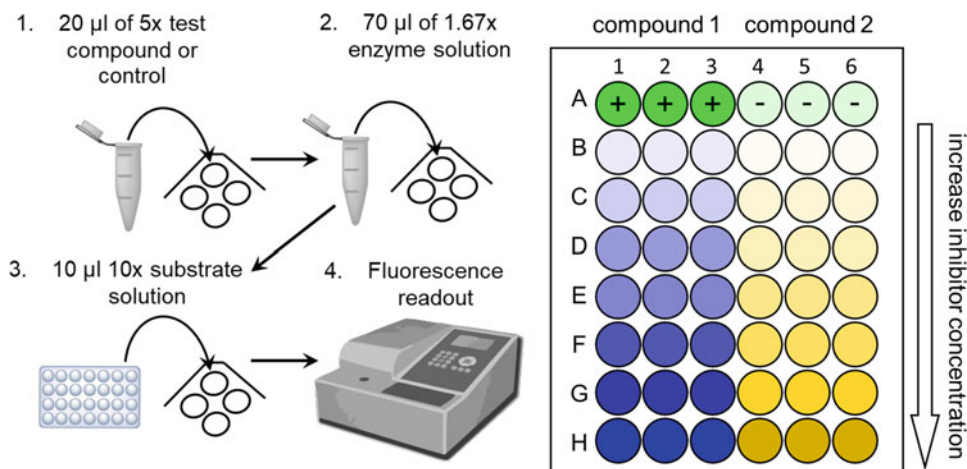


Fig. 4 Schematic pipetting order (left) and pipetting scheme for a 96-well plate for determining a IC_{50} -value for two compounds of interest

4. Add 20 μL of the 25% DMSO solution to the black 96-well fluorescence plate to row A from position 1 to 6 (see Fig. 4). Wells A1 to A3 are the 100% sample (positive control) and wells A4 to A6 represent the 0% sample (negative control, *see Note 12*). Add than 20 μL of your compound of interest solution in triplicates to the same plate. Columns 1 to 3 are for compound of interest 1 and columns 4 to 6 are for compound of interest 2 (*see Note 13*). For example, add 20 μL of compound 1 and the lowest compound concentration (0.02 μM final concentration) to wells B1, B2, and B3. An example of a pipetting scheme is shown in Fig. 4.
5. Prepare 3500 μL of 7.14-nM HDAC11 in HDAC11 assay buffer (1.43 \times) in 5-mL or 15-mL tube, and mix it by pipetting up and down. If you are determining an IC_{50} value for sirtuins, this is the point where you add 500 μM NAD^+ to the enzyme solution (*see Note 14*).
6. Add 70 μL of HDAC11 assay buffer to wells A4 to A6 (negative control without enzyme), and add 70 μL of 1.43 \times HDAC11 to each other well (A1 to A3 and B1 to H6).
7. Incubate the microtiter plate for 5 min at room temperature while shaking the plate. In parallel, prepare 620 μL of 20- μM peptide D in HDAC11 assay buffer (10 \times) by adding 1.24 μL of peptide D stock to 618.8 μL of HDAC11 assay buffer. Add 100 μL to 6 wells of a transparent 96-well plate with V-bottom.
8. Start the reaction by adding 10 μL of 10 \times peptide D with a multichannel pipette from the transparent 96-well plate to the black fluorescence well plate. Start with addition to positive and negative control and then from the lowest to highest inhibitor concentrations.

9. Shake the plate for 1 min, and perform the fluorescence readout at the plate reader with filter settings according to fluorescein fluorescence, for example, with $\lambda_{\text{Excitation}} = 480 \text{ nm}$ and $\lambda_{\text{Emission}} = 520 \text{ nm}$. Perform a readout every 30 s for 20 min (see **Notes 15** and **16**).
10. Plot the fluorescence signal against the time and create a linear fit in for the initial (linear) slope of the plot. This is the activity which you can use to calculate the IC_{50} value. For normalization the sample without inhibitor and with enzyme is set to 100% activity, and the sample without enzyme is set to 0% activity.

3.3 Fluorescence Displacement Assay for SIRT2

1. Thaw the stock solution of your compound of interest at room temperature.
2. Prepare a series of 12 different 0.5-mL tubes (or 1.5 mL) in a rack, and give them a logical labeling for a dilution series. Ten tubes belong to the dilution series, one tube is the 0% bound control and one tube the 100% bound control. Zero percent bound means that no binding of the compound of interest occurs (the fluorescence probe binds 100%). In contrast, 100% bound means that the compound of interest binds completely to SIRT2 (the fluorescence probe is completely displaced and do not bind). The assay principle is shown in Fig. 5.
3. Prepare 800 μL of a 10% DMSO solution in SIRT assay buffer by adding 80 μL of DMSO to 720 μL of SIRT assay buffer. Add 50 μL of this solution to each of the 12 tubes.

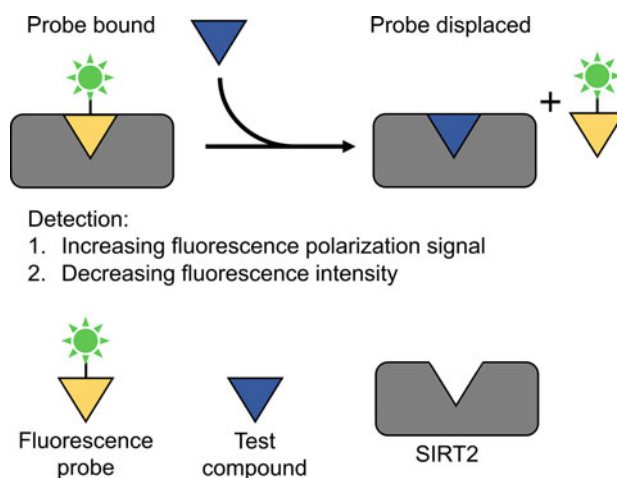


Fig. 5 Principle of the fluorescence indicator displacement assay. The fluorescence probe binds to SIRT2. When adding the compound of interest, the fluorescence probe is displaced by the compound of interest and the signal of the fluorescence polarization increase and the fluorescence intensity decrease

4. Prepare 60 μL of a fourfold compound of interest solution for the highest concentration. For example, the highest compound concentration should be 200 μM , the fourfold solution should be 800 μM with a DMSO concentration of 10%.
5. Add 50 μL of the fourfold inhibitor solution to the tube destined for the highest inhibitor concentration, and mix it by pipetting up and down. Take again 50 μL from this tube, add it to the tube destined for second highest concentration, and mix it by pipetting up and down. Repeat this until you reach the tube designated for the lowest concentration. Take 50 μL from this tube and discard it. There are now ten tubes with twofold inhibitor concentration with a volume of 50 μL and two tubes with 50 μL of a 10% DMSO concentration (*see Note 17*).
6. While preparing the dilution series, thaw the SIRT2 solution on ice and peptide E at room temperature. Peptide E is the fluorescence probe.
7. Prepare 700- μL master mix containing 200 nM of SIRT2 and 20 nM of peptide E (*see Note 18*) in SIRT assay buffer. Add 50 μL of the master mix to each tube except the 100% sample. Prepare 20 nM of peptide E in SIRT assay buffer, and add 50 μL of the 20 nM of peptide E to the 100% bound control (without SIRT2, binding of the fluorescence probe cannot occur, mimics the full displacement of the fluorescence probe). Mix all solutions by pipetting up and down.
8. Incubate the tubes for 10 min at room temperature to allow the reaction mixture to reach equilibrium.
9. Transfer 20 μL to 4 wells (internal replicates) of a 384-well plate with reduced volume. Ensure that you have no bubbles in your wells. Mix the plate for 1 min at high speed (2000 rpm, orbit 2 mm) to ensure that the solution is distributed uniformly to the wells.
10. Read the fluorescence polarization with the plate reader of each well by using settings for fluorescein fluorescence polarization (*see Note 19*).
11. Data could be normalized using the 0% bound control as 0% (with SIRT2, with fluorescence probe, without compound of interest) and the 100% bound control as 100% (with fluorescence probe, without compound of interest, without SIRT2). CD_{50} could be determined by plotting the (normalized) fluorescence polarization against the logarithm of concentration and using a nonlinear fit according to a sigmoidal curve.

4 Notes

1. Purified enzymes should be aliquoted and stored at $-80\text{ }^{\circ}\text{C}$. Repeated thaw/freeze cycles decreases the enzyme activity and should be avoided. Enzymes stocks from the $-80\text{ }^{\circ}\text{C}$ freezer should be aliquoted again after first thawing and could be stored at $-20\text{ }^{\circ}\text{C}$ for further usage.
2. Thioamide-containing compounds are prone to oxidize. Make sure that the substrate solution is thawed directly before use. If you see a higher fluorescence intensity than expected or a lower enzyme activity even if you use a freshly thawed enzyme aliquot, then it is likely that the thioamide quencher is degraded by oxidation or transformation into a normal amide bond. For peptides without a fluorophore, the degradation process is slower. Freeze and thaw cycles also support degradation of the substrates as well as irradiation with UV light. It could be also prevented by using freshly thawed substrate aliquots. It is easy to check the degradation process of the substrate peptides using HPLC and UV-Vis detection or HPLC-MS. The degradation product is more hydrophilic, shows a mass difference of 16 g/mol (sulfur-oxygen exchange), and has no longer the indicative absorbance of the thioamide bond at 260 nm .
3. The enzyme concentrations given in Table 1 are only suggestions to start an assay. Enzyme concentrations to measure peptides A to C are recommended for measurements in a UV cuvette. If it is planned to perform the assay in a 96-well plate, the final enzyme concentration in the assay should be decreased (e.g., by a factor of 5) to have a prolonged readout time.
4. HDACs, especially HDAC11, are strongly dependent on the buffer components. If there are appearing enzyme activity problems, it may help to screen different buffer components like buffer salt and concentration (Tris, phosphate, HEPES), salt additives, and concentration (NaCl, KCl, MgCl_2 ,...), reducing additives in different concentrations (TCEP, DTT) and blocking reagents (BSA, PVP, PEG). It's also useful to check the influence of BSA from different suppliers (Fig. 6). Toro et al. showed that different chelators like EDTA, citrate, and BSA can bind free Zn^{2+} ions in the assay buffer, resulting in increased enzyme activity of HDAC8 [25].
5. It is possible to use 96-well or 384-well plates with a UV transparent bottom to analyze many samples in parallel. In such cases, a plate reader with the possibility to measure UV absorbance in a range of 280 nm (peptide B) or 265 nm (peptide A and C) is necessary. Also, determination of the $v/[S]$ plot could be done using a well plate.

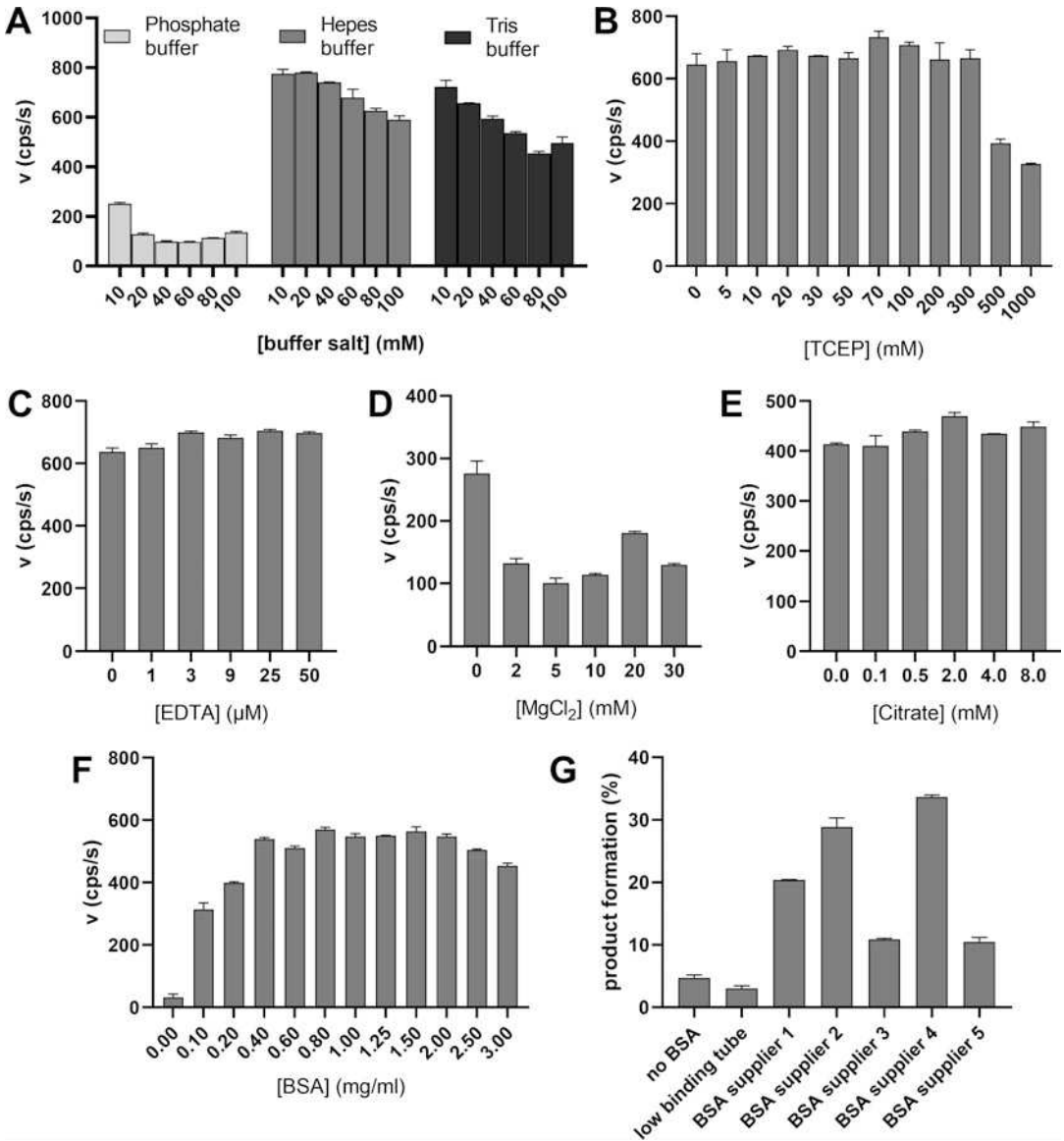


Fig. 6 Testing different buffer components for HDAC11. (a–f) Substrate was peptide D with a concentration of 2 μM, and HDAC11 concentration was 5 nM. The reaction progress was monitored via fluorescence intensity readout at λ_{ex} = 480 nm and λ_{em} = 520 nm. (g) Reaction was done with 50 nM of HDAC11 and 50 μM of trifluoro acetylated peptide as substrate. Enzyme and substrate were incubated for 30 min, and sample was analyzed using analytical HPLC with, and product formation was analyzed using absorbance wavelength at 320 nm

- Enzymes do not always have the same activity even if they come from the same preparation. Starting an activity measurement, you should test the activity of an enzyme with a standard substrate using a known concentration. Define one of the peptides as a standard substrate. Before each measurement series and after finishing your measurements, determine the

enzymatic activity using the standard substrate. If you have significantly changed enzymatic activities, the enzymatic activity has to be corrected.

7. If the enzymatic activity was very high or low, then adjust the enzyme concentration accordingly for the determination of the $v/[S]$ -plot.
8. Sometimes it is necessary to modify the reaction time. If the reaction time should be increased, the enzyme concentration have to be decreased. Please note that the enzyme concentration have to be constant for the complete experiment series.
9. To prepare a completely converted reaction solution for the fluorescence assay for peptides D and E, you could start with a 50- μ M peptide solution, 500-nM NAD^+ , and with 500-nM SIRT2, and incubate for 3 h at 37 °C. HDAC11 is not able to form a fully converted product solution because it is inhibited by the product if it is an analogue of a long-chain fatty acid like myristic acid. For peptide A HDAC8 should be used to create a calibration line.
10. To check, if the product formation of the HDAC4-mediated peptide cleavage for the standard curve was complete, an analytical HPLC analysis or HPLC-MS analysis is necessary. If the product formation was not complete, you can extend the reaction time, increase the enzyme concentration, decrease the peptide concentration, or check the overall enzyme activity on a standard substrate and use a new enzyme aliquot. If there is no access to an HPLC system, you can check full substrate conversion with the UV-signal. If you start the enzyme reaction and you do not see any further decrease in the UV signal, the reaction should be done completely.
11. Taking the whole spectrum from 220 to 320 nm for each concentration allows you to determine calibration lines for each single wavelength in this range.
12. Depending on the used microtiter plate type, plate reader, distance between lamp and well plate, and filter settings, your fluorescence signal can raise or decrease without enzyme. To get the best results, it is recommended to always use a negative control. There is sometimes some lamp, detector, or mixing artifacts which could be eliminated by subtraction of the signal of the negative control from your sample measurement.
13. Avoid formation of air bubbles in the black fluorescence plates. Reverse pipetting is highly recommended. If there are bubbles, it is possible to pierce them with a small pipette tip (e.g., 0.5–10- μ L tip).

14. If necessary, it's possible to change the pipetting pattern for HDACs starting, e.g., with addition of enzyme. Prepare a $10\times$ HDAC11 solution, and start the reaction by adding the enzyme. This could be helpful if you want to check slow binding kinetics or if you have activity problems. For sirtuins you can start the reaction by adding NAD^+ , peptide substrate or enzyme.
15. The fluorescence intensity of the substrate is quenched by $\sim 45\%$, and the measurement will start at a relative high-background fluorescence. Be sure that the settings of your plate reader are optimal for the given concentration range. You can use peptide D or E at different concentrations to optimize the plate reader settings, e.g., detector gain, measurement mode, distance between lamp and well plate, power of excitation light, etc. If you plot the fluorescence intensity against the peptide concentration and you receive a linear relationship, then you are in a good range. Otherwise, the plate reader settings should be optimized.
16. The readout time is dependent on the activity of your enzyme preparation. If you do not have an increase of the fluorescence intensity over the detection period of 20 min and the plate reader settings are already optimized, the enzyme concentration should be increased, or the readout time can be prolonged (e.g., to readout every 60 s or 120 s for 1 h). If the reaction is too fast and already done after a few minutes, the enzyme concentration could be decreased.
17. If there is more than one compound to be tested, it is maybe easier to perform the dilution series in a 96-well plate. One row of the plate (A1 to A12) is for the dilution series of one compound of interest (with 100% and 0% control). To do so add 50 μL of the 10% DMSO solution to all wells of the plate you will need. Fifty μL of the fourfold compound of interest concentration will be added to the first column of the plate for all compounds of interest. The dilutions series is done in parallel with a multichannel pipette.
18. To prepare this master mix, it is better to make one or two intermediate dilution steps. If you plan to test one or more compounds, you can prepare 10 μM of stock in DMSO from the 10-mM stock solution and store it at -20°C .
19. If you do not have the possibility to do the readout with fluorescence polarization, you could also use the fluorescence intensity readout. If you use fluorescence intensity readout, it is necessary to check if the compound of interest itself influences the fluorescence intensity of the peptide substrate.

References

1. Simic Z, Weiwad M, Schierhorn A, Steegborn C, Schutkowski M (2015) The ϵ -amino Group of Protein Lysine Residues is Highly Susceptible to nonenzymatic acylation by several physiological acyl-CoA thioesters. *Chembiochem* 16(16):2337–2347. <https://doi.org/10.1002/cbic.201500364>
2. Smith BC, Hallows WC, Denu JM (2008) Mechanisms and molecular probes of sirtuins. *Chem Biol* 15(10):1002–1013. <https://doi.org/10.1016/j.chembiol.2008.09.009>
3. Feldman JL, Baeza J, Denu JM (2013) Activation of the protein deacetylase SIRT6 by long-chain fatty acids and widespread deacylation by mammalian sirtuins. *J Biol Chem* 288(43):31350–31356. <https://doi.org/10.1074/jbc.C113.511261>
4. Kutil Z, Novakova Z, Meleshin M, Mikesova J, Schutkowski M, Barinka C (2018) Histone deacetylase 11 is a fatty-acid Deacetylase. *ACS Chem Biol* 13(3):685–693. <https://doi.org/10.1021/acscchembio.7b00942>
5. Moreno-Yruela C, Galleano I, Madsen AS, Olsen CA (2018) Histone deacetylase 11 is an ϵ -N-Myristoyllysine hydrolase. *Cell Chem Biol* 25(7):849–856.e8. <https://doi.org/10.1016/j.chembiol.2018.04.007>
6. Cao J, Sun L, Aramsangtienchai P, Spiegelman NA, Zhang X, Huang W, Seto E, Lin H (2019) HDAC11 regulates type I interferon signaling through defatty-acylation of SHMT2. *Proc Natl Acad Sci U S A* 116(12):5487–5492. <https://doi.org/10.1073/pnas.1815365116>
7. Nakajima Y, Kawaguchi M, Ieda N, Nakagawa H (2021) A set of highly sensitive Sirtuin fluorescence probes for screening small-molecular Sirtuin Defatty-Acylase inhibitors. *ACS Med Chem Lett* 12(4):617–624. <https://doi.org/10.1021/acsmchemlett.1c00010>
8. Schuster S, Roessler C, Meleshin M, Zimmermann P, Simic Z, Kambach C, Schiene-Fischer C, Steegborn C, Hottiger MO, Schutkowski M (2016) A continuous sirtuin activity assay without any coupling to enzymatic or chemical reactions. *Sci Rep* 6:22643. <https://doi.org/10.1038/srep22643>
9. Kutil Z, Mikešová J, Zessin M, Meleshin M, Nováková Z, Alquicer G, Kozikowski A, Sippl W, Bařinka C, Schutkowski M (2019) Continuous activity assay for HDAC11 enabling reevaluation of HDAC inhibitors. *ACS Omega* 4(22):19895–19904. <https://doi.org/10.1021/acsomega.9b02808>
10. Kawaguchi M, Ikegawa S, Ieda N, Nakagawa H (2016) A fluorescent probe for imaging Sirtuin activity in living cells, based on one-step cleavage of the Dabcyl quencher. *ChemBioChem* 17(20):1961–1967. <https://doi.org/10.1002/cbic.201600374>
11. Zessin M, Meleshin M, Simic Z, Kalbas D, Arbach M, Gebhardt P, Melesina J, Liebscher S, Bordusa F, Sippl W, Barinka C, Schutkowski M (2021) Continuous Sirtuin/HDAC (histone deacetylase) activity assay using thioamides as PET (Photoinduced Electron Transfer)-based fluorescence quencher. *Bioorg Chem* 117:105425. <https://doi.org/10.1016/j.bioorg.2021.105425>
12. Schutkowski M, Wöllner S, Fischer G (1995) Inhibition of peptidyl-prolyl cis/trans isomerase activity by substrate analog structures: thioxo tetrapeptide-4-nitroanilides. *Biochemistry* 34(40):13016–13026. <https://doi.org/10.1021/bi00040a012>
13. Frank R, Jakob M, Thuncke F, Fischer G, Schutkowski M (2000) Thioxylation as one-atom-substitution generates a Photoswitchable element within the peptide backbone. *Angew Chem Int Ed* 39(6):1120–1122. [https://doi.org/10.1002/\(SICI\)1521-3773\(20000317\)39:6<1120::AID-ANIE1120>3.0.CO;2-H](https://doi.org/10.1002/(SICI)1521-3773(20000317)39:6<1120::AID-ANIE1120>3.0.CO;2-H)
14. Petersson EJ, Goldberg JM, Wissner RF (2014) On the use of thioamides as fluorescence quenching probes for tracking protein folding and stability. *Phys Chem Chem Phys: PCCP* 16(15):6827–6837. <https://doi.org/10.1039/c3cp55525a>
15. Zessin M, Kutil Z, Meleshin M, Nováková Z, Ghazy E, Kalbas D, Marek M, Romier C, Sippl W, Bařinka C, Schutkowski M (2019) One-atom substitution enables direct and continuous monitoring of histone Deacetylase activity. *Biochemistry* 58(48):4777–4789. <https://doi.org/10.1021/acs.biochem.9b00786>
16. Goldberg JM, Batjargal S, Chen BS, Petersson EJ (2013) Thioamide quenching of fluorescent probes through photoinduced electron transfer: mechanistic studies and applications. *J Am Chem Soc* 135(49):18651–18658. <https://doi.org/10.1021/ja409709x>
17. Goldberg JM, Speight LC, Fegley MW, Petersson EJ (2012) Minimalist probes for studying protein dynamics: thioamide quenching of selectively excitable fluorescent amino acids. *J Am Chem Soc* 134(14):6088–6091. <https://doi.org/10.1021/ja3005094>
18. Goldberg JM, Wissner RF, Klein AM, Petersson EJ (2012) Thioamide quenching of intrinsic protein fluorescence. *Chem Commun (Camb)* 48(10):1550–1552. <https://doi.org/10.1039/c1cc14708k>
19. Fatkins DG, Monnot AD, Zheng W (2006) Nepsilon-thioacetyl-lysine: a multi-facet functional probe for enzymatic protein lysine

- Nepsilon-deacetylation. *Bioorg Med Chem Lett* 16(14):3651–3656. <https://doi.org/10.1016/j.bmcl.2006.04.075>
20. Fatkins DG, Zheng W (2008) A spectrophotometric assay for histone deacetylase 8. *Anal Biochem* 372(1):82–88. <https://doi.org/10.1016/j.ab.2007.08.031>
 21. Smith BC, Denu JM (2007) Mechanism-based inhibition of Sir2 deacetylases by thioacetyllysine peptide. *Biochemistry* 46(50):14478–14486. <https://doi.org/10.1021/bi7013294>
 22. He B, Hu J, Zhang X, Lin H (2014) Thiomyristoyl peptides as cell-permeable Sirt6 inhibitors. *Org Biomol Chem* 12(38):7498–7502. <https://doi.org/10.1039/c4ob00860j>
 23. Jing H, Hu J, He B, Abril N, Yashira L, Stupinski J, Weiser K, Carbonaro M, Chiang Y-L, Southard T, Giannakakou P, Weiss RS, Lin H (2016) A SIRT2-selective inhibitor promotes c-Myc Oncoprotein degradation and exhibits broad anticancer activity. *Cancer Cell* 29(3):297–310. <https://doi.org/10.1016/j.ccell.2016.02.007>
 24. Spiegelman NA, Hong JY, Hu J, Jing H, Wang M, Price IR, Cao J, Yang M, Zhang X, Lin H (2019) A small-molecule SIRT2 inhibitor that promotes K-Ras4a lysine fattyacylation. *ChemMedChem* 14(7):744–748. <https://doi.org/10.1002/cmdc.201800715>
 25. Toro TB, Edenfield SA, Hylton BJ, Watt TJ (2018) Chelatable trace zinc causes low, irreproducible KDAC8 activity. *Anal Biochem* 540–541:9–14. <https://doi.org/10.1016/j.ab.2017.10.024>

3.5 Continuous Fluorescent Sirtuin Activity Assay Based on Fatty Acylated Lysines

Matthes Zessin, Marat Meleshin, Sebastian Hilscher, Cordelia Schiene-Fischer, Cyril Barinka, Manfred Jung and Mike Schutkowski

International Journal of Molecular Science 2023, 24, 7416

DOI: <https://doi.org/10.3390/ijms24087416>

Abstract:

Lysine deacetylases, like histone deacetylases (HDACs) and sirtuins (SIRT), are involved in many regulatory processes like control of metabolic pathways, DNA repair and stress response. Besides robust deacetylase activity sirtuin isoforms SIRT2 and SIRT3 show demyristoylase activity as well. Interestingly, most of the inhibitors described so far for SIRT2 are not active if myristoylated substrates are used. Activity assays with myristoylated substrates are either complex because of coupling to enzymatic reactions or time-consuming because of discontinuous formats. Here we describe sirtuin substrates enabling direct recording of fluorescence changes in a continuous format. Fluorescence of the fatty acylated substrate is different as compared to the deacylated peptide product. Additionally, dynamic range of the assay could be improved by the addition of bovine serum albumin which binds the fatty acylated substrate and quenches its fluorescence. Caused by the extraordinary kinetic constants of the new substrates (K_M values in the low nM range, specificity constants between 175 000 and 697 000 $M^{-1}s^{-1}$) reliable determination of IC_{50} and K_i values for different inhibitors in the presence of only 500 pM SIRT2 in different microtiter plate formats was possible.



Article

Continuous Fluorescent Sirtuin Activity Assay Based on Fatty Acylated Lysines

Matthes Zessin¹, Marat Meleshin², Sebastian Hilscher¹, Cordelia Schiene-Fischer², Cyril Barinka³ , Manfred Jung⁴ and Mike Schutkowski^{2,*}

¹ Department of Medicinal Chemistry, Institute of Pharmacy, Martin-Luther-University Halle-Wittenberg, 06120 Halle, Germany

² Department of Enzymology, Charles Tanford Protein Center, Institute of Biochemistry and Biotechnology, Martin-Luther-University Halle-Wittenberg, 06120 Halle, Germany

³ Institute of Biotechnology, Czech Academy of Sciences, BIOCEV, Prumyslova 595, 25250 Vestec, Czech Republic

⁴ Institute of Pharmaceutical Sciences, University of Freiburg, Albertstraße 25, 79104 Freiburg, Germany

* Correspondence: mike.schutkowski@biochemtech.uni-halle.de

Abstract: Lysine deacetylases, like histone deacetylases (HDACs) and sirtuins (SIRT), are involved in many regulatory processes such as control of metabolic pathways, DNA repair, and stress responses. Besides robust deacetylase activity, sirtuin isoforms SIRT2 and SIRT3 also show demyristoylase activity. Interestingly, most of the inhibitors described so far for SIRT2 are not active if myristoylated substrates are used. Activity assays with myristoylated substrates are either complex because of coupling to enzymatic reactions or time-consuming because of discontinuous assay formats. Here we describe sirtuin substrates enabling direct recording of fluorescence changes in a continuous format. Fluorescence of the fatty acylated substrate is different when compared to the deacylated peptide product. Additionally, the dynamic range of the assay could be improved by the addition of bovine serum albumin, which binds the fatty acylated substrate and quenches its fluorescence. The main advantage of the developed activity assay is the native myristoyl residue at the lysine side chain avoiding artifacts resulting from the modified fatty acyl residues used so far for direct fluorescence-based assays. Due to the extraordinary kinetic constants of the new substrates (K_M values in the low nM range, specificity constants between 175,000 and 697,000 $M^{-1}s^{-1}$) it was possible to reliably determine the IC_{50} and K_i values for different inhibitors in the presence of only 50 pM of SIRT2 using different microtiter plate formats.

Keywords: histone deacetylases; sirtuins; fluorescence quenching; sirtuin inhibitors; myristoylated substrates; continuous activity assay; bovine serum albumin effect



Citation: Zessin, M.; Meleshin, M.; Hilscher, S.; Schiene-Fischer, C.; Barinka, C.; Jung, M.; Schutkowski, M. Continuous Fluorescent Sirtuin Activity Assay Based on Fatty Acylated Lysines. *Int. J. Mol. Sci.* **2023**, *24*, 7416. <https://doi.org/10.3390/ijms24087416>

Academic Editor: Santina Bruzzone

Received: 28 February 2023

Revised: 6 April 2023

Accepted: 10 April 2023

Published: 18 April 2023



Copyright: © 2023 by the authors. Licensee MDPI, Basel, Switzerland. This article is an open access article distributed under the terms and conditions of the Creative Commons Attribution (CC BY) license (<https://creativecommons.org/licenses/by/4.0/>).

1. Introduction

Acylation of lysine side chains in proteins is a widespread posttranslational modification that is modulated by the enzymatic activity of acetyltransferases and enzymes known as histone deac(et)ylases (HDACs). HDACs are divided into 4 classes based on their sequence homology. Class I (HDAC1, 2, 3, and 8), class IIa (HDAC4, 5, 7 and 9), class IIb (HDAC6 and 10), and class IV (HDAC11) are grouped within the Zn^{2+} dependent hydrolases. Class III enzymes (called sirtuins; human SIRT1–SIRT7) require NAD^+ as a co-substrate to transfer an acyl moiety from the lysine side chain to the ADP-ribose fragment of the co-substrate generating 2-O-acetyl-ADP-ribose and nicotinamide as the second and third reaction product, respectively [1].

HDACs are involved in a number of patho(physiological) processes including cancer progression, obesity, and immune function. Consequently, several HDAC inhibitors (HDACi) have already been approved by the Food and Drug Administration for the treatment of cancer (including vorinostat, romidepsin, belinostat, and panobinostat) and

a number of clinical trials with sirtuin inhibitors (either natural products or synthetic small molecules) are ongoing. Robust and continuous sirtuin/HDAC activity assays compatible with high-throughput screening (HTS) are, however, required for further drug development.

Several enzymatic assays have been developed to monitor the lysine deacylase activity of HDACs/SIRTs as reviewed in [2,3]. Most of these activity assays are discontinuous (HPLC-based or mass spectrometry-based assays), or suffer from complexity due to coupled enzymatic [4–11] or chemical reactions [12] (reviewed in [13,14]).

Activity assays for lysine deacylase are often linked to a separation step enabling quantification of the peptide substrate and a reaction product. The following separation methods were used: capillary electrophoresis [15], microchip electrophoresis [16], microfluidic mobility [17,18], polyacrylamide gel electrophoresis [19], high-performance liquid chromatography [20–23], thin layer chromatography [24], charcoal binding [25], binding to boronic acid resins [26], and extraction with organic solvents [27]. However, these activity assays are discontinuous and time consuming. Mass spectrometry could be used for quantification of substrates and products subsequent to separation in the gas phase [28–31]. Alternatively, biological reagents and chemical reactions could be used for detection of acetylated substrates, such as acetyllysine-recognizing antibodies [32–37], or reaction products, such as the released primary amino function of the lysine side chain. Described are acylations with biotin-containing compounds or fluorescent dyes [38], alkylations with fluorescamine [39], or intra-molecular reactions, such as transesterification with a coumarin dye [40–42] or release of bioluminescent luciferin subsequent to an intra-molecular cleavage of an ester bond [43] or intramolecular aldimine formation [44,45].

To develop a more robust activity assay that is suitable for the different lysine deacylase isoforms, it is important to consider the influence of the acyl residue on substrate specificity. For example, nearly all sirtuins have demyristoylation activity [46], and it has been shown that HDAC11 also has a high demyristoylase activity [47–49]. We recently demonstrated that the myristoylated lysine residue (Figure 1, R1) in TNF α -derived substrate peptides can be replaced by a 2-aminobenzoylated-11-amino-undecanoylated lysine residue (Figure 1, R4), generating a substrate derivative that enables continuous activity measurement of both sirtuins and HDAC11 [50,51].

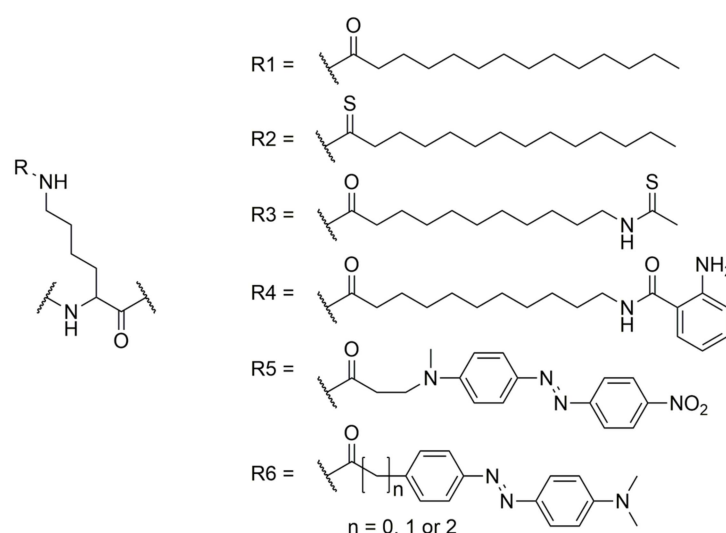


Figure 1. Structure of acyl residues used for different deacylase activity assays.

It has also been shown that an increase in the size of the fluorophore, which allows fluorescence measurements at longer wavelengths, leads to decreased substrate specificity and decreased kinetic properties for sirtuins [50] and HDAC11 [51]. Because sirtuins can accept relatively large fluorophores within the peptide sequence, we addressed this issue by designing substrates where the fluorophore and quencher positions are switched [3].

Replacing the 2-aminobenzoyl residue by a 2-amino-5-nitro-benzoyl quencher resulted in SIRT2 substrates with very similar specificity constants [50]. In the search for smaller quenchers, we exploited the ability thioamides to quench fluorescence by photoinduced electron transfer (PET) [52]. We showed that replacement of the amide scissile bond in fluorescently labeled HDAC substrates by a thioamide bond enabled continuous activity determination of HDAC8 and HDAC11 [53]. Unfortunately, thioamide bonds were poor targets for sirtuins because of the generation of a so-called stalled intermediate [54], and thiomristoyl residues (Figure 1, R2) are components of efficient inhibitors of SIRT1-3 and SIRT6 [55–57]. To overcome this problem, we introduced a thioamide bond into the myristoylated lysine residue (Figure 1, R3) and were able to generate substrates for sirtuins and HDAC11 that showed superior catalytic constants in a continuous and direct activity assay [3].

Additionally, Kawaguchi et al. showed that SIRT1-3 and SIRT6 are able to recognize the sterically more demanding DABCYL moiety in the acyl chain (Figure 1, R5), enabling monitoring of sirtuin activity in living cells [58]. New fluorescence probes for sirtuin activity measurements were generated by replacing the DABCYL quencher with disperse red dye (Figure 1, R6) [59]. Unfortunately, all of the continuous activity assays described suffer from the need for modified acyl moieties on the lysine side chain which can cause assay artifacts [60]. Therefore, to overcome this limitation, we searched for alternative methods to change the fluorescence intensity of a peptide substrate when compared to the corresponding deacylated product. Here, we describe the use of myristoylated peptides, representing the naturally occurring acyl modification, in combination with environmentally sensitive fluorophores for continuous and sensitive detection of sirtuin activity. Furthermore, we show that the use of bovine serum albumin (BSA) as a fluorescence quencher for the substrate dramatically enhances the dynamic range of the defatty acylase activity assay.

2. Results

To test whether the sirtuin/HDAC-mediated release of the hydrophobic myristoyl residue from a peptide substrate could be sensed by fluorophores, we synthesized a TNF α -derived peptide [3,50] that comprised a myristoylated lysine residue in combination with a coumaryl based amino acid at the position -2 (Figure 2, **Mcm1**) or $+2$ (Figure 2, **Mcm2**, **Table S1**). In a systematic fluorophore scan, these two positions were found to be less sensitive to substitution with sterically demanding moieties [3]. Additionally, we synthesized the corresponding fluorescently labeled peptide product of the SIRT/HDAC11-mediated deacylation of **Mcm2** (**Mcm3**, **Figure 2** and **Figure S1–S3**). First, using an HPLC-based activity assay, we analyzed how efficiently **Mcm1** and **Mcm2** were deacylated by different SIRTs and HDAC11 (Figure 2B). Both compounds showed good substrate properties for all the tested sirtuins (including SIRT5) and for HDAC11. Second, we recorded absorbance and fluorescence spectra for **Mcm1-3** (Figure 2C,D), and differences in the latter enabled us to monitor the time-dependent demyristoylation of **Mcm1** by SIRT2 (Figure 2E), which was proportional to the enzyme concentration (Figure 2F). Non-linear analysis of the dependence of the demyristoylation rate on the substrate concentration allowed us to calculate K_M and k_{cat} values (Figure 2G). The K_M value of 17 nM was relatively low, but was in accordance with the low K_M value determined for the structurally related, TNF α -based substrate with the thioacetylated 11-amino undecanoic acyl residue (Figure 1, R3) [3].

The suboptimal spectral properties of **Mcm1** and **Mcm2** prompted us to evaluate substrates where Mcm residues are replaced with fluorescein covalently bound to the side chain of cysteine (Figure 3B). A similar structural element has already been described in combination with acetylated peptides derived from histone H4 to generate fluorescent reporters for monitoring histone acetyltransferase activities [61]. Additionally, we have recently shown that SIRT2 accepts fluorescein-labeled cysteine residue substrates [3]. We synthesized substrates **F1**, **F2**, **F4**, and **F5** that differed in the position of the fluorophore (-2 or $+2$ position) and the nature of the fatty-acyl residue (either myristoyl (**F1** and **F4**) or palmitoyl (**F2** and **F5**)) (Figure 3B and Figure S4–S10). Additionally, we synthesized the

expected fluorescently labeled peptide reaction products F3 (fluorophore in -2 position) and F6 (fluorophore in $+2$ position) (Figure 3B).

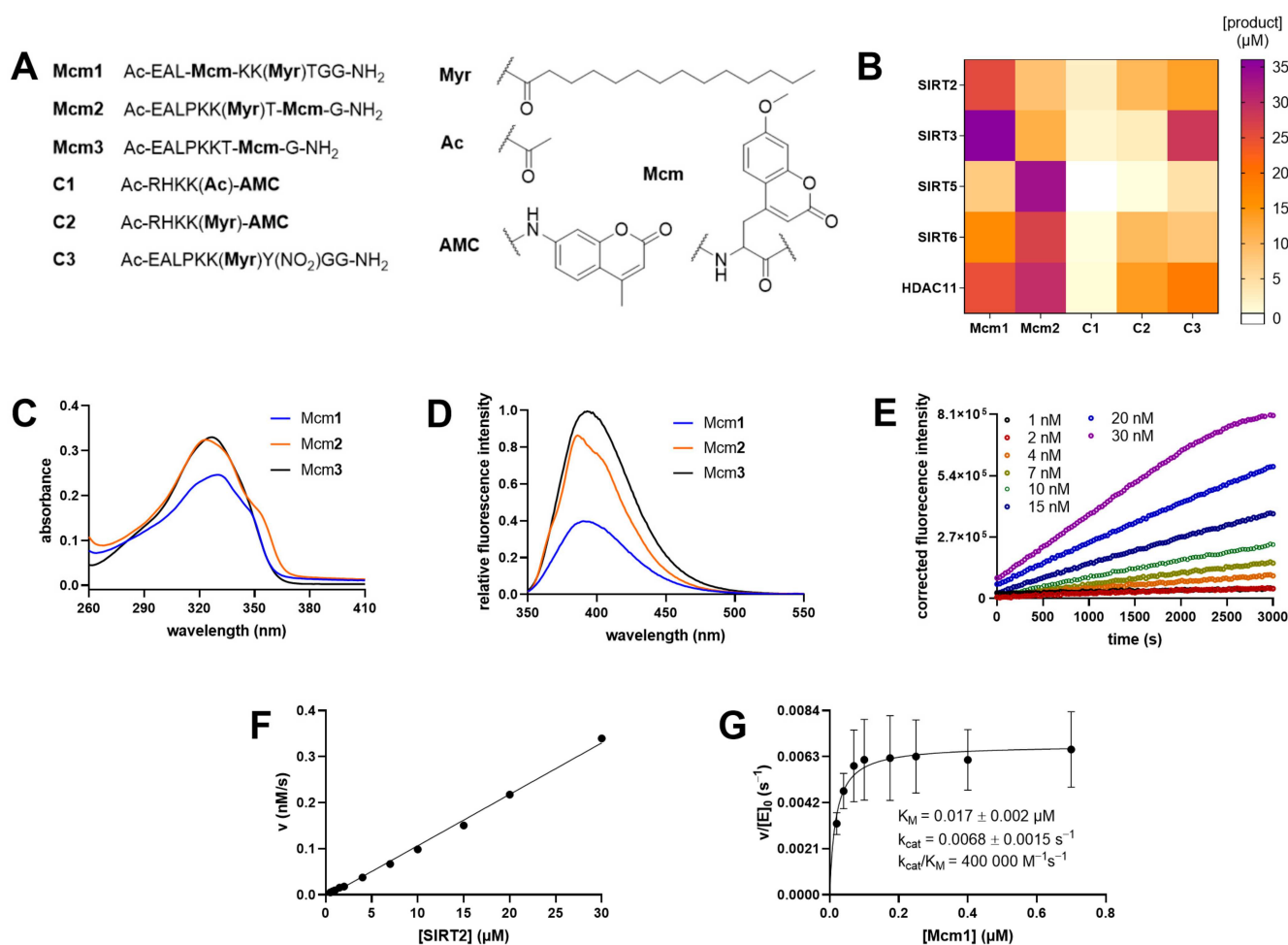


Figure 2. Direct and continuous activity assay for demyristoylation using the environmentally sensitive fluorophore Mcm (7-Methoxycoumarin-4-yl-alanyl). (A) Structures of compounds **Mcm1** to **Mcm3** and control peptides **C1** to **C3**. Y(NO₂) corresponded to *meta*-nitrotyrosine. (B) Peptide substrates at an initial concentration of 50 μM were treated with either 50 nM HDAC11, or with SIRT2 (0.1 μM), SIRT3 (0.1 μM), SIRT5 (0.5 μM), or SIRT6 (0.5 μM) in the presence of 500 μM NAD⁺ at 37 °C for 60 min. Product formation was monitored via HPLC at 320 nm or 360 nm for **C3**. Values were obtained from three independent replicates. (C) Absorbance spectra for **Mcm1** to **Mcm3** at 30 μM concentration. (D) Normalized fluorescence spectra of **Mcm1** to **Mcm3** at 3 μM concentration. (E) Progress curves of **Mcm1** deacylation (1 μM) by SIRT2 (1nM-30nM) at 25 °C ($\lambda_{\text{Ex}} = 330 \pm 75 \text{ nm}$ and $\lambda_{\text{Em}} = 405 \pm 8 \text{ nm}$) monitored in a 96-well plate format. (F) The reaction rate shows a linear correlation with the SIRT2 concentration. (G) Michaelis-Menten kinetic analysis of **Mcm1** deacylation by SIRT2 obtained from three independent replicates.

As a control substrate, we synthesized a myristoylated, TNF α -derived peptide without a fluorophore but with a *meta*-nitrotyrosine residue in the +1 position, allowing more convenient detection in HPLC-based activity assays (**C3** in Figure 3B) [50]. All peptides were then evaluated as putative substrates for sirtuins 2, 3, 5, and 6, and HDAC11 and the results are shown in Figure 3C. Peptides **F4** and **F5**, both containing the fluorophore in the +2 position, turned out to be very good SIRT2 substrates. Additionally, **F4** proved to be a surprisingly good substrate for SIRT5, which is known to be specific for negatively charged acyl residues such as malonyl [62], succinyl [23], and glutaryl [63] residues. Nevertheless,

the enzyme concentration for SIRT5 used was five-fold higher when compared to SIRT2 or SIRT3.

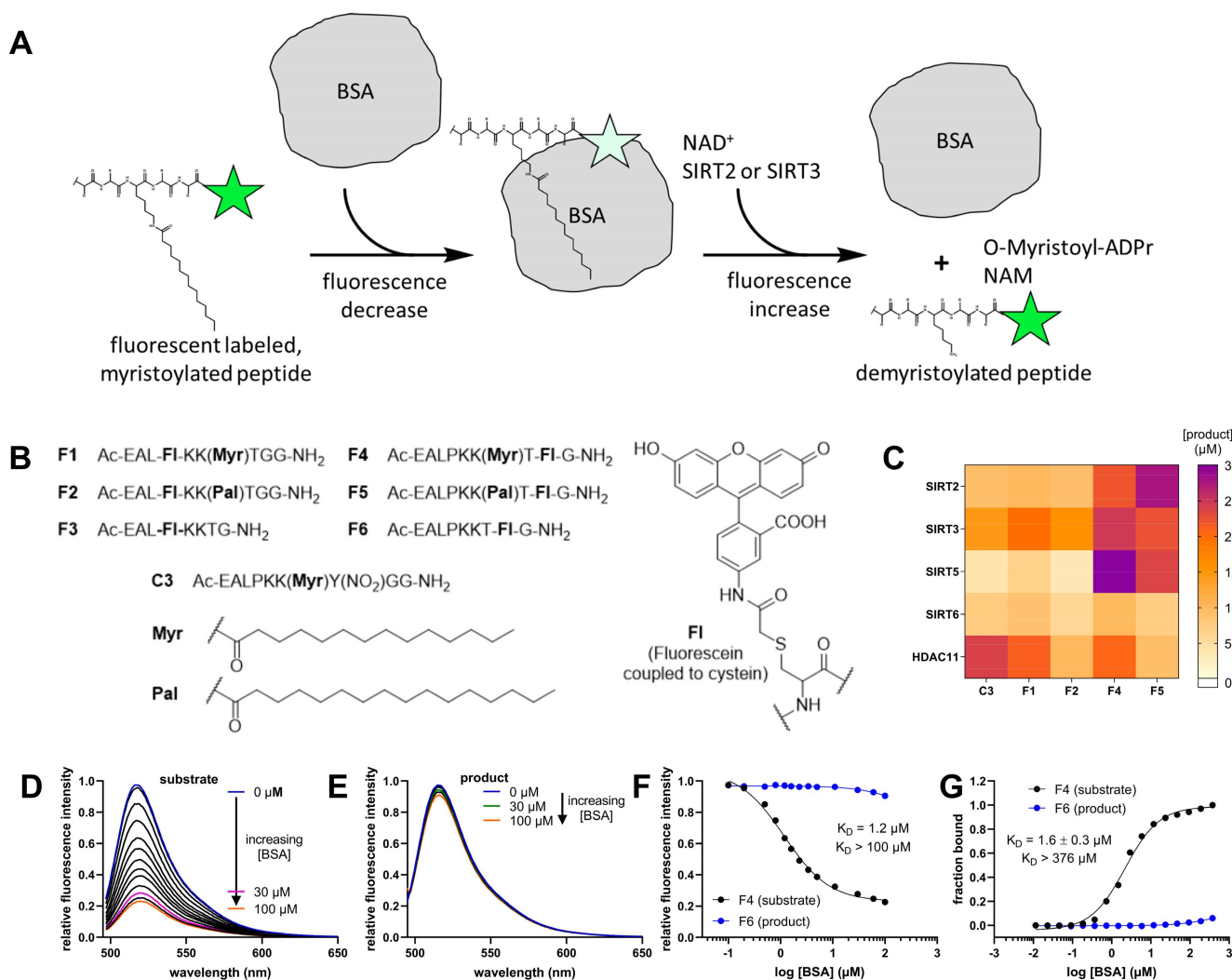


Figure 3. BSA-based activity assay. (A) The principle of the BSA-based assay. A fluorescently labeled and myristoylated peptide binds to BSA and the fluorescence is quenched. SIRT2 separates the myristoyl residue from the fluorescently labeled peptide product, which is not able to bind to BSA so tightly. (B) The structures of the peptides used for these experiments. FI, or fluorescein corresponds to 5-acetamidofluorescein coupled to a cysteine residue. (C) Product formation of different peptide substrates at a concentration of 50 μM with subsequent treatment for 1h at 37 $^{\circ}\text{C}$ with 50 nM HDAC11, or with SIRT2 (0.1 μM), SIRT3 (0.1 μM), SIRT5 (0.5 μM) or SIRT6 (0.5 μM) in the presence of 500 μM NAD⁺. Product formation was monitored via HPLC at 320 nm (or 360 nm for C3). Values were obtained from three independent replicates. (D) Fluorescence spectra of F4 with increasing concentrations of BSA resulting in a decrease in the fluorescence intensity of the substrate. The excitation wavelength was 490 nm. (E) Similar experiment to that in D, with the product F6 showing only a slight decrease in fluorescence. The excitation wavelength was 490 nm. (F) Plotting the relative fluorescence intensities from F4 and F6 directly from (D,E) at $\lambda_{\text{Em}} = 517$ nm against the concentration of BSA yielded a K_{D} value of 1.2 μM for the F4/BSA complex. The K_{D} value was obtained from one experiment ($n = 1$). (G) Determination of the dissociation constants of F4 and F6 complexes with BSA measured via fluorescence polarization. The K_{D} value was obtained from three independent replicates.

In order to develop a continuous fluorescence-based activity assay for SIRTs/HDAC11 using substrates F1, F2, F4, and F5, we compared their fluorescence spectra with the spec-

tra of their respective deacylation products **F3** and **F6** in a protein-free assay buffer, and surprisingly we did not observe any significant differences. However, marked differences in the fluorescence spectra of substrate/product pairs in a buffer containing bovine-serum albumin (BSA), a typical component of our HDAC assay buffers, were noted. This observation suggested interactions between the substrates and BSA that were likely mediated by binding sites for fatty acids on the BSA surface [64].

Figure 3A shows the reaction principle behind the idea to use BSA as a discriminator between the fluorescently labeled substrate and the peptide product of the deacylase-mediated reaction. Here, a fluorescently labeled and myristoylated peptide binds tightly to BSA [64], and its fluorescence is quenched. Following deacylation by SIRT2s, the reaction product is “released” from BSA, leading to a marked increase in fluorescence. Therefore, we first determined the dissociation constant of the **F4**/BSA complex using either fluorescence spectroscopy (Figure 3F) or fluorescence polarization measurements (Figure 3G). The K_D values were 1.2 μM and 1.6 μM , respectively. At the same time, the calculated dissociation constant for the peptide reaction product **F6** was more than 100-fold higher in both cases.

This remarkable discrimination could be visualized by recording fluorescence spectra of **F4** and **F6** in the presence of different BSA concentrations (Figures 3D and 3E, respectively) and demonstrates a strong fluorescence quenching for **F4** bound to BSA. Because of its high K_D value, fluorescence quenching of **F6** caused by binding to BSA was negligible within the concentration range used. Thus, deacylase-mediated removal of the fatty-acyl residue from the lysine side chain resulted in a fluorophore-labeled peptide product that no longer bound to BSA, yielding a robust increase in fluorescence over time (Figure 4A).

Deacylation of the substrate **F4** could also be monitored by measuring differences in the absorbance spectra (Figure 4B) either at 510 nm (signal decrease) or at 489 nm (signal increase) (Figure 4C). Figure 4D shows the progress curves for **F4** deacylation by SIRT2 in the assay buffer in the absence or presence of 30 μM of BSA using a 96-well microtiter plate (MTP) format, which was corrected using a control assay using the same buffer but without SIRT2. Almost no change in fluorescence intensity was observed without BSA in the reaction solution. In contrast, a strong increase in fluorescence over time in the presence of BSA could be detected. We analyzed samples of the reaction solutions with HPLC using both UV-Vis and fluorescence readouts and compared them with the results from the MTP-based format. Our data show that the fluorescence intensity in the presence of BSA in the MTP-based experiment correlated well with the product formation calculated from the HPLC-based experiments (Figure 4E). In contrast, there was no correlation between the MTP-fluorescence and HPLC readouts in the absence of BSA. This discrepancy could be explained by the effect of BSA shown in Figure 3A. SIRT2 was able to cleave the substrate in the absence of BSA, as shown by HPLC measurements, but despite the virtually identical fluorescence intensities of the substrate/product pair, no increase in fluorescence signal could be detected over time in the MTP format.

These positive results prompted us to follow the SIRT2-mediated cleavage of **F4** over a range of enzyme concentrations between 100 pM and 20 nM (Figure 4F,G) using the fluorescence readout (Figure 4F,G). The signal intensity showed a linear correlation with the SIRT2 concentration within the range of 100 pM to 10 nM. To our knowledge, this represents one of the most sensitive SIRT2 activity assays described so far.

In the assay solution, SIRT2 and BSA compete for binding to the fluorescently labeled substrate. Therefore, we next analyzed the binding of the substrate **F4** to SIRT2 in the absence of NAD^+ but in the presence of different BSA concentrations using fluorescence polarization measurements (Figure 4H–K). The aim of this experiment was to elucidate any impact of BSA concentration on the K_D value of the SIRT2/**F4** interaction. The calculated K_D value for binding of **F4** to the active site of SIRT2 was between 7 nM and 18 nM for BSA concentrations varying from zero to 300 μM . Thus, binding to BSA did not influence the formation of the Michaelis complex between SIRT2 and **F4**. Encouraged by these results, we determined the kinetic constants of the novel substrates for SIRT2 and SIRT3

(Table 1). SIRT5, SIRT6, and HDAC11 were not functional in this assay format because of the suboptimal affinities to the substrates F1, F2, F4, and F5.

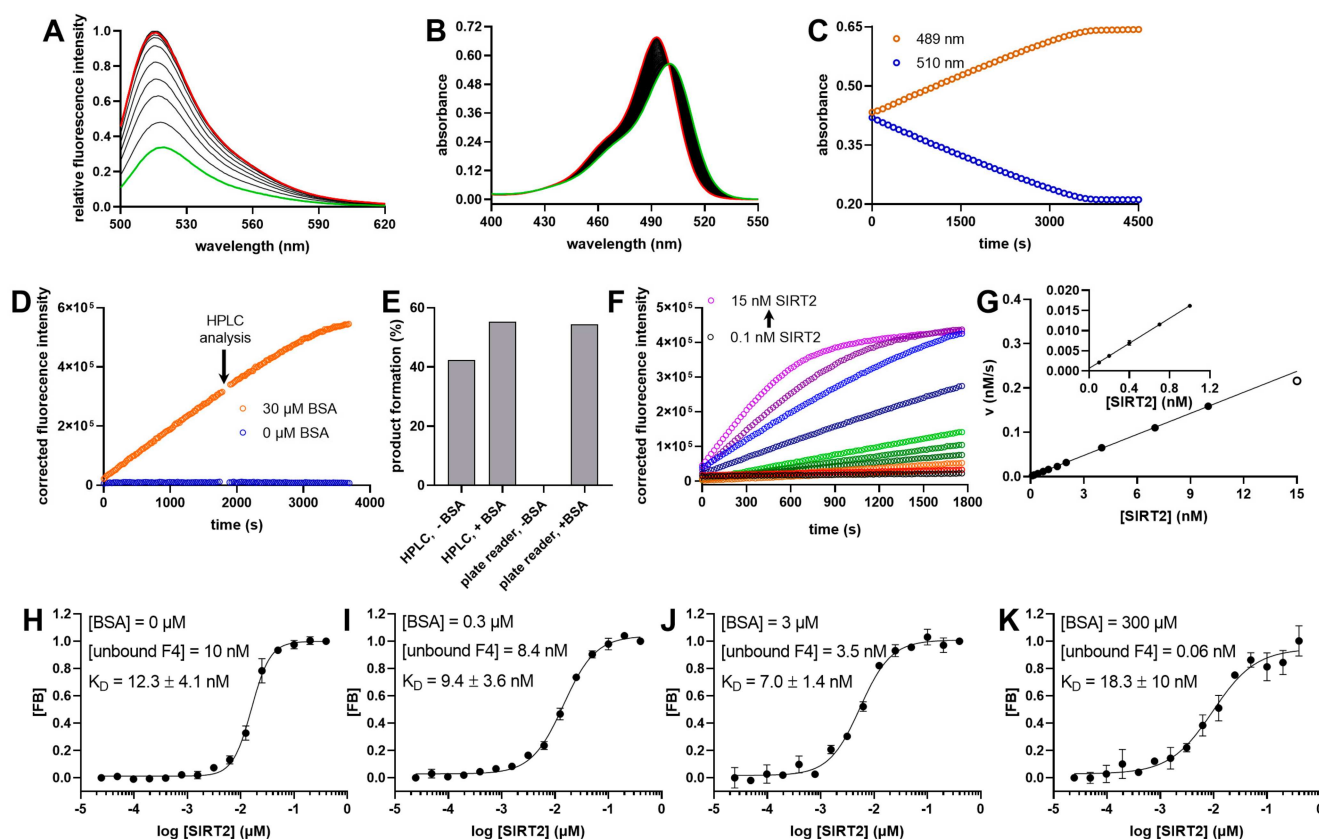


Figure 4. Continuous activity assay for SIRT2 using F4 as a substrate. (A) Fluorescence spectra of 1 μM F4 subsequent to treatment with 30 nM SIRT2 in the presence of 500 μM NAD^+ and 30 μM BSA. The green line shows the first, and the red line the last, spectrum recorded (total recording time 30 min). (B) Absorbance spectra of 10 μM of F4 after the addition of 100 nM of SIRT2 in the presence of 500 μM of NAD^+ . The green line shows the first, and the red line the last, spectrum recorded (total recording time 30 min). (C) Progress curves at two different wavelengths extracted from (B). (D) Progress curves of SIRT2-mediated cleavage of F4 measured in a 96-well plate format as changes in fluorescence intensities. After 1800 s, the measurement was interrupted, and the reaction mixture from individual wells was analyzed by HPLC. The fluorescence detection was continued afterwards. (E) Determination of the product formation of the reaction solution of (D) using HPLC with an absorbance detection at 450 nm and the fluorescence intensity readout of a 96-well MTP reader. Product formation in the MTP experiment was calculated using the total change in the fluorescence intensity as 100%. (F) Cleavage of 0.25 μM of F4 mediated by different concentrations of SIRT2 in the presence of 500 μM of NAD^+ at room temperature. Detection was performed via changes in fluorescence intensity with $\lambda_{\text{Ex}} = 485 \pm 14$ nm and $\lambda_{\text{Em}} = 535 \pm 25$ nm. All fluorescence values were corrected with a negative control without enzymes. The rate of this reaction was plotted as a function of the SIRT2 concentration in (G), and shows a linear relationship up to a SIRT2 concentration of 10 nM. (H–K) Binding curves of F4 (10 nM) to SIRT2 in the absence of NAD^+ at different concentrations of BSA, monitored via fluorescence polarization and with three independent replicates. FB signifies the fraction bound to SIRT2.

Table 1. Kinetic constants for SIRT2, SIRT3, and SIRT5 for selected substrates (Figures 2 and 3). SD denotes the standard deviation of three independent replicates, and n.d. denotes not determined.

Enzyme	Substrate	$K_M \pm SD$ (nM)	$k_{cat} \pm SD \times 10^3$ (s ⁻¹)	k_{cat}/K_M (M ⁻¹ s ⁻¹)
SIRT2	F1	16 ± 3	8.4 ± 1.9	536,000
	F2	39 ± 5	6.7 ± 1.0	175,000
	F4	33 ± 5	23 ± 3	697,000
	F5	43 ± 5	15 ± 2	335,400
	Mcm1	17 ± 2	6.8 ± 1.5	400,000
SIRT3	F1	>20 μM	>17	n.d.
	F2	>20 μM	>6	n.d.
	F4	530 ± 70	23 ± 6	44,000
	F5	990 ± 70	27 ± 6	27,000

Two major conclusions can be drawn from these data. First, palmitoyl residues at the lysine side chain were accepted by SIRT2 and SIRT3, but with slightly increased K_M values, resulting in an approximately 2-3-fold decreased in specificity constants. Acceptance of a palmitoylated lysine residue by SIRT2 has been reported, but was not compared to myristoylated lysines [65]. Second, SIRT3 seemed to be sensitive to the position of the fluorophore in the substrate sequence. While SIRT2 did not distinguish between the -2 and +2 positions, SIRT3 accepted the bulky fluorophore in the +2 position only (Table 1). Determination of the kinetic constants for F4 and SIRT2 using different MTP formats (Figure 5A) revealed a good correlation with excellent Z' -factors and signal to noise (S/N) ratios between 25 (1536-well MTPs) and higher than 90 (96-well and 384-well MTPs) (Figure 5).

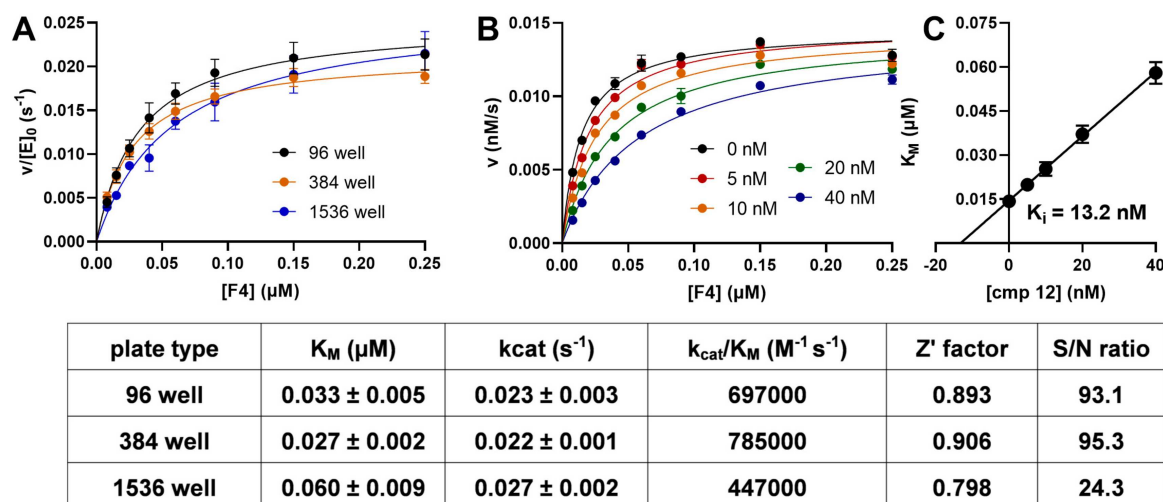


Figure 5. $v/[S]$ plots of SIRT2 with F4 under different conditions. (A) The kinetic parameters for SIRT2 and F4 in a 96-well MTP format compared to 384- and 1536-well MTP formats. The resulting kinetic parameters and the Z' -factors together with the respective S/N ratios for a 90% processed reaction mixture with SIRT2 and F4 at a 1 μM concentration are summarized in the table under the figure. Data points used for the Z' -factor calculation can be found in Figure S11. The values in the table represent the mean of three independent replicates. (B) $v/[S]$ plot of SIRT2 (1 nM) with different concentrations of F4, 500 μM of NAD⁺, and different concentrations of **cmp12** [66]. A nonlinear regression analysis was done according to the Michaelis-Menten equation. Lineweaver-Burk and Hanes-Woolf plots for these data can be found in Figure S14. (C) Plot of the K_M values from panel B as a function of the inhibitor concentration. The intercept with the abscissa represents the negative K_i value.

Several known SIRT2 inhibitors (e.g., **AGK2** and **SirReal2** [67]) are very potent when acetylated substrates are used, but are much less effective with myristoylated substrates [68]. It should therefore be feasible to use the assay developed here to identify inhibitors of sirtuin-mediated defatty acylation in a continuous and direct format using naturally occurring acyl chains in the substrates.

Recently, novel derivatives of SirReal have been described (i.e., **cmp12**; the structure is shown in Figure S13) which potently inhibit SIRT2-mediated demyristoylation reactions in vitro and in cells [66]. We determined the respective K_i value for **cmp12** using the substrate **F4** and SIRT2. Figure 5B shows the $v/[S]$ -plots for different concentrations of the inhibitor, indicating competitive inhibition of SIRT2 when the myristoylated peptide substrate was used. This finding is in line with the proposed binding mode of the inhibitor. Additionally, the calculated K_i value of 13 nM (Figure 5C) for **cmp12** was lower than any other K_i value reported for small molecule SIRT2 inhibitors [66]. In order to validate the substrate **F4**, we compared IC_{50} values of known SIRT2 inhibitors (including **AGK2** [69], **KK-22** [70], **S2iL5** [71], and **SMyr** [55]) using different substrates described in continuous and discontinuous activity assays and with both acetylated and myristoylated lysine residues (Table 2). The substrate **S1** represents a peptide derivative with an aminobenzoylated 11-aminoundecanoylated lysine side chain (Figure 1, R4, and Figure S11) described in [50]. The substrate **S2** represents a fluorescently labeled peptide with a thioacetylated 11-aminoundecanoylated lysine side chain (Figure 1, R3, and Figure S11) as a PET quencher described in [3]. In order to correct for the nanomolar K_M values of the substrates **F4** and **S1** [3], we performed these measurements either at 1 μ M or at concentrations close to the K_M value of the respective substrate. Substrates **C1** and **C2** (Figure 2A) with acetylated and myristoylated lysines, respectively, were included because such fluorescently labeled derivatives are often used in a discontinuous assay format with trypsin as a developer protease. As seen in Table 2, inhibition potency for compounds thought to bind in the vicinity of the lysine channel (i.e., **KK-22**, **SMyr**, **S2iL5**, and **cmp12**) increased with decreasing concentration of myristoylated substrates **F4** or **S2**. In contrast, NAM inhibition showed the opposite effect, specifically for substrates **F4** and **S2** (Table 2).

Table 2. IC_{50} values for SIRT2 using different substrates and SIRT2 inhibitors. The structures of all substrates are shown in Figure S12, and the structures of the inhibitors used are shown in Figure S13. **Mcm1_T** denotes a buffer containing 0.1% Tween20 (*w/v*) instead of BSA. SD values denote the standard deviations of at least two independent replicates.

cmp	IC_{50} Value \pm SD in μ M or Inhibition in % at a Given Concentration								
	[S]	K (μ M)	[E] (nM)	NAM	S2iL5	cmp12	SMyr	KK-22	SirReal2
F4 (1 μ M)	0.033	10	100 \pm 5	0.34 \pm 0.02	0.32 \pm 0.04	0.015 \pm 0.001	16 \pm 1.2	0% @20 μ M	0% @20 μ M
F4 (40 nM)	0.033	1	211 \pm 7	0.034 \pm 0.004	0.015 \pm 0.002	0.00078 \pm 0.00005	1.5 \pm 1	25 \pm 2% @20 μ M	42 \pm 4% @20 μ M
S2 (1 μ M)	0.0053	10	340 \pm 7	1.3 \pm 0.3	0.93 \pm 0.2	0.028 \pm 0.005	30 \pm 2	18 \pm 2% @20 μ M	0% @20 μ M
S2 (10 nM)	0.0053	0.5	600 \pm 70	0.028 \pm 0.015	0.019 \pm 0.006	0.00058 \pm 0.00013	2.1 \pm 0.1	1.1 \pm 0.1	32 \pm 2% @20 μ M
Mcm1 (1 μ M)	0.017	10	43 \pm 6	2.4 \pm 0.5	1.7 \pm 0.2	0.093 \pm 0.002	7 \pm 3% @20 μ M	0% @20 μ M	0% @20 μ M
Mcm1_T (1 μ M)	0.017	10	45 \pm 3	1.9 \pm 0.1	14 \pm 3	0.058 \pm 0.025	0% @20 μ M	0% @20 μ M	0% @20 μ M
S1 (1 μ M)	0.15	10	120 \pm 10	0.56 \pm 0.02	0.41 \pm 0.04	0.0099 \pm 0.003	12 \pm 0.5	5.5 \pm 0.8	33 \pm 5% @20 μ M
C1 (20 μ M)	-	100	12 \pm 1	0.21 \pm 0.01	0.048 \pm 0.005	0.056 \pm 0.011	0.41 \pm 0.03	0.089 \pm 0.009	12 \pm 1
C2 (1 μ M)	-	100	42 \pm 6	0.42 \pm 0.02	0.24 \pm 0.03	0.33 \pm 0.01	24 \pm 1%	22 \pm 3% @20 μ M	6 \pm 6% @ 6 μ M

Interestingly, we detected some weak inhibition for **SirReal2** using substrates **S1** (IC_{50} of 5.5 μ M) and **S2** (IC_{50} = 1 μ M), which both contained a hydrophobic acyl residue which

was structurally related to the myristoylated lysine (Figure S12). Clearly, substrates **S1** and **S2** were more sensitive to inhibition, similar to acetylated substrates. When **SirReal2** was analyzed with histone H3-derived substrates bearing a myristoylated lysine side chain at position 9 using an HPLC-based activity assay, no inhibition could be detected ($IC_{50} \geq 100 \mu\text{M}$) [68]. We analyzed **SirReal2** inhibition using a 100 nM substrate concentration, which was most probably higher than the expected K_M value. Using either **F4** or **Mcm1** at concentrations above their respective K_M constants failed to reveal any inhibition of SIRT2 by **SirReal2** (Table 2, data lines 1, 5, and 6). When we lowered the substrate concentration of **F4** to close to the K_M value, the estimated IC_{50} value for **SirReal2** was close to 20 μM (Table 2, data line 2). These data demonstrate that, in contrast to the substrates **S1** and **S2**, our novel substrates **F4** and **Mcm1** behaved comparably with the themyristoylated peptides used in HPLC-based discontinuous assays, and could be used to determine the inhibition potency of compounds for SIRT2-catalyzed demyristoylation reactions.

3. Discussion

It was demonstrated that enzymes could be used to monitor changes in the substrates or products of sirtuin/HDAC reactions. One of the first continuous sirtuin assays was developed using a combination of nicotinamidase and glutamate dehydrogenase for indirect spectrophotometric determination of sirtuin-mediated release of nicotinamide [11]. In a similar way, a cascade of enzymatic reactions was used to quantify the remaining sirtuin cosubstrate NAD^+ [17]. These two assay principles were shown to be independent of the chemical nature of the acyl residue, thereby allowing activity measurements with the native acyl chain, such as myristoylated substrates. Nevertheless, the combination of several enzymatic reactions with the sirtuin/HDAC reaction resulted in a complex assay setup with a limited linear range which made the assay more susceptible to artifacts by additional modulation of the enzymatic activity of the helper enzymes. This effect was demonstrated for the Sirt5 inhibitor GW5074, which affected the enzymatic activity of the helper enzyme glutamate dehydrogenase [72]. Alternatively, the deacylated peptide product of the sirtuin reaction could be quantified by coupling to the action of a protease specific for free lysine [22,73–75]. A fluorophore in the +1 position of the sirtuin substrate is necessary for such reagents to generate bright fluorescence subsequent to protease-mediated cleavage of the lysyl-fluorophore amide bond [5–10]. Proteolytic instability of different HDACs and sirtuins forced a discontinuous assay format, but for some sirtuin isoforms, this assay could be performed in a continuous manner [76,77]. Nevertheless, the protease-coupled assay format allowed sirtuin activity measurements using native acyl residues at the lysine. For most of the published sirtuin assays, the substrate properties are suboptimal with regard to both K_M and k_{cat} values, resulting in specificity constants in the range of $10 \text{ M}^{-1}\text{s}^{-1}$ – $10,000 \text{ M}^{-1}\text{s}^{-1}$. These constraints result in high substrate and sirtuin concentrations. Assay protocols using enzyme concentrations in the range of 500 nM (sirtuin 2) to 2 μM for sirtuin 6 reduce the validity of the Michaelis-Menten equation and prevent the determination of IC_{50} values for inhibitors binding with affinities below 250 nM.

In contrast to most HDACs, sirtuins are able to accept longer acyl chains at the lysine side chain [46]. Based on the observation that sirtuins are able to recognize fatty acyl chains [46], several direct and fluorescence-based activity assays have been developed [50,58,59]. One of these assays was adapted to monitor HDAC11 activity [51]. A small fluorophore (or a small quencher) was fused to the acyl moiety linked to the lysine side chain (Figure 1, R3 and R4, substrate S1). The resulting substrates had good properties for Sirt2 and HDAC11, with k_{cat}/K_M values up to $175,000 \text{ M}^{-1}\text{s}^{-1}$ and $11,000 \text{ M}^{-1}\text{s}^{-1}$, respectively [50]. Additionally, we replaced the scissile bond with a thioamide bond and were able to show that such a modification was tolerated by HDAC isoforms such as HDAC8 and HDAC11, yielding internally fluorescence-quenched HDAC8 substrates with specificity constants up to $450,000 \text{ M}^{-1}\text{s}^{-1}$. Because a similar thioamide substitution resulted in very slow substrates for sirtuins [54], we wondered if a thioamide bond within the fatty acyl residue (Figure 1, R3) would result in a small quencher. In combination with a respective fluorophore in the

peptide chain, the thioacylated 11-aminoundecanoylated lysine derivatives (Figure 1, R3) showed extremely low K_M values, down to 1 nM for sirtuin 2 [3]. The known K_M values for continuous assay substrates for sirtuin 2 are 120 nM [50], 520 nM [58], and 41 nM [59]. The data presented in Table 2 show that substrates with modified fatty acyl residues such as S1 and S2 do not match the properties of the native myristoyl residue. Determination of the IC_{50} values of SirReal2 for the sirtuin 2-catalyzed reaction showed obvious inhibition when hydrophobic substrates S1 and S2 were used, but no inhibition when F4 or Mcm1 were utilized. Therefore, our novel substrates only reflect the influence of compounds on the demyristoylation activity of sirtuin 2 and other isoforms.

Based on the low K_M value of F4, SIRT2 activity could be reliably detected in microtiter-plate formats with enzyme concentrations as low as 100 pM and a substrate concentration of 40 nM. To the best of our knowledge, this represents one of the most sensitive SIRT2 substrates described so far, enabling highly effective inhibitor screening projects because of the reagent-saving activity assay format. Additionally, substrates F1 and F2 could be used for selective monitoring of sirtuin 2 activity in more complex biological fluids such as cell lysates or within cells, because in contrast to F3 and F4, they could not be cleaved by SIRT3 (Table 1). Nevertheless, metabolic stability must be increased. Cleavages of peptide bonds between the fluorophore and the fatty acylated lysine by proteases yielded a false positive signal. Replacement of amino acid residues by either D-amino acids or N-methyl amino acids are known to prevent proteolytic cleavage. In a systematic study, we were able to demonstrate broad acceptance of such modifications in sirtuin substrates. For cell-based experiments, the metabolically stabilized substrate could be fused to oligo-arginines for better cell penetration. We know that sirtuins recognize peptide substrates fused via the N-terminus to oligo(deca)-D-arginine, opening the way for such substrates to be applied in living cells. Two different methods have been described for sirtuin activity measurements in living cells. Sirtuin activity could either be monitored by spontaneous chromophore maturation after deacetylation of lysine 85 in enhanced green fluorescent protein [78], or by replacing the lysine 529 in the active site by an acetylated lysine in firefly luciferase results in an enzymatically inactive enzyme variant. Sirtuin-mediated deacetylation could be monitored in a continuous assay format by restored luciferase activity [79].

In summary, we were able to demonstrate that environmentally sensitive fluorophores could be helpful for the development of efficient sirtuin substrates, which were useful for continuous activity measurements with microtiter plate-based equipment. The superior kinetic constants of substrate F4 enabled the determination of inhibition constants with substrate concentrations in the low nanomolar range, and SIRT2 concentrations down to 100 pM. Moreover, the developed substrates such as F1 and F2 represent a starting point for the generation of probes enabling monitoring of SIRT2 activity *in vivo*.

4. Materials and Methods

4.1. Enzymes and Chemicals

Sirtuins and HDAC11 were expressed and purified as described previously [3,47]. All chemicals were purchased from Sigma-Aldrich (St. Louis, MO, USA) unless otherwise indicated. N,N-dimethylformamide (DMF), piperidine, ethyl(hydroxyamino)cianoacetate (OxymaPure), pentafluorophenol, and rink amide MBHA were purchased from Iris Biotech (Markredwitz, Germany). The 9-fluorenylmethoxy-carbonyl- (Fmoc)-protected amino acid derivatives and O-(benzotriazol-1-yl)-N,N,N',N'-tetramethyluronium hexafluorophosphate (HBTU) were purchased from Merck (Darmstadt, Germany). Trifluoroacetic acid (TFA) was obtained from Roth (Karlsruhe, Germany). Fmoc-protected β -(7-methoxycoumarin-4-yl)-alanine (Mcm) was purchased from Bachem (Bubendorf, Switzerland). **KK22**, **cmp12**, **S2iL5**, Fmoc-Lys(Ns)-OH, and **SMyr** were synthesized as described previously [50,66,70]. SirReal2 was purchased from Biomol (Hamburg, Germany). **AGK2** was purchased from Selleckchem (Houston, TX, USA).

For all HPLC purifications and analyses, a system of water (solvent A) and acetonitrile (solvent B), both supplemented with 0.1% (*v/v*) trifluoroacetic acid (TFA), was used.

Purification of compounds was done using a Shimadzu LC System (Kyoto, Japan) with a Phenomenex (Torrance, CA, USA) Kinetex™ 5 µm XB-C18 column (250 × 21.1 mm, 100 Å) at a flow rate of 15 mL/min. Different gradients were used depending on the compound, with a runtime of 45 min. Analytical HPLC runs were performed using an Agilent 1100 HPLC system (Santa Clara, CA, USA) with a well plate autosampler and a diode-array detector.

UPLC-MS analysis was carried out using either a Waters Acquity UPLC-MS system or a Waters XEVO-TQD UPLC-MS system (Milford, MA, USA) with a Waters Acquity-UPLC-MS-BEH C18 column of 1.7 µm (2.1 × 50 mm; 30 Å). A system of water (solvent A) and acetonitrile (solvent B) supplemented with 0.1% (*v/v*) formic acid was used for LC analysis, with a typical gradient from 5 to 95% of solvent B within 6 min, and a flowrate of 0.6 mL/min. Data analysis was done using the Waters software MassLynx 4.1.

4.2. Synthesis

The peptides were synthesized using an automated microwave peptide synthesizer, Liberty Blue™ from CEM Corporation (Matthews, NC, USA). A Fmoc-based solid-phase peptide synthesis (SPPS) strategy with rink amide MBHA resin was used. The amino acid coupling was performed twice for every amino acid at 90 °C for 2 min with Oxyma-Pure/DIC in DMF. Fmoc-deprotection was done with 20% (*v/v*) piperidine for 1 min at 90 °C, and the final N-terminal deprotection was done with a 1:2:7 mixture of acetic anhydride/DIPEA/DMF (*v/v*) for 1 h at room temperature.

4.3. Mcm1–Mcm3

The Mcm fluorophore was introduced as a Fmoc-β-(7-methoxy-coumarin-4-yl)-Ala-OH building block via SPPS, and the myristoyl modification of the ε-amino group of the lysine was introduced as a Fmoc-Lys(Myristoyl)-OH building block.

4.4. F1–F6

The peptides were synthesized via SPPS, and the resin modification a 2-nitrobenzenesulfonyl (nosyl) protected lysine (Fmoc-Lys(Ns)-OH) was introduced during synthesis. The nosyl-protecting group was cleaved using a 1,8-diazabicyclo[5.4.0]undec-7-en/thiophenol/DMF solution (1.5/1/7.5 *v/v*) for 90 min, and the procedure was repeated a second time. **F3** and **F6** were cleaved after washing. After washing with DMF, coupling of the myristoyl residue (**F1** and **F4**) was done with 4 equivalents of Myristoyl chloride for 1h, and coupling of the palmitoyl residue (**F2** and **F5**) was done with 4 equivalents of palmitoyl chloride. After washing with DCM (4 × 5 min), methanol (2 × 5 min) and DCM (4 × 5 min) peptides were cleaved of the resin with a TFA/TIPS/H₂O (95/2.5/2.5 *v/v*) solution twice for 1 h. TFA was removed in vacuo, and the residual solution was dissolved in water/acetonitrile solution (1/1 *v/v*) and purified via HPLC. Pure peptide-containing fractions were combined and lyophilized. A total of 5 mg of 5-iodoacetamido fluorescein was coupled with 1.2 equivalents of pure peptide and 6 equivalents of DIPEA in DMF for 1 h. The solution was injected directly into the HPLC system, and peptide-containing fractions were collected, frozen and lyophilized.

4.5. Recording of Fluorescence and Absorbance Spectra

All spectra were recorded in a SIRT assay buffer consisting of 20 mM of Tris-HCl, pH 7.8, 150 mM of NaCl, and 5 mg/mL of MgCl₂. The absorbance spectra were recorded at room temperature in a cuvette with a pathlength of 10 mm using an Agilent CARY 3500 UV-Vis spectrometer. A compound concentration of 30 µM for Mcm-containing compounds or 10 µM for fluorescein-containing compounds was used. The fluorescence spectra were recorded in a fluorescence cuvette with a pathlength of 10 mm × 5 mm with a Horiba Fluoromax 4 (Kyōto, Japan). The compound concentration was 3 µM for Mcm-containing peptides and 1 µM for fluorescein-containing peptides. Excitation wavelengths were chosen according to the absorbance maximum of the individual compounds.

4.6. Quenching Efficiency Determination

Quenching efficiency was determined from the fluorescence emission spectra with the following equation at a wavelength of 515 nm. $F_{i_{acyl}}$ is the fluorescence intensity of the fluorescence peptide with a myristoyl residue, and $F_{i_{free}}$ is the fluorescence intensity of the deacylated counterpart.

$$Q_E = 100 * \left(1 - \frac{F_{i_{acyl}}}{F_{i_{free}}} \right)$$

4.7. HPLC Based Deacylation Analysis

The HPLC analysis was done in a total volume of 70 μ L of SIRT assay buffer (composition above) supplemented with 2 mg/mL BSA for sirtuins, or in HDAC11 assay buffer (20 mM HEPES, 70 μ M TCEP, and 2 mg/mL BSA, pH 7.4 adjusted with NaOH) for HDAC11. The reaction mixture with 50 μ M of peptide and 500 μ M of NAD^+ (only for sirtuins) was incubated for 5 min at 37 $^{\circ}$ C, and the reaction was started with the addition of an enzyme ([SIRT2] and [SIRT3] = 100 nM, [SIRT5] and [SIRT6] = 500 nM, and [HDAC11] = 50 nM final concentration). After 0.5 h and 1 h, the reaction was quenched by adding 20 μ L of a stop solution (5% acetonitrile (*v/v*) and 1% TFA (*v/v*) in water), and the solution was injected directly into the HPLC-system. Separation of the substrate and product was done with a linear gradient from 5% to 95% of solvent B within 6 min and at a flow rate of 0.6 mL/min. Detection was done at a wavelength of 320 nm for **Mcm1**, **Mcm2**, and **C1** and **C2**, at 360 nm for **C3**, and at 450 nm for **F1**, **F2**, **F4**, and **F5**. Product formation was calculated as the ratio of product peak area to total peak area.

4.8. Steady-State Kinetics

The steady-state measurements were done using the sirtuin-mediated fluorescence change through product formation. The reaction took place in a black 96-well fluorescence plate in a total volume of 100 μ L. The peptide was incubated at different concentrations (depending on the substrate properties) with 500 μ M of NAD^+ (final concentration) in SIRT assay buffer (composition above) supplemented with 2 mg/mL of BSA (0.1% (*w/v*) Tween20 for **Mcm1**) for at least 5 min at 25 $^{\circ}$ C. The reaction was started by the addition of an enzyme (1 nM SIRT2 or 10 nM SIRT3 for **F4** and **F5**; 20 nM SIRT3 for **F1**; and 50 nM for **F2**), and the fluorescence change was monitored continuously with a PerkinElmer Envision 2104 multilabel plate reader (Waltham, MA, USA). The excitation wavelength was set to $\lambda_{Ex} = 485 \pm 14$ nm, and the emission wavelength was set to $\lambda_{Em} = 535 \pm 25$ nm for **F1** to **F6**, and to $\lambda_{Ex} = 320 \pm 14$ nm and $\lambda_{Em} = 405 \pm 8$ nm for **Mcm1**. The fluorescence intensities were plotted as a function of time, and the slope of the linear part of this curve represented the reaction rate (steady state velocity). The product concentration was calculated using calibration lines, the reaction rate was plotted against the substrate concentration, and a fit according to the Michaelis-Menten equation was done to determine the K_M and the k_{cat} values.

4.9. Determination of IC_{50} Values

The inhibition experiments were done using different assays depending on the substrate. For peptides **F4**, **Mcm1**, **S1**, and **S2**, the enzyme activity was determined in a continuous manner. For **C1** and **C2**, a trypsin-coupled discontinuous endpoint assay was used. For all assays, a dilution series of the inhibitor was done in DMSO.

The continuous assays were performed in a black 384-well fluorescence plate in a total volume of 40 μ L of SIRT assay buffer (composition above) supplemented with 2 mg/mL of BSA for **F4**, **Mcm1**, **S2**, and **S1**, or 0.1% Tween20 for **Mcm1**. A total of 2 μ L of the inhibitor dilutions were incubated with 14 μ L of the peptide substrate (final concentration 1 μ M for **F4**, **Mcm1**, **S1**, and **S2**, 40 nM for **F4**, or 10 nM for **S2**) and 14 μ L of SIRT2 solution (final concentration 10 nM for **F4**, **Mcm1**, **S1**, and **S2**, 1 nM for **F4**, or 0.5 nM for **S2**) for 5 min at room temperature. In addition to the inhibitor-containing samples, a sample without inhibitors was measured as a positive control, and a sample without enzymes was

measured as a negative control. The DMSO concentration was set to 5 % (*v/v*). The reaction was started with the addition of 10 μL of NAD^+ (final concentration 500 μM), the product formation was monitored by the change of the fluorescence intensity, and the reaction rate (see above) represented the activity. Fluorescence readouts for **S2** were performed at the same wavelengths as **F4**, and readouts for **S1** were performed at the same wavelengths as **Mcm1**. The activity was normalized using the positive control as 100% and the negative control as 0%. The normalized activity (v/v_0) was plotted as a function of the logarithm of the inhibitor concentration [I], and a nonlinear fit was performed according to the following equation to determine the IC_{50} value.

$$\frac{v}{v_0} = \frac{100}{1 + 10^{[\text{I}] - \log \text{IC}_{50}}}$$

The discontinuous fluorescence assay was performed in a black 384-well fluorescence plate in a total volume of 21 μL (for the sirtuin reaction) with **C1** (for the deacetylation reaction) and **C2** (for the demyristoylation reaction) used as peptide substrates. A total of 1.05 μL inhibitor solution was incubated with 9.95 μL SIRT2 solution (final concentration of 100 nM) for 5 min at room temperature, and the reaction was started with the addition of substrate solutions with final concentrations of [**C1**] = 20 μM or [**C2**] = 1 μM and 500 μM NAD^+ . Additionally, a positive control without inhibitor and a negative control without enzyme were performed in the same plate. After 2 h incubation at 37 °C for **C1** and 1 h for **C2**, the reaction was stopped, and the fluorescence signal was developed upon the addition of 21 μL of developer solution containing trypsin (0.5 mg/mL final concentration) and nicotinamide (1 mM final concentration) and additional incubation for 1 h. The fluorescence readout was performed with the 2104 Envision Multilabel plate reader with $\lambda_{\text{Ex}} = 380 \pm 10$ nm and $\lambda_{\text{Em}} = 475 \pm 8$ nm. The fluorescence signal of the positive control was set to 100%, the fluorescence signal of the negative control was set to 0%, and the other values were normalized using these two values. The normalized fluorescence intensities represent the activity. The IC_{50} calculation was done as described above.

4.10. Determination of the K_i Values

Determination of the K_i values was done in the same way as the IC_{50} determination, but with different substrate concentrations and in a black 96-well plate. The total volume was 100 μL per well. The inhibitor was incubated with peptide substrate **S2** or **F4** and 0.5 nM or 1 nM SIRT2 for 5 min at room temperature, and the reaction was started with the addition of NAD^+ . The progress of the reaction was monitored via the fluorescence intensity, as described above. The reciprocal reaction rate was plotted as a function of the reciprocal substrate concentration for each inhibitor concentration to determine the inhibition type. For the competitive inhibitor **cmp12**, the slope of these plots at different inhibitor concentrations was plotted against the inhibitor concentration, and the linearity of these plots determined the inhibition type. The intercept with the abscissa represents the negative K_i value.

4.11. Binding Experiments

All binding experiments were performed in a black 384-well plate with a reduced volume (total volume of 20 μL). The experiment was done in SIRT assay buffer, containing 20 mM of Tris-HCl, pH 7.8, 150 mM of NaCl, and 5 mM of MgCl_2 . The unlabeled binding partner was diluted in serial dilution, starting with 752 μM of BSA and 1.6 μM of SIRT2 in a total volume of 50 μL . The fluorescently labeled peptide was added with a volume of 50 μL to the diluted binding partner with a final concentration of 50 nM of BSA and 10 nM of SIRT2. The solution was transferred to the 384-well plate, and the fluorescence intensity readout was performed with an Envision 2104 Multilabel plate reader with

$\lambda_{Ex} = 485 \pm 14$ nm and $\lambda_{Em} = 535 \pm 40$ nm (one S-polarized and one P-polarized). The anisotropy (A) was calculated with the following equation:

$$A_{obs} = \frac{Fi_S - Fi_P}{Fi_S + 2 \cdot Fi_P}$$

where Fi_S is the measured fluorescence intensity with the parallel filter and Fi_P is the measured fluorescence intensity with the perpendicular filter. The bound fraction [FB] was calculated from the resulting anisotropy (A_{obs}) using the following equation:

$$[FB] = \frac{A_{obs} - A_f}{(A_b - A_{obs}) \cdot Q + A_{obs} - A_f}$$

where A_f represents the anisotropy of free **F4** without a binding partner, A_b the anisotropy of **F4** in the complex with the binding partner at saturation, and Q is the ratio of fluorescence intensities of bound **F4** versus free **F4**, which means that Q is < 1 when fluorescence is quenched upon binding. The total fluorescence intensities (Fi) were calculated with $Fi = Fi(P\text{-channel}) + 2 \cdot Fi(S\text{-channel})$. [FB] was plotted as a function of the binding partner concentration, and the K_D value was determined with a nonlinear curve fit of the quadratic binding equation:

$$[FB] = \frac{(K_D + L_T + R_T) - \sqrt{(K_D + L_T + R_T)^2 - 4R_T L_T}}{L_T}$$

where R_T is the total concentration of the unlabeled binding partner, L_T is the total concentration of the labeled peptide **F4**, and K_D is the dissociation constant. For a better overview, the binding curves are shown in a semi-logarithmic plot where the data were fitted to the following equation. This equation was also used to determine the K_D value of the sirtuin binding curves.

$$[FB] = Y_{min} + \frac{Y_{max} - Y_{min}}{1 + 10^{(\log K_D - R) \cdot n}}$$

4.12. Determination of Z' Value and S/N Ratio

The Z' factor was determined using a full 96-well plate (or 96 wells in a 384-well plate and 96 wells in a 1536-well plate), and half the plate contained a reaction mixture with 1 μ M of **F4**, 500 μ M of NAD^+ , and 10 nM of SIRT2 representing 100%, and the other wells contained the same reaction mixture without SIRT2 and represented the 0% value. Fluorescence readouts were performed with the settings described above after approximately 90% product formation (1 h). The Z' factor was determined with the following equation, where SD indicates the standard deviation of the 100% values and the 0% values.

$$Z' = \frac{3SD_{100\%} + 3SD_{0\%}}{|\text{mean}_{100\%} - \text{mean}_{0\%}|}$$

The signal to noise ratio (S/N) was determined using the values described above in the following equation:

$$S/N = \frac{\text{mean}_{100\%} - \text{mean}_{0\%}}{SD_{0\%}}$$

Supplementary Materials: The following supporting information can be downloaded at: <https://www.mdpi.com/article/10.3390/ijms24087416/s1>.

Author Contributions: Conceptualization and methodology, M.S. and M.Z.; formal analysis, investigation and validation, M.Z., M.M. and S.H.; resources, M.J. and C.B.; writing—original draft preparation, M.S. and M.Z.; writing—review and editing, C.S.-F., M.J. and C.B.; visualization, M.Z.; supervision and project administration, M.S.; funding acquisition, M.S. and C.B. All authors have read and agreed to the published version of the manuscript.

Funding: This work was supported by grants from Deutsche Forschungsgemeinschaft (INST 271/336-1 FUGG) to M.S, and in part by the CAS (RVO: 86652036) and the Czech Science Foundation (21-31806) to C.B. MJ thanks the Deutsche Forschungsgemeinschaft (DFG; Ju-295/18-1) for funding.

Institutional Review Board Statement: Not applicable.

Informed Consent Statement: Not applicable.

Data Availability Statement: Not applicable.

Acknowledgments: The authors thank Gary Sawers for proofreading and language editing of the manuscript, Ilona Kunze for excellent technical support, Sandra Liebscher for providing the sirtuins, Thomas Kiefhaber and Frank Bordusa at the Martin Luther University of Halle-Wittenberg for giving us access to the single-quadrupole LC-MS analyses and the core facility proteomics mass spectrometry of the Martin Luther University of Halle-Wittenberg for technical assistance during the triple-quadrupole LC-MS experiments.

Conflicts of Interest: The authors declare no conflict of interest.

References

1. Smith, B.C.; Hallows, W.C.; Denu, J.M. Mechanisms and molecular probes of sirtuins. *Chem. Biol.* **2008**, *15*, 1002–1013. [[CrossRef](#)] [[PubMed](#)]
2. Schutkowski, M.; Fischer, F.; Roessler, C.; Steegborn, C. New assays and approaches for discovery and design of Sirtuin modulators. *Expert Opin. Drug Discov.* **2014**, *9*, 183–199. [[CrossRef](#)] [[PubMed](#)]
3. Zessin, M.; Meleshin, M.; Simic, Z.; Kalbas, D.; Arbach, M.; Gebhardt, P.; Melesina, J.; Liebscher, S.; Bordusa, F.; Sippl, W.; et al. Continuous Sirtuin/HDAC (histone deacetylase) activity assay using thioamides as PET (Photoinduced Electron Transfer)-based fluorescence quencher. *Bioorg. Chem.* **2021**, *117*, 105425. [[CrossRef](#)]
4. Riester, D.; Hildmann, C.; Grünewald, S.; Beckers, T.; Schwienhorst, A. Factors affecting the substrate specificity of histone deacetylases. *Biochem. Biophys. Res. Commun.* **2007**, *357*, 439–445. [[CrossRef](#)] [[PubMed](#)]
5. Wegener, D.; Hildmann, C.; Riester, D.; Schober, A.; Meyer-Almes, F.-J.; Deubzer, H.E.; Oehme, I.; Witt, O.; Lang, S.; Jaensch, M.; et al. Identification of novel small-molecule histone deacetylase inhibitors by medium-throughput screening using a fluorogenic assay. *Biochem. J.* **2008**, *413*, 143–150. [[CrossRef](#)]
6. Ciossek, T.; Julius, H.; Wieland, H.; Maier, T.; Beckers, T. A homogeneous cellular histone deacetylase assay suitable for compound profiling and robotic screening. *Anal. Biochem.* **2008**, *372*, 72–81. [[CrossRef](#)] [[PubMed](#)]
7. Wegener, D.; Wirsching, F.; Riester, D.; Schwienhorst, A. A fluorogenic histone deacetylase assay well suited for high-throughput activity screening. *Chem. Biol.* **2003**, *10*, 61–68. [[CrossRef](#)] [[PubMed](#)]
8. Wegener, D.; Hildmann, C.; Riester, D.; Schwienhorst, A. Improved fluorogenic histone deacetylase assay for high-throughput-screening applications. *Anal. Biochem.* **2003**, *321*, 202–208. [[CrossRef](#)]
9. Bradner, J.E.; West, N.; Grachan, M.L.; Greenberg, E.F.; Haggarty, S.J.; Warnow, T.; Mazitschek, R. Chemical phylogenetics of histone deacetylases. *Nat. Chem. Biol.* **2010**, *6*, 238–243. [[CrossRef](#)]
10. Lahm, A.; Paolini, C.; Pallaoro, M.; Nardi, M.C.; Jones, P.; Neddermann, P.; Sambucini, S.; Bottomley, M.J.; Lo Surdo, P.; Carfi, A.; et al. Unraveling the hidden catalytic activity of vertebrate class IIa histone deacetylases. *Proc. Natl. Acad. Sci. USA* **2007**, *104*, 17335–17340. [[CrossRef](#)]
11. Smith, B.C.; Hallows, W.C.; Denu, J.M. A continuous microplate assay for sirtuins and nicotinamide-producing enzymes. *Anal. Biochem.* **2009**, *394*, 101–109. [[CrossRef](#)]
12. Wei, W.; Zhang, J.; Xu, Z.; Liu, Z.; Huang, C.; Cheng, K.; Meng, L.; Matsuda, Y.; Hao, Q.; Zhang, H.; et al. Universal Strategy to Develop Fluorogenic Probes for Lysine Deacylase/Demethylase Activity and Application in Discriminating Demethylation States. *ACS Sens.* **2023**, *8*, 28–39. [[CrossRef](#)]
13. Tan, S.; Li, X. Small-Molecule Fluorescent Probes for Detecting HDAC Activity. *Chem. Asian J.* **2022**, *17*, e202200835. [[CrossRef](#)] [[PubMed](#)]
14. Hori, Y.; Kikuchi, K. Chemical Tools with Fluorescence Switches for Verifying Epigenetic Modifications. *Acc. Chem. Res.* **2019**, *52*, 2849–2857. [[CrossRef](#)] [[PubMed](#)]
15. Fan, Y.; Scriba, G.K.E. Electrophoretically mediated microanalysis assay for sirtuin enzymes. *Electrophoresis* **2010**, *31*, 3874–3880. [[CrossRef](#)] [[PubMed](#)]
16. Ohla, S.; Beyreiss, R.; Scriba, G.K.E.; Fan, Y.; Belder, D. An integrated on-chip sirtuin assay. *Electrophoresis* **2010**, *31*, 3263–3267. [[CrossRef](#)] [[PubMed](#)]
17. Liu, Y.; Gerber, R.; Wu, J.; Tsuruda, T.; McCarter, J.D. High-throughput assays for sirtuin enzymes: A microfluidic mobility shift assay and a bioluminescence assay. *Anal. Biochem.* **2008**, *378*, 53–59. [[CrossRef](#)]
18. Blackwell, L.; Norris, J.; Suto, C.M.; Janzen, W.P. The use of diversity profiling to characterize chemical modulators of the histone deacetylases. *Life Sci.* **2008**, *82*, 1050–1058. [[CrossRef](#)]

19. Khan, A.N.; Lewis, P.N. Unstructured conformations are a substrate requirement for the Sir2 family of NAD-dependent protein deacetylases. *J. Biol. Chem.* **2005**, *280*, 36073–36078. [[CrossRef](#)]
20. Jackson, M.D.; Denu, J.M. Structural identification of 2'- and 3'-O-acetyl-ADP-ribose as novel metabolites derived from the Sir2 family of beta -NAD+-dependent histone/protein deacetylases. *J. Biol. Chem.* **2002**, *277*, 18535–18544. [[CrossRef](#)]
21. Tanner, K.G.; Landry, J.; Sternglanz, R.; Denu, J.M. Silent information regulator 2 family of NAD- dependent histone/protein deacetylases generates a unique product, 1-O-acetyl-ADP-ribose. *Proc. Natl. Acad. Sci. USA* **2000**, *97*, 14178–14182. [[CrossRef](#)] [[PubMed](#)]
22. Marcotte, P.A.; Richardson, P.L.; Guo, J.; Barrett, L.W.; Xu, N.; Gunasekera, A.; Glaser, K.B. Fluorescence assay of SIRT protein deacetylases using an acetylated peptide substrate and a secondary trypsin reaction. *Anal. Biochem.* **2004**, *332*, 90–99. [[CrossRef](#)]
23. Du, J.; Zhou, Y.; Su, X.; Yu, J.J.; Khan, S.; Jiang, H.; Kim, J.; Woo, J.; Kim, J.H.; Choi, B.H.; et al. Sirt5 is a NAD-dependent protein lysine demalonylase and desuccinylase. *Science* **2011**, *334*, 806–809. [[CrossRef](#)] [[PubMed](#)]
24. Khan, A.N.; Lewis, P.N. Use of substrate analogs and mutagenesis to study substrate binding and catalysis in the Sir2 family of NAD-dependent protein deacetylases. *J. Biol. Chem.* **2006**, *281*, 11702–11711. [[CrossRef](#)]
25. Borra, M.T.; Denu, J.M. Quantitative assays for characterization of the Sir2 family of NAD(+)-dependent deacetylases. *Methods Enzymol.* **2004**, *376*, 171–187. [[CrossRef](#)] [[PubMed](#)]
26. McDonagh, T.; Hixon, J.; DiStefano, P.S.; Curtis, R.; Napper, A.D. Microplate filtration assay for nicotinamide release from NAD using a boronic acid resin. *Methods* **2005**, *36*, 346–350. [[CrossRef](#)]
27. Hoffmann, K.; Heltweg, B.; Jung, M. Improvement and Validation of the Fluorescence-Based Histone Deacetylase Assay Using an Internal Standard. *Arch. Pharm. Pharm. Med. Chem.* **2001**, *334*, 248–252. [[CrossRef](#)]
28. Shao, D.; Yao, C.; Kim, M.H.; Fry, J.; Cohen, R.A.; Costello, C.E.; Matsui, R.; Seta, F.; McComb, M.E.; Bachschmid, M.M. Improved mass spectrometry-based activity assay reveals oxidative and metabolic stress as sirtuin-1 regulators. *Redox Biol.* **2019**, *22*, 101150. [[CrossRef](#)]
29. Holzhauser, S.; Freiwald, A.; Weise, C.; Multhaup, G.; Han, C.-T.; Sauer, S. Discovery and characterization of protein-modifying natural products by MALDI mass spectrometry reveal potent SIRT1 and p300 inhibitors. *Angew. Chem. Int. Ed. Engl.* **2013**, *52*, 5171–5174. [[CrossRef](#)]
30. Rye, P.T.; Frick, L.E.; Ozbal, C.C.; Lamarr, W.A. Advances in label-free screening approaches for studying sirtuin-mediated deacetylation. *J. Biomol. Screen.* **2011**, *16*, 1217–1226. [[CrossRef](#)]
31. Fischer, F.; Gertz, M.; Suenkel, B.; Lakshminarasimhan, M.; Schutkowski, M.; Steegborn, C. Sirt5 deacetylation activities show differential sensitivities to nicotinamide inhibition. *PLoS ONE* **2012**, *7*, e45098. [[CrossRef](#)]
32. Machleidt, T.; Robers, M.B.; Hermanson, S.B.; Dudek, J.M.; Bi, K. TR-FRET cellular assays for interrogating posttranslational modifications of histone H3. *J. Biomol. Screen.* **2011**, *16*, 1236–1246. [[CrossRef](#)]
33. Degorce, F.; Card, A.; Soh, S.; Trinquet, E.; Knapik, G.P.; Xie, B. HTRF: A technology tailored for drug discovery—A review of theoretical aspects and recent applications. *Curr. Chem. Genomics* **2009**, *3*, 22–32. [[CrossRef](#)] [[PubMed](#)]
34. Dudek, J.M.; Horton, R.A. TR-FRET biochemical assays for detecting posttranslational modifications of p53. *J. Biomol. Screen.* **2010**, *15*, 569–575. [[CrossRef](#)]
35. Robers, M.B.; Loh, C.; Carlson, C.B.; Yang, H.; Frey, E.A.; Hermanson, S.B.; Bi, K. Measurement of the cellular deacetylase activity of SIRT1 on p53 via LanthaScreen® technology. *Mol. Biosyst.* **2011**, *7*, 59–66. [[CrossRef](#)]
36. Rauh, D.; Fischer, F.; Gertz, M.; Lakshminarasimhan, M.; Bergbrede, T.; Aladini, F.; Kambach, C.; Becker, C.F.W.; Zerweck, J.; Schutkowski, M.; et al. An acetyloyme peptide microarray reveals specificities and deacetylation substrates for all human sirtuin isoforms. *Nat. Commun.* **2013**, *4*, 2327. [[CrossRef](#)] [[PubMed](#)]
37. Kutil, Z.; Skultetyova, L.; Rauh, D.; Meleshin, M.; Snajdr, L.; Novakova, Z.; Mikesova, J.; Pavlicek, J.; Hadzima, M.; Baranova, P.; et al. The unraveling of substrate specificity of histone deacetylase 6 domains using acetyloyme peptide microarrays and peptide libraries. *FASEB J.* **2019**, *33*, 4035–4045. [[CrossRef](#)]
38. Heltweg, B.; Dequiedt, F.; Verdin, E.; Jung, M. Nonisotopic substrate for assaying both human zinc and NAD+-dependent histone deacetylases. *Anal. Biochem.* **2003**, *319*, 42–48. [[CrossRef](#)]
39. Toro, T.B.; Watt, T.J. KDAC8 substrate specificity quantified by a biologically relevant, label-free deacetylation assay. *Protein Sci.* **2015**, *24*, 2020–2032. [[CrossRef](#)] [[PubMed](#)]
40. Xie, Y.; Ge, J.; Lei, H.; Peng, B.; Zhang, H.; Wang, D.; Pan, S.; Chen, G.; Chen, L.; Wang, Y.; et al. Fluorescent Probes for Single-Step Detection and Proteomic Profiling of Histone Deacetylases. *J. Am. Chem. Soc.* **2016**, *138*, 15596–15604. [[CrossRef](#)]
41. Baba, R.; Hori, Y.; Kikuchi, K. Intramolecular long-distance nucleophilic reactions as a rapid fluorogenic switch applicable to the detection of enzymatic activity. *Chemistry* **2015**, *21*, 4695–4702. [[CrossRef](#)]
42. Baba, R.; Hori, Y.; Mizukami, S.; Kikuchi, K. Development of a fluorogenic probe with a transesterification switch for detection of histone deacetylase activity. *J. Am. Chem. Soc.* **2012**, *134*, 14310–14313. [[CrossRef](#)] [[PubMed](#)]
43. Wang, C.; Du, W.; Zhang, T.; Liang, G. A Bioluminescent Probe for Simultaneously Imaging Esterase and Histone Deacetylase Activity in a Tumor. *Anal. Chem.* **2020**, *92*, 15275–15279. [[CrossRef](#)] [[PubMed](#)]
44. Rooker, D.R.; Klyubka, Y.; Gautam, R.; Tomat, E.; Buccella, D. Peptide-Based Fluorescent Probes for Deacetylase and Decrotonylase Activity: Toward a General Platform for Real-Time Detection of Lysine Deacylation. *ChemBiochem* **2018**, *19*, 496–504. [[CrossRef](#)]
45. Rooker, D.R.; Buccella, D. Real-time detection of histone deacetylase activity with a small molecule fluorescent and spectrophotometric probe. *Chem. Sci.* **2015**, *6*, 6456–6461. [[CrossRef](#)]

46. Feldman, J.L.; Baeza, J.; Denu, J.M. Activation of the protein deacetylase SIRT6 by long-chain fatty acids and widespread deacylation by mammalian sirtuins. *J. Biol. Chem.* **2013**, *288*, 31350–31356. [[CrossRef](#)]
47. Kutil, Z.; Novakova, Z.; Meleshin, M.; Mikesova, J.; Schutkowski, M.; Barinka, C. Histone Deacetylase 11 Is a Fatty-Acid Deacylase. *ACS Chem. Biol.* **2018**, *13*, 685–693. [[CrossRef](#)] [[PubMed](#)]
48. Moreno-Yruela, C.; Galleano, I.; Madsen, A.S.; Olsen, C.A. Histone Deacetylase 11 Is an ϵ -N-Myristoyllysine Hydrolase. *Cell Chem. Biol.* **2018**, *25*, 849–856. [[CrossRef](#)]
49. Cao, J.; Sun, L.; Aramsangtienchai, P.; Spiegelman, N.A.; Zhang, X.; Huang, W.; Seto, E.; Lin, H. HDAC11 regulates type I interferon signaling through defatty-acylation of SHMT2. *Proc. Natl. Acad. Sci. USA* **2019**, *116*, 5487–5492. [[CrossRef](#)]
50. Schuster, S.; Roessler, C.; Meleshin, M.; Zimmermann, P.; Simic, Z.; Kambach, C.; Schiene-Fischer, C.; Steegborn, C.; Hottiger, M.O.; Schutkowski, M. A continuous sirtuin activity assay without any coupling to enzymatic or chemical reactions. *Sci. Rep.* **2016**, *6*, 22643. [[CrossRef](#)]
51. Kutil, Z.; Mikešová, J.; Zessin, M.; Meleshin, M.; Nováková, Z.; Alquicer, G.; Kozikowski, A.; Sippl, W.; Bařinka, C.; Schutkowski, M. Continuous Activity Assay for HDAC11 Enabling Reevaluation of HDAC Inhibitors. *ACS Omega* **2019**, *4*, 19895–19904. [[CrossRef](#)]
52. Petersson, E.J.; Goldberg, J.M.; Wissner, R.F. On the use of thioamides as fluorescence quenching probes for tracking protein folding and stability. *Phys. Chem. Chem. Phys.* **2014**, *16*, 6827–6837. [[CrossRef](#)]
53. Zessin, M.; Kutil, Z.; Meleshin, M.; Nováková, Z.; Ghazy, E.; Kalbas, D.; Marek, M.; Romier, C.; Sippl, W.; Bařinka, C.; et al. One-Atom Substitution Enables Direct and Continuous Monitoring of Histone Deacetylase Activity. *Biochemistry* **2019**, *58*, 4777–4789. [[CrossRef](#)]
54. Smith, B.C.; Denu, J.M. Mechanism-based inhibition of Sir2 deacetylases by thioacetyl-lysine peptide. *Biochemistry* **2007**, *46*, 14478–14486. [[CrossRef](#)] [[PubMed](#)]
55. He, B.; Hu, J.; Zhang, X.; Lin, H. Thiomyristoyl peptides as cell-permeable Sirt6 inhibitors. *Org. Biomol. Chem.* **2014**, *12*, 7498–7502. [[CrossRef](#)] [[PubMed](#)]
56. Jing, H.; Hu, J.; He, B.; Negrón Abril, Y.L.; Stupinski, J.; Weiser, K.; Carbonaro, M.; Chiang, Y.-L.; Southard, T.; Giannakakou, P.; et al. A SIRT2-Selective Inhibitor Promotes c-Myc Oncoprotein Degradation and Exhibits Broad Anticancer Activity. *Cancer Cell* **2016**, *29*, 297–310. [[CrossRef](#)]
57. Spiegelman, N.A.; Hong, J.Y.; Hu, J.; Jing, H.; Wang, M.; Price, I.R.; Cao, J.; Yang, M.; Zhang, X.; Lin, H. A Small-Molecule SIRT2 Inhibitor That Promotes K-Ras4a Lysine Fatty-Acylation. *ChemMedChem* **2019**, *14*, 744–748. [[CrossRef](#)] [[PubMed](#)]
58. Kawaguchi, M.; Ikegawa, S.; Ieda, N.; Nakagawa, H. A Fluorescent Probe for Imaging Sirtuin Activity in Living Cells, Based on One-Step Cleavage of the Dabcyl Quencher. *Chembiochem* **2016**, *17*, 1961–1967. [[CrossRef](#)] [[PubMed](#)]
59. Nakajima, Y.; Kawaguchi, M.; Ieda, N.; Nakagawa, H. A Set of Highly Sensitive Sirtuin Fluorescence Probes for Screening Small-Molecular Sirtuin Defatty-Acylase Inhibitors. *ACS Med. Chem. Lett.* **2021**, *12*, 617–624. [[CrossRef](#)]
60. Kannan, S.; Melesina, J.; Hauser, A.-T.; Chakrabarti, A.; Heimbürg, T.; Schmidtkunz, K.; Walter, A.; Marek, M.; Pierce, R.J.; Romier, C.; et al. Discovery of inhibitors of *Schistosoma mansoni* HDAC8 by combining homology modeling, virtual screening, and in vitro validation. *J. Chem. Inf. Model.* **2014**, *54*, 3005–3019. [[CrossRef](#)]
61. Wu, J.; Zheng, Y.G. Fluorescent reporters of the histone acetyltransferase. *Anal. Biochem.* **2008**, *380*, 106–110. [[CrossRef](#)]
62. Peng, C.; Lu, Z.; Xie, Z.; Cheng, Z.; Chen, Y.; Tan, M.; Luo, H.; Zhang, Y.; He, W.; Yang, K.; et al. The first identification of lysine malonylation substrates and its regulatory enzyme. *Mol. Cell. Proteom.* **2011**, *10*, M111.012658. [[CrossRef](#)] [[PubMed](#)]
63. Tan, M.; Peng, C.; Anderson, K.A.; Chhoy, P.; Xie, Z.; Dai, L.; Park, J.; Chen, Y.; Huang, H.; Zhang, Y.; et al. Lysine glutarylation is a protein posttranslational modification regulated by SIRT5. *Cell Metab.* **2014**, *19*, 605–617. [[CrossRef](#)] [[PubMed](#)]
64. Spector, A.A. Fatty acid binding to plasma albumin. *J. Lipid Res.* **1975**, *16*, 165–179. [[CrossRef](#)]
65. Moniot, S.; Schutkowski, M.; Steegborn, C. Crystal structure analysis of human Sirt2 and its ADP-ribose complex. *J. Struct. Biol.* **2013**, *182*, 136–143. [[CrossRef](#)]
66. Vogelmann, A.; Schiedel, M.; Wössner, N.; Merz, A.; Herp, D.; Hammelmann, S.; Colcerasa, A.; Komaniecki, G.; Hong, J.Y.; Sum, M.; et al. Development of a NanoBRET assay to validate inhibitors of Sirt2-mediated lysine deacetylation and defatty-acylation that block prostate cancer cell migration. *RSC Chem. Biol.* **2022**, *3*, 468–485. [[CrossRef](#)]
67. Rumpf, T.; Schiedel, M.; Karaman, B.; Roessler, C.; North, B.J.; Lehotzky, A.; Oláh, J.; Ladwein, K.I.; Schmidtkunz, K.; Gajer, M.; et al. Selective Sirt2 inhibition by ligand-induced rearrangement of the active site. *Nat. Commun.* **2015**, *6*, 6263. [[CrossRef](#)]
68. Spiegelman, N.A.; Price, I.R.; Jing, H.; Wang, M.; Yang, M.; Cao, J.; Hong, J.Y.; Zhang, X.; Aramsangtienchai, P.; Sadhukhan, S.; et al. Direct Comparison of SIRT2 Inhibitors: Potency, Specificity, Activity-Dependent Inhibition, and On-Target Anticancer Activities. *ChemMedChem* **2018**, *13*, 1890–1894. [[CrossRef](#)] [[PubMed](#)]
69. Outeiro, T.F.; Kontopoulos, E.; Altmann, S.M.; Kufareva, I.; Strathearn, K.E.; Amore, A.M.; Volk, C.B.; Maxwell, M.M.; Rochet, J.-C.; McLean, P.J.; et al. Sirtuin 2 inhibitors rescue alpha-synuclein-mediated toxicity in models of Parkinson's disease. *Science* **2007**, *317*, 516–519. [[CrossRef](#)]
70. Kalbas, D.; Meleshin, M.; Liebscher, S.; Zessin, M.; Melesina, J.; Schiene-Fischer, C.; Bülbül, E.F.; Bordusa, F.; Sippl, W.; Schutkowski, M. Small Changes Make the Difference for SIRT2: Two Different Binding Modes for 3-Arylmercapto-Acylated Lysine Derivatives. *Biochemistry* **2022**, *61*, 1705–1722. [[CrossRef](#)]

71. Yamagata, K.; Goto, Y.; Nishimasu, H.; Morimoto, J.; Ishitani, R.; Dohmae, N.; Takeda, N.; Nagai, R.; Komuro, I.; Suga, H.; et al. Structural basis for potent inhibition of SIRT2 deacetylase by a macrocyclic peptide inducing dynamic structural change. *Structure* **2014**, *22*, 345–352. [[CrossRef](#)]
72. Suenkel, B.; Fischer, F.; Steegborn, C. Inhibition of the human deacetylase Sirtuin 5 by the indole GW5074. *Bioorg. Med. Chem. Lett.* **2013**, *23*, 143–146. [[CrossRef](#)] [[PubMed](#)]
73. Dose, A.; Jost, J.O.; Spieß, A.C.; Henklein, P.; Beyermann, M.; Schwarzer, D. Facile synthesis of colorimetric histone deacetylase substrates. *Chem. Commun.* **2012**, *48*, 9525–9527. [[CrossRef](#)] [[PubMed](#)]
74. Halley, F.; Reinshagen, J.; Ellinger, B.; Wolf, M.; Niles, A.L.; Evans, N.J.; Kirkland, T.A.; Wagner, J.M.; Jung, M.; Gribbon, P.; et al. A bioluminogenic HDAC activity assay: Validation and screening. *J. Biomol. Screen.* **2011**, *16*, 1227–1235. [[CrossRef](#)]
75. Milne, J.C.; Lambert, P.D.; Schenk, S.; Carney, D.P.; Smith, J.J.; Gagne, D.J.; Jin, L.; Boss, O.; Perni, R.B.; Vu, C.B.; et al. Small molecule activators of SIRT1 as therapeutics for the treatment of type 2 diabetes. *Nature* **2007**, *450*, 712–716. [[CrossRef](#)]
76. Roessler, C.; Tüting, C.; Meleshin, M.; Steegborn, C.; Schutkowski, M. A Novel Continuous Assay for the Deacetylase Sirtuin 5 and Other Deacetylases. *J. Med. Chem.* **2015**, *58*, 7217–7223. [[CrossRef](#)]
77. Galleano, I.; Schiedel, M.; Jung, M.; Madsen, A.S.; Olsen, C.A. A Continuous, Fluorogenic Sirtuin 2 Deacetylase Assay: Substrate Screening and Inhibitor Evaluation. *J. Med. Chem.* **2016**, *59*, 1021–1031. [[CrossRef](#)]
78. Xuan, W.; Yao, A.; Schultz, P.G. Genetically Encoded Fluorescent Probe for Detecting Sirtuins in Living Cells. *J. Am. Chem. Soc.* **2017**, *139*, 12350–12353. [[CrossRef](#)]
79. Spinck, M.; Ecke, M.; Sievers, S.; Neumann, H. Highly Sensitive Lysine Deacetylase Assay Based on Acetylated Firefly Luciferase. *Biochemistry* **2018**, *57*, 3552–3555. [[CrossRef](#)] [[PubMed](#)]

Disclaimer/Publisher’s Note: The statements, opinions and data contained in all publications are solely those of the individual author(s) and contributor(s) and not of MDPI and/or the editor(s). MDPI and/or the editor(s) disclaim responsibility for any injury to people or property resulting from any ideas, methods, instructions or products referred to in the content.

3.6 Uncovering robust delactoylase and depyruvoylase activities of HDAC isoforms

Matthes Zessin, Marat Meleshin, Lucas Praetorius, Wolfgang Sippl, Cyril Bařinka und Mike Schutkowski

ACS Chemical Biology, 2022, 17, 1364-1375
DOI: <https://doi.org/10.1021/acscchembio.1c00863>

Abstract:

Zinc-dependent histone deacetylases (HDACs) and sirtuins (SIRT) represent two different classes of enzymes which are responsible for deacylation of modified lysine side chains. The repertoire of acyl residues on lysine side chains identified *in vivo* is rapidly growing, and very recently lysine lactoylation was described to be involved in metabolic reprogramming. Additionally, lysine pyruvoylation represents a marker for aging and liver cirrhosis. Here, we report a systematic analysis of acyl-specificity of human zinc-dependent HDAC and sirtuin isoforms. We identified HDAC3 as a robust delactoylase with several-thousand-fold higher activity as compared to SIRT2, which was claimed to be the major *in vivo* delactoylase. Additionally, we systematically searched for enzymes, capable of removing pyruvoyl residues from lysine side chains. Using model peptides, we uncovered high depyruvoylase activity for HDAC6 and HDAC8. Interestingly, such substrates have extremely low K_M values for both HDAC isoforms, pointing to possible *in vivo* functions.

Reprinted (adapted) with permission from Uncovering Robust Delactoylase and Depyruvoylase Activities of HDAC Isoforms, Matthes Zessin, Marat Meleshin, Lucas Praetorius, Wolfgang Sippl, Cyril Bařinka, and Mike Schutkowski, ACS Chemical Biology 2022 17 (6), 1364-1375 DOI: 10.1021/acscchembio.1c00863. Copyright 2022 American Chemical Society."

Uncovering Robust Delactoylase and Depyruvoylase Activities of HDAC Isoforms

Published as part of the ACS Chemical Biology special issue "Epigenetics 2022".

Matthes Zessin, Marat Meleshin, Lucas Praetorius, Wolfgang Sippl, Cyril Bařinka, and Mike Schutkowski*



Cite This: *ACS Chem. Biol.* 2022, 17, 1364–1375



Read Online

ACCESS |



Metrics & More

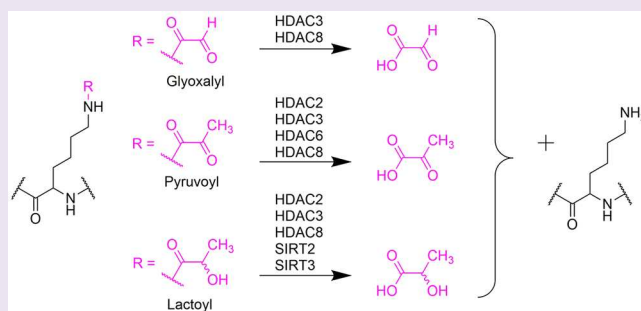


Article Recommendations



Supporting Information

ABSTRACT: Zinc-dependent histone deacetylases (HDACs) and sirtuins (SIRT) represent two different classes of enzymes which are responsible for deacylation of modified lysine side chains. The repertoire of acyl residues on lysine side chains identified *in vivo* is rapidly growing, and very recently lysine lactoylation was described to be involved in metabolic reprogramming. Additionally, lysine pyruvoylation represents a marker for aging and liver cirrhosis. Here, we report a systematic analysis of acyl-specificity of human zinc-dependent HDAC and sirtuin isoforms. We identified HDAC3 as a robust delactoylase with several-thousand-fold higher activity as compared to SIRT2, which was claimed to be the major *in vivo* delactoylase. Additionally, we systematically searched for enzymes, capable of removing pyruvoyl residues from lysine side chains. Using model peptides, we uncovered high depyruvoylase activity for HDAC6 and HDAC8. Interestingly, such substrates have extremely low K_M values for both HDAC isoforms, pointing to possible *in vivo* functions.



Acylation of lysine side chains in proteins is a widespread post-translational modification regulated by the action of histone acetyltransferases (HATs) or by the respective metabolic situation. Figure 1 shows examples of various acylations that are introduced by the action of HATs, such as acetyltransferase p300, which can use a plethora of cofactors. For p300 (besides acetylation), the transfer of propionyl,¹ butyryl,¹ succinyl,² glutaryl,³ crotonyl,⁴ lactoyl,⁵ 2-hydroxyisobutyryl,⁶ and β -hydroxybutyryl⁷ residues to lysine side chains has been reported.

Figure 2 summarizes modifications of lysine side chains resulting from spontaneous reactions of metabolites, like chemical acylation by acyl-CoAs in mitochondria⁸ or ketoamidation mediated by 4-oxo-2-nonenal, a degradation product of arachidonic acid.⁹

Recently, spontaneous lysine lactoylation by lactoylglutathione was reported.¹⁰ Lactoylglutathione is formed by the reaction of glutathione with methylglyoxal via the glyoxalase pathway. Lactoylation of lysine residues seems to be involved in metabolic reprogramming⁵ and could be induced by neural excitation and social stress.¹¹ Pyruvoylation, a modification very similar to lactoylation, was reported as an amide advanced glycation endproduct¹² enriched in aging mice liver tissue and liver cirrhosis.¹³ Chemical diversity of acyl residues generated by the reaction of lysines with α -dicarbonyls and acylphosphates was reviewed recently.¹⁴

Generally, reversal of lysine acetylations is mediated by evolutionarily conserved enzymes introduced as histone deacetylases (HDACs). On the basis of sequence homology, HDACs can be divided into four classes. Members of class I (HDAC1, -2, -3, and -8), class IIa (HDAC4, -5, -7, and -9), class IIb (HDAC6 and -10), and class IV (HDAC11) are Zn²⁺-dependent hydrolases, while class III proteins (called sirtuins; SIRT1–7) use NAD⁺ as a cosubstrate.¹⁵

Robust deacetylase activity is reported for sirtuins 1–3 and for HDACs1–3, -6, and -8. Additionally, nearly all sirtuins have demyristoylation activity,¹⁶ and recently it was shown that HDAC11 is a demyristoylase as well.^{17–19} SIRT5 is a robust demalonylase, desuccinylase, and deglutarylase.^{3,20,21} SIRT4 seems to be specialized to reverse hydroxymethylglutarylations.²² SIRT2 accepts a relatively broad panel of acyl residues including benzoyl moieties²³ and is the only enzyme removing 4-oxo-nonanoylations.²⁴ Recently, delactoylase activity was reported for SIRT2 but with very low catalytic efficiency ($k_{cat}/$

Received: October 31, 2021

Accepted: May 10, 2022

Published: May 31, 2022



Table 1. Compounds (1–6) and Control Substrates (C1–C5) Used in This Work^a

compound	peptide sequence	acyl residue (R)
1	Abz-SRGGK(R)FFRR-NH ₂	
1a	ARTKQTARK(R)STGGWW-NH ₂	
2	Abz-SRGGK(R)FFRR-NH ₂	
3	Abz-SRGGK(R)FFRR-NH ₂	
3a	ARTKQTARK(R)STGGWW-NH ₂	
4	Abz-SRGGK(R)FFRR-NH ₂	
4a	ARTKQTARK(R)STGGWW-NH ₂	
5	Abz-SRGGK(R)FFRR-NH ₂	
6	Abz-SRGGK(R)FFRR-NH ₂	
C1	Ac-RHKK(R)-AMC	
C2	Abz-SRGGK(R)FFRR-NH ₂	
C3	Bz-GVLK(R)EYGV-NH ₂	
C4	Ac-EALPKK(R)Y(NO ₂)GG-NH ₂	
C5	Abz-SRGGKFFRR-NH ₂	-

^aAbz = 2-aminobenzoyl; Ac = acetyl; AMC = 7-amino-4-methylcoumarin; Bz = benzoyl; Y(NO₂) = 3-nitrotyrosyl, NH₂ = C-terminal amide.

(Figures S1–S8). We tested the stability by treatment with an assay buffer for 3 h. All peptide derivatives are stable at 30 °C.

We screened the activity of HDAC2–9 and HDAC11, and SIRT2, -3, -5, and -6 against compound 3 and compared it to the acetylated (1) and propionylated (2) counterpart using an HPLC-based end point assay. As apparent from Figure 3, HDAC2 and HDAC3 accept 2 slightly better than 1. In contrast, HDAC6 and HDAC8 showed reduced activity against 2 as compared to 1. Class IIa HDACs and HDAC11 are not able to hydrolyze derivatives 1–3, and class IIb HDAC6 cannot handle lactoylated peptide derivative 3, at least *in vitro*. HDAC2 and HDAC3 and to some extent HDAC8 can remove the lactoyl residue from 3. This HDAC8 activity is somehow surprising because Moreno-Yruela et al. found no HDAC8-mediated turnover of lactoylated peptide derivatives.²⁹ We repeated the HDAC8 experiments in the presence of RGFP966 and Mocetinostat, which are known inhibitors of HDAC1, HDAC2, and HDAC3, but not for HDAC8. If contaminating HDACs in the HDAC8 preparation would be the source of the detected delactoylase activity, much less

activity could be expected. Nevertheless, we were able to detect delactoylase activity for HDAC8 in the presence of these inhibitors, pointing to a direct HDAC8-mediated cleavage of lactoyl amide bonds (Figure S27).

We used an HPLC-based assay to determine the velocity of deacylation at different substrate concentrations.^{15,21,31–33} Therefore, we stopped the enzymatic reaction at four different time points and separated the substrate and peptidic product using RP-HPLC. Plotting the amount of product formed against the reaction time yielded linear relationships (Figure S9), and respective slopes enable calculation of reaction velocities. Determination of kinetic constants (Table 2) revealed that HDAC2, HDAC3, and HDAC8 have approximately 10-fold reduced specificity constants for the lactoylated substrate 3 as compared to the propionylated version. This difference is caused by an increased K_M value for HDAC2 and HDAC3 but by a clearly lower k_{cat} value for HDAC8, pointing to subtle differences in the enzymatic mechanisms of class I HDACs. It seems likely that the presence of the hydroxyl group (when compared to 2) directly influences the proposed

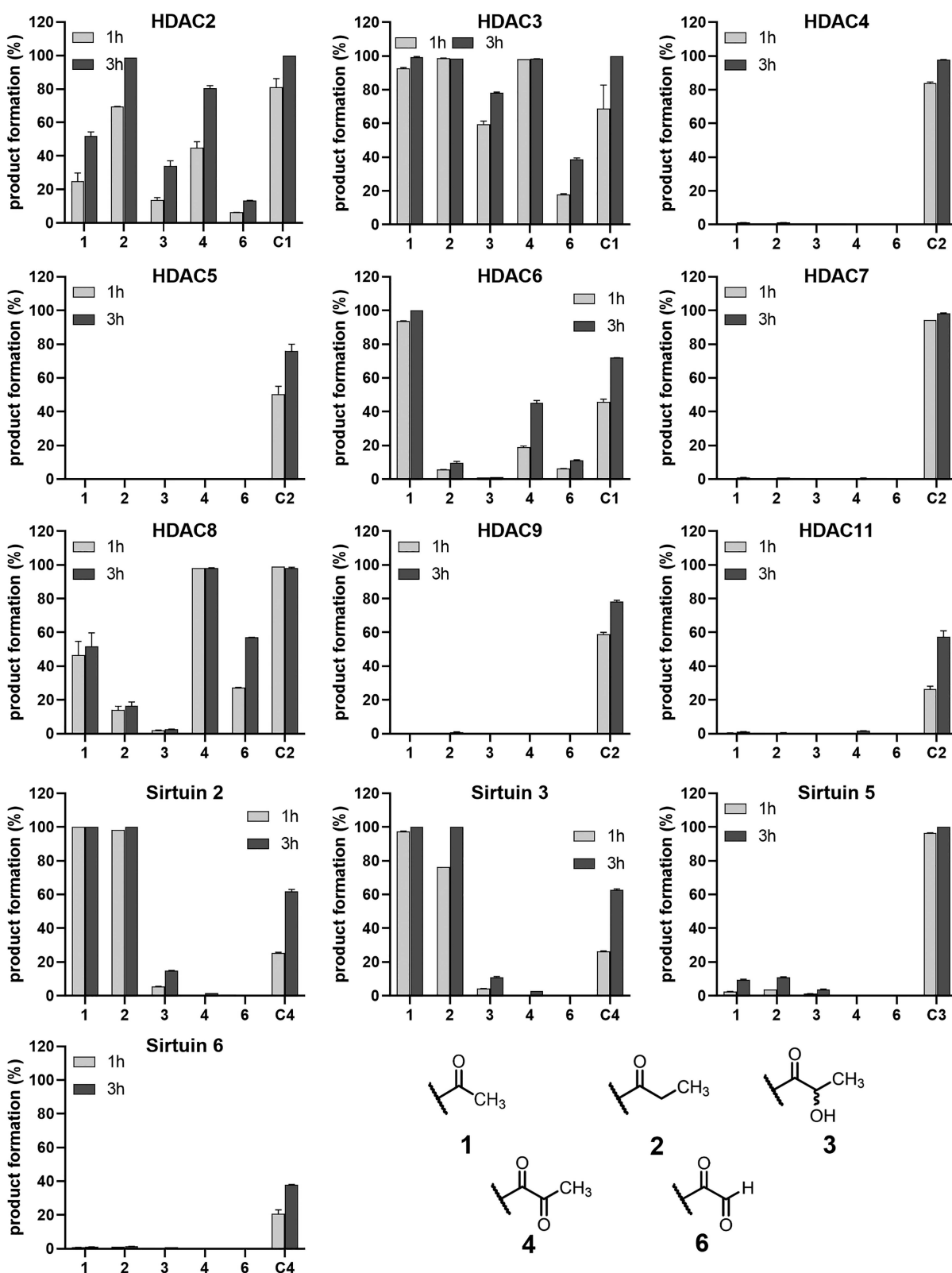


Figure 3. Deacylation profile of peptide derivatives 1 to 6 by HDAC1–9, HDAC11, and sirtuins 2, 3, 5, and 6. Data are presented in % of product formation subsequent to treatment of 50 μM compound for 1 and 3 h at 37 $^{\circ}\text{C}$ (25 $^{\circ}\text{C}$ HDAC8) with 0.1 μM HDAC or with 0.5 μM sirtuin in the presence of 500 μM NAD $^{+}$. The product formation was monitored via separation of the product and substrate using analytical HPLC. The compound detection was done at 320 nm (360 nm for C4). Product concentration was calculated as the ratio of product peak area to total peak area.

Table 2. Kinetic Constants k_{cat} and K_{M} and Resulting Specificity Constant for Different HDAC Isoforms and Compounds 1 to 4 Including 1a, 3a, and 4a^a

enzyme	compound	acyl residue	K_{M} (μM)	k_{cat} (s^{-1})	$k_{\text{cat}}/K_{\text{M}}$ ($\text{M}^{-1} \text{s}^{-1}$)	fold change in $k_{\text{cat}}/K_{\text{M}}$ ^a
HDAC2	1	acetyl	1100 \pm 400	1.1 \pm 0.3	1000	1
	1a	acetyl	1100 \pm 300	2.0 \pm 0.6	1800	1
	2	propionyl	75 \pm 12	0.51 \pm 0.05	6800	6.8
	3	lactoyl	370 \pm 80	0.24 \pm 0.05	640	0.64
	3a	lactoyl	610 \pm 80	0.31 \pm 0.02	510	0.28
	4	pyruvoyl	960 \pm 210	1.6 \pm 0.2	1700	1.7
	4a	pyruvoyl	1000 \pm 200	1.6 \pm 0.2	1600	0.89
	HDAC3	1	acetyl	58 \pm 16	0.83 \pm 0.04	14 000
1a		acetyl	56 \pm 14	1.6 \pm 0.2	29 000	1
2		propionyl	14 \pm 2	0.77 \pm 0.19	55 000	3.9
3		lactoyl	45 \pm 18	0.35 \pm 0.05	7800	0.56
3a		lactoyl	110 \pm 18	0.57 \pm 0.11	5200	0.18
4		pyruvoyl	26 \pm 5	1.8 \pm 0.2	69 000	4.9
4a		pyruvoyl	43 \pm 19	1.3 \pm 0.5	30 000	1.0
6		glyoxalyl	27 \pm 7	0.023 \pm 0.004	850	0.061
HDAC6	1	acetyl	12.2 ^b	2.28 ^b	187 490 ^b	1
	2	propionyl	190 \pm 30	0.063 \pm 0.01	330	0.0018
	4	pyruvoyl	1.7 \pm 1.1	0.016 \pm 0.006	9400	0.050
	HDAC8	1	acetyl	440 \pm 150	2.4 \pm 0.5	5400
1a		acetyl	620 \pm 60	0.86 \pm 0.18	1400	1
2		propionyl	180 \pm 30	0.25 \pm 0.02	1400	0.26
3		lactoyl	46 \pm 5	0.005 \pm 0.001	110	0.020
4		pyruvoyl	6.1 \pm 1.9	1.0 \pm 0.1	164 000	30
4 ^a		pyruvoyl	4.5 \pm 0.7	1.1 \pm 0.1	240 000	44
4a		pyruvoyl	9.2 \pm 1.7	4.7 \pm 1.1	510 000	364
6		glyoxalyl	33 \pm 9	0.051 \pm 0.009	1550	0.29
SIRT2	1	acetyl	25 \pm 2	0.36 \pm 0.06	14 000	1
	2	propionyl	12 \pm 1	0.12 \pm 0.02	10 000	0.71
	3	lactoyl	950 \pm 150	0.035 \pm 0.002	38	0.0027
SIRT3	1	acetyl	6.8 \pm 1.1	0.15 \pm 0.01	22 000	1
	2	propionyl	4.9 \pm 0.3	0.028 \pm 0.002	5700	0.26
	3	lactoyl	1580 \pm 370	0.030 \pm 0.005	19	0.00086

^aSpecificity constants relative to the respective acetylated substrate are given as ratio in the last column of the table. Kinetic constants were determined using an alternative, fluorescence-based activity assay (Figure 5). ^bResults taken from ref 30.

rate-limiting step of HDAC8 catalysis, which is assumed to be the formation of the transition state.³⁴

SIRT2, -3, and -5 can act as delactoylases but with reduced kinetic constants as compared to corresponding acetylated substrates, while SIRT6 cannot accept lactoylated peptide derivative 3 as a substrate (Figure 3, Table 2). As expected, sirtuins are generally poor delactoylases because the branching in the α -position causes steric hindrance during the formation of the bicyclic intermediate.³⁵ Compound 3 represents a mixture of two possible diastereomers distinguished by the L-lactoyl and D-lactoyl moiety. The 100% cleavage of 3 (subsequent to a prolonged incubation time with higher enzyme concentrations) demonstrates that both, HDACs and sirtuins, accept both acyl isomers.

The other natural occurring 3-carbon acyl residue pyruvoyl in compound 4 is well accepted by HDAC2, HDAC3, HDAC6, and HDAC8 (Figure 3). HDAC6 and HDAC8 clearly prefer 4 to its propionylated counterpart 2. Looking more closely to the kinetic data, obviously 4 is a highly efficient substrate for HDAC8 yielding a $k_{\text{cat}}/K_{\text{M}}$ value of 164,000 $\text{M}^{-1} \text{s}^{-1}$ (Table 2). The superior specificity constant is mainly caused by the low K_{M} value, which is approximately 70-fold lower compared to the acetylated substrate 1 and approximately 30-fold lower than for the propionylated substrate 2

(Table 2 and Figure 4B). The Michaelis constant of HDAC6 for 4 is 110-fold lower compared to the propionylated peptide 2 and, surprisingly, 7-fold lower than for the acetylated compound 1. In contrast the k_{cat} value of HDAC6 for 4 decreased about 140 times compared to 1. HDAC2 and -3 are able to accept 4 but with catalytic constants similar to the propionylated substrate 2 (Table 2 and Figure 4A). HDAC11 is not able to depyruvoylate compound 4.

We synthesized peptides derived from the biological substrate histone H3. We generated the N-terminal H3 sequence 1–13 with the lysine residue number 9 in the acetylated (compound 1a), lactoylated (compound 3a), and pyruvoylated (compound 4a) forms (Table 1). To improve the detection in the HPLC-based activity measurements, we added two tryptophan residues, as described Jiang et al.³¹ We treated these substrates with HDAC2, HDAC3, and HDAC8 and determined kinetic constants k_{cat} and K_{M} using HPLC-based activity assay.^{21,31} Histone H3-derived substrates 1a, 3a, and 4a follow the trend we observed for the substrates 1, 3, and 4. Lactoylated 3a is well accepted by HDAC2 and HDAC3, and pyruvoylated 4a is a good HDAC8 substrate with a $k_{\text{cat}}/K_{\text{M}}$ value of 510 000 $\text{M}^{-1} \text{s}^{-1}$ (Figure 4C and Table 2). Again, similar to compound 4, the K_{M} value is very low for HDAC8 (Table 2).

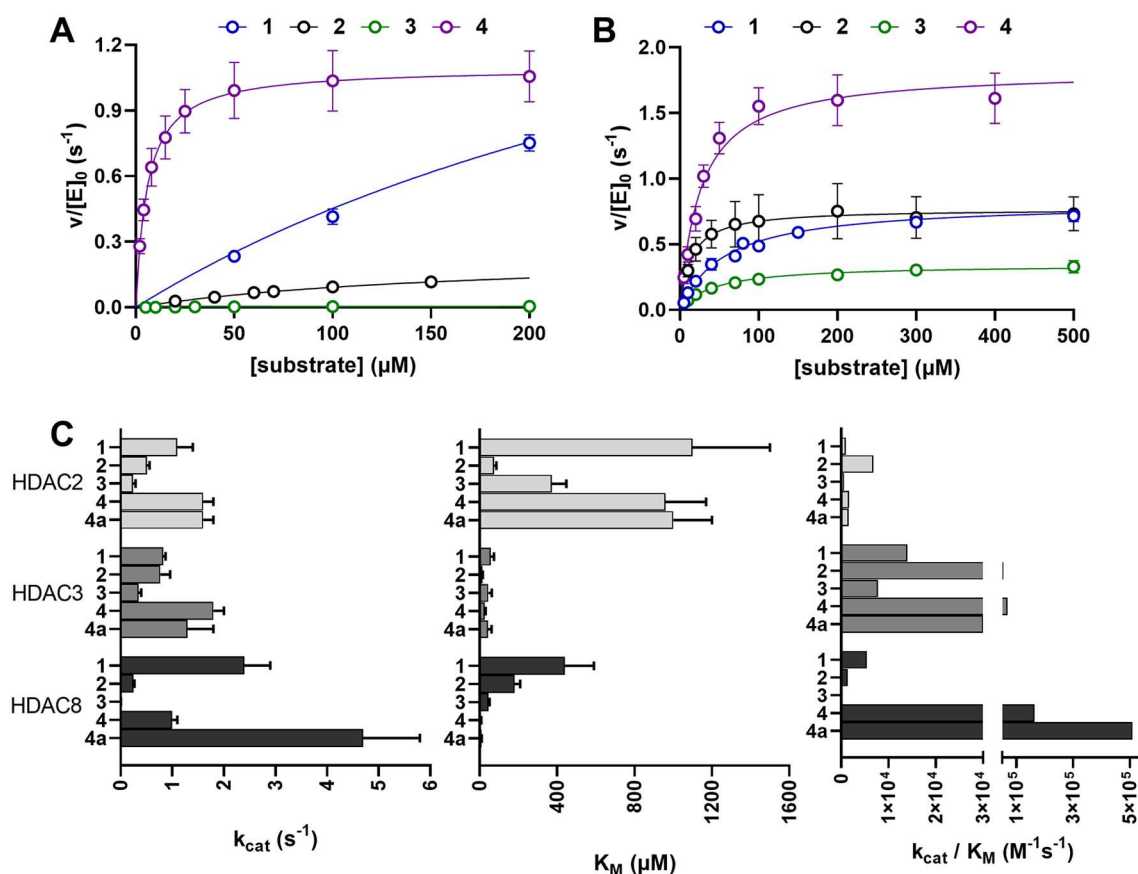


Figure 4. $v/[S]$ plots and the resulting kinetic compounds for different HDAC isoforms and substrates. (A) Steady state kinetics of HDAC8 (A) and HDAC3 (B) with compounds 1–4. Reactions were performed at 37 °C for HDAC3 and at 25 °C for HDAC8. HDAC3 concentrations were 10 nM for 1, 2, and 3 and 4 nM for 4. HDAC8 concentrations of 25 nM for 1, 20 nM for 2, 100 nM for 3, and 4 nM for 4. Data were obtained from analytical HPLC measurements. (C) Overview of the kinetic parameters of HDAC2, HDAC3, and HDAC8.

Removal of the methyl group from the pyruvoyl moiety results in naturally occurring glyoxylated lysine (compound 6), which is recognized by HDAC2, HDAC3, HDAC6, and HDAC8 but with reduced efficacy as compared to 4 and the acetylated counterpart 1 (Figure 3 and Table 2). HDAC8 is known to accept larger acyl residues, like D-phenylalanyl residues in inhibitor structures, because of the architecture of the foot pocket.³⁶ Inspired by this fact, we synthesized and analyzed phenylglyoxalyl derivative 5 to get additional interactions with the active site. However, neither HDAC8 nor any of the other HDACs and sirtuins can accept 5 as a substrate.

As a quality control for our enzymes, we analyzed dose dependent inhibition of deacylation reactions of compounds 1–4 for HDAC2 (Table S1 and Figure S23), HDAC3 (Table 2 and Figure S24), HDAC6 (Table S3 and Figure S24), and HDAC8 (Table S4 and Figure S25) using selective inhibitors HI7.3 (compound 21a in ref 37), RFGP966,³⁸ Tubastatin A,³⁹ and PCI-34051,⁴⁰ respectively. The determined IC₅₀ values are in a similar range for the different substrates excluding the possibility that contaminating HDACs are responsible for the newly discovered deacylation activity.

If a peptide derivative is not a substrate for an HDAC, there are two possible reasons; either it could not enter the active site or it acts as a competitive inhibitor. Recently, lactic amide derivatives were described as Zn²⁺ chelators for HDAC.⁴¹ Therefore, we analyzed possible inhibition of class IIa HDACs

by 1–4 and 6 (Figures S19–S22). We performed dose–response experiments and found no influence on the catalytic activity up to a 1 mM concentration of compounds 2, 3, and 4. In contrast, weak binding could be detected for the acetylated compound 1 and the glyoxylated compound 6. Obviously, class IIa HDACs could not accommodate acyl moieties with more than two carbon atoms in the active site.

The superior HDAC8 substrate properties of 4 and 4a encouraged us to determine kinetic constants with an alternative activity assay. Careful inspection of the UV–vis and fluorescence spectra of 4 and C5 uncovered differences (Figure 5) useful for the continuous monitoring of depyruvoylase activity. The $n-\pi^*$ transition of 2-oxo-amides is in the range of 310–350 nm,⁴² perfectly overlapping with the excitation of aminobenzoic amide (Abz) fluorescence. Therefore, we were able to monitor HDAC8-mediated depyruvoylation via increasing fluorescence in a continuous format with many more data points per progress curve as compared to the HPLC-based assay. As can be seen in Figure 5C and Table 2, the resulting kinetic constants are very similar, underlying the accuracy of the HPLC-based assay.

In order to understand the recognition of 3 and 4 by different HDACs, we docked these derivatives into the individual HDAC isoforms, and the top-ranked docking poses were compared with the crystal structure of HDAC8 complexed with the acetylated tetrapeptide RHKacKac-4-

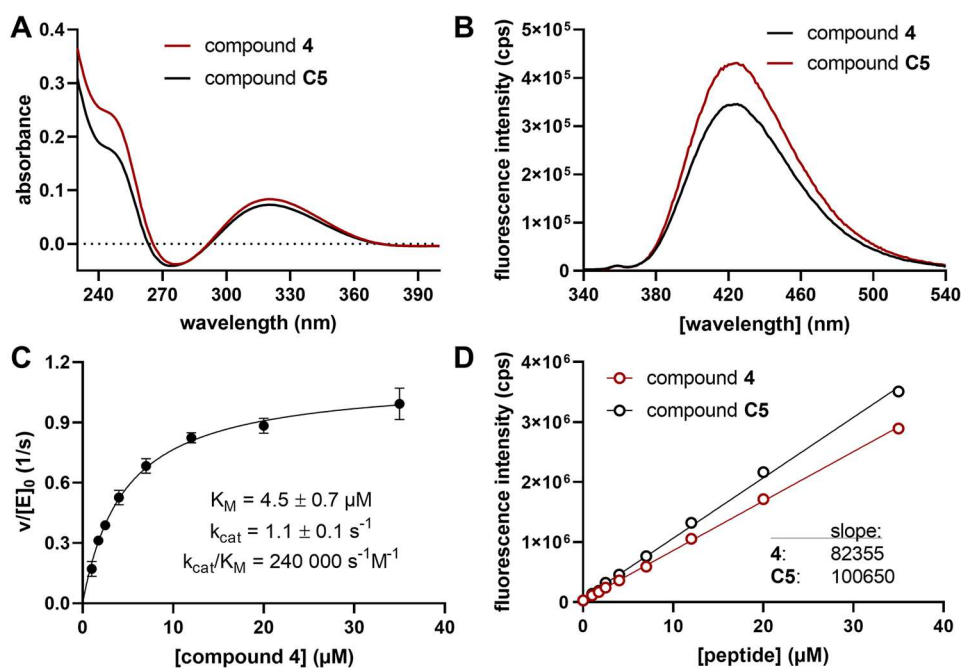


Figure 5. Absorbance and fluorescence measurements of compound 4 with HDAC8. (A) Absorbance spectra of compound 4 and compound C5. The spectra were recorded at 25 °C with a compound concentration of 30 μM and a UV cuvette with a path length of 10 mm. The spectra were corrected against a buffer background. (B) Fluorescence emission spectra of 4 and C5. The fluorescence was monitored at 25 °C, with a compound concentration of 5 μM and with an excitation wavelength of 320 nm. The excitation slit was set to 1 nm and the emission slit to 5 nm. (C) $v/[E]_0$ plot of HDAC8 and compound 4 using the increase of fluorescence intensity caused by HDAC8-mediated depyruvoylation of compound 4. The HDAC8 concentration was 5 nM with varying concentrations of 4. The fluorescence intensity was monitored using a 96-well plate reader (Envision, PerkinElmer) with $\lambda_{\text{ex}} = 320 \pm 75$ nm and $\lambda_{\text{em}} = 430 \pm 8$ nm. Values shown are the means of three independent replicates. Product concentration was calculated using the calibration lines of D. (D) Calibration line of 4 (substrate) and C5 (product) monitored at 25 °C with a 96-well plate reader with the same settings as above with varying peptide concentrations.

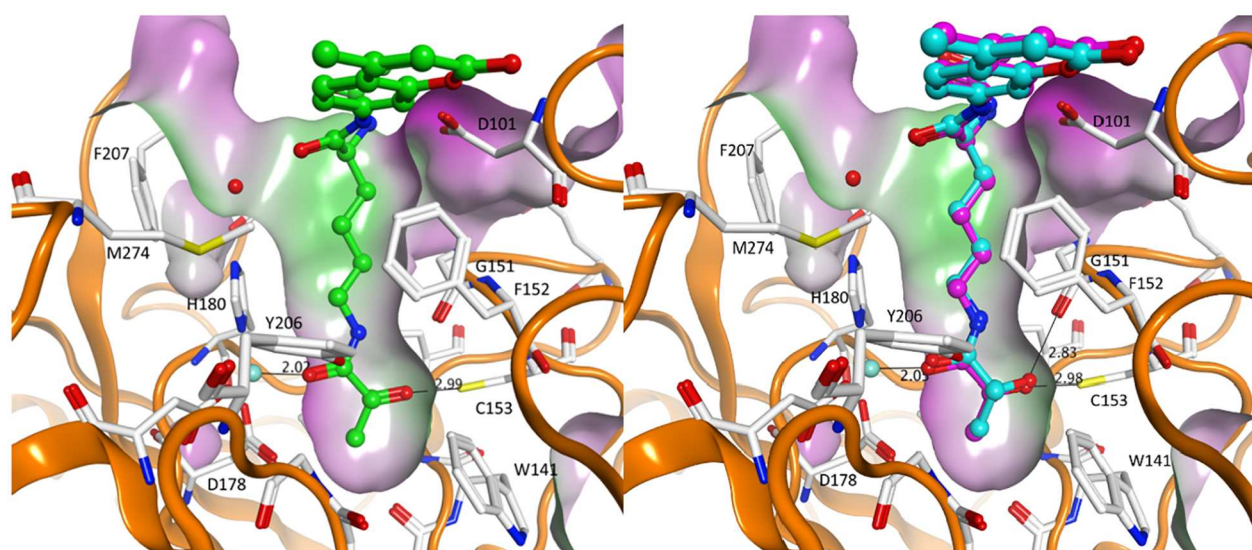


Figure 6. Docking poses of K-pyruvoyl (left site, colored green) and K-lactoyl (right site, R isomer colored magenta, S isomer colored cyan) peptide in HDAC8 (PDB ID 3EWF).⁴³ Only 4-methylcoumarin and acylated lysine are shown for clarity. The molecular surface of the substrate pocket is colored according to the hydrophobicity (green) and hydrophilicity (magenta). Distances between the acyl group and HDAC8 are given in Ångströms. The conserved water molecule bound to His180 and the catalytic zinc ion are shown as red and cyan spheres, respectively.

methylcoumarin (see Figures S29–S32 for controls and results).

For all docked substrates, the amide carbonyl group coordinates with the Zn^{2+} ion of the HDACs (distances between 1.65 and 2.03 Å). Binding pockets of HDAC6/8 and HDAC2/3 differ significantly in the so-called foot pocket. In

the case of HDAC6/8, the foot pocket size is restricted by the bulky residue Pro608 (HDAC6, Figure S30) or Trp141 (HDAC8, Figure 6), whereas in HDAC 2/3 the foot pocket is widened due to a different course of the backbone and the more flexible methionine (Met35 in HDAC2, Figure S32, and Met24 in HDAC3, Figure S31) at this position. This leads to

<https://doi.org/10.1021/acschembio.1c00863>
ACS Chem. Biol. 2022, 17, 1364–1375

different docking solutions for the substrates with residues that can form hydrogen bonds, i.e., pyruvoyl and lactoyl residues. In the case of the good HDAC6/8 substrate **4**, a hydrogen bond to a conserved cysteine in the foot pocket (Cys621 in HDAC6, Cys153 in HDAC8) is observed, whereas in the case of HDAC2/3, the pyruvoyl carbonyl group is rotated 180° and does not show an interaction with the conserved cysteine (Cys145 in HDAC2, Cys156 in HDAC3). This cysteine residue is conserved in HDACs and involved in the stabilization of the substrate transition state.³⁴ Due to the spatial restriction of the foot pocket, the carbonyl group of the pyruvoyl residue is directed into the position for an optimal hydrogen bond to Cys153 (Figure 6). In the case of HDAC2/3, this interaction is not evident due to the altered geometry of the foot pocket. In the case of the lactoyl derivative **3**, both isomers show the same hydrogen bond to the conserved cysteine in HDAC6/8 and additionally a hydrogen bond to a neighboring glycine (Gly619 in HDAC6, Gly154 in HDAC8). In HDAC2/3, the hydroxyl function of the lactoyl residue points in the same direction as that of the pyruvoyl residue (Figures S31 and S32). Thus, the modified geometry of the foot pocket (HDAC6/8 compared to HDAC2/3) and the preferential hydrogen bonds calculated for pyruvoyl moieties could explain the good substrate properties of compound **4** for HDAC6/8.

DISCUSSION

In the cytoplasm, the source of D-lactoyl lysine residues is the nonenzymatic acyl transfer from D-lactoylglutathione which is formed by the reaction of the glycolytic byproduct methylglyoxal and glutathione.¹⁰ In contrast, it was demonstrated that acetyltransferase p300 is able to generate L-lactoylated histone residues in the nucleus using L-lactoyl-CoA.⁵ While the generation of reactive lactoyl derivatives and lactoylated lysine residues is relatively well understood, the enzymes responsible for the removal of these modifications were not known. First, SIRT2 was reported to be the *in vivo* delactoylase with a specificity constant for the two lactoylated lysine isomers of approximately $1 \text{ M}^{-1} \text{ s}^{-1}$,²⁵ but this constant seems to be too low to be relevant *in vivo*. The specificity constant of HDAC3 for lactoylated substrate **3** determined in this work is more than 7500-fold higher than the reported one and more than 200-fold higher as compared to the specificity constant of SIRT2 and **3** determined here. On the basis of these findings, it could be assumed that HDAC3 is the more relevant *in vivo* delactoylase. These data correspond well with the findings of Moreno-Yruela et al., who showed that HDAC1–3 are delactoylases with model peptides and reinforced their results with *in cellulo* delactoylase activities of HDAC1–3. They found only weak to no delactoylase activity for SIRT1 to SIRT3.²⁹ Additionally, HDAC2 also has a much higher (640-fold) catalytic efficiency for **3** as compared to the reported values for SIRT2. Our delactoylase results were generated with short peptide derivatives and could not easily be transferred to similar modifications in a full-length protein context. But model peptides have served well in the past to find substrate peptides for HDACs/sirtuins. For instance, the unique selectivity of Sirtuin 5 for negatively charged acyl residues (like malonyl, succinyl, and glutaryl residues) was detected using peptide substrates.^{3,20,21} Later, it could be confirmed that desuccinylase and deglutarylase activity is the major *in vivo* activity of sirtuin 5. Additionally, defatty acylase activity of sirtuin 6 again was discovered first using peptide

substrates in combination with HPLC-based activity assays.³¹ In addition, the unique defatty acylase activity of HDAC11 was uncovered using peptide substrates,^{17,18} and in later studies, *in vivo* defatty acylase substrates for HDAC11 could be identified.^{19,44} This shows that novel acyl residues, which are removed with several-hundred-fold higher efficacy *in vitro* as compared to acetylated lysine substrates, represent with high probability novel *in vivo* substrates. Moreover, in a recent publication, lactoylated histone H2Bs were incorporated into nucleosomes, and both the nucleosomes and isolated lactoylated histone H2Bs were treated with a variety of multiprotein complexes containing HDAC1. It was demonstrated that protein complexes CoREST and MIER were able to remove the lactoyl residue from H2Bs and that complexes MiDAC and RERE have delactoylase activities in the nucleosome context.⁴⁵

Considering the proposed enzymatic mechanism, it can be expected that sirtuins should not be able to handle pyruvoyl modifications efficiently and that HDACs, especially class IIa HDACs, should accept such a modification because of the higher reactivity of the amide carbonyl carbon.⁴⁶ Class IIa HDACs are known to be poor deacetylases but are able to hydrolyze very efficiently more activated trifluoromethylacetylated substrates.⁴⁷ Common for all members of class IIa HDACs is the substitution of a conserved tyrosine residue in the active site by a histidine.⁴⁷ The histidine residue is not able to stabilize the tetrahedral intermediate like the tyrosine residue, and so class IIa HDACs need more reactive lysine modifications like the trifluoroacetyl amides to perform the deacylation reaction. Pyruvoylated lysine residues, as in compound **4**, are activated in a similar manner because of the electron-withdrawing effect of the α -carbonyl function. Therefore, we expected that **4** represents the naturally occurring equivalent to the artificial trifluoroacetylated substrate. To our surprise, no member of the class IIa HDACs but HDAC8 and HDAC6 are able to remove the pyruvoyl residue from the derivatives **4** and **4a**. The very low K_M values for HDAC8 point to a probable function *in vivo* as an eraser for the spontaneously occurring protein pyruvoylation.^{12,14} Peptide derivatives **4** and **4a** represent the best substrates described for HDAC8 so far. Such differences in affinities to the active site of enzymes (i.e., K_M values for **1a** and **4a**) could dramatically influence the substrate specificity *in vivo*. Recently, it could be demonstrated for N-myristoyltransferases that these enzyme act exclusively as fatty acyl transferases *in vivo*.⁴⁸ This is surprising because, *in vitro*, the same enzymes are able to transfer acetyl residues from acetyl-CoA to the N-terminus of a protein with very similar specificity constants. The authors could demonstrate that the extremely different affinities of the cosubstrates to the active site of the enzyme are the only reason for the exclusive specificity within cells.⁴⁸ We analyzed HDAC8-mediated depyruvoylation of **4** in the presence of an acetylated HDAC8 substrate via HPLC at several time points (Figure S28). As expected from the very different K_M values, we found at the beginning of the enzymatic reaction exclusive depyruvoylation and no deacetylation. Even after more than 90% turnover of **4**, there was no product of deacetylation reaction visible.

It remains to be discovered if lactoylated and/or pyruvoylated lysine residues could be recognized by so-called reader domains in a specific manner. Binding of proteins to acylated lysines (in addition to acetylated lysines) is described for succinylated lysines,⁴⁹ propionylated lysines,⁴⁹ butyrylated

lysines,^{49,50} and crotonylated lysines.^{51–53} In summary, we uncovered delactoylase and depyruvylase activity for different HDAC isoforms. The superior kinetic constants determined for compounds **3**, **3a**, **4**, and **4a** point to the potential biological significance of these lysine acylations.

EXPERIMENTAL SECTION

Chemicals and General Methods. Most of the Fmoc-protected amino acids and *O*-(benzotriazol-1-yl)-*N,N,N',N'*-tetramethyluronium hexafluorophosphate (HBTU) were purchased from GL Biochem Ltd. (Shanghai, China). Acetonitrile (ACN) was purchased from VWR. *N,N*-Dimethylformamide (DMF), ethyl (hydroxyimino)-cyanoacetate (OxymaPure), and Rink amide MBHA resin were purchased from Iris Biotech (Marktredwitz, Germany). *N,N*-Diisopropylethylamine (DIPEA), trifluoroacetic acid (TFA), and dichloromethane (DCM) were purchased from Carl Roth (Karlsruhe, Germany).

UPLC-MS analysis was performed using the Waters ACQUITY UPLC-MS system (Milford, MA) with a Waters ACQUITY-UPLC-MS-BEH C18 1.7 μm (2.1 \times 50 mm; 30 \AA) column. As a mobile phase, 0.1% formic acid in H_2O (solvent A) and 0.1% formic acid in ACN (solvent B) solutions were used. A typical gradient from 95:5 (v/v) of H_2O /ACN to 5:95 (v/v) of H_2O /ACN in 6 min was used for most of the experiments. Data analysis was performed using Waters MassLynx software. Purification of peptides was done on the Shimadzu LC System with a Phenomenex Kinetex 5 μm XB-C18 (250 \times 21.1 mm, 100 \AA) column using different gradients of 0.1% TFA in H_2O (solvent A) and 0.1% TFA in ACN (solvent B) solutions.

Solid-Phase Peptide Synthesis. The substrates **1**, **1a**, **2**, **3a**, **4a**, and **C2** were synthesized from the fully protected polymer-bound peptides (Boc)Abz-SRGGK(Ns)FFRR-NH-(Rink amide resin) and Boc-ARTKQTARK(Ns)STGGWW-(Rink amide resin), using the strategy published before.¹⁷ Acetyl, glyoxalyl, lactoyl, pyruvyl, and phenylglyoxalyl peptides **1a**, **3a**, **4a**, and **3–6** were prepared from the same resin-bound peptide according to the methods below. Substrates **C1**, **C3**, and **C4** were prepared as described elsewhere.^{54,55,21}

Acetyl Peptide 1a. For the acetylation, the resin was treated with acetic anhydride and DIPEA in DMF (0.2:0.4:10, v/v/v) for 20 min. After washing of the resin, global deprotection (TFA/ H_2O 9:1, for 2 \times 1 h) was used to remove protecting groups and to cleave the crude peptide from the solid support. TFA was removed *in vacuo*, and the crude peptide was dissolved in ACN/ H_2O mixture and purified using preparative HPLC.

Lactoyl Peptides 3 and 3a. A total of 45 mg of the crude pyruvyl-peptide **4** was dissolved in H_2O , and 1 mg of NaBH_4 was added. After 30 min, the solution was acidified with acetic acid and directly used for preparative HPLC.

Pyruvyl Peptides 4 and 4a. 2,2-Diethoxypropionic acid⁵⁶ was activated with HBTU (3 equiv) and DIPEA (6 equiv) in DMF, and this solution was incubated with the resin-bound peptide for 1 h. Next, the peptide was cleaved from the resin using the same protocol described before (peptide **1a**).

Phenylglyoxalyl Peptide 5. The same procedure as above was used to couple phenylglyoxylic acid (Sigma-Aldrich) to the polymer-bound peptide using HBTU/DIPEA followed by deprotection and HPLC purification.

Glyoxalyl Peptide 6. Diethoxyacetic acid (prepared from ethyl diethoxyacetate (Aldrich) and NaOH) was coupled to the resin-bound peptide and cleaved from the resin as described above. Volatiles were removed *in vacuo*, and the crude peptide was dissolved in the minimal volume of concentrated hydrochloric acid. After 1 h, acid was removed in the stream of N_2 , and the residue was purified with preparative HPLC.

Enzymes. Recombinant HDAC4, HDAC5, HDAC6, HDAC7, HDAC8, HDAC9,⁵⁷ and HDAC11¹⁷ were cloned, expressed, and purified as described previously. Recombinant HDAC2 (BML-SE500, activity = 2585 U/ μg) and HDAC3/NCOR1 (BML-SE515, activity = 1590 U/ μg) were purchased from ENZO Life Science GmbH (Lörrach, Germany). One unit is defined as 1 pmol/min at 37 $^\circ\text{C}$

using 100 μM of the FLOUR DE LYS-SIRT1 deacetylase substrate. Sirtuins 2, 3, 5, and 6 were cloned, expressed, and purified as described.⁵⁸

HPLC-Based Deacylation Assay. Reactions were performed in a total volume of 70 μL in HDAC assay buffer containing 50 mM HEPES (pH 7.4), 140 mM NaCl, 10 mM KCl, 1 mM TCEP, and 0.2 mg mL^{-1} BSA for HDAC1, -2, -3, -4, -5, -6, -7, -8, -9, and -11 or in SIRT assay buffer containing 20 mM Tris-HCl (pH 7.8), 150 mM NaCl, 5 mM MgCl_2 , and 0.2 mg mL^{-1} BSA for SIRT2, SIRT3, SIRT5, and SIRT6. The peptides with a final concentration of 50 μM and 500 μM NAD^+ (only for sirtuins) were preincubated for 5 min at 37 $^\circ\text{C}$ (25 $^\circ\text{C}$ for HDAC8), and the reaction was started by the addition of enzymes ([HDAC1–9] = 0.1 μM , [HDAC11] = 0.1 μM , and [sirtuins] = 0.5 μM final concentrations for **1–6** and [HDAC1] = 0.1 μM , [HDAC2–3, HDAC6] = 10 nM, [HDAC4,5,7] = 5 nM, [HDAC8] = 2 nM, [HDAC9] = 20 nM, [HDAC11] = 50 nM, [SIRT2,3,5] = 0.1 μM , and [SIRT6] = 0.5 μM for controls **C1–C4**). At time points 1 and 3 h, the reaction was quenched by addition of 1% TFA (final concentration at least 0.2%). The HDAC/sirtuin mediated reaction was monitored via analytical HPLC.

All analytical HPLC analyses were performed with a system of water supplemented with 0.1% TFA (solvent A) and acetonitrile (ACN) supplemented with 0.1% TFA (solvent B) on an Agilent 1100 system (Boeblingen, Germany) with a quaternary pump, a well-plate autosampler, and a diode array detector or a fluorescence detector. The reaction solution was injected in the HPLC system (40 μL), and separation was done with a linear gradient from 10% to 60% (for compounds **C1**, **C2**, **C3**, and **5**), 5% to 95% (for compound **C4**), and 16% to 32% (for compound **1–4** and **6**) solvent B within 6 min and a flow rate of 0.6 mL/min on a 3.0 \times 50 mm reversed phase column (Phenomenex, Kinetex XB C-18, 2.6 μm). Analysis of the substrate and product peak area was done with Chemstation software (Agilent, Boeblingen, Germany) at 320 nm or with fluorescence detection of amino benzoic acid with λ_{ex} = 320 \pm 4 nm and λ_{em} = 420 \pm 4 nm. Product formation was calculated as a ratio of product peak area to total peak area. Peptides **4** and **6** were corrected against a negative control without enzymes.

Determination of Kinetic Constants k_{cat} and K_{M} . The peptides were preincubated in HDAC assay buffer (see above, for HDACs) or in SIRT assay buffer (see above, for sirtuins) at eight different concentrations (0.25 μM up to 2 mM depending on the substrate and the enzyme) in a 1.5 or 0.5 mL reaction vessel at 37 $^\circ\text{C}$ (25 $^\circ\text{C}$ HDAC8), for 5 min. Depending on the substrate concentration, the reaction volume was 30 μL up to 400 μL . For sirtuin reactions, 500 μM NAD^+ for **1** and **2** or 2000 μM NAD^+ for **3** (final concentration) was added to the reaction mixture. The reaction was started by the addition of a 10 \times enzyme solution (4 nM up to 0.5 μM final concentration depending on the peptide and the enzyme). After four different time points (5, 10, 15, and 20 min or 10, 20, 30, and 40 min), a sample was taken from the reaction solution and was added to a 96-well plate, where a stop solution (5% acetonitrile, 1% TFA in water, final TFA concentration at least 0.2%) was provided to quench the reaction. The quenched reaction solution was injected into the HPLC system (Agilent 1100 series, Boblingen, Germany), and separation was done with a linear water/acetonitrile (both supplemented with 0.1% TFA) gradient ($t = 0$ min, 16% acetonitrile; $t = 6$ min, 32% acetonitrile) with a flow rate of 0.6 mL/min. For samples less concentrated than 5 μM , the injection volume was 100 μL ; for all other samples, it was 40 μL . For peptide **1a**, **3a**, and **4a**, separation was done with a linear water/acetonitrile (both supplemented with 0.1% TFA) gradient ($t = 0$ min, 14% acetonitrile; $t = 6$ min, 28% acetonitrile) with a flow rate of 0.8 mL/min at 40 $^\circ\text{C}$. Product and substrate detection was done with a fluorescence detector with λ_{ex} = 320 nm and λ_{em} = 420 nm. For compounds **1a**, **3a**, and **4a**, chromatograms were recorded at 282 nm (tryptophane absorbance). Product and substrate peak area were integrated using ChemStation software (Agilent, Boblingen, Germany). Product formation was calculated as the ratio of substrate peak area to total peak area (substrate + product peak area). The product concentration was plotted as a function of time. A linear regression analysis was

done following the linear trend of the plot. The slopes obtained of these plots (reaction rate v) at the appropriate substrate concentration were used to create a $v/[S]$ plot. A nonlinear regression analysis, according to the Michaelis–Menten equation, was used to determine k_{cat} and K_{M} values. The substrate fluorescence intensity of compound 4 was different as compared to the fluorescence intensity of the reaction product C5. A calibration line was recorded for compound 4, and the appropriate product and substrate concentrations were corrected using this calibration line.

Fluorescence and Absorbance Measurements for 4 and C5. The absorbance spectra of compound 4 and C5 were recorded in a UV cuvette with a path length of 10 mm and a compound concentration of 30 μM in HDAC assay buffer (as described above). The spectra were recorded using a CARY 3500 UV–vis spectrophotometer (Agilent, Boblingen, Germany). The fluorescence spectra were recorded in a fluorescence cuvette with path lengths of 5 mm \times 10 mm and a compound concentration of 5 μM at 25 $^{\circ}\text{C}$. A Fluoromax 4 fluorescence spectrometer (Horiba, Kyoto, Japan) was used with an excitation wavelength of 320 nm.

Determination of Kinetic Constants of HDAC8 and Compound 4 Using Fluorescence Intensity Readout. The kinetic measurements were carried out in a black 96-well fluorescence plate at 25 $^{\circ}\text{C}$ in HDAC assay buffer (as described above). The reaction volume per well was 100 μL . The substrate was diluted to eight different concentrations (ranging from 0.5 to 35 μM) and incubated for 5 min at 25 $^{\circ}\text{C}$. Each concentration was measured in triplicate on the plate. The reaction was started with the addition of 10 μL of 10-fold HDAC8 solution (final HDAC8 concentration 5 nM), and a negative control for each concentration (also in triplicates) was started using 10 μL of HDAC assay buffer. The product formation was monitored via fluorescence intensity readout and was done on a Envision 2104 Multilabel plate reader (PerkinElmer, Waltham, USA) with $\lambda_{\text{Ex}} = 320 \pm 75$ nm and $\lambda_{\text{Em}} = 430 \pm 8$ nm. The fluorescence intensity was recorded every 30 s for 1 h. The fluorescence intensity was corrected using the negative control, and the corrected values were plotted as a function of time. A linear regression analysis was done following the initial slope (reaction rate v_0) of the data points. The fluorescence intensities were transformed to product concentration using a calibration line (as the difference of substrate and product fluorescence). The reaction rate was plotted as a function of substrate concentration, and a nonlinear regression analysis according to the Michaelis–Menten equation was done to determine k_{cat} and K_{M} values using GraphPad Prism 8 software (San Diego, CA).

Computational Methods. The available X-ray structure of human HDAC8 complexed with a tetrapeptide (PDB ID 3EWF), human HDAC6 (PDB ID 5EDU), human HDAC3 (PDB ID 4A69), and human HDAC2 (PDB ID 6G3O) were downloaded from the Protein Data Bank (PDB; www.rcsb.org). Protein preparation was done using the protein preparation wizard implemented in Schrödinger, version 2019.1, by adding hydrogen atoms, assigning protonation states, and minimizing the protein. Substrate peptide structures were generated in MOE.⁵⁹ A conserved water molecule bound to His180 in HDAC8 (His651 in HDAC6, H172 in HDAC3, His183 in HDAC2) was included for the docking studies. The ligands were subsequently prepared for docking using the LigPrep tool as implemented in Schrödinger's software (version 2019.1) and energy minimized using the OPLS3e force field. In total, 100 conformers of all ligands were subsequently generated with ConfGen. Docking of the generated conformers into the prepared protein structures was performed using the program Glide (Schrödinger-release 2019.1) in the Standard Precision mode. Docking was also carried out using the program GOLD3.8.1. The Zn^{2+} ion was used to define the size of the grid box (20 Å radius). Protein hydrogen bonds to Asp104 (HDAC2), Asp93 (HDAC3), Asp101 (HDAC8), and the corresponding Ser668 in HDAC6 were used as docking constraints. These residues make hydrogen bonds to the backbone of the peptide substrates in the corresponding crystal structures and are known to stabilize the substrate binding. A total of 100 docking poses were calculated for each molecule. All other docking options were left at

their default values. Top-ranked docking solutions were analyzed using the program MOE. Since both docking programs yielded highly similar top-ranked docking poses (Figure S29) only results from GLIDE are shown in Figures 6 and S30–S32.

■ ASSOCIATED CONTENT

Supporting Information

The Supporting Information is available free of charge at <https://pubs.acs.org/doi/10.1021/acscchembio.1c00863>.

HPLC/MS runs of the peptides, $v/[S]$ plots, dose response curves, additional HPLC experiments, additional docking poses (PDF)

■ AUTHOR INFORMATION

Corresponding Author

Mike Schutkowski – Department of Enzymology, Charles Tanford Protein Center, Institute of Biochemistry and Biotechnology, Martin-Luther-University Halle-Wittenberg, Halle/Saale 06120, Germany; orcid.org/0000-0003-0919-7076; Email: mike.schutkowski@biochemtech.uni-halle.de

Authors

Matthes Zessin – Department of Medicinal Chemistry, Institute of Pharmacy, Martin-Luther-University Halle-Wittenberg, Halle/Saale 06120, Germany

Marat Meleshin – Department of Enzymology, Charles Tanford Protein Center, Institute of Biochemistry and Biotechnology, Martin-Luther-University Halle-Wittenberg, Halle/Saale 06120, Germany

Lucas Praetorius – Department of Medicinal Chemistry, Institute of Pharmacy, Martin-Luther-University Halle-Wittenberg, Halle/Saale 06120, Germany

Wolfgang Sippl – Department of Medicinal Chemistry, Institute of Pharmacy, Martin-Luther-University Halle-Wittenberg, Halle/Saale 06120, Germany; orcid.org/0000-0002-5985-9261

Cyril Bařinka – Institute of Biotechnology of the Czech Academy of Sciences, BIOCEV, Vestec 252 50, Czech Republic; orcid.org/0000-0003-2751-3060

Complete contact information is available at: <https://pubs.acs.org/doi/10.1021/acscchembio.1c00863>

Funding

This work was supported by grants from Deutsche Forschungsgemeinschaft (INST 271/336-1 FUGG) to M.S., SI868/22-1 to W.S., and in part by the CAS (RVO: 86652036) and the Czech Science Foundation (21-31806) to C.B.

Notes

The authors declare no competing financial interest.

■ ACKNOWLEDGMENTS

The authors thank Ilona Kunze for excellent technical support, T. Kiefhaber at the Martin-Luther University Halle-Wittenberg for giving us access to the single-quadrupole LC-MS analyses, and the core facility proteomics mass spectrometry of the Martin-Luther University Halle-Wittenberg for technical assistance during the triple-quadrupole LC-MS experiments.

<https://doi.org/10.1021/acscchembio.1c00863>
ACS Chem. Biol. 2022, 17, 1364–1375

■ ABBREVIATIONS

TFA, trifluoroacetic acid; AMC, 7-amino-4-methylcoumarin; Abz, 2-aminobenzoyl; Ac, acetyl; HDAC, histone deacetylase; SIRT, sirtuin

■ REFERENCES

- (1) Chen, Y.; Sprung, R.; Tang, Y.; Ball, H.; Sangras, B.; Kim, S. C.; Falck, J. R.; Peng, J.; Gu, W.; Zhao, Y. Lysine propionylation and butyrylation are novel post-translational modifications in histones. *Molecular & cellular proteomics: MCP* **2007**, *6* (5), 812–819.
- (2) Xie, Z.; Dai, J.; Dai, L.; Tan, M.; Cheng, Z.; Wu, Y.; Boeke, J. D.; Zhao, Y. Lysine succinylation and lysine malonylation in histones. *Molecular & cellular proteomics: MCP* **2012**, *11* (5), 100–107.
- (3) Tan, M.; Peng, C.; Anderson, K. A.; Chhoy, P.; Xie, Z.; Dai, L.; Park, J.; Chen, Y.; Huang, H.; Zhang, Y.; et al. Lysine glutarylation is a protein posttranslational modification regulated by SIRT5. *Cell metabolism* **2014**, *19* (4), 605–617.
- (4) Sabari, B. R.; Tang, Z.; Huang, H.; Yong-Gonzalez, V.; Molina, H.; Kong, H. E.; Dai, L.; Shimada, M.; Cross, J. R.; Zhao, Y.; et al. Intracellular Crotonyl-CoA Stimulates Transcription through p300-Catalyzed Histone Crotonylation. *Molecular cell* **2018**, *69* (3), 533.
- (5) Zhang, Di; Tang, Z.; Huang, H.; Zhou, G.; Cui, C.; Weng, Y.; Liu, W.; Kim, S.; Lee, S.; Perez-Neut, M.; et al. Metabolic regulation of gene expression by histone lactylation. *Nature* **2019**, *574* (7779), 575–580.
- (6) Huang, H.; Tang, S.; Ji, M.; Tang, Z.; Shimada, M.; Liu, X.; Qi, S.; Locasale, J. W.; Roeder, R. G.; Zhao, Y.; et al. p300-Mediated Lysine 2-Hydroxyisobutyrylation Regulates Glycolysis. *Molecular cell* **2018**, *70* (5), 984.
- (7) Kaczmarek, Z.; Ortega, E.; Goudarzi, A.; Huang, H.; Kim, S.; Márquez, J. A.; Zhao, Y.; Khochbin, S.; Panne, D. Structure of p300 in complex with acyl-CoA variants. *Nat. Chem. Biol.* **2017**, *13* (1), 21–29.
- (8) Simic, Z.; Weiwad, M.; Schierhorn, A.; Steegborn, C.; Schutkowski, M. The ϵ -Amino Group of Protein Lysine Residues Is Highly Susceptible to Nonenzymatic Acylation by Several Physiological Acyl-CoA Thioesters. *Chembiochem: a European journal of chemical biology* **2015**, *16* (16), 2337–2347.
- (9) Galligan, J. J.; Rose, K. L.; Beavers, W. N.; Hill, S.; Tallman, K. A.; Tansey, W. P.; Marnett, L. J. Stable histone adduction by 4-oxo-2-nonenal: a potential link between oxidative stress and epigenetics. *J. Am. Chem. Soc.* **2014**, *136* (34), 11864–11866.
- (10) Gaffney, D. O.; Jennings, E. Q.; Anderson, C. C.; Marentette, J. O.; Shi, T.; Schou Oxvig, A.-M.; Streeter, M. D.; Johannsen, M.; Spiegel, D. A.; Chapman, E.; Roede, J. R.; Galligan, J. J. Non-enzymatic Lysine Lactoylation of Glycolytic Enzymes. *Cell Chem. Biol.* **2020**, *27* (2), 206–213.
- (11) Hagihara, H.; Shoji, H.; Otabi, H.; Toyoda, A.; Katoh, K.; Namihira, M.; Miyakawa, T. Protein lactylation induced by neural excitation. *Cell Reports* **2021**, *37* (2), 109820.
- (12) Baldensperger, T.; Jost, T.; Zipprich, A.; Glomb, M. A. Novel α -Oxoamide Advanced-Glycation Endproducts within the N6-Carboxymethyl Lysine and N6-Carboxyethyl Lysine Reaction Cascades. *Journal of agricultural and food chemistry* **2018**, *66* (8), 1898–1906.
- (13) Baldensperger, T.; Eggen, M.; Kappen, J.; Winterhalter, P. R.; Pfirrmann, T.; Glomb, M. A. Comprehensive analysis of posttranslational protein modifications in aging of subcellular compartments. *Sci. Rep.* **2020**, *10* (1), 7596.
- (14) Baldensperger, T.; Glomb, M. A. Pathways of Non-enzymatic Lysine Acylation. *Frontiers in cell and developmental biology* **2021**, *9*, 664553.
- (15) Smith, B. C.; Hallows, W. C.; Denu, J. M. Mechanisms and molecular probes of sirtuins. *Chemistry & biology* **2008**, *15* (10), 1002–1013.
- (16) Feldman, J. L.; Baeza, J.; Denu, J. M. Activation of the protein deacetylase SIRT6 by long-chain fatty acids and widespread deacylation by mammalian sirtuins. *J. Biol. Chem.* **2013**, *288* (43), 31350–31356.
- (17) Kutil, Z.; Novakova, Z.; Meleshin, M.; Mikesova, J.; Schutkowski, M.; Barinka, C. Histone Deacetylase 11 Is a Fatty-Acid Deacylase. *ACS Chem. Biol.* **2018**, *13* (3), 685–693.
- (18) Moreno-Yruela, C.; Galleano, I.; Madsen, A. S.; Olsen, C. A. Histone Deacetylase 11 Is an ϵ -N-Myristoyllysine Hydrolase. *Cell chemical biology* **2018**, *25* (7), 849–856.
- (19) Cao, J.; Sun, L.; Aramsangtienchai, P.; Spiegelman, N. A.; Zhang, X.; Huang, W.; Seto, E.; Lin, H. HDAC11 regulates type I interferon signaling through defatty-acylation of SHMT2. *Proc. Natl. Acad. Sci. U.S.A.* **2019**, *116* (12), 5487–5492.
- (20) Du, J.; Zhou, Y.; Su, X.; Yu, J. J.; Khan, S.; Jiang, H.; Kim, J.; Woo, J.; Kim, J. H.; Choi, B. H.; et al. Sirt5 is a NAD-dependent protein lysine demalonylase and desuccinylase. *Science (New York, N.Y.)* **2011**, *334* (6057), 806–809.
- (21) Roessler, C.; Nowak, T.; Pannek, M.; Gertz, M.; Nguyen, G. T. T.; Scharfe, M.; Born, I.; Sippl, W.; Steegborn, C.; Schutkowski, M. Chemical probing of the human sirtuin 5 active site reveals its substrate acyl specificity and peptide-based inhibitors. *Angewandte Chemie (International ed. in English)* **2014**, *53* (40), 10728–10732.
- (22) Pannek, M.; Simic, Z.; Fuszard, M.; Meleshin, M.; Rotili, D.; Mai, A.; Schutkowski, M.; Steegborn, C. Crystal structures of the mitochondrial deacylase Sirtuin 4 reveal isoform-specific acyl recognition and regulation features. *Nat. Commun.* **2017**, *8* (1), 1513.
- (23) Huang, H.; Zhang, Di; Wang, Y.; Perez-Neut, M.; Han, Z.; Zheng, Y. G.; Hao, Q.; Zhao, Y. Lysine benzoylation is a histone mark regulated by SIRT2. *Nat. Commun.* **2018**, *9* (1), 3374.
- (24) Jin, J.; He, B.; Zhang, X.; Lin, H.; Wang, Y. SIRT2 Reverses 4-Oxononoyl Lysine Modification on Histones. *J. Am. Chem. Soc.* **2016**, *138* (38), 12304–12307.
- (25) Jennings, E. Q.; Ray, J. D.; Zerito, C. J.; Trujillo, M. N.; McDonald, D. M.; Chapman, E.; Spiegel, D. A.; Galligan, J. J. Sirtuin 2 Regulates Protein Lactoyllys Modifications. *Chembiochem: a European journal of chemical biology* **2021**, *22* (12), 2102–2106.
- (26) Madsen, A. S.; Olsen, C. A. Profiling of substrates for zinc-dependent lysine deacylase enzymes: HDAC3 exhibits decrotonylase activity in vitro. *Angewandte Chemie (International ed. in English)* **2012**, *51* (36), 9083–9087.
- (27) Wei, W.; Liu, X.; Chen, J.; Gao, S.; Lu, L.; Zhang, H.; Ding, G.; Wang, Z.; Chen, Z.; Shi, T.; et al. Class I histone deacetylases are major histone decrotonylases: evidence for critical and broad function of histone crotonylation in transcription. *Cell Research* **2017**, *27* (7), 898–915.
- (28) Huang, H.; Zhang, D.; Weng, Y.; Delaney, K.; Tang, Z.; Yan, C.; Qi, S.; Peng, C.; Cole, P. A.; Roeder, R. G.; Zhao, Y. The regulatory enzymes and protein substrates for the lysine β -hydroxybutyrylation pathway. *Sci. Adv.* **2021**, *7* (9), DOI: 10.1126/sciadv.abe2771.
- (29) Moreno-Yruela, C.; Zhang, Di; Wei, W.; Bæk, M.; Liu, W.; Gao, J.; Danková, D.; Nielsen, A. L.; Bolding, J. E.; Yang, L.; et al. Class I histone deacetylases (HDAC1–3) are histone lysine deacetylases. *Science advances* **2022**, *8* (3), eabi6696.
- (30) Kutil, Z.; Skultetyova, L.; Rauh, D.; Meleshin, M.; Snajdr, I.; Novakova, Z.; Mikesova, J.; Pavlicek, J.; Hadzima, M.; Baranova, P.; et al. The unraveling of substrate specificity of histone deacetylase 6 domains using acetylome peptide microarrays and peptide libraries. *FASEB journal: official publication of the Federation of American Societies for Experimental Biology* **2019**, *33* (3), 4035–4045.
- (31) Jiang, H.; Khan, S.; Wang, Y.; Charron, G.; He, B.; Sebastian, C.; Du, J.; Kim, R.; Ge, E.; Mostoslavsky, R.; et al. SIRT6 regulates TNF- α secretion through hydrolysis of long-chain fatty acyl lysine. *Nature* **2013**, *496* (7443), 110–113.
- (32) Dancy, B. C. R.; Ming, S. A.; Papazyan, R.; Jelinek, C. A.; Majumdar, A.; Sun, Y.; Dancy, B. M.; Drury, W. J.; Cotter, R. J.; Taverna, S. D.; et al. Azalysine analogues as probes for protein lysine deacetylation and demethylation. *J. Am. Chem. Soc.* **2012**, *134* (11), 5138–5148.

- (33) He, Y.; Yan, L.; Zang, W.; Zheng, W. Novel sirtuin inhibitory warheads derived from the N(ϵ)-acetyl-lysine analog L-2-amino-7-carboxamidoheptanoic acid. *Organic & biomolecular chemistry* **2015**, *13* (42), 10442–10450.
- (34) Gantt, S. M. L.; Decroos, C.; Lee, M. S.; Gullett, L. E.; Bowman, C. M.; Christianson, D. W.; Fierke, C. A. General Base-General Acid Catalysis in Human Histone Deacetylase 8. *Biochemistry* **2016**, *55* (5), 820–832.
- (35) Borra, M. T.; Langer, M. R.; Slama, J. T.; Denu, J. M. Substrate specificity and kinetic mechanism of the Sir2 family of NAD⁺-dependent histone/protein deacetylases. *Biochemistry* **2004**, *43* (30), 9877–9887.
- (36) Whitehead, L.; Dobler, M. R.; Radetich, B.; Zhu, Y.; Atadja, P. W.; Claiborne, T.; Grob, J. E.; McRiner, A.; Pancost, M. R.; Patnaik, A.; et al. Human HDAC isoform selectivity achieved via exploitation of the acetate release channel with structurally unique small molecule inhibitors. *Bioorg. Med. Chem.* **2011**, *19* (15), 4626–4634.
- (37) Ibrahim, H. S.; Abdelsalam, M.; Zeyn, Y.; Zessin, M.; Mustafa, A.-H. M.; Fischer, M. A.; Zeyen, P.; Sun, P.; Bülbül, E. F.; Vecchio, A. Synthesis, Molecular Docking and Biological Characterization of Pyrazine Linked 2-Aminobenzamides as New Class I Selective Histone Deacetylase (HDAC) Inhibitors with Anti-Leukemic Activity. *International Journal of Molecular Sciences* **2022**, *23* (1), 369.
- (38) Malvaez, M.; McQuown, S. C.; Rogge, G. A.; Astarabadi, M.; Jacques, V.; Carreiro, S.; Rusche, J. R.; Wood, M. A. HDAC3-selective inhibitor enhances extinction of cocaine-seeking behavior in a persistent manner. *Proc. Natl. Acad. Sci. U.S.A.* **2013**, *110* (7), 2647–2652.
- (39) Butler, K. V.; Kalin, J.; Brochier, C.; Vistoli, G.; Langley, B.; Kozikowski, A. P. Rational design and simple chemistry yield a superior, neuroprotective HDAC6 inhibitor, tubastatin A. *J. Am. Chem. Soc.* **2010**, *132* (31), 10842–10846.
- (40) Balasubramanian, S.; Ramos, J.; Luo, W.; Sirisawad, M.; Verner, E.; Buggy, J. J. A novel histone deacetylase 8 (HDAC8)-specific inhibitor PCI-34051 induces apoptosis in T-cell lymphomas. *Leukemia* **2008**, *22* (5), 1026–1034.
- (41) Kurohara, T.; Tanaka, K.; Takahashi, D.; Ueda, S.; Yamashita, Y.; Takada, Y.; Takeshima, H.; Yu, S.; Itoh, Y.; Hase, K. Identification of Novel Histone Deacetylase 6-Selective Inhibitors Bearing 3,3,3-Trifluorolactic Amide (TFLAM) Motif as a Zinc Binding Group. *Chembiochem: a European journal of chemical biology* **2021**, *22*, 3158.
- (42) Fischer, G.; Oehme, G.; Schellenberger, A. Zur theorie der α -ketosäuren. *Tetrahedron* **1971**, *27* (22), 5683–5696.
- (43) Dowling, D. P.; Gantt, S. L.; Gattis, S. G.; Fierke, C. A.; Christianson, D. W. Structural studies of human histone deacetylase 8 and its site-specific variants complexed with substrate and inhibitors. *Biochemistry* **2008**, *47* (51), 13554–13563.
- (44) Bagchi, R. A.; Robinson, E. L.; Hu, T.; Cao, J.; Hong, J. Y.; Tharp, C. A.; Qasim, H.; Gavin, K. M.; Pires da Silva, J.; Major, J. L.; McConnell, B. K.; Seto, E.; Lin, H.; McKinsey, T. A. Reversible lysine fatty acylation of an anchoring protein mediates adipocyte adrenergic signaling. *Proc. Natl. Acad. Sci. U.S.A.* **2022**, *119* (7), e2119678119.
- (45) Wang, Z. A.; Whedon, S. D.; Wu, M.; Wang, S.; Brown, E. A.; Anmangandla, A.; Regan, L.; Lee, K.; Du, J.; Hong, J. Y.; et al. Histone H2B Deacylation Selectivity: Exploring Chromatin's Dark Matter with an Engineered Sortase. *J. Am. Chem. Soc.* **2022**, *144* (8), 3360–3364.
- (46) Smith, B. C.; Denu, J. M. Acetyl-lysine analog peptides as mechanistic probes of protein deacetylases. *J. Biol. Chem.* **2007**, *282* (51), 37256–37265.
- (47) Lahm, A.; Paolini, C.; Pallaoro, M.; Nardi, M. C.; Jones, P.; Neddermann, P.; Sambucini, S.; Bottomley, M. J.; Lo Surdo, P.; Carfi, A.; et al. Unraveling the hidden catalytic activity of vertebrate class IIa histone deacetylases. *Proc. Natl. Acad. Sci. U.S.A.* **2007**, *104* (44), 17335–17340.
- (48) Su, D.; Kosciuk, T.; Yang, M.; Price, I. R.; Lin, H. Binding Affinity Determines Substrate Specificity and Enables Discovery of Substrates for N-Myristoyltransferases. *ACS catalysis* **2021**, *11* (24), 14877–14883.
- (49) Barnes, C. E.; English, D. M.; Cowley, S. M. Acetylation & Co: an expanding repertoire of histone acylations regulates chromatin and transcription. *Essays in Biochemistry* **2019**, *63* (1), 97–107.
- (50) Flynn, E. M.; Huang, O. W.; Poy, F.; Oppikofer, M.; Bellon, S. F.; Tang, Y.; Cochran, A. G. A Subset of Human Bromodomains Recognizes Butyryllysine and Crotonyllysine Histone Peptide Modifications. *Structure* **2015**, *23* (10), 1801–1814.
- (51) Li, Y.; Sabari, B. R.; Panchenko, T.; Wen, H.; Zhao, D.; Guan, H.; Wan, L.; Huang, H.; Tang, Z.; Zhao, Y.; et al. Molecular Coupling of Histone Crotonylation and Active Transcription by AF9 YEATS Domain. *Molecular cell* **2016**, *62* (2), 181–193.
- (52) Zhao, D.; Guan, H.; Zhao, S.; Mi, W.; Wen, H.; Li, Y.; Zhao, Y.; Allis, C. D.; Shi, X.; Li, H. YEATS2 is a selective histone crotonylation reader. *Cell Research* **2016**, *26* (5), 629–632.
- (53) Andrews, F. H.; Shinsky, S. A.; Shanle, E. K.; Bridgers, J. B.; Gest, A.; Tsun, I. K.; Krajewski, K.; Shi, X.; Strahl, B. D.; Kutateladze, T. G. The Taf14 YEATS domain is a reader of histone crotonylation. *Nat. Chem. Biol.* **2016**, *12* (6), 396–398. DOI: .
- (54) Borra, M. T.; Smith, B. C.; Denu, J. M. Mechanism of human SIRT1 activation by resveratrol. *J. Biol. Chem.* **2005**, *280* (17), 17187–17195.
- (55) Schuster, S.; Roessler, C.; Meleshin, M.; Zimmermann, P.; Simic, Z.; Kambach, C.; Schiene-Fischer, C.; Steegborn, C.; Hottiger, M. O.; Schutkowski, M. A continuous sirtuin activity assay without any coupling to enzymatic or chemical reactions. *Sci. Rep.* **2016**, *6*, 22643.
- (56) Pankaskie, M.; Abdel-Monem, M. M. Inhibitors of polyamine biosynthesis VII: Evaluation of pyruvate derivatives as inhibitors of S-adenosyl-L-methionine decarboxylase. *J. Pharm. Sci.* **1980**, *69* (9), 1000–1004.
- (57) Zessin, M.; Kutil, Z.; Meleshin, M.; Nováková, Z.; Ghazy, E.; Kalbas, D.; Marek, M.; Romier, C.; Sippl, W.; Bařinka, C.; et al. One-Atom Substitution Enables Direct and Continuous Monitoring of Histone Deacylase Activity. *Biochemistry* **2019**, *58* (48), 4777–4789.
- (58) Zessin, M.; Meleshin, M.; Simic, Z.; Kalbas, D.; Arbach, M.; Gebhardt, P.; Melesina, J.; Liebscher, S.; Bordusa, F.; Sippl, W.; et al. Continuous Sirtuin/HDAC (histone deacetylase) activity assay using thioamides as PET (Photoinduced Electron Transfer)-based fluorescence quencher. *Bioorganic Chemistry* **2021**, *117*, 105425.
- (59) *Molecular Operating Environment (MOE)*, 2019.01; Chemical Computing Group ULC: Montreal, QC, Canada, 2021.

4 Diskussion und Zusammenfassung der Ergebnisse

4.1 Messung der HDAC-Aktivität

Die Messung der Enzymaktivität wird vor allem genutzt, um den aktivierenden bzw. inhibierenden Einfluss verschiedener Verbindungen auf die Enzyme zu untersuchen. Die ideale Messmethode soll reproduzierbare Ergebnisse liefern (Robustheit), eine klare Identifizierung aktiver Verbindungen (Hits) ermöglichen, wenig störanfällig, einfach anzuwenden und kostengünstig sein. Die Entwicklung von Messmethoden zur Charakterisierung und Analyse der HDAC-Aktivität gestattet die Untersuchung der enzymatischen Eigenschaften dieser Enzyme hinsichtlich ihrer Spezifität für verschiedene Substrate. Dies betrifft sowohl die Acylmodifikation als auch den Träger der Modifikation, also das Peptid oder das Polyamid. Wie in Kapitel 1.6 beschrieben, gibt es für die Messung der Enzymaktivität der HDACs verschiedene Ansätze, welche unterschiedliche Vor- und Nachteile aufweisen.

Die erste Möglichkeit ist die Kopplung der Aktivitätsmessung an einen zusätzlichen Separationsschritt, wobei das Substrat vom Reaktionsprodukt getrennt wird (siehe Abschnitt 1.6.1). Übliche Methoden sind z.B. die Polyacrylamid-Elektrophorese, Dünnschichtchromatographie, Extraktion mit organischen Lösungsmitteln und klassische Methoden wie Kapillarelektrophorese, HPLC und MS. Aufgrund des Designs sind diese Messmethoden diskontinuierlich. Vorteile sind die hohe Robustheit und damit einhergehende gute Reproduzierbarkeit. Außerdem können Substrate mit natürlichem Acylrest und grundsätzlich ohne weitere Markierungen, wie Fluoreszenz-tags genutzt werden. Dennoch werden bei einigen Ansätzen zusätzliche Fluoreszenz-tags oder ähnliche Markierungen an Substrate gekoppelt, um eine komfortablere Quantifizierbarkeit per HPLC oder Kapillarelektrophorese zu erreichen (45, 169). Nachteile dieser Methoden sind die meist aufwendige Probenpräparation, eine hohe Analysezeit und die Notwendigkeit von komplexen Analysegeräten. Durch verschiedene Ansätze zur Entwicklung von HTS Systemen konnte sowohl die Messzeit, (wenige Sekunden pro Probe bei MS (184) oder Mikrochipelektrophorese (182)) als auch der Aufwand der Probenpräparation deutlich gesenkt werden.

Eine weitere Möglichkeit ist die Verwendung von verschiedenen optischen Assays. Dabei wird in einer Lösung durch eine Reaktion ein messbares Signal erzeugt, welches proportional zur Produktbildung ist. Bei der den optischen Assays zugrundeliegenden HDAC-Reaktion wird kein messbares Signal erzeugt. Deswegen müssen entweder die Substrate modifiziert oder an eine weitere Reaktion gekoppelt werden. Diese Art der Reaktion kann eine oder mehrere enzymatische Reaktionen (siehe 1.6.2), chemische Kopplungsschritte (siehe 1.6.3) oder eine intramolekulare Reaktion (siehe 1.6.4) beinhalten. Es können auch mehrere Reaktionsschritte hintereinander miteinander kombiniert werden.

Die Kopplung der Enzymreaktion an einen chemischen Reaktionsschritt ist normalerweise diskontinuierlich. Sie erfordert dementsprechend zusätzliche Arbeitsschritte nach der Enzymreaktion. Dies liegt an den zugegebenen Reagenzien, welche die Enzymreaktion stören können, Kreuzreaktionen hervorrufen können oder auch dafür sorgen können, dass die Reaktionsbedingungen, wie zum Beispiel der pH-Wert geändert werden müssen (110, 210).

Die Nutzung von Enzym-gekoppelten Assays erlaubt zwar teilweise kontinuierliche Messungen, aber diese Art der Assays weist einen großen Nachteil auf. Durch die Zugabe von weiteren Enzymen und deren Substraten wird die Reaktionslösung deutlich komplexer und die Messmethode wird damit anfälliger für Störungen.

Die einfachste Möglichkeit für einen Assayansatz ist die der kontinuierlichen und direkten Assays (siehe 1.6.5). Bei diesen Assays wird das Messsignal direkt durch die enzymatische Reaktion hervorgerufen, wodurch es keine Einflüsse auf das Messsignal durch nachgelagerte Reaktionen gibt. Dieser Assayansatz ist wenig komplex und ist daher wenig stör anfällig. Zusätzlich besticht diese Methode durch eine sehr einfache Anwendung. Aufgrund dieser Vorteile gegenüber den anderen Messmethoden ist die Entwicklung direkter und kontinuierlicher Messmethoden von besonderem Interesse. Es eignen sich hierfür besonders Fluorophor/Quencherpaare, die sich durch die Deacylierungsreaktion so trennen lassen, dass eine räumliche Separierung stattfindet, welche die Fluoreszenzlöschung aufhebt. Damit diese Fluorophor/Quencherpaare die Substrateigenschaften nicht maßgeblich verändern, muss das entsprechende Substrat exakt für das untersuchte Enzym modifiziert sein oder die Modifikation muss so unbedeutend sein, dass sie die Substrateigenschaften nicht verändern.

4.1.1 FRET-basierter HDAC11 Assay

Wie wichtig die richtige Wahl des Substrats für die entsprechende Isoform ist, konnte in der hier vorliegenden Arbeit für HDAC11 gezeigt werden (Manuskript 3.1). HDAC11 weist nahezu keine Deacetylaseaktivität, aber eine hohe Aktivität bei der Hydrolyse des artifiziellen TFA-Rests auf (61, 62). Ebenso hydrolysiert HDAC11 längere Fettsäurereste an Lysinen sehr effizient (61–63). Im Rahmen dieser Arbeit wurde ein Assay etabliert, mit dem Ziel, diese Substratspezifität der HDAC11 zu nutzen. Dafür wurde ein bekanntes Sirtuinsubstrat genutzt, welches eine direkte und kontinuierliche Messung erlaubt (Manuskript 3.1, Verbindung 1). Seine Peptidsequenz ist von TNF α abgeleitet und enthält einen Quencher. Der Acylrest ist dem Myristoylrest strukturell deutlich ähnlicher als einem Acetylrest (236). Durch die Hydrolyse des den Fluorophor enthaltenden Acylrests steigt die Fluoreszenzintensität.

Die ermittelten kinetischen Konstanten von HDAC11 für dieses Peptid mit einem K_M von 12,2 μM , einem k_{cat} von 0,16 s^{-1} und einer katalytischen Effizienz von 13 000 $\text{M}^{-1}\text{s}^{-1}$ sind vergleichbar mit bekannten myristoylierten Peptidsubstraten von HDAC11. Für diese myristoylierten Peptide besitzt HDAC11 eine katalytische Effizienz von 15 400 $\text{M}^{-1}\text{s}^{-1}$ für ein H3K9 abgeleitetes Peptid (63), 15 000 $\text{M}^{-1}\text{s}^{-1}$ für ein Dihydrolipoyl-Transacetylase (DLAT) abgeleitetes Peptid (62) und 72 000 $\text{M}^{-1}\text{s}^{-1}$ für ein artifizielles Peptid (61). Die höhere katalytische Effizienz für das artifizielle Peptid ergibt sich vor allem durch den geringen K_M -Wert von 1,4 μM .

Die in Manuskript 3.1 erfolgte Untersuchung verschiedener HDACi, welche teilweise als niedrige nanomolare HDAC11-Inhibitoren beschrieben sind, zeigte, dass diese Ergebnisse bei der Verwendung des in dieser Arbeit entwickelten Assays nur teilweise reproduzierbar waren. Für fünf der elf getesteten Verbindungen konnten zuvor publizierte IC_{50} -Werte reproduziert werden. Dazu gehörten die niedrigen IC_{50} -Werte von Trapoxin A (62) und Fimepinostat (255), sowie die geringe Inhibition durch Ricolinostat (256), Trichostatin A (TSA), (62) und Romidepsin (257). Das in dieser Arbeit durchgeführte Kontrollexperiment mit dem kommerziell erhältlichen fluorogenen Lysinderivat Boc-Lys(TFA)-AMC zeigte, dass alle gemessenen IC_{50} -Werte in diesen Fällen vergleichbar waren.

Die reproduzierten Werte für TSA und Trapoxin A wurden in der Originalarbeit mit einem myristoylierten Peptid gemessen (62). Sofern beschrieben, wurden alle anderen IC_{50} -Werte aus den Vergleichsstudien mit acetylierten Peptiden gemessen. Alternativ wurden die IC_{50} -Werte durch kommerzielle Anbieter bestimmt, weshalb meist keine Beschreibung des Substrats in der entsprechenden Publikation zu finden ist. Ein erwähnenswertes Beispiel ist der Inhibitor

Romidepsin. In beiden Publikationen wurden die IC_{50} -Werte für HDAC11 von BPS Bioscience bestimmt. Im Jahr 2014 wurde für HDAC11 ein IC_{50} -Wert von 0,3 nM bestimmt (258). In 2015 wurde für den gleichen Inhibitor durch die gleiche Firma ein IC_{50} -Wert für HDAC11 von > 10 μ M bestimmt (257).

Für die deutlichen Unterschiede zwischen den in dieser Arbeit gemessenen IC_{50} -Werte und den Literaturwerten gibt es zwei Möglichkeiten. Zum einen könnte HDAC11 abhängig vom verwendeten Substrat verschieden inhibiert werden, wie zum Beispiel SIRT2 (195). Zum anderen besteht die Möglichkeit, dass bei den Messungen von HDAC11 mit dem acetylierten Substrat verschiedene systematische Fehler aufgetreten sind, welche die hohen Abweichungen erklären. Die meisten der untersuchten Verbindungen sind pan-Inhibitoren, weisen also ein breites Aktivitätsspektrum gegen alle HDAC-Isoformen auf. Durch die sehr niedrige katalytische Effizienz von HDAC11 für acetylierte Substrate muss eine hohe Enzymkonzentration eingesetzt werden, um den Substratumsatz zu detektieren. Dabei könnten Verunreinigungen von anderen HDACs, welche eine deutlich höhere katalytische Effizienz für acetylierte Substrate aufweisen, für die gemessenen Umsätze verantwortlich sein. Eine Verunreinigung von 0,1 % würde vermutlich ausreichen, um ein falsch positives Signal zu erzeugen und könnte mit den gängigen Methoden schwer detektiert werden. Die meisten der Vergleichswerte aus der Literatur wurden mit kommerziell erhältlicher HDAC11 oder direkt von den entsprechenden Anbietern gemessen. Daher ist das Auftreten einer Verunreinigung wahrscheinlicher, da diese Proteine oft nur unzureichend gereinigt vertrieben werden.

Bei der Verwendung von Verbindung 3 (Manuskript 3.1) als Substrat für HDAC11, welche einen TFA-Rest trägt, sind solche Kreuzreaktionen deutlich unwahrscheinlicher, da HDAC11 gegen diesen Acylrest eine weitaus höhere Aktivität aufweist (61). Es ist entsprechend weniger Enzym im Ansatz notwendig. Eine Kreuzkontamination könnte in diesem Fall mit den HDACs der Klasse IIa und der HDAC8 möglich sein, da diese deutlich höhere Aktivitäten für die Hydrolyse von TFA-Resten aufweisen als HDAC11 (57). Die Verbindung 1 (Manuskript 3.1) hingegen ist optimal als Substrat für die Messung der HDAC11-Aktivität. HDAC8, als einziger Vertreter der Zn^{2+} -abhängigen HDACs, der ebenso in der Lage ist längere Fettsäurereste zu hydrolysieren (51), spaltete Verbindung 1 (Manuskript 3.1) nicht. Damit ist HDAC11 die einzige Isoform, welche diesen Acylrest hydrolysieren kann. Sirtuine können diesen Acylrest hydrolysieren, brauchen aber NAD^+ als Cosubstrat für die Reaktion und unter Verwendung von NAM sind Sirtuine sehr spezifisch zu inhibieren.

Zusammenfassend zeigt sich also, dass sich der hier beschriebene Assay, der hochspezifisch die Aktivität von HDAC11 bestimmen kann, anbietet, bekannte HDACi zu überprüfen, ob sie in der Lage sind dieses Isoenzym zu inhibieren.

Auch bei der Untersuchung anderer HDACs zeigte sich ein Einfluss des verwendeten Substrats auf die inhibitorischen Eigenschaften verschiedener Verbindungen. Zum Beispiel inhibiert der Inhibitor SirReal2 SIRT2 nur effektiv, wenn ein acetyliertes Peptid als Substrat genutzt wird. Wird ein myristoyliertes Substrat genutzt, kann keine oder nur eine geringe Inhibition gemessen werden (259). Ein weiteres Beispiel ist der Inhibitor TM, welcher ein Thiomyristoylderivat ist und designt wurde, um die Demyristoylaseaktivität von SIRT2 zu inhibieren (260). Wurde der IC_{50} -Wert von TM mit einem myristoylierten von H3K9 abgeleiteten Peptidsubstrat analysiert, ergibt sich ein IC_{50} -Wert von 0,05 μ M (259). Wurde hingegen ein kontinuierlicher und direkter SIRT2-Assay genutzt, welcher ein Peptid mit sehr artifiziellem Acylrest Substrat verwendete (239), wurde ein 920-fach höherer IC_{50} -Wert von 46 μ M gemessen. Um diese Nachteile zu minimieren,

wurde für diese Arbeit die Strategie gewählt, Acylreste zu nutzen, welche strukturell möglichst geringe Abweichungen zum natürlichen Acylrest aufweisen.

4.1.2 Messung der HDAC-Aktivität durch Hydrolyse des Thioacylrests

Eine weitere Möglichkeit einen Assay mit Spezifität für eine bestimmte Isoform bzw. eine Gruppe von HDACs zu entwickeln, ergibt sich aus der Tatsache, dass HDAC8 in der Lage ist, Thioamidbindungen zu spalten (209). In der hier vorliegenden Arbeit wurde gezeigt, dass die Spaltung der Thioamidbindung durch die HDACs deren spezifische Absorption bei 260 nm eliminiert (251). Über die daraus resultierende Intensitätsabnahme kann die Enzymaktivität der HDACs direkt und kontinuierlich gemessen werden. Das gleiche Messprinzip wurde bereits für die Messung der Enzymaktivität der Carboxypeptidase A genutzt (261). Der Vorteil dieser Methode ist, dass die Substitution von nur einem Atom im Acylrest die Möglichkeit bietet, die Enzymaktivität direkt und kontinuierlich zu messen. Diese Messmethode eignet sich ausschließlich für die Zn^{2+} -abhängigen HDACs, da Sirtuine durch Thioamidbindungen als zu hydrolysierende Bindung inhibiert werden.

Die verschiedenen HDAC-Isoformen unterscheiden sich hinsichtlich ihrer Aktivität bei der Hydrolyse der Thioamidbindung. HDAC1 zeigte in dieser Arbeit nur eine geringe Deacetylaseaktivität (Manuskript 3.2). Gegen das thioacetylierte Peptid konnte kein Substratumsatz gemessen werden, weder mittels HPLC noch im optischen Assay. HDAC2 und HDAC3 wurden in dieser Arbeit nicht untersucht. Jedoch zeigten Fatkins *et al.* in Übereinstimmung mit den hier erhaltenen Daten, dass HDAC1 und auch HDAC2 keine Thioacetylreste hydrolysieren kann (209). HDAC3 gehört zwar ebenso zur Klasse I der HDACs, weist allerdings eine von der HDAC1 und HDAC2 etwas abweichende Substratspezifität für verschiedene Acylreste auf. Beispielsweise war HDAC3 in der Lage Crotonyl- und TFA-Reste zu hydrolysieren, wohingegen HDAC1 und HDAC2 diese Reste nicht bzw. schlecht als Substrate akzeptierten (52). Deswegen besteht die Möglichkeit, dass HDAC3 ebenso wie HDAC8 in der Lage ist, Thioacetylreste zu hydrolysieren.

Die HDACs der Klasse IIa und HDAC6 sind ebenfalls in der Lage, Thio-TFA-Reste zu hydrolysieren (Manuskript 3.2). Diese Enzyme weisen für die Hydrolyse der Thioamidbindung einen 5 bis 8-fach niedrigeren k_{cat} -Wert im Vergleich zur Hydrolyse der Amidbindung auf. Der K_M -Wert hingegen bleibt für HDAC5 und HDAC7 gleich und wurde bei HDAC4, HDAC6 und HDAC9 etwas niedriger. Dahingegen wies HDAC11 eine ähnliche Aktivität gegenüber Thiomyristoylresten auf, jedoch mit einem 6-fach erhöhten K_M -Wert. HDAC6 zeigte eine Verschlechterung des K_M -Werts und des k_{cat} -Werts. HDAC8 ist die einzige Isoform, die eine 3-fach höhere Dethioacetylaseaktivität als Deacetylaseaktivität aufweist (Manuskript 3.2 und 0). Dieser Effekt konnte bei der Hydrolyse des den TFA-Rest enthaltenden Substrats und beim entsprechenden Thioxo-Substrat nicht beobachtet werden, wobei die Grundaktivität von HDAC8 für TFA-Reste deutlich erhöht ist im Vergleich zum Acetylrest (52).

Die Fähigkeit einiger Zn^{2+} -abhängiger HDAC-Isoformen, thioacetylierte Lysine als Substrate zu erkennen, ist bemerkenswert. Andere Enzyme, welche Amidbindungen spalten bzw. an Amidbindungen agieren, sind oft nicht in der Lage, Reaktionen an Thioamidbindungen zu katalysieren. Zum Beispiel werden Peptidsubstrate von Cyclophilin und Pin1 mit thioxylierter Peptidyl-Prolyl-Bindung zu kompetitiven Inhibitoren (262, 263). Auch für die NAD^+ -abhängigen Sirtuine sind Thioxoacyllysine (wie z.B. Thiosuccinyllysine für SIRT5 oder Thiomyristoyllysine für SIRT2 und SIRT6) effektive Inhibitoren (254, 264–266). Eigentlich handelt es sich bei Thioxoacyl-

Lysinen um sehr langsame, kompetitive Substrate. Dies liegt an einer deutlichen Verringerung der Reaktionsgeschwindigkeit und einer Verlagerung des geschwindigkeits-bestimmenden Schritts von der Produktfreisetzung zu der Dekomposition des Imidats (Abbildung 6, Schritt 2). Dies führt dazu, dass die Sirtuine nach dem ersten Reaktionsschritt als 1-S-Alkylimidat „verbleiben“ und deswegen auch *stalled intermediate* genannt werden (254).

Aspartatproteasen wie z.B. die HIV-Protease waren nicht in der Lage, Peptide mit Thioamidbindungen an verschiedenen Positionen und an der zu spaltenden Bindung, zu hydrolysieren (267). Auch Serinproteasen, wie Chymotrypsin oder Subtilisin, können keine Thioamidbindungen spalten (268, 269). Die Prolin-spezifischen Serinproteasen, wie die Dipeptidylpeptidase IV oder die Prolyl-Oligopeptidase, können Thioarylamidbindungen spalten. Die Dipeptidylpeptidase IV besitzt einen 25-fach geringeren k_{cat} -Wert für das thioxylierte Peptid im Vergleich zum entsprechenden Gegenpart (270). Die Prolyl-Oligopeptidase spaltet die Thioarylamidbindung mit einer um das 5 600-fache reduzierten Spezifitätskonstante (271), akzeptiert aber keine „normale“ thioxylierten Peptidbindung und auch keine Thioamidbindung zwischen der P2- und P1-Position (271, 272).

Auch Serin- β -Lactamasen können Thioamidbindungen nicht effektiv spalten (273). Cysteinproteasen, wie Papain, konnten aktiviert thioxylierte Bindungen, wie bei Thioxoestern (274) oder thioxylierten 4-Nitroaniliden (275) spalten. Sie können jedoch keine „normalen“ thioxylierten Peptidbindungen, wie in Ac-Phe-Gly-Amid oder Ac-Phe-Gly-Methylamid, umsetzen (275, 276). Insgesamt lässt sich sagen, dass Serin- und Cysteinproteasen tendenziell nicht in der Lage sind, Thioamidbindungen zu hydrolysieren. Vor allem die richtige Positionierung des Oxyanion-Lochs und die Stabilisierung des tetrahedralen Intermediats durch Wasserstoffbrückenbindung zum Peptidrückgrat des Enzyms wurde durch den Schwefelaustausch gestört. Als mögliche Ursachen dafür werden die längere Bindungslänge der C-S-Bindung im Vergleich zur C-O-Bindung und der größere Van-der-Waals-Radius des Schwefels diskutiert.

Die Situation der Metallion-abhängigen Amidohydrolasen und Proteasen gestaltet sich etwas diverser. Peptiddeformylasen akzeptierten keine thioformylierte Derivate als Substrate (277). Thiono-Cephalosporine sind Substrate mit um das 16,7-fach verringerter Spezifitätskonstante im Vergleich zum Oxo-Gegenpart für die Zn^{2+} -abhängige β -Lactamase aus *Bacillus cereus* (278). Sie wirken als schwache kompetitive Inhibitoren (279) und binden ähnlich wie die Oxo-Verbindungen im aktiven Zentrum. Die Metalloprotease Leucin-Amino-peptidase ist ebenfalls nicht in der Lage, Thioamidbindungen in Peptiden zu spalten. Die thioxylierten Peptide sind schwache kompetitive Inhibitoren der Protease (280). Die Metalloprotease Angiotensin-konvertierendes Enzym (ACE) akzeptiert Thioamide als Substrate bei einem N-Furylacroylierten Tripeptidderivat mit vergleichbaren kinetischen Konstanten wie der Oxo-Gegenpart. Ändert sich die zu spaltende Thioamidbindung von Phe-Gly zu Phe-Ala wird das Peptid nicht mehr durch ACE hydrolysiert (281).

Die Metalloprotease Carboxypeptidase A spaltete Thioamidbindungen in Dipeptiden mit leicht verringerten k_{cat} -Werten (282, 261). Wird das Zn^{2+} -Ion im aktiven Zentrum durch thiophilere Metallionen substituiert (z.B. Co^{2+} und Cd^{2+}), steigt die Aktivität gegenüber den Thioxopeptiden an (282, 261). Im Gegensatz dazu hydrolysierte die Amino-peptidase P Thioamidbindungen mit 1 000-fach geringeren k_{cat} -Werten (270). Auch bei der Amino-peptidase aus *Aeromonas proteolytica* änderte sich die Aktivität enzymatisch gegenüber Thioamidbindungen, wenn das Zn^{2+} -Ion im aktiven Zentrum durch Cd^{2+} ersetzt wurde. Das Zn^{2+} -Enzym spaltete die

Thiopeptide mit ähnlichen kinetischen Konstanten wie die entsprechenden Peptide. Das Cd²⁺-Enzym spaltete ausschließlich das thioxylierte Peptid (283).

Auch für HDAC8 wird diskutiert, ob sie *in vivo* mit einem anderen Metallion als Zn²⁺ im aktiven Zentrum beladen ist. Es existieren Kristallstrukturen mit Co²⁺, Mn²⁺ oder Fe²⁺ als Metallion im aktiven Zentrum der HDAC8 (121, 242, 284). Wäre die HDAC8-Präparation mit einem anderen Metallion als Zn²⁺ beladen, welches die Spaltung der Thioamidbindung begünstigt, könnte dies die gute Aktivität der HDAC8 gegenüber der Thioamidbindung erklären.

Tabelle 1. Verschiedene Peptidsubstrate mit den entsprechenden kinetischen Konstanten für HDAC8. n.B. bedeutet, dass die entsprechenden Konstanten nicht bestimmt wurden, nicht vergleichbar sind oder nicht angegeben wurde. *Das zweiwertige Metallion ist das katalytische Ion der HDAC8. Wenn nicht anders angegeben, wird davon ausgegangen, dass es sich um Zn²⁺ handelt.

Sequenz	K _M (μM)	k _{cat} (s ⁻¹)	k _{cat} /K _M (M ⁻¹ s ⁻¹)	Referenz
Ac-FRK(Ac)RW-NH ₂	950 ± 110	0,162 ± 0,007	171 ± 13	(210)
Ac-FAK(Ac)WR-NH ₂	730 ± 170	0,037 ± 0,004	51 ± 8	(210)
Ac-RHKK(Ac)-AMC	1 270 ± 190	0,21 ± 0,02	164	(210)
Ac-RHKK(Ac)-AMC	650 ± 20	0,007 ± 0,001	10,8	(241)
Ac-RHK(Ac)K(Ac)-AMC (Co ²⁺) *	160	1,2	7 500	(121)
Ac-RHK(Ac)K(Ac)-AMC (Fe ²⁺) *	210	0,48	2 300	(121)
Ac-RHK(Ac)K(Ac)-AMC (Zn ²⁺) *	1100	0,9	800	(121)
Ac-RHK(Ac)K(Ac)-AMC (Ni ²⁺) *	n.b.	n.b.	110	(121)
Ac-RHK(Ac)K(Ac)-AMC (Mn ²⁺) *	n.b.	n.b.	40	(121)
Ac-K(Ac)	800 ± 400	0,011 ± 0,003	1.4 ± 0.3	(285)
Ac-K(Ac)-AMC	4 200 ± 1700	0,07 ± 0,02	16.3 ± 1.5	(285)
Ac-RHK(Ac)K(Ac)	3 100 ± 1100	0,10 ± 0,03	34 ± 4	(285)
Ac-RHK(Ac)K(Ac)W	1 200 ± 300	0,131 ± 0,014	106 ± 13	(285)
Ac-RHK(Ac)K(Ac)-AMC	1 300 ± 300	0,34 ± 0,06	259 ± 19	(285)
Ac-RHK(Ac)K(Ac)-AMC	90	0,017	190	(52)
Ac-TARK(Ac)STG-NH ₂	n.b.	n.b.	56 ± 6	(286)
Ac-ARTKQTARK(Ac)STGGKAPR-NH ₂	n.b.	n.b.	120	(286)
KKGQSTSRHKK(S-Ac)LMFKTEG	33,7	0,0043	128	(209)
Ac-KGGAK(Ac)-AMC	320 ± 20	0.90 ± 0.06	2 800 ± 100	(124)
KQTARK(Ac)STGGWW	>600 μM	n.b.	58	(51)
Ac-RHKK(Ac)-AMC	251	0,021	80,1	(287)
Boc-K(TFA)-AMC	247	n.b.	n.b.	(288)
Ac-LGK(TFA)-AMC	440	16,5	38 000	(52)
Abz-SRGGK(TFA)FFRR-NH ₂	1 400 ± 200	440 ± 40	320 000	Manuskript 3.2
Abz-SRGGK(S-TFA)FFRR-NH ₂	550 ± 50	260 ± 20	470 000	Manuskript 3.2
Abz-SRGGK(Ac)FFRR-NH ₂	440 ± 150	2,4 ± 0,5	5 400	Manuskript 0
Abz-SRGGK(S-Ac)FFRR-NH ₂	710 ± 10	13 ± 1	18 000	Manuskript 3.2
Abz-SRGGK(Pyruvoyl)FFRR-NH ₂	4,5 ± 0.7	1,1 ± 0,1	240 000	Manuskript 0

Typische HDAC8-Substrate haben geringe katalytische Effizienzen (Tabelle 1). Zum Beispiel konnten für HDAC8, unter Verwendung eines chemisch gekoppelten Assays, die katalytischen Effizienzen für einige acetylierte Pentapeptide bestimmt werden. Diese liegen im Bereich von $16 - 171 \text{ M}^{-1}\text{s}^{-1}$ (210). Im Vergleich dazu wies HDAC8 für das in dieser Arbeit verwendete acetylierte Modellpeptid eine katalytische Effizienz von $5\,400 \text{ M}^{-1}\text{s}^{-1}$ auf (Manuskript 5.6, Verbindung 1). Diese Unterschiede ergeben sich vor allem aus dem 13-fach höheren k_{cat} -Wert. HDAC8 weist für die acetylierten Peptide, bis auf wenige Ausnahmen, einen K_{M} -Wert im hohen mikromolaren bzw. im niedrigen millimolaren Bereich auf. Eine Ausnahme bildet beispielsweise der K_{M} -Wert von HDAC8 für das kommerziell erhältliche HDAC8-Fluor-de-Lys (Ac-RHK(Ac)K(Ac)-AMC) von $90 \mu\text{M}$ (52). Allerdings wurden für das gleiche Peptid in anderen Arbeiten auch K_{M} -Werte von $1\,100 \mu\text{M}$ und $1\,300 \mu\text{M}$ gemessen (121, 285). In der Arbeit von Fatkins *et al.* wurde ein K_{M} -Wert von $33,7 \mu\text{M}$ bestimmt für ein von p53 abgeleitetes 18-meres Peptid. Der niedrige K_{M} -Wert könnte durch das lange Peptidrückgrat erklärt werden. Für HDAC8 wird vermutet, dass Wechselwirkungen mit Teilen des Substrats, welche weiter entfernt vom aktiven Zentrum liegen, eine wichtige Rolle in der Substraterkennung spielen (286).

Die K_{M} -Werte von HDAC8 für trifluoracetylierte Substrate sind mit denen für acetylierte Substrate vergleichbar, der k_{cat} -Wert ist deutlich erhöht, was in einer höheren katalytischen Effizienz resultiert (Tabelle 1). Zum Beispiel wurde für ein H4 abgeleitetes Substrat (Ac-LGK(TFA)-AMC) eine katalytische Effizienz von $38\,000 \text{ M}^{-1}\text{s}^{-1}$ bestimmt (52). Die Kombination des reaktiveren TFA-Rests mit der Thioamidbindung ermöglicht die optische Verfolgbarkeit des Reaktionsfortschritts. Im Vergleich zum bisher effizientesten Substrat konnte ein Substrat für HDAC8 erzeugt werden, welches sich durch eine mehr als 10-fach so hohe katalytische Effizienz auszeichnet. Dieses weist einen $k_{\text{cat}}/K_{\text{M}}$ -Wert von $450\,000 \text{ M}^{-1}\text{s}^{-1}$ auf und bietet die Möglichkeit der direkten und kontinuierlichen Messbarkeit. Diese ausgezeichneten katalytischen Konstanten konnten ebenso auf ein p53 abgeleitetes Peptidsubstrat (Peptid 13, Manuskript 5.2) übertragen werden.

Durch die N-terminale Einführung des Fluorophors Abz (Peptid 4, Manuskript 5.2) und durch Tryptophan (Peptid 13, Manuskript 5.2) ergab sich die Möglichkeit, neben der UV-Absorption auch die Fluoreszenzintensität als Detektionsmethode zu verwenden. Hierbei ist die Thioamidbindung der Quencher für die Fluorophore. Dies ermöglichte eine komfortable Messung der Enzymaktivität in Mikrotiterplatten im 96-well, 384-well und 1536-well Format.

4.1.3 Substrate mit Thioamiden als PET-basierte Fluoreszenzquencher

Die Spaltung der Thioamidbindung zu messen, kam für Sirtuine nicht in Betracht, weil Thioacylreste Inhibitoren für Sirtuine darstellen (254, 264). Der Thiomyristoylrest stellt z.B. das strukturelle Kernstück des potenten SIRT2-Inhibitors TM dar (260). Nach dem ersten Reaktionsschritt der Sirtuinreaktion, der Freisetzung von NAM, (Abbildung 6) bildet sich anstelle des 1-O-Alkylimidat-Intermediats ein relativ stabiles 1-S-Alkylimidat-Intermediat und die Reaktion bleibt an diesem Punkt hängen (254).

Wie in der vorherigen Studie gezeigt (Manuskript 3.2), sind Thioamidbindungen fähig, als Quencher für den Fluorophor Abz und die fluorogene AS Tryptophan zu fungieren. Thioamide können ebenso Quencher für andere Fluorophore sein, wie zum Beispiel verschiedene Cumarinderivate oder Fluorescein (252, 253). Das Quenching dieser Fluorophore durch Thioamide beruht auf dem PET-Mechanismus (252). Das Quenching durch PET basiert auf der Übertragung von Elektronen vom Donor zum Akzeptor. Dabei müssen, im Gegensatz zum FRET,

die Emissionsbande des Fluorophors nicht mit der Absorptionsbande der Quencher überlappen. Deswegen können auch langwelligere Fluorophore wie Fluorescein durch Thioamide gequencht werden (252). Die vergleichsweise geringe Größe von Thioamiden erlaubte das Design eines N-Thioacetylaminoundecanoyl-Acylrests (SAC-Aun) als Quencher, welcher strukturell ähnlich zum natürlichen Myristoylrest ist (Abbildung 13, Manuskript 3.3).

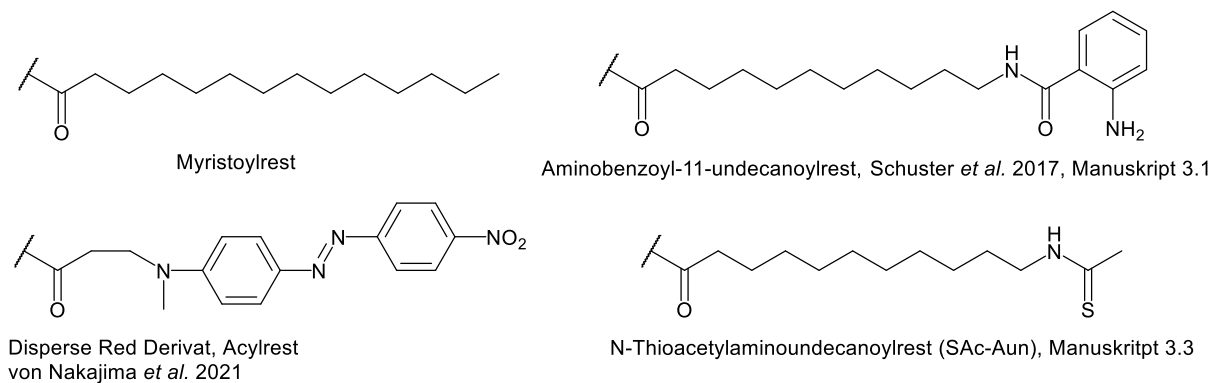


Abbildung 13. Struktur des Myristoylrests als natürliches Substrat für verschiedene HDAC-Isoformen. Im Vergleich dazu ist die Struktur ähnlicher artifizieller Acylreste aus verschiedenen HDAC-Assays dargestellt. Das ist der N-Thioacetylaminoundecanoylrest aus dieser Arbeit (Manuskript 3.3), der Aminobenzoyl-11-undecanoylrest entwickelt von Schuster *et al.* (236) und der DisperseRed-Rest entwickelt von Nakajima *et al.* als Acylreste für Sirtuin Substrate (239).

In einer systematischen Studie haben Goldberg *et al.* Thioacetamid als Quencher für verschiedene Fluorophore in Lösung untersucht. Dabei wurden die Fluoresceinderivate und die BODIPY-Derivate BODIPY FL und BODIPY R6G effizient durch Thioacetamid gequencht. NBD wurde mäßig gequencht (252). Außerdem konnte in einer weiteren Arbeit von Goldberg *et al.* gezeigt werden, dass 7-Methoxycoumarin (MCA) gut durch Thioacetamid gequencht wurde (289). Wurden MCA und die Thioamidbindung in einem Peptid integriert wurde MCA intramolekular durch die Thioamidbindung gequencht. Dieses Quenching ließ sich durch die Spaltung des Moleküls durch eine Protease und die damit verbundene räumliche Trennung aufheben (289). Die beschriebenen Quencheffizienzen (Q_E) stimmen gut mit den in dieser Arbeit ermitteltem Werten des intramolekularen Quenching überein. Das Peptid mit MCA (Peptid 12, Manuskript 5.3) wurde am besten mit einer Q_E von 55,1 % durch eine einfache Thioamidbindung gequencht. Das Peptid mit BODIPY FL wurde zu 52,6 % gequencht (Manuskript 3.3, Verbindung 9). Wie in der Arbeit von Goldberg *et al.*, wies auch hier das Peptid mit NBD als Fluorophor mit 12,2 % eine geringe Q_E auf (252).

Die Peterson-Gruppe hat Thioamide nicht nur als Quencher in Proteaseassays eingesetzt, sondern auch als Sonden, um die Proteinfaltung zu untersuchen (290, 291). Diese Anwendung ist möglich, da das PET-Quenching stark von der räumlichen Entfernung abhängig ist. Damit ein effektives PET-Quenching stattfinden kann, muss der Quencher bei vielen Fluorophoren im Van-der-Waals-Kontakt mit dem angeregten Fluorophor stehen, um den Elektronenübergang zu ermöglichen (252). So zeigten in Arbeiten der Peterson-Gruppe unterschiedlich lange Polyprolin-Peptide mit einem C-terminalen Tryptophan und einer N-terminale Thioamidbindung eine deutliche Abhängigkeit der Q_E von der Anzahl der Prolinreste bzw. vom Abstand zwischen Quencher und Fluorophor (253, 292). Eine deutliche Abhängigkeit der Q_E vom Abstand zwischen Fluorophor und Quencher konnte in dieser Arbeit nicht beobachtet werden. Die Untersuchung der Q_E in Abhängigkeit der Position des Fluorophors Fluorescein ("Fluorescein-Scan") im Substratpeptid Ac-EALPKK(SAC-Aun)TGG-NH₂ zeigte keine deutliche Veränderung. Die Q_E lag für

diese Peptide zwischen 35,7 % und 48,3 %. Es konnte auch kein Einfluss festgestellt werden, ob sich der Fluorophor N-terminal oder C-terminal vom modifizierten Lysin befand. Möglicherweise liegt das am flexiblen Acylrest, der den Quencher trägt. So zeigten Goldberg *et al.*, dass die Q_E für die untersuchten Fluorophore mit einem Diprolyl-Linker zwischen Thioamidbindung und Fluorophor deutlich niedriger war, im Vergleich zu Peptiden mit einem flexibleren Diglycyl-Linker. Durch den flexiblen Linker wird laut den Autoren der Studie dynamisches Quenching ermöglicht, was die Q_E erhöht (291).

Der Acylrest SAC-Aun dient als Träger der zur Fluoreszenzlöschung genutzten Thioamidbindung. SAC-Aun ist dem Myristoylrest strukturell ähnlich. Durch diese Ähnlichkeit ist der Assay besonders zur Detektion der enzymatischen Aktivität von denjenigen HDACs geeignet, die die Fähigkeit besitzen, lange Acylketten vom Lysin zu hydrolysieren. Daher wurde der Assay für HDAC11 und die Sirtuine SIRT2, SIRT3 und SIRT6 genutzt. Zusätzlich wurde SIRT5 zum Vergleich mit seiner alternativen Acylspezifität untersucht.

Alle untersuchten Sirtuine und HDAC11 haben die artifizialen SAC-Aun Lysin Acylierungen als Substrate erkannt. Die Enzymaktivität von SIRT2, SIRT3, SIRT5 und HDAC11 konnte direkt über die Änderung der Fluoreszenzintensität gemessen werden (Manuskript 3.3). Dies ist damit die zweite Messmethode für HDAC11, die in dieser Arbeit entwickelt wurde und die Möglichkeit der direkten und kontinuierlichen Messung der HDAC11-Aktivität eröffnet. Durch die Verwendung von Fluorescein als Fluorophor und durch die Bestimmung der optimalen Position des Fluorophors im Peptidrückgrat konnte die katalytische Effizienz von HDAC11 für das Peptid 1 (Manuskript 5.1) von $13\,000\text{ M}^{-1}\text{s}^{-1}$ auf $61\,000\text{ M}^{-1}\text{s}^{-1}$ bei Peptid 4 (Manuskript 3.3) verbessert werden. Durch die verbesserten Substrateigenschaften und die besseren optischen Eigenschaften von Fluorescein im Vergleich zu Abz (eine höhere Quantenausbeute und der höhere Extinktionskoeffizient), konnten die Aktivitätsmessungen mit einer HDAC11 Konzentration von 2 nM statt 20 nM durchgeführt werden. Dies ermöglicht die genauere Bestimmung der IC_{50} -Werte für potente Inhibitoren.

Für Sirtuine existieren drei direkte und kontinuierliche Assays, welche keinen zusätzlichen Reaktionsschritt benötigen. Die katalytischen Effizienzen von SIRT3 für die Assaypeptide waren $2\,800\text{ M}^{-1}\text{s}^{-1}$ (236), $240\text{ M}^{-1}\text{s}^{-1}$ (238) und $37\,000\text{ M}^{-1}\text{s}^{-1}$ (239). Verglichen mit den ersten beiden Substraten weist SIRT3 mit einer katalytischen Effizienz von $76\,000\text{ M}^{-1}\text{s}^{-1}$ für das in dieser Arbeit entwickelte Peptid 1 (Manuskript 3.3) eine deutlich höhere und im Vergleich zum dritten bekannten Substratpeptid eine ähnliche katalytische Effizienz auf. Auch in diesem Fall konnte die SIRT3 Assaykonzentration im Vergleich zum von Schuster *et al.* entwickelten Assay von 100 nM auf 10 nM SIRT3 gesenkt werden (236). Damit liegt die eingesetzte SIRT3-Konzentration in einem ähnlichen Bereich, wie in dem hier benannten dritten, von Nakajima *et al.* entwickelten, Assay mit 5,98 nM (239).

SIRT2 wies für alle SAC-Aun Peptide mit Fluorophor sehr niedrige K_M -Werte auf. Für Peptid 7 (Manuskript 3.3) wurde ein K_M -Wert von 5,3 nM gemessen. Durch leichte Modifikationen am Acylrest und mit MCA als Fluorophor konnte sogar ein K_M -Wert von SIRT2 für Peptid 14 (Manuskript 3.3) von 1,1 nM gemessen werden. Für die drei direkten und kontinuierlichen Assays wurde für SIRT2 für die Substrate ein K_M -Wert von 120 nM (236), 520 nM (238) und 41 nM (239) bestimmt. Im Vergleich mit diesen Substraten weist SIRT2 für Peptid 7 (Manuskript 5.3) einen 8 bis 40-fach niedrigeren K_M -Wert auf. Dahingegen ist der k_{cat} -Wert von SIRT2 für Peptid 7 (Manuskript 3.3) mit $0,36\text{ s}^{-1}$ mit dem von SIRT2 für das aminobenzoyl-11-aminoundecanoylierte Substrat vergleichbar (236). Die K_M -Werte für die Peptide 12-16 waren in Verbindung mit MCA als Fluorophor so niedrig, dass sie bei einer Konzentration am K_M -Wert nicht als Assaysubstrat in

Betracht kamen. Ursache hierfür sind die suboptimalen spektroskopischen Eigenschaften von MCA. Dafür konnte mit 10 nM Peptid 7 (Manuskript 3.3) mit einer SIRT2 Konzentration von 100 pM die SIRT2 Aktivität gemessen werden. Dadurch ergibt sich die Möglichkeit, potente SIRT2-Inhibitoren im niedrigen nanomolaren Bereich zuverlässig zu charakterisieren.

Im Vergleich dazu weist SIRT2 für Peptide mit einer Myristoylmodifikation am Lysin deutlich höhere K_M -Werte auf. Mittels HPLC wurde ein K_M -Wert von SIRT2 für ein von TNF α abgeleitetes Peptid von 0,69 μ M (236) und für ein H4 abgeleitetes Peptid von 0,5 μ M bestimmt (248). Für myristoylierte AMC-haltige Peptide wurden K_M -Werte von SIRT2 für ein von TNF α und ein von p53 abgeleitetes Peptid von kleiner als 0,5 μ M bestimmt (194). Dies war die untere Detektionsgrenze des Assays. Für ein von der DLAT abgeleitetes myristoyliertes Peptid wies SIRT2 einen K_M -Wert von 1,8 μ M auf (195).

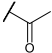
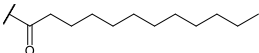
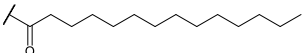
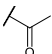
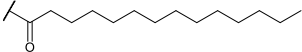
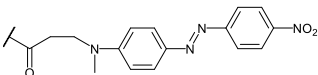
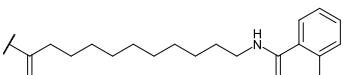
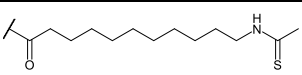
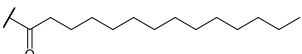
Eine besondere Bedeutung besitzt vor allem die Entwicklung von Assays, welche zuverlässig die Demyristoylaseaktivität von SIRT2 detektieren können. SIRT2 ist das einzige Sirtuin, welches abhängig vom Acylrest inhibiert wird (195, 259). Die meisten bekannten SIRT2 Inhibitoren hemmen die SIRT2-Aktivität nur, wenn diese mit einem acetylierten Peptidsubstrat gemessen wird. Historisch bedingt beruhen die meisten Inhibitoren auf Untersuchungen mit acetylierten Substraten, da die Deacetylaseaktivität von SIRT2 deutlich vor deren Demyristoylaseaktivität entdeckt wurde. Somit inhibieren die meisten bekannten kompetitiven SIRT2 Inhibitoren (wie SirReal2 und AGK-2) nur die Deacetylaseaktivität und nicht oder nur sehr schwach die Demyristoylaseaktivität. In Tabelle 2 ist eine Übersicht über die Inhibition der SIRT2-Aktivität durch bekannte Inhibitoren unter Verwendung verschiedener Substrate dargestellt.

Die Demyristoylaseaktivität von SIRT2 wird durch ein thiomyristoyliertes Peptid (SMyr) sehr effektiv inhibiert durch die Bildung des *stalled intermediate*. Der SIRT2 Inhibitor TM wurde mit dieser Information entwickelt und der wirksame Teil ist strukturell ein modifizierter Thiomyristoylrest (293). TM inhibiert neben der Deacetylaseaktivität von SIRT2 (293) auch die Demyristoylaseaktivität (259). Vor Kurzem konnten Vogelmann *et al.* SirReal2-Derivate erzeugen, welche ebenso die Demyristoylase Aktivität inhibieren (294). Für die Validierung der Messmethoden wurden in dieser Arbeit verschiedene bekannte Inhibitoren, wie SirReal2 (295), AGK-2 (296), NAM und SMyr (236), getestet. Dabei stellte sich heraus, dass die SIRT2-Aktivität unter Verwendung des Peptids 7 (Manuskript 5.3) und des aminobenzoylierten-11-aminoundecanoylierten Peptids ((236) durch SirReal2 und AGK-2 inhibiert werden, obwohl die Acylreste dieser Substrate strukturell dem Myristoylrest sehr ähnlich sind (Abbildung 13). Das heißt, der Umsatz dieser beiden Substrate durch SIRT2 wurde wie bei einem acetylierten Substrat und nicht wie bei einem myristoylierten Substrat inhibiert.

Einen anderen Effekt beobachteten Nakajima *et al.* in dem von ihnen entwickelten Assay (239). Bei einem Screening von 9 600 Verbindungen wurde eine Verbindung identifiziert (Verbindung C), welche SIRT2 inhibiert. Durch eine Messung mit einem myristoylierten Substrat Ac-RHKK(My)-AMC wurde bestätigt, dass dieser Inhibitor auch die Demyristoylaseaktivität von SIRT2 inhibiert. Deswegen ist der Assay grundsätzlich geeignet, um Inhibitoren der SIRT2 Demyristoylaseaktivität zu identifizieren. Allerdings wurde für den bekannten SIRT2 Demyristoylase Inhibitor TM mit diesem Assay ein IC_{50} -Wert von 47 μ M gemessen, während unter Verwendung eines myristoylierten H3K9-Peptids mit einem HPLC-basierten Assay ein um das 1 000-fache niedrigerer IC_{50} -Wert von 0,05 μ M bestimmt wurde. Im Gegensatz dazu konnte die SIRT2-Aktivität mit dem Assay von Nakajima *et al.* durch AGK-2 inhibiert werden (IC_{50} = 20 μ M),

während dieser Inhibitor im HPLC-basierten Assay die Demyristoylaseaktivität von SIRT2 nicht inhibieren konnte (259).

Tabelle 2. Inhibition der SIRT2-Aktivität durch bekannte Inhibitoren in Abhängigkeit des Acylrests des verwendeten Substrats. Das Zeichen „+“ bedeutet, dass die SIRT2-Aktivität inhibiert wird und „-“ bedeutet, dass die SIRT2-Aktivität nicht inhibiert wird. n.u. bedeutet, dass diese Kombination nicht untersucht wurde. * aminobenzoylierten-11-aminoundecanoylierten, # Manuskript 0.

Name	Acylrest Struktur	K _M (μ M)	SirReal2	AGK-2	TM	SMyr	Ref
Acetyl		750	+	n.u.	n.u.	n.u.	(195)
Dodecyl		4,5	+	n.u.	n.u.	n.u.	(195)
Myristoyl		1,8	—	n.u.	n.u.	n.u.	(195)
Acetyl		n.u.	+	+	+	n.u.	(259)
Myristoyl		n.u.	—	—	+	n.u.	(259)
Disperse Red-Derivat		0,057	—	—	—	n.u.	(239)
Abz-Aun*		0,1	+	+	n.u.	+	0#
SAc-Aun		0,0053	+	+	n.u.	+	0#
Myristoyl		0,033	—	—	n.u.	+	0#

4.1.4 Fluoreszenzbasierter Assays mit Myristoylrest

Aufgrund der unterschiedlichen und abweichenden Ergebnisse der Inhibition der SIRT2-Aktivität unter Nutzung von Substraten mit artifiziellen Acylresten im Vergleich zum natürlich auftretenden Myristoylrest wurde in der vorliegenden Arbeit ein Assay entwickelt, der die Messung der SIRT2-Aktivität mit dem natürlichen Myristoylrest ermöglicht (Manuskript 0). Dabei wurde die Umgebungssensitivität von den Fluorophoren MCA (Mcm1, Manuskript 0) und Fluorescein (F4, Manuskript 0) ausgenutzt. Unter der Nutzung von Mcm1 konnte ein direkter und kontinuierlicher Assay für SIRT2 entwickelt werden. SIRT2 wies, wie für die in Manuskript 5.3 entwickelten Substrate, einen sehr geringen K_M-Wert von 17 nM für Mcm1 auf (Manuskript 0). Die K_M-Werte von SIRT2 für das Peptid Mcm1 waren in Verbindung mit MCA als Fluorophor so niedrig, dass sie bei einer Konzentration am K_M-Wert nicht als Assaysubstrat in Betracht kamen. Deswegen wurde MCA als Fluorophor durch Fluorescein ersetzt (F4, Manuskript 0).

Fluorescein wird im Peptid nicht durch den Myristoylrest gequencht. Das Quenching ergibt sich durch die Bindung von dem fluoreszenzmarkierten Peptid F4 an Albumin aus Rinderserum (BSA). Wird der Myristoylrest durch SIRT2 gespalten, bindet das Produkt nicht mehr an BSA und die Fluoreszenz nimmt zu. Es handelte sich bei diesem Ansatz also um eine gekoppelte Messmethode. Dieses Assayprinzip funktioniert nur, wenn der K_M-Wert des Enzyms für das Substrat deutlich niedriger ist als der K_D-Wert von BSA für das Substrat. Ist dies nicht der Fall wird

die Bindung von BSA an das Peptid bevorzugt und die kinetischen Konstanten vom Enzym für das Substrat werden verfälscht. In diesem Fall war die Messmethode für die Bestimmung der enzymatischen Aktivität von SIRT2 und SIRT3 geeignet. Ein ähnliches Messprinzip wurde bereits für HATs durch Lanyon-Hogg *et al.* entwickelt. Ein Fluorescein-markiertes Peptid wird durch eine HAT am N-Terminus palmitoyliert. Das markierte Peptid bindet anschließend an BSA oder an Mizelle. Dadurch erhöhte sich die Fluoreszenzpolarisation deutlich (297). Die Fluoreszenzpolarisation als Detektionsmethode würde bei dem in dieser Arbeit entwickelten Messprinzip (mit F4, Manuskript 5.5) ebenso funktionieren. Durch die BSA-Bindung des Substrats ändert sich die Fluoreszenzpolarisation deutlich im Vergleich zum ungebundenen Produkt. Dies könnte eine deutlichere Unterscheidung des Substratsignals und des Produktsignals ermöglichen. Mit der in dieser Arbeit entwickelten Messmethode war es möglich, die SIRT2-Aktivität mit einer Enzymkonzentration von 0,1 nM und die SIRT3-Aktivität mit 10 nM zu bestimmen.

Bei der Analyse der bekannten Inhibitoren konnte gezeigt werden, dass die spezifischen SIRT2 Deacetylase-Inhibitoren SirReal2 und AGK-2 die Demyristoylierung des Peptids F4 nicht bzw. nur partiell inhibieren (Manuskript 0). Dahingegen konnten die SIRT2 Demyristoylase-Inhibitoren SMyr und Verbindung 12 (294) die SIRT2-Aktivität inhibieren. Damit konnte ein kontinuierlicher Assay entwickelt werden, der die Demyristoylaseaktivität von SIRT2 detektieren kann und für das zukünftige Screening von SIRT2 Demyristoylase-Inhibitoren von SIRT2 eingesetzt werden kann. Bei der Bestimmung der *in vitro* Aktivität von Verbindung 12 wurde ein Trypsin-gekoppelter Assay eingesetzt, bei dem das ZMML (Z-Schutzgruppe-K(Myristoyl)-AMC) Lysinderivat als Substrat genutzt wurde. Es wurde ein IC_{50} -Wert von 2,4 μ M gemessen, was an der unteren Detektionsgrenze des Assays von ca. 1 μ M liegt (294). Die *in vitro* Testung von TM wurde mit 200 nM SIRT2 durchgeführt und der ermittelte IC_{50} -Wert lag bei 0,05 μ M. Dies ist nahe der theoretischen unteren Detektionsgrenze des genutzten HPLC-Assays von 0,1 μ M und lässt die Vermutung zu, dass TM, unter Verwendung eines sensitiveren Assays, einen niedrigeren IC_{50} -Wert aufweisen würde. Die hervorragenden Substrateigenschaften von SIRT2 für F4 mit einer katalytischen Effizienz von 697 000 $M^{-1}s^{-1}$ (Manuskript 0) ermöglichten die Messung der Demyristoylaseaktivität von SIRT2 mit 100 pM. Dadurch konnte, unter Verwendung von F4, der Inhibitionstyp von Verbindung 12 (kompetitiv gegenüber dem Peptidsubstrat) bestimmt werden und der K_i -Wert von 13,2 nM gemessen werden.

Die HDAC-Isoformen weisen große Unterschiede in der Spezifität gegenüber der zu entfernenden Acylgruppe und des Trägermoleküls dieser Acylgruppe auf. Im Vergleich der verschiedenen Methoden zur Bestimmung der enzymatischen Aktivität der HDACs zeigt sich, dass es sich aufgrund dieser Unterschiede empfiehlt, statt eines universalen Assaysystems individuelle Assays zu nutzen. Diese individuellen Assaysysteme sollten das Wissen über die Besonderheiten der einzelnen HDAC-Isoformen nutzen. Auf diese Weise gelang es in dieser Arbeit, personalisierte Assays zu etablieren, welche die spezifischen Eigenschaften der HDACs ausnutzen. So konnten vor allem für die HDACs der Klasse IIa, für HDAC8, HDAC11, SIRT2 und SIRT3 Assays etabliert werden. Diese etablierten Assays sind besonders gut geeignet, um die entsprechenden Isoformen weiter zu untersuchen.

4.1.5 Betrachtung bekannter HDAC-Assays

Die publizierten und genutzten Arten von HDAC-Assays weisen verschiedene Probleme auf, die bei den in dieser Arbeit entwickelten Assays nicht auftreten bzw. durch das Methodendesign umgangen werden. Einige dieser Probleme werden im folgenden Abschnitt diskutiert.

Das Problem von allen gekoppelten Assays ist grundsätzlich, dass die komplexere Reaktionslösung die Störanfälligkeit erhöht. Das geschieht normalerweise durch die Interaktion oder Kreuzreaktion von zu testenden Verbindungen mit anderen Substanzen, die für die weiteren Reaktionen im Assay benötigt werden. Durch die Verwendung von kontinuierlichen Messmethoden wird die Wahrscheinlichkeit durch weniger Komponenten im Reaktionsansatz gesenkt. Zusätzlich wirkt sich nachteilig aus, dass gekoppelte Assays zumeist diskontinuierlich genutzt werden müssen, wodurch der experimentelle Aufwand steigt und die Datendichte geringer ist als bei einer kontinuierlichen Messung. Ein grundsätzlicher Vorteil von gekoppelten Assays besteht in der Verwendung von natürlichen Acylresten für die Aktivitätsmessung. Dadurch können durch den Acylrest keine negativen Effekte, wie im Fall der SIRT2-Assays, entstehen.

Bei der Verwendung von chemisch gekoppelten Assays kann es bei der Markierungsreaktion zu Nebenprodukten kommen, z.B. beim Vorhandensein mehrerer, gleicher funktioneller Gruppen im zu markierenden Produkt oder Substrat. Zum Beispiel erfolgt bei der HDAC10 katalysierten Deacetylierungsreaktion des Substrats N⁸-Acetylspermidin eine Dansylmarkierung der Spermidinderivate an sekundären und primären Aminen (110). Wenn unter den gewählten Reaktionsbedingungen keine vollständige Markierung stattfindet, ergeben sich für das Substrat N⁸-Acetylspermidin drei mögliche Markierungsprodukte und für das entstehende Spermidin sieben mögliche Markierungsprodukte (110). Diese müssen nach der Markierungsreaktion getrennt, identifiziert und quantifiziert werden. Durch die Verwendung von spezifischeren Reagenzien, die selektiv nur primäre Amine modifizieren, wie zum Beispiel die Markierung durch Fluorescamin, ließen sich die Mehrfachmodifikationen verhindern (210, 212).

Beim Screening von potenziellen Inhibitoren ergibt sich ein Nachteil für alle Enzym-gekoppelten Assays. Es muss sichergestellt werden, dass die nachgeschalteten Enzyme nicht durch die zu testenden Verbindungen inhibiert werden. Bestimmte Verbindungen bzw. Strukturelemente, die bei verschiedenen Assays problematische Nebeneffekte hervorrufen, lassen sich durch *Pan Assay Interference Compounds* (PAINS)-Analysen von vornherein ausschließen (298). Trotzdem müssen Hits auf Inhibierung aller in den entsprechenden Assays für die gekoppelten Reaktionen genutzten Enzyme getestet werden. Diese Testung bedeutet einen erheblichen Mehraufwand. So ist zum Beispiel der SIRT5-Inhibitor GW5074 nicht mit dem Assay für NAM produzierende Enzyme (Abbildung 7A) kompatibel, da er ebenso das nachgeschaltete Enzym GDH inhibiert (183, 299).

Beim Acetat-Assay, einem Enzym-gekoppelten Assay, werden drei weitere Enzymreaktionen an die Deacetylierungsreaktion gekoppelt (Abbildung 7B). Durch diese Enzymreaktionen wird die Bildung des Produkts Acetat an die detektierbare NADH-Bildung gekoppelt (186). Auf dieser Grundlage ergibt sich, dass der Assay ausschließlich für Enzyme geeignet ist, die eine gute Deacetylaseaktivität aufweisen. Zum Beispiel weist HDAC8 *in vitro* eine nur mäßige Deacetylaseaktivität auf im Vergleich zu der deutlich höheren Deacetylaseaktivität von artifiziellen TFA-Resten (Tabelle 1). Bei der Nutzung des Acetat-Assays wurde eine HDAC8-Konzentration von 0,5 µM bis 1 µM verwendet (186). Bei dem in dieser Arbeit entwickelten Assay (Manuskript 3.2) für die Aktivitätsmessungen der HDAC8 konnte eine Enzymkonzentration von

2 nM verwendet werden (300). Durch die geringe Enzymkonzentration im Reaktionsansatz ergibt sich die Möglichkeit, IC₅₀-Werte für potentere Inhibitoren zuverlässig bis zu deutlich geringeren Werten bestimmen zu können.

Assays, bei denen die Inaktivierung von Enzymen oder Proteinen durch eine Lysinacetylierung genutzt wird, bieten eine weitere Möglichkeit der Aktivitätsmessung von HDACs. Die Verwendung von Cas12a, der Firefly Luciferase und EGFP sind bekannte Beispiele für HDAC-Assays (188–190, 235). Durch die HDAC vermittelte Deacetylierung wird die Inaktivierung aufgehoben. Die Enzyme können zugesetzte, lumineszierende bzw. fluoreszierende Substrate umsetzen bzw. EGFP kann korrekt falten. Der große Vorteil dieser Methoden ist, dass sie sehr starke Messsignale erzeugen, da die Reaktion der aktivierten Reporterenzyme kontinuierlich weiterläuft, bis das Reportersubstrat vollständig umgesetzt wurde. Die starre Substratstruktur, vorgegeben durch die Struktur des Enzyms, kann sich wiederum nachteilig auswirken und somit suboptimale Substrateigenschaften für HDACs besitzen. Beispielweise konnte keine Fluoreszenzzunahme bei HDAC3 Überexpression im EGFP-Assay beobachtet werden (235). Dies könnte im Fall von HDAC3 auch am Fehlen vom entsprechenden Deacetylase-Aktivator NCOR liegen, welcher nicht in *E. coli* überexprimiert wurde (55, 235). Mit dem Luciferase-Assay konnte in einem Screening von 168 000 Verbindungen ein SIRT1-Inhibitor identifiziert werden, welcher durch verschiedene Modifikationen verbessert wurde (190). Dabei wiesen die Ergebnisse aus dem Luciferase-Assay starke Abweichungen von den etablierten kommerziell erhältlichen Fluor-de-Lys- und SIRT-Glo-Assays auf. Es wurde nur eine Verbindung der neun initialen Hits als Inhibitor für SIRT1 bestätigt. Die Autoren erklären diese Abweichung durch substratabhängige Inhibierung (190).

Eine weitere Assay-Möglichkeit ist die Kopplung der HDAC-Reaktion an eine proteolytische Spaltung (siehe 1.6.2, Abbildung 8) durch Trypsin, die nur nach der Deacylierung erfolgt. Ein großer Vorteil dieses Ansatzes ist, dass er durch die kommerzielle Verfügbarkeit als Fluor-de-Lys-Assay gut etabliert wurde (auch durch sehr viele nicht kommerzielle Varianten) und viele Varianten für die einzelnen HDAC-Isoformen entwickelt wurden (191–199). Durch die Trypsin-vermittelte AMC-Abspaltung ergibt sich eine starke Fluoreszenzzunahme, wodurch eine sehr gute Sensitivität dieses Ansatzes gegeben ist. Die Fluoreszenzzunahme ergibt sich aus der Spaltung der Lysinyl-Coumaryl Amidbindung. Deswegen muss sich der AMC-Rest direkt C-terminal vom modifizierten Lysin im Substratpeptid befinden. Durch diese, dem Assay innewohnende Limitation, ist es nicht möglich, mit Hilfe dieses Assays die Substratspezifität der Positionen im Peptidsubstrat C-terminal zum modifizierten Lysin zu untersuchen.

Zusätzlich konnte für die Zn²⁺-abhängigen HDACs durch verschiedene Arbeitsgruppen gezeigt werden, dass der artifizielle AMC-Rest die Substrateigenschaften im Vergleich zu eher natürlichen Substraten stark beeinflusst. Beispielweise wurde die Substrataffinität der HDAC6 durch den AMC-Rest deutlich erhöht. Für HDAC4 hingegen ging die Substratspezifität verloren (285). Auch HDAC3 zeigte eine deutlich abweichende katalytische Effizienz zwischen Peptiden mit und ohne AMC-Rest. So wies HDAC3 für das H4 abgeleitete Peptid Ac-WGKGLGK(Ac)GGAKW-NH₂ eine katalytische Effizienz von 2 900 M⁻¹s⁻¹ auf. Für das H4 abgeleitete Ac-LGK(Ac)-AMC Peptid wies HDAC3 mit 690 000 M⁻¹s⁻¹ eine 238-fach höhere katalytische Effizienz auf (50). Diese hohe Abweichung in der katalytischen Effizienz ergab sich aus einem 12,8-fach höheren k_{cat}-Wert und einem 18,5-fach geringerem K_M-Wert des AMC-haltigen Peptids. Ebenso nachteilig ist, dass die AMC-gekoppelten Substrate suboptimale Substrateigenschaften für Sirtuine besitzen und daher mit sehr hohen Sirtuinkonzentrationen (0,5 µM für SIRT2 und 2 µM für SIRT6) gemessen werden muss. Dadurch erreicht man die Limitierung für die Anwendung der Michaelis-Menten-Gleichung

und die korrekte Bestimmung der IC_{50} -Werte für hochaffine Inhibitoren wird dadurch erschwert. Um diese Limitierungen zu umgehen, wurde ein Fluorophor/Quencherpaar N- und C-terminal am Peptid gekoppelt. Durch die zugegebene Protease und die daraus resultierende räumliche Trennung von Quencher und Fluorophor wurde das Quenching vermindert (201, 205). Durch den größeren Abstand zum modifizierten Lysin sollten Fluorophor und Quencher einen geringeren Einfluss auf die Substrataffinität haben. So ergibt sich durch viele bekannte FRET-Paare die Möglichkeit zur Nutzung verschiedener Fluorophore.

Diese Assayvarianten werden normalerweise diskontinuierlich genutzt. Für verschiedene HDAC-Isoformen, z.B. für HDAC1-3, HDAC11, SIRT2 und SIRT5 konnte der Assay auch kontinuierlich genutzt werden (50, 62, 192, 195, 201). Dies setzt voraus, dass die HDACs über den Messzeitraum stabil gegenüber der Protease sind und die Trypsin-Reaktion schneller als die HDAC katalysierte Reaktion abläuft. Beide Voraussetzungen können gegenläufig sein. Außerdem muss auf zusätzliche Arginine und Lysine in der Peptidsequenz verzichtet werden.

Die Kopplung der HDAC-Reaktion an eine intramolekulare Umlagerung (auch *self-immolative* genannt) umgeht einige Nachteile der gekoppelten Assays (siehe 1.6.4). Da die Reaktion intramolekular stattfindet, kann auf weitere Enzyme bzw. Substrate verzichtet werden, so dass ein weniger komplexer Assayansatz genutzt werden kann. Außerdem stören Aminogruppen bzw. andere reaktive Gruppen im Substrat und auch in der Reaktionslösung, welche die intramolekulare Reaktion ausführen können, den Assay und müssen vermieden werden. Bei manchen Arten dieser Messmethoden war eine mäßige Zunahme bzw. eine Abnahme der Fluoreszenz auf die Hälfte der Ursprungsfluoreszenz zu beobachten (230, 231). Durch Verwendung alternativer Fluorophore, wie NBD oder einem Cumarinderivat, war ein enormer Anstieg der Fluoreszenzintensität infolge der intramolekularen Umlagerung zu beobachten (222–224, 232, 246, 301). Dadurch konnte bei Assays mit diesen Substraten eine sehr gute Sensitivität erreicht werden. Nach SIRT1 Zugabe bzw. durch HDAC6-Zugabe konnte zum Beispiel eine Fluoreszenzzunahme um das 6,7-fache (229) bis hin zum 70-fachen beobachtet werden (232). Durch systematische Verbesserung des Fluorophors und des Substrats zu einer Infrarot-Sonde konnte die HDAC-Aktivität sogar im Tumorgewebe einer lebenden Maus gemessen werden. Diese Fluoreszenzzunahme konnte durch die Zugabe von TSA deutlich gesenkt werden (234). Ein weiterer Vorteil dieses Substratdesigns ist, dass der natürliche Acylrest verwendet werden kann und das Substratdesign die Messung mit jedem Acylrest ermöglichen sollte. Die Funktionalität wurde unter anderem mit Acetyl-, Succinyl-, Malonyl-, Crotonyl-, und Lactoylresten gezeigt (88, 224). Ein Nachteil dieses Assaydesigns ist, dass die nachgeschalteten intramolekularen Reaktionen eine geringere Reaktionsgeschwindigkeit aufweisen als die enzymatische Reaktion und somit keine Linearität in den Progresskurven beobachtet werden kann. Dadurch wird die Analyse von kinetischen Ereignissen, welche durch die Analyse von Progresskurven zu entdecken sind (wie z.B. *tight binding*), erschwert.

4.2 Lactoyl- und Pyruvoylmodifikationen an Lysinen

In den letzten Jahren wurden neben Acetylierungen viele Acylmodifikationen der ϵ -Aminogruppe von Lysinen nachgewiesen. Für einige dieser Acylierungen ist weder geklärt, welche Funktionen sie besitzen, noch durch welche *reader* bzw. *eraser* sie reguliert werden. Eine dieser Modifikationen ist die Lysinlactoylierung (oder auch Lysinlactylierung). Die Lysinlactoylierung entsteht durch verschiedene Stoffwechselwege. Es gibt zwei Wege über den MGO-Abbau, wodurch D-Lactoyllysin durch Lactoglutathion und L-Lactoyllysin als AGE entsteht.

Lactoyllysin wurde 2015 erstmals als Lysinmodifikation *in vivo* nachgewiesen und später bestätigt (30, 65, 82, 86). Aufgrund des methodischen Designs war es nicht möglich, konkrete Aussagen über die modifizierten Proteine zu treffen. 2019 wurde Lactoyllysin als Histonmodifizierung mit Hilfe von Lactoyll Lysin-ysin-spezifischen Antikörpern nachgewiesen (34), wobei die Delactoylasen noch unbekannt waren. Die erste *in vitro* und *in vivo* beschriebene Delactoylase war SIRT2. Für D- und L-lactoylierte Undecapeptide, welche von der PKM-2 Lactoylierungsstelle abgeleitet wurden (86), weist SIRT2 eine sehr geringe katalytische Effizienz von ca. $1 \text{ M}^{-1}\text{s}^{-1}$ auf (65). Hier zeigte sich ein erhöhtes Lactoylierungs-Level bei SIRT2 *knockdown* Zellen. Die katalytische Effizienz von SIRT2 für das acetylierte Peptid war in dieser Studie 36-fach bzw. 50-fach höher als für das L-Lactoyl bzw. das D-Lactoylpeptid. Diese geringe Aktivität scheint zu niedrig zu sein, um die einzige relevante *in vivo* Delactoylase zu sein.

In einer weiteren Arbeit konnten für SIRT2 mit lactoylierten Histon-Peptiden deutlich höhere katalytische Effizienzen (höchste: H4K91-Lac-Peptid mit $666 \text{ M}^{-1}\text{s}^{-1}$) gemessen werden (88). SIRT2 weist in dieser Publikation deutlich geringere Unterschiede in der katalytischen Effizienz zwischen acetylierten und lactoylierten Peptiden auf (Tabelle 3).

Angeregt durch diese Erkenntnisse wurden in der vorliegenden Arbeit die Zn^{2+} -abhängigen HDACs 2-9 und HDAC11, sowie die Sirtuine SIRT2, 3, 5 und 6 hinsichtlich ihrer enzymatischen Aktivität gegenüber Lactoyl-, Pyruvoyl-, und Glyoxalresten untersucht. Diese enzymatische Aktivität wurde mit der Deacylaseaktivität gegenüber Acetyl- und Propionylresten verglichen. Die Reste wurden an den Peptidsequenzen Abz-SRGGK(Acyl)FFRR-NH₂ und ARTKQTARK(Acyl)STGGWW-NH₂ untersucht.

Für SIRT3 wurde in der hier vorliegenden Arbeit eine ähnliche katalytische Effizienz wie für SIRT2 gemessen. Eine von Jin *et al.* kürzlich publizierte Arbeit konnte durch *stable isotope labeling by amino acids in cell culture* (SILAC) Experimente in HCC-Zellen verschiedene durch SIRT3 regulierte Lactoylierungsstellen ermitteln (302). Eines der Substrate war Cyclin E2, das am Lys347 und Lys348 lactoyliert vorliegen kann und in der lactoylierten Form die Tumorprogression verstärkt. Jin *et al.* zeigten ebenso, dass die Überexpression von SIRT3 durch Honokiolgabe (303) die Lysinlactoylierung von Cyclin E2 in HCC-Zellen verringerte und die Honokiolgabe die Apoptose der HCC-Zellen induzierte (302). In Mäusen mit induziertem HCC wurde durch die Honokiolgabe die SIRT3-Expression in der Leber erhöht und das Tumorwachstum unterdrückt (302).

In dieser Arbeit wurde für HDAC2 und HDAC3 eine deutlich höhere Delactoylaseaktivität, im Vergleich zu SIRT2, gemessen (Manuskript 0). Die katalytische Effizienz von HDAC3 für das lactoylierte Peptid (Manuskript 0, Verbindung 3) war um das 7 800-fache größer im Vergleich zu SIRT2 für das PKM-2-Lac Peptid (65), um das 205-fache größer als bei SIRT2 für Verbindung 3 (Manuskript 0) und 12-fach größer als von SIRT2 für das H4K91-Lac Peptid (88). Ebenso zeigte sich HDAC2 in der hier vorliegenden Arbeit als eine effizientere *in vitro* Delactoylase als SIRT2 und SIRT3.

Dies kann auf eine größere *in vivo* Relevanz für HDAC3 und HDAC2 hindeuten. Ähnliches konnte durch Moreno-Yruela *et al.* gezeigt werden (50). Hier wurden zwar keine kinetischen Konstanten für SIRT2 bestimmt, da diese nur sehr geringe Umsätze im Aktivitätstest zeigten. HDAC2 und HDAC3 wiesen jedoch in diesem Aktivitätstest deutlich höhere Umsätze auf. Ebenso wurden für H3K9 lactoylierte Peptide ähnliche kinetische Konstanten erhalten wie in dieser Arbeit (50). Diese Ergebnisse an Modellpeptiden konnten auch an lactoylierten Histonen, an lactoylierten Nucleosomen und durch *in cellulo* Delactoylase Aktivität von HDAC1-3 durch Moreno-Yruela *et al.* bestätigt werden (50).

Neben der Lysinlactoylierung wurden Pyruvoyllysin und Glyoxalyllysin als neue Modifikationen untersucht. Diese entstehen durch die Reaktion von Glyoxal (GO, für Glyoxalyl) und MGO (für Pyruvoyl) mit Lysinen als AGEs unter oxidativem Stress (30). Pyruvoylreste und Glyoxalylreste besitzen durch den α -Carbonylrest einen reaktiveren Carbonylkohlenstoff der Amidbindung. Aufgrund des Reaktionsmechanismus der Sirtuine sollten Sirtuine Pyruvoyllysin und Glyoxalyllysin nicht oder nur schlecht als Substrate erkennen. Auch andere Verbindungen, die einen aktivierten Carbonylkohlenstoff des Amids besitzen, werden von Sirtuinen schlecht bzw. nicht umgesetzt. Zum Beispiel sind trifluoracetylierte Peptide keine Substrate sondern Inhibitoren für Sirtuine (254, 304, 305).

Zn²⁺-abhängige HDACs hingegen, vor allem diejenigen der Klasse IIa, sollten solche Modifikationen aufgrund des reaktiveren Carbonylkohlenstoffs des Amids als Substrate erkennen. Die HDACs der Klasse IIa besitzen nahezu keine Deacetylaseaktivität *in vitro*. Die reaktiveren TFA-Reste werden hingegen effizient hydrolysiert. Dies liegt an dem Austausch eines konservierten Tyrosins im aktiven Zentrum durch Histidin, welcher für die HDACs der Klasse IIa typisch ist (57, 127). Da durch den α -Carbonylrest eine ähnliche Aktivierung bei Pyruvoyl- und Glyoxalylresten vorliegt, wurde die Überlegung angestellt, dass diese Reste die natürlichen Substrate für die HDACs der Klasse IIa darstellen könnten. Diese These konnte nicht bestätigt werden, da keine der HDACs der Klasse IIa Depyruvoylase- oder Deglyoxalylaseaktivität zeigten. Dafür konnten HDAC2, HDAC3, HDAC6 und HDAC8 diese Reste effektiv spalten. Alle untersuchten Enzyme hydrolysierten den Pyruvoylrest effizienter als den Glyoxalylrest. Dies ist auf einen deutlich verringerten k_{cat} -Wert bei den Glyoxalylresten zurückzuführen (Manuskript 0).

Tabelle 3. Übersicht über bekannte *in vitro* acetylierte und lactoylierte Peptidsubstrate für SIRT2 und SIRT3. * Die „Änderung zum Acetylrest“ bedeutet die Änderung der katalytischen Effizienz des acetylierten Peptids im Vergleich zum lactoylierten Peptid.

SIRT2	K_M (μM)	k_{cat} (s^{-1})	k_{cat}/K_M ($M^{-1}s^{-1}$)	Änderung zu Acetylrest*	Referenz
H2A-K115-Ac	182	0,52	2 800	1	(88)
H2A-K115-Lac	190	0,065	342	0,12	(88)
H2B-K85-Ac	120	0,47	3 900	1	(88)
H2B-K85-Lac	328	0,073	224	0,057	(88)
H3K18-Ac	99	0,17	1 700	1	(88)
H3K18-Lac	245	0,050	203	0,12	(88)
H4K91-Ac	165	0,35	2 100	1	(88)
H4K91-Lac	188	0,013	666	0,32	(88)
PKM-2-Ac	115	0,0045	39,6	1	(65)
PKM-2-D-Lac	1 426	0,0012	0,8	0,020	(65)
PKM-2-L-Lac	486	0,0005	1,1	0,028	(65)
sLogo-Ac (1)	25	0,36	14 000	1	Manuskript 0
sLogo-Lac (3)	950	0,035	38	0,0027	Manuskript 0
SIRT3	K_M (μM)	k_{cat} (s^{-1})	k_{cat}/K_M ($M^{-1}s^{-1}$)	Änderung zu Acetylrest*	Referenz
sLogo-Ac (1)	6,8	0,15	22 000	1	Manuskript 0
sLogo-Lac (3)	1 580	0,030	19	0,00086	Manuskript 0

Die K_M -Werte von HDAC6 für das pyruvoylierte Peptid sind niedriger und von HDAC8 deutlich niedriger im Vergleich zum acetylierten Peptid: 620 μM für den Acetylrest und 9,2 μM für den Pyruvoylrest am gleichen Peptidrückgrat für HDAC8. Eine Verringerung der K_M -Werte konnte für die HDAC2 und HDAC3 nicht beobachtet werden. Simulationen basierend auf Dockingmethoden zeigten mögliche Ursachen dafür, dass der K_M -Wert für HDAC2 und HDAC3 im Gegensatz zu HDAC6 und HDAC8 nicht verringert ist. Bei HDAC6 und HDAC8 ging der Carbonylsauerstoff des α -Carbonylrests eine Wasserstoffbrückenbindung mit einem konservierten Cystein (Cys621 in HDAC6 und Cys153 in HDAC8) ein. Diese zusätzliche Interaktion kann den niedrigen K_M -Wert von HDAC6 und HDAC8 erklären. Bei HDAC2 und HDAC3 war die Carbonylgruppe vom Pyruvoylrest um 180° gedreht und konnte die Wasserstoffbrückenbindung nicht ausbilden. Dadurch kann keine zusätzliche Interaktion zustande kommen und der K_M -Wert ist ähnlich dem K_M -Wert für acetylierte bzw. propionylierte Peptide. Der Cysteinrest ist in allen Zn^{2+} -abhängigen HDACs konserviert und stabilisiert den Übergangszustand des Substrats (124).

Dieser niedrige K_M -Wert kann auf eine mögliche *in vivo* Funktion von HDAC8 als *eraser* für Pyruvoylreste hindeuten. Besonders auffällig ist der niedrige K_M -Wert der HDAC8 für diesen Rest, wenn man ihn mit K_M -Werten für bekannte acetylierte HDAC8-Substrate vergleicht, welche ausnahmslos um ein Vielfaches größer sind (Tabelle 1). Solche großen Unterschiede in der Affinität für das aktive Zentrum von Enzymen können einen großen Einfluss auf die Substratspezifität *in vivo* haben. Für Substrate mit geringer Konzentration *in vivo* ist dies von besonderer Bedeutung. Die Abundanz der Pyruvoylmodifikationen scheint *in vivo* relativ gering zu sein. So war bei aus der Leber von drei Monate alten Mäusen isolierten Histonen die Acetylmodifikation um das 438-fache höher als die Pyruvoylmodifikation. Im gleichen Gewebe konnte in Mitochondrien und im Cytosol die Pyruvoylmodifikation nachgewiesen, aber aufgrund der geringen Konzentration nicht quantifiziert werden (306). Kürzlich konnte für N-Myristoyltransferasen gezeigt werden, dass diese Enzyme *in vivo* exklusiv Fettsäurereste übertragen (307). Überraschend ist dabei, dass die Transferasen *in vitro* ähnliche Spezifitätskonstanten für die Übertragung des Acetylrests und des Myristoylrests von CoA auf den N-Terminus aufweisen. Die Autoren dieser Studie wiesen die deutlichen Unterschiede der Affinitäten des aktiven Zentrums zum Cosubstrat als einzige Ursache für die exklusive Aktivität in Zellen nach (307).

Die Ergebnisse dieser Arbeit stammen aus *in vitro* Messungen mit Modellpeptiden. Dadurch lassen sich die Ergebnisse nicht direkt auf vollständige Proteinsubstrate und auf *in cellulo* Messungen übertragen. Für die in dieser Arbeit nachgewiesenen *in vitro* Delactoylaseaktivitäten der HDACs wurden mittlerweile entsprechende *in vivo* Aktivitäten nachgewiesen (50, 65, 88, 302). Auch in anderen Fällen wurden für die Untersuchung der Acylspezifitäten von HDACs Modellpeptide genutzt, welche anschließend auf Proteinebene übertragen und *in vivo* bestätigt werden konnten. Zum Beispiel wurde die bis jetzt einzigartige Spezifität von SIRT5 für negativ geladene Acylreste (Malonyl-, Succinyl-, Glutarylreste) zuerst auf Peptidebene gezeigt. Später konnte bestätigt werden, dass die Desuccinylase- und Deglutarylaseaktivität die Hauptaktivität von SIRT5 *in vivo* ist (36, 69, 70). Ähnliches gilt für die Demyristoylaseaktivität von HDAC11 (61, 62) oder SIRT6 (41) und SIRT2 (64), welche später *in vivo* als Deacylaseaktivität für Fettsäurereste bestätigt wurde (63, 71, 308–310). Es besteht die Möglichkeit, dass verschiedene Acylspezifitäten an Peptidsubstraten nicht erkannt werden. Zum Beispiel zeigte sich für die Deacylaseaktivität von SIRT7, dass SIRT7 DNA oder ganze Nukleosomen benötigt, um als Deacylase zu arbeiten (75–81). SIRT6 zeigt keine Deacetylaseaktivität an Peptiden, jedoch wurde Deacetylaseaktivität nachgewiesen wenn acetylierte Nukleosomen die Substrate waren (72–74). Dass eine hohe

Aktivität fälschlicherweise gemessen wurde und dafür die Verwendung von Peptiden als Substrate die singuläre Ursache war, wurde noch nicht nachgewiesen. Für die Zn²⁺-abhängigen HDACs zeigt sich, dass diese verschiedene Aktivitäten aufweisen, in Abhängigkeit vom Bindungspartner (56, 311). HDAC1 im CoREST- und MIER-Komplex konnte den Lactoylrest von H2B entfernen. HDAC1 im MiDAC- und RERE-Komplex wiesen Delactoylaseaktivität nur auf, wenn die Histone im Nukleosom verpackt waren. Dies muss für zukünftige Untersuchung und der Interpretation der Daten beachtet werden.

5 Zusammenfassung und Ausblick

Um neue HDAC-Effektoren zu entdecken und diese zuverlässig zu charakterisieren, sind robuste und reproduzierbare Messmethoden notwendig. Da die bestehenden und etablierten Messmethoden verschiedene Schwächen aufweisen, war das Ziel dieser Arbeit, neue Messverfahren für die enzymatische Aktivität der HDACs zu entwickeln. Dabei wurde ein besonderer Fokus auf HDACs gelegt, die nur eine geringe Deacetylaseaktivität aufweisen, sodass sie mit etablierten Messmethoden besonders schwer zu untersuchen sind.

Unter Nutzung eines bekannten Sirtuinsubstrats konnte ein direkter und kontinuierlicher Assay für die HDAC11 entwickelt werden. Dabei wurde der Umstand genutzt, dass es sich bei der HDAC11 um eine Demyristoylase handelt. HDAC11 zeigte eine katalytische Effizienz von $13\,000\text{ M}^{-1}\text{s}^{-1}$. Dadurch war es möglich, die Inhibitionswerte für beschriebene HDAC11-Inhibitoren zu evaluieren. Verifiziert wurden die niedrigen IC_{50} -Werte von Fimepinostat und Trapoxin A, sowie die hohen IC_{50} -Werte von TSA, Romidepsin und Ricolinostat. Die potente Inhibition von HDAC11 durch Dacinostat, Mocetinostat, Elevenostat, Pracinostat und Quisinostat konnte unter Nutzung dieses Assays nicht verifiziert werden. Die erhaltenen Ergebnisse konnten durch Kontrollmessungen mit einem TFA-Lysinderivat überprüft und verifiziert werden.

Weiterhin konnte ein direkter und kontinuierlicher UV-Assay für HDACs der Klasse IIa, für HDAC11 und HDAC8 entwickelt werden. Dies war möglich, durch den Austausch eines einzigen Atoms (Sauerstoff zu Schwefel) in der zu spaltenden Amidbindung, wodurch ein Thioacylrest entstand. Durch die HDAC vermittelte Spaltung der Thioamidbindung konnte die HDAC-Aktivität bei der Absorption von 262 nm bzw. 275 nm detektiert werden. Durch die N-terminale Einführung des Fluorophors Abz in Kombination mit thiotrifluoracetylierten Lysinen konnte ein fluoreszenzbasierter Assay entwickelt werden. HDAC8 zeigte für die entwickelten Peptide eine extrem hohe katalytische Effizienz von $450\,000\text{ M}^{-1}\text{s}^{-1}$.

Für Sirtuine und HDAC11 konnte ein weiteres fluoreszenzbasiertes Assayprinzip etabliert werden. Es wurde ein dem Myristoylrest strukturell ähnlicher Thioacetylaminoundecanoylrest eingeführt, welcher in der Lage war, verschiedene Fluorophore im Peptidrückgrat zu quenchen.

Im Vergleich zu bestehenden Assays wurden die katalytischen Konstanten von HDAC11, SIRT2 und SIRT3 für diese Peptide durch dieses Design deutlich verbessert. Vor allem SIRT2 wies für diese Substrate extrem niedrige K_M -Werte im niedrigen nanomolaren Bereich auf. Dadurch ergab sich eine katalytische Effizienz von $6\,800\,000\text{ M}^{-1}\text{s}^{-1}$ für ein fluoresceinhaltiges Peptid und $15\,000\,000\text{ M}^{-1}\text{s}^{-1}$ für ein MCA-haltiges Peptid. Durch diese niedrigen K_M -Werte konnten die Substrate für SIRT2 auch als Fluoreszenzindikator für ein FID-Assay genutzt werden. Unter Verwendung dieser Peptide wurde die SIRT2-Aktivität, trotz der strukturellen Ähnlichkeit des Acylrests zum Myristoylrest, durch spezifische SIRT2-Deacetylaseinhibitoren inhibiert. Aufbauend auf diesen Ergebnissen wurde ein weiterer Assay etabliert, wobei MCA- und fluoresceinmarkierte Peptide mit Myristoylrest als Assaysubstrate genutzt wurden.

Dadurch konnte ein direkter und kontinuierlicher SIRT2-Assay entwickelt werden, welcher spezifisch die Demyristoylaseaktivität von SIRT2 detektiert. Durch die ausgezeichnete katalytische Konstante von $697\,000\text{ M}^{-1}\text{s}^{-1}$ für das Peptid F4 konnte die Demyristoylaseaktivität von SIRT2 mit 1 nM SIRT2 im Ansatz gemessen werden, was die Sensitivität im Vergleich zu anderen Assays deutlich verbesserte.

Für HDACs als diejenigen Enzyme, die die Deacylierung der Acylmodifikationen der Lysinseitenketten katalysieren, ergibt sich neben den bereits bekannten Substraten eine große

Anzahl möglicher neuer Substrate. Die Anzahl der Modifikationen und deren Position, die *in vivo* identifiziert werden, nimmt immer weiter zu und die Deacylasen sind oft nicht bekannt. Deswegen wurde die Fähigkeit der HDACs, verschiedene neu entdeckte Lysinmodifikationen (Lactoyl-, Pyruvoyl-, Glyoxalylreste) zu hydrolysieren, systematisch untersucht und mit bekannten Lysinmodifikationen (Acetyl- und Propionylreste) verglichen. Dabei konnten vor allem HDAC3 und HDAC2 als effektive *in vitro* Delactoylasen identifiziert werden. Die katalytische Effizienz der Delactoylierungsreaktion dieser beiden HDACs war deutlich höher als von der bis dato einzigen bekannten Delactoylase SIRT2. Zusätzlich konnte gezeigt werden, dass HDAC2, HDAC3, HDAC6 und HDAC8 Pyruvoyllysinreste in Modellpeptiden als Substrat akzeptieren. Vor allem HDAC8 wies einen extrem niedrigen K_M -Wert für das pyruvoylierte Peptid auf, was in einer 30-fach (artifizielles Peptid) bzw. in einer 364-fach (H3K9-Peptid) höheren katalytischen Effizienz im Vergleich zum acetylierten Peptid resultierte. Mit einer katalytischen Effizienz von $510\,000\text{ M}^{-1}\text{s}^{-1}$ von HDAC8 für das pyruvoylierte H3K9-Peptid, ist es das beste Substrat, soweit bekannt, für HDAC8, mit einem *in vivo* Acylrest. Zusätzlich konnte das pyruvoylierte Peptid genutzt werden, um die HDAC8-Aktivität direkt und kontinuierlich mittels Fluoreszenzintensität zu messen.

Die in dieser Arbeit neu entwickelten Substrate für die HDACs und die damit verbundenen Assays für die einzelnen HDAC-Isoformen ermöglichen neue Möglichkeiten für direkte und kontinuierliche Messungen der HDAC-Aktivität für einige Isoformen. Die ausgezeichneten kinetischen Konstanten, vor allem für SIRT2, SIRT3, HDAC8, HDAC11 und die HDACs der Klasse IIa und die damit verbundene niedrige eingesetzte Enzymkonzentration erlaubt eine zuverlässige Bestimmung der Inhibitionskonstanten im niedrigen nanomolaren Bereich. Zusätzlich können alle entwickelten Assays in den gängigen Mikrotiterplatten-Formaten genutzt werden, was sie für zukünftige Inhibitorscreenings nutzbar macht.

Die in dieser Arbeit erhaltenen Informationen über die Sequenzspezifitäten der einzelnen Sirtuine (Manuskript 3.3 und 0) können genutzt werden, um für verschiedene Sirtuine neue und Isoform-spezifische Assaysubstrate zu entwickeln. Auch die hochaffinen Sirtuinsubstrate aus Manuskript 3.3 eignen sich mit dem niedrigen K_M -Wert ideal als Ausgangspunkt für die Entwicklung von hochaffinen und spezifischen SIRT2-Inhibitoren. Um zu verstehen, durch welche Interaktionen die hohe Affinität von SIRT2 zu den in Manuskript 3.3 entwickelten Peptiden entsteht, können Röntgenkristallstrukturanalysen helfen. Auch diese Information kann zur Entwicklung von hochaffinen SIRT2-Inhibitoren beitragen.

Das Prinzip des Quenchings der Fluoreszenz durch die Ausnutzung der Umgebungssensitivität des Fluorophors, wie in Manuskript 0 gezeigt, bietet die Möglichkeit zur Entwicklung neuer Deacylaseassays. Dafür können myristoylierte Peptide in Kombination mit alternativen Fluorophoren, die stark von der umgebenden Hydrophobizität abhängen, genutzt werden.

Ebenso kann das Prinzip der Spaltung Thioamidbindung des entwickelten HDAC8-Assays genutzt werden, um einen kontinuierlichen und direkten Assay für HDAC10 zu entwickeln. Ein mögliches Substrat für die kontinuierliche Messung der HDAC10-Aktivität ist N^1 -Abz- N^8 -Thiotrifluoracetyl-Spermidin.

Die Ergebnisse der Untersuchung der Substrateigenschaften der lactoylierten und pyruvoylierten Peptide in Manuskript 0 deuten auf eine *in vivo* Relevanz der HDACs als Delactoylasen und Depyruvoylasen hin. *In vivo* Untersuchungen mit dem Fokus auf diese Reste und die spezielle Rolle der HDACs als *eraser* dieser Reste können interessante und neue Erkenntnisse über den biologischen Wirkmechanismus der HDACs bringen.

6 Literaturverzeichnis

1. Moore, L. D.; Le, T.; Fan, G. DNA methylation and its basic function. *Neuropsychopharmacology : official publication of the American College of Neuropsychopharmacology* **2013**, *38* (1), 23–38. DOI: 10.1038/npp.2012.112.
2. Zhang, G.; Pradhan, S. Mammalian epigenetic mechanisms. *IUBMB life* **2014**, *66* (4), 240–256. DOI: 10.1002/iub.1264.
3. Luger, K.; Mäder, A. W.; Richmond, R. K.; Sargent, D. F.; Richmond, T. J. Crystal structure of the nucleosome core particle at 2.8 Å resolution. *Nature* **1997**, *389* (6648), 251–260. DOI: 10.1038/38444.
4. Jenuwein, T.; Allis, C. D. Translating the histone code. *Science (New York, N.Y.)* **2001**, *293* (5532), 1074–1080. DOI: 10.1126/science.1063127.
5. Strahl, B. D.; Allis, C. D. The language of covalent histone modifications. *Nature* **2000**, *403* (6765), 41–45. DOI: 10.1038/47412.
6. Zhang, Y.; Sun, Z.; Jia, J.; Du, T.; Zhang, N.; Tang, Y.; Fang, Y.; Fang, D. Overview of Histone Modification. In: *Histone Mutations and Cancer*; Springer, Singapore, 2021, pp 1–16. DOI: 10.1007/978-981-15-8104-5_1.
7. ALLFREY, V. G.; FAULKNER, R.; MIRSKY, A. E. ACETYLATION AND METHYLATION OF HISTONES AND THEIR POSSIBLE ROLE IN THE REGULATION OF RNA SYNTHESIS. *Proceedings of the National Academy of Sciences of the United States of America* **1964**, *51* (5), 786–794. DOI: 10.1073/pnas.51.5.786.
8. Verdin, E.; Ott, M. 50 years of protein acetylation: from gene regulation to epigenetics, metabolism and beyond. *Nat Rev Mol Cell Biol* **2015**, *16* (4), 258–264. DOI: 10.1038/nrm3931.
9. Xia, C.; Tao, Y.; Li, M.; Che, T.; Qu, J. Protein acetylation and deacetylation: An important regulatory modification in gene transcription (Review). *Experimental and Therapeutic Medicine* **2020**, *20* (4), 2923–2940. DOI: 10.3892/etm.2020.9073.
10. Marmorstein, R.; Zhou, M.-M. Writers and readers of histone acetylation: structure, mechanism, and inhibition. *Cold Spring Harbor perspectives in biology* **2014**, *6* (7), a018762. DOI: 10.1101/cshperspect.a018762.
11. Shvedunova, M.; Akhtar, A. Modulation of cellular processes by histone and non-histone protein acetylation. *Nat Rev Mol Cell Biol* **2022**, *23* (5), 329–349. DOI: 10.1038/s41580-021-00441-y.
12. Yap, K. L.; Zhou, M.-M. Keeping it in the family: diverse histone recognition by conserved structural folds. *Critical reviews in biochemistry and molecular biology* **2010**, *45* (6), 488–505.
13. Gregoret, I. V.; Lee, Y.-M.; Goodson, H. V. Molecular evolution of the histone deacetylase family: functional implications of phylogenetic analysis. *Journal of molecular biology* **2004**, *338* (1), 17–31. DOI: 10.1016/j.jmb.2004.02.006.
14. Frye, R. A. Phylogenetic classification of prokaryotic and eukaryotic Sir2-like proteins. *Biochemical and biophysical research communications* **2000**, *273* (2), 793–798. DOI: 10.1006/bbrc.2000.3000.
15. Hubbert, C.; Guardiola, A.; Shao, R.; Kawaguchi, Y.; Ito, A.; Nixon, A.; Yoshida, M.; Wang, X.-F.; Yao, T.-P. HDAC6 is a microtubule-associated deacetylase. *Nature* **2002**, *417* (6887), 455–458. DOI: 10.1038/417455a.
16. Seto, E.; Yoshida, M. Erasers of histone acetylation: the histone deacetylase enzymes. *Cold Spring Harbor perspectives in biology* **2014**, *6* (4), a018713. DOI: 10.1101/cshperspect.a018713.
17. Sinnott-Smith, J.; Ni, Y.; Wang, J.; Ming, M.; Young, S. H.; Rozengurt, E. Protein kinase D1 mediates class IIa histone deacetylase phosphorylation and nuclear extrusion in intestinal epithelial cells: role in mitogenic signaling. *American journal of physiology. Cell physiology* **2014**, *306* (10), C961-71. DOI: 10.1152/ajpcell.00048.2014.
18. Grozinger, C. M.; Schreiber, S. L. Regulation of histone deacetylase 4 and 5 and transcriptional activity by 14-3-3-dependent cellular localization. *Proceedings of the National Academy of Sciences of the United States of America* **2000**, *97* (14), 7835–7840. DOI: 10.1073/pnas.140199597.
19. Li, J.; Chen, S.; Cleary, R. A.; Wang, R.; Gannon, O. J.; Seto, E.; Tang, D. D. Histone deacetylase 8 regulates cortactin deacetylation and contraction in smooth muscle tissues. *American journal of physiology. Cell physiology* **2014**, *307* (3), C288-95. DOI: 10.1152/ajpcell.00102.2014.

20. Chakrabarti, A.; Oehme, I.; Witt, O.; Oliveira, G.; Sippl, W.; Romier, C.; Pierce, R. J.; Jung, M. HDAC8: a multifaceted target for therapeutic interventions. *Trends in pharmacological sciences* **2015**, *36* (7), 481–492. DOI: 10.1016/j.tips.2015.04.013.
21. Verdel, A.; Curtet, S.; Brocard, M. P.; Rousseaux, S.; Lemerrier, C.; Yoshida, M.; Khochbin, S. Active maintenance of mHDA2/mHDAC6 histone-deacetylase in the cytoplasm. *Current biology : CB* **2000**, *10* (12), 747–749. DOI: 10.1016/s0960-9822(00)00542-x.
22. Wu, Q.-J.; Zhang, T.-N.; Chen, H.-H.; Yu, X.-F.; Lv, J.-L.; Liu, Y.-Y.; Liu, Y.-S.; Zheng, G.; Zhao, J.-Q.; Wei, Y.-F.; Guo, J.-Y.; Liu, F.-H.; Chang, Q.; Zhang, Y.-X.; Liu, C.-G.; Zhao, Y.-H. The sirtuin family in health and disease. *Sig Transduct Target Ther* **2022**, *7* (1), 402. DOI: 10.1038/s41392-022-01257-8.
23. North, B. J.; Verdin, E. Interphase nucleo-cytoplasmic shuttling and localization of SIRT2 during mitosis. *PloS one* **2007**, *2* (8), e784. DOI: 10.1371/journal.pone.0000784.
24. Vaquero, A.; Scher, M. B.; Lee, D. H.; Sutton, A.; Cheng, H.-L.; Alt, F. W.; Serrano, L.; Sternglanz, R.; Reinberg, D. SirT2 is a histone deacetylase with preference for histone H4 Lys 16 during mitosis. *Genes & Development* **2006**, *20* (10), 1256–1261. DOI: 10.1101/gad.1412706.
25. Tanno, M.; Sakamoto, J.; Miura, T.; Shimamoto, K.; Horio, Y. Nucleocytoplasmic shuttling of the NAD⁺-dependent histone deacetylase SIRT1. *The Journal of biological chemistry* **2007**, *282* (9), 6823–6832. DOI: 10.1074/jbc.M609554200.
26. Schwer, B.; North, B. J.; Frye, R. A.; Ott, M.; Verdin, E. The human silent information regulator (Sir)2 homologue hSIRT3 is a mitochondrial nicotinamide adenine dinucleotide-dependent deacetylase. *The Journal of cell biology* **2002**, *158* (4), 647–657. DOI: 10.1083/jcb.200205057.
27. Haigis, M. C.; Mostoslavsky, R.; Haigis, K. M.; Fahie, K.; Christodoulou, D. C.; Murphy, A. J.; Valenzuela, D. M.; Yancopoulos, G. D.; Karow, M.; Blander, G.; Wolberger, C.; Prolla, T. A.; Weindruch, R.; Alt, F. W.; Guarente, L. SIRT4 inhibits glutamate dehydrogenase and opposes the effects of calorie restriction in pancreatic beta cells. *Cell* **2006**, *126* (5), 941–954. DOI: 10.1016/j.cell.2006.06.057.
28. Nakagawa, T.; Lomb, D. J.; Haigis, M. C.; Guarente, L. SIRT5 Deacetylates carbamoyl phosphate synthetase 1 and regulates the urea cycle. *Cell* **2009**, *137* (3), 560–570. DOI: 10.1016/j.cell.2009.02.026.
29. Jiang, T.; Zhou, X.; Taghizadeh, K.; Dong, M.; Dedon, P. C. N-formylation of lysine in histone proteins as a secondary modification arising from oxidative DNA damage. *Proceedings of the National Academy of Sciences of the United States of America* **2007**, *104* (1), 60–65. DOI: 10.1073/pnas.0606775103.
30. Baldensperger, T.; Jost, T.; Zipprich, A.; Glomb, M. A. Novel α -Oxoamide Advanced-Glycation Endproducts within the N6-Carboxymethyl Lysine and N6-Carboxyethyl Lysine Reaction Cascades. *Journal of agricultural and food chemistry* **2018**, *66* (8), 1898–1906. DOI: 10.1021/acs.jafc.7b05813.
31. Garrity, J.; Gardner, J. G.; Hawse, W.; Wolberger, C.; Escalante-Semerena, J. C. N-lysine propionylation controls the activity of propionyl-CoA synthetase. *The Journal of biological chemistry* **2007**, *282* (41), 30239–30245. DOI: 10.1074/jbc.M704409200.
32. Chen, Y.; Sprung, R.; Tang, Y.; Ball, H.; Sangras, B.; Kim, S. C.; Falck, J. R.; Peng, J.; Gu, W.; Zhao, Y. Lysine propionylation and butyrylation are novel post-translational modifications in histones. *Molecular & cellular proteomics : MCP* **2007**, *6* (5), 812–819. DOI: 10.1074/mcp.M700021-MCP200.
33. Tan, M.; Luo, H.; Lee, S.; Jin, F.; Yang, J. S.; Montellier, E.; Buchou, T.; Cheng, Z.; Rousseaux, S.; Rajagopal, N.; Lu, Z.; Ye, Z.; Zhu, Q.; Wysocka, J.; Ye, Y.; Khochbin, S.; Ren, B.; Zhao, Y. Identification of 67 histone marks and histone lysine crotonylation as a new type of histone modification. *Cell* **2011**, *146* (6), 1016–1028. DOI: 10.1016/j.cell.2011.08.008.
34. Di Zhang; Tang, Z.; Huang, H.; Zhou, G.; Cui, C.; Weng, Y.; Liu, W.; Kim, S.; Lee, S.; Perez-Neut, M.; Ding, J.; Czyz, D.; Hu, R.; Ye, Z.; He, M.; Zheng, Y. G.; Shuman, H. A.; Dai, L.; Ren, B.; Roeder, R. G.; Becker, L.; Zhao, Y. Metabolic regulation of gene expression by histone lactylation. *Nature* **2019**, *574* (7779), 575–580. DOI: 10.1038/s41586-019-1678-1.
35. Xie, Z.; Dai, J.; Dai, L.; Tan, M.; Cheng, Z.; Wu, Y.; Boeke, J. D.; Zhao, Y. Lysine succinylation and lysine malonylation in histones. *Molecular & Cellular Proteomics* **2012**, *11* (5), 100–107. DOI: 10.1074/mcp.M111.015875.
36. Tan, M.; Peng, C.; Anderson, K. A.; Chhoy, P.; Xie, Z.; Dai, L.; Park, J.; Chen, Y.; Huang, H.; Zhang, Y.; Ro, J.; Wagner, G. R.; Green, M. F.; Madsen, A. S.; Schmiesing, J.; Peterson, B. S.; Xu, G.; Ilkayeva, O. R.; Muehlbauer, M. J.; Braulke, T.; Mühlhausen, C.; Backos, D. S.; Olsen, C. A.;

- McGuire, P. J.; Pletcher, S. D.; Lombard, D. B.; Hirschey, M. D.; Zhao, Y. Lysine glutarylation is a protein posttranslational modification regulated by SIRT5. *Cell metabolism* **2014**, *19* (4), 605–617. DOI: 10.1016/j.cmet.2014.03.014.
37. Xie, Z.; Di Zhang; Chung, D.; Tang, Z.; Huang, H.; Dai, L.; Qi, S.; Li, J.; Colak, G.; Chen, Y.; Xia, C.; Peng, C.; Ruan, H.; Kirkey, M.; Wang, D.; Jensen, L. M.; Kwon, O. K.; Lee, S.; Pletcher, S. D.; Tan, M.; Lombard, D. B.; White, K. P.; Zhao, H.; Li, J.; Roeder, R. G.; Yang, X.; Zhao, Y. Metabolic Regulation of Gene Expression by Histone Lysine β -Hydroxybutyrylation. *Molecular cell* **2016**, *62* (2), 194–206. DOI: 10.1016/j.molcel.2016.03.036.
 38. Dai, L.; Peng, C.; Montellier, E.; Lu, Z.; Chen, Y.; Ishii, H.; Debernardi, A.; Buchou, T.; Rousseaux, S.; Jin, F.; Sabari, B. R.; Deng, Z.; Allis, C. D.; Ren, B.; Khochbin, S.; Zhao, Y. Lysine 2-hydroxyisobutyrylation is a widely distributed active histone mark. *Nature chemical biology* **2014**, *10* (5), 365–370. DOI: 10.1038/nchembio.1497.
 39. Anderson, K. A.; Huynh, F. K.; Fisher-Wellman, K.; Stuart, J. D.; Peterson, B. S.; Douros, J. D.; Wagner, G. R.; Thompson, J. W.; Madsen, A. S.; Green, M. F.; Sivley, R. M.; Ilkayeva, O. R.; Stevens, R. D.; Backos, D. S.; Capra, J. A.; Olsen, C. A.; Campbell, J. E.; Muoio, D. M.; Grimsrud, P. A.; Hirschey, M. D. SIRT4 Is a Lysine Deacylase that Controls Leucine Metabolism and Insulin Secretion. *Cell metabolism* **2017**, *25* (4), 838–855.e15. DOI: 10.1016/j.cmet.2017.03.003.
 40. Huang, H.; Di Zhang; Wang, Y.; Perez-Neut, M.; Han, Z.; Zheng, Y. G.; Hao, Q.; Zhao, Y. Lysine benzoylation is a histone mark regulated by SIRT2. *Nature communications* **2018**, *9* (1), 3374. DOI: 10.1038/s41467-018-05567-w.
 41. Jiang, H.; Khan, S.; Wang, Y.; Charron, G.; He, B.; Sebastian, C.; Du, J.; Kim, R.; Ge, E.; Mostoslavsky, R.; Hang, H. C.; Hao, Q.; Lin, H. SIRT6 regulates TNF- α secretion through hydrolysis of long-chain fatty acyl lysine. *Nature* **2013**, *496* (7443), 110–113. DOI: 10.1038/nature12038.
 42. Mathias, R. A.; Greco, T. M.; Oberstein, A.; Budayeva, H. G.; Chakrabarti, R.; Rowland, E. A.; Kang, Y.; Shenk, T.; Cristea, I. M. Sirtuin 4 is a lipoamidase regulating pyruvate dehydrogenase complex activity. *Cell* **2014**, *159* (7), 1615–1625. DOI: 10.1016/j.cell.2014.11.046.
 43. Goudarzi, A.; Di Zhang; Huang, H.; Barral, S.; Kwon, O. K.; Qi, S.; Tang, Z.; Buchou, T.; Vitte, A.-L.; He, T.; Cheng, Z.; Montellier, E.; Gaucher, J.; Curtet, S.; Debernardi, A.; Charbonnier, G.; Puthier, D.; Petosa, C.; Panne, D.; Rousseaux, S.; Roeder, R. G.; Zhao, Y.; Khochbin, S. Dynamic Competing Histone H4 K5K8 Acetylation and Butyrylation Are Hallmarks of Highly Active Gene Promoters. *Molecular cell* **2016**, *62* (2), 169–180. DOI: 10.1016/j.molcel.2016.03.014.
 44. Moreno-Yruela, C.; Bæk, M.; Vrsanova, A.-E.; Schulte, C.; Maric, H. M.; Olsen, C. A. Hydroxamic acid-modified peptide microarrays for profiling isozyme-selective interactions and inhibition of histone deacetylases. *Nat Commun* **2021**, *12* (1), 62. DOI: 10.1038/s41467-020-20250-9.
 45. Kutil, Z.; Skultetyova, L.; Rauh, D.; Meleshin, M.; Snajdr, I.; Novakova, Z.; Mikesova, J.; Pavlicek, J.; Hadzima, M.; Baranova, P.; Havlinova, B.; Majer, P.; Schutkowski, M.; Barinka, C. The unraveling of substrate specificity of histone deacetylase 6 domains using acetylome peptide microarrays and peptide libraries. *The FASEB Journal* **2019**, *33* (3), 4035–4045. DOI: 10.1096/fj.201801680R.
 46. Kutil, Z.; Meleshin, M.; Baranova, P.; Havlinova, B.; Schutkowski, M.; Barinka, C. Characterization of the class IIa histone deacetylases substrate specificity. *The FASEB Journal* **2022**, *36* (5), e22287. DOI: 10.1096/fj.202101663R.
 47. Bheda, P.; Jing, H.; Wolberger, C.; Lin, H. The Substrate Specificity of Sirtuins. *Annual review of biochemistry* **2016**, *85*, 405–429. DOI: 10.1146/annurev-biochem-060815-014537.
 48. Rauh, D.; Fischer, F.; Gertz, M.; Lakshminarasimhan, M.; Bergbrede, T.; Aladini, F.; Kambach, C.; Becker, C. F. W.; Zerweck, J.; Schutkowski, M.; Steegborn, C. An acetylome peptide microarray reveals specificities and deacetylation substrates for all human sirtuin isoforms. *Nat Commun* **2013**, *4* (1), 2327. DOI: 10.1038/ncomms3327.
 49. McClure, J. J.; Inks, E. S.; Zhang, C.; Peterson, Y. K.; Li, J.; Chundru, K.; Lee, B.; Buchanan, A.; Miao, S.; Chou, C. J. Comparison of the Deacylase and Deacetylase Activity of Zinc-Dependent HDACs. *ACS chemical biology* **2017**, *12* (6), 1644–1655. DOI: 10.1021/acschembio.7b00321.
 50. Moreno-Yruela, C.; Di Zhang; Wei, W.; Bæk, M.; Liu, W.; Gao, J.; Danková, D.; Nielsen, A. L.; Bolding, J. E.; Yang, L.; Jameson, S. T.; Wong, J.; Olsen, C. A.; Zhao, Y. Class I histone deacetylases (HDAC1-3) are histone lysine delactylases. *Science advances* **2022**, *8* (3), eabi6696. DOI: 10.1126/sciadv.abi6696.

51. Aramsangtienchai, P.; Spiegelman, N. A.; He, B.; Miller, S. P.; Dai, L.; Zhao, Y.; Lin, H. HDAC8 Catalyzes the Hydrolysis of Long Chain Fatty Acyl Lysine. *ACS chemical biology* **2016**, *11* (10), 2685–2692. DOI: 10.1021/acschembio.6b00396.
52. Madsen, A. S.; Olsen, C. A. Profiling of substrates for zinc-dependent lysine deacylase enzymes: HDAC3 exhibits decrotonylase activity in vitro. *Angewandte Chemie (International ed. in English)* **2012**, *51* (36), 9083–9087. DOI: 10.1002/anie.201203754.
53. Wei, W.; Liu, X.; Chen, J.; Gao, S.; Lu, L.; Zhang, H.; Ding, G.; Wang, Z.; Chen, Z.; Shi, T.; Li, J.; Yu, J.; Wong, J. Class I histone deacetylases are major histone decrotonylases: evidence for critical and broad function of histone crotonylation in transcription. *Cell research* **2017**, *27* (7), 898–915. DOI: 10.1038/cr.2017.68.
54. Huang, H.; Di Zhang; Weng, Y.; Delaney, K.; Tang, Z.; Yan, C.; Qi, S.; Peng, C.; Cole, P. A.; Roeder, R. G.; Zhao, Y. The regulatory enzymes and protein substrates for the lysine β -hydroxybutyrylation pathway. *Science advances* **2021**, *7* (9). DOI: 10.1126/sciadv.abe2771.
55. Guenther, M. G.; Barak, O.; Lazar, M. A. The SMRT and N-CoR corepressors are activating cofactors for histone deacetylase 3. *Molecular and cellular biology* **2001**, *21* (18), 6091–6101. DOI: 10.1128/MCB.21.18.6091-6101.2001.
56. Wang, Z. A.; Whedon, S. D.; Wu, M.; Wang, S.; Brown, E. A.; Anmangandla, A.; Regan, L.; Lee, K.; Du, J.; Hong, J. Y.; Fairall, L.; Kay, T.; Lin, H.; Zhao, Y.; Schwabe, J. W. R.; Cole, P. A. Histone H2B Deacylation Selectivity: Exploring Chromatin's Dark Matter with an Engineered Sortase. *Journal of the American Chemical Society* **2022**, *144* (8), 3360–3364. DOI: 10.1021/jacs.1c13555.
57. Lahm, A.; Paolini, C.; Pallaoro, M.; Nardi, M. C.; Jones, P.; Neddermann, P.; Sambucini, S.; Bottomley, M. J.; Lo Surdo, P.; Carfí, A.; Koch, U.; Francesco, R. de; Steinkühler, C.; Gallinari, P. Unraveling the hidden catalytic activity of vertebrate class IIa histone deacetylases. *Proceedings of the National Academy of Sciences of the United States of America* **2007**, *104* (44), 17335–17340. DOI: 10.1073/pnas.0706487104.
58. Luo, L.; Martin, S. C.; Parkington, J.; Cadena, S. M.; Zhu, J.; Ibebunjo, C.; Summermatter, S.; Londraville, N.; Patora-Komisarska, K.; Widler, L.; Zhai, H.; Trendelenburg, A.-U.; Glass, D. J.; Shi, J. HDAC4 Controls Muscle Homeostasis through Deacetylation of Myosin Heavy Chain, PGC-1 α , and Hsc70. *Cell Reports* **2019**, *29* (3), 749-763.e12. DOI: 10.1016/j.celrep.2019.09.023.
59. Baas, T. Closer to class IIa HDAC inhibitors. *Science-Business eXchange* **2013**, *6* (13), 301. DOI: 10.1038/scibx.2013.301.
60. Zhang, Y.; Andrade, R.; Hanna, A. A.; Pflum, M. K. H. Evidence that HDAC7 acts as an epigenetic "reader" of AR acetylation through NCoR-HDAC3 dissociation. *Cell chemical biology* **2022**, *29* (7), 1162-1173.e5. DOI: 10.1016/j.chembiol.2022.05.008.
61. Kutil, Z.; Novakova, Z.; Meleshin, M.; Mikesova, J.; Schutkowski, M.; Barinka, C. Histone Deacetylase 11 Is a Fatty-Acid Deacylase. *ACS chemical biology* **2018**, *13* (3), 685–693. DOI: 10.1021/acschembio.7b00942.
62. Moreno-Yruela, C.; Galleano, I.; Madsen, A. S.; Olsen, C. A. Histone Deacetylase 11 Is an ϵ -N-Myristoyllysine Hydrolase. *Cell chemical biology* **2018**, *25* (7), 849-856.e8. DOI: 10.1016/j.chembiol.2018.04.007.
63. Cao, J.; Sun, L.; Aramsangtienchai, P.; Spiegelman, N. A.; Zhang, X.; Huang, W.; Seto, E.; Lin, H. HDAC11 regulates type I interferon signaling through defatty-acylation of SHMT2. *Proceedings of the National Academy of Sciences of the United States of America* **2019**, *116* (12), 5487–5492. DOI: 10.1073/pnas.1815365116.
64. Feldman, J. L.; Baeza, J.; Denu, J. M. Activation of the protein deacetylase SIRT6 by long-chain fatty acids and widespread deacylation by mammalian sirtuins. *Journal of Biological Chemistry* **2013**, *288* (43), 31350–31356. DOI: 10.1074/jbc.C113.511261.
65. Jennings, E. Q.; Ray, J. D.; Zerio, C. J.; Trujillo, M. N.; McDonald, D. M.; Chapman, E.; Spiegel, D. A.; Galligan, J. J. Sirtuin 2 Regulates Protein LactoylLys Modifications. *Chembiochem : a European journal of chemical biology* **2021**, *22* (12), 2102–2106. DOI: 10.1002/cbic.202000883.
66. Jin, J.; He, B.; Zhang, X.; Lin, H.; Wang, Y. SIRT2 Reverses 4-Oxononanoyl Lysine Modification on Histones. *Journal of the American Chemical Society* **2016**, *138* (38), 12304–12307. DOI: 10.1021/jacs.6b04977.
67. Laurent, G.; German, N. J.; Saha, A. K.; Boer, V. C. J. de; Davies, M.; Koves, T. R.; Dephoure, N.; Fischer, F.; Boanca, G.; Vaitheesvaran, B.; Lovitch, S. B.; Sharpe, A. H.; Kurland, I. J.; Steegborn,

- C.; Gygi, S. P.; Muoio, D. M.; Ruderman, N. B.; Haigis, M. C. SIRT4 coordinates the balance between lipid synthesis and catabolism by repressing malonyl CoA decarboxylase. *Molecular cell* **2013**, *50* (5), 686–698. DOI: 10.1016/j.molcel.2013.05.012.
68. Pannek, M.; Simic, Z.; Fuszard, M.; Meleshin, M.; Rotili, D.; Mai, A.; Schutkowski, M.; Steegborn, C. Crystal structures of the mitochondrial deacylase Sirtuin 4 reveal isoform-specific acyl recognition and regulation features. *Nature communications* **2017**, *8* (1), 1513. DOI: 10.1038/s41467-017-01701-2.
 69. Du, J.; Zhou, Y.; Su, X.; Yu, J. J.; Khan, S.; Jiang, H.; Kim, J.; Woo, J.; Kim, J. H.; Choi, B. H.; He, B.; Chen, W.; Zhang, S.; Cerione, R. A.; Auwerx, J.; Hao, Q.; Lin, H. Sirt5 is a NAD-dependent protein lysine demalonylase and desuccinylase. *Science (New York, N.Y.)* **2011**, *334* (6057), 806–809. DOI: 10.1126/science.1207861.
 70. Roessler, C.; Nowak, T.; Pannek, M.; Gertz, M.; Nguyen, G. T. T.; Scharfe, M.; Born, I.; Sippl, W.; Steegborn, C.; Schutkowski, M. Chemical probing of the human sirtuin 5 active site reveals its substrate acyl specificity and peptide-based inhibitors. *Angewandte Chemie (International ed. in English)* **2014**, *53* (40), 10728–10732. DOI: 10.1002/anie.201402679.
 71. Zhang, X.; Spiegelman, N. A.; Nelson, O. D.; Jing, H.; Lin, H. SIRT6 regulates Ras-related protein R-Ras2 by lysine defatty-acylation. *eLife* **2017**, *6*. DOI: 10.7554/eLife.25158.
 72. Michishita, E.; McCord, R. A.; Berber, E.; Kioi, M.; Padilla-Nash, H.; Damian, M.; Cheung, P.; Kusumoto, R.; Kawahara, T. L. A.; Barrett, J. C.; Chang, H. Y.; Bohr, V. A.; Ried, T.; Gozani, O.; Chua, K. F. SIRT6 is a histone H3 lysine 9 deacetylase that modulates telomeric chromatin. *Nature* **2008**, *452* (7186), 492–496. DOI: 10.1038/nature06736.
 73. Michishita, E.; McCord, R. A.; Boxer, L. D.; Barber, M. F.; Hong, T.; Gozani, O.; Chua, K. F. Cell cycle-dependent deacetylation of telomeric histone H3 lysine K56 by human SIRT6. *Cell cycle (Georgetown, Tex.)* **2009**, *8* (16), 2664–2666. DOI: 10.4161/cc.8.16.9367.
 74. Gil, R.; Barth, S.; Kanfi, Y.; Cohen, H. Y. SIRT6 exhibits nucleosome-dependent deacetylase activity. *Nucleic acids research* **2013**, *41* (18), 8537–8545. DOI: 10.1093/nar/gkt642.
 75. Barber, M. F.; Michishita-Kioi, E.; Xi, Y.; Tasselli, L.; Kioi, M.; Moqtaderi, Z.; Tennen, R. I.; Paredes, S.; Young, N. L.; Chen, K.; Struhl, K.; Garcia, B. A.; Gozani, O.; Li, W.; Chua, K. F. SIRT7 links H3K18 deacetylation to maintenance of oncogenic transformation. *Nature* **2012**, *487* (7405), 114–118. DOI: 10.1038/nature11043.
 76. Ryu, D.; Jo, Y. S.; Lo Sasso, G.; Stein, S.; Zhang, H.; Perino, A.; Lee, J. U.; Zeviani, M.; Romand, R.; Hottiger, M. O.; Schoonjans, K.; Auwerx, J. A SIRT7-dependent acetylation switch of GABP β 1 controls mitochondrial function. *Cell metabolism* **2014**, *20* (5), 856–869. DOI: 10.1016/j.cmet.2014.08.001.
 77. Tong, Z.; Wang, Y.; Zhang, X.; Kim, D. D.; Sadhukhan, S.; Hao, Q.; Lin, H. SIRT7 Is Activated by DNA and Deacetylates Histone H3 in the Chromatin Context. *ACS Chem. Biol.* **2016**, *11* (3), 742–747. DOI: 10.1021/acscchembio.5b01084.
 78. Tong, Z.; Wang, M.; Wang, Y.; Kim, D. D.; Grenier, J. K.; Cao, J.; Sadhukhan, S.; Hao, Q.; Lin, H. SIRT7 Is an RNA-Activated Protein Lysine Deacylase. *ACS Chem. Biol.* **2017**, *12* (1), 300–310. DOI: 10.1021/acscchembio.6b00954.
 79. Tanabe, K.; Liu, J.; Kato, D.; Kurumizaka, H.; Yamatsugu, K.; Kanai, M.; Kawashima, S. A. LC-MS/MS-based quantitative study of the acyl group- and site-selectivity of human sirtuins to acylated nucleosomes. *Sci Rep* **2018**, *8* (1), 2656. DOI: 10.1038/s41598-018-21060-2.
 80. Kuznetsov, V. I.; Liu, W. H.; Klein, M. A.; Denu, J. M. Potent Activation of NAD⁺-Dependent Deacetylase Sirt7 by Nucleosome Binding. *ACS chemical biology* **2022**, *17* (8), 2248–2261. DOI: 10.1021/acscchembio.2c00348.
 81. Wang, W. W.; Angulo-Ibanez, M.; Lyu, J.; Kurra, Y.; Tong, Z.; Wu, B.; Zhang, L.; Sharma, V.; Zhou, J.; Lin, H.; Gao, Y. Q.; Li, W.; Chua, K. F.; Liu, W. R. A Click Chemistry Approach Reveals the Chromatin-Dependent Histone H3K36 Deacylase Nature of SIRT7. *Journal of the American Chemical Society* **2019**, *141* (6), 2462–2473. DOI: 10.1021/jacs.8b12083.
 82. Smuda, M.; Henning, C.; Raghavan, C. T.; Johar, K.; Vasavada, A. R.; Nagaraj, R. H.; Glomb, M. A. Comprehensive analysis of maillard protein modifications in human lenses: effect of age and cataract. *Biochemistry* **2015**, *54* (15), 2500–2507. DOI: 10.1021/bi5013194.
 83. Li, Z.; Wang, Q.; Huang, X.; Yang, M.; Zhou, S.; Li, Z.; Fang, Z.; Tang, Y.; Chen, Q.; Hou, H.; Li, L.; Fei, F.; Wang, Q.; Wu, Y.; Gong, A. Lactate in the tumor microenvironment: A rising star for targeted tumor therapy. *Frontiers in Nutrition* **2023**, *10*, 1113739. DOI: 10.3389/fnut.2023.1113739.

84. Fan, M.; Yang, K.; Wang, X.; Chen, L.; Gill, P. S.; Ha, T.; Liu, L.; Lewis, N. H.; Williams, D. L.; Li, C. Lactate promotes endothelial-to-mesenchymal transition via Snail1 lactylation after myocardial infarction. *Science advances* **2023**, *9* (5), eadc9465. DOI: 10.1126/sciadv.adc9465.
85. Wang, J.; Yang, P.; Yu, T.; Gao, M.; Liu, D.; Zhang, J.; Lu, C.; Chen, X.; Zhang, X.; Liu, Y. Lactylation of PKM2 Suppresses Inflammatory Metabolic Adaptation in Pro-inflammatory Macrophages. *Int. J. Biol. Sci.* **2022**, *18* (16), 6210–6225. DOI: 10.7150/ijbs.75434.
86. Gaffney, D. O.; Jennings, E. Q.; Anderson, C. C.; Marentette, J. O.; Shi, T.; Schou Oxvig, A.-M.; Streeter, M. D.; Johannsen, M.; Spiegel, D. A.; Chapman, E.; Roede, J. R.; Galligan, J. J. Non-enzymatic Lysine Lactoylation of Glycolytic Enzymes. *Cell chemical biology* **2020**, *27* (2), 206–213.e6. DOI: 10.1016/j.chembiol.2019.11.005.
87. Hagihara, H.; Shoji, H.; Otabi, H.; Toyoda, A.; Katoh, K.; Namihira, M.; Miyakawa, T. Protein lactylation induced by neural excitation. *Cell reports* **2021**, *37* (2), 109820. DOI: 10.1016/j.celrep.2021.109820.
88. Zu, H.; Li, C.; Dai, C.; Pan, Y.; Ding, C.; Sun, H.; Zhang, X.; Yao, X.; Zang, J.; Mo, X. SIRT2 functions as a histone delactylase and inhibits the proliferation and migration of neuroblastoma cells. *Cell discovery* **2022**, *8* (1), 54. DOI: 10.1038/s41421-022-00398-y.
89. Yu, J.; Chai, P.; Xie, M.; Ge, S.; Ruan, J.; Fan, X.; Jia, R. Histone lactylation drives oncogenesis by facilitating m6A reader protein YTHDF2 expression in ocular melanoma. *Genome biology* **2021**, *22* (1), 85. DOI: 10.1186/s13059-021-02308-z.
90. Yang, D.; Yin, J.; Shan, L.; Yi, X.; Zhang, W.; Ding, Y. Identification of lysine-lactylated substrates in gastric cancer cells. *iScience* **2022**, *25* (7), 104630. DOI: 10.1016/j.isci.2022.104630.
91. Dong, H.; Zhang, J.; Zhang, H.; Han, Y.; Lu, C.; Chen, C.; Tan, X.; Wang, S.; Bai, X.; Zhai, G.; Tian, S.; Zhang, T.; Cheng, Z.; Li, E.; Xu, L.; Zhang, K. YiaC and CobB regulate lysine lactylation in Escherichia coli. *Nat Commun* **2022**, *13* (1), 6628. DOI: 10.1038/s41467-022-34399-y.
92. Feldman, J. L.; Dittenhafer-Reed, K. E.; Denu, J. M. Sirtuin catalysis and regulation. *The Journal of biological chemistry* **2012**, *287* (51), 42419–42427. DOI: 10.1074/jbc.R112.378877.
93. Kaeberlein, M.; McVey, M.; Guarente, L. The SIR2/3/4 complex and SIR2 alone promote longevity in Saccharomyces cerevisiae by two different mechanisms. *Genes & Development* **1999**, *13* (19), 2570–2580. DOI: 10.1101/gad.13.19.2570.
94. Sinclair, D. A.; Guarente, L. Extrachromosomal rDNA circles--a cause of aging in yeast. *Cell* **1997**, *91* (7), 1033–1042. DOI: 10.1016/S0092-8674(00)80493-6.
95. Liang, T.; Wang, F.; Elhassan, R. M.; Cheng, Y.; Tang, X.; Chen, W.; Fang, H.; Hou, X. Targeting histone deacetylases for cancer therapy: Trends and challenges. *Acta Pharmaceutica Sinica B* **2023**, *13* (6), 2425–2463. DOI: 10.1016/j.apsb.2023.02.007.
96. Gao, L.; Cueto, M. A.; Asselbergs, F.; Atadja, P. Cloning and functional characterization of HDAC11, a novel member of the human histone deacetylase family. *The Journal of biological chemistry* **2002**, *277* (28), 25748–25755. DOI: 10.1074/jbc.M111871200.
97. Deubzer, H. E.; Schier, M. C.; Oehme, I.; Lodrini, M.; Haendler, B.; Sommer, A.; Witt, O. HDAC11 is a novel drug target in carcinomas. *International journal of cancer* **2013**, *132* (9), 2200–2208. DOI: 10.1002/ijc.27876.
98. Li, M.-Y.; Zhu, M.; Linghu, E.-Q.; Feng, F.; Zhu, B.; Wu, C.; Guo, M.-Z. Interleukin-13 suppresses interleukin-10 via inhibiting A20 in peripheral B cells of patients with food allergy. *Oncotarget* **2016**, *7* (48), 79914–79924. DOI: 10.18632/oncotarget.13107.
99. Liu, S.-S.; Wu, F.; Jin, Y.-M.; Chang, W.-Q.; Xu, T.-M. HDAC11: a rising star in epigenetics. *Biomedicine & pharmacotherapy = Biomedecine & pharmacotherapie* **2020**, *131*, 110607. DOI: 10.1016/j.biopha.2020.110607.
100. Villagra, A.; Cheng, F.; Wang, H.-W.; Suarez, I.; Glozak, M.; Maurin, M.; Nguyen, D.; Wright, K. L.; Atadja, P. W.; Bhalla, K.; Pinilla-Ibarz, J.; Seto, E.; Sotomayor, E. M. The histone deacetylase HDAC11 regulates the expression of interleukin 10 and immune tolerance. *Nature immunology* **2009**, *10* (1), 92–100. DOI: 10.1038/ni.1673.
101. Yang, H.; Chen, L.; Sun, Q.; Yao, F.; Muhammad, S.; Sun, C. The role of HDAC11 in obesity-related metabolic disorders: A critical review. *Journal of Cellular Physiology* **2021**, *236* (8), 5582–5591. DOI: 10.1002/jcp.30286.
102. Bagchi, R. A.; Ferguson, B. S.; Stratton, M. S.; Hu, T.; Cavaasin, M. A.; Sun, L.; Lin, Y.-H.; Liu, D.; Londono, P.; Song, K.; Pino, M. F.; Sparks, L. M.; Smith, S. R.; Scherer, P. E.; Collins, S.; Seto, E.; McKinsey, T. A. HDAC11 suppresses the thermogenic program of adipose tissue via BRD2. *JCI Insight* **2018**, *3* (15). DOI: 10.1172/jci.insight.120159.

103. Sun, L.; Marin de Evsikova, C.; Bian, K.; Achille, A.; Telles, E.; Pei, H.; Seto, E. Programming and Regulation of Metabolic Homeostasis by HDAC11. *EBioMedicine* **2018**, *33*, 157–168. DOI: 10.1016/j.ebiom.2018.06.025.
104. Imai, S.; Armstrong, C. M.; Kaeberlein, M.; Guarente, L. Transcriptional silencing and longevity protein Sir2 is an NAD-dependent histone deacetylase. *Nature* **2000**, *403* (6771), 795–800. DOI: 10.1038/35001622.
105. Landry, J.; Sutton, A.; Tafrov, S. T.; Heller, R. C.; Stebbins, J.; Pillus, L.; Sternglanz, R. The silencing protein SIR2 and its homologs are NAD-dependent protein deacetylases. *Proceedings of the National Academy of Sciences of the United States of America* **2000**, *97* (11), 5807–5811. DOI: 10.1073/pnas.110148297.
106. Frye, R. A. Characterization of five human cDNAs with homology to the yeast SIR2 gene: Sir2-like proteins (sirtuins) metabolize NAD and may have protein ADP-ribosyltransferase activity. *Biochemical and biophysical research communications* **1999**, *260* (1), 273–279. DOI: 10.1006/bbrc.1999.0897.
107. Tanny, J. C.; Dowd, G. J.; Huang, J.; Hilz, H.; Moazed, D. An Enzymatic Activity in the Yeast Sir2 Protein that Is Essential for Gene Silencing. *Cell* **1999**, *99* (7), 735–745. DOI: 10.1016/S0092-8674(00)81671-2.
108. Kowieski, T. M.; Lee, S.; Denu, J. M. Acetylation-dependent ADP-ribosylation by *Trypanosoma brucei* Sir2. *The Journal of biological chemistry* **2008**, *283* (9), 5317–5326. DOI: 10.1074/jbc.M707613200.
109. Dsilva, P.; Pai, P.; Shetty, M. G.; Babitha, K. S. The role of histone deacetylases in embryonic development. *Molecular Reproduction and Development* **2023**, *90* (1), 14–26. DOI: 10.1002/mrd.23659.
110. Hai, Y.; Shinsky, S. A.; Porter, N. J.; Christianson, D. W. Histone deacetylase 10 structure and molecular function as a polyamine deacetylase. *Nature communications* **2017**, *8*, 15368. DOI: 10.1038/ncomms15368.
111. Hai, Y.; Christianson, D. W. Histone deacetylase 6 structure and molecular basis of catalysis and inhibition. *Nature chemical biology* **2016**, *12* (9), 741–747. DOI: 10.1038/nchembio.2134.
112. Kanyo, Z. F.; Scolnick, L. R.; Ash, D. E.; Christianson, D. W. Structure of a unique binuclear manganese cluster in arginase. *Nature* **1996**, *383* (6600), 554–557. DOI: 10.1038/383554a0.
113. Lombardi, P. M.; Cole, K. E.; Dowling, D. P.; Christianson, D. W. Structure, mechanism, and inhibition of histone deacetylases and related metalloenzymes. *Current opinion in structural biology* **2011**, *21* (6), 735–743. DOI: 10.1016/j.sbi.2011.08.004.
114. Finnin, M. S.; Donigian, J. R.; Cohen, A.; Richon, V. M.; Rifkind, R. A.; Marks, P. A.; Breslow, R.; Pavletich, N. P. Structures of a histone deacetylase homologue bound to the TSA and SAHA inhibitors. *Nature* **1999**, *401* (6749), 188–193. DOI: 10.1038/43710.
115. Dowling, D. P.; Di Costanzo, L.; Gennadios, H. A.; Christianson, D. W. Evolution of the arginase fold and functional diversity. *Cellular and molecular life sciences : CMLS* **2008**, *65* (13), 2039–2055. DOI: 10.1007/s00018-008-7554-z.
116. Gantt, S. L.; Joseph, C. G.; Fierke, C. A. Activation and inhibition of histone deacetylase 8 by monovalent cations. *Journal of Biological Chemistry* **2010**, *285* (9), 6036–6043. DOI: 10.1074/jbc.M109.033399.
117. Dowling, D. P.; Gattis, S. G.; Fierke, C. A.; Christianson, D. W. Structures of metal-substituted human histone deacetylase 8 provide mechanistic inferences on biological function. *Biochemistry* **2010**, *49* (24), 5048–5056. DOI: 10.1021/bi1005046.
118. Vannini, A.; Volpari, C.; Gallinari, P.; Jones, P.; Mattu, M.; Carfi, A.; Francesco, R. de; Steinkühler, C.; Di Marco, S. Substrate binding to histone deacetylases as shown by the crystal structure of the HDAC8-substrate complex. *EMBO reports* **2007**, *8* (9), 879–884. DOI: 10.1038/sj.embor.7401047.
119. Vannini, A.; Volpari, C.; Filocamo, G.; Casavola, E. C.; Brunetti, M.; Renzoni, D.; Chakravarty, P.; Paolini, C.; Francesco, R. de; Gallinari, P.; Steinkühler, C.; Di Marco, S. Crystal structure of a eukaryotic zinc-dependent histone deacetylase, human HDAC8, complexed with a hydroxamic acid inhibitor. *Proceedings of the National Academy of Sciences of the United States of America* **2004**, *101* (42), 15064–15069. DOI: 10.1073/pnas.0404603101.
120. Somoza, J. R.; Skene, R. J.; Katz, B. A.; Mol, C.; Ho, J. D.; Jennings, A. J.; Luong, C.; Arvai, A.; Buggy, J. J.; Chi, E.; Tang, J.; Sang, B.-C.; Verner, E.; Wynands, R.; Leahy, E. M.; Dougan, D. R.; Snell, G.; Navre, M.; Knuth, M. W.; Swanson, R. V.; McRee, D. E.; Tari, L. W. Structural snapshots

- of human HDAC8 provide insights into the class I histone deacetylases. *Structure (London, England : 1993)* **2004**, *12* (7), 1325–1334. DOI: 10.1016/j.str.2004.04.012.
121. Gantt, S. L.; Gattis, S. G.; Fierke, C. A. Catalytic activity and inhibition of human histone deacetylase 8 is dependent on the identity of the active site metal ion. *Biochemistry* **2006**, *45* (19), 6170–6178. DOI: 10.1021/bi060212u.
 122. Porter, N. J.; Christianson, D. W. Structure, mechanism, and inhibition of the zinc-dependent histone deacetylases. *Current opinion in structural biology* **2019**, *59*, 9–18. DOI: 10.1016/j.sbi.2019.01.004.
 123. Dowling, D. P.; Gantt, S. L.; Gattis, S. G.; Fierke, C. A.; Christianson, D. W. Structural studies of human histone deacetylase 8 and its site-specific variants complexed with substrate and inhibitors. *Biochemistry* **2008**, *47* (51), 13554–13563. DOI: 10.1021/bi801610c.
 124. Gantt, S. M. L.; Decroos, C.; Lee, M. S.; Gullett, L. E.; Bowman, C. M.; Christianson, D. W.; Fierke, C. A. General Base-General Acid Catalysis in Human Histone Deacetylase 8. *Biochemistry* **2016**, *55* (5), 820–832. DOI: 10.1021/acs.biochem.5b01327.
 125. Wu, R.; Wang, S.; Zhou, N.; Cao, Z.; Zhang, Y. A proton-shuttle reaction mechanism for histone deacetylase 8 and the catalytic role of metal ions. *Journal of the American Chemical Society* **2010**, *132* (27), 9471–9479. DOI: 10.1021/ja103932d.
 126. Herbst-Gervasoni, C. J.; Christianson, D. W. X-ray Crystallographic Snapshots of Substrate Binding in the Active Site of Histone Deacetylase 10. *Biochemistry* **2021**, *60* (4), 303–313. DOI: 10.1021/acs.biochem.0c00936.
 127. Schuetz, A.; Min, J.; Allali-Hassani, A.; Schapira, M.; Shuen, M.; Loppnau, P.; Mazitschek, R.; Kwiatkowski, N. P.; Lewis, T. A.; Maglathin, R. L.; McLean, T. H.; Bochkarev, A.; Plotnikov, A. N.; Vedadi, M.; Arrowsmith, C. H. Human HDAC7 harbors a class IIa histone deacetylase-specific zinc binding motif and cryptic deacetylase activity. *The Journal of biological chemistry* **2008**, *283* (17), 11355–11363. DOI: 10.1074/jbc.M707362200.
 128. Wambua, M. K.; Nalawansha, D. A.; Negmeldin, A. T.; Pflum, M. K. H. Mutagenesis studies of the 14 Å internal cavity of histone deacetylase 1: insights toward the acetate-escape hypothesis and selective inhibitor design. *Journal of medicinal chemistry* **2014**, *57* (3), 642–650. DOI: 10.1021/jm401837e.
 129. Sun, Z.; Feng, D.; Fang, B.; Mullican, S. E.; You, S.-H.; Lim, H.-W.; Everett, L. J.; Nabel, C. S.; Li, Y.; Selvakumaran, V.; Won, K.-J.; Lazar, M. A. Deacetylase-independent function of HDAC3 in transcription and metabolism requires nuclear receptor corepressor. *Molecular cell* **2013**, *52* (6), 769–782. DOI: 10.1016/j.molcel.2013.10.022.
 130. Rossmann, M. G.; Argos, P. The taxonomy of binding sites in proteins. *Mol Cell Biochem* **1978**, *21* (3), 161–182. DOI: 10.1007/BF00240135.
 131. Sanders, B. D.; Jackson, B.; Marmorstein, R. Structural basis for sirtuin function: what we know and what we don't. *Biochimica et biophysica acta* **2010**, *1804* (8), 1604–1616. DOI: 10.1016/j.bbapap.2009.09.009.
 132. Borra, M. T.; Langer, M. R.; Slama, J. T.; Denu, J. M. Substrate specificity and kinetic mechanism of the Sir2 family of NAD⁺-dependent histone/protein deacetylases. *Biochemistry* **2004**, *43* (30), 9877–9887. DOI: 10.1021/bi049592e.
 133. Avalos, J. L.; Boeke, J. D.; Wolberger, C. Structural basis for the mechanism and regulation of Sir2 enzymes. *Molecular cell* **2004**, *13* (5), 639–648. DOI: 10.1016/s1097-2765(04)00082-6.
 134. Avalos, J. L.; Celic, I.; Muhammad, S.; Cosgrove, M. S.; Boeke, J. D.; Wolberger, C. Structure of a Sir2 enzyme bound to an acetylated p53 peptide. *Molecular cell* **2002**, *10* (3), 523–535. DOI: 10.1016/s1097-2765(02)00628-7.
 135. Zhao, K.; Chai, X.; Clements, A.; Marmorstein, R. Structure and autoregulation of the yeast Hst2 homolog of Sir2. *Nature structural biology* **2003**, *10* (10), 864–871. DOI: 10.1038/nsb978.
 136. Feldman, J. L.; Dittenhafer-Reed, K. E.; Kudo, N.; Thelen, J. N.; Ito, A.; Yoshida, M.; Denu, J. M. Kinetic and Structural Basis for Acyl-Group Selectivity and NAD(+) Dependence in Sirtuin-Catalyzed Deacylation. *Biochemistry* **2015**, *54* (19), 3037–3050. DOI: 10.1021/acs.biochem.5b00150.
 137. Cosgrove, M. S.; Bever, K.; Avalos, J. L.; Muhammad, S.; Zhang, X.; Wolberger, C. The structural basis of sirtuin substrate affinity. *Biochemistry* **2006**, *45* (24), 7511–7521. DOI: 10.1021/bi0526332.

138. Jin, L.; Wei, W.; Jiang, Y.; Peng, H.; Cai, J.; Mao, C.; Dai, H.; Choy, W.; Bemis, J. E.; Jirousek, M. R.; Milne, J. C.; Westphal, C. H.; Perni, R. B. Crystal structures of human SIRT3 displaying substrate-induced conformational changes. *The Journal of biological chemistry* **2009**, *284* (36), 24394–24405. DOI: 10.1074/jbc.M109.014928.
139. Min, J.; Landry, J.; Sternglanz, R.; Xu, R. M. Crystal structure of a SIR2 homolog-NAD complex. *Cell* **2001**, *105* (2), 269–279. DOI: 10.1016/s0092-8674(01)00317-8.
140. Chang, J.-H.; Kim, H.-C.; Hwang, K.-Y.; Lee, J.-W.; Jackson, S. P.; Bell, S. D.; Cho, Y. Structural basis for the NAD-dependent deacetylase mechanism of Sir2. *The Journal of biological chemistry* **2002**, *277* (37), 34489–34498. DOI: 10.1074/jbc.M205460200.
141. Pan, P. W.; Feldman, J. L.; Devries, M. K.; Dong, A.; Edwards, A. M.; Denu, J. M. Structure and biochemical functions of SIRT6. *The Journal of biological chemistry* **2011**, *286* (16), 14575–14587. DOI: 10.1074/jbc.M111.218990.
142. Sauve, A. A.; Celic, I.; Avalos, J.; Deng, H.; Boeke, J. D.; Schramm, V. L. Chemistry of gene silencing: the mechanism of NAD⁺-dependent deacetylation reactions. *Biochemistry* **2001**, *40* (51), 15456–15463. DOI: 10.1021/bi011858j.
143. Landry, J.; Slama, J. T.; Sternglanz, R. Role of NAD(+) in the deacetylase activity of the SIR2-like proteins. *Biochemical and biophysical research communications* **2000**, *278* (3), 685–690. DOI: 10.1006/bbrc.2000.3854.
144. Tanner, K. G.; Landry, J.; Sternglanz, R.; Denu, J. M. Silent information regulator 2 family of NAD- dependent histone/protein deacetylases generates a unique product, 1-O-acetyl-ADP-ribose. *Proceedings of the National Academy of Sciences of the United States of America* **2000**, *97* (26), 14178–14182. DOI: 10.1073/pnas.250422697.
145. Sauve, A. A. Sirtuin chemical mechanisms. *Biochimica et biophysica acta* **2010**, *1804* (8), 1591–1603. DOI: 10.1016/j.bbapap.2010.01.021.
146. Smith, B. C.; Denu, J. M. Sir2 deacetylases exhibit nucleophilic participation of acetyl-lysine in NAD⁺ cleavage. *Journal of the American Chemical Society* **2007**, *129* (18), 5802–5803. DOI: 10.1021/ja070162w.
147. Zhao, K.; Harshaw, R.; Chai, X.; Marmorstein, R. Structural basis for nicotinamide cleavage and ADP-ribose transfer by NAD(+)-dependent Sir2 histone/protein deacetylases. *Proceedings of the National Academy of Sciences of the United States of America* **2004**, *101* (23), 8563–8568. DOI: 10.1073/pnas.0401057101.
148. Sauve, A. A.; Wolberger, C.; Schramm, V. L.; Boeke, J. D. The biochemistry of sirtuins. *Annual review of biochemistry* **2006**, *75*, 435–465. DOI: 10.1146/annurev.biochem.74.082803.133500.
149. Hu, P.; Wang, S.; Zhang, Y. Highly dissociative and concerted mechanism for the nicotinamide cleavage reaction in Sir2Tm enzyme suggested by ab initio QM/MM molecular dynamics simulations. *Journal of the American Chemical Society* **2008**, *130* (49), 16721–16728. DOI: 10.1021/ja807269j.
150. Jackson, M. D.; Schmidt, M. T.; Oppenheimer, N. J.; Denu, J. M. Mechanism of nicotinamide inhibition and transglycosidation by Sir2 histone/protein deacetylases. *The Journal of biological chemistry* **2003**, *278* (51), 50985–50998. DOI: 10.1074/jbc.M306552200.
151. Sauve, A. A.; Schramm, V. L. Sir2 regulation by nicotinamide results from switching between base exchange and deacetylation chemistry. *Biochemistry* **2003**, *42* (31), 9249–9256. DOI: 10.1021/bi034959l.
152. Sauve, A. A.; Moir, R. D.; Schramm, V. L.; Willis, I. M. Chemical activation of Sir2-dependent silencing by relief of nicotinamide inhibition. *Molecular cell* **2005**, *17* (4), 595–601. DOI: 10.1016/j.molcel.2004.12.032.
153. Hawse, W. F.; Hoff, K. G.; Fatkins, D. G.; Daines, A.; Zubkova, O. V.; Schramm, V. L.; Zheng, W.; Wolberger, C. Structural insights into intermediate steps in the Sir2 deacetylation reaction. *Structure (London, England : 1993)* **2008**, *16* (9), 1368–1377. DOI: 10.1016/j.str.2008.05.015.
154. Hoff, K. G.; Avalos, J. L.; Sens, K.; Wolberger, C. Insights into the sirtuin mechanism from ternary complexes containing NAD⁺ and acetylated peptide. *Structure (London, England : 1993)* **2006**, *14* (8), 1231–1240. DOI: 10.1016/j.str.2006.06.006.
155. Smith, B. C.; Denu, J. M. Sir2 protein deacetylases: evidence for chemical intermediates and functions of a conserved histidine. *Biochemistry* **2006**, *45* (1), 272–282. DOI: 10.1021/bi052014t.

156. Sauve, A. A.; Youn, D. Y. Sirtuins: NAD(+)-dependent deacetylase mechanism and regulation. *Current opinion in chemical biology* **2012**, *16* (5-6), 535–543. DOI: 10.1016/j.cbpa.2012.10.003.
157. Jackson, M. D.; Denu, J. M. Structural identification of 2'- and 3'-O-acetyl-ADP-ribose as novel metabolites derived from the Sir2 family of beta -NAD+-dependent histone/protein deacetylases. *The Journal of biological chemistry* **2002**, *277* (21), 18535–18544. DOI: 10.1074/jbc.M200671200.
158. Haberland, M.; Montgomery, R. L.; Olson, E. N. The many roles of histone deacetylases in development and physiology: implications for disease and therapy. *Nature reviews. Genetics* **2009**, *10* (1), 32–42. DOI: 10.1038/nrg2485.
159. Ghazy, E.; Abdelsalam, M.; Robaa, D.; Pierce, R. J.; Sippl, W. Histone Deacetylase (HDAC) Inhibitors for the Treatment of Schistosomiasis. *Pharmaceuticals* **2022**, *15* (1), 80. DOI: 10.3390/ph15010080.
160. Bondarev, A. D.; Attwood, M. M.; Jonsson, J.; Chubarev, V. N.; Tarasov, V. V.; Schiöth, H. B. Recent developments of HDAC inhibitors: Emerging indications and novel molecules. *British Journal of Clinical Pharmacology* **2021**, *87* (12), 4577–4597. DOI: 10.1111/bcp.14889.
161. Bedalov, A.; Gathbonton, T.; Irvine, W. P.; Gottschling, D. E.; Simon, J. A. Identification of a small molecule inhibitor of Sir2p. *Proceedings of the National Academy of Sciences of the United States of America* **2001**, *98* (26), 15113–15118. DOI: 10.1073/pnas.261574398.
162. Kölle, D.; Brosch, G.; Lechner, T.; Lusser, A.; Loidl, P. Biochemical methods for analysis of histone deacetylases. *Methods* **1998**, *15* (4), 323–331. DOI: 10.1006/meth.1998.0636.
163. Borra, M. T.; Denu, J. M. Quantitative Assays for Characterization of the Sir2 Family of NAD+-Dependent Deacetylases. In: *Methods in Enzymology : Chromatin and Chromatin Remodeling Enzymes, Part B*; Academic Press, 2003, pp 171–187. DOI: 10.1016/S0076-6879(03)76011-X.
164. Zhu, A.; Su, X.; Lin, H. Detecting sirtuin-catalyzed deacylation reactions using ³²P-labeled NAD and thin-layer chromatography. *Methods in molecular biology (Clifton, N.J.)* **2013**, *1077*, 179–189. DOI: 10.1007/978-1-62703-637-5_12.
165. Du, J.; Jiang, H.; Lin, H. Investigating the ADP-ribosyltransferase activity of sirtuins with NAD analogues and 32P-NAD. *Biochemistry* **2009**, *48* (13), 2878–2890. DOI: 10.1021/bi802093g.
166. Khan, A. N.; Lewis, P. N. Unstructured conformations are a substrate requirement for the Sir2 family of NAD-dependent protein deacetylases. *The Journal of biological chemistry* **2005**, *280* (43), 36073–36078. DOI: 10.1074/jbc.M508247200.
167. Fan, Y.; Ludewig, R.; Scriba, G. K. E. 9-Fluorenylmethoxycarbonyl-labeled peptides as substrates in a capillary electrophoresis-based assay for sirtuin enzymes. *Analytical biochemistry* **2009**, *387* (2), 243–248. DOI: 10.1016/j.ab.2009.01.038.
168. Fan, Y.; Scriba, G. K. E. Electrophoretically mediated microanalysis assay for sirtuin enzymes. *Electrophoresis* **2010**, *31* (23-24), 3874–3880. DOI: 10.1002/elps.201000336.
169. Fan, Y.; Hense, M.; Ludewig, R.; Weisgerber, C.; Scriba, G. K. E. Capillary electrophoresis-based sirtuin assay using non-peptide substrates. *Journal of Pharmaceutical and Biomedical Analysis* **2011**, *54* (4), 772–778. DOI: 10.1016/j.jpba.2010.10.010.
170. Ohla, S.; Beyreiss, R.; Scriba, G. K. E.; Fan, Y.; Belder, D. An integrated on-chip sirtuin assay. *Electrophoresis* **2010**, *31* (19), 3263–3267. DOI: 10.1002/elps.201000220.
171. Blackwell, L.; Norris, J.; Suto, C. M.; Janzen, W. P. The use of diversity profiling to characterize chemical modulators of the histone deacetylases. *Life Sciences* **2008**, *82* (21-22), 1050–1058. DOI: 10.1016/j.lfs.2008.03.004.
172. Liu, Y.; Gerber, R.; Wu, J.; Tsuruda, T.; McCarter, J. D. High-throughput assays for sirtuin enzymes: a microfluidic mobility shift assay and a bioluminescence assay. *Analytical biochemistry* **2008**, *378* (1), 53–59. DOI: 10.1016/j.ab.2008.02.018.
173. Rahnasto-Rilla, M.; Kokkola, T.; Jarho, E.; Lahtela-Kakkonen, M.; Moaddel, R. N-Acylethanolamines Bind to SIRT6. *ChemBioChem* **2016**, *17* (1), 77–81. DOI: 10.1002/cbic.201500482.
174. Rahnasto-Rilla, M.; Lahtela-Kakkonen, M.; Moaddel, R. Sirtuin 6 (SIRT6) Activity Assays. *Methods in molecular biology (Clifton, N.J.)* **2016**, *1436*, 259–269. DOI: 10.1007/978-1-4939-3667-0_17.

175. McDonagh, T.; Hixon, J.; DiStefano, P. S.; Curtis, R.; Napper, A. D. Microplate filtration assay for nicotinamide release from NAD using a boronic acid resin. *Methods* **2005**, *36* (4), 346–350. DOI: 10.1016/j.ymeth.2005.03.005.
176. Di Shao; Yao, C.; Kim, M. H.; Fry, J.; Cohen, R. A.; Costello, C. E.; Matsui, R.; Seta, F.; McComb, M. E.; Bachschmid, M. M. Improved mass spectrometry-based activity assay reveals oxidative and metabolic stress as sirtuin-1 regulators. *Redox Biology* **2019**, *22*, 101150. DOI: 10.1016/j.redox.2019.101150.
177. Fischer, F.; Gertz, M.; Suenkel, B.; Lakshminarasimhan, M.; Schutkowski, M.; Steegborn, C. Sirt5 deacylation activities show differential sensitivities to nicotinamide inhibition. *PLoS one* **2012**, *7* (9), e45098. DOI: 10.1371/journal.pone.0045098.
178. Holzhauser, S.; Freiwald, A.; Weise, C.; Multhaup, G.; Han, C.-T.; Sauer, S. Discovery and characterization of protein-modifying natural products by MALDI mass spectrometry reveal potent SIRT1 and p300 inhibitors. *Angewandte Chemie International Edition* **2013**, *52* (19), 5171–5174. DOI: 10.1002/anie.201207325.
179. Gurard-Levin, Z. A.; Kim, J.; Mrksich, M. Combining mass spectrometry and peptide arrays to profile the specificities of histone deacetylases. *ChemBioChem* **2009**, *10* (13), 2159–2161. DOI: 10.1002/cbic.200900417.
180. Gurard-Levin, Z. A.; Kilian, K. A.; Kim, J.; Bähr, K.; Mrksich, M. Peptide arrays identify isoform-selective substrates for profiling endogenous lysine deacetylase activity. *ACS Chem. Biol.* **2010**, *5* (9), 863–873. DOI: 10.1021/cb100088g.
181. Rye, P. T.; Frick, L. E.; Ozbal, C. C.; Lamarr, W. A. Advances in label-free screening approaches for studying sirtuin-mediated deacetylation. *Journal of biomolecular screening* **2011**, *16* (10), 1217–1226. DOI: 10.1177/1087057111420291.
182. Guetschow, E. D.; Kumar, S.; Lombard, D. B.; Kennedy, R. T. Identification of sirtuin 5 inhibitors by ultrafast microchip electrophoresis using nanoliter volume samples. *Analytical and bioanalytical chemistry* **2016**, *408* (3), 721–731. DOI: 10.1007/s00216-015-9206-0.
183. Smith, B. C.; Hallows, W. C.; Denu, J. M. A continuous microplate assay for sirtuins and nicotinamide-producing enzymes. *Analytical biochemistry* **2009**, *394* (1), 101–109. DOI: 10.1016/j.ab.2009.07.019.
184. Hubbard, B. P.; Gomes, A. P.; Dai, H.; Li, J.; Case, A. W.; Considine, T.; Riera, T. V.; Lee, J. E.; E, S. Y.; Lamming, D. W.; Pentelute, B. L.; Schuman, E. R.; Stevens, L. A.; Ling, A. J. Y.; Armour, S. M.; Michan, S.; Zhao, H.; Jiang, Y.; Sweitzer, S. M.; Blum, C. A.; Disch, J. S.; Ng, P. Y.; Howitz, K. T.; Rolo, A. P.; Hamuro, Y.; Moss, J.; Perni, R. B.; Ellis, J. L.; Vlasuk, G. P.; Sinclair, D. A. Evidence for a common mechanism of SIRT1 regulation by allosteric activators. *Science (New York, N.Y.)* **2013**, *339* (6124), 1216–1219. DOI: 10.1126/science.1231097.
185. Sugawara, K.; Oyama, F. Fluorogenic reaction and specific microdetermination of ammonia. *Journal of biochemistry* **1981**, *89* (3), 771–774. DOI: 10.1093/oxfordjournals.jbchem.a133257.
186. Wolfson, N. A.; Pitcairn, C. A.; Sullivan, E. D.; Joseph, C. G.; Fierke, C. A. An enzyme-coupled assay measuring acetate production for profiling histone deacetylase specificity. *Analytical biochemistry* **2014**, *456*, 61–69. DOI: 10.1016/j.ab.2014.03.012.
187. Krämer, A.; Herzer, J.; Overhage, J.; Meyer-Almes, F.-J. Substrate specificity and function of acetylpolyamine amidohydrolases from *Pseudomonas aeruginosa*. *BMC Biochem* **2016**, *17* (1), 4. DOI: 10.1186/s12858-016-0063-z.
188. Kang, W.; Liu, L.; Yu, P.; Zhang, T.; Lei, C.; Nie, Z. A switchable Cas12a enabling CRISPR-based direct histone deacetylase activity detection. *Biosensors & bioelectronics* **2022**, *213*, 114468. DOI: 10.1016/j.bios.2022.114468.
189. Spinck, M.; Ecke, M.; Sievers, S.; Neumann, H. Highly Sensitive Lysine Deacetylase Assay Based on Acetylated Firefly Luciferase. *Biochemistry* **2018**, *57* (26), 3552–3555. DOI: 10.1021/acs.biochem.8b00483.
190. Spinck, M.; Bischoff, M.; Lampe, P.; Meyer-Almes, F.-J.; Sievers, S.; Neumann, H. Discovery of Dihydro-1,4-Benzoxazine Carboxamides as Potent and Highly Selective Inhibitors of Sirtuin-1. *Journal of medicinal chemistry* **2021**, *64* (9), 5838–5849. DOI: 10.1021/acs.jmedchem.1c00017.
191. Wegener, D.; Wirsching, F.; Riester, D.; Schwienhorst, A. A fluorogenic histone deacetylase assay well suited for high-throughput activity screening. *Chemistry & biology* **2003**, *10* (1), 61–68. DOI: 10.1016/s1074-5521(02)00305-8.

192. Moreno-Yruela, C.; Olsen, C. A. High-throughput screening of histone deacetylases and determination of kinetic parameters using fluorogenic assays. *STAR protocols* **2021**, *2* (1), 100313. DOI: 10.1016/j.xpro.2021.100313.
193. Yuan, T.; Keijer, J.; Guo, A. H.; Lombard, D. B.; Boer, V. C. J. de. An optimized desuccinylase activity assay reveals a difference in desuccinylation activity between proliferative and differentiated cells. *Sci Rep* **2020**, *10* (1), 17030. DOI: 10.1038/s41598-020-72833-7.
194. Chiang, Y.-L.; Lin, H. An improved fluorogenic assay for SIRT1, SIRT2, and SIRT3. *Org. Biomol. Chem.* **2016**, *14* (7), 2186–2190. DOI: 10.1039/C5OB02609A.
195. Galleano, I.; Schiedel, M.; Jung, M.; Madsen, A. S.; Olsen, C. A. A Continuous, Fluorogenic Sirtuin 2 Deacylase Assay: Substrate Screening and Inhibitor Evaluation. *Journal of medicinal chemistry* **2016**, *59* (3), 1021–1031. DOI: 10.1021/acs.jmedchem.5b01532.
196. Hoffmann, K.; Brosch, G.; Loidl, P.; Jung, M. A non-isotopic assay for histone deacetylase activity. *Nucleic Acids Res* **1999**, *27* (9), 2057–2058. DOI: 10.1093/nar/27.9.2057.
197. Hu, J.; He, B.; Bhargava, S.; Lin, H. A fluorogenic assay for screening Sirt6 modulators. *Org. Biomol. Chem.* **2013**, *11* (32), 5213–5216. DOI: 10.1039/c3ob41138a.
198. Yang, L.-L.; Wang, H.-L.; Yan, Y.-H.; Liu, S.; Yu, Z.-J.; Huang, M.-Y.; Luo, Y.; Zheng, X.; Yu, Y.; Li, G.-B. Sensitive fluorogenic substrates for sirtuin deacylase inhibitor discovery. *European Journal of Medicinal Chemistry* **2020**, *192*, 112201. DOI: 10.1016/j.ejmech.2020.112201.
199. Bradner, J. E.; West, N.; Grachan, M. L.; Greenberg, E. F.; Haggarty, S. J.; Warnow, T.; Mazitschek, R. Chemical phylogenetics of histone deacetylases. *Nat Chem Biol* **2010**, *6* (3), 238–243. DOI: 10.1038/nchembio.313.
200. Dose, A.; Jost, J. O.; Spieß, A. C.; Henklein, P.; Beyermann, M.; Schwarzer, D. Facile synthesis of colorimetric histone deacetylase substrates. *Chem. Commun.* **2012**, *48* (76), 9525–9527. DOI: 10.1039/c2cc34422j.
201. Roessler, C.; Tüting, C.; Meleshin, M.; Steegborn, C.; Schutkowski, M. A Novel Continuous Assay for the Deacylase Sirtuin 5 and Other Deacetylases. *Journal of medicinal chemistry* **2015**, *58* (18), 7217–7223. DOI: 10.1021/acs.jmedchem.5b00293.
202. Li, Y.; You, L.; Huang, W.; Liu, J.; Zhu, H.; He, B. A FRET-based assay for screening SIRT6 modulators. *European Journal of Medicinal Chemistry* **2015**, *96*, 245–249. DOI: 10.1016/j.ejmech.2015.04.008.
203. Li, Y.; Zhao, Y.; Cao, Z.; Wang, J.; Liu, T.; Li, Y.; Wang, Y.; He, B. Development of a mitochondrial sirtuin 4 FRET assay based on its activity for removing 3-hydroxy-3-methylglutaryl (HMG) modification. *RSC Adv.* **2021**, *11* (5), 2677–2681. DOI: 10.1039/d0ra09424b.
204. Schultz, B. E.; Misialek, S.; Wu, J.; Tang, J.; Conn, M. T.; Tahilramani, R.; Wong, L. Kinetics and comparative reactivity of human class I and class IIb histone deacetylases. *Biochemistry* **2004**, *43* (34), 11083–11091. DOI: 10.1021/bi0494471.
205. Marcotte, P. A.; Richardson, P. L.; Guo, J.; Barrett, L. W.; Xu, N.; Gunasekera, A.; Glaser, K. B. Fluorescence assay of SIRT protein deacetylases using an acetylated peptide substrate and a secondary trypsin reaction. *Analytical biochemistry* **2004**, *332* (1), 90–99. DOI: 10.1016/j.ab.2004.05.039.
206. Padige, G.; Negmeldin, A. T.; Pflum, M. K. H. Development of an ELISA-Based HDAC Activity Assay for Characterization of Isoform-Selective Inhibitors. *Journal of biomolecular screening* **2015**, *20* (10), 1277–1285. DOI: 10.1177/1087057115598118.
207. Halley, F.; Reinshagen, J.; Ellinger, B.; Wolf, M.; Niles, A. L.; Evans, N. J.; Kirkland, T. A.; Wagner, J. M.; Jung, M.; Gribbon, P.; Gul, S. A bioluminogenic HDAC activity assay: validation and screening. *Journal of biomolecular screening* **2011**, *16* (10), 1227–1235. DOI: 10.1177/10870571111416004.
208. Wang, S.; Zeng, P.; Zhu, X.; Lei, C.; Huang, Y.; Nie, Z. Chimeric Peptides Self-Assembling on Titanium Carbide MXenes as Biosensing Interfaces for Activity Assay of Post-translational Modification Enzymes. *Anal. Chem.* **2020**, *92* (13), 8819–8826. DOI: 10.1021/acs.analchem.0c00243.
209. Fatkins, D. G.; Zheng, W. A spectrophotometric assay for histone deacetylase 8. *Analytical biochemistry* **2008**, *372* (1), 82–88. DOI: 10.1016/j.ab.2007.08.031.
210. Toro, T. B.; Watt, T. J. KDAC8 substrate specificity quantified by a biologically relevant, label-free deacetylation assay. *Protein science : a publication of the Protein Society* **2015**, *24* (12), 2020–2032. DOI: 10.1002/pro.2813.

211. Swyter, S.; Schiedel, M.; Monaldi, D.; Szunyogh, S.; Lehotzky, A.; Rumpf, T.; Ovádi, J.; Sippl, W.; Jung, M. New chemical tools for probing activity and inhibition of the NAD⁺-dependent lysine deacetylase sirtuin 2. *Philosophical Transactions of the Royal Society B: Biological Sciences* **2018**, *373* (1748). DOI: 10.1098/rstb.2017.0083.
212. Herp, D.; Ridinger, J.; Robaa, D.; Shinsky, S. A.; Schmidtkunz, K.; Yesiloglu, T. Z.; Bayer, T.; Steimbach, R. R.; Herbst-Gervasoni, C. J.; Merz, A.; Romier, C.; Sehr, P.; Gunkel, N.; Miller, A. K.; Christianson, D. W.; Oehme, I.; Sippl, W.; Jung, M. First Fluorescent Acetylspermidine Deacetylation Assay for HDAC10 Identifies Selective Inhibitors with Cellular Target Engagement. *ChemBioChem* **2022**, *23* (14), e202200180. DOI: 10.1002/cbic.202200180.
213. Heltweg, B.; Jung, M. A homogeneous nonisotopic histone deacetylase activity assay. *Journal of biomolecular screening* **2003**, *8* (1), 89–95. DOI: 10.1177/1087057102239644.
214. Feng, Y.; Wu, J.; Chen, L.; Luo, C.; Shen, X.; Chen, K.; Jiang, H.; Liu, D. A fluorometric assay of SIRT1 deacetylation activity through quantification of nicotinamide adenine dinucleotide. *Analytical biochemistry* **2009**, *395* (2), 205–210. DOI: 10.1016/j.ab.2009.08.011.
215. Hu, J.; Pan, L.; Li, Y.; Zou, X.; Liu, B.; Jiang, B.; Zhang, C. Deacetylation-activated construction of single quantum dot-based nanosensor for sirtuin 1 assay. *Talanta* **2021**, *224*, 121918. DOI: 10.1016/j.talanta.2020.121918.
216. Garske, A. L.; Denu, J. M. SIRT1 top 40 hits: use of one-bead, one-compound acetyl-peptide libraries and quantum dots to probe deacetylase specificity. *Biochemistry* **2006**, *45* (1), 94–101. DOI: 10.1021/bi052015l.
217. Minoshima, M.; Matsumoto, T.; Kikuchi, K. Development of a fluorogenic probe based on a DNA staining dye for continuous monitoring of the histone deacetylase reaction. *Analytical Chemistry* **2014**, *86* (15), 7925–7930. DOI: 10.1021/ac501881s.
218. Han, Y.; Li, H.; Hu, Y.; Li, P.; Wang, H.; Nie, Z.; Yao, S. Time-resolved luminescence biosensor for continuous activity detection of protein acetylation-related enzymes based on DNA-sensitized terbium(III) probes. *Anal. Chem.* **2015**, *87* (18), 9179–9185. DOI: 10.1021/acs.analchem.5b01338.
219. Dhara, K.; Hori, Y.; Baba, R.; Kikuchi, K. A fluorescent probe for detection of histone deacetylase activity based on aggregation-induced emission. *Chem. Commun.* **2012**, *48* (94), 11534–11536. DOI: 10.1039/C2CC36591J.
220. Yu, C.; Wu, Y.; Zeng, F.; Li, X.; Shi, J.; Wu, S. Hyperbranched polyester-based fluorescent probe for histone deacetylase via aggregation-induced emission. *Biomacromolecules* **2013**, *14* (12), 4507–4514. DOI: 10.1021/bm401548u.
221. Gao, L.; Zhou, Y.; Cao, L.; Cui, X.; Zheng, Y.; Yin, H.; Ai, S. Photoelectrochemical Biosensor for Histone Deacetylase Sirt1 Detection Based on Polyaspartic Acid-Engaged and Triggered Redox Cycling Amplification and Enhanced Photoactivity of BiVO₄ by Gold Nanoparticles and SnS₂. *Anal. Chem.* **2022**, *94* (48), 16936–16944. DOI: 10.1021/acs.analchem.2c04380.
222. Baba, R.; Hori, Y.; Mizukami, S.; Kikuchi, K. Development of a fluorogenic probe with a transesterification switch for detection of histone deacetylase activity. *Journal of the American Chemical Society* **2012**, *134* (35), 14310–14313. DOI: 10.1021/ja306045j.
223. Baba, R.; Hori, Y.; Kikuchi, K. Intramolecular long-distance nucleophilic reactions as a rapid fluorogenic switch applicable to the detection of enzymatic activity. *Chemistry – A European Journal* **2015**, *21* (12), 4695–4702. DOI: 10.1002/chem.201406093.
224. Hori, Y.; Nishiura, M.; Tao, T.; Baba, R.; Bull, S. D.; Kikuchi, K. Fluorogenic probes for detecting deacetylase and demethylase activity towards post-translationally-modified lysine residues. *Chemical Science* **2021**, *12* (7), 2498–2503. DOI: 10.1039/d0sc06551j.
225. Wang, P.; Di Chen; An, J.; Lin, S.; Liu, T.; Li, Y.; Chen, L.; He, B. Development of a single-step fluorogenic sirtuin assay and its applications for high-throughput screening. *Organic & Biomolecular Chemistry* **2022**, *20* (6), 1243–1252. DOI: 10.1039/d1ob02347k.
226. Xie, Y.; Ge, J.; Lei, H.; Peng, B.; Zhang, H.; Wang, D.; Pan, S.; Chen, G.; Chen, L.; Wang, Y.; Hao, Q.; Yao, S. Q.; Sun, H. Fluorescent Probes for Single-Step Detection and Proteomic Profiling of Histone Deacetylases. *Journal of the American Chemical Society* **2016**, *138* (48), 15596–15604. DOI: 10.1021/jacs.6b07334.
227. Xie, Y.; Chen, L.; Wang, R.; Wang, J.; Li, J.; Xu, W.; Li, Y.; Yao, S. Q.; Zhang, L.; Hao, Q.; Sun, H. Chemical Probes Reveal Sirt2's New Function as a Robust "Eraser" of Lysine Lipoylation. *Journal of the American Chemical Society* **2019**, *141* (46), 18428–18436. DOI: 10.1021/jacs.9b06913.

228. Xie, Y.; Yang, L.; Chen, Q.; Zhang, J.; Feng, L.; Chen, J. L.; Hao, Q.; Zhang, L.; Sun, H. Single-step fluorescent probes to detect decrotonylation activity of HDACs through intramolecular reactions. *European Journal of Medicinal Chemistry* **2021**, *212*, 113120. DOI: 10.1016/j.ejmech.2020.113120.
229. Li, R.; Xue, F.; Cao, C.; Wei, P.; Zhong, Y.; Xiao, S.; Li, F.; Yi, T. A near infrared fluorescent probe for one-step detection of histone deacetylase activity based on an intramolecular FRET. *Sensors and Actuators B: Chemical* **2019**, *297*, 126791. DOI: 10.1016/j.snb.2019.126791.
230. Rooker, D. R.; Buccella, D. Real-time detection of histone deacetylase activity with a small molecule fluorescent and spectrophotometric probe. *Chemical Science* **2015**, *6* (11), 6456–6461. DOI: 10.1039/C5SC02704G.
231. Rooker, D. R.; Klyubka, Y.; Gautam, R.; Tomat, E.; Buccella, D. Peptide-Based Fluorescent Probes for Deacetylase and Decrotonylase Activity: Toward a General Platform for Real-Time Detection of Lysine Deacylation. *ChemBioChem* **2018**, *19* (5), 496–504. DOI: 10.1002/cbic.201700582.
232. Liu, X.; Xiang, M.; Tong, Z.; Luo, F.; Chen, W.; Liu, F.; Wang, F.; Yu, R.-Q.; Jiang, J.-H. Activatable Fluorescence Probe via Self-Immolative Intramolecular Cyclization for Histone Deacetylase Imaging in Live Cells and Tissues. *Anal. Chem.* **2018**, *90* (9), 5534–5539. DOI: 10.1021/acs.analchem.8b00709.
233. Li, M.; Liu, J.; Chen, X.; Dang, Y.; Shao, Y.; Xu, Z.; Zhang, W. An activatable and tumor-targeting NIR fluorescent probe for imaging of histone deacetylase 6 in cancer cells and in vivo. *Chem. Commun.* **2022**, *58* (12), 1938–1941. DOI: 10.1039/D1CC04640C.
234. Liu, F.; Ding, X.; Xu, X.; Wang, F.; Chu, X.; Jiang, J.-H. A Reactivity-Tunable Self-Immolative Design Enables Histone Deacetylase-Targeted Imaging and Prodrug Activation. *Angewandte Chemie International Edition* **2022**, *61* (47), e202203243. DOI: 10.1002/anie.202203243.
235. Xuan, W.; Yao, A.; Schultz, P. G. Genetically Encoded Fluorescent Probe for Detecting Sirtuins in Living Cells. *Journal of the American Chemical Society* **2017**, *139* (36), 12350–12353. DOI: 10.1021/jacs.7b05725.
236. Schuster, S.; Roessler, C.; Meleshin, M.; Zimmermann, P.; Simic, Z.; Kambach, C.; Schiene-Fischer, C.; Steegborn, C.; Hottiger, M. O.; Schutkowski, M. A continuous sirtuin activity assay without any coupling to enzymatic or chemical reactions. *Sci Rep* **2016**, *6* (1), 22643. DOI: 10.1038/srep22643.
237. Dai, Q.; Zheng, Z.; Xia, F.; Liu, P.; Li, M. A one-step specific assay for continuous detection of sirtuin 2 activity. *Acta Pharmaceutica Sinica B* **2019**, *9* (6), 1183–1192. DOI: 10.1016/j.apsb.2019.05.007.
238. Kawaguchi, M.; Ikegawa, S.; Ieda, N.; Nakagawa, H. A Fluorescent Probe for Imaging Sirtuin Activity in Living Cells, Based on One-Step Cleavage of the Dabcyl Quencher. *ChemBioChem* **2016**, *17* (20), 1961–1967. DOI: 10.1002/cbic.201600374.
239. Nakajima, Y.; Kawaguchi, M.; Ieda, N.; Nakagawa, H. A Set of Highly Sensitive Sirtuin Fluorescence Probes for Screening Small-Molecular Sirtuin Defatty-Acylase Inhibitors. *ACS medicinal chemistry letters* **2021**, *12* (4), 617–624. DOI: 10.1021/acsmedchemlett.1c00010.
240. Mazitschek, R.; Patel, V.; Wirth, D. F.; Clardy, J. Development of a fluorescence polarization based assay for histone deacetylase ligand discovery. *Bioorganic & medicinal chemistry letters* **2008**, *18* (9), 2809–2812. DOI: 10.1016/j.bmcl.2008.04.007.
241. Singh, R. K.; Mandal, T.; Balasubramanian, N.; Cook, G.; Srivastava, D. K. Coumarin-suberoylanilide hydroxamic acid as a fluorescent probe for determining binding affinities and off-rates of histone deacetylase inhibitors. *Analytical biochemistry* **2011**, *408* (2), 309–315. DOI: 10.1016/j.ab.2010.08.040.
242. Kim, B.; Pithadia, A. S.; Fierke, C. A. Kinetics and thermodynamics of metal-binding to histone deacetylase 8. *Protein science : a publication of the Protein Society* **2015**, *24* (3), 354–365. DOI: 10.1002/pro.2623.
243. Meng, Q.; Liu, Z.; Li, F.; Ma, J.; Wang, H.; Huan, Y.; Li, Z. An HDAC-Targeted Imaging Probe LBH589-Cy5.5 for Tumor Detection and Therapy Evaluation. *Molecular Pharmaceutics* **2015**, *12* (7), 2469–2476. DOI: 10.1021/acs.molpharmaceut.5b00167.
244. Fleming, C. L.; Natoli, A.; Schreuders, J.; Devlin, M.; Yoganantharajah, P.; Gibert, Y.; Leslie, K. G.; New, E. J.; Ashton, T. D.; Pfeffer, F. M. Highly fluorescent and HDAC6 selective scriptaid analogues. *European Journal of Medicinal Chemistry* **2019**, *162*, 321–333. DOI: 10.1016/j.ejmech.2018.11.020.

245. Tang, C.; Du, Y.; Liang, Q.; Cheng, Z.; Tian, J. Development of a Novel Histone Deacetylase-Targeted Near-Infrared Probe for Hepatocellular Carcinoma Imaging and Fluorescence Image-Guided Surgery. *Mol Imaging Biol* **2020**, *22* (3), 476–485. DOI: 10.1007/s11307-019-01389-4.
246. Zhang, K.; Liu, Z.; Yao, Y.; Qiu, Y.; Li, F.; Chen, D.; Hamilton, D. J.; Li, Z.; Jiang, S. Structure-Based Design of a Selective Class I Histone Deacetylase (HDAC) Near-Infrared (NIR) Probe for Epigenetic Regulation Detection in Triple-Negative Breast Cancer (TNBC). *Journal of medicinal chemistry* **2021**, *64* (7), 4020–4033. DOI: 10.1021/acs.jmedchem.0c02161.
247. Riester, D.; Hildmann, C.; Schwienhorst, A.; Meyer-Almes, F.-J. Histone deacetylase inhibitor assay based on fluorescence resonance energy transfer. *Analytical biochemistry* **2007**, *362* (1), 136–141. DOI: 10.1016/j.ab.2006.12.019.
248. Bi, D.; Yang, J.; Hong, J. Y.; Parikh, P.; Hinds, N.; Infanti, J.; Lin, H.; Weiser, B. P. Substrate-Dependent Modulation of SIRT2 by a Fluorescent Probe, 1-Aminoanthracene. *Biochemistry* **2020**, *59* (40), 3869–3878. DOI: 10.1021/acs.biochem.0c00564.
249. Hong, J. Y.; Cassel, J.; Yang, J.; Lin, H.; Weiser, B. P. High-Throughput Screening Identifies Ascorbyl Palmitate as a SIRT2 Deacetylase and Defatty-Acylase Inhibitor. *ChemMedChem* **2021**, *16* (22), 3484–3494. DOI: 10.1002/cmdc.202100343.
250. Géraldy, M.; Morgen, M.; Sehr, P.; Steimbach, R. R.; Moi, D.; Ridinger, J.; Oehme, I.; Witt, O.; Malz, M.; Nogueira, M. S.; Koch, O.; Gunkel, N.; Miller, A. K. Selective Inhibition of Histone Deacetylase 10: Hydrogen Bonding to the Gatekeeper Residue is Implicated. *Journal of medicinal chemistry* **2019**, *62* (9), 4426–4443. DOI: 10.1021/acs.jmedchem.8b01936.
251. Frank, R.; Jakob, M.; Thunecke, F.; Fischer, G.; Schutkowski, M. Thioxylation as One-Atom-Substitution Generates a Photoswitchable Element within the Peptide Backbone. *Angewandte Chemie International Edition* **2000**, *39* (6), 1120–1122. DOI: 10.1002/(SICI)1521-3773(20000317)39:6<1120:AID-ANIE1120>3.0.CO;2-H.
252. Goldberg, J. M.; Batjargal, S.; Chen, B. S.; Petersson, E. J. Thioamide quenching of fluorescent probes through photoinduced electron transfer: mechanistic studies and applications. *Journal of the American Chemical Society* **2013**, *135* (49), 18651–18658. DOI: 10.1021/ja409709x.
253. Petersson, E. J.; Goldberg, J. M.; Wissner, R. F. On the use of thioamides as fluorescence quenching probes for tracking protein folding and stability. *Phys. Chem. Chem. Phys.* **2014**, *16* (15), 6827–6837. DOI: 10.1039/C3CP55525A.
254. Smith, B. C.; Denu, J. M. Mechanism-based inhibition of Sir2 deacetylases by thioacetyl-lysine peptide. *Biochemistry* **2007**, *46* (50), 14478–14486. DOI: 10.1021/bi7013294.
255. Chen, Y.; Wang, X.; Xiang, W.; He, L.; Tang, M.; Wang, F.; Wang, T.; Yang, Z.; Yi, Y.; Wang, H.; Niu, T.; Zheng, L.; Lei, L.; Li, X.; Song, H.; Chen, L. Development of Purine-Based Hydroxamic Acid Derivatives: Potent Histone Deacetylase Inhibitors with Marked in Vitro and in Vivo Antitumor Activities. *Journal of medicinal chemistry* **2016**, *59* (11), 5488–5504. DOI: 10.1021/acs.jmedchem.6b00579.
256. Yang, Z.; Wang, T.; Wang, F.; Niu, T.; Liu, Z.; Chen, X.; Long, C.; Tang, M.; Cao, D.; Wang, X.; Xiang, W.; Yi, Y.; Ma, L.; You, J.; Chen, L. Discovery of Selective Histone Deacetylase 6 Inhibitors Using the Quinazoline as the Cap for the Treatment of Cancer. *Journal of medicinal chemistry* **2016**, *59* (4), 1455–1470. DOI: 10.1021/acs.jmedchem.5b01342.
257. Yao, Y.; Tu, Z.; Liao, C.; Wang, Z.; Li, S.; Yao, H.; Li, Z.; Jiang, S. Discovery of Novel Class I Histone Deacetylase Inhibitors with Promising in Vitro and in Vivo Antitumor Activities. *Journal of medicinal chemistry* **2015**, *58* (19), 7672–7680. DOI: 10.1021/acs.jmedchem.5b01044.
258. Salvador, L. A.; Park, H.; Al-Awadhi, F. H.; Liu, Y.; Kim, B.; Zeller, S. L.; Chen, Q.-Y.; Hong, J.; Luesch, H. Modulation of Activity Profiles for Largazole-Based HDAC Inhibitors through Alteration of Prodrug Properties. *ACS medicinal chemistry letters* **2014**, *5* (8), 905–910. DOI: 10.1021/ml500170r.
259. Spiegelman, N. A.; Price, I. R.; Jing, H.; Wang, M.; Yang, M.; Cao, J.; Hong, J. Y.; Zhang, X.; Aramsangtienchai, P.; Sadhukhan, S.; Lin, H. Direct Comparison of SIRT2 Inhibitors: Potency, Specificity, Activity-Dependent Inhibition, and On-Target Anticancer Activities. *ChemMedChem* **2018**, *13* (18), 1890–1894. DOI: 10.1002/cmdc.201800391.
260. Jing, H.; Hu, J.; He, B.; Negrón Abril, Y. L.; Stupinski, J.; Weiser, K.; Carbonaro, M.; Chiang, Y.-L.; Southard, T.; Giannakakou, P.; Weiss, R. S.; Lin, H. A SIRT2-Selective Inhibitor Promotes c-Myc Oncoprotein Degradation and Exhibits Broad Anticancer Activity. *Cancer Cell* **2016**, *29* (3), 297–310. DOI: 10.1016/j.ccell.2016.02.007.

261. Bond, M. D.; Holmquist, B.; Vallee, B. L. Thioamide substrate probes of metal-substrate interactions in carboxypeptidase A catalysis. *Journal of inorganic biochemistry* **1986**, *28* (2-3), 97–105. DOI: 10.1016/0162-0134(86)80074-5.
262. Schutkowski, M.; Wöllner, S.; Fischer, G. Inhibition of peptidyl-prolyl cis/trans isomerase activity by substrate analog structures: thioxo tetrapeptide-4-nitroanilides. *Biochemistry* **1995**, *34* (40), 13016–13026. DOI: 10.1021/bi00040a012.
263. Zhang, Y.; Füssel, S.; Reimer, U.; Schutkowski, M.; Fischer, G. Substrate-based design of reversible Pin1 inhibitors. *Biochemistry* **2002**, *41* (39), 11868–11877. DOI: 10.1021/bi0262395.
264. Fatkins, D. G.; Monnot, A. D.; Zheng, W. Nepsilon-thioacetyl-lysine: a multi-facet functional probe for enzymatic protein lysine Nepsilon-deacetylation. *Bioorganic & medicinal chemistry letters* **2006**, *16* (14), 3651–3656. DOI: 10.1016/j.bmcl.2006.04.075.
265. He, B.; Du, J.; Lin, H. Thiosuccinyl peptides as Sirt5-specific inhibitors. *Journal of the American Chemical Society* **2012**, *134* (4), 1922–1925. DOI: 10.1021/ja2090417.
266. He, B.; Hu, J.; Zhang, X.; Lin, H. Thiomyristoyl peptides as cell-permeable Sirt6 inhibitors. *Org. Biomol. Chem.* **2014**, *12* (38), 7498–7502. DOI: 10.1039/c4ob00860j.
267. Yao, S.; Zutshi, R.; Chmielewski, J. Endothiopeptide inhibitors of HIV-1 protease. *Bioorganic & medicinal chemistry letters* **1998**, *8* (6), 699–704. DOI: 10.1016/s0960-894x(98)00100-0.
268. Asbóth, B.; Polgár, L. Transition-state stabilization at the oxyanion binding sites of serine and thiol proteinases: hydrolyses of thiono and oxygen esters. *Biochemistry* **1983**, *22* (1), 117–122. DOI: 10.1021/bi00270a017.
269. Campbell, P.; Nashed, N. T.; Lapinskas, B. A.; Gurrieri, J. Thionesters as a probe for electrophilic catalysis in the serine protease mechanism. *The Journal of biological chemistry* **1983**, *258* (1), 59–66.
270. Schutkowski, M.; Neubert, K.; Fischer, G. Influence on proline-specific enzymes of a substrate containing the thioxoaminoacyl-prolyl peptide bond. *European journal of biochemistry* **1994**, *221* (1), 455–461. DOI: 10.1111/j.1432-1033.1994.tb18758.x.
271. Polgár, L.; Kollt, E.; Hollósi, M. Prolyl oligopeptidase catalysis. Reactions with thiono substrates reveal substrate-induced conformational change to be the rate-limiting step. *FEBS letters* **1993**, *322* (3), 227–230. DOI: 10.1016/0014-5793(93)81575-k.
272. Schutkowski, M.; Jakob, M.; Landgraf, G.; Born, I.; Neubert, K.; Fischer, G. Probing substrate backbone function in prolyl oligopeptidase catalysis--large positional effects of peptide bond monothioxylation. *European journal of biochemistry* **1997**, *245* (2), 381–385. DOI: 10.1111/j.1432-1033.1997.00381.x.
273. Curley, K.; Pratt, R. F. The Oxyanion Hole in Serine beta-Lactamase Catalysis: Interactions of Thiono Substrates with the Active Site. *Bioorganic chemistry* **2000**, *28* (6), 338–356. DOI: 10.1006/bioo.2000.1184.
274. Hussain, S.; Pinitglang, S.; Bailey, T. S. F.; Reid, J. D.; Noble, M. A.; Resmini, M.; Thomas, E. W.; Greaves, R. B.; Verma, C. S.; Brocklehurst, K. Variation in the pH-dependent pre-steady-state and steady-state kinetic characteristics of cysteine-proteinase mechanism: evidence for electrostatic modulation of catalytic-site function by the neighbouring carboxylate anion. *The Biochemical journal* **2003**, *372* (Pt 3), 735–746. DOI: 10.1042/BJ20030177.
275. Foje, K. L.; Hanzlik, R. P. Peptidyl thioamides as substrates and inhibitors of papain, and as probes of the kinetic significance of the oxyanion hole. *Biochimica et biophysica acta* **1994**, *1201* (3), 447–453. DOI: 10.1016/0304-4165(94)90075-2.
276. Thompson, S. A.; Andrews, P. R.; Hanzlik, R. P. Carboxyl-modified amino acids and peptides as protease inhibitors. *Journal of medicinal chemistry* **1986**, *29* (1), 104–111. DOI: 10.1021/jm00151a018.
277. Meinnel, T.; Patiny, L.; Ragusa, S.; Blanquet, S. Design and synthesis of substrate analogue inhibitors of peptide deformylase. *Biochemistry* **1999**, *38* (14), 4287–4295. DOI: 10.1021/bi982622r.
278. Murphy, B. P.; Pratt, R. F. A thiono-beta-lactam substrate for the beta-lactamase II of *Bacillus cereus*. Evidence for direct interaction between the essential metal ion and substrate. *The Biochemical journal* **1989**, *258* (3), 765–768. DOI: 10.1042/bj2580765.
279. Tsang, W. Y.; Dhanda, A.; Schofield, C. J.; Frère, J.-M.; Galleni, M.; Page, M. I. The inhibition of metallo-beta-lactamase by thioxo-cephalosporin derivatives. *Bioorganic & medicinal chemistry letters* **2004**, *14* (7), 1737–1739. DOI: 10.1016/j.bmcl.2004.01.047.

280. Beattie, R. E.; Elmore, D. T.; Williams, C. H.; Guthrie, D. J. The behaviour of leucine aminopeptidase towards thiono-peptides. *The Biochemical journal* **1987**, *245* (1), 285–288. DOI: 10.1042/bj2450285.
281. Maziak, L.; Lajoie, G.; Belleau, B. Productive conformation in the bound state and hydrolytic behavior of thiopeptide analogs of angiotensin-converting enzyme substrates. *Journal of the American Chemical Society* **1986**, *108* (1), 182–183. DOI: 10.1021/ja00261a034.
282. Mock, W. L.; Chen, J. T.; Tsang, J. W. Hydrolysis of a thiopeptide by cadmium carboxypeptidase A. *Biochemical and biophysical research communications* **1981**, *102* (1), 389–396. DOI: 10.1016/0006-291X(81)91533-3.
283. Bienvenue, D. L.; Gilner, D.; Holz, R. C. Hydrolysis of thiono-peptides by the aminopeptidase from *Aeromonas proteolytica*: insight into substrate binding. *Biochemistry* **2002**, *41* (11), 3712–3719. DOI: 10.1021/bi011752o.
284. Castaneda, C. A.; Lopez, J. E.; Joseph, C. G.; Scholle, M. D.; Mrksich, M.; Fierke, C. A. Active Site Metal Identity Alters Histone Deacetylase 8 Substrate Selectivity: A Potential Novel Regulatory Mechanism. *Biochemistry* **2017**, *56* (42), 5663–5670. DOI: 10.1021/acs.biochem.7b00851.
285. Toro, T. B.; Bryant, J. R.; Watt, T. J. Lysine Deacetylases Exhibit Distinct Changes in Activity Profiles Due to Fluorophore Conjugation of Substrates. *Biochemistry* **2017**, *56* (34), 4549–4558. DOI: 10.1021/acs.biochem.7b00270.
286. Castañeda, C. A.; Wolfson, N. A.; Leng, K. R.; Kuo, Y.-M.; Andrews, A. J.; Fierke, C. A. HDAC8 substrate selectivity is determined by long- and short-range interactions leading to enhanced reactivity for full-length histone substrates compared with peptides. *Journal of Biological Chemistry* **2017**, *292* (52), 21568–21577. DOI: 10.1074/jbc.M117.811026.
287. Yoo, H.; Polsinelli, G. A. Kinetic Characterization of Human Histone Deacetylase 8 With Medium-Chain Fatty Acyl Lysine. *Epigenetics insights* **2021**, *14*, 25168657211065685. DOI: 10.1177/25168657211065685.
288. Riester, D.; Wegener, D.; Hildmann, C.; Schwienhorst, A. Members of the histone deacetylase superfamily differ in substrate specificity towards small synthetic substrates. *Biochemical and biophysical research communications* **2004**, *324* (3), 1116–1123. DOI: 10.1016/j.bbrc.2004.09.155.
289. Goldberg, J. M.; Chen, X.; Meinhardt, N.; Greenbaum, D. C.; Petersson, E. J. Thioamide-based fluorescent protease sensors. *Journal of the American Chemical Society* **2014**, *136* (5), 2086–2093. DOI: 10.1021/ja412297x.
290. Goldberg, J. M.; Batjargal, S.; Petersson, E. J. Thioamides as fluorescence quenching probes: minimalist chromophores to monitor protein dynamics. *Journal of the American Chemical Society* **2010**, *132* (42), 14718–14720. DOI: 10.1021/ja1044924.
291. Goldberg, J. M.; Speight, L. C.; Fegley, M. W.; Petersson, E. J. Minimalist probes for studying protein dynamics: thioamide quenching of selectively excitable fluorescent amino acids. *Journal of the American Chemical Society* **2012**, *134* (14), 6088–6091. DOI: 10.1021/ja3005094.
292. Goldberg, J. M.; Wissner, R. F.; Klein, A. M.; Petersson, E. J. Thioamide quenching of intrinsic protein fluorescence. *Chem. Commun.* **2012**, *48* (10), 1550–1552. DOI: 10.1039/C1CC14708K.
293. Jing, H.; Hu, J.; He, B.; Negrón Abril, Y. L.; Stupinski, J.; Weiser, K.; Carbonaro, M.; Chiang, Y.-L.; Southard, T.; Giannakakou, P.; Weiss, R. S.; Lin, H. A SIRT2-Selective Inhibitor Promotes c-Myc Oncoprotein Degradation and Exhibits Broad Anticancer Activity. *Cancer Cell* **2016**, *29* (3), 297–310. DOI: 10.1016/j.ccell.2016.02.007.
294. Vogelmann, A.; Schiedel, M.; Wössner, N.; Merz, A.; Herp, D.; Hammelmann, S.; Colcerasa, A.; Komaniecki, G.; Hong, J. Y.; Sum, M.; Metzger, E.; Neuwirt, E.; Zhang, L.; Einsle, O.; Groß, O.; Schüle, R.; Lin, H.; Sippl, W.; Jung, M. Development of a NanoBRET assay to validate inhibitors of Sirt2-mediated lysine deacetylation and defatty-acylation that block prostate cancer cell migration. *RSC Chemical Biology* **2022**, *3* (4), 468–485. DOI: 10.1039/d1cb00244a.
295. Rumpf, T.; Schiedel, M.; Karaman, B.; Roessler, C.; North, B. J.; Lehotzky, A.; Oláh, J.; Ladwein, K. I.; Schmidtkunz, K.; Gajer, M.; Pannek, M.; Steegborn, C.; Sinclair, D. A.; Gerhardt, S.; Ovádi, J.; Schutkowski, M.; Sippl, W.; Einsle, O.; Jung, M. Selective Sirt2 inhibition by ligand-induced rearrangement of the active site. *Nat Commun* **2015**, *6*, 6263. DOI: 10.1038/ncomms7263.
296. Outeiro, T. F.; Kontopoulos, E.; Altmann, S. M.; Kufareva, I.; Strathearn, K. E.; Amore, A. M.; Volk, C. B.; Maxwell, M. M.; Rochet, J.-C.; McLean, P. J.; Young, A. B.; Abagyan, R.; Feany, M. B.;

- Hyman, B. T.; Kazantsev, A. G. Sirtuin 2 inhibitors rescue alpha-synuclein-mediated toxicity in models of Parkinson's disease. *Science (New York, N.Y.)* **2007**, *317* (5837), 516–519. DOI: 10.1126/science.1143780.
297. Lanyon-Hogg, T.; Ritzefeld, M.; Sefer, L.; Bickel, J. K.; Rudolf, A. F.; Panyain, N.; Bineva-Todd, G.; Ocasio, C. A.; O'Reilly, N.; Siebold, C.; Magee, A. I.; Tate, E. W. Acylation-coupled lipophilic induction of polarisation (Acyl-cLIP): a universal assay for lipid transferase and hydrolase enzymes. *Chem. Sci.* **2019**, *10* (39), 8995–9000. DOI: 10.1039/c9sc01785b.
298. Baell, J. B.; Holloway, G. A. New substructure filters for removal of pan assay interference compounds (PAINS) from screening libraries and for their exclusion in bioassays. *Journal of medicinal chemistry* **2010**, *53* (7), 2719–2740. DOI: 10.1021/jm901137j.
299. Suenkel, B.; Fischer, F.; Steegborn, C. Inhibition of the human deacylase Sirtuin 5 by the indole GW5074. *Bioorganic & medicinal chemistry letters* **2013**, *23* (1), 143–146. DOI: 10.1016/j.bmcl.2012.10.136.
300. Sun, P.; Wang, J.; Khan, K. S.; Yang, W.; Ng, B. W.-L.; Ilment, N.; Zessin, M.; Bülbül, E. F.; Robaa, D.; Erdmann, F.; Schmidt, M.; Romier, C.; Schutkowski, M.; Cheng, A. S.-L.; Sippl, W. Development of Alkylated Hydrazides as Highly Potent and Selective Class I Histone Deacetylase Inhibitors with T cell Modulatory Properties. *Journal of medicinal chemistry* **2022**, *65* (24), 16313–16337. DOI: 10.1021/acs.jmedchem.2c01132.
301. Wei, W.; Zhang, J.; Xu, Z.; Liu, Z.; Huang, C.; Cheng, K.; Meng, L.; Matsuda, Y.; Hao, Q.; Zhang, H.; Sun, H. Universal Strategy to Develop Fluorogenic Probes for Lysine Deacetylase/Demethylase Activity and Application in Discriminating Demethylation States. *ACS sensors* **2023**, *8* (1), 28–39. DOI: 10.1021/acssensors.2c01345.
302. Jin, J.; Bai, L.; Wang, D.; Ding, W.; Cao, Z.; Yan, P.; Li, Y.; Xi, L.; Wang, Y.; Zheng, X.; Wei, H.; Ding, C.; Wang, Y. SIRT3-dependent deacetylation of cyclin E2 prevents hepatocellular carcinoma growth. *EMBO reports* **2023**, e56052. DOI: 10.15252/embr.202256052.
303. Pillai, V. B.; Samant, S.; Sundaresan, N. R.; Raghuraman, H.; Kim, G.; Bonner, M. Y.; Arbisser, J. L.; Walker, D. I.; Jones, D. P.; Gius, D.; Gupta, M. P. Honokiol blocks and reverses cardiac hypertrophy in mice by activating mitochondrial Sirt3. *Nat Commun* **2015**, *6*, 6656. DOI: 10.1038/ncomms7656.
304. Morimoto, J.; Hayashi, Y.; Suga, H. Discovery of Macrocyclic Peptides Armed with a Mechanism-Based Warhead: Isoform-Selective Inhibition of Human Deacetylase SIRT2. *Angew. Chem.* **2012**, *124* (14), 3479–3483. DOI: 10.1002/ange.201108118.
305. Patel, K. D.; Mohid, S. A.; Dutta, A.; Arichthota, S.; Bhunia, A.; Haldar, D.; Sarojini, V. Synthesis and antibacterial study of cell-penetrating peptide conjugated trifluoroacetyl and thioacetyl lysine modified peptides. *European Journal of Medicinal Chemistry* **2021**, *219*, 113447. DOI: 10.1016/j.ejmech.2021.113447.
306. Baldensperger, T.; Eggen, M.; Kappen, J.; Winterhalter, P. R.; Pfirrmann, T.; Glomb, M. A. Comprehensive analysis of posttranslational protein modifications in aging of subcellular compartments. *Sci Rep* **2020**, *10* (1), 7596. DOI: 10.1038/s41598-020-64265-0.
307. Su, D.; Kosciuk, T.; Yang, M.; Price, I. R.; Lin, H. Binding Affinity Determines Substrate Specificity and Enables Discovery of Substrates for N-Myristoyltransferases. *ACS Catalysis* **2021**, *11* (24), 14877–14883. DOI: 10.1021/acscatal.1c03330.
308. Bagchi, R. A.; Robinson, E. L.; Hu, T.; Cao, J.; Hong, J. Y.; Tharp, C. A.; Qasim, H.; Gavin, K. M.; Da Pires Silva, J.; Major, J. L.; McConnell, B. K.; Seto, E.; Lin, H.; McKinsey, T. A. Reversible lysine fatty acylation of an anchoring protein mediates adipocyte adrenergic signaling. *Proceedings of the National Academy of Sciences of the United States of America* **2022**, *119* (7). DOI: 10.1073/pnas.2119678119.
309. Jing, H.; Zhang, X.; Wisner, S. A.; Chen, X.; Spiegelman, N. A.; Linder, M. E.; Lin, H. SIRT2 and lysine fatty acylation regulate the transforming activity of K-Ras4a. *eLife* **2017**, *6*. DOI: 10.7554/eLife.32436.
310. Spiegelman, N. A.; Zhang, X.; Jing, H.; Cao, J.; Kotliar, I. B.; Aramsangtienchai, P.; Wang, M.; Tong, Z.; Rosch, K. M.; Lin, H. SIRT2 and Lysine Fatty Acylation Regulate the Activity of RalB and Cell Migration. *ACS Chem. Biol.* **2019**, *14* (9), 2014–2023. DOI: 10.1021/acscchembio.9b00492.
311. Wang, Z. A.; Millard, C. J.; Lin, C.-L.; Gurnett, J. E.; Wu, M.; Lee, K.; Fairall, L.; Schwabe, J. W.; Cole, P. A. Diverse nucleosome Site-Selectivity among histone deacetylase complexes. *eLife* **2020**, *9*. DOI: 10.7554/eLife.57663.

Danksagung

An dieser Stelle möchte ich mich bei allen Personen bedanken, die zum Gelingen dieser Arbeit beigetragen haben.

Besonderer Dank gilt hierbei Prof. Dr. Mike Schutkowski, der es mir ermöglicht hat in seiner Arbeitsgruppe die Promotion anzufertigen. Weiterhin möchte ich mich bei ihm für die gute Betreuung, für das stetige Interesse an meiner Arbeit und die vielen guten Ratschläge und gemeinsamen Diskussionen danken, die zur Vollendung der Arbeit beigetragen haben.

Mein Dank gilt ebenso Prof. Dr. Wolfgang Sippl der die finanzielle Möglichkeit geschaffen hat meine Promotion durchzuführen. Außerdem möchte ich mich bei ihm dafür bedanken, dass er jederzeit zur Verfügung stand, um mir bei wissenschaftlichen oder organisatorischen Anliegen zu helfen.

Auch möchte ich mich an dieser Stelle bei Dr. Cordelia Schiene-Fischer dafür bedanken, dass ich jederzeit mit ihr über wissenschaftliche Fragestellungen diskutieren konnte und dass sie sich auch im Nachgang der Diskussion oft den Kopf über aufgetretene Probleme zerbrochen hat und anschließend einige Tage später mit einer ausgezeichneten Idee aufwarten konnte. Außerdem möchte ich ihr für die Hilfe bei der Finalisierung der Dissertation danken.

Ich bedanke mich ganz herzlich bei Dr. Cyril Barinka und Dr. Zsofia Kutil für die wunderbare Zusammenarbeit und die Bereitstellung der HDACs. Ebenso gilt mein Dank Dr. Sandra Liebscher und Mareike Leidig für die Bereitstellung der Sirtuine.

Ganz besonderer Dank geht an Dr. Marat Meleshin und Dr. Diana Kalbas. Mit Diana konnte ich mich im Büro jederzeit über wissenschaftliche und auch nicht ganz so wissenschaftliche Themen unterhalten. Bei Marat möchte ich mich für jede Hilfe bedanken, die er mir zukommen ließ, sei es ein wissenschaftlicher Rat oder ein synthetisiertes Peptid, was ich ganz schnell brauchte. Ebenso möchte ich mich bei Sebastian Hilscher für jeden Plausch bedanken und dafür, dass er meine entwickelten Assays für seine Arbeit weiterhin nutzt.

Auch bei Ilona Kunze bedanke ich mich für die Reinigung diverser Peptide, für die netten Pausengespräche und für jede Süßigkeit, die mir zugesteckt wurde, wenn es mal wieder etwas spät wurde.

Ich bedanke mich ganz herzlich bei allen nicht genannten Personen, die mir bei der Arbeit geholfen haben, bei allen Mitgliedern der AG Enzymologie für das angenehme Arbeitsklima. Auch bei allen Studierenden, die während meiner Zeit in der AG Enzymologie dort ihre Abschlussarbeit angefertigt haben, bedanke ich mich für die gemeinsame Zeit.

Auch bei meiner Familie und Freunden, und besonders bei meinen Eltern und Geschwistern bedanke ich mich für jegliche Unterstützung. Vor allem möchte ich mich bei Alex und meiner Schwester Johanna bedanken, die beim Finalisieren der Arbeit besonderen Enthusiasmus gezeigt haben.

Zum Schluss möchte ich mich von tiefsten Herzen bei meiner Partnerin Katharina Jansen bedanken, die mich beim Anfertigen dieser Arbeit immer unterstützt hat.

Publikationsliste

Publikationen im Zusammenhang mit der Dissertation:

- Continuous Activity Assay for HDAC11 Enabling Reevaluation of HDAC Inhibitors
ACS OMEGA. **2019**, 22 (4), 19895–19904, <https://doi.org/10.1021/acsomega.9b02808>
- One-Atom Substitution Enables Direct and Continuous Monitoring of Histone Deacetylase Activity
Biochemistry. **2019**, 58 (48), 4777–4789, <https://doi.org/10.1021/acs.biochem.9b00786>
- Continuous Sirtuin/HDAC (histone deacetylase) activity assay using thioamides as PET (Photoinduced Electron Transfer)-based fluorescence quencher
Bioorg Chem, **2021**, 117, 105425, <https://doi.org/10.1016/j.bioorg.2021.105425>
- Continuous Histone Deacetylase Activity Assays
Methods mol. biol. **2022**, 2589, 411–428, https://doi.org/10.1007/978-1-0716-2788-4_27
- Continuous Fluorescent Sirtuin Activity Assay Based on Fatty Acylated Lysines
Int. J. Mol. Sci. **2023**, 24 (8), 7416, <https://doi.org/10.3390/ijms24087416>
- Uncovering Robust Delactoylase and Depyruvoylase Activities of HDAC Isoforms
ACS Chem. Biol. **2022**, 17 (6), 1364–1375, <https://doi.org/10.1021/acscchembio.1c00863>

Publikationen, die nicht direkt im Zusammenhang mit der Dissertation stehen:

- Synthesis, Molecular Docking and Biological Characterization of Pyrazine Linked 2-Aminobenzamides as New Class I Selective Histone Deacetylase (HDAC) Inhibitors with Anti-Leukemic Activity
Int. J. Mol. Sci. **2022**, 23 (1), 369, <https://doi.org/10.3390/ijms23010369>
- Docking, Binding Free Energy Calculations and In Vitro Characterization of Pyrazine Linked 2-Aminobenzamides as Novel Class I Histone Deacetylase (HDAC) Inhibitors.
Molecules **2022**; 27 (8), 2526. <https://doi.org/10.3390/molecules27082526>
- Development of New Inhibitors of HDAC1–3 Enzymes Aided by In Silico Design Strategies
J. Chem. Inf. Model. **2022**, 62 (10), 2387–2397, <https://doi.org/10.1021/acs.jcim.1c01557>
- Small Changes Make the Difference for SIRT2: Two Different Binding Modes for 3-Arylmercapto-Acylated Lysine Derivatives
Biochemistry **2022**, 61 (17), 1705–1722, <https://doi.org/10.1021/acs.biochem.2c00211>
- Development of Alkylated Hydrazides as Highly Potent and Selective Class I Histone Deacetylase Inhibitors with T cell Modulatory Properties
J. Med. Chem. **2022**, 65 (24), 16313–16337, <https://doi.org/10.1021/acs.jmedchem.2c01132>

Development of Pyrazine-Anilinobenzamides as Histone Deacetylase HDAC1-3 Selective Inhibitors and Biological Testing Against Pancreas Cancer Cell Lines

Methods mol. biol. **2023**, 2589, 145–155, https://doi.org/10.1007/978-1-0716-2788-4_10

Application of Ligand- and Structure-Based Prediction Models for the Design of Alkylhydrazide-Based HDAC3 Inhibitors as Novel Anti-Cancer Compounds

Pharmaceuticals. **2023**; 16 (7), 968, <https://doi.org/10.3390/ph16070968>

Novel hydroxamic acid derivative induces apoptosis and constrains autophagy in leukemic cells

J. Adv. Res. **2023**, <https://doi.org/10.1016/j.jare.2023.07.005>

Lebenslauf

Persönliche Daten:

Name: Matthes Zessin
Nationalität: deutsch

Studium:

12/2017 – 11/2022 **Promotionsstudium,
angestrebter Abschluss Dr. rer. nat.**
Martin-Luther-Universität Halle-Wittenberg,
Institut für Biochemie und Biotechnologie,
Abteilung Enzymologie

10/2014 – 05/2017 **Master of Science (Biochemie)**
Martin-Luther-Universität Halle-Wittenberg
Masterarbeit, Abteilung Enzymologie
Thema: „Synthese und Charakterisierung von
Sirtuin-Substraten“

10/2011 – 09/2014 **Bachelor of Science (Biochemie)**
Martin-Luther-Universität Halle-Wittenberg
Bachelorarbeit, Abteilung Pflanzenbiochemie
Thema: „Analyse der entwicklungsabhängigen
Veränderung im Chloroplasten-Proteom von
Arabidopsis thaliana“

Schule:

07/2001 – 05/2010 **Allgemeine Hochschulreife**
„Glückauf“-Gymnasium Dippoldiswalde/Altenberg

Selbstständigkeitserklärung

Hiermit erkläre ich eidesstattlich, dass ich die vorliegende Arbeit selbstständig und ohne fremde Hilfe verfasst habe. Ich habe keine anderen Quellen oder Hilfsmittel genutzt als die in dieser Arbeit angegebenen und die den benutzten Werken wörtlich oder inhaltlichen entnommenen Stellen als Solche kenntlich gemacht.

Ich versichere hiermit, dass ich mich mit dieser eingereichten Arbeit das erste Mal um die Erlangung des Doktorgrades bewerbe.

Ort, Datum

Unterschrift